MICROBIAL STRESS: FROM MODEL ORGANISMS TO APPLICATIONS IN FOOD, MICROBIOTECHNOLOGY AND MEDICINE

EDITED BY: Aleksandra P. Djukic-Vukovic, Daniela De Biase, Peter Adrian Lund, Nuno Pereira Mira and Jana Sedlakova-Kadukova

PUBLISHED IN: Frontiers in Microbiology

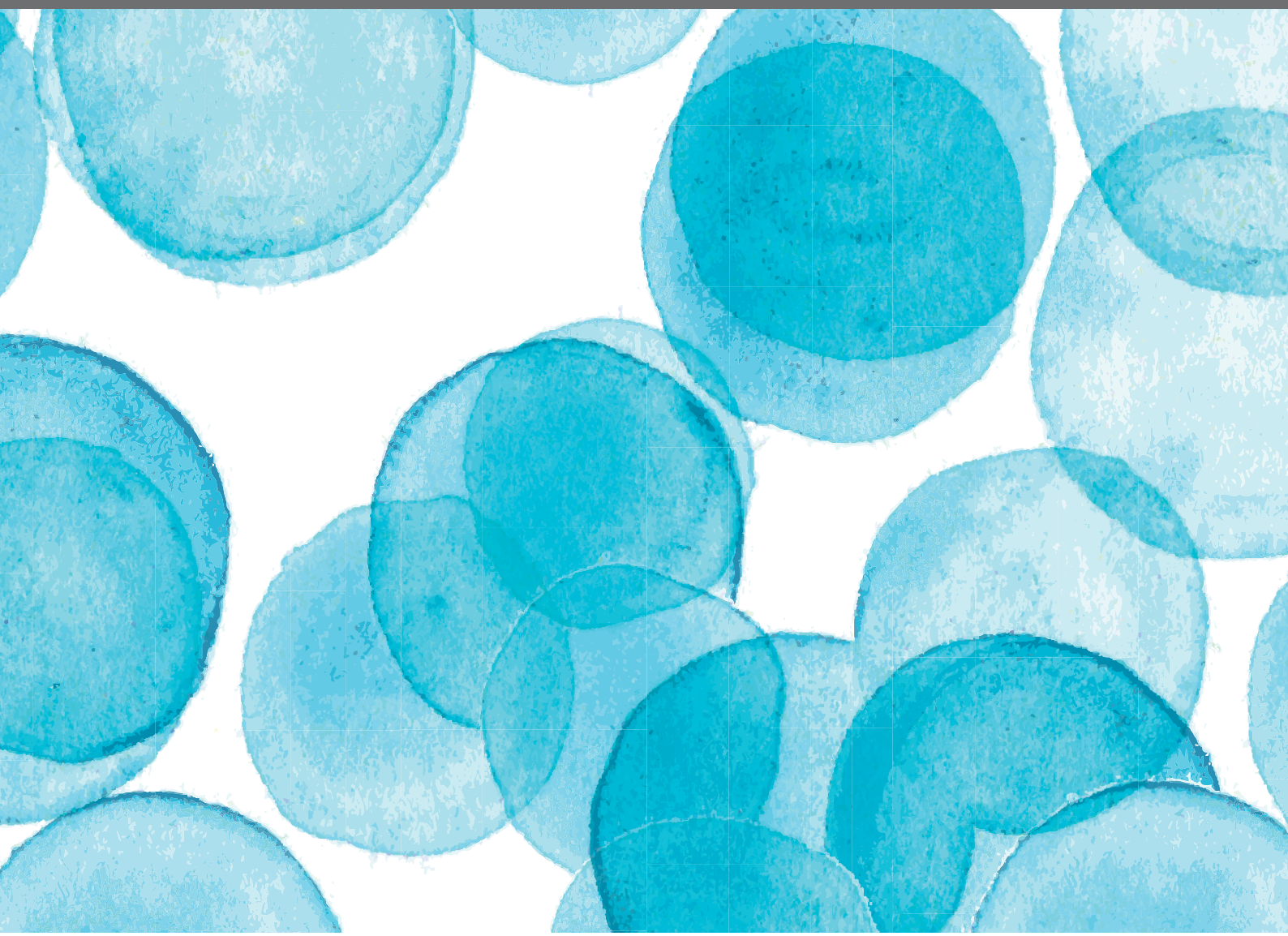

frontiers Research Topics

ISSN 1664-8714
ISBN 978-2-88976-619-2
DOI 10.3389/978-2-88976-619-2

About Frontiers

Frontiers is more than just an open-access publisher of scholarly articles: it is a pioneering approach to the world of academia, radically improving the way scholarly research is managed. The grand vision of Frontiers is a world where all people have an equal opportunity to seek, share and generate knowledge. Frontiers provides immediate and permanent online open access to all its publications, but this alone is not enough to realize our grand goals.

Frontiers Journal Series

The Frontiers Journal Series is a multi-tier and interdisciplinary set of open-access, online journals, promising a paradigm shift from the current review, selection and dissemination processes in academic publishing. All Frontiers journals are driven by researchers for researchers; therefore, they constitute a service to the scholarly community. At the same time, the Frontiers Journal Series operates on a revolutionary invention, the tiered publishing system, initially addressing specific communities of scholars, and gradually climbing up to broader public understanding, thus serving the interests of the lay society, too.

Dedication to Quality

Each Frontiers article is a landmark of the highest quality, thanks to genuinely collaborative interactions between authors and review editors, who include some of the world's best academicians. Research must be certified by peers before entering a stream of knowledge that may eventually reach the public - and shape society; therefore, Frontiers only applies the most rigorous and unbiased reviews.
Frontiers revolutionizes research publishing by freely delivering the most outstanding research, evaluated with no bias from both the academic and social point of view. By applying the most advanced information technologies, Frontiers is catapulting scholarly publishing into a new generation.

What are Frontiers Research Topics?

Frontiers Research Topics are very popular trademarks of the Frontiers Journals Series: they are collections of at least ten articles, all centered on a particular subject. With their unique mix of varied contributions from Original Research to Review Articles, Frontiers Research Topics unify the most influential researchers, the latest key findings and historical advances in a hot research area! Find out more on how to host your own Frontiers Research Topic or contribute to one as an author by contacting the Frontiers Editorial Office: frontiersin.org/about/contact

MICROBIAL STRESS: FROM MODEL ORGANISMS TO APPLICATIONS IN FOOD, MICROBIOTECHNOLOGY AND MEDICINE

Topic Editors:
Aleksandra P. Djukic-Vukovic, University of Belgrade, Serbia
Daniela De Biase, Sapienza University of Rome, Italy
Peter Adrian Lund, University of Birmingham, United Kingdom
Nuno Pereira Mira, University of Lisbon, Portugal
Jana Sedlakova-Kadukova, University of St. Cyril and Methodius, Slovakia

Citation: Djukic-Vukovic, A. P., De Biase, D., Lund, P. A., Mira, N. P., Sedlakova-Kadukova, J., eds. (2022). Microbial Stress: From Model Organisms to Applications in Food, Microbiotechnology and Medicine. Lausanne: Frontiers Media SA. doi: 10.3389/978-2-88976-619-2

Table of Contents

frontiers | Frontiers in Microbiology

EDITORIAL
published: 27 June 2022
doi: 10.3389/fmicb.2022.945573

Editorial: Microbial Stress: From Model Organisms to Applications in Food, Microbiotechnology and Medicine

Aleksandra Djukić-Vuković[1]*, *Nuno P. Mira*[2,3], *Jana Sedlakova-Kadukova*[4], *Daniela De Biase*[5] *and Peter A. Lund*[6]

[1] Department of Biochemical Engineering and Biotechnology, Faculty of Technology and Metallurgy, University of Belgrade, Belgrade, Serbia, [2] Institute for Bioengineering and Biosciences, Instituto Superior Técnico—Department of Bioengineering, Universidade de Lisboa, Lisboa, Portugal, [3] Associate Laboratory i4HB—Institute for Health and Bioeconomy at Instituto Superior Técnico, Universidade de Lisboa, Lisboa, Portugal, [4] Department of Ecochemistry and Radioecology, Faculty of Natural Sciences, University of St. Cyril and Methodius in Trnava, Trnava, Slovakia, [5] Department of Medico-Surgical Sciences and Biotechnologies, Sapienza University of Rome, Latina, Italy, [6] Institute of Microbiology and Infection, School of Biosciences, University of Birmingham, Birmingham, United Kingdom

Keywords: methodologies in microbial stress studies, adaptive responses in microbial stress and tolerance, structure-function relationship in stress adaptation, acid stress, OMICS stress responses, food safety, stress responses and bioremediation, antimicrobial stress responses

Editorial on the Research Topic

Microbial Stress: From Model Organisms to Applications in Food, Microbiotechnology and Medicine

OPEN ACCESS

Edited and reviewed by:
Biswarup Mukhopadhyay, Virginia Tech, United States

***Correspondence:**
Aleksandra Djukić-Vuković
adjukic@tmf.bg.ac.rs

Specialty section:
This article was submitted to Microbial Physiology and Metabolism, a section of the journal Frontiers in Microbiology

Received: *16 May 2022*
Accepted: *10 June 2022*
Published: *27 June 2022*

Citation:
Djukić-Vuković A, Mira NP, Sedlakova-Kadukova J, De Biase D and Lund PA (2022) Editorial: Microbial Stress: From Model Organisms to Applications in Food, Microbiotechnology and Medicine. Front. Microbiol. 13:945573. doi: 10.3389/fmicb.2022.945573

Within this Research Topic (RT) we have collected articles addressing microbial stress with special attention on methodology and applications in food technology, medicine or microbiotechnology. We anticipated contributions from members of COST action CA18113 EuroMicropH "*Understanding and exploiting the impact of low pH on micro-organism*" (COST, 2019), but in the final collection (which attracted 85 authors from 17 countries), we were happy to see many contributing authors from outside this network. This shows the breadth and importance of the topic and also the potential for expansion of the COST network. With 14 original research articles, 1 methods and 1 review article, this RT shows that microbial stress in the above contexts is mostly a result of a combination of stressors. This makes it challenging to understand mechanisms and exploit this knowledge although significant efforts are dedicated to it (De Biase et al., 2020a,b; Lund et al., 2020). The main goal of our EuroMicropH community is to translate research on low pH in particular, and microbial stress in general, between fields, and to identify conceptual and methodological gaps in that knowledge. Our RT helps to address this. We hope it will help the development of new approaches to infection control, while improving food and drink processing and the use of microorganisms in green industrial processes.

NEW METHODOLOGIES TO STUDY MICROORGANISMS UNDER STRESS

Modeling microbial growth under stress conditions is crucial to ensure food safety. Lag phase is one important component that can be hard to model. Akkermans and Van Impe present a new method combining improved sampling to reduce error, and simulations to identify which parameters are

most important in providing accurate estimates of lag phase under different conditions. Beyond food safety applications, monitoring of the growth and cellular metabolic state helps increase bioprocess productivity. To accelerate the design of high-performing yeast strains, Pianale et al. developed a toolbox of intracellular biosensors to monitor pH, redox state, ATP levels, glycolytic flux, and ribosome production, all important for a robust stress response. They demonstrated how these biosensors can be used to show how these parameters are affected by stress during fermentation of a synthetic wheat straw hydrolysate.

FERMENTATION STRESS

Microbe-based hydrolysis and fermentation of lignocellulose is a key target for green economies, but it can be hampered by compounds such as furfural that arise during biomass pretreatment. A furfural-resistant *Zymomonas mobilis* strain was characterized by Hu et al. using complementation and RNA-seq, and they identified several aspects of its resistance mechanism, including increased breakdown of furfural, increased flocculation, increased chaperone production, and down-regulation of energy-intensive transporters. Didak Ljubas et al. also identified furfural as an important inhibitor of *Paenibacillus polymyxa* DSM 742, a newly-used bacterial strain for the production of 2,3-butanediol, lactic acid and ethanol. Fermentation stress caused by changes in pH of media, presence of furfural and oxygen caused changes in metabolic activity which can be valorized by process optimization and strain adaptation. This should help future engineering of improved strains.

Fermentation stress is caused by combination of a stressors, and adaptive laboratory evolution is a convenient technique to study it and get more resistant strains. Resistance to fermentation stress in the acetic acid bacterium *Komagataeibacter medellinensis* was studied in this way by Kataoka et al.. Through this approach they obtained strains with improved growth and fermentation yield at high temperatures in the presence of ethanol and acetic acid. Whole genome sequencing revealed mutations in *gyrB*, *spoT*, and *degP*. The effects of mutation of the latter two genes alone were studied by making further targeted mutations, the analysis of which suggested they have roles in cell surface stability and cell elongation. More in depth analysis of oxidative stress, which is often seen in bioprocesses and can cause problems with yield, was provided by Kocaefe-Özşen et al.. They also used adaptive laboratory evolution, in this case to produce strains of the yeast *Saccharomyces cerevisiae* that showed enhanced resistance to oxidative stress. A full physiological and genomic characterization of the resistant strains showed many adaptations, including elevated trehalose and glycogen synthesis, and also showed the strains had become resistant to other additional stresses such as heat, high salt, and ethanol. Although these studies were performed for intensification of bioprocesses, results may also be useful in the food industry, where these stressors are applied intentionally with aim of inactivating food-borne pathogens, or in hurdle technology approaches.

LOW pH, NaCl, AND NITROSATIVE STRESS IN HEALTH AND DISEASE

Pathogenic microorganisms are exposed to low pH or NaCl in food by means of preservation, to low pH, bile salts and varying oxygen concentration in the gastrointestinal tract (GIT), and to nitrosative stress as a defense mechanism in GIT, skin, and other mucosal surfaces. Under physiological conditions, or during infection or food processing, selective environments force microorganisms to adapt, and this will determine their abilities to colonize and survive. This is the case both with pathogens (e.g., *L. monocytogenes*, *S. aureus*, etc.) or with organisms that are beneficial (e.g., as probiotics) for the host.

Among food-borne pathogens, *Listeria monocytogenes* has an important place, causing even fatal outcomes. Lakićević et al. describe the mechanisms that *L. monocytogenes* can employ to persist in different habitats, such as farms, food production environments, and foods. The authors focused on the stress response genes that allow *L. monocytogenes* to grow at low pH, low temperature, high salt concentrations as well as on the virulence genes that contribute to the high degree of strain divergence. In the case of one particular strain, *L. monocytogenes* F2365, Chakravarty et al. studied transcription variations when exposed to acid and bile salts under anaerobic and aerobic conditions. Upon exposure to anaerobiosis in acidic conditions, variations in the transcript levels for the virulence factors including internalins and listeriolysin O were determined as well as for many histidine sensory kinases, helping to understand strain response to varying oxygen concentration throughout GIT.

Brucella species are another important group of pathogens, which can be transmitted in contaminated foods as well as *via* other routes, and acid resistance is an important factor determining the their prevalence. de la Garza-García et al. used RNAseq to compare acid responses of two species, one of which (*B. microti*) is particularly resistant to acid, and identified a wide range of responses, some in common and some unique to *B. microti*. These included induction of the cold shock protein CspA and the general stress protein Dps, together with other changes which may be relevant to the survival of these organisms in soil or foods. Although NaCl is commonly used for food preservation, it is identified as a risk factor for cardiovascular diseases and significant effort is being made to decrease its level in food. However, work of Etter et al. showed the important influence of NaCl on the expression of staphylococcal enterotoxin C (SEC), a cause of foodborne intoxication. By using qRT-PCR and analyzing protein expression levels, they found that mild NaCl stress as a hurdle can cause a decrease in SEC levels in different *Staphylococcus aureus* strains. Therefore, while lowering salt content in food is regarded as a positive way to reduce cardiovascular diseases, it could lead to an increase in SEC production and therefore food poisoning.

The neurotransmitter NO_2 can accumulate in high concentrations and lead to nitrosative stress. Nasuno et al. described how pathogenic *Candida glabrata* cells cope with nitrosative stress through the activity of the riboflavin biosynthesis gene *RIB1*. It was also shown that expression

of *RIB1* increases survival of *C. glabrata* in the presence of macrophage-like cells. Genes that, like *RIB1*, mediate tolerance of *C. glabrata* to stress are an interesting target for the development of new therapeutic targets. Gu et al. reported also potential therapeutic agents produced by *Bacillus* sp. YJ17 isolated from the deep-sea cold seep. Two compounds belonging to family of fengycin and surfactin showed stronger antibacterial properties when compared to the commercial food preservative nisin, and were efficient against multidrug-resistant bacteria. Synergies between stressors could be important for antimicrobial activity as confirmed by Masoura et al. for honey. The authors used genome-wide transposon mutagenesis combined with high-throughput sequencing (TraDIS) to identify genes in *E. coli* K-12 MG1655 which are needed for resistance to honey's antimicrobial effects. They include genes which encode membrane proteins like those involved in uptake of essential molecules, and components of the electron transport chain. They are enriched for pathways involved in intracellular homeostasis and redox activity. Moreover, Lovšin et al. obtained interesting results showing that exposure to abiotic stress by electroporation, a phenomenon mainly related to cell membranes, can modulate the susceptibility of *E. coli* to antibiotics with mechanisms which go beyond membrane permeabilization.

METALS AS MICROBIAL STRESSORS IN THE ENVIRONMENT

Joudeh et al. reported that Pd-stress induced wide changes in *E. coli* genomic expression, resulting in drastic alterations in the expression of transporters of inorganic ion complexes. Additionally, up-regulation of genes encoding multidrug-efflux pumps was suggested to improve tolerance to Pd by reducing intracellular accumulation due to reduced influx and improved efflux. Other detoxification strategies included intracellular chelation of Pd by histidine and histidine-rich proteins and enzyme-mediated formation of less toxic nanoparticles. The generated knowledge is expected to contribute to the design of Pd-tolerant *E. coli* strains, accelerating microbial production of this important catalyst. Šimonovičová et al. reported on potential of *Aspergillus niger* as a Ni-bioleaching microorganism for treatment of hazardous ash waste with *Chlorella vulgaris* biomass being used for the biosorption of Ni. The total process efficiency reached 46% suggesting a new route not only for waste reduction, but also for recovery of valuable metals for industry.

AUTHOR CONTRIBUTIONS

AD-V, DD, NM, JS-K, and PL did literature survey, wrote the section of the manuscript, and reviewed and corrected the manuscript. AD-V prepared draft version of the manuscript. All authors agreed on the final version of the manuscript.

FUNDING

This work was supported by the COST Action CA18113 and for AD-V by the Ministry of Education, Science and Technological Development of the Republic of Serbia (Contract No. 451-03-68/2022-14/200135).

ACKNOWLEDGMENTS

The work of AD-V, DD, NM, JS-K, and PL was done within the framework of EuroMicropH-COST Action CA18113.

REFERENCES

COST (2019). *EuroMicropH – COST Action 18113 – CA18113 – Understanding and Exploiting the Impacts of low pH on Micro-Organisms*. Available online at: https://euromicroph.eu/ (accessed May 9, 2022).

De Biase, D., Mira, N., and Lund, P. (2020a). Genes | special issue : mechanisms of microbial adaptation to low pH. *Genes* 12, 53. doi: 10.3390/genes12010053

De Biase, D., Morrissey, J. P., and O'Byrne, C. P. (2020b). Editorial: microbial stress: from sensing to intracellular and population responses. *Front. Microbiol.* 11, 1667. doi: 10.3389/fmicb.2020.01667

Lund, P. A., De Biase, D., Liran, O., Scheler, O., Mira, N. P., Cetecioglu, Z., et al. (2020). Understanding how microorganisms respond to acid pH is central to their control and successful exploitation. *Front. Microbiol.* 11, 556140. doi: 10.3389/fmicb.2020.556140

Conflict of Interest: The authors declare that the research was conducted in the absence of any commercial or financial relationships that could be construed as a potential conflict of interest.

Publisher's Note: All claims expressed in this article are solely those of the authors and do not necessarily represent those of their affiliated organizations, or those of the publisher, the editors and the reviewers. Any product that may be evaluated in this article, or claim that may be made by its manufacturer, is not guaranteed or endorsed by the publisher.

frontiers in Microbiology

ORIGINAL RESEARCH
published: 08 October 2021
doi: 10.3389/fmicb.2021.741836

Transcriptomic Response Analysis of *Escherichia coli* to Palladium Stress

*Nadeem Joudeh[1], Athanasios Saragliadis[1], Christian Schulz[2], André Voigt[2], Eivind Almaas[2] and Dirk Linke[1]**

[1] Department of Biosciences, University of Oslo, Oslo, Norway, [2] Department of Biotechnology and Food Science, Norwegian University of Science and Technology (NTNU), Trondheim, Norway

Palladium (Pd), due to its unique catalytic properties, is an industrially important heavy metal especially in the form of nanoparticles. It has a wide range of applications from automobile catalytic converters to the pharmaceutical production of morphine. Bacteria have been used to biologically produce Pd nanoparticles as a new environmentally friendly alternative to the currently used energy-intensive and toxic physicochemical methods. Heavy metals, including Pd, are toxic to bacterial cells and cause general and oxidative stress that hinders the use of bacteria to produce Pd nanoparticles efficiently. In this study, we show in detail the Pd stress-related effects on *E. coli*. Pd stress effects were measured as changes in the transcriptome through RNA-Seq after 10 min of exposure to 100 μM sodium tetrachloropalladate (II). We found that 709 out of 3,898 genes were differentially expressed, with 58% of them being up-regulated and 42% of them being down-regulated. Pd was found to induce several common heavy metal stress-related effects but interestingly, Pd causes unique effects too. Our data suggests that Pd disrupts the homeostasis of Fe, Zn, and Cu cellular pools. In addition, the expression of inorganic ion transporters in *E. coli* was found to be massively modulated due to Pd intoxication, with 17 out of 31 systems being affected. Moreover, the expression of several carbohydrate, amino acid, and nucleotide transport and metabolism genes was vastly changed. These results bring us one step closer to the generation of genetically engineered *E. coli* strains with enhanced capabilities for Pd nanoparticles synthesis.

Keywords: RNA-seq, heavy metal stress, palladium, precious metals, nanoparticles, oxidative stress, *Escherichia coli*, transcriptional response

OPEN ACCESS

Edited by:
Nuno Pereira Mira, University of Lisbon, Portugal

Reviewed by:
Ricardo Jasso-Chávez, Instituto Nacional de Cardiologia Ignacio Chavez, Mexico
C. French, University of Edinburgh, United Kingdom

***Correspondence:**
Dirk Linke
dirk.linke@ibv.uio.no

Specialty section:
This article was submitted to Microbial Physiology and Metabolism, a section of the journal Frontiers in Microbiology

Received: *15 July 2021*
Accepted: *03 September 2021*
Published: *08 October 2021*

Citation:
Joudeh N, Saragliadis A, Schulz C, Voigt A, Almaas E and Linke D (2021) Transcriptomic Response Analysis of Escherichia coli to Palladium Stress. Front. Microbiol. 12:741836. doi: 10.3389/fmicb.2021.741836

INTRODUCTION

The International Union of Pure and Applied Chemistry (IUPAC) reported in 2002 that there were more than 30 different definitions used in literature for a heavy metal (Duffus, 2002; Pourret, 2018). Nevertheless, density in most cases is considered to be the defining criterion, and heavy metals are commonly defined by a density higher than 5 g/cm^3 (Lozet and Mathieu, 1993; Nies, 1999; Järup, 2003). Most heavy metals are transition metals with partially filled d orbitals. These d orbitals provide the cations of heavy metals with the ability to form complex compounds which may be redox-active (Nies, 1999). Hence, heavy-metal cations play an important role as trace elements in biological systems.

From a physiological point of view, heavy metals are placed in two categories: (1) essential ones, also known as trace elements, and (2) toxic heavy metals. The essential heavy metals [Co, Cu, Fe, Mn, Mo, Ni, V, W, and Zn (Nies and Silver, 2007)] are required in smaller amounts than the bulk metals (Na, K, Mg, and Ca). The essential heavy metals have to be acquired by bacteria from their surrounding environments as inorganic ions (Nies and Silver, 2007). These cations are required for functions that include stabilizing biological molecules (Nies and Silver, 2007), electron transfer and redox processes (Bruins et al., 2000), and as components of metalloenzymes, which account for approximately 30% of all enzymes in bacterial cells (Wackett et al., 2004). The toxic heavy metals are elements that have no known beneficial roles and can be damaging to the cell if taken up (Nies and Silver, 2007). The list of toxic heavy metals includes e.g., Ag, Au, Bi, Cd, Cr, Hg, In, Ir, Pb, Pd, Pt, Sn, and Tl (Nies, 1999; Nies and Silver, 2007).

Both excessive levels of essential heavy-metal ions and the presence of toxic heavy-metal ions cause cellular stress (Nies and Silver, 2007). Unlike organic molecules, heavy metals cannot be broken down by enzymatic reactions, and due to the wide range of toxic effects of some heavy metals, strategies for dealing with those toxic heavy metals are limited (Nies and Silver, 2007). Those strategies include (1) the extracellular detoxification and sequestration of the metal, (2) the prevention of the metal from entering the cell by reducing cell permeability, (3) the active transport of the metal out of the cell, (4) the intracellular sequestration of the metal by binding to proteins, and (5) the enzymatic alteration of the metal to a less toxic form (Rouch et al., 1995).

Bacterial cellular responses to stress caused by metal ions can be measured as changes in the transcription of genes involved in the detoxification processes or metal ion homeostasis. Bacterial transcriptional responses to excessive levels of essential heavy metals have been intensively studied in literature (Kershaw et al., 2005; Lee et al., 2005; Fantino et al., 2010; Gault et al., 2016), but for the toxic heavy metals, this information is often lacking or only exists for key environmental pollutants (Wang and Crowley, 2005; LaVoie and Summers, 2018).

Palladium (Pd), element number 46 in the periodic table, belongs to the platinum group metals and is an industrially important heavy metal due to its unique catalytic properties. It is primarily used as a key component in catalysts for different carbon-carbon coupling reactions such as Heck and Suzuki coupling reactions (Cui et al., 2017; Miller et al., 2017; Biffis et al., 2018). The unique ground-state structure of Pd ($4d^{10}5s^0$) and the square-planar geometry of Pd(II) complexes (d^8) give Pd unique properties in C-C bond formation and C-O bond cleavage (Jbara et al., 2017). Moreover, Pd is also known for its uniquely high capacity for hydrogen gas absorption (Gavia and Shon, 2015). Besides its major application in automobile catalytic converters (Zereini and Alt, 2006), it is used in versatile applications in catalysis (Biffis et al., 2018), sensors (Kundu et al., 2015), fuel cells (Feliciano-Ramos et al., 2014), and electronics (Zhang G. et al., 2019). Due to its increased industrial use and limited supply, its price has increased more than 27 times in the last 30 years (3,000$/kg in 1990 to 83,000$/kg in 2021)[1]. Consequently, the recovery of waste Pd has become of prime importance. The current techniques for Pd recovery include costly and non-environmentally friendly processes, such as pyrometallurgy, solvent extraction, chemical treatment and electrochemical recovery (Baxter-Plant et al., 2002). Therefore, alternative eco-friendly processes for Pd recovery, such as biomineralization, are of high interest (Lloyd et al., 2020).

Pd ions can be taken up and reduced to Pd nanoparticles by living organisms, such as plants (Vishnukumar et al., 2017), fungi (Tarver et al., 2019), and microorganisms (De Corte et al., 2012). Microorganisms and especially bacteria, due to their fast growth rate and inexpensive cultivation media, are considered one of the most efficient systems for the reduction of Pd (Matsumoto et al., 2020). The formation of Pd nanoparticles through bioreductive deposition of Pd^{2+} ions was intensively studied in different bacteria (De Corte et al., 2012). This metabolic side process is believed to happen during hydrogen production through anaerobic fermentation in *E. coli* (Deplanche et al., 2010) and other obligate and facultative anaerobes (Hennebel et al., 2011), or in the process of sulfate and metal reduction in sulfate-reducing (Lloyd et al., 1998) and metal-reducing bacteria (De Windt et al., 2005). Due to its advantageous properties and its status as a model organism, *E. coli* has been widely used in the recovery of heavy metals and the reduction of metal ions for nanoparticles synthesis (Du et al., 2007; Gurunathan et al., 2009; Quintelas et al., 2009).

The use of *E. coli* whether for Pd recovery or Pd nanoparticles synthesis requires a deep understanding of the exposure effects that Pd causes to *E. coli*. In addition, the genetic engineering of *E. coli* strains that are capable of performing Pd reduction for different applications, requires information about the genes and pathways that are involved in Pd ion uptake from the surrounding environment, in the reduction of Pd ions to form Pd nanoparticles, and in Pd detoxification processes. In this study, we measured the bacterial transcriptional response to the exposure to sublethal levels of Pd^{2+} ions in *E. coli* K-12 BW25113 strain and compared our results with published transcriptional responses to other heavy metals. Anaerobic conditions were approximated in our experiment since Pd nanoparticles synthesis is typically performed in the absence of oxygen.

MATERIALS AND METHODS

Bacterial Strains and Growth Conditions

The bacterial strain used in this study was *E. coli* K-12 BW25113 (Baba et al., 2006). For each biological replicate, a single colony of bacteria was used to inoculate a 10 ml starter culture in M63 minimal medium [$(NH_4)_2SO_4$ 2 g/L, KH_2PO_4 13.6 g/L, and $FeSO_4.7H_2O$ 0.5 mg/L were mixed together, pH was adjusted to 7 with KOH, the solution was autoclaved and then 1 ml of 1 M sterile $MgSO_4.7H_2O$ and sterile glucose to a final concentration of 0.4% were added before use] (Miller et al., 1992) incubated overnight at 37°C with shaking at 200 rpm. On the next day, the overnight starter

[1]https://www.macrotrends.net/2542/palladium-prices-historical-chart-data

cultures were diluted 1:100 to inoculate 58 ml of the same medium in 50 ml falcon centrifuge tubes and incubated at 37°C with shaking at 200 rpm until the OD_{600} reached 0.3. The falcon centrifuge tubes were filled to the top with 58 ml medium in order to create an anaerobic atmosphere as far as possible. Please note that some residual oxygen availability cannot be excluded as polypropylene tubes are potentially allowing some minimal oxygen diffusion into the sample (Karian, 2003). A total of 8 samples, 4 palladium-treated and 4 controls, were prepared. Ammonium sulfate, potassium phosphate, ferrous sulfate heptahydrate, potassium hydroxide, magnesium sulfate heptahydrate, and D(+)-Glucose were purchased from Merck Life Science AS, Oslo, Norway.

Determination of Palladium Toxicity

The lethality of Pd to *E. coli* was measured using the alamarBlue™ Cell Viability Kit (Life Technologies AS, Oslo, Norway). The AlamarBlue™ Cell Viability kit uses the reducing power of living cells to quantitatively measure the metabolic activity of bacteria. Resazurin, the active compound of the kit, is a cell permeable compound that is blue in color and non-fluorescent. Upon entering living cells, resazurin is reduced to resorufin, a compound that is red in color and highly fluorescent. Viable cells continuously convert resazurin to resorufin, increasing the overall fluorescence and color of the media surrounding cells.

Two hundred microliter of *E. coli* bacterial suspension of OD_{600} 0.3 in M63 minimal medium were mixed with different Pd concentrations (0.1, 1, and 10 mM) in a 96-well transparent plate. Immediately after that, the cell suspensions were mixed with 10 μl of the resazurin reagent (1 mg/ml stock concentration, which corresponds to 4 mM). Three controls with the same concentrations of Pd in 200 μl M63 medium were also mixed with 10 μl resazurin reagent and used for determination of fluorescence background. Then, the fluorescence was measured every 10 min continuously for 8 h at 37°C using a SYNERGY H1 microplate reader (BioTek, United States). The measurements were fluorescence endpoint with excitation at 530 nm, emission at 590 nm, and 100 gain. The intensity of fluorescence is proportional to the number of living cells and corresponds to the metabolic activity. Fluorescence intensity values (after the subtraction of fluorescence background) were used for the comparison of cell viability between different samples.

Palladium Challenge

When the OD_{600} reached 0.3, 4 biological replicates were challenged with 100 μM Pd^{2+} in the form of sodium tetrachloropalladate (II) dissolved in 0.01 M nitric acid (similar amounts of Milli-Q water were added to the 4 control replicates). The pH of the samples was not affected (data not shown). The cultures were incubated at 37°C with shaking at 200 rpm for 10 min. The cells were harvested by centrifuging at 4200 × *g* for 10 min at 4°C. Then, the pellets were resuspended in 1 ml of 20 mM MOPS buffer (pH 7) and transferred to 2 ml Eppendorf tubes to remove excess heavy metal ions that might impact the subsequent RNA isolation and analysis. The tubes were centrifuged at 6000 × *g* for 2 min at 4°C. The supernatant was removed, and the tubes were immediately dipped into liquid nitrogen, stored at −80°C, and later shipped on dry ice. Sodium tetrachloropalladate (II) 98%, 5.6 M nitric acid, and MOPS were purchased from Merck Life Science AS, Oslo, Norway.

RNA Sequencing

Total RNA isolation, RNA quality control, library preparation, sequencing, and data analysis were performed by Eurofins Scientific, Konstanz, Germany (INVIEW Transcriptome Bacteria package). Eurofins protocol contained the following steps: total RNA isolation by RNeasy kit (Qiagen, Hilden, Germany), rRNA depletion by NEBNext kit (New England Biolabs, Frankfurt, Germany), and RNA quality measurement by a fragment analyzer (Agilent Technologies, Ratingen, Germany). Then, the mRNA was fragmented and random hexamer primers were used for cDNA synthesis. Adapter ligation and adapter-specific PCR amplification were used to generate libraires of 150 bp reads. More than 10 million reads were generated per sample. The reads were paired-end sequenced by an Illumina sequencing platform.

Data Analysis

The reads were mapped by Eurofins Scientific against the *E. coli* K-12 MG1655 strain reference genome (the closest *E. coli* reference genome to *E. coli* K-12 BW25113 genome) using the software BWA-MEM (version 0.7.12-r1039) (Li, 2013). Transcripts were identified and quantified. Then, pairwise comparison of expression levels and statistical analysis were carried out.

Raw read counts were created using featureCounts (version 1.5.1) (Liao et al., 2014). Only reads overlapping "CDS" features in the reference genome were counted. All reads mapping to features with the same meta-feature attribute were summed. Only reads with unique mapping positions and a mapping quality score of at least 10 were considered for read counting. Supplementary alignments were ignored for read counting. Paired-end reads that mapped with unexpected strandedness were ignored. Reads mapping to multiple features were assigned to the feature that has the largest number of overlapping bases.

A Trimmed Mean of M-values (TMM) normalization was performed using the edgeR package (version 3.16.5) (Robinson et al., 2009; Robinson and Oshlack, 2010). The basic assumption of this normalization technique is that most features (e.g., genes) should not be differentially expressed between samples. For each sample a normalization factor is calculated as the weighted mean of feature-wise log ratios between this sample and a reference sample.

Bioinformatics Analysis

For the interpretation of the results based on gene functions, the differentially expressed genes with p-value < 0.05 were manually categorized by Clusters of Orthologous Groups (COGs) using NCBI COGs database[2]. Next, the differentially expressed genes were furtherly manually subcategorized based on their encoded functions into separate biological processes and pathways by

[2]https://www.ncbi.nlm.nih.gov/research/cog

Gene Ontology (GO) terms using UniProt[3] and Quick GO databases[4], and BioCyc pathway/genome database collection[5].

Genome-Scale Metabolic Modeling

We applied gene-expression flux balance analysis (gx-FBA) methodology (Navid and Almaas, 2012) to the genome-scale metabolic model *E. coli* *i*ML1515 (Monk et al., 2017) in Matlab 2020a (The Math Works Inc., 1991) using Cobra toolbox v3 (Heirendt et al., 2019) with Gurobi (Gurobi Optimization, 2014) as solver. The gx-FBA method integrates gene expression data with the *i*ML1515 model, allowing for response-modeling of environmental perturbations. In short, the cellular metabolic fluxes are scaled in relation to the mRNA expression data in the stress state of the cell. By optimizing for similarity between differentially expressed genes (and hence reaction fluxes) and the provided transcriptomics data, a flux distribution consistent with the constraints and gene expression values of the stressed state is calculated. The flux distribution of the reference state can then be compared with the flux distribution of the stress state. The predicted relative flux changes as a response to Pd stress are used as proxies for metabolic responses.

For modeling the cellular environment corresponding to the biocide environments, we allowed aerobic growth on the default *i*ML1515 medium, using glucose as the sole carbon source. For modeling the cellular environment corresponding to the Pd-stress environment, we set conditions to anaerobic growth and restricted carbon, phosphate and sulfate sources only to those available in the biomass (proteins and glycogen) in minimal amounts necessary to ensure survival, representing the cell using its reserves simply to satisfy ATP maintenance requirements. Secretion fluxes were not changed in the model. Reactions regulated by non-differentially expressed genes are not directly limited in their flux as they are not part of the gx-FBA objective function, but are nonetheless restricted by substrate availability (and ability for other reactions to consume their products), and therefore, indirectly restricted according to constraints applied to the reaction system. Given a set of constraints, which in our case is imposed by nutrient availability, gene expression, non-depletion/accumulation of metabolites and stoichiometry, an FBA optimal solution (including gx-FBA) will typically not be unique; rather, multiple different flux solutions might satisfy the objective function equally well. Therefore, flux values for a reaction are not necessarily fixed, but can be said to fall between a pair of upper and lower bounds, with some degree of uncertainty in the flux predictions given by a model.

In each of the gx-FBA simulations, we classify reactions into four categories. The first category, which we call "no flux," consists of reactions which do not carry flux in the unstressed environment and are also unable to carry flux in stress conditions. The second category, "ambiguous," consists of reactions for which the unstressed reaction flux falls between the upper and lower bounds returned by the gx-FBA optimization, meaning that up- or down-regulation of the flux is not a necessary consequence of the gene expression values. The last two categories are down-regulated and up-regulated reaction fluxes. Down-regulated fluxes are reaction fluxes for which the upper bound in the gx-FBA solution is smaller than the unstressed reaction flux, and which must therefore necessarily carry lower reaction flux in stress conditions. Conversely, up-regulated reaction fluxes are those for which the lower bound of the gx-FBA solution are larger than the unstressed reaction flux, which means that the expression values in stress conditions necessarily require an increase in the flux.

[3]https://www.uniprot.org/

[4]https://www.ebi.ac.uk/QuickGO/

[5]https://biocyc.org/

RESULTS

Palladium Sublethal Concentration

We have tested several Pd concentrations. Out of the three Pd concentrations used in the viability assay, the highest one (10 mM Pd) resulted in the complete inhibition of metabolism (the green graph in **Figure 1**). For 1 mM Pd, the cells seemed to be adversely impacted by this concentration, as the fluorescence signal was 22% less than the control in average. After 200 min of incubation at this concentration, the cells went through a phase of adaptation (the shoulder in the blue graph in **Figure 1**) for ca. 100 min. After that the cells start dying fast. For 0.1 mM Pd, the cells did not appear to be strongly affected, the reduction in fluorescence signal was 7% (the red graph in **Figure 1**). This concentration was used for Pd exposure in this study.

A Transcriptomic View of Pd Stress

The RNA-Seq results showed that 709 genes, which account for 18.2% of the genes mapped in our experiment, were differentially expressed after 10 min of exposure to 100 μM Pd

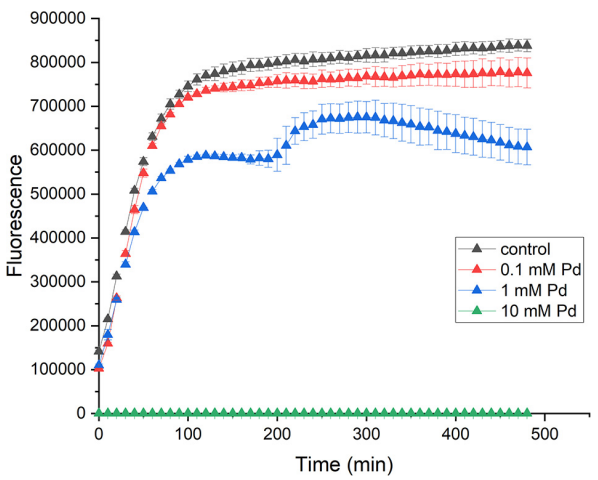

FIGURE 1 | Effect of Pd on the viability on *E. coli*. *E. coli* cells were incubated with 10 mM (green triangles), 1 mM (blue triangles), and 0.1 mM (red triangles) sodium tetrachloropalladate (II) or with water as a control (black triangles). The viability of cells was measured for 8 h. The error bars represent the standard deviation of the mean for three replicates.

TABLE 1 | Number of genes that were differentially expressed after 10 min of exposure to 100 μM Pd.

Category	Number	Percentage
Non-differentially expressed genes	3189	81.8%
Differentially expressed genes	709	18.2%
Up-regulated	411	58%
Down-regulated	298	42%
The cut-off *p*-value was 0.05		

From 100% differentially expressed genes 58% were up-regulated and 42% were down-regulated.

(p-value < 0.05). From those genes, 411 (58%) were up-regulated and 298 (42%) were down-regulated. The results are summarized in **Table 1**.

Differentially Expressed Genes Grouped by Functional Categories

The differentially expressed genes were grouped based on Clusters of Orthologous Groups (COGs) to identify expression differences based on gene functions (**Figure 2** and **Supplementary Data Sheet 1**). Raw RNA-Seq data can be found in **Supplementary Data Sheet 2, Tabs 1–28**. In this paper, the COG category names are used together with their international one-letter code (Tatusov et al., 2000).

The top five COG categories with the highest number of differentially expressed genes were amino acid transport and metabolism (D) with 85 genes (50 up-regulated and 35 down-regulated); carbohydrate transport and metabolism (G) with 78 genes (56 up-regulated and 22 down-regulated); transcription (K) with 76 genes (59 up-regulated and 17 down-regulated); genes of unknown function (S) with 76 genes (49 up-regulated and 27 down-regulated); and post-translational modification, protein turnover, and chaperones (O) with 56 genes (47 up-regulated and 9 down-regulated). The five COG categories with the lowest number of differentially expressed genes were RNA processing and modification (A) with 0 genes affected; mobilome, prophages, and transposons (X) with 1 up-regulated gene; extracellular structures (W) with 3 down-regulated genes; intracellular trafficking, secretion, and vesicular transport (U) with 3 genes (2 up-regulated and 1 down-regulated); and cell cycle control, cell division, and chromosome partitioning (D) with 5 genes (3 up-regulated and 2 down-regulated).

The functional categorization of differentially expressed genes showed that there were categories that had a high up-regulation

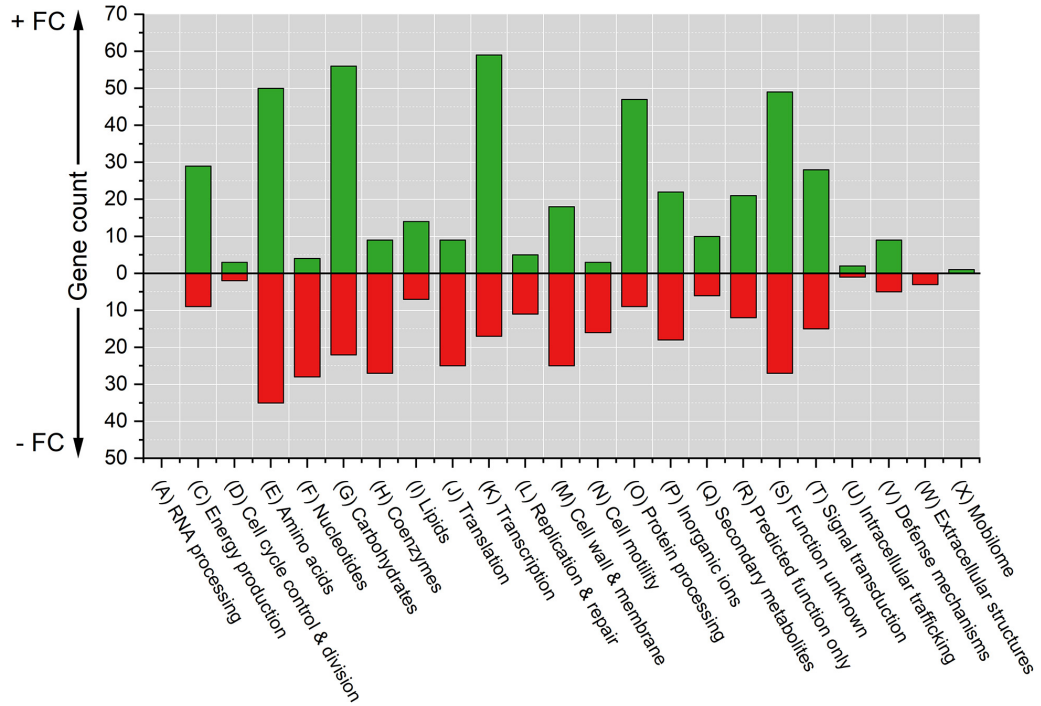

FIGURE 2 | Counts of differentially expressed genes due to Pd stress grouped by COG functional categories. The cut-off *p*-value was 0.05. Positive counts represent observed up-regulated genes (green bars) and negative counts represent observed down-regulated genes (red bars). COG code, number of proteins encoded by *E. coli* genome and category description: (A, 3) RNA processing and modification; (C, 284) Energy production and conversion; (D, 43) Cell cycle control, cell division, and chromosome partitioning; (E, 356) Amino acid transport and metabolism; (F, 107) Nucleotide transport and metabolism; (G, 384) Carbohydrate transport and metabolism; (H, 180) Coenzyme transport and metabolism; (I, 122) Lipid transport and metabolism; (J,236) Translation, ribosomal structure and biogenesis; (K, 301) Transcription; (L, 140) Replication, recombination, and repair; (M, 254) Cell wall, membrane, and envelop biogenesis; (N,110) Cell motility; (O, 178) Post-translational modification, protein turnover, and chaperones; (P, 223) Inorganic ion transport and metabolism; (Q, 72) Secondary metabolites biosynthesis, transport, and catabolism; (R, 261) General function prediction only; (S, 255) Function unknown; (T, 193) Signal transduction mechanisms; (U, 50) Intracellular trafficking, secretion, and vesicular transport; (V, 93) Defense mechanisms; (W, 31) Extracellular structures; and (X, 60) Mobilome, prophages, and transposons.

trend [energy production and conversion (C), transcription (K), and post-translational modification, protein turnover, and chaperones (O)] and other categories with a high down-regulation trend [nucleotide transport and metabolism (F), coenzyme transport and metabolism (H), translation, ribosomal structure and biogenesis (J), and cell motility (N)].

Top Differentially Expressed Genes

The majority of differentially expressed genes (640 out 709 genes) had an absolute fold change (FC) value of 3.5-30 compared to the control (**Supplementary Data Sheet 1**). **Tables 2**, **3** show the top 20 highest up- and down-regulated genes, respectively.

Detailed Results of Differentially Expressed Genes Based on Clusters of Orthologous Groups Categorization and Gene Ontology Terms

Genes Related to Information Macromolecules

DNA replication, recombination, and repair (L)

Of the genes responsible for initiation, maintenance, and termination of chromosome replication, only one gene was down-regulated (*recQ*) and one was up-regulated (*smbC*). Of the genes encoding polymerase subunits, no genes were differentially expressed. Finally, of the genes responsible for DNA repair and recombination, 8 genes were down-regulated and 2 were up-regulated. Detailed information can be found in **Supplementary Data Sheet 3, Tab 1**.

Transcription (K)

The genes for RNA polymerase subunits were not affected by Pd exposure. The same applies to the termination factors and degradosome complex genes. Of the genes responsible for RNA processing enzymes and RNases, 2 were down-regulated (*ghoS* and *rnb*). Three out of the 7 sigma factors were differentially expressed, FecI (ferric citrate sigma factor) was down-regulated, RpoS (stationary phase and stress response sigma factor) and RpoH (heat shock sigma factor) were up-regulated. Detailed information can be found in **Supplementary Data Sheet 3, Tab 2**. Many transcriptional regulators were differentially expressed due to Pd exposure, 50 were up-regulated and 10 were down-regulated (**Supplementary Data Sheet 3, Tab 3**). Of all COG categories, transcription had the highest number of up-regulated genes (59 genes).

Translation, ribosomal structure and biogenesis (J)

Six out of the genes responsible for ribosome-assembly proteins (r-proteins) were down-regulated, 5 of them were from the *rpsJ* operon. Of the other r-proteins, 7 gene were down-regulated (several methyltransferases) and 4 were up-regulated (stress-related proteins responsible for ribosome stabilization). Moreover, 3 genes responsible for ribosome recycling and stalled-ribosome rescue were up-regulated. The translation initiation and termination factors were unchanged, while 2 of the elongation factors were down-regulated. For the genes of tRNA synthetases/ligases, only one was down-regulated (proline-tRNA ligase). While for tRNA processing genes, 8 were down-regulated and 2 were up-regulated. Detailed information can be found in **Supplementary Data Sheet 3, Tab 4**. This shows that the ribosome assembly process and translation overall is repressed due to Pd stress, while at the same time genes for recycling and rescuing present ribosomes are up-regulated.

Post-translational modification, protein turnover, and chaperones (O)

Intoxication with several heavy metals can cause protein cross-linking (Rouch et al., 1995), which disrupts their 3D structures and allosteric movements. The proteases and chaperones of the heat shock response repair or degrade misfolded proteins (Georgopoulos and Welch, 1993). Pd stress induced these repair mechanisms, as 28 different genes for proteases, heat shock proteins, and chaperones were highly up-regulated. Five of them were in the top 20 most up-regulated genes, namely *spy* (6447-fold), *ibpB* (565-fold), *cpxP* (330-fold), *ves* (151-fold), and *ibpA* (70-fold). Of the RNases and RNA processing enzyme genes, only one was down-regulated (*rnb* RNase II, responsible for mRNA degradation). Detailed information can be found in **Supplementary Data Sheet 3, Tab 5**.

Genes Related to Central Metabolism

Carbohydrate transport and metabolism (G)

This COG category had the 2nd highest number of up-regulated genes (56 genes). Most of the up-regulated genes are related to carbohydrate transport. For the transport of disaccharides, *malEKX* and the regulator gene *mlc* involved in maltose transporter complex; *mglA* and *mglB* involved in galactose transporter complex; and *treB* and *treC* involved in trehalose transport and hydrolysis systems, respectively, were up-regulated. For the transport of hexoses, *frwA* fructose transporter gene; *gntP* gluconate transporter gene; *ytfQRT* galactofuranose transporter genes; *srlABE* sorbitol transporter genes; *manXY* mannose transporter genes; *garP* galactarate transporter gene; and L-fucose-proton symporter gene *fucP* were all up-regulated. The expression of some hexoses metabolic enzymes was also increased. All the genes (*fucAIKOR*) from L-fucose degradation pathway to make L-lactate and pyruvate; *dgoADK* genes involved in making pyruvate from D-galactonate; and *garD* involved in galactarate degradation pathway to make pyruvate were up-regulated.

For the transport of pentoses, *xylF* xylose transporter gene; *rbsA* and *rbsB* involved in the ribose uptake system; and *araF* L-arabinose transporter gene were up-regulated. The sugar efflux transporter gene *ydeA* responsible for L-arabinose level maintenance was down-regulated. In addition to transport, several genes from pentose and glucuronate interconversion pathways were up-regulated (*uxaABC* and *uxuAB*). For the transport of other kinds of sugars, *glpT* and *glpF* glycerol transporter genes and *lsrABCDK* from autoinducer 2 carbohydrate import system were up-regulated. The function of *lsr* system is not clear, but it has been suggested to have functions in quorum sensing (Xavier and Bassler, 2005).

The other genes that were down-regulated were from unconnected parts of pathways or were poorly defined. Detailed information can be found in **Supplementary Data Sheet 4, Tab 1**. The systematic up-regulation of carbohydrate transport genes

TABLE 2 | Top 20 most up-regulated genes after 10 min of exposure to 100 μM Pd.

Gene ID	Gene name	Product description	FC	Error
b1743	*spy*	Periplasmic ATP-independent protein refolding chaperone	6447	± 2830
b1970	*hiuH*	5-hydroxyisourate hydrolase, zinc metal-binding	1465	± 986
b3686	*ibpB*	Chaperone, heat shock protein of HSP20 family	565	± 94
b4002	*zraP*	Important component of the zinc-balancing mechanism	357	± 45
b4484	*cpxP*	Part of the cpx two-component envelope stress response system	330	± 92
b4062	*soxS*	Transcriptional activator of the superoxide response regulon	240	± 28
b2074	*mdtA*	Part of *mdt*ABC-*tol*C efflux pump, multidrug resistance	188	± 47
b4140	*fxsA*	Suppresses F exclusion of phage T7	163	± 35
b3263	*yhdU*	Function unknown	160	± 148
b1742	*ves*	Cold and stress-inducible protein	151	± 88
b2162	*rihB*	Pyrimidine-specific ribonucleoside hydrolase	133	± 17
b3501	*arsR*	Arsenate resistance operon repressor	132	± 20
b1972	*yedZ*	Protein-methionine-sulfoxide reductase heme-binding subunit MsrQ	112	± 15
b0484	*copA*	Copper-, silver-translocating ATPase efflux pump; involved in copper resistance	101	± 10
b3828	*metR*	Positive activator of the metA, metE and metH genes	100	± 4
b1971	*yedY*	Protein-methionine-sulfoxide reductase catalytic subunit MsrP	96	± 8
b3708	*tnaA*	Tryptophanase, synthesis of pyruvate from L-tryptophan pathway	94	± 3
b4670	*yjeV*	Function unknown	81	± 63
b3502	*arsB*	Arsenite pump; resistance to arsenate, arsenite, and antimonite	76	± 8
b3687	*ibpA*	Chaperone, heat-inducible protein of HSP20 family	70	± 7

TABLE 3 | Top 20 most down-regulated genes after 10 min of exposure to 100 μM Pd.

Gene ID	Gene name	Product description	FC	Error
b2725	*hycA*	Regulatory protein for the formate hydrogenlyase system	−520	± 151
b1038	*csgF*	Curli production assembly/transport component	−338	± 60
b3215	*yhcA*	Required for the biogenesis of putative fimbria	−197	± 32
b0336	*codB*	Required for cytosine transport into the cell	−130	± 23
b2145	*yeiS*	Function unknown	−130	± 103
b2269	*elaD*	Protease, capable of cleaving an AMC-ubiquitin model substrate	−119	± 13
b4665	*ibsC*	Toxic component of a type I toxin-antitoxin (TA) system	−117	± 28
b2345	*yfdF*	Function unknown	−117	± 19
b4128	*ghoS*	Antitoxin component of a type V toxin-antitoxin (TA) system	−110	± 12
b1520	*yneE*	Predicted inner membrane protein, bestrophin family; possible chloride channel	−109	± 27
b0945	*pyrD*	Dihydroorotate dehydrogenase, UMP biosynthesis	−106	± 21
b3622	*waaL*	LPS core biosynthesis; O-antigen ligase	−85	± 13
b0991	*ymcE*	Cold shock protein, function unknown	−80	± 64
b2352	*gtrS*	Serotype-specific glucosyl transferase, CPS-53/KpLE1 prophage	−70	± 16
b2497	*uraA*	Uracil permease, uracil transport into the cell	−59	± 4
b2669	*stpA*	RNA chaperone and DNA-binding protein	−50	± 14
b0564	*appY*	Induces the synthesis of acid phosphatase (AppA) and several other polypeptides	−49	± 23
b4345	*mcrC*	McrBC restriction endonuclease	−44	± 5
b3508	*yhiD*	Putative magnesium transporter	−41	± 16
b1018	*efeO*	Involved in Fe^{2+} uptake	−41	± 7

suggests that the cells were in high demand for sugars as they were trying to make energy through different pathways simultaneously to cope with Pd stress.

Energy production and conversion (C)

Several metabolic processes related to energy production were highly modulated upon Pd exposure (shown in detail in **Figure 3**). For glucose transport and metabolism (**Figure 3A**), glucose transport was up-regulated through the up-regulation of one the outer membrane porins, OmpC, and three of the seven glucose transporter systems (Alva et al., 2020). *E. coli* has three native glycolytic pathways: the Embden-Meyerhof pathway (EMP), the oxidative pentose-phosphate pathway (OPPP), and the Entner-Doudoroff pathway (EDP) (Hollinshead et al., 2016). None of these pathways were highly modulated, but one enzyme from the EMP, TpiA, was down-regulated. For OPPP,

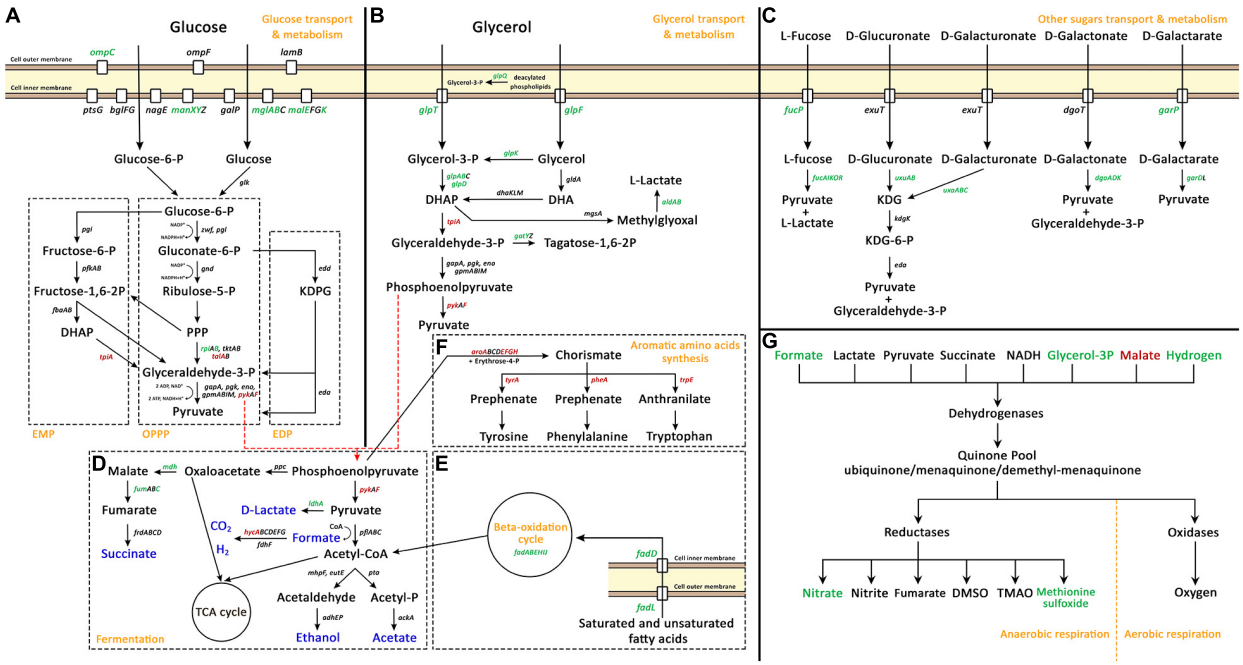

FIGURE 3 | Palladium (Pd) stress effects on genes related to carbohydrate transport, carbohydrate metabolism and energy production pathways, namely, glucose transport and metabolism **(A)**, glycerol transport and metabolism **(B)**, other sugars transport and metabolism **(C)**, fermentation **(D)**, beta-oxidation cycle **(E)**, aromatic amino acids synthesis **(F)**, and anaerobic respiration **(G)**. In panels **(A–F)**, green gene names represent up-regulated genes, red names represent down-regulated genes, and black names represent unaffected genes. In panel **(D)**, blue color represents fermentation end products. In panel **(G)**, green and red colors represent up-regulated and down-regulated parts of anaerobic respiration pathways, respectively. In panel **(A)**, the three native glycolytic pathways in *E. coli* are demonstrated: Embden-Meyerhof pathway (EMP), oxidative pentose-phosphate pathway (OPPP), and Entner-Doudoroff pathway (EDP). The full names of abbreviated compounds are DHAP, dihydroxyacetone phosphate; KDPG, 2-Keto-3-deoxy-6-phosphogluconate; DHA, dihydroxyacetone; KDG, 2-dehydro-3-deoxy-D-gluconate; TCA, tricarboxylic acid cycle; DMSO, dimethyl sulfoxide; and TMAO, Trimethylamine N-oxide.

2 enzymes were down-regulated, TalA and PykF, and one was up-regulated, RpiB. Interestingly, the expression of the genes responsible for the transport and metabolism of glycerol (**Figure 3B**) and other sugars (**Figure 3C**) was highly increased despite the fact that these sugars were not present in the culture medium. Glycerol transport and metabolism genes had a high up-regulated trend; its two transport systems, GlpQ enzyme (glycerophosphoryl diester phosphodiesterase which hydrolyzes deacylated phospholipids to glycerol-3-phosphate), and several of its metabolic enzymes were up-regulated. For the transport and metabolism of other sugars, five sugar degradation pathways to make pyruvate were up-regulated (from L-fucose, D-glucuronate, D-galacturonate, D-galactonate, and D-galactarate) together with the transporters of L-fucose and D-galactarate.

Fermentation processes (**Figure 3D**) were also modulated. The production of D-lactate, malate, and fumarate was increase thought the up-regulation of *ldhA*, *mdh*, and *fumC*, respectively. The production of H_2 was highly modulated thought the massive down-regulation of the transcriptional repressor of hydrogenase 3 operon, HycA, which was the most down-regulated gene due to Pd exposure, decreasing 520-fold. Moreover, two other pathways that are related to fermentation were highly modulated. The beta-oxidation cycle (**Figure 3E**) that produces acetyl-CoA was highly up-regulated through the up-regulation of the outer membrane protein FadL and the inner membrane protein FadD responsible for the transport of saturated and unsaturated fatty acids, together with the beta-oxidation cycle genes, *fadABEHIJ*.

Phosphoenolpyruvate enters two separate pathways; it is either converted to oxaloacetate or to pyruvate. In addition, phosphoenolpyruvate is also the precursor for aromatic amino acids synthesis (**Figure 3F**) together with erythrose-4-P. This pathway was massively down-regulated on two levels, firstly, through the down-regulation of *aroAEFGH* genes which encode enzymes that convert phosphoenolpyruvate and erythrose-4-P to chorismate, and secondly, through the down-regulation of aromatic amino acids individual pathways, through *tyrA*, *pheA*, and *trpE* genes.

Besides the modulation of glycolysis and fermentation processes, the anaerobic respiration process was also modulated. In this study, HNO_3 was used a solvent for sodium tetrachloropalladate (II). The addition of HNO_3 (0.291 μL from 0.01 M stock concentration to 58 mL medium) created a 50 μM HNO_3 concentration in the medium. *E. coli* can use the nitrate of HNO_3 as terminal electron acceptor for anaerobic respiration. The nitrate reductase operons of *E. coli* are optimally expressed at higher nitrate concentrations. Genes such as *napF*, *nrfA*, and *nirB* are optimally expressed at 1 mM nitrate while *narG* is optimally expressed at 10 mM nitrate concentration (Wang et al., 1999; Wang and Gunsalus, 2000). However, the

minimal HNO_3 concentration added might be the cause for this modulation, at least partially (**Figure 3G**).

For respiration in *E. coli,* dehydrogenases transfer electrons from various substrates to the quinone pool. Then, terminal reductases and oxidases transfer these electrons to different electron acceptors. For aerobic respiration, the terminal electron acceptor is O_2, while for anaerobic respiration there are different electron acceptors. On the dehydrogenases level, the expression of formate and glycerol-3-P dehydrogenases and the expression of hydrogenase 2 was increased, while the expression of malate dehydrogenase was decreased. On the reductases level, the expression of nitrate and methionine sulfoxide reductases was up-regulated.

In addition to all this, the expression of the glucose dehydrogenase gene *gcd* and 4 of the 6 genes of the *rsx* operon (ion-translocating oxidoreductase complex) were down-regulated. This complex is a membrane-bound complex that couples electron transfer with translocation of protons across the membrane. Detailed information about energy production and conversion modulated genes can be found in **Supplementary Data Sheet 4, Tab 2**.

Amino acid transport and metabolism (E)

This category of COGs was modulated the most under Pd stress with 85 genes being differentially expressed, 50 up-regulated and 35 down-regulated. We found particular amino acid pathways that were heavily modulated (more than 5 genes of the pathway), others that were slightly modulated with 2-3 genes being affected, and the rest had only one or no genes being modulated. The amino acid synthesis pathways that were heavily modulated are shown in **Figure 4**. The modulation is divided into two parts: biosynthesis pathways and uptake pathways. On the biosynthesis level, arginine biosynthesis was highly up-regulated, with all the 8 genes involved in its biosynthesis from glutamate (*argABCDEGHI*) were up-regulated. Arginine could alternatively be synthesized from glutamine by converting glutamine to carbamoyl phosphate by the products of the *carA* and *carB* genes; but we found this pathway was down-regulated. Glutamate together with putrescine can be also converted to succinate by the products of *puuABCDE* genes, this pathway was dramatically down-regulated. It appears that bacteria are saving all the glutamate for arginine biosynthesis, and particularly through this pathway and not from glutamine (**Figure 4A**).

The biosynthesis of histidine (**Figure 4B**) and methionine (**Figure 4C**) was also highly up-regulated, where the genes *hisABCDGH* and *metABCFL* were up-regulated, respectively. Moreover, the expression of the positive regulator of the methionine operon, MetR, increased 100-fold. At the same time, the biosynthesis of aromatic amino acids was severely down-regulated. For their biosynthesis, phosphoenolpyruvate

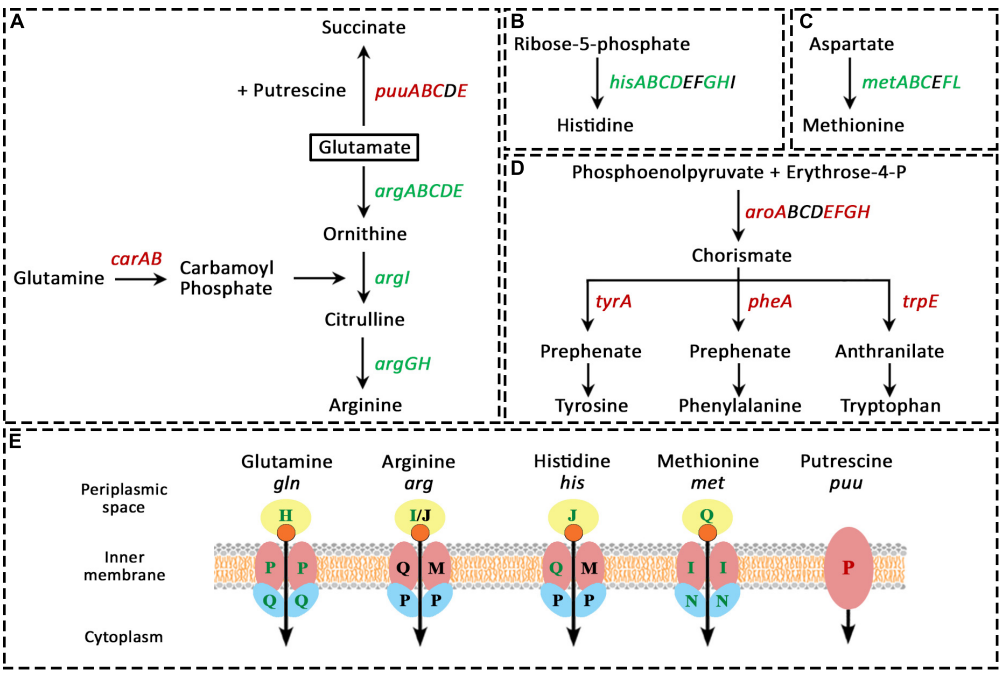

FIGURE 4 | Amino acid-related pathways that were heavily modulated due to Pd stress. In panels **(A–D)**, green gene names represent up-regulated genes, red names represent down-regulated genes, and black names represent unaffected genes. In figure **(E)**, green, red, and black letters represent up-regulated, down-regulated, and unaffected genes, respectively. **(A)**, arginine biosynthesis from glutamate (*argABCDEGHI*) was highly up-regulated, but the biosynthesis of arginine from glutamine was down-regulated (*carA* and *carB* genes). The conversion of glutamate and putrescine to succinate by the products *puuABCDE* genes was also heavily down-regulated. The biosynthesis of histidine **(B)** and methionine **(C)** was also highly up-regulated. **(D)**, the biosynthesis of aromatic amino acids was drastically down-regulated on two levels, firstly, thought the down-regulation of the production of their common precursor (chorismate) from erythrose-4-phosphate by the products of *aroABCDEFGH* genes, and secondly, through the down-regulation of their individual pathways. **(E)**, the pathways involved in the transport of glutamine, arginine, histidine, and methionine were up-regulated. Lastly, the putrescine importer gene *puuP* was down-regulated.

and erythrose-4-P have to be converted to chorismate by the products of *aroABCDEFGH* genes, then, chorismate can be converted to the three aromatic amino acids through three different pathways. For tyrosine and phenylalanine, the first step in their biosynthesis is that chorismate is converted to prephenate by the products of *tyrA* and *pheA* genes, respectively, while for tryptophan, chorismate is converted to anthranilate by the product of *trpE* gene. The majority of all these genes were down-regulated (**Figure 4D**).

On the uptake level (**Figure 4E**), a comparable behavior was found. The pathways involved in the transport of glutamine, arginine, histidine, and methionine were up-regulated as well. For glutamine and methionine, all the three genes involved in their transporter complex were up-regulated (the periplasmic binding protein (GlnH and MetQ, respectively), the membrane permease (GlnP and MetI, respectively), and the ATP-binding import protein [GlnQ and MetN, respectively)]. For histidine, the genes for the periplasmic binding protein HisJ and the permease HisQ were up-regulated. For arginine, only the periplasmic binding protein ArgI was up-regulated. Lastly, the putrescine importer PuuP was down-regulated.

For the amino acid pathways that were slightly modulated, 2 genes involved in the serine biosynthesis pathway were down-regulated, *serA* and *serC*. Two genes involved in the isoleucine biosynthesis pathway were down-regulated, *ilvC* and *ilvD*. The three genes involved in the transporter complex of glycine betaine, *yehWXY*, were down-regulated. The genes encoding the S-methylmethionine permease, *mmuP*, and homocysteine S-methyltransferase, *mmuM*, were up-regulated. Lastly, two genes involved in the catabolism of tryptophan, *tnaA* and *tnaB*, were up-regulated. Detailed information can be found in **Supplementary Data Sheet 5, Tab 1**.

Inorganic ion transport and metallochaperones (P)

Escherichia coli has several systems for importing, balancing, and exporting bulk and trace metal ions. Some of these systems are very specific to one metal ion while others can transport a variety of ions. **Figure 5** shows the well-studied systems in *E. coli*, the upper half of the figure shows the systems responsible for ion import while the lower half shows the systems responsible for ion export. Ten of the 17 systems responsible for importing inorganic ions were differentially expressed, 8 down-regulated and 2 up-regulated. The periplasmic binding protein gene *nikA* of the nickel transporter complex operon *nikABCDE* was down-regulated. The uptake protein gene *trkG* of the potassium transporter complex operon *trkAEG* was down-regulated. Interestingly, all the 6 systems responsible for iron import were down-regulated, namely, the ferric citrate sigma factor gene *fecI* and the regulator gene *fecR* responsible for the *ficABCDE* operon of the Fe^{3+}-citrate import system; the periplasmic binding protein gene *feoA* and the GTP-binding channel protein gene *feoB* of *feoABC* operon of the Fe^{2+} import

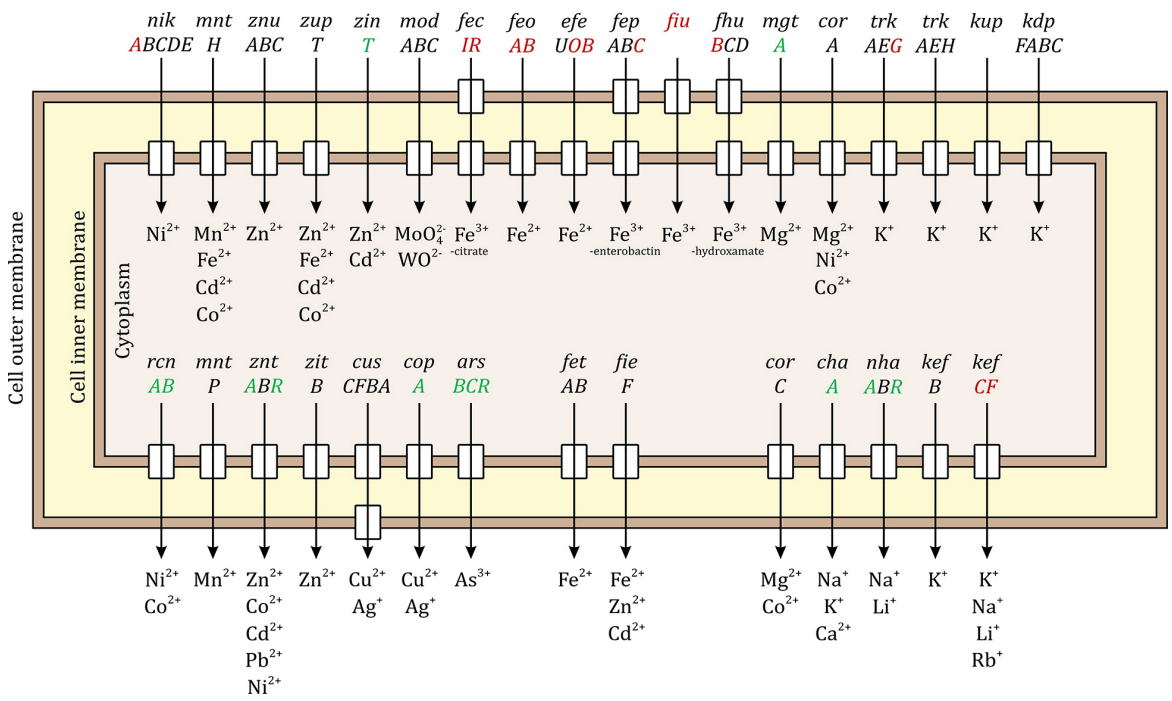

FIGURE 5 | Palladium (Pd) stress effects on inorganic metal ion import and export systems in *E. coli*. The upper half of the figure shows the systems responsible for ion import and the lower half shows the systems responsible for ion export. Some systems are specific to one metal ion while other can transport a variety of ions. The small rectangles in the inner membrane indicate that the system has an inner member permease protein and the rectangles in the outer membrane indicate that the system includes an outer membrane porin. The up-regulated genes due to Pd stress are shown in green, the down-regulated genes in red, and the unaffected genes in black. Ten of the importing systems were modulated, 8 of them were down-regulated. All the iron importing systems were down-regulated. Seven of the exporting systems were modulated, 6 of them were up-regulated.

system; the periplasmic binding protein gene *efeO* and the deferrochelatase gene *efeB* of the *efeUOB* operon of the Fe^{2+} import system; the ATP-binding protein gene *febC* of *fepABCDG* operon of the Fe^{3+}-enterobactin import system; the siderophore receptor gene *fiu* responsible for iron transport across the outer membrane complexed with catecholate siderophores such as dihydroxybenzoylserine and dihydroxybenzoate; and the permease protein gene *fhuB* of *fhuBCD* operon of the Fe^{3+}-hydroxamate import system. The up-regulated genes were the magnesium-transporting ATPase gene *mgtA* and periplasmic zinc chaperon gene *zinT*.

Seven of the 14 systems responsible for exporting inorganic ions were differentially expressed, 6 up-regulated and 1 down-regulated. The up-regulated genes were *rcnA* and *rcnB* of the nickel/cobalt efflux system; the transporting ATPase gene *zntA* and the regulator gene *zntR* of the zinc/cadmium/lead system; the copper-exporting ATPase gene *copA*; the channel protein gene *arsB*, arsenate reductase gene *arsC*, and the regulator gene *arsR* of the arsenical resistance system; the sodium-potassium/proton antiporter gene *chaA*; and the sodium/proton antiporter gene *nhaA* together with its regulator gene *nhaR*. The down-regulated genes were the glutathione-regulated potassium-efflux system gene *kefC* and its regulator gene *kefF*.

In addition to the transporter complexes, several other metal-related pathways were modulated as well. The genes involved in the biosynthesis of the enterobactin siderophore, a low-molecular mass compound that is secreted extracellularly by *E. coli* to chelate Fe^{3+} from the environment and then it is brought back to the cell through the FepABCDG system (Gehring et al., 1997), were down-regulated (*entC* and *entE*). The iron storage system was up-regulated through *ftnB* gene. All the genes of the *iscARSU* operon involved in Fe-S cluster assembly were up-regulated. The gene for copper oxidase, *cueO*, was highly up-regulated, increasing 44-fold.

Three other non-metal transporters were also modulated. The phosphate transporter complex permease gene *pstA* was down-regulated, the nitrate/nitrite transporter genes *narK* and *narU* were down-regulated, and the periplasmic binding protein gene *tauA* and the ATP-binding protein gene *tauB* of taurine import system were up-regulated. Detailed information can be found in **Supplementary Data Sheet 5, Tab 2**.

Coenzyme transport and metabolism (H)

This COG category had a high down-regulation trend, mainly on the vitamin biosynthesis level. Nine of the 11 genes involved in vitamin B1 (thiamine) biosynthesis were down-regulated (*thiCDEFGHIMS*). Two genes involved in vitamin B2 (riboflavin) biosynthesis pathway were down-regulated (*ribA* and *yigB*). For vitamin B3 (nicotinamide riboside), its transporter gene *pnuC*, and one gene involved in its biosynthesis (*pncB*) were down-regulated. Of the vitamin B6 (pyridoxal phosphate) biosynthesis pathway, 2 genes were down-regulated (*pdxK* and *pdxY*). Of the vitamin B9 (folate) biosynthesis pathway, 2 gene were down-regulated (*folE* and *folK*). For vitamin B12 (cobalamin), one gene of its transporter complex to the cell was down-regulated (the ATP-binding protein gene *btuD*), but one gene of its biosynthesis pathway was up-regulated (*btuR*).

In addition to vitamins, the synthesis of quinones was modulated. Two genes involved in ubiquinone biosynthesis pathway were up-regulated (*ubiA* and *ubiC*), but 2 genes involved in menaquinone/demethyl-menaquinone biosynthesis pathway were down-regulated (*menF* and *menH*). Moreover, the biosynthesis of iminosuccinic acid through the oxidation of aspartate was down-regulated through *nadB*. Phenylacetate degradation pathway was up-regulated through *paaJ* and *paaK*. Detailed information can be found in **Supplementary Data Sheet 5, Tab 3**.

Nucleotide transport and metabolism (F)

This COG category had a high down-regulation trend too, 28 genes were down-regulated (3 of them were in top 20 most down-regulated genes) compared to only 4 up-regulated genes. For purine biosynthesis pathway from phosphoribosyl pyrophosphate (PRPP), 9 genes were down-regulated, *purBCEFHKMNU*. For pyrimidine biosynthesis pathway from bicarbonate, 4 genes were down-regulated, *pyrBCDI*. For uridine monophosphate (UMP) biosynthesis pathway, 2 genes were down-regulated, *carA* and *carB*. Finally, for guanosine monophosphate (GMP) biosynthesis pathway, 2 genes were down-regulated, *guaA* and *guaB*. Of purine and pyrimidine hydrolysis pathways, 3 genes were drastically up-regulated, *rihB*, *rihC* and *hiuH*, the first being the 11th and last being the 2nd highest up-regulated genes with 133- and 1465-fold, respectively.

The genes involved for the biosynthesis of nucleotides through the nucleotide salvage pathway were also down-regulated: for adenosine monophosphate (AMP), *apt* was down-regulated; for cytidine monophosphate (CMP), *codA* was down-regulated; for GMP and xanthosine monophosphate (XMP), *gpt* was down-regulated; for inosine monophosphate (IMP), *gsk* was down-regulated; and for UMP, *upp* was down-regulated.

For the transport of nucleotides, all the permeases involved in the uptake of nucleobases were down-regulated. Adenine permease gene *adeP*, cytosine permease gene *codB*, guanine/hypoxanthine permease gene *ghxP*, uracil permease gene *uraA*, xanthine permease gene *xanP,* and the nucleoside permease gene *nupC*. Detailed information can be found in **Supplementary Data Sheet 5, Tab 4**.

Lipid transport and metabolism (I)

This category had a low number of modulated genes, 14 up-regulated and 7 down-regulated. The key pathway that was affected was the fatty acid beta-oxidation cycle, where 6 of its genes, *fadABEHIJ*, were up-regulated. The fatty acid transport protein genes *fadL* and *fadD* were also up-regulated. Two genes of isopentenyl diphosphate biosynthesis via DXP pathway, *ispD* and *ispF*, were down-regulated. Detailed information can be found in **Supplementary Data Sheet 5, Tab 5**.

Cell Cycle Control, Cell Division, and Chromosome Partitioning (D)

For this category, only a few genes were differentially expressed. The cell death peptidase gene *lit* and the cell division protein gene *yedR* were down-regulated. The toxic component gene *ibsC* of type I toxin-antitoxin (TA) system (Fozo et al., 2008) and the antitoxin component gene *ghoS* of type V TA system

(Cheng et al., 2014) were heavily down-regulated, being the 7th and 9th most down-regulated, decreasing 117- and 110-fold, respectively. The toxic component gene *mokC* of the type I TA system (Pedersen and Gerdes, 1999) was up-regulated.

Cell Wall Functions

Cell wall biogenesis, defense mechanisms, and extracellular structures (M, V, and W)

For cell wall biogenesis, several genes involved in LPS biosynthesis were down-regulated, *arnC*, *eptC*, *IptD*, *lpxH*, *waaC*, *waaL* and *wza*. Several genes involved in enterobacterial common antigen biosynthesis pathway were also down-regulated, *rffG*, *rffH*, *wecB* and *wecC*. Moreover, *osmB* gene of the osmotically inducible lipoprotein B, which provides resistance to osmotic stress, was up-regulated.

More importantly, *E. coli* encodes multiple antibiotic efflux systems that increase drug efflux and limit passive uptake by decreasing porin expression (Alekshun and Levy, 1999). These genes are activated in response to antibiotics and general stress. We found that Pd stress activates them too. From the multiple antibiotic resistance MarRAB system, 3 out of 4 genes were highly up-regulated, *marABR*. Several TolC-dependent systems were modulated too. From the multidrug resistance MdtABC system, 5 genes were vastly up-regulated, *mdtABCDG*, *mdtA* was the 7th highest up-regulated gene, increasing 188-fold. While for the anaerobic multidrug efflux transporter genes *mdtEF*, *mdtE* was down-regulated. From the AcrAB system, 2 genes were up-regulated, *arcD* and *arcR*. From the EmrAB energy-dependent system, *emr*B was down-regulated. This might suggest that *E. coli* is trying to use the passive efflux systems and not the active ones, to save energy for other crucial systems. Finally, from the outer membrane porins (Omp) system, *ompC* was up-regulated. OmpC imports extracellular glucose to the periplasmic space (Alva et al., 2020), the high need for energy is possibly the reason for this up-regulation. Detailed information can be found in **Supplementary Data Sheet 6, Tab 1**.

Motility and biofilm (N)

This category had a heavy down-regulation trend with a total of 16 genes being down-regulated compared to only 3 up-regulated genes. Of the *flg* operon responsible for flagellar synthesis, 8 genes, *flgBCDEFGHI*, were down-regulated. The same effect was found on type 1 fimbriae, which are filamentous pili that are attached to the cell surface and mediate biofilm formation and adhesion onto host cells. *FimBCDFG*, encoding proteins responsible for the assembly of FimA fimbrial subunit, its export across the outer membrane, and its regulation, were all down-regulated. Moreover, *ecp*B was also down-regulated, which is a member of *ecpRABCDE* operon that encodes the *E. coli* common pilus (ECP) and plays a role in early-stage biofilm development and host cell recognition. In addition, genes involved in curli organelles biogenesis were heavily down-regulated, the expression of *csgE* and *csgF* was 16- and 338-fold lower, respectively. At the same time, the 3 genes that were up-regulated were *bssS* (a biofilm repressor gene), *tomB* (a biofilm formation regulator gene), and *glgS* (a negative regulator gene of motility, adhesion, and synthesis of biofilm exopolysaccharides). In summary, this all shows that the bacteria were intentionally avoiding the structurally and energetically intensive motility and biofilm formation systems. Detailed information can be found in **Supplementary Data Sheet 6, Tab 2**.

Stress Responses

Oxidative stress response and repair

There are two oxidative stress response systems in *E. coli*, the OxyRS and SoxRS regulons (Seo et al., 2015), explained in **Figure 6**. OxyR is a member of the LysR transcriptional regulators family, which uses a cysteine-pair to sense the oxidative damage

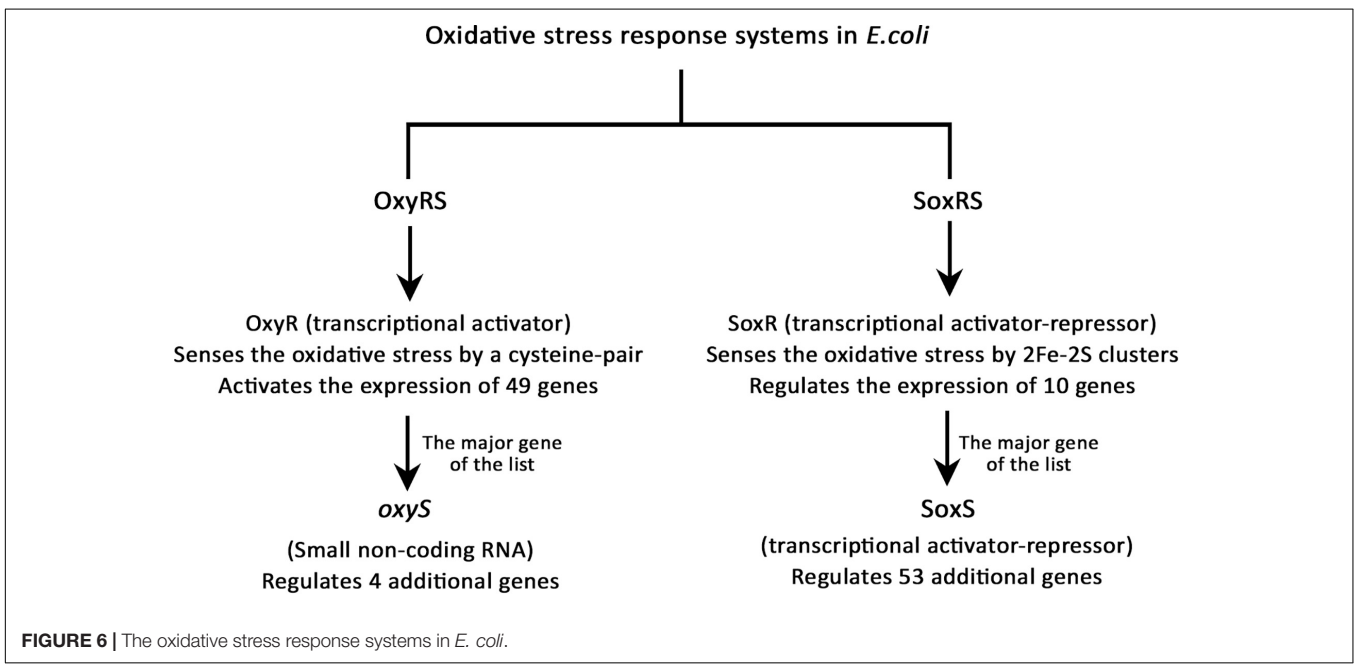

FIGURE 6 | The oxidative stress response systems in *E. coli*.

and regulates 49 genes when oxidized (Choi et al., 2001). Nine genes out of those 49 were up-regulated due to Pd stress and no genes were down-regulated. *oxyS* is a small non-coding RNA (ncRNA) regulated by OxyR, which represses *rpoS* (stationary phase and stress response sigma factor gene), *fhlABC* flagellar proteins genes, and other genes to prevent redundant induction of stress response genes (Altuvia et al., 1998). Our RNA purification and library preparation methods were not optimized for the enrichment of nc-RNAs; therefore, we were not able to detect any of them. Despite being unable to detect the expression of *oxyS*, several genes regulated by it were modulated. The expression of *flhA* and *flhC* was down-regulated but the expression of *rpoS* was up-regulated. The up-regulation of *rpoS* might be a due to the low number of OxyR stress response activated genes (9 out of 49), which resulted in no redundant induction of stress response genes.

The SoxRS regulon is the other oxidative stress response system in *E. coli*. SoxR is a member of the MerR repressor-activator family, which uses the oxidation state of 2Fe-2S clusters to sense the oxidative damage and regulates 10 stress-related genes (Watanabe et al., 2008). The most important gene of SoxR regulated genes is *soxS*, which is responsible for the regulation of additional 53 genes (Seo et al., 2015). Out of the 10 genes regulated by SoxR, 4 genes were up-regulated and 3 were down-regulated. *soxS* was modulated the highest in this list, its expression was up-regulated 240-fold. Then, of the 53 genes regulated by SoxS, 15 genes were up-regulated and 4 were down-regulated. This altogether shows that Pd exposure caused a serious oxidative stress to *E. coli*. Detailed information can be found in **Supplementary Data Sheet 7**.

Genome-Scale Metabolic Modeling

First, we note that 306 of the 709 differentially expressed genes are present in the genome-scale metabolic model *i*ML1515 (Monk et al., 2017). In **Figures 7**, **8**, we present the *E. coli* K-12 MG1655 KEGG (Kyoto Encyclopedia of Genes and Genomes) (Kanehisa, 2019; Kanehisa et al., 2019) pathway map. Colored in green and red are the up- and down-regulated reaction flux predictions based on the *i*ML1515 genome- scale metabolic model, respectively, with yellow representing non-zero reaction fluxes that are not required to be regulated.

In **Table 4** we present the individual regulation pattern for ten different biocides (Pereira et al., 2020) as well as for Pd. We found that the general distribution of reactions into different categories is fairly consistent between biocides, with between 50 and 125 up-regulated reactions, 550 to 600 down-regulated reactions, and eight to 15 ambiguous reactions. There are approximately 2,000 reactions in the metabolic network that do not carry flux. The Pd flux distribution differs substantially from the others, with the majority of reactions (1,485 out of 2,712) being categorized as ambiguous, 1,090 not carrying flux, 17 up-regulated, and 120 down-regulated reactions.

Comparing the stress responses between the Pd stress environment and the biocide set as a whole (using the median flux values and upper and lower bounds of each reaction across biocides as a proxy for a generic response), we found the most significant commonality between the down-regulated sets (**Table 5**). Almost all reactions down-regulated in Pd (105 out of 120) are also being generically down-regulated under biocide stress conditions. However, we also found several major differences: in particular, ambiguous reactions are far more common in the Pd set, representing more than half (1,485 out of 2,712, or 55%) of all of the reactions. This is also reflected in **Figures 7**, **8**, where we can see that the Pd condition is dominated by ambiguous fluxes, whereas biocide stress in general corresponds to consistently down-regulated fluxes.

DISCUSSION

The general and oxidative stress-related effects of Pd stress to *E. coli* were compared to published work on the transcriptomic response of *E. coli* to other heavy metal stresses, namely, Ni (Gault et al., 2016), Co (Fantino et al., 2010), Cu (Kershaw et al., 2005), Zn (Lee et al., 2005), Ag (McQuillan and Shaw, 2014), Hg (LaVoie and Summers, 2018), and Cd (Helbig et al., 2008; A. Wang and Crowley, 2005), and to the response of the *Enterobacteriaceae* bacterium LSJC7 to As stress (Zhang et al., 2016). Pd-induced oxidative stress effects were also compared to other non-heavy metal-related oxidative stresses, namely, Cl (Wang et al., 2009) and biocide (Pereira et al., 2020) stresses. We found that several Pd stress-related effects are similar to the effects of other heavy metal or oxidative stresses (discussed in the section on common transcriptional changes, below). Interestingly, Pd stress caused unique effects that were not reported in the aforementioned heavy metal and oxidative stress studies (discussed in uncommon transcriptional changes, below).

Common Transcriptional Changes

This section discusses transcriptional changes that have been shown to occur in heavy metal stress responses previously. Overall, the challenge with Pd ions induced a multitude of expected changes in general stress response mechanisms and especially in efflux systems. A number of changes in basic energy metabolism were also observed in other heavy metal stress responses previously.

Protein Synthesis Arrest

Protein synthesis uses most of the cellular ATP (Pontes et al., 2015). The global down-regulation of the translation apparatus including the expression of the r-proteins, the elongation factors, and the tRNA processing genes suggests that the cells are trying to save energy for stress-related pathways rather than translation. This process of energy conservation was also found in other heavy metal stresses including Ni (Gault et al., 2016), Hg (LaVoie and Summers, 2018), Ag (McQuillan and Shaw, 2014) and Cd (Wang and Crowley, 2005).

RpoH and RpoS Sigma Factor Up-Regulation

When *E. coli* is exposed to high temperatures or any other condition that results in unfolded proteins, including exposure to heavy metals, the heat shock sigma factor, RpoH, is induced (Foster, 2005). RpoH regulates the expression of approximately 30 genes encoding heat shock response proteins. In contrast to

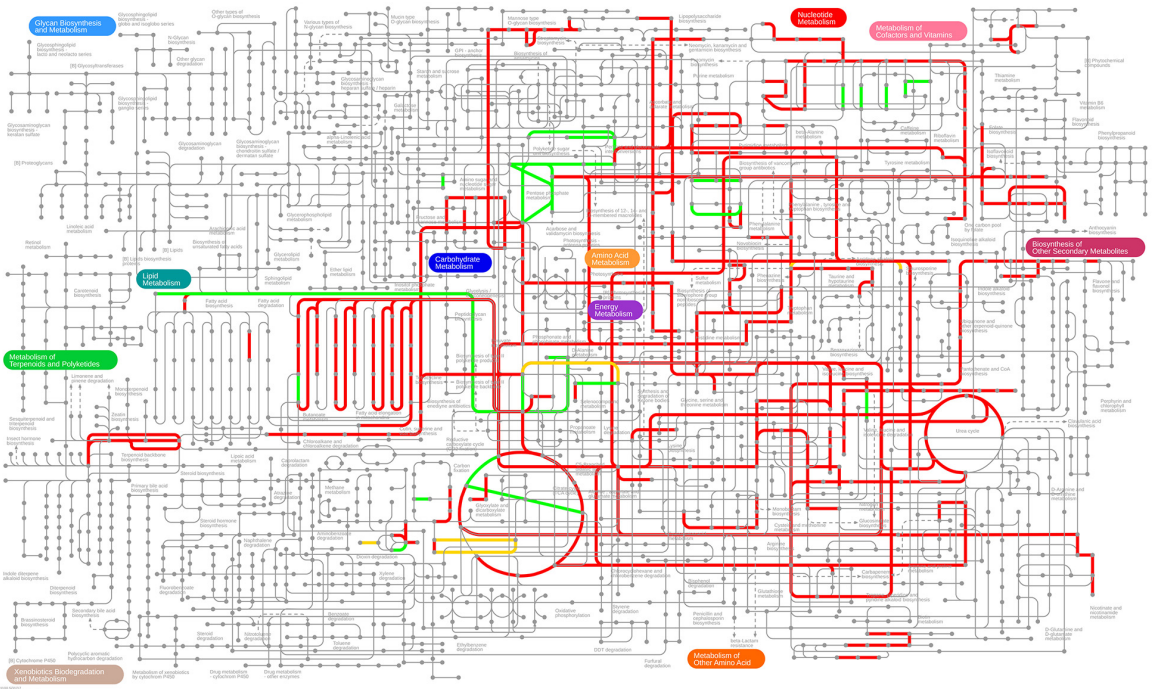

FIGURE 7 | Predicted up- and down-regulated median fluxes across ten biocides (Pereira et al., 2020) using the *i*ML1515 model, presented in the KEGG pathway map of *E. coli*. Up-regulated fluxes are green, down regulated fluxes red, and fluxes without a regulation requirement are colored yellow. No-flux reactions and reactions without KEGG IDs are omitted.

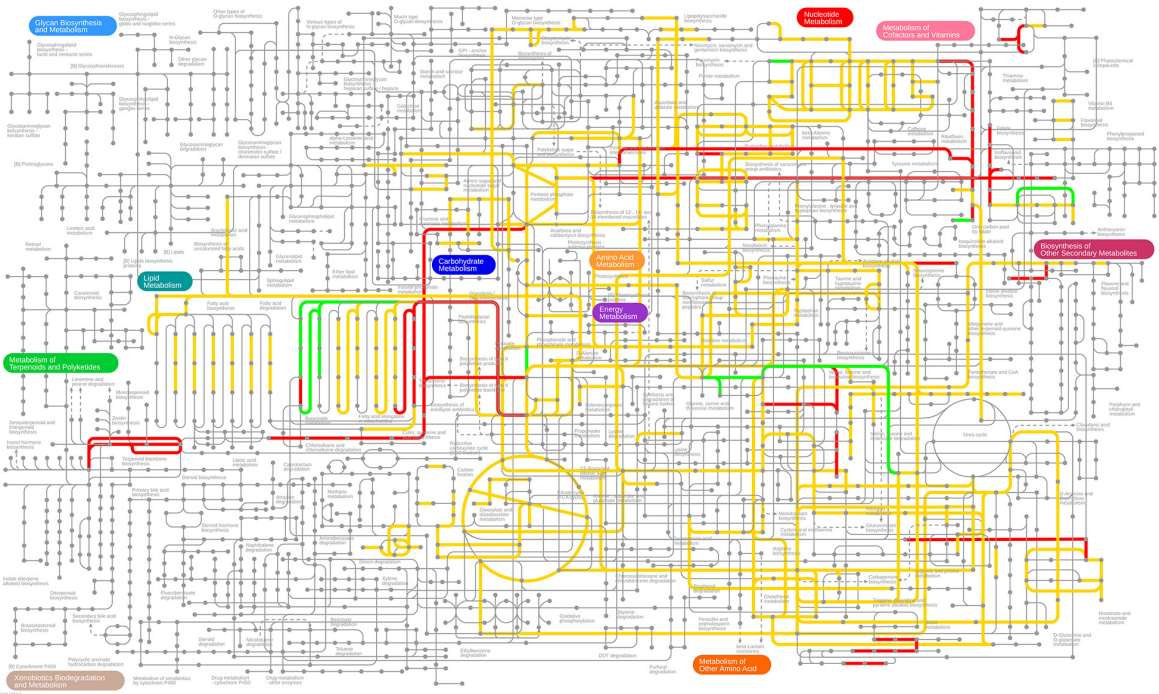

FIGURE 8 | Predicted up- and down-regulated fluxes in response to Pd stress using the *i*ML1515 genome-scale metabolic model, presented for the KEGG pathway map of *E. coli*. Up-regulated fluxes are green, down regulated fluxes red, and fluxes without a regulation requirement are colored yellow. No-flux reactions and reactions without KEGG IDs are omitted.

TABLE 4 | Differentially regulated flux predictions for the given condition.

	BENZ	XID	PHE	GLUTA	H_2O_2	ETOH	ISOP	PERA	POV	SOD	PAL
Up-regulation	122	72	80	48	103	84	79	76	71	55	17
Down-regulation	558	575	590	593	555	580	573	563	585	590	120
Ambiguous	12	14	9	9	11	13	15	10	8	11	1485

The table shows differentially regulated flux predictions for multiple biocides employing the E. coli model iML1515. The listed chemicals are Benzalkonium chloride BENZ, Chlorhexidine XID, Chlorophene PHE, Glutaraldehyde GLUTA, Hydrogen peroxide H2O2, Ethanol ETOH, Isopropanol ISOP, Peracetic acid PERA, Povidone- iodine POV, Sodium hypochlorite SOD, and Palladium PAL (Pereira et al., 2020). Note that we used the transcriptomic response after twelve hours.

this, the stationary phase and stress response sigma factor, RpoS, is triggered by other stress conditions that have the common property of arresting growth (Prabhakaran et al., 2016), such as oxidative stress (Eisenstark et al., 1996). Pd stress induced both sigma factors, this was also the case in Ag (McQuillan and Shaw, 2014) and Hg (LaVoie and Summers, 2018) stresses. Ni (Gault et al., 2016) and Cl (Wang et al., 2009) stresses induced only RpoS.

Heat Shock Response and Stress Proteins

Several heavy metals cause protein damage through cross-linking, disrupting their 3D structures and allosteric movements. The heat shock and stress-related proteolytic enzymes and chaperones help in the stabilization, re-folding, or the proteolysis of misfolded proteins. Five of the known heat shock and stress proteins were in top 20 highest up-regulated genes. The total number of up-regulated genes encoding heat shock and stress proteins due to Pd stress (28 genes) is very high compared to other heavy metal stresses. Ag stress (McQuillan and Shaw, 2014) comes in second where 17 genes were up-regulated. Other heavy metal stresses had less than 10 up-regulated genes, including Hg (LaVoie and Summers, 2018) and Cd (Helbig et al., 2008). Ni (Gault et al., 2016), Zn (Lee et al., 2005), Cu (Kershaw et al., 2005), Cl (Wang et al., 2009). Biocide stress (Pereira et al., 2020) induced only stress proteins and not heat shock proteins, based on RpoH and RpoS up-regulation explained in the previous section. This suggests that the damage caused by Pd on the protein level is even higher than by other heavy metals and requires a high number proteases and chaperones to deal with it.

Multi-Drug Efflux Systems

These systems are up-regulated in various stress conditions. The genes of these systems induce the expression of drug/toxin efflux system genes and limit passive uptake by decreasing porin expression (Alekshun and Levy, 1999). Pd stress induced the major three multiple drug efflux systems, MarRAB, MdtABC, and AcrAB. A similar effect was induced by Hg stress (LaVoie and Summers, 2018), while other heavy metal and oxidative stresses induced less than 3 efflux systems; 2 in case of Zn (Lee et al., 2005); 1 in case of Cd (Helbig et al., 2008) and Cl (Wang et al., 2009); and none in case of Ni (Gault et al., 2016), Ag (McQuillan and Shaw, 2014), As (Zhang et al., 2016), Co (Fantino et al., 2010), and Cu (Kershaw et al., 2005). This might suggest that Pd toxicity is highly unwanted for the cells or potentially the cells do not know what they are dealing with, and as a result, all the multi-drug efflux systems are up-regulated.

TABLE 5 | Similarity of stress responses.

Biocides \ Palladium	Up	Down	Ambiguous	No flux
Up-regulation	2	7	175	12
Down-regulation	10	105	299	21
Ambiguous	0	0	11	1
No flux	5	8	1000	1056

The table shows the similarity of the predicted stress responses. We summarized the biocide stress response and compared it to the palladium stress response. Here, we list the number of reactions in the respective categories.

Oxidative Stress Response

The formation of reactive intermediates, mainly radicals that react with oxygen and produce reactive oxygen species (ROS) is a common effect of heavy metal stresses (metal-induced oxidative stress), as a result of changing the redox state of the cell and their ability to self-oxidation (Kappus, 1987). These ROS interact with thiols, metal centers, nucleotide bases and lipids (Fang, 2004), which results in damages to nucleic acids, proteins, and lipids, and therefore, disrupting the normal cellular function (Ray et al., 2012). The two oxidative stress response systems in *E. coli* were up-regulated due to Pd stress, OxyRS and SoxRS. These two systems modulate a cascade of more than 100 genes encoding proteins with diverse stress-related biological functions including superoxide scavenging, DNA and protein repair, recycling of macromolecules, xenobiotics efflux, carbon metabolism, and NADPH regeneration (Pomposiello and Demple, 2001; Blanchard et al., 2007). Pd stress induced 32 genes from these pathways, including the *soxS* regulator gene that was the 6th highest up-regulated gene, increasing 240-fold. Similar effects are found in other heavy metal stresses including Ag (McQuillan and Shaw, 2014), As (Zhang et al., 2016), Cd (Helbig et al., 2008), Cu (Kershaw et al., 2005), Hg (LaVoie and Summers, 2018), Ni (Gault et al., 2016), and Zn (Lee et al., 2005).

Fe-S Clusters Biogenesis

Many genes encode proteins that contain Fe-S clusters. These redox-active proteins have prominent roles in several important cellular processes, including respiration, central metabolism, and gene regulation (Y. Zhang et al., 2016). Fe-S proteins can by damaged by oxidative stress (Py and Barras, 2010). *E. coli* has two systems that are responsible for Fe-S clusters assembly and repair, the *isc* and *suf* operons (Outten et al., 2004). All genes of the *iscARSU* system were up-regulated due to Pd stress, together with the *nfuA* gene that is involved in Fe-S biogenesis under iron starvation conditions. This suggests that Pd-induced oxidative

stress is damaging the Fe-S proteins and hence, the need to repair these proteins is increased. The *sufABC* operon was not modulated. Similar behavior was observed with As (Zhang et al., 2016), Cd (Helbig et al., 2008), Co (Fantino et al., 2010), and Zn (Lee et al., 2005) stresses. Copper stress (Kershaw et al., 2005) had the opposite effect, where the *suf* operon was up-regulated and not the *isc* operon. There are other heavy metal stresses that induced both *isc* and *suf* operons, including Ag (McQuillan and Shaw, 2014), Hg (LaVoie and Summers, 2018), and Cl (Wang et al., 2009) stresses. Ni stress (Gault et al., 2016) did not induce either of these operons.

Energy Production

In this study, *E. coli* was cultivated anaerobically, and accordingly, the cells are predicted to mainly use anaerobic respiration and fermentation for energy production. It is worth noting though that complete absence of oxygen cannot be guaranteed because closed tubes might still allow minimal diffusion of oxygen into the sample (see section "DISCUSSION"). The M63 minimal culture medium used to cultivate *E. coli* did not include any known amounts of terminal electron acceptors for anaerobic respiration (**Figure 3G**), except the minimal concentrations of HNO_3 solvent added, this leaves *E. coli* with fermentation as the main energy production process.

The first step of energy production is the degradation of carbohydrates to make pyruvate (glycolysis). *E. coli* has three native pathways to make pyruvate from glucose (EMP, OPPP, and EDP). None of these pathways were heavily modulated due to Pd stress. Interestingly, the genes involved in making pyruvate from other sugars such as glycerol, L-fucose, D-glucuronate, D-galacturonate, D-galactonate, and D-galactarate were highly up-regulated (summarized in **Figures 3B,C**). None of these carbohydrates were included in the culture medium either, where the sole carbon source was glucose. Glycerol-3-P can be synthesized from deacetylated phospholipids in the periplasm by the enzyme GlpQ (periplasmic glycerophosphoryl diester phosphodiesterase). These deacetylated phospholipids are released from dying cells and imported through the outer membrane by FadL and through the inner membrane by FadD proteins. GlpQ, FadL, and FadD were all up-regulated upon Pd exposure. This suggests that *E. coli* is generating energy through glycerol metabolism simultaneously with glucose metabolism to cope with Pd stress. A similar effect was reported in the same *E. coli* strain when it was exposed to atmospheric pollution (Zhang T. et al., 2019) and heavy metal mixtures (Trchounian et al., 2016). Regarding the other aforementioned carbohydrates, we assume that the cells up-regulated the transport systems for 14 different sugars out of a desperate, general need for energy.

The second step is making energy from pyruvate through fermentation. *E. coli* has different fermentative pathways to generate energy (marked in blue color in **Figure 3D**). The fermentative pathways of D-lactate, succinate and hydrogen were up-regulated. The *hycA* gene encoding the transcriptional repressor of the formate regulon was the strongest down-regulated gene due to Pd stress, decreasing 520-fold. This regulon includes the genes *hycBCDEFGHI* of hydrogenlyase FHL (also called [Ni-Fe] hydrogenase 3), and the gene for formate dehydrogenase H, *fdhF* (Skibinski et al., 2002). These 2 enzymes form a formate hydrogenlyase complex, which is responsible for the vast majority of H_2 production that occurs during fermentation in *E. coli* (McDowall et al., 2014). The bioreduction of Pd^{2+} ions requires the involvement of [Ni-Fe] hydrogenases. Deplanche et al. showed that a negligible Pd^{2+} ions reduction happens in an *E. coli* mutant strain genetically deprived of all hydrogenase activity (Deplanche et al., 2010). This might suggest that *E. coli* was detoxifying Pd ions through reduction in addition to the modulation of ion transporters.

Phosphoenolpyruvate, the starting molecule for the fermentation process, is also the precursor for aromatic amino acids synthesis together with erythrose-4-P. Aromatic amino acid synthesis pathways were massively down-regulated due to Pd stress (**Figure 4F**). This suggests that *E. coli* was trying to save phosphoenolpyruvate for energy production. In addition, the synthesis of acetyl-CoA, another pathway feeding into fermentation processes, though beta-oxidation cycle was up-regulated. This demonstrates that *E. coli* has modulated its gene expression for energy production over multiple pathways to cope with Pd stress (**Figures 3A–E**).

Interestingly, the anaerobic respiration genes were modulated too, despite the absence of terminal electron acceptors (**Figure 3G**). Upon Pd exposure, the genes encoding formate and glycerol-3-P dehydrogenases and hydrogenase 2 were up-regulated together with nitrate reductase, but glucose and malate dehydrogenases were down-regulated. The up-regulation of nitrate reductase might be due to signaling induced through the addition of minimal amounts of HNO_3, and this could partly explain the modulation of the dehydrogenases. However, the up-regulation of nitrate reductase could also be a general stress effect, as a similar effect was reported in As stress (Zhang et al., 2016).

Similar to Fe-S clusters, the sulfur-containing amino acids, cysteine and methionine, are vulnerable to oxidation. Methionine residues are extremely sensitive to oxidative stress and they are easily oxidized to methionine sulfoxide (Liu et al., 2018). The oxidation of these amino acids makes them unavailable for metabolic processes (Drazic and Winter, 2014). *E. coli* has a dedicated system for methionine oxidation repair, methionine sulfoxide reductase YedYZ (or MsrPQ) that are expressed under oxidative stress conditions (Yin et al., 2015). This reductase takes electrons from the quinone pool and gives it to methionine sulfoxide as a terminal electron acceptor (Ezraty et al., 2005). The expression of these genes was vastly up-regulated due to Pd stress, both were in the top 20 up-regulated genes, with *yedY* increasing 96-fold and *yedZ* increasing 112-fold. A similar behavior was seen in *E. coli* (S. Wang et al., 2009), *Enterococcus faecalis* (Zhao et al., 2010), *Pseudomonas fluorescens* (Lipus et al., 2019), and *Staphylococcus aureus* (Singh and Singh, 2010) when they were exposed to oxidative stress. The up-regulation of methionine sulfoxide reductase might suggest that *E. coli* was using methionine sulfoxide also as a terminal electron acceptor for the anaerobic respiration as another way to generate energy, and this could also partly explain the modulation of the anaerobic respiration dehydrogenases.

For the respiratory quinone pool, the expression of ubiquinone was up-regulated but the expression of menaquinone

TABLE 6 | Summary of anaerobic respiration differentially expressed genes.

Electron donor	Respiratory dehydrogenase	Quinone pool	Terminal reductase/oxidase	Electron acceptor
Formate	*fdnGHI* *fdoGHI*	Ubiquinone	*cyoABCD* *cydAB* *cyxAB*	Oxygen
Lactate	*lldD* *dld*		*narGHI* *narVYZ* *napABCGH*	Nitrate
Pyruvate	*poxB*			
Succinate	*sdhABCD*			
NADH	*ndh (NDH-1)* *nuo (NDH-2)*	Menaquinone	*nrfABCD*	Nitrite
			frdABCD	Fumarate
G3P	*glpABC* *glpD*	Demethyl-menaquinone	*dmsABC* *ynfFGH*	DMSO
Malate	*mqo*		*torABC* *torYZ*	TMAO
Hydrogen	*hyaABC* *hybABCO*			
Glucose	*gcd*		*yedYZ*	Methionine sulfoxide

The green color indicates up-regulation and the red color indicates down-regulation.

and demethyl-menaquinone was down-regulated. Ubiquinone is known to be a universal electron acceptor, accepting electrons from all the dehydrogenases, while menaquinone and demethyl-menaquinone accept electrons only from hydrogen, formate, glycerol-3-P, and NADH dehydrogenases (Søballe and Poole, 1999). The biosynthesis of one universal quinone that serves all the dehydrogenases instead of biosynthesizing three, from an energy perspective, could be the reason for this modulation. All the modulated genes related to anaerobic respiration are summarized in **Table 6**.

Amino Acid Biosynthesis and Transport

Possibly due to methionine oxidation, the biosynthesis and uptake of methionine were heavily up-regulated in parallel to the up-regulation of methionine sulfoxide repair system. The biosynthesis and uptake of arginine and histidine was also highly up-regulated due to Pd stress. Arginine biosynthesis is elevated in nutrient limitation and stress conditions (Weerasinghe et al., 2006), and has been suggested to help bacteria in adaptation to oxidative stress (Tiwari et al., 2018; Barrientos-Moreno et al., 2019). The biosynthesis of histidine was also reported to be elevated in heavy metal stresses. Histidine helps the bacteria in the detoxification of metal ions through the sequestration and complexation of ions by histidine-rich peptides (Isarankura-Na-Ayudhya et al., 2018). Cysteine biosynthesis was not up-regulated due to Pd exposure despite being an easy target for oxidation. Interestingly, the same behavior was also found in $HgCl_2$ stress (LaVoie and Summers, 2018) despite the fact that mercury has a strong affinity for thiol groups (Syversen and Kaur, 2012). Under $HgCl_2$ exposure, the biosynthesis of methionine and histidine was up-regulated but the biosynthesis of cysteine was unchanged. The biosynthesis of most other amino acids was down-regulated or unchanged for Pd, $HgCl_2$, Ni (Gault et al., 2016), Ag (McQuillan and Shaw, 2014) and, As (Zhang et al., 2016) stresses.

Inorganic Ion Transport Modulation

The most common bacterial strategies to deal with heavy metal stresses are the prevention of the metal ion from entering the cell and/or the active transport of the metal ion out of the cell (Nies and Silver, 2007). Both strategies were found to be applied by *E. coli* for Pd detoxification. For the first strategy, 8 metal ion import systems were down-regulated. The nickel-binding periplasmic protein NikA from the nickel transporter complex was down-regulated. Similar behavior was also found in Hg (LaVoie and Summers, 2018) and Co (Fantino et al., 2010) stresses. This shows that this system might be involved more generally in divalent heavy metal ion transport to the *E. coli*. For unknown reasons, this system was not down-regulated in Ni stress (Gault et al., 2016). Interestingly, all Fe^{2+} and Fe^{3+} import systems were down-regulated. This strongly suggests that Pd stress causes the disruption of Fe homeostasis and suggest that these systems could also be more directly involved in Pd transport to the cell. In oxidative stress conditions, iron import systems are usually up-regulated to take up more Fe for the biogenesis and repair of Fe-S clusters. Four of these systems were up-regulated in Ag stress (McQuillan and Shaw, 2014), while in As (Zhang et al., 2016), Cu (Kershaw et al., 2005) and biocide (Pereira et al., 2020) stresses, 3 or fewer systems were up-regulated. Other heavy metal stresses also caused Fe homeostatic disruption and therefore, some of the Fe import systems were down-regulated, including Co (Fantino et al., 2010), Cd (Helbig et al., 2008), Hg (LaVoie and Summers, 2018), and Ni (Gault et al., 2016) stresses. In addition to Fe import systems, the biosynthesis of enterobactin siderophore required for Fe^{3+} import was down-regulated, while the iron storage system was up-regulated. Similar findings were observed in Ni stress (Gault et al., 2016), where the cellular Fe content of Ni-treated *E. coli* was found to be less than the control. The zinc import system ZinT was up-regulated together with zinc resistance-associated protein ZraP (the latter is the 4th highest up-regulated, increasing 357-fold). This suggests that Pd might cause Zn homeostasis disruption too, supported by the fact that Zn homeostasis gene *zraP* was highly up-regulated. In addition, the magnesium import system MgtA was up-regulated. This up-regulation together with the down-regulation of potassium uptake protein TrkG could be based on the disturbance of cellular electrolyte balance caused by Pd stress, and as a result the cells try to maintain this balance by modulating these systems. The up-regulation of the osmotically inducible lipoprotein B, OsmB, supports this proposition. The magnesium import system MgtA was also up-regulated in Hg stress (LaVoie and Summers, 2018).

For the second strategy (the active transport of the metal ions out of the cell), 6 metal ion export systems were up-regulated. The nickel/cobalt efflux system RcnAB was up-regulated, comparable to up-regulation in Ni (Gault et al., 2016), Co (Fantino et al., 2010), and Hg (LaVoie and Summers, 2018) stresses. This suggests that this efflux system is involved more generally in divalent heavy metal ion detoxification in *E. coli*. The genes of the low-affinity ZntABR system were also up-regulated. This system is known to export ions with the following selectivity: Pb, Zn, Cd, Cu, Ni, and Co (Dutta et al., 2007). This system was up-regulated in Hg (LaVoie and Summers, 2018), Cd (Helbig et al., 2008), Co (Fantino et al., 2010), and Zn (Lee et al., 2005), but not in Ni (Gault et al., 2016) and Cu (Kershaw et al., 2005) stresses. This suggests that this system might also bind Pd ions, but this has to be confirmed. The copper-exporting ATPase CopA and

the copper oxidase CueO were also up-regulated. These genes are involved in copper detoxification through efflux and through oxidizing Cu^{+} to Cu^{2+}, respectively, and are up-regulated in many heavy metal stress situations (Grass and Rensing, 2001). This common heavy metal effect might be explained as an attempt to detoxify heavy metals by oxidation. It might also be that heavy metal exposure disrupts Cu homeostasis. Interestingly, Ni (Gault et al., 2016), Zn (Lee et al., 2005), Cu (Kershaw et al., 2005), and Ag (McQuillan and Shaw, 2014) stresses induced the *cus*ABC genes encoding a copper export system, but Pd exposure did not. This might suggest that Pd does not cause a disruption of Cu homeostasis as strongly as Fe and Zn. The arsenical resistance system ArsBCR was heavily up-regulated, with two of these genes in the top 20 up-regulated genes. This system was also up-regulated in As (Zhang et al., 2016), Hg (LaVoie and Summers, 2018), and Cd (Helbig et al., 2008) stresses. Moreover, the Ca^{2+}/H^{+} antiporter ChaA and Na^{+}/H^{+} antiporter NhaABR were both up-regulated. Similar behavior was found in Hg stress (LaVoie and Summers, 2018). The reason of this modulation could be the cellular attempt to restore the pH balance disturbed by Pd stress. Finally, the potassium efflux system KefCF system was down-regulated, which could be implicated in electrolyte and osmotic balancing together with TrkG and MgtA discussed above.

Down-Regulation of Motility and Biofilm Structures

Flagellar motility, fimbriae, and curli fibers are energetically costly structures (LaVoie and Summers, 2018). Like with protein synthesis arrest, Pd stress resulted in the down-regulation of these structures that are maybe less critical to immediate survival. For flagellar proteins, 8 genes were down-regulated upon Pd exposure, similar down-regulation was also found in Ni (Gault et al., 2016), Hg (LaVoie and Summers, 2018), Cu (Kershaw et al., 2005) and biocide (Pereira et al., 2020) stresses. The genes encoding biofilm structures suffered from a huge down-regulation too, the list includes the *yhcA* gene required for fimbriae biogenesis that was the 3rd strongest down-regulated gene, decreasing 197-fold, and the *csgE* gene required for curli production and assembly that was the 2nd strongest down-regulated gene, decreasing 338-fold. For biofilm synthesis, Cu (Kershaw et al., 2005) and Zn (Lee et al., 2005) stresses resulted in the down-regulation of the genes encoding fimbriae and curli proteins, but Ni (Gault et al., 2016), Hg (LaVoie and Summers, 2018), Cl (Wang et al., 2009), and biocide (Pereira et al., 2020) stresses induced them.

Uncommon Transcriptional Changes

This section discusses transcriptional changes that have not previously been observed or discussed in other heavy metal stresses, and that might be specific to Pd stress. It also discusses changes that are counterintuitive or opposite to what has been described previously for other heavy metal stress conditions.

Down-Regulation of DNA Repair Genes

Heavy metal and oxidative stresses cause damage to nucleic acids through ROS. An up-regulation in DNA repair genes was found in Hg (LaVoie and Summers, 2018), Cd (Helbig et al., 2008), Zn (Lee et al., 2005), As (Y. Zhang et al., 2016), Cl (Wang et al., 2009), and biocide (Pereira et al., 2020) stresses. DNA repair genes were unchanged in Ni (Gault et al., 2016), Cu (Kershaw et al., 2005), or Co (Fantino et al., 2010) stresses. Pd exposure, surprisingly, caused a down-regulation of DNA repair genes.

Nucleotide Transport and Metabolism

Purine and pyrimidine transport and metabolism genes were severely down-regulated due to Pd stress. All the permeases responsible for nucleotide import were down-regulated. The genes involved in the biosynthesis of nucleotides through both the *de novo* synthesis and salvage pathways were down-regulated. At the same time, the metabolic pathways for nucleotide hydrolysis were highly up-regulated, including the *hiuH* gene that was the 2nd highest up-regulated gene, increasing 1465-fold. Interestingly, Ni (Gault et al., 2016) and Cd (Pan et al., 2017) stresses included a similar effect, but an opposite effect was seen in *Desulfovibrio vulgaris* when it was exposed to oxidative stress (Zhang et al., 2006). Nevertheless, this is not a common heavy metal or oxidative stress-related effect. Some microorganisms, e.g., *Klebsiella pneumoniae* can utilize purines as carbon or nitrogen source (Tyler, 1978). *E. coli* can utilize purines as nitrogen source (Xi et al., 2000). This major down-regulation in nucleotide metabolism might suggest that *E. coli* is using nucleotides as nitrogen source instead of using them as building blocks for DNA and RNA. This could also explain the down-regulation of DNA repair genes (see section above).

Coenzyme Transport and Metabolism

Palladium stress resulted in the down-regulation of several genes related to the biosynthesis and transport of vitamins, including vitamins B1, B2, B3, B6, B9, and B12. A modulation in the genes of any of these or other vitamins to the best of our knowledge was not reported before in any heavy metal or oxidative stress study. The reason for such modulation remains unclear.

Cell Division and Cell Wall Biogenesis

Some cell cycle control, cell division, and cell wall biogenesis genes were down-regulated due to Pd stress. Many of these genes were related to LPS biosynthesis. This effect might be explained by the general poor health status of the bacterial cells, that prefer to shut down these genes in order to conserve energy for stress related pathways. LPS also has high affinity to divalent metallic ions (Ferris and Beveridge, 1986; Kotrba et al., 1999), and the down-regulation of LPS biosynthesis genes might also contribute to a reduction in Pd binding and uptake.

Sulfur Transport and Metabolism

The genes of the transporter complex of sulfate/thiosulfate, *cysAWTP*, and the hydrogen sulfide biosynthesis genes, *cysCDHIJN,* are differentially expressed in heavy metal and oxidative stresses. Some of these genes were up-regulated in Ag (McQuillan and Shaw, 2014), Cd (Helbig et al., 2008), Zn (Lee et al., 2005), and Cl (S. Wang et al., 2009) stresses, and down-regulated in Hg (LaVoie and Summers, 2018), Ni (Gault et al., 2016), and Co (Fantino et al., 2010) stresses. None of these genes were modulated due to Pd stress. This might show that Pd

does not affect sulfur homeostasis in *E. coli*, unlike the situation with Fe, Cu and Zn.

Carbohydrate Transport

Palladium stress induced the up-regulation of 14 different sugar transport systems. The uptake of maltose, galactose, trehalose, fructose, gluconate, galactofuranose, sorbitol, mannose, galactarate, L-fucose, xylose, ribose, L-arabinose, and glycerol was up-regulated. Such a systematic up-regulation was not found as an effect to any heavy metal stress before, in fact, the heavy metal and oxidative stress studies used in this paper did not record an up-regulation of any single sugar transport system. On the contrary, in Hg stress (LaVoie and Summers, 2018), the expression of several carbohydrate transport genes was down-regulated. The reasons for this remain unclear, but we speculate that under the anaerobic conditions approximated in our experiments, *E. coli* markedly tries to take up different possible fermentation substrates for energy, despite the fact that these sugars are not present in the medium.

Genome-Scale Metabolic Modeling

Our RNA-Seq data was used in genome-scale metabolic modeling and the results that represent changes in metabolic pathways and fluxes were compared to our (manual) analysis of up- and down-regulation of individual genes and operons. The genome-scale analysis was also compared to a dataset where 10 different biocides that were analyzed under comparable experimental conditions (Pereira et al., 2020). This was done to narrow down what of the observed responses under Pd stress are general stress responses to a toxic substance, and what effects are indeed specific to Pd stress.

As shown in **Figure 7** and **Table 4**, most of the metabolic reactions are either not affected (not shown in **Figure 7**) or down-regulated overall. **Figure 8** shows that the Pd stress response does not require most reactions to be differentially regulated for an optimal match with the experimental expression data.

Note however, that the *i*ML1515 metabolic model only contains a subset of the experimentally determined differentially expressed genes. Nevertheless, several similarities in down-regulation were found in the pathways of cofactor and vitamin metabolism (highlighted in pink in **Figures 7**, **8**), carbohydrate metabolism (highlighted in blue), and terpenoid metabolism (highlighted in green) to mention a few.

Especially for Pd stress response, many reactions are classified as ambiguous in our calculations. While it might be tempting to presume that this difference is a result of comparing a median (across multiple biocides) to a single value, we also see that the distribution of reactions in each of the individual biocide environments is generally similar to that of the median, and widely different from the Pd response. It seems more plausible that the difference in observed regulation is influenced by the environmental differences between the starting point for the biocide and Pd experiments. One such difference relates to available carbon and resulting capability of the cell to grow in the unstressed state. In the biocide experiments, the unstressed cell is able to allocate much of its input to biomass growth, which requires the production of a varied set of metabolites in fixed proportions. Any reduction in growth due to a limited set of bottlenecks would also reduce the necessary production of other metabolites. In contrast, the Pd environment has no external carbon source, and metabolism is simply directed toward survival, which from a model point of view primarily involves producing a sufficient amount of ATP, using whatever carbon source is available. If the cell has a wider set of alternative states available to meet such a requirement, this would lead to a greater uncertainty in possible flux distributions.

The conditions between Pd and biocides are also different as the latter are grown in an aerobic environment for 12 h in a defined medium. Hence, the organism has likely achieved a degree of adaptation to the new environment containing the stressor, possibly resulting in a lower growth rate (Pereira et al., 2020). In contrast, for Pd stress with short exposure time, the immediate stress response to the heavy metal is assessed. This results in many genes in comparison not being as significantly regulated based on the experimental data. For the biocides however, possibly due to the longer adaptation time, more genes are differentially expressed, resulting in an increased overlap with the model. Thus, the gx-FBA methodology is more likely to generate results of higher quality and result in a clearer pattern of up- and down- regulated reactions in comparison to the Pd stress response.

In summary, we observe that the biocide and Pd stress responses share certain commonalities, in particular with regards to a significant amount of down-regulated reactions; we also see a substantial difference evidenced by the large amount of reactions that are down-regulated under biocide stress conditions, but ambiguous under Pd stress, which may in part be a result of the differences in environmental conditions.

CONCLUSION

The introduction of Pd stress to *E. coli* resulted in common heavy metal and oxidative stress effects as well as effects that seem to be unique for Pd exposure. The commons effects were: energy conservation through protein synthesis arrest and the down-regulation of motility and biofilm structures; cellular detoxication through the up-regulation of multi-drug efflux systems and inorganic ion transport complexes; the stabilization, re-folding, and degradation of misfolded proteins through up-regulation of heat-shock and stress sigma factors and proteins; the induction of OxyRS and SoxRS oxidative stress response systems; and the up-regulation of energy production and conversion pathways. Pd^{2+} has a standard reduction potential of + 0.95 V, which is higher than all the other heavy metal ions used for the comparison in this study (Zn^{2+} is −0.76 V, Cd^{2+} is −0.40 V, Co^{2+} is −0.28 V, Ni^{2+} is −0.26 V, As^{3+} is −0.22 V, Cu^{2+} is + 0.34 V, Ag^{+} is 0.80 V, and Hg^{2+} is + 0.85 V) (Mayer and Holze, 2001). The higher the reduction potential, the easier it is for the metal ions to get reduced and therefore, the higher the oxidative stress caused. This might explain the high oxidative stress levels that resulted from Pd exposure, compared to other heavy metals.

Interestingly, Pd stress resulted in some unique effects, namely, the down-regulation of DNA repair genes, massive down-regulation of nucleotide transport and metabolism genes, down-regulation of coenzyme transport and metabolism genes especially for the B vitamins, down-regulation of cell wall biogenesis genes, and a massive up-regulation of carbohydrate transport genes. We previously observed that Pd stress might cause *E. coli* to go into viable but non-culturable (VBNC) state (data not shown). In this state, the cells are metabolically active (confirmed by colorimetric assays and viability assay kits) but unable to grow on agar plates. The massive down-regulation of nucleotide transport and metabolism, coenzyme transport and metabolism, and cell wall biogenesis genes might explain the reason behind *E. coli* going into this state.

In addition, Pd stress was found to disrupt the homeostasis of iron, copper, and zinc. Furthermore, the cells were found to detoxify Pd ions through four different strategies: the prevention of metal ions from entering the cells through the down-regulation of several inorganic ion transporter complexes, the active transport of the metal ions out of the cell through the up-regulation of multi-drug efflux systems and inorganic ion transporter complexes, the enzymatic alteration of the metal ions to a less toxic form (Pd nanoparticles) through the up-regulation of hydrogenases (Deplanche et al., 2010), and the potential intracellular sequestration of the metal ions by binding to proteins such as histidine-rich peptides through the up-regulation of histidine transport and biosynthesis genes. Pd is not a trace metal relevant to the growth of *E. coli*, and it seems improbable that the bacteria harbor sensory systems that would directly respond to the presence of Pd ions. More likely, the observed responses and changes in gene expression were mainly caused by the secondary effects of general heavy metal toxicity. It is interesting to note that *E. coli* shows some responses that seem to be specific for Pd, and further research is needed to elucidate the underlying signaling processes. The results presented here are important for efforts to use bacteria in bioremediation of heavy metal wastes (Foulkes et al., 2016; Murray et al., 2020), or to produce metal nanoparticles. Engineering strains for such purposes is only possible based on a thorough understanding of the physiological processes induced by the presence of Pd and other heavy metal ions, both on a single-gene and a systems level.

DATA AVAILABILITY STATEMENT

The data that supports the findings of this study are available in the **Supplementary Material** of this article. The raw data is publicly available on ArrayExpress database, https://www.ebi.ac.uk/arrayexpress/experiments/E-MTAB-10803/.

AUTHOR CONTRIBUTIONS

NJ performed experiments, analyzed data, and wrote the manuscript. AS, CS, and AV analyzed data and edited the manuscript. EA acquired funding, supervised data analysis, and edited the manuscript. DL acquired funding, supervised experiments and data analysis, and edited the manuscript. All authors contributed to the article and approved the submitted version.

FUNDING

This work was supported by the Research Council of Norway, grant 294605 (Center for Digital Life).

ACKNOWLEDGMENTS

The authors wish to thank Hawzeen Salah Khalil and Anders Kristian Krabberød for their contribution to this work.

SUPPLEMENTARY MATERIAL

The Supplementary Material for this article can be found online at: https://www.frontiersin.org/articles/10.3389/fmicb.2021.741836/full#supplementary-material

REFERENCES

Alekshun, M. N., and Levy, S. B. (1999). The mar regulon: multiple resistance to antibiotics and other toxic chemicals. *Trends Microbiol.* 7, 410–413. doi: 10.1016/S0966-842X(99)01589-9

Altuvia, S., Zhang, A., Argaman, L., Tiwari, A., and Storz, G. (1998). The *Escherichia coli* oxyS regulatory RNA represses fhlA translation by blocking ribosome binding. *EMBO J.* 17, 6069–6075. doi: 10.1093/emboj/17.20.6069

Alva, A., Sabido-Ramos, A., Escalante, A., and Bolívar, F. (2020). New insights into transport capability of sugars and its impact on growth from novel mutants of *Escherichia coli*. *Appl. Microbiol. Biotechnol.* 104, 1463–1479. doi: 10.1007/s00253-019-10335-x

Baba, T., Ara, T., Hasegawa, M., Takai, Y., Okumura, Y., Baba, M., et al. (2006). Construction of *Escherichia coli* K-12 in-frame, single-gene knockout mutants: the keio collection. *Mol. Syst. Biol.* 2:2006.0008. doi: 10.1038/msb4100050

Barrientos-Moreno, L., Molina-Henares, M. A., Pastor-García, M., Ramos-González, M. I., and Espinosa-Urgel, M. (2019). Arginine biosynthesis modulates pyoverdine production and release in *Pseudomonas* putida as part of the mechanism of adaptation to oxidative stress. *J. Bacteriol.* 201:e00454.

Baxter-Plant, V. S., Mabbett, A. N., and Macaskie, L. E. (2002). Bacteria, their precious metal armour, and a new weapon against waste. *Microbiol. Today* 29, 80–81.

Biffis, A., Centomo, P., Del Zotto, A., and Zecca, M. (2018). Pd metal catalysts for cross-couplings and related reactions in the 21st century: a critical review. *Chem. Rev.* 118, 2249–2295. doi: 10.1021/acs.chemrev.7b00443

Blanchard, J. L., Wholey, W. Y., Conlon, E. M., and Pomposiello, P. J. (2007). Rapid changes in gene expression dynamics in response to superoxide reveal SoxRS-dependent and independent transcriptional networks. *PLoS One* 2:e1186. doi: 10.1371/journal.pone.0001186

Bruins, M. R., Kapil, S., and Oehme, F. W. (2000). Microbial resistance to metals in the environment. *Ecotoxicol. Environ. Saf.* 45, 198–207. doi: 10.1006/eesa.1999.1860

Cheng, H. Y., Soo, V. W. C., Islam, S., McAnulty, M. J., Benedik, M. J., and Wood, T. K. (2014). Toxin GhoT of the GhoT/GhoS toxin/antitoxin system damages the cell membrane to reduce adenosine triphosphate and to reduce growth

under stress. *Environ. Microbiol.* 16, 1741–1754. doi: 10.1111/1462-2920.12373

Choi, H. J., Kim, S. J., Mukhopadhyay, P., Cho, S., Woo, J. R., Storz, G., et al. (2001). Structural basis of the redox switch in the OxyR transcription factor. *Cell* 105, 103–113. doi: 10.1016/S0092-8674(01)00300-2

Cui, Z., Bai, X., Liu, Y., and Li, S. (2017). Synthesis of palladium concave nanocubes with high−index facets and their catalytic properties. *Appl. Organometallic Chem.* 31:e3887. doi: 10.1002/aoc.3887

De Corte, S., Hennebel, T., De Gusseme, B., Verstraete, W., and Boon, N. (2012). Bio−palladium: from metal recovery to catalytic applications. *Microb. Biotechnol.* 5, 5–17. doi: 10.1111/j.1751-7915.2011.00265.x

De Windt, W., Aelterman, P., and Verstraete, W. (2005). Bioreductive deposition of palladium (0) nanoparticles on Shewanella oneidensis with catalytic activity towards reductive dechlorination of polychlorinated biphenyls. *Environ. Microbiol.* 7, 314–325. doi: 10.1111/j.1462-2920.2004.00696.x

Deplanche, K., Caldelari, I., Mikheenko, I. P., Sargent, F., and Macaskie, L. E. (2010). Involvement of hydrogenases in the formation of highly catalytic Pd(0) nanoparticles by bioreduction of Pd(II) using *Escherichia coli* mutant strains. *Microbiology* 156, 2630–2640. doi: 10.1099/mic.0.036681-0

Drazic, A., and Winter, J. (2014). The physiological role of reversible methionine oxidation. *Biochim. Biophys. Acta* 1844, 1367–1382. doi: 10.1016/j.bbapap.2014.01.001

Du, L., Jiang, H., Liu, X., and Wang, E. (2007). Biosynthesis of gold nanoparticles assisted by *Escherichia coli* DH5α and its application on direct electrochemistry of hemoglobin. *Electrochem. Commun.* 9, 1165–1170. doi: 10.1016/j.elecom.2007.01.007

Duffus, J. H. (2002). " Heavy metals" a meaningless term?(IUPAC Technical Report). *Pure Appl. Chem.* 74, 793–807. doi: 10.1351/pac200274050793

Dutta, S. J., Liu, J., Stemmler, A. J., and Mitra, B. (2007). Conservative and nonconservative mutations of the transmembrane CPC motif in ZntA: effect on metal selectivity and activity. *Biochemistry* 46, 3692–3703. doi: 10.1021/bi0616394

Eisenstark, A., Calcutt, M. J., Becker-Hapak, M., and Ivanova, A. (1996). Role of *Escherichia coli* rpoS and associated genes in defense against oxidative damage. *Free Radic. Biol. Med.* 21, 975–993. doi: 10.1016/S0891-5849(96)00154-2

Ezraty, B., Aussel, L., and Barras, F. (2005). Methionine sulfoxide reductases in prokaryotes. *Biochim. Biophys. Acta* 1703, 221–229. doi: 10.1016/j.bbapap.2004.08.017

Fang, F. C. (2004). Antimicrobial reactive oxygen and nitrogen species: concepts and controversies. *Nat. Rev. Microbiol.* 2, 820–832. doi: 10.1038/nrmicro1004

Fantino, J. R., Py, B., Fontecave, M., and Barras, F. (2010). A genetic analysis of the response of *Escherichia coli* to cobalt stress. *Environ. Microbiol.* 12, 2846–2857. doi: 10.1111/j.1462-2920.2010.02265.x

Feliciano-Ramos, I., Casañas-Montes, B., García-Maldonado, M. M., Menéndez, C. L., Mayol, A. R., Díaz-Vázquez, L. M., et al. (2014). Assembly of a cost-effective anode using palladium nanoparticles for alkaline fuel cell applications. *J. Chem. Educ.* 92, 360–363. doi: 10.1021/ed500230y

Ferris, F. G., and Beveridge, T. J. (1986). Site specificity of metallic ion binding in *Escherichia coli* K-12 lipopolysaccharide. *Can. J. Microbiol.* 32, 52–55. doi: 10.1139/m86-010

Foster, P. L. (2005). Stress responses and genetic variation in bacteria. *Mutat. Res.* 569, 3–11. doi: 10.1016/j.mrfmmm.2004.07.017

Foulkes, J. M., Deplanche, K., Sargent, F., Macaskie, L. E., and Lloyd, J. R. (2016). A novel aerobic mechanism for reductive palladium biomineralization and recovery by *escherichia coli*. *Geomicrobiol. J.* 33, 230–236. doi: 10.1080/01490451.2015.1069911

Fozo, E. M., Kawano, M., Fontaine, F., Kaya, Y., Mendieta, K. S., Jones, K. L., et al. (2008). Repression of small toxic protein synthesis by the Sib and OhsC small RNAs (Molecular Microbiology (2008) 70, (1076-1093)). *Mol. Microbiol.* 70:1305. doi: 10.1111/j.1365-2958.2008.06529.x

Gault, M., Effantin, G., and Rodrigue, A. (2016). Ni exposure impacts the pool of free Fe and modifies DNA supercoiling via metal-induced oxidative stress in *Escherichia coli* K-12. *Free Radic. Biol. Med.* 97, 351–361. doi: 10.1016/j.freeradbiomed.2016.06.030

Gavia, D. J., and Shon, Y.-S. (2015). Catalytic properties of unsupported palladium nanoparticle surfaces capped with small organic ligands. *ChemCatChem* 7:892. doi: 10.1002/cctc.201402865

Gehring, A. M., Bradley, K. A., and Walsh, C. T. (1997). Enterobactin biosynthesis in *escherichia coli*: Isochorismate lyase (EntB) is a bifunctional enzyme that is phosphopantetheinylated by EntD and then acylated by ente using ATP and 2,3-dihydroxybenzoate. *Biochemistry* 36, 8495–8503. doi: 10.1021/bi970453p

Georgopoulos, C., and Welch, W. J. (1993). Role of the major heat shock proteins as molecular chaperones. *Annu. Rev. Cell Biol.* 9, 601–634. doi: 10.1146/annurev.cb.09.110193.003125

Grass, G., and Rensing, C. (2001). Genes involved in copper homeostasis in *Escherichia coli*. *J. Bacteriol.* 183, 2145–2147. doi: 10.1128/JB.183.6.2145-2147.2001

Gurobi Optimization (2014). *Gurobi Optimizer Reference Manual, 2015*. Available online at: http://www.gurobi.com.

Gurunathan, S., Kalishwaralal, K., Vaidyanathan, R., Venkataraman, D., Pandian, S. R. K., Muniyandi, J., et al. (2009). Biosynthesis, purification and characterization of silver nanoparticles using *Escherichia coli*. *Colloids Surf. B Biointerfaces* 74, 328–335. doi: 10.1016/j.colsurfb.2009.07.048

Heirendt, L., Arreckx, S., Pfau, T., Mendoza, S. N., Richelle, A., Heinken, A., et al. (2019). Creation and analysis of biochemical constraint-based models using the COBRA Toolbox v.3.0. *Nat. Protoc.* 14, 639–702. doi: 10.1038/s41596-018-0098-2

Helbig, K., Grosse, C., and Nies, D. H. (2008). Cadmium toxicity in glutathione mutants of *Escherichia coli*. *J. Bacteriol.* 190, 5439–5454. doi: 10.1128/JB.00272-08

Hennebel, T., Van Nevel, S., Verschuere, S., De Corte, S., De Gusseme, B., Cuvelier, C., et al. (2011). Palladium nanoparticles produced by fermentatively cultivated bacteria as catalyst for diatrizoate removal with biogenic hydrogen. *Appl. Microbiol. Biotechnol.* 91, 1435–1445. doi: 10.1007/s00253-011-3329-9

Hollinshead, W. D., Rodriguez, S., Martin, H. G., Wang, G., Baidoo, E. E. K., Sale, K. L., et al. (2016). Examining *Escherichia coli* glycolytic pathways, catabolite repression, and metabolite channeling using Δ pfk mutants. *Biotechnol. Biofuels* 9:212.

Isarankura-Na-Ayudhya, P., Thippakorn, C., Pannengpetch, S., Roytrakul, S., Isarankura-Na-Ayudhya, C., Bunmee, N., et al. (2018). Metal complexation by histidine-rich peptides confers protective roles against cadmium stress in *Escherichia coli* as revealed by proteomics analysis. *PeerJ* 6:e5245.

Järup, L. (2003). Hazards of heavy metal contamination. *Br. Med. Bull.* 68, 167–182. doi: 10.1093/bmb/ldg032

Jbara, M., Maity, S. K., and Brik, A. (2017). Palladium in the chemical synthesis and modification of proteins. *Angew. Chem. Int. Ed.* 56, 10644–10655. doi: 10.1002/anie.201702370

Kanehisa, M. (2019). Toward understanding the origin and evolution of cellular organisms. *Protein Sci.* 28, 1947–1951. doi: 10.1002/pro.3715

Kanehisa, M., Sato, Y., Furumichi, M., Morishima, K., and Tanabe, M. (2019). New approach for understanding genome variations in KEGG. *Nucleic Acids Res.* 47, D590–D595. doi: 10.1093/nar/gky962

Kappus, H. (1987). Oxidative stress in chemical toxicity. *Arch. Toxicol.* 60, 144–149. doi: 10.1007/BF00296968

Karian, H. (2003). *Handbook of Polypropylene and Polypropylene Composites, Revised and Expanded*. Boca Raton, FL: CRC Press.

Kershaw, C. J., Brown, N. L., Constantinidou, C., Patel, M. D., and Hobman, J. L. (2005). The expression profile of *Escherichia coli* K-12 in response to minimal, optimal and excess copper concentrations. *Microbiology* 151, 1187–1198. doi: 10.1099/mic.0.27650-0

Kotrba, P., Dolečková, L., De Lorenzo, V., and Ruml, T. (1999). Enhanced bioaccumulation of heavy metal ions by bacterial cells due to surface display of short metal binding peptides. *Appl. Environ. Microbiol.* 65, 1092–1098. doi: 10.1128/aem.65.3.1092-1098.1999

Kundu, S., Kalees Warran, P., Mursalin, S. M., and Narjinary, M. (2015). Synergistic effect of Pd and Sb incorporation on ethanol vapour detection of La doped tin oxide sensor. *J. Materi. Sci. Mater. Electron.* 26, 9865–9872. doi: 10.1007/s10854-015-3662-3

LaVoie, S. P., and Summers, A. O. (2018). Correction: transcriptional responses of *Escherichia coli* during recovery from inorganic or organic mercury exposure. *BMC Genomics* 19:268. doi: 10.1186/s12864-018-4631-z

Lee, L. J., Barrett, J. A., and Poole, R. K. (2005). Genome-wide transcriptional response of chemostat-cultured *Escherichia coli* to zinc. *J. Bacteriol.* 187, 1124–1134. doi: 10.1128/JB.187.3.1124-1134.2005

Li, H. (2013). Aligning sequence reads, clone sequences and assembly contigs with BWA-MEM. *ArXiv* [Preprint] Available online at: http://arxiv.org/abs/1303.3997. ArXiv:1303.3997

Liao, Y., Smyth, G. K., and Shi, W. (2014). FeatureCounts: an efficient general purpose program for assigning sequence reads to genomic features. *Bioinformatics* 30, 923–930. doi: 10.1093/bioinformatics/btt656

Lipus, D., Vikram, A., Gulliver, D., and Bibby, K. (2019). Upregulation of peroxide scavenging enzymes and multidrug efflux proteins highlight an active sodium hypochlorite response in *Pseudomonas* fluorescens biofilms. *Biofouling* 35, 329–339. doi: 10.1080/08927014.2019.1605357

Liu, G., Huang, Y., and Zhai, L. (2018). Impact of nutritional and environmental factors on inflammation, oxidative stress, and the microbiome. *Biomed. Res. Int.* 2018:5606845.

Lloyd, J. R., Coker, V. S., Kimber, R. L., Pearce, C. I., Watts, M. P., Omajali, J. B., et al. (2020). New frontiers in metallic bio-nanoparticle catalysis and green products from remediation processes. *RSC Green Chem.* 2020, 244–265. doi: 10.1039/9781788016353-00244

Lloyd, J. R., Yong, P., and Macaskie, L. E. (1998). Enzymatic recovery of elemental palladium by using sulfate-reducing bacteria. *Appl. Environ. Microbiol.* 64, 4607–4609. doi: 10.1128/aem.64.11.4607-4609.1998

Lozet, J., and Mathieu, C. (1993). "Dictionary of soil science," in *Soil Science*, eds J. Lozet and C. Mathieu (Paris: Technique et Documentation-Lavoisier).

Matsumoto, T., Kamino, M., Yamada, R., Konishi, Y., and Ogino, H. (2020). Identification of genes responsible for reducing palladium ion in *Escherichia coli*. *J, Biotechnol,* 324, 7–10. doi: 10.1016/j.jbiotec.2020.09.015

Mayer, P., and Holze, R. (2001). Electrocatalysis of redox reactions by metal nanoparticles on graphite electrodes. *J. Solid State Electrochem.* 5, 402–411. doi: 10.1007/s100080000169

McDowall, J. S., Murphy, B. J., Haumann, M., Palmer, T., Armstrong, F. A., and Sargent, F. (2014). Bacterial formate hydrogenlyase complex. *Proc. Natl. Acad. Sci. U.S.A.* 111, E3948–E3956. doi: 10.1073/pnas.1407927111

McQuillan, J. S., and Shaw, A. M. (2014). Differential gene regulation in the Ag nanoparticle and Ag +-induced silver stress response in *Escherichia coli*: a full transcriptomic profile. *Nanotoxicology* 8(Suppl. 1), 177–184. doi: 10.3109/17435390.2013.870243

Miller, J., Schuler, C., Ward, J., Wylie, F., Frea, T., Delbene, R., et al. (1992). A short course. *Bact. Genet.* 37, 509–509.

Miller, M. A., Askevold, B., Mikula, H., Kohler, R. H., Pirovich, D., and Weissleder, R. (2017). Nano-palladium is a cellular catalyst for in vivo chemistry. *Nat. Commun.* 8:15906. doi: 10.1038/ncomms15906

Monk, J. M., Lloyd, C. J., Brunk, E., Mih, N., Sastry, A., King, Z., et al. (2017). iML1515, a knowledgebase that computes *Escherichia coli* traits. *Nat. Biotechnol.* 35, 904–908. doi: 10.1038/nbt.3956

Murray, A. J., Mikheenko, I. P., Deplanche, K., Omajali, J. B., Gomez-Bolivar, J., Merroun, M. L., et al. (2020). Chapter 9: biorefining of metallic wastes into new nanomaterials for green chemistry, environment and energy. *RSC Green Chem.* 63, 213–243. doi: 10.1039/9781788016353-00213

Navid, A., and Almaas, E. (2012). Genome-level transcription data of yersinia pestis analyzed with a new metabolic constraint-based approach. *BMC Syst. Biol.* 6:150. doi: 10.1186/1752-0509-6-150

Nies, D. H. (1999). Microbial heavy-metal resistance. *Appl. Microbiol. Biotechnol.* 51, 730–750. doi: 10.1007/s002530051457

Nies, D. H., and Silver, S. (2007). "Molecular microbiology of heavy metals," in *Molecular Microbiology of Heavy Metals*, eds D. H. Nies and S. Silver (Berlin: Springer Science & Business Media), 460.

Outten, F. W., Djaman, O., and Storz, G. (2004). A suf operon requirement for Fe-S cluster assembly during iron starvation in *Escherichia coli*. *Mol. Microbiol.* 52, 861–872. doi: 10.1111/j.1365-2958.2004.04025.x

Pan, J., Huang, X., Li, Y., Li, M., Yao, N., Zhou, Z., et al. (2017). Zinc protects against cadmium-induced toxicity by regulating oxidative stress, ions homeostasis and protein synthesis. *Chemosphere* 188, 265–273. doi: 10.1016/j.chemosphere.2017.08.106

Pedersen, K., and Gerdes, K. (1999). Multiple hok genes on the chromosome of *Escherichia coli*. *Mol. Microbiol.* 32, 1090–1102. doi: 10.1046/j.1365-2958.1999.01431.x

Pereira, B. M. P., Wang, X., and Tagkopoulos, I. (2020). Short-and long-term transcriptomic responses of *escherichia coli* to biocides: a systems analysis. *Applied and Environmental Microbiology* 86, e00708. doi: 10.1128/AEM.00708-20

Pomposiello, P. J., and Demple, B. (2001). Redox-operated genetic switches: the SoxR and OxyR transcription factors. *Trends Biotechnol.* 19, 109–114. doi: 10.1016/S0167-7799(00)01542-0

Pontes, M. H., Sevostyanova, A., and Groisman, E. A. (2015). When too much ATP is bad for protein synthesis. *J. Mol. Biol.* 427, 2586–2594. doi: 10.1016/j.jmb.2015.06.021

Pourret, O. (2018). On the necessity of banning the term "heavy metal" from the scientific literature. *Sustainability* 10:2879. doi: 10.3390/su10082879

Prabhakaran, P., Ashraf, M. A., and Aqma, W. S. (2016). Microbial stress response to heavy metals in the environment. *RSC Adv.* 6, 109862–109877. doi: 10.1039/c6ra10966g

Py, B., and Barras, F. (2010). Building Feg-S proteins: bacterial strategies. *Nat. Rev. Microbiol.* 8, 436–446. doi: 10.1038/nrmicro2356

Quintelas, C., Rocha, Z., Silva, B., Fonseca, B., Figueiredo, H., and Tavares, T. (2009). Removal of Cd(II), Cr(VI), Fe(III) and Ni(II) from aqueous solutions by an E. coli biofilm supported on kaolin. *Chem. Eng. J.* 149, 319–324. doi: 10.1016/j.cej.2008.11.025

Ray, P. D., Huang, B. W., and Tsuji, Y. (2012). Reactive oxygen species (ROS) homeostasis and redox regulation in cellular signaling. *Cell. Signal.* 24, 981–990. doi: 10.1016/j.cellsig.2012.01.008

Robinson, M. D., McCarthy, D. J., and Smyth, G. K. (2009). edgeR: a bioconductor package for differential expression analysis of digital gene expression data. *Bioinformatics* 26, 139–140. doi: 10.1093/bioinformatics/btp616

Robinson, M. D., and Oshlack, A. (2010). A scaling normalization method for differential expression analysis of RNA-seq data. *Genome Biol.* 11:R25. doi: 10.1186/gb-2010-11-3-r25

Rouch, D. A., Lee, B. T. O., and Morby, A. P. (1995). Understanding cellular responses to toxic agents: a model for mechanism-choice in bacterial metal resistance. *J. Ind. Microbiol.* 14, 132–141. doi: 10.1007/BF01569895

Seo, S. W., Kim, D., Szubin, R., and Palsson, B. O. (2015). Genome-wide reconstruction of OxyR and SoxRS transcriptional regulatory networks under oxidative stress in *Escherichia coli* K-12 MG1655. *Cell Rep.* 12, 1289–1299. doi: 10.1016/j.celrep.2015.07.043

Singh, K., and Singh, V. K. (2010). Expression of four methionine sulfoxide reductases in Staphylococcus aureus. *Int. J. Microbiol.* 2012:719594.

Skibinski, D. A. G., Golby, P., Chang, Y. S., Sargent, F., Hoffman, R., Harper, R., et al. (2002). Regulation of the hydrogenase-4 operon of *Escherichia coli* by the σ54-dependent transcriptional activators FhlA and HyfR. *J. Bacteriol.* 184, 6642–6653. doi: 10.1128/JB.184.23.6642-6653.2002

Søballe, B., and Poole, R. K. (1999). Microbial ubiquinones: multiple roles in respiration, gene regulation and oxidative stress management. *Microbiology* 145, 1817–1830. doi: 10.1099/13500872-145-8-1817

Syversen, T., and Kaur, P. (2012). The toxicology of mercury and its compounds. *J. Trace Elements Med. Biol.* 26, 215–226. doi: 10.1016/j.jtemb.2012.02.004

Tarver, S., Gray, D., Loponov, K., Das, D. B., Sun, T., and Sotenko, M. (2019). Biomineralization of Pd nanoparticles using Phanerochaete chrysosporium as a sustainable approach to turn platinum group metals (PGMs) wastes into catalysts. *Int. Biodeterior. Biodegr.* 143:104724. doi: 10.1016/j.ibiod.2019.104724

Tatusov, R. L., Galperin, M. Y., Natale, D. A., and Koonin, E. V. (2000). The COG database: a tool for genome-scale analysis of protein functions and evolution. *Nucleic Acids Res.* 28, 33–36. doi: 10.1093/nar/28.1.33

The Math Works Inc. (1991). The math works inc. *Simulation* 57:240. doi: 10.1177/003754979105700407

Tiwari, S., Van Tonder, A. J., Vilchèze, C., Mendes, V., Thomas, S. E., Malek, A., et al. (2018). Arginine-deprivation–induced oxidative damage sterilizes mycobacterium tuberculosis. *Proc. Natl. Acad. Sci. U.S.A.* 115, 9779–9784. doi: 10.1073/pnas.1808874115

Trchounian, K., Poladyan, A., and Trchounian, A. (2016). Optimizing strategy for *Escherichia coli* growth and hydrogen production during glycerol fermentation in batch culture: effects of some heavy metal ions and their mixtures. *Appl. Energy* 177, 335–340. doi: 10.1016/j.apenergy.2016.05.129

Tyler, B. (1978). Regulation of the assimilation of nitrogen compounds. *Annu. Rev. Biochem.* 47, 1127–1162. doi: 10.1146/annurev.bi.47.070178.005403

Vishnukumar, P., Vivekanandhan, S., and Muthuramkumar, S. (2017). Plant-mediated biogenic synthesis of palladium nanoparticles: recent trends and emerging opportunities. *ChemBioEng. Rev.* 4, 18–36. doi: 10.1002/cben.201600017

Wackett, L. P., Dodge, A. G., and Ellis, L. B. M. (2004). Microbial genomics and the periodic table. *Appl. Environ. Microbiol.* 70, 647–655. doi: 10.1128/AEM.70.2.647-655.2004

Wang, A., and Crowley, D. E. (2005). Global gene expression responses to cadmium toxicity in *Escherichia coli*. *J. Bacteriol.* 187, 3259–3266. doi: 10.1128/JB.187.9.3259-3266.2005

Wang, H., and Gunsalus, R. P. (2000). The nrfA and nirB nitrite reductase operons in *Escherichia coli* are expressed differently in response to nitrate than to nitrite. *J. Bacteriol.* 182, 5813–5822. doi: 10.1128/jb.182.20.5813-5822.2000

Wang, H., Tseng, C.-P., and Gunsalus, R. P. (1999). The napF and narG nitrate reductase operons in *Escherichia coli* are differentially expressed in response to submicromolar concentrations of nitrate but not nitrite. *J. Bacteriol.* 181, 5303–5308. doi: 10.1128/jb.181.17.5303-5308.1999

Wang, S., Deng, K., Zaremba, S., Deng, X., Lin, C., Wang, Q., et al. (2009). Transcriptomic response of *Escherichia coli* O157:H7 to oxidative stress. *Appl. Environ. Microbiol.* 75, 6110–6123. doi: 10.1128/AEM.00914-09

Watanabe, S., Kita, A., Kobayashi, K., and Miki, K. (2008). Crystal structure of the [2Fe-2S] oxidative-stress sensor SoxR bound to DNA. *Proc. Natl. Acad. Sci. U.S.A.* 105, 4121–4126. doi: 10.1073/pnas.0709188105

Weerasinghe, J. P., Dong, T., Schertzberg, M. R., Kirchhof, M. G., Sun, Y., and Schellhorn, H. E. (2006). Stationary phase expression of the arginine biosynthetic operon argCBH in *Escherichia coli*. *BMC Microbiol.* 6:14. doi: 10.1186/1471-2180-6-14

Xavier, K. B., and Bassler, B. L. (2005). Regulation of uptake and processing of the quorum-sensing autoinducer AI-2 in *Escherichia coli*. *J. Bacteriol.* 187, 238–248. doi: 10.1128/JB.187.1.238-248.2005

Xi, H., Schneider, B. L., and Reitzer, L. (2000). Purine catabolism in *Escherichia coli* and function of xanthine dehydrogenase in purine salvage. *J. Bacteriol.* 182, 5332–5341. doi: 10.1128/JB.182.19.5332-5341.2000

Yin, C., Zheng, L., Zhu, J., Chen, L., and Ma, A. (2015). Enhancing stress tolerance by overexpression of a methionine sulfoxide reductase A (MsrA) gene in Pleurotus ostreatus. *Appl. Microbiol. Biotechnol.* 99, 3115–3126. doi: 10.1007/s00253-014-6365-4

Zereini, F., and Alt, F. (2006). *Palladium Emissions in the Environment*. Berlin: Springer-Verlag.

Zhang, G., Amani, M., Chaturvedi, A., Tan, C., Bullock, J., Song, X., et al. (2019). Optical and electrical properties of two-dimensional palladium diselenide. *Appl. Phys. Lett.* 114:253102. doi: 10.1063/1.5097825

Zhang, T., Shi, X. C., Xia, Y., Mai, L., and Tremblay, P. L. (2019). *Escherichia coli* adaptation and response to exposure to heavy atmospheric pollution. *Sci. Rep.* 9:10879. doi: 10.1038/s41598-019-47427-7

Zhang, W., Culley, D. E., Hogan, M., Vitiritti, L., and Brockman, F. J. (2006). Oxidative stress and heat-shock responses in Desulfovibrio vulgaris by genome-wide transcriptomic analysis. *Antonie van Leeuwenhoek* 90, 41–55. doi: 10.1007/s10482-006-9059-9

Zhang, Y., Chen, S., Hao, X., Su, J. Q., Xue, X., Yan, Y., et al. (2016). Transcriptomic analysis reveals adaptive responses of an *enterobacteriaceae* strain LSJC7 to arsenic exposure. *Front. Microbiol.* 7:636. doi: 10.3389/fmicb.2016.00636

Zhao, C., Hartke, A., La Sorda, M., Posteraro, B., Laplace, J. M., Auffray, Y., et al. (2010). Role of methionine sulfoxide reductases A and B of *Enterococcus faecalis* in oxidative stress and virulence. *Infect. Immun.* 78, 3889–3897. doi: 10.1128/IAI.00165-10

Conflict of Interest: The authors declare that the research was conducted in the absence of any commercial or financial relationships that could be construed as a potential conflict of interest.

Publisher's Note: All claims expressed in this article are solely those of the authors and do not necessarily represent those of their affiliated organizations, or those of the publisher, the editors and the reviewers. Any product that may be evaluated in this article, or claim that may be made by its manufacturer, is not guaranteed or endorsed by the publisher.

frontiers in Microbiology

ORIGINAL RESEARCH
published: 18 October 2021
doi: 10.3389/fmicb.2021.722232

Electroporation as an Efficacy Potentiator for Antibiotics With Different Target Sites

*Žana Lovšin[1], Anja Klančnik[2] and Tadej Kotnik[1]**

[1] Faculty of Electrical Engineering, University of Ljubljana, Ljubljana, Slovenia, [2] Biotechnical Faculty, University of Ljubljana, Ljubljana, Slovenia

Antibiotic resistance is a global health threat, and there is ample motivation for development of novel antibacterial approaches combining multiple strategies. Electroporation is among the promising complementary techniques – highly optimizable, effective against a broad range of bacteria, and largely impervious to development of resistance. To date, most studies investigating electroporation as an efficacy potentiator for antibacterials used substances permissible in food industry, and only few used clinical antibiotics, as acceptable applications are largely limited to treatment of wastewaters inherently contaminated with such antibiotics. Moreover, most studies have focused mainly on maximal achievable effect, and less on underlying mechanisms. Here, we compare *Escherichia coli* inactivation potentiation rates for three antibiotics with different modes of action: ampicillin (inhibits cell wall synthesis), ciprofloxacin (inhibits DNA replication), and tetracycline (inhibits protein synthesis). We used concentrations for each antibiotic from 0 to 30× its minimum inhibitory concentration, a single 1-ms electric pulse with amplitude from 0 to 20 kV/cm, and post-pulse pre-dilution incubation either absent ($\lesssim$1 min) or lasting 60 min, 160 min, or 24 h. Our data show that with incubation, potentiation is significant for all three antibiotics, increases consistently with pulse amplitude, and generally also with antibiotic concentration and incubation time. With incubation, potentiation for ampicillin was rather consistently (although with weak statistical significance) superior to both ciprofloxacin and tetracycline: ampicillin was superior to both in 42 of 48 data points, including 7 with significance with respect to both, while at 60- and 160-min incubation, it was superior in 31 of 32 data points, including 6 with significance with respect to both. This suggests that electroporation potentiates wall-targeting antibiotics more than those with intracellular targets, providing motivation for in-depth studies of the relationship between the mode of action of an antibiotic and its potentiation by electroporation. Identification of substances permissible in foods and targeting the cell wall of both Gram-negative and Gram-positive bacteria might provide candidate antibacterials for broad and strong potentiation by electroporation applicable also for food preservation.

Keywords: electroporation, antibiotics, mode of action, combined antibacterial treatments, wastewater treatment, treatment time

OPEN ACCESS

Edited by:
Aleksandra P. Djukic-Vukovic, University of Belgrade, Serbia

Reviewed by:
Allen L. Garner, Purdue University, United States
Guiying Li, Guangdong University of Technology, China

****Correspondence:***
Tadej Kotnik
tadej.kotnik@fe.uni-lj.si

Specialty section:
This article was submitted to Microbial Physiology and Metabolism, a section of the journal Frontiers in Microbiology

Received: *08 June 2021*
Accepted: *29 September 2021*
Published: *18 October 2021*

Citation:
Lovšin Ž, Klančnik A and Kotnik T (2021) Electroporation as an Efficacy Potentiator for Antibiotics With Different Target Sites. Front. Microbiol. 12:722232. doi: 10.3389/fmicb.2021.722232

INTRODUCTION

Antibiotic resistance is a global health threat associated with increased morbidity, mortality, hospitalization, and healthcare costs (Laxminarayan et al., 2013; Frieri et al., 2017; Klein et al., 2019). There is thus high motivation for development of novel approaches combining multiple antibacterial strategies that have different modes of action (Alexopoulos et al., 2019; Berdejo et al., 2019; Douafer et al., 2019; Juma et al., 2020). Among the promising complementary techniques for such approaches is electroporation, in which exposure of bacteria to short electric pulses of sufficient strength permeabilizes their membranes, thereby facilitating the uptake of diverse compounds, including antibiotics (Garner, 2019). Electroporation is highly optimizable through adjustment of pulse amplitude and duration, reproducible, and effective across a broad range of microorganisms [see Table 1 in Kotnik et al. (2015)]. Moreover, due to the physical nature of the main underlying mechanism – formation of aqueous pores in the membranes (Kotnik et al., 2019) – bacteria cannot develop resistance against it.

Electroporation alone can also cause bacterial death, but the levels of inactivation typically achieved are insufficient for general stand-alone use, providing motivation for development of synergistic treatments (Martín-Belloso and Sobrino-López, 2011; Berdejo et al., 2019). For food and beverage preservation, the combination of electroporation with antibacterials has been shown to decrease required pulse amplitudes and increase achievable inactivation rates (Berdejo et al., 2019). However, the range of antibacterials permissible for such applications is in practice limited to substances that either occur also naturally in food (e.g., acetic acid, citric acid, lactic acid, cinnamaldehyde, and linalool) or are registered as food additives (e.g., nisin, triethyl citrate).

For any application outside clinical and veterinary medicine, addition of antibiotics is generally problematic due to the involved health risks and/or the resulting environmental burden. However, wastewaters from hospitals and livestock farms are already inherently contaminated with clinical and veterinary antibiotics, respectively (Diwan et al., 2013; Kim et al., 2020), as well as with a broad range of bacteria including strains resistant to different antibiotics (Hocquet et al., 2016). As a result, downstream wastewater treatment plants where all these antibiotics and bacteria accumulate become hotbeds for cross-acquisition of bacterial antibiotic resistance and for release of resistance genes into the environment, where they can further contribute to the spread of resistance (Rizzo et al., 2013). The ensuing problem is further aggravated by hospitals' use and subsequent release into wastewater of novel and last-resort antibiotics, for which it is of paramount importance to retain the absence of bacterial resistance.

These problems are increasingly recognized as being critical both for human health and for the environment, and thus approaches to reduce the concentration of viable bacteria, antibiotics, and/or antibiotic resistance genes – preferably all three – in wastewaters are now being proposed and tested. For on-site treatment of wastewaters prior to their release into the communal sewage, various designs have been proposed based on ozonation, ultraviolet light, and/or microalgal biodegradation (Paulus et al., 2019; Leng et al., 2020).

With wastewaters already containing various bacteria and antibiotics, methods that render the bacterial envelope permeable, thus facilitating the permeation of antibiotics into the bacteria and potentiating their efficacy, emerge as straightforward candidates for the first "line of attack." Once the bacterial load is sufficiently reduced, subsequent treatment can focus on degradation/removal of the antibiotics and the bacterial resistance genes. As permeabilization based on additives (e.g., detergents, enzymes, and microbeads) would cause additional pollution of the treated wastewater, the acceptable options are limited to green techniques, such as ultrasonication, freeze-thawing, and electroporation. Among these, electroporation is most widely recognized and used due to its general effectiveness, efficiency, and applicability to a broad range of microorganisms (Aune and Aachmann, 2010; Kotnik et al., 2015; Eleršek et al., 2020). Furthermore, in contrast to the mainstream water treatment method of chlorination, which in wastewaters can create genotoxic adsorbable organic chlorides (Emmanuel et al., 2004), delivery of electric pulses does not increase wastewater genotoxicity even at highest amplitudes and durations used in practice for electroporation (Gusbeth et al., 2009).

To date, the majority of studies that have combined electroporation and antibacterials [see **Table 2** in Garner (2019)] have focused on substances permissible in food and beverage processing. Still, five recent studies have quantified the potentiation of inactivation rates for combination of electroporation and clinical antibiotics (Korem et al., 2018; Novickij et al., 2018a; Vadlamani et al., 2018, 2020; Rubin et al., 2019), with their exposure parameters and results summarized in **Table 1**. Two further studies (Kuyukina et al., 2020; Martens et al., 2020) used the disk diffusion test to study electroporation-induced increase in susceptibility of *Rhodococcus ruber* to five and *Escherichia coli* to four different antibiotics, at increasing concentrations, and confirmed that such susceptibility increases are generally achievable.

As summarized in **Table 1**, the studies to date have shown that electroporation generally potentiates the efficacy of antibiotics, and that potentiation is achievable whether the antibiotic targets the synthesis of nucleic acids (ciprofloxacin, rifampicin), proteins (doxycycline, erythromycin, gentamicin, mupirocin, streptomycin, and tobramycin), or the cell wall (oxacillin, penicillin G, and vancomycin). Still, a systematic evaluation of the possible dependence of this potentiation on the antibiotic's mode of action is lacking, yet needed for a broader understanding and recognition of electroporation as an effective potentiator of antibiotics, and for its implementation in practice. Moreover, for cross-comparison of potentiation rates achievable for different antibiotics, the most informative approach is to proceed for each investigated antibiotic from its minimum inhibitory concentration (MIC), which has to date only been used in one study to investigate a single antibiotic (Korem et al., 2018).

Also, where stated in these previous studies, the post-pulse incubation times before diluting out of the antibiotics

TABLE 1 | Summary of the five reports on combined antibacterial use of clinical antibiotics and electroporation.

Study	Bacteria	Antibiotic		Pulse parameters				Maximum effect (IR = inactivation rate; VR = viability rate)
		Type	Concentration (μg/mL)	Pulse duration (μs)	Number of pulses	Pulse amplitude (kV/cm)	Repetition frequency (Hz)	
Novickij et al., 2018a	*Staphylococcus aureus* (MRSA)	Ciprofloxacin	1, 10, 100, and 1,000	100	8	5, 10, 15, 20	1,000	<25% VR @ 20 kV/cm, 1,000 μg/ml
		Doxycycline	1, 10, 100, and 1,000					<3% VR @ 20 kV/cm, 1,000 μg/ml
		Gentamicin	1, 10, 100, and 1,000					<1% VR @ 15 kV/cm, 10 μg/ml
		Sulfamethoxazole	1, 10, 100, and 1,000					<5% VR @ 20 kV/cm, ≥1 μg/ml
		Vancomycin	1, 10, 100, and 1,000					<16% VR @ 20 kV/cm, 1,000 μg/ml
Rubin et al., 2019	*Pseudomonas aeruginosa*	Mix of penicillin G (500–5,000 U/mL), streptomycin (0.5–5 mg/mL), nystatin (antimycotic, 62.5–625 U/mL)		60	200	≤∼3.1	2.8	Same IR @ ∼30–45% lower pulse amplitude
	Staphylococcus epidermidis					≤∼3.8		Same IR @ ∼8–13% lower pulse amplitude
Korem et al., 2018	*Staphylococcus aureus* (oxacillin-sensitive)	Oxacillin	0.5×, 1×, 2 × MIC (MIC = 0.38 μg/mL)	100	∼50 pulses 2.0 kV and ∼50 pulses 1.5 kV		1	No detectable VR @ ≥0.5 × MIC
Vadlamani et al., 2018	*Staphylococcus aureus*	Tobramycin	0.2, 2, and 20	0.3	1,000 pulses 20 kV/cm, 445 pulses 30 kV/cm, or 250 pulses 40 kV/cm		1	>5.5 $\log_{10}$ IR @ 40 kV/cm, 20 μg/ml
	Escherichia coli							>4.2 $\log_{10}$ IR @ 30 kV/cm, 20 μg/ml
	Staphylococcus aureus	Rifampicin	0.2, 2, 20					>5.2 $\log_{10}$ IR @ 30 kV/cm, 20 μg/ml
	Escherichia coli							>8.5 $\log_{10}$ IR @ 30 kV/cm, 20 μg/ml
Vadlamani et al., 2020	*Staphylococcus aureus* (MRSA)	Mupirocin	2, 20	0.3	500 pulses 20 kV/cm or 222 pulses 30 kV/cm		1	≤6.5 $\log_{10}$ IR
	Escherichia coli							≤4.5 $\log_{10}$ IR
	Pseudomonas aeruginosa							≤1.3 $\log_{10}$ IR
	Staphylococcus aureus (MRSA)	Rifampicin	2, 20					≤6.3 $\log_{10}$ IR
	Escherichia coli							≤6.4 $\log_{10}$ IR
	Pseudomonas aeruginosa							≤2.1 $\log_{10}$ IR
	Staphylococcus aureus (MRSA)	Erythromycin	2, 20					≤4.8 $\log_{10}$ IR
	Escherichia coli							≤4.4 $\log_{10}$ IR
	Pseudomonas aeruginosa							≤1.0 $\log_{10}$ IR
	Staphylococcus aureus (MRSA)	Vancomycin	2, 20					≤5.3 $\log_{10}$ IR
	Escherichia coli							≤4.5 $\log_{10}$ IR
	Pseudomonas aeruginosa							≤1.4 $\log_{10}$ IR

have been as long as 24 h (Novickij et al., 2018a; Kuyukina et al., 2020; Martens et al., 2020). Implementation of such a long incubation for on-site hospital wastewater treatment would require a reservoir in which the undiluted antibiotic concentration would be retained until release into the communal sewage (and thus dilution), and the required reservoir volume would likely be prohibitive. Lastly, in these previous studies, bacteria were subjected to at least 8 and up to 1,000 consecutive pulses per treatment, which maximized the effect, but at the cost of adding to the list of parameters (bacterial strain, antibiotic type, antibiotic concentration, pulse duration, pulse amplitude, and post-treatment incubation time) two more – the number of pulses and their repetition frequency.

Here, we compared the *E. coli* inactivation potentiation by electroporation for three antibiotics with different modes of action: ampicillin (inhibits cell wall synthesis), ciprofloxacin (inhibits DNA replication), and tetracycline (inhibits protein synthesis). The inactivation rates were investigated at antibiotic concentrations from the MIC to 30-fold the MIC, exposure to a single 1-ms electric pulse with amplitudes from 5 to 20 kV/cm, and a post-pulse pre-dilution incubation from $\lesssim$ 1 min to 24 h.

MATERIALS AND METHODS

Bacterial Strain and Growth Conditions

To exclude the effect of resistance and virulence genes, the non-resistant and non-pathogenic *E. coli* K12 ER1821 strain was used (New England BioLabs, Ipswitch, MA, United States), and was propagated according to the protocol of the supplier. The cells were cultured in lysogeny broth rich medium (Sigma-Aldrich, St. Louis, MO, United States) at 37°C, with agitation. The growth curve was measured from a starting culture with optical density at 600 nm (OD_{600}) of 0.01, and the middle exponential phase was determined at 3.5 h of incubation.

Antibiotics and Minimum Inhibitory Concentration Determination

Three antibiotics with different modes of action were used in this study: (i) ampicillin (#A9518; Sigma-Aldrich), which inhibits cell wall synthesis by binding to bacterial penicillin-binding protein transpeptidases, thus preventing them from catalyzing cross-linking of peptidoglycan chains (Wright, 1999); (ii) ciprofloxacin (#17850; Sigma-Aldrich), which inhibits DNA replication by binding to and thus blocking bacterial DNA gyrase and topoisomerase IV (Madurga et al., 2008); and (iii) tetracycline (#T3383; Sigma-Aldrich), which inhibits protein synthesis by preventing the attachment of aminoacyl-tRNA to the A-site of the bacterial 30S ribosomal subunit (Chopra and Roberts, 2001).

To allow for cross-comparisons of the potentiation achievable for each of these antibiotics, the minimum inhibitory concentration (MIC) for each antibiotic was determined against the *E. coli* strain used, as the lowest concentration of the antibiotic that inhibited visible growth of the *E. coli* during the incubation. This is to be distinguished from the minimum bactericidal concentration, MBC, which is higher and is defined as the lowest concentration of an antibiotic that kills at least 99.9% of the bacteria. The standard protocol of agar dilution and overnight incubation was followed for MIC determination (Andrews, 2001), with the MIC values so determined given in section "Antibiotics Minimum Inhibitory Concentrations." Experiments were then carried out at the antibiotic concentrations corresponding to MIC, 3 × MIC, 10 × MIC, and 30 × MIC, with the multiples of MIC used to compensate for the shorter post-pulse pre-dilution incubation times used in these experiments compared to the overnight incubation used for MIC determination.

Sample Preparation

Overnight *E. coli* cultures were initiated by inoculation of one colony from lysogeny broth agar plate to 50 mL lysogeny broth, with overnight incubation at 37°C, with agitation. The following morning OD_{600} was measured, and fresh 250 mL lysogeny broth was inoculated for the starting OD_{600} of 0.01. The cultures were grown to the middle exponential growth phase, which occurred at 3.5 h at 37°C, with agitation. The cells were then centrifuged, washed with 250 mM sucrose, centrifuged again, and resuspended in 16 mL 250 mM sucrose.

Treatment: Antibiotic Concentrations, Electric Pulse Amplitudes, and Post-pulse Pre-dilution Incubation Times

For each antibiotic, the concentrations used were 0 (no antibiotic), MIC, 3 × MIC, 10 × MIC, and 30 × MIC. For the electric pulse, the amplitudes used were 0 (no pulse delivery), 5, 10, 15, and 20 kV/cm. For post-pulse pre-dilution incubation at room temperature with the same antibiotic at the same concentration as in the treatment, the incubation times used were $\lesssim$1 min (dilution right after pulse delivery), 60 min, 160 min, and 24 h.

For each combination of parameters, the experiments were performed three times on different days, with altered order in which the parameters were varied for each of three repetitions of the experiment. The treatment with no antibiotic and no pulse delivery was considered as the control.

A 3-mL volume of prepared washed culture was added to 3 mL of 250 mM sucrose (for control and electroporation-only experiments), or to 3 mL of 250 mM sucrose supplemented with an antibiotic at the final concentration required (i.e., MIC or multiples thereof) as stated above. Electroporation was performed using the HVP-VG square wave pulse generator (IGEA, Carpi, Italy). The samples (140 μL) were placed between two parallel stainless-steel electrodes with a 1-mm gap, and a single 1-ms rectangular electric pulse was delivered. The voltages applied were 500, 1,000, 1,500, and 2,000 V, for electric pulse amplitude (i.e., voltage-to-distance ratio) of 5, 10, 15, and 20 kV/cm, respectively, with the actual time courses of the voltage for each pulse amplitude as measured with LeCroy HDO4104A oscilloscope and HVD3206A voltage probe (Teledyne Technologies, Thousand Oaks, CA, United States) shown in **Figure 1**. Then, a 100-μL volume

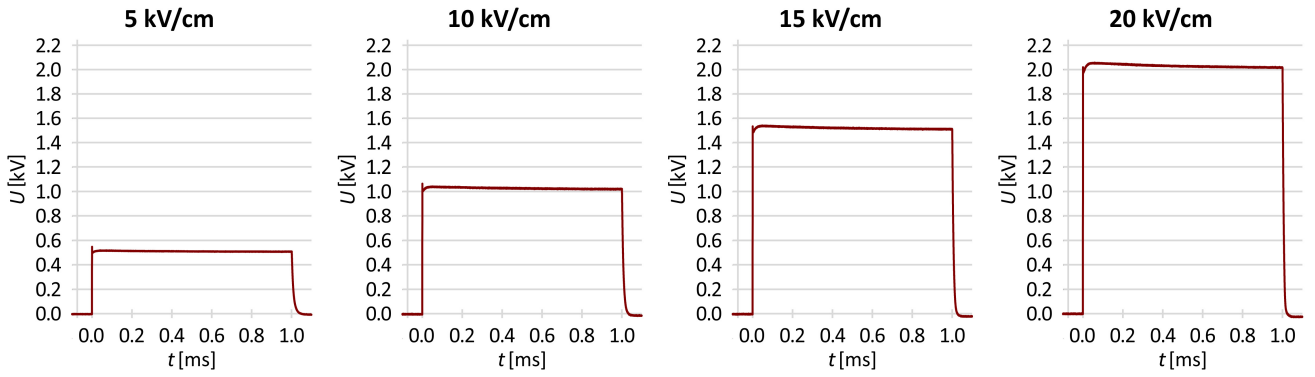

FIGURE 1 | The actual time courses of the voltage delivered in this study by the 5, 10, 15, and 20 kV/cm pulse.

was taken from each sample, and mixed with 100 μL of either lysogeny broth (for control and electroporation-only experiments) or lysogeny broth supplemented with the antibiotic at the final concentration required for the post-pulse pre-dilution incubation.

Determination of Inactivation Rate

After the treatment and the post-treatment incubation, the *E. coli* samples were serially diluted in 0.9% NaCl, and for each dilution, three drops of 10 μL were plated on a lysogeny broth agar plate. After the drops dried, the plates were incubated overnight at 37°C. The *E. coli* counts were recorded for each dilution (colony counts from 3 to 30), and the colony forming units (CFU)/mL were calculated from the mean number of colonies (mean of the three drops). The *E. coli* inactivation rates were calculated as $-\log_{10}(N/N_0)$, where N is the *E. coli* CFU/mL of the sample, and N_0 is the *E. coli* CFU/mL of the control ($\log_{10}$ will henceforth be referred to as log).

Statistical Analysis

The experiments were repeated three times on different days for each antibiotic, and the treatment data were normalized to the control (i.e., sample with no antibiotic and no pulse delivery) and expressed as mean ± standard deviation. The data were post-processed in R Commander 2.6 (developed by John Fox at McMaster University, Hamilton, Canada, and available under the GNU General Public License). To compare the effects of the three antibiotics, one-way analysis of variance was used (ANOVA; $p < 0.05$) for each combination of electric pulse amplitude, antibiotic concentration, and post-pulse pre-dilution incubation time. Tukey's HSD multiple comparison test for evaluation of the difference was used when ANOVA indicated a statistically significant difference ($p < 0.05$). In **Figure 2**, asterisks indicate data points where the effect with one antibiotic was statistically significantly different from each of the other two (e.g., a data point for ampicillin was assigned an asterisk if it was significantly different from both ciprofloxacin and tetracycline, and similarly with data points for the other two antibiotics).

RESULTS

Antibiotics Minimum Inhibitory Concentrations

The minimum inhibitory concentrations (MICs) against *E. coli* were determined initially, using the standard protocol of agar dilution and overnight incubation of the *E. coli* with each antibiotic. The MICs were 30 μg/mL for ampicillin, 0.025 μg/mL for ciprofloxacin, and 2 μg/mL for tetracycline. As to compensate for the much shorter incubation times used in most of our subsequent experiments combining antibiotics with electroporation, we performed these at MIC as well as at 3 × MIC, 10 × MIC, and 30 × MIC, with corresponding concentrations in μg/mL given in **Table 2**.

Of note, even the highest antibiotic concentrations used here (i.e., 30 × MIC, as determined in overnight *E. coli* cultures) were not bactericidal even after 24 h of incubation with each of the antibiotics. This was because while the growth of *E. coli* cells was inhibited throughout the incubation, after the transfer to rich growth medium they recovered (e.g., see **Figure 2E4**).

Inactivation With Antibiotics and Electroporation

The *E. coli* inactivation rates obtained in the absence of antibiotics and for each of the three antibiotics at the MIC, 3 × MIC, 10 × MIC, and 30 × MIC, combined with a single 1-ms electric pulse at amplitude of 0 (no pulse), 5, 10, 15, and 20 kV/cm, are presented in **Figure 2**, with the raw experimental data and further statistical analysis provided in the **Supplementary Material**.

Electroporation Treatment Alone

When the *E. coli* cells were treated with electroporation alone (**Figures 2A1–A4**), 5 kV/cm amplitude had only a minor and statistically non-significant effect on inactivation rate ($\lesssim$0.2 log) regardless of post-pulse incubation time, while as the amplitude was increased (to 10, 15, and 20 kV/cm), the inactivation rate gradually increased. This was expected, as empirically for most bacteria, a single 1-ms electric pulse with an amplitude of ∼5 kV/cm causes only mild and reversible electroporation, while amplitudes of 10, 15, and 20 kV/cm are roughly at the lower

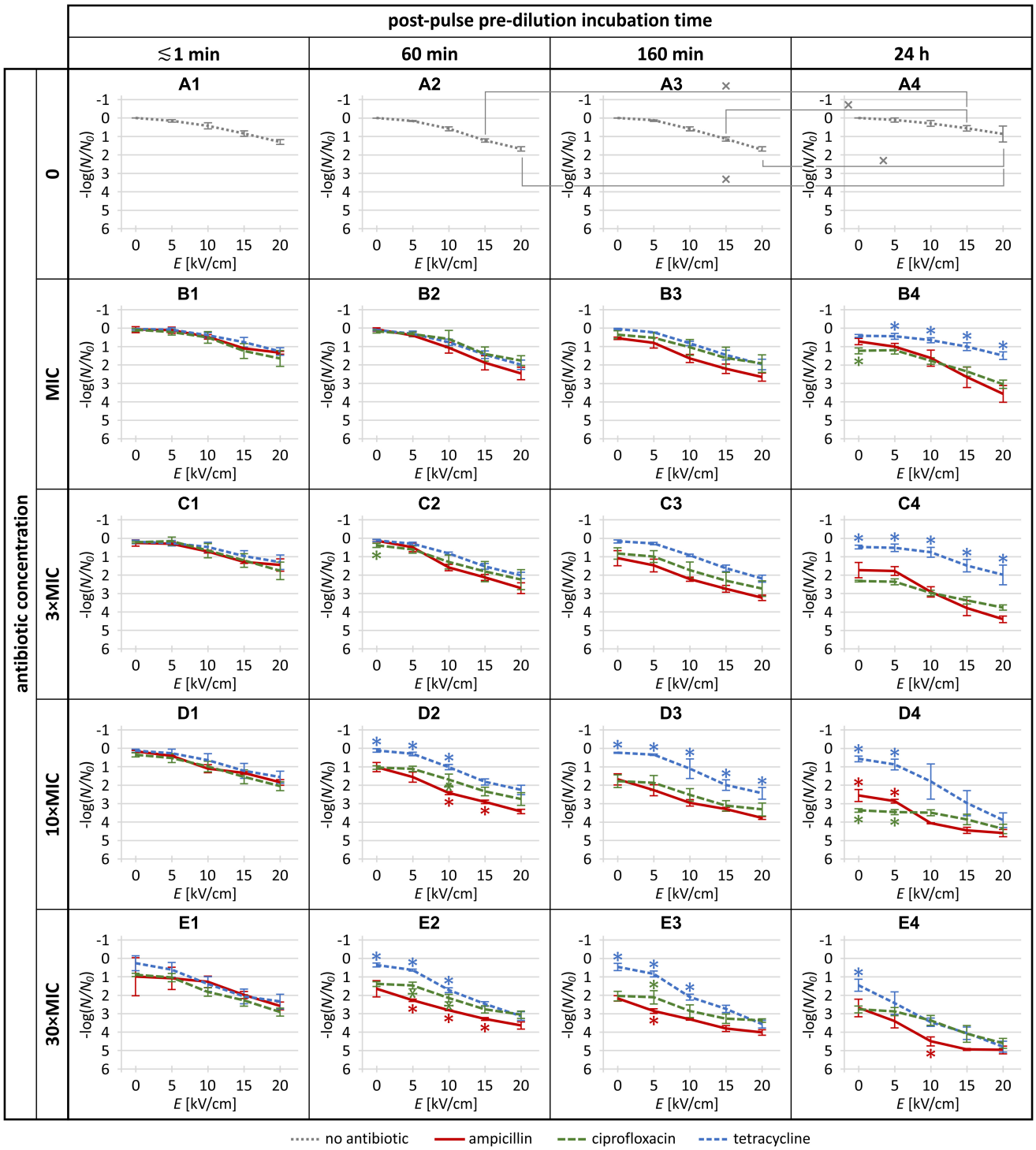

FIGURE 2 | The *Escherichia coli* inactivation rates in the absence of antibiotics (gray dotted) and for each of the three investigated antibiotics (red solid: ampicillin; green long-dashed: ciprofloxacin; blue short-dashed: tetracycline) at the MIC, 3 × MIC, 10 × MIC, and 30 × MIC, combined with a single 1-ms electric pulse at amplitude (*E*) of 0 (i.e., no pulse), 5, 10, 15, and 20 kV/cm. The plot labels **(A1–E4)** are provided to facilitate the referencing of individual plots in the body text. Each data point is represented as mean ± standard deviation of 3 replicates. In panels **(A1–A4)**, tilted crosses (×) mark pairs of data points where the inactivation rate achieved with the same pulse amplitude was statistically significantly different ($p < 0.05$) for different incubation times. In panels **(B1–E4)**, asterisks (*) mark data points where the inactivation rate was statistically significantly different ($p < 0.05$) for one antibiotic versus both others (red *: ampicillin vs. both ciprofloxacin and tetracycline; green *: ciprofloxacin vs. both ampicillin and tetracycline; blue *: tetracycline vs. both ampicillin and ciprofloxacin). Raw data and further statistical analysis are provided in the **Supplementary Material**.

TABLE 2 | Antibiotics and concentrations used in the experiment.

Antibiotic	Concentration (μg/mL)			
	MIC	3 × MIC	10 × MIC	30 × MIC
Ampicillin	30	90	300	900
Ciprofloxacin	0.025	0.075	0.25	0.75
Tetracycline	2.0	6.0	20	60

MIC, minimal inhibitory concentration.

end, middle, and higher end, respectively, of the range of non-thermal irreversible electroporation [e.g., see Figure 1A in Kotnik et al. (2015)]. More precisely, for each of the four post-pulse incubation times, the maximum inactivation rate was obtained at the maximum amplitude used, 20 kV/cm, reaching ∼1.3 log for the $\lesssim$1-min post-pulse incubation, ∼1.7 log for 60- and 160-min post-pulse incubations, and ∼0.9 log for 24-h post-pulse incubation. This relative recovery for the longest post-pulse incubation indicates that in the absence of antibiotics, the *E. coli* were gradually starting to grow and proliferate again.

We note here that in comparison to these bacterial inactivation rates obtained by electroporation alone, many studies report much higher rates, for two reasons. First, most studies have aimed for the maximum achievable effect, and have thus applied tens, hundreds, or even up to 1,000 consecutive pulses per treatment (see **Table 1**), while our aim was to investigate whether efficacy potentiation by electroporation for an antibiotic depends on the latter's mode of action; thus we used a single pulse to keep the analysis of the investigated dependence straightforward. Second, again to maximize the inactivation rates, some studies have applied pulse amplitudes of 30 or even 40 kV/cm, while here we used amplitudes up to 20 kV/cm, to assure that the contribution of electroporation was not entangled with those of electric arcing (with accompanying mechanical shockwaves and ultraviolet light) and thermal damage that can occur at higher pulse amplitudes.

Electroporation as an Efficacy Potentiator for Antibiotics

As stated previously, our main aim was to investigate whether efficacy potentiation by electroporation for an antibiotic depends on its mode of action. However, as outlined in the penultimate paragraph of the Introduction, from the perspective of limitations in practical applications, a post-pulse pre-dilution incubation time as long as 24 h is prohibitive from the aspect of the required reservoir volume, so we first tested whether this incubation time can perhaps be eliminated altogether, or at least shortened considerably. Thus, we initially considered whether reasonable potentiation can be achieved even with dilution performed right after the treatment (after $\lesssim$1 min incubation), and then we focused on the roles of (longer) post-pulse pre-dilution incubation time and of antibiotic concentrations.

Potentiation with dilution right after pulse delivery

With the antibiotic dilution right after the electroporation pulse treatment (i.e., $\lesssim$1 min incubation), no significant difference was seen between ampicillin, tetracycline, and ciprofloxacin (**Figures 2B1–E1**). With the lowest pulse amplitude (5 kV/cm), the increase in *E. coli* inactivation rate was small, particularly for the antibiotic concentrations up to 10 × MIC, and although at 30 × MIC (**Figure 2E1**) ampicillin and ciprofloxacin appeared more effective than tetracycline, the differences did not reach statistical significance. These data indicate that irrespective of their mode of action, efficacy of antibiotics is not significantly potentiated by electroporation when the antibiotic is diluted out within a minute or less after pulse delivery.

Potentiation with dilution after post-pulse incubation of 60 min, 160 min, and 24 h

When post-pulse pre-dilution incubation time was increased to 60 min, 160 min, and 24 h, relative to the $\lesssim$1 min incubation the potentiation also increased for each antibiotic. Specifically, three observed parametric dependences can be inferred.

First, the antibiotic potentiation consistently increased with the increase of pulse amplitude (i.e., in each of the panels of **Figure 2**, each of the curves has a downward slope).

Second, the antibiotic potentiation generally also increased with the increase of antibiotic concentrations at each of these three post-pulse incubation times (**Figures 2B2 ↘ C2 ↘ D2 ↘ E2**; **B3 ↘ C3 ↘ D3 ↘ E3**; **B4 ↘ C4 ↘ D4 ↘ E4**). A single exception here was for ciprofloxacin at 24-h post-pulse incubation for the 5 kV/cm pulse, with indication of lower *E. coli* inactivation for 30 × MIC compared to 10 × MIC, although this did not reach statistical significance (i.e., in **Figure 2**, the second data point of the green curve is higher in **E4** than in **D4**).

Third, the antibiotic potentiation generally also increased with the increase of the post-pulse incubation time at each of the four antibiotic concentrations (**Figures 2B2 ↘ B3 ↘ B4**; **C2 ↘ C3 ↘ C4**; **D2 ↘ D3 ↘ D4**; **E2 ↘ E3 ↘ E4**). Here the exception was tetracycline at MIC and 3 × MIC, with indications of lower *E. coli* inactivation for 24-h than for 60- or 160-min post-pulse incubations; however, again, none of these reached statistical significance (i.e., in **Figure 2**, the blue curve is partly higher in **B4** vs. **B2** and **B3**, and partly higher in **C4** vs. **C2** and **C3**).

As seen in **Figure 2**, in many data points the differences did not reach statistical significance, although we note, as elaborated in section "Statistical Analysis," that we only marked by an asterisk those data points for an antibiotic for which its *E. coli* inactivation rate differed statistically significantly from both other antibiotics. Despite this, there was a relatively clear general trend of superior inactivation rates for ampicillin compared to ciprofloxacin and tetracycline (i.e., in **Figure 2**, the red curves are rather consistently below the green and blue ones), particularly for the intermediate post-pulse incubation times of 60 and 160 min. On the opposite end, potentiation of *E. coli* inactivation rates was generally the weakest with tetracycline, although at the highest concentrations combined with the highest pulse amplitude this was less pronounced (**Figures 2D4,E2–E4**).

In quantitative terms, all the data presented in **Figure 2** for the combination of an antibiotic, electric pulse, and post-pulse incubation (60 min, 160 min, or 24 h), can be summarized into two aspects.

First, for all three incubation times, i.e., considering in **Figures 2B2–E4** on all the curves the 48 data points for pulse amplitudes from 5 to 20 kV/cm, for ampicillin 42 of these data points were superior to both ciprofloxacin and tetracycline, of which 7 reached statistical significance with respect to both.

Second, if we restrict this analysis to only the 60- and 160-min post-pulse incubations, of the 32 data points that thus remain on the relevant curves (**Figures 2B2–E3**), for ampicillin 31 of these data points were superior to both ciprofloxacin and tetracycline, of which 6 reached statistical significance with respect to both. The only exception here was for 3 × MIC with 5 kV/cm pulse and 60 min post-pulse incubation (**Figure 2C2**, second data point), where ampicillin appeared to be inferior to ciprofloxacin but still superior to tetracycline, although these apparent differences did not reach statistical significance.

DISCUSSION

Considering the different target sites of the three antibiotics, the rather consistently superior efficacy potentiation for ampicillin can be explained by its easier access to its particular target: the bacterial cell wall. Namely, ampicillin targets the sites of peptidoglycan chains cross-linkage by inhibiting the transpeptidase enzyme that catalyzes this cross-linkage, which destabilizes the local structure and the cell wall as a whole. Thus, for ampicillin to exhibit its antibacterial activity, permeation-enabling disruption of the inner (cytoplasmic) bacterial membrane is not required, in contrast to both ciprofloxacin and tetracycline that have intracellular targets (the sites of DNA replication and protein synthesis, respectively), for access to which they must permeate through all the layers of the bacterial envelope.

The data for dilution right after pulse delivery (i.e., $\lesssim$1 min incubation) imply, however, that even for ampicillin, substantial efficacy potentiation requires time, with *E. coli* inactivation rates improved by an order of magnitude when the dilution of the antibiotic was delayed by 60 or 160 min, while the 24-h delay resulted in more sporadic further improvements and mostly at the highest pulse amplitudes. This suggests that shortening the post-pulse incubation time with the antibiotic from 24 h (as used in many previous studies) to one or several hours is feasible, with proportionally reduced reservoir volume required in applications for wastewater treatment.

The small and sporadic further improvements in inactivation rates with the 24-h incubation are most likely due to the physiological uptake of the antibiotics, which would occur even without electroporation by gradual permeation through the intact bacterial envelope. This is reflected in the small but rather consistent improvement of the inactivation rates for all three antibiotics at 0 kV/cm (i.e., without electric pulse delivery) at 24-h incubation compared to 60- or 160-min incubation, which is detectable also for MIC and 3 × MIC, but is more evident for 10 × MIC and even more so for 30 × MIC. The role of physiological permeation on longer time scales is also consistent with the empirical fact that in medical and veterinary therapies with an antibiotic alone, its concentration must be maintained at a suprainhibitory level for days, and for some infections even for weeks to achieve an effective outcome (Wormser et al., 2004).

Regarding the generally weakest potentiation for tetracycline, we note that of the three antibiotics used in our study, tetracycline has the highest molecular weight (444 g/mol, vs. 331 and 349 g/mol for ciprofloxacin and ampicillin, respectively) and therefore likely requires stronger and/or more extensive electroporation for similarly potentiated permeation into bacteria. However, we stop short of postulating this as the main reason for the relatively inferior *E. coli* inactivation rates observed here for tetracycline compared to both ampicillin and ciprofloxacin.

Our finding that for a wall-targeting antibiotic, the efficacy against *E. coli* can be potentiated by electroporation to a greater extent – and/or more readily – compared to two antibiotics that target intracellular sites, is also in empirical agreement with findings from a recent study of Kuyukina et al. (2020). Although their study did not focus on the role of the antibiotic target site, for post-pulse incubation times up of to 240 min they found generally superior antibiotic potentiation by electroporation for benzylpenicillin and cefazolin (which also target cell wall synthesis) compared to gentamicin, kanamycin, and neomycin (which target protein synthesis). This is particularly relevant for the more general validity of the thesis that electroporation provides superior potentiation for antibiotics that target the cell wall compared to those with intracellular targets, as *E. coli* (used in the present study) is Gram-negative, while *Rhodococcus ruber* (used by Kuyukina and colleagues) is Gram-positive, and thus the structure of their envelope differs significantly.

However, there are still some obvious and possibly other unforeseen obstacles for the application of this finding in practice. Adding antibiotics is universally problematic in terms of the resulting environmental burden, and in many applications also from the resulting risks to human health. Conversely, the applications utilizing the inherently present antibiotics, such as treatment of wastewaters from hospitals and livestock farms, are dependent on the persistently fluctuating compositions and concentrations of antibiotics, which are also generally well below their MICs (Martinez, 2009; Diwan et al., 2013; Cheng et al., 2020). Thus, although the results presented here show that at the MIC and multiples thereof, a post-pulse incubation time of 1 or 2 h may be sufficient for substantial (∼3–4 log) inactivation rates, this may not be true for the antibiotic concentrations that occur inherently in such wastewaters.

For use in clinical or veterinary applications, and in general for combining antibiotics with electroporation against bacterial infections of eukaryotic organisms, a major and perhaps largely unsurmountable obstacle lies in the fact that most eukaryotic cells are an order of magnitude larger than bacteria. Since the transmembrane voltage induced by exposing a cell to an electric pulse of a fixed amplitude (electric field strength, that can be approximated by the voltage-to-distance ratio) is proportional to the cell size (Pauly and Schwan, 1959; Kotnik et al., 1998; Kotnik and Miklavčič, 2000), a significantly higher transmembrane

voltage is induced by the same pulse on eukaryotic cells than on bacteria. As the intensity of electroporation is strongly correlated to the induced transmembrane voltage (Kotnik et al., 2010), the application of electroporating pulses to a eukaryotic tissue infected with bacteria, or in general to a mix of eukaryotic cells and bacteria, will typically result in extensive damage to the eukaryotic tissue (through irreversible electroporation) before achieving electroporation of bacteria.

For use in food industry, the range of permissible antibacterials is limited to those that either occur naturally in foods or are approved as food additives, but if superior potentiation by electroporation for substances targeting the bacterial cell wall holds generally true for antibacterials, applications for food and beverage preservation can (re)focus on those among the permissible substances that target the wall. Currently, one such substance widely recognized as targeting the wall is nisin (Malanovic and Lohner, 2016; Modugno et al., 2018), and there is at least one report of its potentiation by electroporation, achieving moderate (∼2–3 log) inactivation rates against *E. coli* (Novickij et al., 2018b). However, at least one study found no potentiating effect of electroporation for nisin against either *E. coli* or *Salmonella typhimurium* (Saldaña et al., 2012), while the efficacy of nisin alone is largely limited to Gram-positive bacteria (Asaduzzaman and Sonomoto, 2009) and can only be extended to Gram-negative bacteria by artificially modifying the nisin molecule (Field et al., 2015; Zhou et al., 2016) or by binding nanocomposites to it (Vukomanović et al., 2017). There is thus ample motivation for systematic search and identification of antibacterials that are permissible in foods and target the cell wall of Gram-negative as well as Gram-positive bacteria, as this class of compounds should provide optimal candidates for broad and strong potentiation by electroporation applicable also in food and beverage preservation.

CONCLUSION

For the understanding of the dependence of the antibiotic efficacy potentiation by electroporation on the antibiotic's target site, our results presented above suggest that for antibiotics targeting the bacterial cell wall, this potentiation can be higher than for antibiotics with intracellular targets. For broader testing and a deeper understanding of this thesis, further studies are needed, performed with a broader range of antibiotics and on a broader range of bacteria, including comparisons for antibiotic-sensitive vs. antibiotic-resistant strains, and for bacteria in different growth stages. Identification of substances permissible in foods and targeting the cell wall of both Gram negative and Gram positive bacteria might provide candidate antibacterials for broad and strong potentiation by electroporation applicable also in food industry.

DATA AVAILABILITY STATEMENT

The original contributions presented in the study are included in the article/**Supplementary Material**, further inquiries can be directed to the corresponding author.

AUTHOR CONTRIBUTIONS

ŽL set up the experimental plan, conducted the experiments, processed, analyzed, interpreted the results, and wrote part of the manuscript. TK set up the concept of the experiments, supervised the work, interpreted the results, and wrote part of the manuscript. AK wrote part of the manuscript. All authors have reviewed and approved the final manuscript.

FUNDING

The authors acknowledge the financial support for this research from the Slovenian Research Agency (Javna Agencija za Raziskovalno Dejavnost – ARRS) within the Research Programme "Electroporation-Based Technologies and Treatments" (Grant No. P2-0249) and the Junior Researcher funding for ŽL (Grant No. MR-53516). The experiments were performed within the Infrastructure Programme "Network of research infrastructure centers at the University of Ljubljana (MRIC UL)" (Grant No. IP-0510).

ACKNOWLEDGMENTS

The authors would like to thank Saša Haberl Meglič for practical advice, and Duša Hodžić and Lea Vukanović for technical assistance.

SUPPLEMENTARY MATERIAL

The Supplementary Material for this article can be found online at: https://www.frontiersin.org/articles/10.3389/fmicb.2021.722232/full#supplementary-material

REFERENCES

Alexopoulos, A., Kimbaris, A. C., Plessas, S., Mantzourani, I., Voidarou, C., Pagonopoulou, O., et al. (2019). Combined action of piperitenone epoxide and antibiotics against clinical isolates of *Staphylococcus aureus* and *Escherichia coli*. *Front. Microbiol.* 10:2607. doi: 10.3389/fmicb.2019.02607

Andrews, J. M. (2001). Determination of minimum inhibitory concentrations. *J. Antimicrob. Chemother.* 48, 5–16. doi: 10.1093/jac/48.suppl_1.5

Asaduzzaman, S. M., and Sonomoto, K. (2009). Lantibiotics: diverse activities and unique modes of action. *J. Biosci. Bioeng.* 107, 475–487. doi: 10.1016/j.jbiosc.2009.01.003

Aune, T. E. V., and Aachmann, F. L. (2010). Methodologies to increase the transformation efficiencies and the range of bacteria that can be transformed. *Appl. Microbiol. Biotechnol.* 85, 1301–1313. doi: 10.1007/s00253-009-2349-1

Berdejo, D., Pagán, E., García-Gonzalo, D., and Pagán, R. (2019). Exploiting the synergism among physical and chemical processes for improving

food safety. *Curr. Opin. Food Sci.* 30, 14–20. doi: 10.1016/j.cofs.2018.08.004

Cheng, D., Ngo, H. H., Guo, W., Chang, S. W., Nguyen, D. D., Liu, Y., et al. (2020). A critical review on antibiotics and hormones in swine wastewater: water pollution problems and control approaches. *J. Hazard. Mater.* 387:121682. doi: 10.1016/j.jhazmat.2019.121682

Chopra, I., and Roberts, M. (2001). Tetracycline antibiotics: mode of action, applications, molecular biology, and epidemiology of bacterial resistance. *Microbiol. Mol. Biol. Rev.* 65, 232–260. doi: 10.1128/MMBR.65.2.232-260.2001

Diwan, V., Stålsby Lundborg, C., and Tamhankar, A. J. (2013). Seasonal and temporal variation in release of antibiotics in hospital wastewater: estimation using continuous and grab sampling. *PLoS One* 8:e68715. doi: 10.1371/journal.pone.0068715

Douafer, H., Andrieu, V., Phanstiel, O., and Brunel, J. M. (2019). Antibiotic adjuvants: make antibiotics great again! *J. Med. Chem.* 62, 8665–8681. doi: 10.1021/acs.jmedchem.8b01781

Eleršek, T., Flisar, K., Likozar, B., Klemenčič, M., Golob, J., Kotnik, T., et al. (2020). Electroporation as a solvent-free green technique for non-destructive extraction of proteins and lipids from *Chlorella vulgaris*. *Front. Bioeng. Biotechnol.* 8:443. doi: 10.3389/fbioe.2020.00443

Emmanuel, E., Keck, G., Blanchard, J. M., Vermande, P., and Perrodin, Y. (2004). Toxicological effects of disinfections using sodium hypochlorite on aquatic organisms and its contribution to AOX formation in hospital wastewater. *Environ. Int.* 30, 891–900. doi: 10.1016/j.envint.2004.02.004

Field, D., Cotter, P. D., Hill, C., and Ross, R. P. (2015). Bioengineering lantibiotics for therapeutic success. *Front. Microbiol.* 6:1363. doi: 10.3389/fmicb.2015.01363

Frieri, M., Kumar, K., and Boutin, A. (2017). Antibiotic resistance. *J. Infect. Public Health* 10, 369–378. doi: 10.1016/j.jiph.2016.08.007

Garner, A. L. (2019). Pulsed electric field inactivation of microorganisms: from fundamental biophysics to synergistic treatments. *Appl. Microbiol. Biotechnol.* 103, 7917–7929. doi: 10.1007/s00253-019-10067-y

Gusbeth, C., Frey, W., Volkmann, H., Schwartz, T., and Bluhm, H. (2009). Pulsed electric field treatment for bacteria reduction and its impact on hospital wastewater. *Chemosphere* 75, 228–233. doi: 10.1016/j.chemosphere.2008.11.066

Hocquet, D., Muller, A., and Bertrand, X. (2016). What happens in hospitals does not stay in hospitals: antibiotic-resistant bacteria in hospital wastewater systems. *J. Hosp. Infect.* 93, 395–402. doi: 10.1016/j.jhin.2016.01.010

Juma, A., Lemoine, P., Simpson, A. B. J., Murray, J., O'Hagan, B. M. G., Naughton, P. J., et al. (2020). Microscopic investigation of the combined use of antibiotics and biosurfactants on methicillin resistant *Staphylococcus aureus*. *Front. Microbiol.* 11:1477. doi: 10.3389/fmicb.2020.01477

Kim, J.-P., Jin, D. R., Lee, W., Chae, M., and Park, J. (2020). Occurrence and removal of veterinary antibiotics in livestock wastewater treatment plants, South Korea. *Processes* 8:720. doi: 10.3390/pr8060720

Klein, E. Y., Tseng, K. K., Pant, S., and Laxminarayan, R. (2019). Tracking global trends in the effectiveness of antibiotic therapy using the Drug Resistance Index. *BMJ Glob. Health* 4:e001315. doi: 10.1136/bmjgh-2018-001315

Korem, M., Goldberg, N. S., Cahan, A., Cohen, M. J., Nissenbaum, I., and Moses, A. E. (2018). Clinically applicable irreversible electroporation for eradication of micro-organisms. *Lett. Appl. Microbiol.* 67, 15–21. doi: 10.1111/lam.12996

Kotnik, T., Frey, W., Sack, M., Haberl Meglič, S., Peterka, M., and Miklavčič, D. (2015). Electroporation-based applications in biotechnology. *Trends Biotechnol.* 33, 480–488. doi: 10.1016/j.tibtech.2015.06.002

Kotnik, T., and Miklavčič, D. (2000). Analytical description of transmembrane voltage induced by electric fields on spheroidal cells. *Biophys. J.* 79, 670–679. doi: 10.1016/S0006-3495(00)76325-9

Kotnik, T., Miklavčič, D., and Slivnik, T. (1998). Time course of transmembrane voltage induced by time-varying electric fields – a method for theoretical analysis and its application. *Bioelectrochem. Bioenerg.* 45, 3–16. doi: 10.1016/S0302-4598(97)00093-7

Kotnik, T., Pucihar, G., and Miklavčič, D. (2010). Induced transmembrane voltage and its correlation with electroporation-mediated molecular transport. *J. Membr. Biol.* 236, 3–13. doi: 10.1007/s00232-010-9279-9

Kotnik, T., Rems, L., Tarek, M., and Miklavčič, D. (2019). Membrane electroporation and electropermeabilization: mechanisms and models. *Annu. Rev. Biophys.* 48, 63–91. doi: 10.1146/annurev-biophys-052118-115451

Kuyukina, M. S., Varushkina, A. M., and Ivshina, I. B. (2020). Effects of electroporation on antibiotic susceptibility and adhesive activity to n-hexadecane in *Rhodococcus ruber* IEGM 231. *Appl. Biochem. Microbiol.* 56, 729–735. doi: 10.1134/S0003683820060083

Laxminarayan, R., Duse, A., Wattal, C., Zaidi, A. K. M., Wertheim, H. F. L., Sumpradit, N., et al. (2013). Antibiotic resistance-the need for global solutions. *Lancet Infect. Dis.* 13, 1057–1098. doi: 10.1016/S1473-3099(13)70318-9

Leng, L., Wei, L., Xiong, Q., Xu, S., Li, W., Lv, S., et al. (2020). Use of microalgae based technology for the removal of antibiotics from wastewater: a review. *Chemosphere* 238:124680. doi: 10.1016/j.chemosphere.2019.124680

Madurga, S., Sánchez-Céspedes, J., Belda, I., Vila, J., and Giralt, E. (2008). Mechanism of binding of fluoroquinolones to the quinolone resistance-determining region of DNA gyrase: towards an understanding of the molecular basis of quinolone resistance. *ChemBioChem* 9, 2081–2086. doi: 10.1002/cbic.200800041

Malanovic, N., and Lohner, K. (2016). Gram-positive bacterial cell envelopes: the impact on the activity of antimicrobial peptides. *Biochim. Biophys. Acta Biomembr.* 1858, 936–946. doi: 10.1016/j.bbamem.2015.11.004

Martens, S. L., Klein, S., Barnes, R. A., TrejoSanchez, P., Roth, C. C., and Ibey, B. L. (2020). 600-ns pulsed electric fields affect inactivation and antibiotic susceptibilities of *Escherichia coli* and *Lactobacillus acidophilus*. *AMB Express* 10:55. doi: 10.1186/s13568-020-00991-y

Martín-Belloso, O., and Sobrino-López, A. (2011). Combination of pulsed electric fields with other preservation techniques. *Food Bioprocess Technol.* 4, 954–968. doi: 10.1007/s11947-011-0512-z

Martinez, J. L. (2009). Environmental pollution by antibiotics and by antibiotic resistance determinants. *Environ. Pollut.* 157, 2893–2902. doi: 10.1016/j.envpol.2009.05.051

Modugno, C., Loupiac, C., Bernard, A., Jossier, A., Neiers, F., Perrier-Cornet, J. M., et al. (2018). Effect of high pressure on the antimicrobial activity and secondary structure of the bacteriocin nisin. *Innov. Food Sci. Emerg. Technol.* 47, 9–15. doi: 10.1016/j.ifset.2018.01.006

Novickij, V., Švedienė, J., Paškevičius, A., Markovskaja, S., Lastauskienė, E., Zinkevičienė, A., et al. (2018a). Induction of different sensitization patterns of MRSA to antibiotics using electroporation. *Molecules* 23:1799. doi: 10.3390/molecules23071799

Novickij, V., Zinkevičienė, A., Stanevičienė, R., Gruškienė, R., Servienė, E., Vepštaitė-Monstavičė, I., et al. (2018b). Inactivation of *Escherichia coli* using nanosecond electric fields and nisin nanoparticles: a kinetics study. *Front. Microbiol.* 9:3006. doi: 10.3389/fmicb.2018.03006

Paulus, G. K., Hornstra, L. M., Alygizakis, N., Slobodnik, J., Thomaidis, N., and Medema, G. (2019). The impact of on-site hospital wastewater treatment on the downstream communal wastewater system in terms of antibiotics and antibiotic resistance genes. *Int. J. Hyg. Environ. Health* 222, 635–644. doi: 10.1016/j.ijheh.2019.01.004

Pauly, H., and Schwan, H. P. (1959). Über die Impedanz einer Suspension von kugelförmigen Teilchen mit einer Schale. *Z. Naturforsch. B* 14b, 125–131.

Rizzo, L., Manaia, C., Merlin, C., Schwartz, T., Dagot, C., Ploy, M. C., et al. (2013). Urban wastewater treatment plants as hotspots for antibiotic resistant bacteria and genes spread into the environment: a review. *Sci. Total Environ.* 447, 345–360. doi: 10.1016/j.scitotenv.2013.01.032

Rubin, A. E., Usta, O. B., Schloss, R., Yarmush, M., and Golberg, A. (2019). Selective inactivation of *Pseudomonas aeruginosa* and *Staphylococcus epidermidis* with pulsed electric fields and antibiotics. *Adv. Wound Care* 8, 136–148. doi: 10.1089/wound.2018.0819

Saldaña, G., Monfort, S., Condón, S., Raso, J., and Álvarez, I. (2012). Effect of temperature, pH and presence of nisin on inactivation of *Salmonella Typhimurium* and *Escherichia coli* O157:H7 by pulsed electric fields. *Food Res. Int.* 45, 1080–1086. doi: 10.1016/j.foodres.2011.03.059

Vadlamani, A., Detwiler, D. A., Dhanabal, A., and Garner, A. L. (2018). Synergistic bacterial inactivation by combining antibiotics with nanosecond electric pulses. *Appl. Microbiol. Biotechnol.* 102, 7589–7596. doi: 10.1007/s00253-018-9215-y

Vadlamani, R. A., Dhanabal, A., Detwiler, D. A., Pal, R., McCarthy, J., Seleem, M. N., et al. (2020). Nanosecond electric pulses rapidly enhance the inactivation of Gram-negative bacteria using Gram-positive antibiotics. *Appl. Microbiol. Biotechnol.* 104, 2217–2227. doi: 10.1007/s00253-020-10365-w

Vukomanović, M., Žunič, V., Kunej, Š, Jančar, B., Jeverica, S., Podlipec, R., et al. (2017). Nano-engineering the antimicrobial spectrum of lantibiotics: activity of nisin against Gram negative bacteria. *Sci. Rep.* 7:4324. doi: 10.1038/s41598-017-04670-0

Wormser, G. P., Nadelman, R. B., Dattwyler, R. J., Dennis, D. T., Shapiro, E. D., Steere, A. C., et al. (2004). Practice guidelines for the treatment of Lyme disease. *Clin. Infect. Dis.* 31, S1–S14. doi: 10.1086/314053

Wright, A. J. (1999). The penicillins. *Mayo Clin. Proc.* 74, 290–307. doi: 10.4065/74.3.290

Zhou, L., van Heel, A. J., Montalban-Lopez, M., and Kuipers, O. P. (2016). Potentiating the activity of nisin against *Escherichia coli*. *Front. Cell Dev. Biol.* 4:7. doi: 10.3389/fcell.2016.00007

Conflict of Interest: The authors declare that the research was conducted in the absence of any commercial or financial relationships that could be construed as a potential conflict of interest.

frontiers in Microbiology

METHODS
published: 04 November 2021
doi: 10.3389/fmicb.2021.725499

An Accurate Method for Studying Individual Microbial Lag: Experiments and Computations

Simen Akkermans[1,2,3] *and Jan F. M. Van Impe*[1,2,3]*

[1] BioTeC, Chemical and Biochemical Process Technology and Control, Department of Chemical Engineering, KU Leuven, Ghent, Belgium, [2] Optimization in Engineering Center-of-Excellence (OPTEC), KU Leuven, Leuven, Belgium, [3] Flemish Cluster Predictive Microbiology in Foods (CPMF2), Ghent, Belgium

OPEN ACCESS

Edited by:
Peter Adrian Lund,
University of Birmingham,
United Kingdom

Reviewed by:
Xiaomei SU,
Zhejiang Normal University, China
Lihan Huang,
Agricultural Research Service,
United States Department
of Agriculture (USDA), United States
Laurent Guillier,
Agence Nationale de Sécurité
Sanitaire de l'Alimentation,
de l'Environnement et du Travail
(ANSES), France

***Correspondence:**
Jan F. M. Van Impe
jan.vanimpe@kuleuven.be

Specialty section:
This article was submitted to
Food Microbiology,
a section of the journal
Frontiers in Microbiology

Received: 15 June 2021
Accepted: 15 October 2021
Published: 04 November 2021

Citation:
Akkermans S and Van Impe JFM
(2021) An Accurate Method
for Studying Individual Microbial Lag:
Experiments and Computations.
Front. Microbiol. 12:725499.
doi: 10.3389/fmicb.2021.725499

Variability in the behavior of microbial foodborne pathogens and spoilers causes difficulties in predicting the safety and quality of food products during their shelf life. Therefore, the quantification of the individual microbial lag phase distribution is of high relevance to the field of quantitative microbial risk assessment. To construct models that predict the effect of changes in environmental conditions on the individual lag, an accurate determination of these distributions is required. Therefore, the current research focuses on the development of an experimental and computational method for accurate determination of individual lag phase distribution. The experimental method is unique in the sense that full liquid volumes are sampled without using dilutions to detect the final population, thereby minimizing experimental errors. Moreover, the method does not aim at the isolation of single cells but at a low number of cells. The fact that several cells can be present in the initial samples instead of having a single cell is considered by the computational method. This method relies on Monte Carlo simulation to predict the individual lag phase distribution for a given set of distribution parameters and maximum likelihood estimation to find the parameters that describe the experimental data best. The method was validated both through simulation and experiments and was found to deliver a desired accuracy.

Keywords: individual lag, method development, maximum likelihood estimation, Monte Carlo simulation, *Escherichia coli*

INTRODUCTION

Microbial risks associated with the consumption of food products are studied using quantitative microbial risk assessments. These risk assessments rely on mathematical models from the field of predictive microbiology to simulate microbial behavior. The risk that undesired events will take place is calculate by including different source of variation in these model predictions through techniques such as Monte Carlo simulation. The variation comes from several different sources, e.g., experimental uncertainty and variability in processing conditions. Another important source of variability comes from the microorganism, which includes the variability in the lag phase duration

(Lianou and Koutsoumanis, 2013). The lag phase duration and variability in a microbial population is a result of the lag phase duration and variability of its individuals. Therefore, the characterization of the variability in the individual lag phase duration under various environmental stresses is of high importance for improving microbial food safety and quality (Guillier et al., 2005). Future research could aim to construct mathematical models that describe the effect of changes in environmental conditions on the individual lag phase distribution. Therefore, accurate approximations of these distributions are required. The current research deals with the development and validation of an experimental and computational method for the accurate determination of the individual lag phase distribution.

Studying process variability requires a large amount of experimental data. Therefore, researchers often turn to high-throughput methods, such as optical density (OD) measurements, for studying microbial variability (Francois et al., 2005; D'Arrigo et al., 2006; Dupont and Augustin, 2009; Stringer et al., 2011; Aguirre et al., 2013; Xu et al., 2015). However, this technique comes with some limitations. First, the detection limit is high, at about 10^6–10^7 CFU/mL for bacterial cells (Baka et al., 2014). This means that measurements are taken close to the stationary phase and require a long period of growth when starting from low inoculum sizes. Secondly, the relationship between the OD and the true number of viable cells is influenced by the environmental conditions that the cells are subjected to. As such, using calibration curves between these measures reduces the method's accuracy (Métris et al., 2006). Finally, there are several common practical issues when working with the microplates that are needed for these studies. They often suffer from problems with respect to evaporation of the liquid from the plate and condensation on the lid of the plates (Brewster, 2003; Walzl et al., 2012). Other high throughput methods are available, such as the analysis of time laps microscopy imaging or the ScanLag system (Pin and Baranyi, 2006; Levin-Reisman et al., 2010). However, these methods are not frequently used since they require equipment that is too expensive or not available for many labs.

Based on the downsides and difficulties with respect to OD methods, the first criterion was that the new method should work with viable plate counts. Plate count methods deliver a great accuracy by using a direct measurement of the number of living microorganisms in a sample. The downside of this technique is the high experimental load. Moreover, when considering the inoculation methods that are commonly used to isolate individual cells, the yield of experimental data over the total number of samples is relatively low. This is because most samples either contain no cells at all or have to be discarded for likely containing too many cells. The first goal will be therefore to select the most suitable inoculation method out of two conventional methods.

Two methods are commonly applied to isolate single cells. In the first method, an inoculum is serially diluted in a microplate such that the chance of achieving single cells in the last columns is maximized (Francois et al., 2003). In the other method, a solution is diluted to such a low concentration that, when distributed over a microplate, the chance of isolating single cells is maximized (Robinson et al., 2001). Both methods have a few things in common. It is inevitable that some of the samples may contain more than 1 cell. However, the computational methods that are typically used to process the data from these experiments assume that there is only a single cell in each sample that contains cells. Therefore, to increase the chance of obtaining single cells as opposed to multiple cells, the inoculum concentration should be low. A low inoculum concentration will also increase the chance of having no cells at all and therefore decreases the yield of experimental data. As such, a trade of exists between the quantity of experimental data and the quality of that data (quality being a high likelihood of having a single cell in the samples containing cells). Therefore, a computational method is required that considers the initial distribution of the population size in the calculation of the distribution of the individual cell lag. Baranyi et al. (2009) published a methodology that takes the initial concentration into account based on the method of moments. However, this method does not allow to determine the accuracy of the estimation results. In contrast, maximum likelihood estimation allows the calculation of confidence bounds on distribution parameters, which is of high importance in a modeling context. The second goal is therefore the development of a suitable computational method and comparison with the existing moments-based method.

The overall goal of this work is the development of an experimental and computational method that allows the accurate determination of the distribution of the individual cell lag. The experimental method will be designed in such a way that experimental errors are decreased to an absolute minimum by analyzing the total cell content of samples without dilutions. The computational method will be developed so that there is no longer a need to aim for single cell isolation in the experimental method, but rather to include the initial cell distribution in an accurate description of the uncertainty propagation.

MATERIALS AND METHODS

Bacterial Strain

Escherichia coli K12 MG1655 (CGSC#6300) was acquired from the *E. coli* Genetic Stock Center at Yale University. A stock culture was stored at −80°C in Brain Hearth Infusion broth (BHI, Oxoid, Hampshire, United Kingdom), supplemented with 20 % (w/v) glycerol (Acros Organics, Geel, Belgium). This strain was used for all microbiological experiments in this study.

Inoculum Preparation

The inoculum was prepared in a three step procedure: (i) A loop (10 μL) of the stock culture was spread onto a BHI agar plate, (BHIA, containing 14 g/L technical agar, VWR, Radnor, PA, United States) and incubated overnight at 37°C. (ii) Then, a single colony was transferred to a 50 mL Erlenmeyer containing 20 mL BHI broth and stored at 37°C for 9 h. (iii) Finally, 20 μL of the stationary phase culture was inoculated in 20 mL of fresh BHI broth and incubated at 37°C for 17 h.

Detection Limit

The detection limit of the optical density (OD) measurement was defined as three time the standard deviation on the mean of a repeated measurement. The OD was measured at 595 nm using a FilterMax F5 microplate reader (Molecular Devices). The OD of a 1/8 dilution of the second preculture, was measured 24 times at a volume of 150 μL per well.

Calibration Curve

The method used to obtain the calibration curve was based on Francois et al. (2003). All wells of a 96-well microplate were filled with 150 μL of BHI broth, except for the first column. The first and last well of the first column were filled with 300 μL of BHI solution. These will cause the first and last row to serve as blanks. The remaining 6 wells of the first column were filled 300 μL of the second preculture, after mixing it thoroughly. A 1:2 dilution series was made by transferring 150 μL from all wells of the first column to all wells of the second column. This process is repeated 10 times until 150 μL is taken from the last column and discarded. After measuring the OD, one sample of each dilution was decimally diluted and plated on BHIA plates for enumeration. BHIA plates were incubated overnight at 37°C. This entire process was performed in duplicate. A linear regression was applied to the natural logarithm of the cell density vs. the natural logarithm of the OD, yielding the following equation:

$$\mathbf{ln\,(N)} \;=\; \mathbf{a} + \mathbf{b} \cdot \mathbf{ln(OD)} \tag{1}$$

with N [CFU/mL] the cell density, OD [−] the OD and a and b the linear regression parameters. Given the low variance on the measurements of OD compared to viable plate counts, the former variance was considered negligible and the parameters *a* and *b* were estimated using a simple least squares regression. More details on the regression and calculation of uncertainty on the parameters and predictions is provided in section "Parameter Estimations."

Serial Dilution Inoculation Method

This method is based on the work of Francois et al. (2003) and aims at obtaining single cells in the last four or five rows of a microplate after serial dilutions. The concentration of the preculture was measured at 595 nm using six 150 μL samples of a 1:10 dilution of the preculture in BHI broth, using a FilterMax F5 microplate reader. The OD of the cells in these samples was calculated by subtracting the OD of six 150 μL samples of pure BHI solution. The concentration of viable cells (CFU/mL) was calculated using the calibration curve that is described in section "Calibration Curve." Based on this calculated cell density, the preculture was further diluted to obtain 100 CFU per well containing 150 μL. Therefore, the preculture was first serially decimal diluted in BHI broth and a final dilution was made by transferring the appropriate volume of diluted preculture to 8 mL of BHI broth in a 15 mL centrifuge tube. The diluted culture (300 μL) was transferred from the Falcon tube to each well of the first row of a microplate. The remaining wells were filled with 150 μL of BHI broth each. Using a multichannel pipette, 150 μL was transferred from each well of the first to the second row of the microplate and mixed. This process was repeated for the remaining rows and 150 μL was discarded from each well of the last row. This process resulted in a 1:2 dilution series throughout the rows of the microplate with the following expected number of cells per well: 100.00, 50.00, 25.00, 12.50, 6.25, 3.13, 1.56, 0.78, 0.39, 0.20, 0.10, and 0.10 CFU.

Low Cell Density Inoculation Method

An alternative method for the inoculation of single cells in a microplate was based on the inoculation of the entire plate with the same concentration of diluted preculture. The concentration is typically chosen below one CFU per well to have a high likelihood of obtaining single cells in those wells that contain cells. To initiate this method, the cell density of the preculture was measured and calculated in the same way as described in section "Serial Dilution Inoculation Method." Then, the appropriate volume to achieve the desired final concentration was transferred from a serial decimal dilution of the preculture to 40 mL of BHI broth in a 50 mL centrifuge tube. Using a multichannel pipette, 150 μL of this solution was placed in every well of a microplate.

Experimental Study of the Population Variability

Starting from streak plates, three sets of preculture Erlenmeyer's were prepared the day before the experiments were inoculated. When diluting the preculture into the final concentration, cells were transferred in BHI broth containing 56 g/L NaCl to induce a lag phase. Three sets of 96-well plates were inoculated in the morning at different intended population sizes: (i) 4 96-well plates at 0.48 CFU/well, (ii) 4 96-well plates at 4.80 CFU/well and (iii) 2 96-well plates at 48.00 CFU/well. The method used for inoculation was the low cell density method explained in section "Low Cell Density Inoculation Method" and all wells were inoculated with a volume of 150 μL. The time of inoculation of each plate was noted down. After inoculation, all plates were sealed with a polyester microplate sealing film before closing the lid. The decimal dilution series that was used to inoculate the BHI and salt broth was also used to plate 9 drops of 20 μL of the 6th decimal dilution of the preculture for the calculation of the concentration of cells in the BHI and salt broth. The first two sets of plates were incubated overnight at 25°C. Then, all samples were transferred entirely to individual BHI agar plates that had been left to dry at atmospheric conditions for several days to allow fast absorption of the liquid and fixation of the individual cells on the agar surface. Before transferring the samples to the agar plates, they were pipetted up and down several times to make sure all cells were in suspension. The time of sampling was noted down for each sample. These plates were incubated overnight at 37°C. The number of colonies on these plates represented exactly the number of cells in the population that had developed from the low initial number of cells. The third set of plates was used to quantify the exponential growth rate of the population under identical conditions as those used for the low inoculum levels. After inoculation, three entire samples were taken and plated at three time points to be able to quantify the initial population density. During the following days, 50 μL samples were taken,

diluted and plated every hour in triplicate during working hours. As such, the full growth curve from lag until stationary phase was included in the data.

Two- and Three-Phase Linear Model

To determine the lag phase duration and maximum specific growth rate of experimental or simulation data, the following simple three-phase linear model was used:

$$\ln(N(t)) = N_0 + \mu \cdot (t-\lambda) \cdot 1(t-\lambda) - \mu \cdot (t-t_{max}) \cdot 1(t-t_{max}) \quad (2)$$

In this equation N is the number of cells at time t, N_0 is the initial number of cells, is the exponential growth rate, is the lag phase duration of the population and t_{max} is the time at which the maximum population density is obtained. The function $1(\cdot)$ represents the unit step function, which is 0 for all arguments smaller than 0 and 1 for all arguments greater or equal than 0. If no stationary phase behavior was included in the data, the last term of this equation was omitted. This will be referred to as the two-phase linear model. This equation was based on the work of Buchanan et al. (1997), (McKellar and Lu, 2004).

Monte Carlo Simulations

Monte Carlo simulation was used in this research. Data were generated with the function *random* of MATLAB 9.7 (MathWorks), according to the appropriate distribution. The number of iterations varied depending on the desired accuracy or the experimental system that was described by the simulation. The number of iterations when describing inoculations according to the Poisson [*Pois*(*cell concentration* · *sample volume*)] distribution is expressed as the number of 96-well plates, in equivalence with the experimental methods represented by these simulations.

Parameter Estimations

Parameter estimations were carried out based on least squares regressions using the *lsqnonlin* routine of the optimization toolbox of MATLAB 9.7. Probability density functions were fitted to data using the *fitdist* function of the same software. The method for calculating the uncertainty on the model parameters and output with the linear approximation is described in Akkermans et al. (2018).

RESULTS AND DISCUSSION

The current research aims to determine the parameters of the probability distribution of the individual cell lag, based on the measurement of the population density after a certain period of growth. Specifically, the method should deliver a high accuracy while requiring a reasonable experimental effort and being applicable in most microbiological labs. Based on the explanation in the introduction, it was decided that a sample inoculation method had to be selected that provides a high yield of experimental data. Computational and experimental comparison of two inoculation methods is presented in section "Comparison of Conventional Inoculation Methods." Section "Detection Limit and Calibration Curve" will first present the results of the determination of the detection limit and calibration curve, which are essential for each of the inoculation methods. The computational method to process the experimental data requires a mathematical model that describes the stochastic process of cell division in the lag and exponential phases of growth. Therefore, section "Probabilistic Individual-Based Model" starts with presenting an individual-based model that considers the life cycle of each individual cell to predict the population growth. This model is simplified until a population-based model with much lower computational load is obtained in section "Probabilistic Population-Level Model." The parameters of the individual lag phase distribution that minimize the difference between the simulated and experimental distributions of the population size are then selected. This requires that the type of distribution of the population size is known. Therefore, several types of probability distributions will be compared in section "Population Size Distribution" to select the most suitable one. Section "Proposed Experimental and Computational Method" presents an overview of the complete experimental and computational method that is proposed. This method is validated based on simulations in section "Simulation Validation" and on experiments in section "Experimental Validation."

Detection Limit and Calibration Curve

Any method relying on the use of OD measurements should start with the determination of the measurement's detection limit and making a calibration between the measured OD values and the underlying quantity of colony forming units. Based on the method explained in section "Detection Limit," the standard deviation of the measurement was calculated to be 1.55×10^{-3} OD units. This corresponds with a detection limit of 4.65×10^{-3} OD units above the measurement blank. This detection limit includes pipetting errors because the standard deviation was determined based on replicates that were independently pipetted.

Only the seven most concentrated samples of the calibration curve had OD values above this detection limit. The remaining samples were therefore discarded from the calibration curve. The parameters *a* and *b* of the calibration curve were estimated to be 22.55 ln(CFU/mL) and 1.07 ln(CFU/mL)/ln(OD). The 95 % confidence bounds of these parameters were [22.38; 22.72] and [1.02; 1.12]. The mean squared error of the regression was just 0.01 $\ln(CFU/mL)^2$, demonstrating a good quality of fit. Based on this calibration curve, the detection limit of 4.65×10^{-3} OD units corresponds with 1.98×10^7 CFU/mL. This reflects the high cell density level that is required for applying OD measurements. In comparison, the detection limit for viable plate counts is generally between 10^2 and 10^3 CFU/mL.

Comparison of Conventional Inoculation Methods

This section deals with the selection of an experimental method that is suitable for high throughput data collection. This method is needed because the study of the variation of the lag phase (or any other process) requires large amounts of data. As such,

experimental protocol for this method needs to be selected in such a way that the quantity of useful data is maximized. In both inoculation methods, there is no guarantee of obtaining single cells in the different samples (wells of the microplate). However, the idea is to maximize the chance that single cells are obtained. The amount of useful data can be quantified by evaluating (i) the number of wells that contain cells compared to the total amount of wells and (ii) the number of wells containing exactly a single cell compared to the total number of wells containing cells.

The experimental methods that are reported, respectively, in section "Serial Dilution Inoculation Method" and section "Low Cell Density Inoculation Method" were first implemented in two sets of Monte Carlo simulation. The first set of simulation only used the Poisson distribution to determine the random number of cells that is transferred in each pipetting step. For each experimental protocol, 10^5 iterations were run in which a 96-well microplate was inoculated with a Poisson distributed number of cells per well. In these first simulations, the number of cells in the first column was fixed to 100 for the serial dilution method. When evaluating the number of cells in the last five rows, 10.86 % of the total number of wells were found to contain cells and 77.93 % of those contained a single cell. (**Table 1 part A**). This latest measure was taken as a benchmark to determine the concentration of the diluted preculture for the low concentration inoculation method. As such, it was found that at a concentration of 0.48 CFU/well, the same fraction of wells with cells contained a single cell. On the other hand, from the total number of wells, almost four times as many contained cells (38.13 %). As such, the low concentration inoculation method delivers a much higher quantity of useful data for the same number of microplates and a slightly lower workload (as the serial dilutions require more effort).

To further evaluate the difference between these methods, a second set of Monte Carlo simulation was performed. In this set of simulation, the variability that was due to the error related to the calibration curve and the pipetting errors was included as well. For these calculations, the number of cells in the first row of the microplate was no longer fixed to 200 CFU in 300 μL (of which on average half are transferred to the following wells). Instead, the model prediction error on the calibration curve was used to determine the probability distribution of the number of cells in the 1:10 diluted preculture (see calculation in section "Parameter Estimations"). Moreover, for all dilution steps, the pipetting errors were considered as well. According to the manufacturer specifications the pipetted volumes were assigned normal distributions with relative standard deviations of, respectively, 0.20, 0.25, 0.25 and 0.50 % for a single channel 200 μL pipette, a multichannel 200 μL pipette, a single channel 1,000 μL pipette and a single channel 5,000 μL pipette. As in the previous simulations, the quantity of cells in the pipetted samples followed the Poisson distribution. The resulting evaluation of the two inoculation methods is presented in **Table 1 part B**. These results are similar to the Monte Carlo simulation that only considered the variance due to the cell distribution over pipetted volumes. The low inoculation method is more susceptible to the effect of pipetting errors and the error on the calibration curve than the serial dilution method. This is probably because the former method relies more on the accuracy of the obtained calibration curve to perform the inoculation of the microplate at the correct cell concentration. On the other hand, the low inoculation method will always yield more wells containing cells and will have less variability on the percentage of wells that contains a single cell. As such, when considering all significant stochastic processes in these methods, it was found that the low inoculation method yielded the highest amount of useful experimental data.

To prove the conclusions of the simulation study, an experimental validation was performed on four independent biological replicates for each protocol. This resulted in 384 inoculated wells for each inoculation method. The evaluation of the experimental results is presented in **Table 1 part C**. Compared to the simulation studies, there was a lower yield of wells containing cells and a higher percentage of wells containing a single cell. This was found to be due to having a lower inoculation in practice, than was calculated from the calibration curve. Irrespective of this, the experimental results are in line with the Monte Carlo simulation and confirm the conclusion that the low concentration inoculation method delivers more useful experimental data. Moreover, the experimental work demonstrated that the low inoculation method required the same amount of lab consumables and had a slightly lower workload. Based on these results, the low concentration inoculation method was selected to be most suitable as part of an efficient and accurate method to determine single cell lag.

TABLE 1 | Evaluation of the serial dilution and low concentration method for the inoculation of microplate wells with single cells.

Origin of variability	Evaluation measure	Serial dilution inoculation method (%)	Low concentration inoculation method (%)
A) Cell distribution	Wells with cells	10.86 ± 5.07	38.13 ± 9.71
	Wells with 1 cell	77.93 ± 26.76	77.93 ± 13.55
B) Cell distribution, error on calibration, pipetting errors	Wells with cells	10.25 ± 5.08	37.99 ± 12.09
	Wells with 1 cell	77.93 ± 27.02	77.93 ± 14.50
C) Experimental uncertainty and microbial variability	Wells with cells	9.90	27.86
	Wells with 1 cell	84.21	82.24

Percentages of (i) wells containing cells compared to the total number of wells and (ii) wells containing a single cell compared to the wells containing cells. ***A*** *and* ***B*** *were calculated from Monte Carlo simulations and results are provided with 95 % confidence intervals.* ***C*** *was obtained experimentally.*

Probabilistic Individual-Based Model

The computational method that will be developed requires a mathematical model that is suitable for simulating cell growth and its variability, starting from a single cell. Individual-based models are perfectly suitable for this task, as they describe every cell individual and the variation between these cells can be included in that description. As such, the next step in the method

development is to propose and test a very simple individual-based model that can be used to simulate the lag phase and growth starting from a single or few cells. The first step in this process was to create a probabilistic simulation of the growth of a population starting from a single cell. This simulation is illustrated in **Figure 1**. The simulation assumes that cells have a specific distribution for their generation time in the lag phase and the exponential phase. The lag phase is considered to be the time until the first division after a cell enters a new environment. This assumption is supported by the research of Pin and Baranyi (2006) in which individual cell division times were observed through microscopy experiments. For a specific set of experiments with *E. coli* K12, the time for the first, second, third and fourth division were found to be 3.30, 1.04, 0.98 and 0.92 h. This demonstrates that the lag phase duration is mainly related to the time until the first division for single cells. For the current paper, this time until first division is taken equal to the individual lag time. It should be noted that some researchers consider the time until the first division to be the sum of the lag time and the generation time. When the generation time is known, a simple conversion between the two definitions is possible. To create a simulation case study for the model development, the distribution parameters for the lag phase duration and generation time were based on the data of Pin and Baranyi (2006). The individual lag phase duration was assumed to have a mean of 3.30 h and standard deviation of 1.02 h, and the generation time a mean of 0.92 h and standard deviation of 0.29 h. Given that the lag and generation time can never be negative, these growth parameters cannot be described by a normal distribution and a lognormal distribution was assumed for these processes (Koch, 1966). In the past, researchers have also used other distributions such as the Weibull, gamma and exponential distribution to describe individual cell lag (Standaert et al., 2007). It is important to stress that the results from this study would not be different if a different probability distribution for the individual cell lag was assumed.

The individual-based simulation starts from a single cell that is assigned a lag time from the lognormal distribution of the individual lag phase. Once this timepoint is reached, the cell is replaced by two daughter cells. Each of these daughter cells is assigned a random generation time according to the lognormal distribution for the generation time in the exponential phase of growth. When these daughter cells reach their individually assigned generation times they are replaced in the same manner and so on. This simple simulation can also be made by starting from a set of multiple cells, each with a randomly assigned individual lag time. Following this random process, it is, however, not possible to estimate the parameters from both the distribution of the individual lag time and the generation time because they would be highly correlated. Therefore, it is desirable that these two probability distributions can be simplified to a single distribution. This simplification is only possible if the model with a single probability distribution can accurately describe the variability of the process. To test this possibility, a Monte Carlo simulation with 10^5 iterations was performed. Each iteration simulated the inoculation and growth of a microorganism in the well of a microplate, according to the low concentration inoculation method established in section "Comparison of Conventional Inoculation Methods" (0.48 CFU/well). In each well containing cells, the growth occurred according to the individual-based simulation with random distributions for both the individual lag

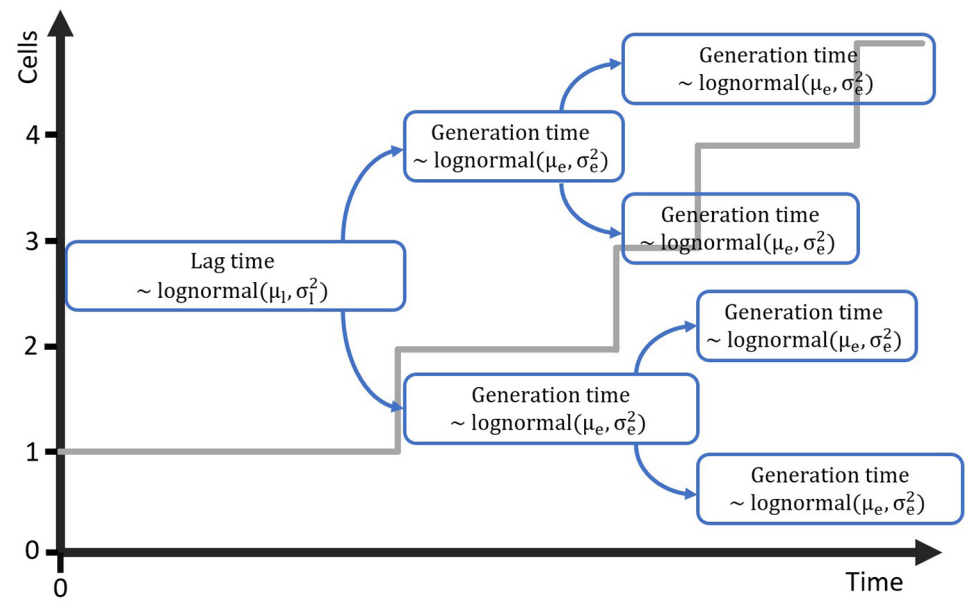

FIGURE 1 | Probabilistic simulation of the growth of a population starting from a single cell with generation time in the lag phase distributed according to the lognormal distribution with parameters μ_l and σ_l^2. Each of the daughter cells is assigned a generation time for the exponential phase from the lognormal distribution with parameters μ_e and σ_e^2.

time and exponential generation time. After obtaining all growth curves, they were transformed to a logarithmic scale and the mean and standard deviation were calculated as a function of time (**Figure 2**). The evolution of the standard deviation of the population size shows a sigmoidal behavior. This is because once the population reaches a certain size, the fast and slow growing cells will balance each other out and different populations all grow at approximately the same rate. As such, when a certain population size is reached, there is no further evolution of the variability of the population growth on a logarithmic scale.

The evaluation of the variability was further assessed by defining the population size where the variability settled to a near-constant value. The Monte Carlo simulations were carried out in parallel for increasing time values and the simulation was stopped at the point where the relative increase of the standard deviation of the population size was less than 0.01%. As such, the final standard deviation of the population size can be taken equal to the maximum standard deviation that could be reached. Then, the population sizes were calculated at which 95 and 99 % of the increase from the initial to the final standard deviation were achieved. As such, it was found that under the simulation conditions, the variability of the population size settled to a constant value between population sizes of just 6–18 CFU on average. Although these values depend on the simulation parameters, they illustrate that the variability reaches an equilibrium at very low population sizes. This is in agreement with the results of, e.g., Kutalik et al. (2005) who found the standard deviation of the division time to decrease after the first division.

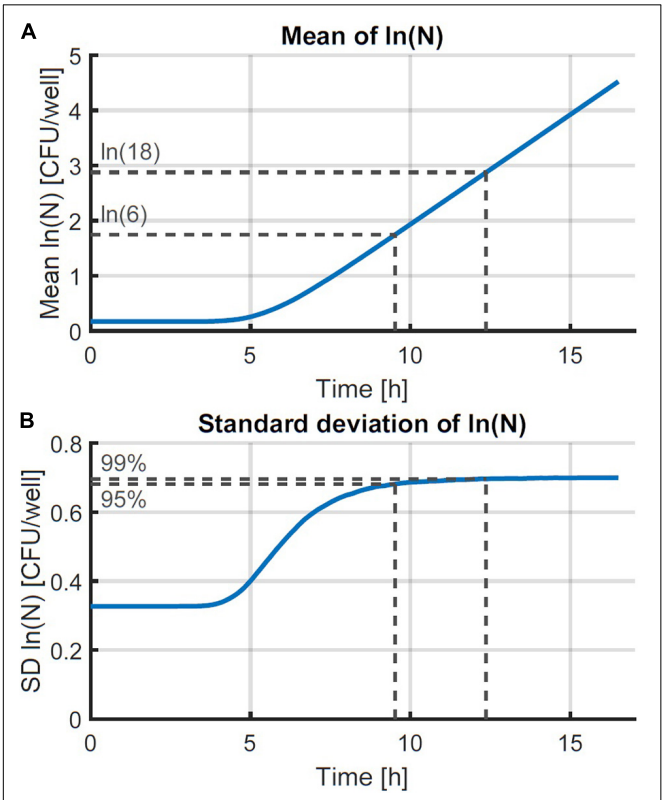

FIGURE 2 | Monte Carlo simulation of the growth of small microbial populations with random lag time and exponential generation time. The mean **(A)** and standard deviation (SD) **(B)** of the obtained populations are shown as a function of time. The striped lines indicate the point at which 95 and 99 % of the maximum variability are reached at 6 and 18 CFU, respectively.

These results demonstrate that the probabilistic simulation model can be simplified from a model that has separate distributions for the individual lag time and exponential generation time to a model that only has a distribution for the individual lag time and a constant generation time in the exponential phase. This simplification holds under the assumption that the model will be used to describe the variability on the population size after a few generations. As such, the variability of the initial phases of population growth can be studied by analyzing the variability on the population size after just a few generations.

Probabilistic Population-Level Model

The simulations with the individual-based model of section "Probabilistic Individual-Based Model" provide a very accurate description of the variation of population growth. However, given the algorithm that needs to calculated with a high number of iterations, simulating this model is slow. To allow the proposed method to work, a model should be constructed that approximates the individual-based model but can be computed much faster. The model will be incorporated as part of a Monte Carlo method within a parameter estimation and will therefore be computed a high number of times. Therefore, a population-level model should be constructed that can be expressed by a simple mathematical expression. The following simple mathematical expression is proposed for the growth of a population starting from a single cell:

$$\ln(N_s(t)) = 1(t-\lambda_i)\cdot\mu\cdot(t-\lambda_i) \quad (3)$$

with N_s [CFU] the number of cells originating form a single cell, t [h] the time, $_i$ [h] the individual lag time and [h^{-1}] the maximum specific growth rate in the exponential phase of growth. The function $1(\cdot)$ represents the unit step function, which is 0 for all arguments smaller than 0 and 1 for all arguments greater or equal than 0. As such, Equation 3 remains constant at 0 during the individual lag time (t $_i$) and predicts log-linear growth for all times larger than $_i$. For populations, N, starting from multiple cells, N_0, the equation can be written as:

$$\ln(N(t)) = \ln(N_0)\sum_{i=0}^{N_0} 1(t-\lambda_i)\cdot\mu\cdot(t-\lambda_i) \quad (4)$$

The summation is used in this equation since the individual lag times are not equal but obtained from a random distribution. The population-level model in Equation 4 was compared with the individual-based model with probability distribution for the individual lag time and fixed generation times. This comparison was done by performing a Monte Carlo simulation with 10^5 iterations and the same parameters for the lag time distribution as the simulation in section "Probabilistic Individual-Based

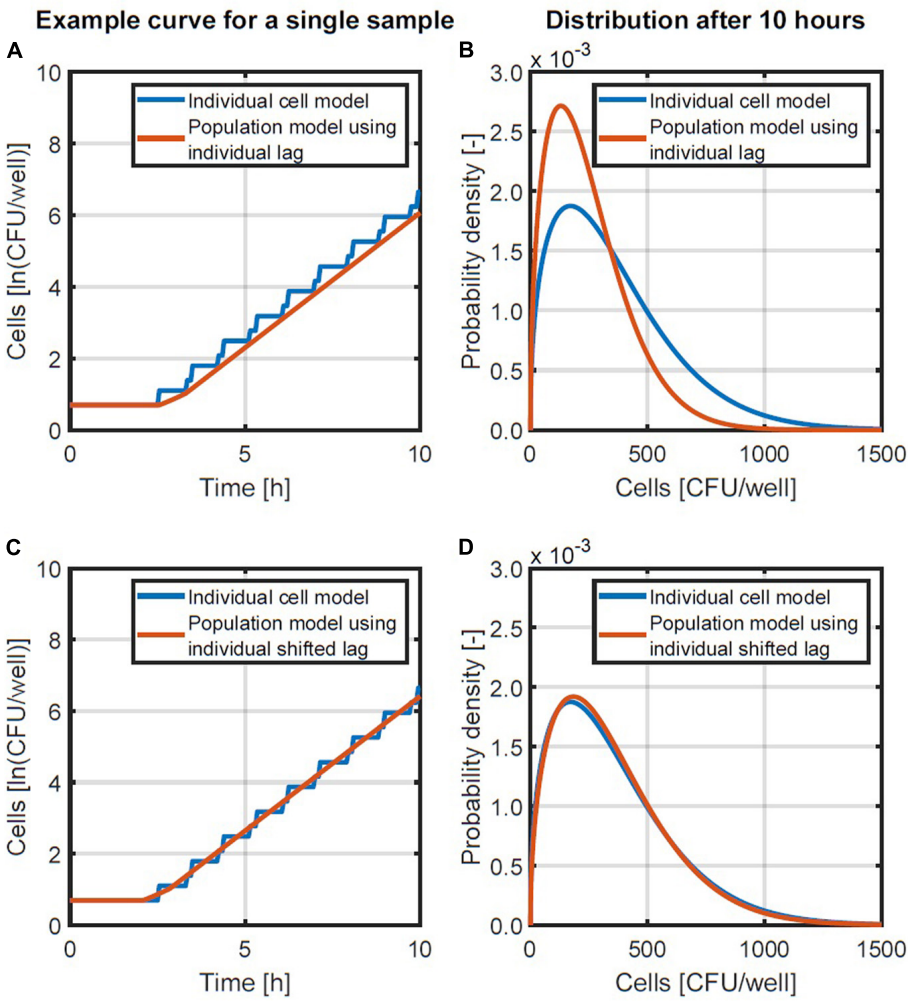

FIGURE 3 | Examples of the individual-based and population-level models **(A,C)** and the probability density functions of population sizes after 10 h **(B,D)**. A comparison is made between a population-level model using the individual lag time directly **(A,B)** and a population-level model in which the lag time is reduced with half of the generation time **(C,D)**.

Model." The simulation results are presented in **Figures 3A,B**. **Figure 3A** compares an example simulation from the two different models for the same initialization parameters (initial number of cells and their individual lag times). **Figure 3B** provides the lognormal probability density functions that were fitted to the population size data after 10 h, when the variability on the population size has long settled. As can be seen from these results, there is a discrepancy between the obtained probability distributions. This discrepancy in the probability distributions was because the predicted population size with the population-level model was always lower than that of the individual-based model (**Figure 3A**). This difference in the predicted growth curves of each model originates from the stepwise evolution of the individual-based model whereas the population-level model lags behind with a gradual increase that starts at the end of the lag time. This difference can be balanced out by shortening the lag phase duration in the population-level model by half the generation time in the exponential phase. This correction essentially applies a time shift to the exponential phase so that the log-linear increase ends up halfway of the stepwise increase (see **Figures 3A,C**). Since the generation time can be expressed as $\ln(2)/$, the model in Equation 4 is than converted to the following expression:

$$\ln(N(t)) = \ln(N_0) + \sum_{i=1}^{N_0} 1\left(t - \lambda_i + \frac{\ln(2)}{2\mu}\right) \cdot \mu \cdot \left(t - \lambda_i + \frac{\ln(2)}{2\mu}\right) \quad (5)$$

A comparison of the population model in Equation 5 and the individual-based model is presented in **Figures 3C,D**. **Figure 3C** demonstrates with an example that the new population model is a linear approximation of the stepwise

behavior of the individual-based model. **Figure 3D** illustrates that this change in the population model results in a good approximation of the distribution of the population size that is obtained. As such, the model in Equation 5 will be used to simulate the distribution of the population density.

Without proving this point, it is worth mentioning that it is possible to calculate the final population size, as done in Equation 5, by first calculating the population lag, $_p$, using the following equation:

$$\lambda_p = -\frac{1}{\mu} \cdot \ln\left(\frac{1}{N_0}\sum_{i=1}^{N_0} \exp\left(\frac{\ln(2)}{2\mu} + \lambda_i\right) \cdot \mu\right) \quad (6)$$

The mean population density is then calculated as:

$$\ln(N(t)) = \ln(N_0) + 1\left(t - \lambda_p\right) \cdot \mu \quad (7)$$

Although seemingly simpler, the fact that the summation remained necessary through Equation 6, meant that the computational load did not decrease in the current study. As such, all calculations of the population size were carried out with Equation 5 as a population model.

Population Size Distribution

Now that the population-based model has been proposed, all that remains to finalize the method is to find the probability density function that is most suitable to describe the population size at a given time point. This probability density function is required within the parameter estimation to compare the simulated model output with the experimentally measured probability distribution of the population size. The optimal parameters of the distribution of the individual cell lag are those parameters that minimize the difference between the simulated and experimental distributions of the population size.

To test which probability density function would be most suitable, a set of simulation data was generated. The data was generated for 1,000 96-well plates, inoculated at intended concentrations of 0.5, 1.0, 2.0 and 4.0 CFU/well according to a Poisson distribution. In each sample containing cells, the population growth was simulated for a period of 6 h, using the individual-based model of **Figure 1** with the parameters of Pin and Baranyi (2006) as mentioned in section "Probabilistic Individual-Based Model." At each time point, the Weibull, gamma and lognormal distribution were fitted to the distribution of the population size. The mean squared errors between the data and the distributions were calculated based on the cumulative distributions and plotted as a function of time in **Figure 4**. As can be seen from this figure, the Weibull distribution achieves a better approximation of the distribution of the population size for all inoculum sizes and at all time points. As such, the Weibull distribution was selected as the most suitable distribution to describe the population size and was used within the following parameter estimations to determine the individual lag phase distribution. The small differences between the approximation by the different distributions is in line with the results of Huang (2016) who found little difference between simulation results using the normal, lognormal, Gumbel, gamma, Weibull, and exponential distributions.

Proposed Experimental and Computational Method

The current section describes all experimental and computational steps that are proposed in the current method for the estimation of the individual lag time distribution. The following steps are taken: (i) determine the OD detection limit and calibration curve between OD and colony forming units, (ii) perform a growth experiment to find the growth rate in the exponential phase, (iii) inoculate microplates with several cells per well and quantify the number of cells after a period of time, (iv) correct all measurements to the exact same sampling time and (v) perform a parameter estimation to find the distribution of the individual lag time that results in the same distribution of the cells at the sampling time.

Even though the proposed method relies primarily on the use of viable plate counts, OD measurements are a useful tool for the inoculation procedure. The availability of a calibration curve between the OD and the number of viable plate counts allows the estimation of the cell density of the preculture or one of its dilutions. This cell density should be known for the calculation of the desired dilutions to start the actual experiments. Since the cell density of the preculture will often vary, the OD can provide a fast measurement of the cell density before starting the inoculation. The detection limit is needed to know the lower bound of the calibration curve. If it is not specifically desired to aim at the same initial cell density among replicates, this step can also be omitted. The initial concentration needs to be verified in any case based on plate counts for a more accurate determination.

The next experimental and computational steps require knowledge on the growth of the microorganism under the relevant conditions. To this end, a growth curve is constructed under the same conditions as during the actual experiments. In the current research, the growth curve is therefore also constructed using the same 96-well plates. Once the growth curve is available, a parameter estimation with the simple three-phase linear model (Equation 2) will provide the exponential growth rate which is essential information for the computational part.

The next step is to inoculate samples with a relatively low quantity of cells. The idea is to have a high chance of obtaining at least one cell in every sample while not exaggerating with the number of cells per sample either. After all, too high a number of cells could cause the cells to influence each other during the first stages of the microbial growth, which is not desirable in this type of experiments. Before inoculating the samples, it is also important to determine the concentration of the inoculum using viable plate counts. After a certain period of time, the quantity of cells in each sample is determined using the viable plate count method. The fastest and most accurate method is to transfer the entire sample volume to petri plates. This is possible when using small sample sizes (e.g., 100 μL) and if the total number of cells in the sample is kept limited (e.g., maximum 300 cells). As such, the time point of sampling should be selected in such a way that the individual lag phase has most likely passed but the number of

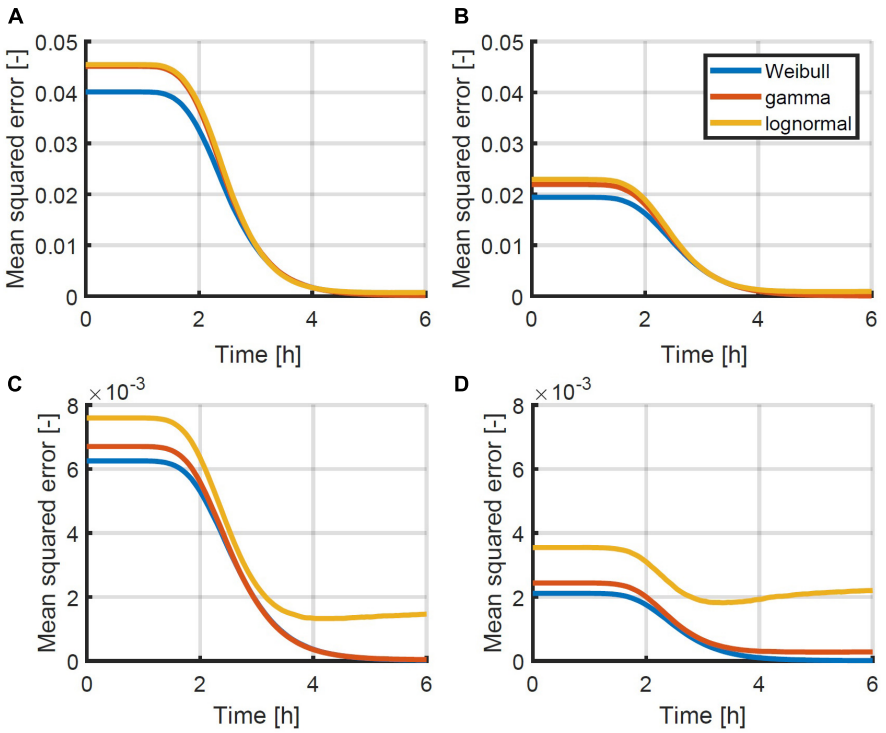

FIGURE 4 | Mean squared error between the simulated cumulative distribution of the population size as a function of time and the approximated Weibull, gamma and lognormal distribution for initial population sizes: **(A)** 0.5, **(B)** 1.0, **(C)** 2.0, and **(D)** 4.0 CFU/well. Simulations were performed using the individual-based model of **Figure 1** with the parameters described in section "Probabilistic Individual-Based Model".

cells has not yet increased by too much. The growth experiment from the previous step will indicate the appropriate time point.

The fact that the current method relies on plating the entire undiluted volume of each sample, yields a relatively fast experimental method. That is to say, samples from a full 96-well plate can be transferred directly to 96 agar plates. However, compared to OD methods, it is important to understand that there is a significant additional work load involved. Obtaining an OD measurement in a microplate reader takes only a few minutes. On the other hand, even this efficient protocol for plate counts would take at least about 1 h and could extend to several hours, depending on the approach. The method can be done in less than an hour when using ready-to-use agar plates in combination with an automatic colony counter. When using self-prepared agar plates and performing manual plate counts, the method requires at least 2 h for a single 96-well plate.

After incubating the petri plates and counting colonies, the final number of cells in each sample is known. However, depending on the number of samples, there can be a significant difference in the time between inoculation and sampling. As such, it is important to determine the time t between inoculation and sampling for each sample. All sample quantities can then be recalculated for the mean sampling time $\bar{t}$. The logarithm of the sample quantity n [ln(CFU)] is then converted to $n - \mu \cdot (t - \bar{t})$, with μ being the previously estimated exponential growth rate. After this correction, a distribution of the cell population size is obtained at a specific time point $\bar{t}$.

At this point, the following is known: (i) the distribution of the initial quantity of cells at the time of inoculation, which follows a Poisson distribution with the average number of cells per sample as its only parameter, (ii) the exponential growth rate μ, (iii) the time of sampling $\bar{t}$ and (iv) the distribution of the population size at that point in time. It should be noted that the Poisson distribution of the initial quantity of cells is valid in this case because the experimental method relies on the distribution of samples from a single suspension with a random distribution of bacteria. If the experimental method were to be changed, it should be considered if this distribution needs to be changed as well. It is also possible to simulate a distribution of the population size by using the population-based model of Equation 5 in a Monte Carlo simulation with randomly generated initial cell quantities from the known Poisson distribution and randomly generated individual lag phase durations from a the lognormal distribution. The parameters of this lognormal distribution are, however, unknown. These parameters can therefore be found by selecting them in such a way that the simulated and measured distributions of the population size approximate each other best. To quantify the distance between both probability distributions, a Weibull distribution is fitted to the simulated distribution and the difference between the cumulative form of that Weibull distribution and the cumulative probability density of the data is calculated. Finding the parameters of the lognormal distribution of the individual lag phase can be achieved by solving this optimization problem with the function *lsqnonlin* of MATLAB.

Simulation Validation

Methods to determine the variation of a lag phase distribution are difficult to validate because testing the reliability of these methods requires high amounts of experimental data. Therefore, the first step in validating the proposed method is to validate based on the theoretical simulations. These simulations allow the repeated calculation of a simulated experiment to test the reproducibility of the results. To obtain representative simulations, the same steps are followed that would be applied in an experimental study. This validation was carried out using these steps: (i) a first dataset was generated to estimate the growth rate, (ii) two datasets were generated at different initial concentrations to determine the lag phase distribution by using the individual-based growth model, (iii) the lag phase distribution was estimated for both datasets, (iv) a Monte Carlo simulation of the population growth was made using the population-based model and estimated parameters, and (v) the results were compared with those of a Monte Carlo simulation of the original individual-based model.

When following the proposed method, the first step is the estimation of the microbial growth rate. This step was simulated by generating inoculation data for a 96-well plate with liquid samples of approximately 48 CFU/well according to a Poisson distribution. For each sample, the growth was simulated according to the individual-based model that is described in **Figure 1**. The mean and standard deviation for the generation time of both the lag phase and exponential growth were again taken from Pin and Baranyi (2006) to obtain realistic simulations: 3.30 and 1.02 h, and 0.92 and 0.29 h respectively. The growth of all samples was simulated for a period of 12 h. Three random samples were taken every hour out of the simulated results and their averages were calculated as a function of time. These data were used to estimate the lag phase duration and exponential growth rate by fitting the three-phase linear model (Equation 2) to the simulated data (**Figure 5**). The lag phase duration of the population was found to be 2.24 h and the exponential growth rate was 0.834 1/h. This exponential growth rate is essential to determine the lag phase distribution in the following step.

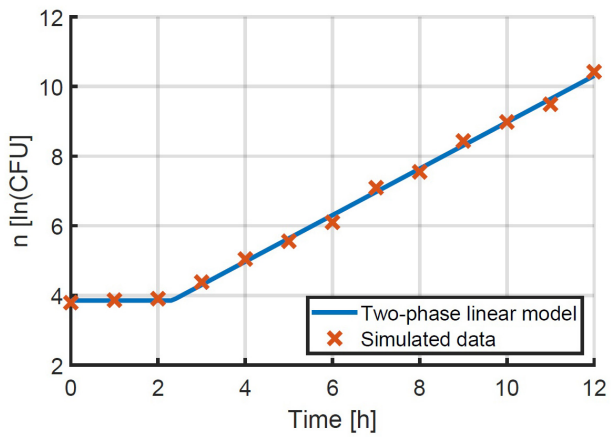

FIGURE 5 | Simulated data starting at Poisson distributed initial concentrations and following growth according to the individual-based model of **Figure 1**. The two-phase linear model was fitted to this data (Equation 2).

In the second step, two datasets were simulated, each consisting of 4 96-well plates. These datasets were inoculated with intended concentrations of 0.48 and 4.80 CFU/well according to a Poisson distribution. In all wells containing cells, growth was simulated according to the same individual-based model to obtain the population size after 6 h. These simulated data correspond to the experimental data that would be obtained when determining the viable plate counts of each sample after a given time. As such, these data were used as inputs for two parameter estimation problems to estimate the parameters of the lognormal distribution that describes the individual lag phase duration. The mean and standard deviation of this distribution were calculated to be, respectively, 3.17 (3.14; 3.20) and 1.18 (1.14; 1.23) h, and 3.27 (3.25; 3.28) and 1.12 (1.08; 1.17) h for initial population sizes of 0.48 and 4.80 CFU/well. These parameter values are close to the mean and standard deviation of the individual lag phase duration that were used in the individual-based model to generate the data (3.30 and 1.02 h). It can be noted that the standard deviations were found to be higher than that specified to run the simulation with the individual-based model. This is due to the fact that the standard deviation of the individual lag phase duration in the population-based model captures the variability of both the lag phase duration and the generation time in the exponential phase. The small difference between the parameters used to simulate the data and the estimated parameters is already a first indication of the successful implementation of the proposed method.

Baranyi et al. (2009) have published a methodology that is based on the method of moments for calculating the individual lag phase distribution from the same type of data as described here. This method has a much lower computational burden than the method proposed in this work, which requires solving a maximum likelihood estimation problem that involves a Monte Carlo simulation. As such, this moments-based method was compared on exactly the same simulation data. To this end, the mathematical formulation to solve this problem was taken directly from Baranyi et al. (2009). For the data at 4.80 CFU/well, a decent estimate of the individual lag phase distribution was obtained, with a mean of 2.90 and standard deviation of 1.16 CFU/well. However, no reasonable solution could be obtained for the low concentration data of 0.48 CFU/well. Upon further examination, it was found that the accuracy of the estimated distribution decreased with decreasing initial concentrations. Combining this inaccuracy with the fact that this method provides no uncertainty on the parameter estimates, the moments-based method was found to be unsuitable for solving the current problem.

A more thorough validation of the obtained method and parameter estimation results was done by comparing a simulation of the individual-based model using the original parameters with a simulation of the population-based model using the estimated parameters. The simulations were performed for 10 96-well plates at the original average inoculation densities and the resulting mean and standard deviation of the population size as a function of time are presented in **Figure 6**. The number of plates (iterations) was chosen to obtain an accurate

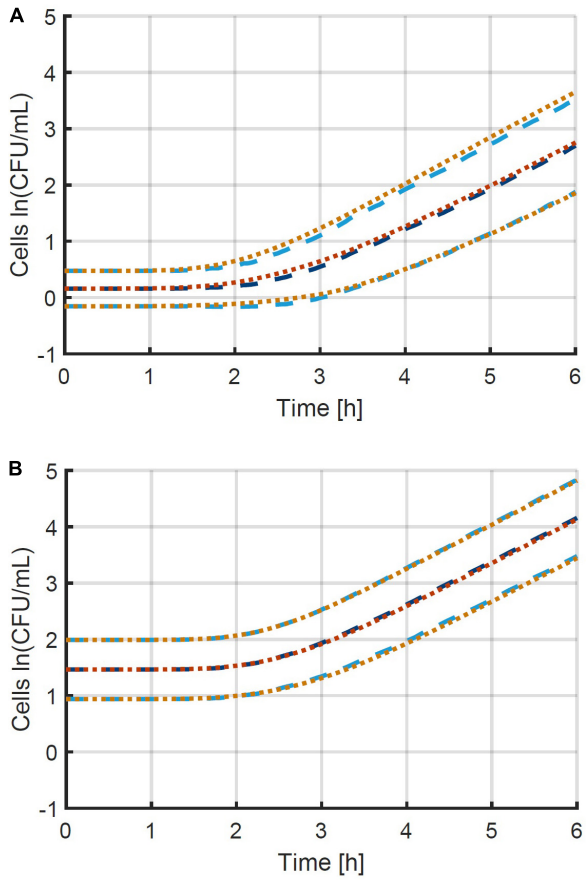

FIGURE 6 | Comparison between the mean and standard deviation of the population size according to (i) the individual-based model used to generate simulation data (— and . . .) and (ii) the population-based model that approximates this data (— and . . .). This information is represented for the two case studies with initial population sizes according to a Poisson distribution with means of **(A)** 0.48 and **(B)** 4.80 CFU/well. The individual-based model and parameters are described in section "Probabilistic Individual-Based Model".

estimation of the standard deviation as a function of time, as indicated by smooth curves. Comparing the two model simulations in the figure demonstrates that the newly developed method enables the population-based model to provide a very good approximation of both the average population behavior and the individual cell variability. Specifically, the ability of the method and the population-based model to describe the variability is remarkable. Even though the model completely ignores the variability between individual cells in the exponential phase of growth, a good approximation is achieved, starting from the initial concentration of cells, all the way into the exponential phase of growth. This validation study proves that it is indeed possible to capture the combined variability of the cells in the lag and exponential phase of growth into a single variable, being the individual lag phase duration. The prerequisites to obtain the current results are that both the mean initial population size and the exponential growth rate are determined accurately. The final step in the method development is the experimental validation.

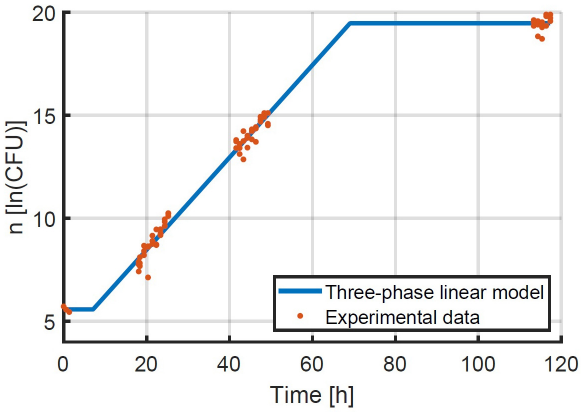

FIGURE 7 | Data on the growth of *E. coli* at 25°C after being transferred to BHI medium with 56 g/L NaCl at an average quantity of 48 CFU/well. The three-phase linear model of Equation 2 was fitted to the data.

Experimental Validation

Given that the simulation validation was successful, an experimental validation was performed specifically to test the assumption that the method can be used at higher inoculation levels and therefore at higher yields of experimental data. The method for the experimental validation study is explained in detail in section "Experimental Study of the Population Variability." The first step in the evaluation of the experimental data was to estimate the exponential growth rate based on the experiments that were inoculated at an intended concentration or 48 CFU/well. The exponential growth rate μ was estimated to be 0.224 1/h with 95 % confidence bounds of 0.216–0.232 1/h. This experimental data and the fitted model are illustrated in **Figure 7**. The 95 % confidence bounds indicate a high level of confidence in the estimated growth rate, because of the large number of samples. The lag phase duration was estimated to be 7.10 h (4.88; 9.33).

The next step was to process the data on the distribution of the population size. Given the difference in inoculation and sampling times between all samples, it was considered that not all samples were taken after the same period of time. The average sampling time $\bar{t}$ was calculated for all samples and the logarithm of the sample quantity n was corrected to $n - \mu \cdot (t - \bar{t})$. In this manner, all sample quantities were obtained at the exact same time point, which was 26.79 h for the experiments at 0.48 CFU/well and 21.97 h for the experiments at 4.80 CFU/well. Based on the quantification of the concentration of the diluted inoculum, the real average initial concentrations were calculated to be 0.35 and 3.07 CFU/well. Based on the known exponential growth rate, sampling time and initial concentrations, the parameter estimation to determine the distribution of the individual lag phase duration could be performed as explained in section "Proposed Experimental and Computational Method." These parameter estimations led to the identification of the mean and standard deviation of the lognormal distribution of the individual lag phase duration with 95 % confidence bounds to be 9.72 (9.65; 9.79) and

1.77 (1.62; 1.93), and 9.80 (9.78; 9.82) and 1.95 (1.90; 2.00) for the lower and higher inoculation level, respectively. These parameter estimates were in good agreement between the experiments at different inoculum levels and they were relatively accurate. The parameter accuracy of the experiments started at the low inoculum level was lower than those started at a high level. This is simply due to the much lower number of wells that contained cells for the low inoculum level (95 wells compared to 375 wells). As such, these experiments demonstrated first of all that the characterization of the individual lag phase duration is possible with the current method at various inoculum levels. More importantly even, these experiments have shown that this new method allows for the determination of the individual lag phase variability with the same precision, while requiring a much lower experimental effort by starting the experiments at inoculum levels that are more likely to place at least one cell in every well instead of aiming at a high chance of having no more than 1 cell per well.

A final step in this validation was to predict the lag phase duration for the experiment with the highest inoculum level that was used to estimate the exponential growth rate, based on the estimated distributions of the individual lag phase. This was done using the population-based model at the same inoculum level of 39.76 CFU/well for 1,000 iteration. The lag phase durations were estimated by approximating the simulation data with the two-phase linear model. Based on the distribution from the inoculum of 0.35 CFU/well the lag phase was estimated to be 7.68 h and for the distribution from the inoculum of 3.07 CFU/well it was 7.61 h. The predicted lag phase durations were close to each other because of the probability distributions being very similar. Moreover, the predicted population lag times were in line with the lag phase duration of 7.10 h that was estimated from the growth data at the highest inoculum level. Both the data and simulations demonstrated a reduction of the population lag phase duration with increasing population size. This reduction of the lag phase duration can be understood from the larger likelihood of having fast growing cells that will dominate the population lag. Moreover, this phenomenon has been demonstrated in previous research. For example, Robinson et al. (2001) demonstrated this effect experimentally for *L. monocytogenes* at increased NaCl concentrations.

CONCLUSION

This research presents a combined experimental and computational method for the determination of the individual lag phase variability. The experimental method can readily be implemented in most microbiology labs and the computational combines robust techniques such as Monte Carlo simulation and maximum likelihood parameter estimation, which are familiar to researchers in the domains of predictive microbiology and quantitative microbial risk assessment. The experimental method requires an accurate estimation of the average initial concentration and the growth rate under the given conditions. By demonstrating that the variability on the logarithmic concentration of the population settles after just a few generations, it is possible to quantify this variability of the population size as a measure for the variability on the initial growth phases. The further simulations demonstrated that a simple population-based model can accurately approximate and predict this growth variability as a consequence of individual cell variability. The experimental validation demonstrated the ability of the proposed methodology to determine the probability distribution of the individual lag phase through experiments at higher inoculum levels (>1 CFU/sample). The advantage of these higher inoculum levels is that a larger amount of useful data (wells containing cells) can be obtained from the same experimental effort and cost. Moreover, by plating full undiluted samples in the experimental method, the experimental error is reduced to a minimum. As such, the proposed method delivers high accuracy while minimizing the experimental load.

DATA AVAILABILITY STATEMENT

The raw data supporting the conclusions of this article will be made available by the authors, without undue reservation.

AUTHOR CONTRIBUTIONS

SA performed the experimental and computational work. SA and JV coordinated the research and contributed to the writing. Both authors contributed to the article and approved the submitted version.

FUNDING

SA was supported by the Research Foundation – Flanders (FWO), under grant 1224620N. This work was supported by the KU Leuven Research Fund through project C24/18/046 and by the Research Foundation – Flanders (FWO) through project G0B4121N.

SUPPLEMENTARY MATERIAL

The Supplementary Material for this article can be found online at: https://www.frontiersin.org/articles/10.3389/fmicb.2021.725499/full#supplementary-material

REFERENCES

Aguirre, J. S., González, A., Özçelik, N., Rodríguez, M. R., and García de Fernando, G. D. (2013). Modeling the *Listeria innocua* micropopulation lag phase and its variability. *Int. J. Food Microbiol.* 164, 60–69. doi: 10.1016/j.ijfoodmicro.2013.03.003

Akkermans, S., Nimmegeers, P., and Van Impe, J. F. (2018). A tutorial on uncertainty propagation techniques for predictive microbiology: a critical analysis of state-of-the-art techniques. *Int. J. Food Microbiol.* 282, 1–8. doi: 10.1016/j.ijfoodmicro.2018.05.027

Baka, M., Noriega, E., Stamati, I., Logist, F., and Van Impe, J. F. M. (2014). Critical assessment of the time-to-detection method for accurate estimation of

microbial growth parameters. *J. Food Saf.* 35, 179–192. doi: 10.1186/s13054-016-1208-6

Baranyi, J., George, S. M., and Kutalik, Z. (2009). Parameter estimation for the distribution of single cell lag times. *J. Theor. Biol.* 259, 24–30. doi: 10.1016/j.jtbi.2009.03.023

Brewster, J. D. (2003). A simple micro-growth assay for enumerating bacteria. *J. Microbiol. Methods* 53, 77–86. doi: 10.1016/s0167-7012(02)00226-9

Buchanan, R. L., Whiting, R. C., and Damert, W. C. (1997). When is simple good enough: a comparison of the Gompertz, Baranyi and three-phase linear models for fitting bacterial growth curves. *Food Microbiol.* 14, 313–326. doi: 10.1006/fmic.1997.0125

D'Arrigo, M., García de Fernando, G. D., Velasco de Diego, R., Ordónez, J. A., George, S. M., and Pin, C. (2006). Indirect measurement of the lag time distribution of single cells of *Listeria innocua* in food. *Appl. Env. Microbiol.* 72, 2533–2538. doi: 10.1128/AEM.72.4.2533-2538.2006

Dupont, C., and Augustin, J.-C. (2009). Influence of stress on single-cell lag time and growth probability of *Listeria monocytogenes* in half Fraser broth. *Appl. Env. Microbiol.* 75, 3069–3076. doi: 10.1128/AEM.02864-08

Francois, K., Devlieghere, F., Smet, K., Standaert, A. R., Geeraerd, A. H., Van Impe, J. F., et al. (2005). Modelling the individual cell lag phase: effect of temperature and pH on the individual cell lag distribution of *Listeria monocytogenes*. *Int. J. Food Microbiol.* 100, 41–53. doi: 10.1016/j.ijfoodmicro.2004.10.032

Francois, K., Devlieghere, F., Standaert, A. R., Geeraerd, A. H., Van Impe, J. F., and Debevere, J. (2003). Modelling the individual cell lag phase. Isolating single cells: protocol development. *Lett. Appl. Microbiol.* 37, 26–30. doi: 10.1046/j.1472-765x.2003.01340.x

Guillier, L., Pardon, P., and Augustin, J.-C. (2005). Influence of stress on individual lag time distributions of *Listeria monocytogenes*. *Appl. Env. Microbiol.* 71, 2940–2948. doi: 10.1128/AEM.71.6.2940-2948.2005

Koch, A. L. (1966). The logarithm in Biology 1. Mechanisms generating the log-normal distribution exactly. *J. Theor. Biol.* 12, 276–290. doi: 10.1016/0022-5193(66)90119-6

Kutalik, Z., Razaz, M., Elfwing, A., Ballagi, A., and Baranyi, J. (2005). Stochastic modelling of individual cell growth using flow chamber microscopy images. *Int. J. Food Microbiol.* 105, 177–190. doi: 10.1016/j.ijfoodmicro.2005.04.026

Levin-Reisman, I., Gefen, O., Fridman, O., Ronin, I., Shwa, D., Sheftel, H., et al. (2010). Automated imaging with ScanLag reveals previously undetectable bacterial growth phenotypes. *Nat. Methods* 7, 737–739. doi: 10.1038/nmeth.1485

Lianou, A., and Koutsoumanis, K. P. (2013). Strain variability of the behaviour of foodborne bacterial pathogens: a review. *Int. J. Food Microbiol.* 167, 310–321.

Huang, L. (2016). Simulation and evaluation of different statistical functions for describing lag time distributions of a bacterial growth curve. *Microb. Risk Anal.* 1, 47–55.

McKellar, R. C., and Lu, X. (2004). "Primary models," in *Modeling Microbial Responses in Food*, eds R. C. McKellar and X. Lu (Boca Raton, FL: CRC Press), 21–62.

Métris, A., George, S. M., and Baranyi, J. (2006). Use of optical density detection times to assess the effect of acetic acid on single-cell kinetics. *Appl. Env. Microbiol.* 72, 6674–6679. doi: 10.1128/aem.00914-06

Pin, C., and Baranyi, J. (2006). Kinetics of single cells: observation and modelling of a stochastic process. *Appl. Env. Microbiol.* 72, 2163–2169. doi: 10.1128/aem.72.3.2163-2169.2006

Robinson, T. P., Aboaba, O. O., Kaloti, A., Ocio, M. J., Baranyi, J., and Mackey, B. (2001). The effect of inoculum size on the lag phase of *Listeria monocytogenes*. *Int. J. Food Microbiol.* 70, 163–173. doi: 10.1016/s0168-1605(01)00541-4

Standaert, R. A., Francois, K., Devlieghere, F., Debevere, J., Van Impe, J. F., and Geeraerd, A. H. (2007). Modeling individual cell lag time distributions for *Listeria monocytogenes*. *Risk Anal.* 27, 241–254. doi: 10.1111/j.1539-6924.2006.00873.x

Stringer, S. C., Webb, M. D., and Peck, M. W. (2011). Lag time variability in individual spores of *Clostridium botulinum*. *Food Microbiol.* 28, 228–235. doi: 10.1016/j.fm.2010.03.003

Walzl, A., Kramer, N., Mazza, G., Rosner, M., Falkenhagen, D., Hengstschläger, M., et al. (2012). A simple and cost efficient method to avoid unequal evaporation in cellular screening assays, which restores cellular metabolic activity. *Int. J. Appl. Sci.* 2, 17–25.

Xu, Y. Z., Métris, A., Stasinopoulos, D. M., Forsythe, S. J., and Sutherland, J. P. (2015). Effect of heat shock and recovery temperature on variability of single cell lag time of *Cronobacter turicensis*. *Food Microbiol.* 45, 195–204. doi: 10.1016/j.fm.2014.04.003

Conflict of Interest: The authors declare that the research was conducted in the absence of any commercial or financial relationships that could be construed as a potential conflict of interest.

Publisher's Note: All claims expressed in this article are solely those of the authors and do not necessarily represent those of their affiliated organizations, or those of the publisher, the editors and the reviewers. Any product that may be evaluated in this article, or claim that may be made by its manufacturer, is not guaranteed or endorsed by the publisher.

frontiers in Microbiology

ORIGINAL RESEARCH
published: 11 November 2021
doi: 10.3389/fmicb.2021.754748

Transcriptomic Analysis of *Listeria monocytogenes* in Response to Bile Under Aerobic and Anaerobic Conditions

*Damayanti Chakravarty[1], Gyan Sahukhal[1], Mark Arick II[2], Morgan L. Davis[3] and Janet R. Donaldson[1]**

[1] Cell and Molecular Biology, The University of Southern Mississippi, Hattiesburg, MS, United States, [2] Institute for Genomics, Biocomputing & Biotechnology, Mississippi State University, Mississippi State, MS, United States, [3] Department of Biological Sciences, Mississippi State University, Mississippi State, MS, United States

Listeria monocytogenes is a gram-positive facultative anaerobic bacterium that causes the foodborne illness listeriosis. The pathogenesis of this bacterium depends on its survival in anaerobic, acidic, and bile conditions encountered throughout the gastrointestinal (GI) tract. This transcriptomics study was conducted to analyze the differences in transcript levels produced under conditions mimicking the GI tract. Changes in transcript levels were analyzed using RNA isolated from *L. monocytogenes* strain F2365 at both aerobic and anaerobic conditions, upon exposure to 0 and 1% bile at acidic and neutral pH. Transcripts corresponding to genes responsible for pathogenesis, cell wall associated proteins, DNA repair, transcription factors, and stress responses had variations in levels under the conditions tested. Upon exposure to anaerobiosis in acidic conditions, there were variations in the transcript levels for the virulence factors internalins, listeriolysin O, etc., as well as many histidine sensory kinases. These data indicate that the response to anaerobiosis differentially influences the transcription of several genes related to the survival of *L. monocytogenes* under acidic and bile conditions. Though further research is needed to decipher the role of oxygen in pathogenesis of *L. monocytogenes*, these data provide comprehensive information on how this pathogen responds to the GI tract.

Keywords: ***Listeria monocytogenes*, transcriptomics, anaerobiosis, bile, stress response, anaerobic**

OPEN ACCESS

Edited by:
Aleksandra P. Djukic-Vukovic, University of Belgrade, Serbia

Reviewed by:
Stephan Schmitz-Esser, Iowa State University, United States
Yvonne Sun, University of Dayton, United States

***Correspondence:**
Janet R. Donaldson
janet.donaldson@usm.edu

Specialty section:
This article was submitted to Food Microbiology, a section of the journal Frontiers in Microbiology

Received: *06 August 2021*
Accepted: *18 October 2021*
Published: *11 November 2021*

Citation:
Chakravarty D, Sahukhal G, Arick M II, Davis ML and Donaldson JR (2021) Transcriptomic Analysis of Listeria monocytogenes in Response to Bile Under Aerobic and Anaerobic Conditions. Front. Microbiol. 12:754748. doi: 10.3389/fmicb.2021.754748

INTRODUCTION

Listeria monocytogenes is a gram-positive foodborne pathogen that is responsible for the disease listeriosis (Scallan et al., 2011). Pregnant women, infants, elderly, and immunocompromised individuals are more susceptible to listeriosis, with meningitis, septicemia, and spontaneous abortions being possible manifestations of the disease (Thigpen et al., 2011). Being a foodborne pathogen, this bacterium must be able to respond to the stressors encountered following ingestion of contaminated food. Low pH, bile, and hypoxic/anoxic environments are some of the key stressors that are encountered by *L. monocytogenes* within the gastrointestinal (GI) tract (Davis et al., 1996).

Low pH of the stomach is one of the initial stressors encountered by *L. monocytogenes* upon ingestion (White et al., 2015). The low pH of the gastric secretion is a roadblock to invasion by the bacteria. *Listeria's* acid response involves the SOS response, LisRK (a two-component regulatory system that regulates listerial osmotolerance), components of sigma B regulon, ATPase proton pump, and enzymatic systems that regulate internal hydrogen ion concentration (Sleator and Hill, 2005). A transcriptomic study that was performed on *Listeria* grown in the presence of organic acids revealed an increase in the transcript levels of sigma B and *prfA* regulated genes, which included internalins, phospholipases, and other virulence genes. This previous study also indicated an up-regulation of oxidative stress defenses, DNA repair, intermediary metabolism, cell wall modification, and cofactor and fatty acid biosynthesis (Tessema et al., 2012). A proteomic study performed on *Listeria* grown in the presence of organic salts demonstrated an up-regulation of oxidoreductases and lipoproteins. Upon exposure to hydrochloric acid, it was also observed that proteins involved in respiration (enzyme dehydrogenases and reductases), osmolyte transport, protein folding and repair, general stress resistance, flagella synthesis and metabolism were expressed in the response to the acidic conditions (Bowman et al., 2012).

Listeria is also exposed to bile within the GI tract (White et al., 2015). Bile is synthesized by the liver and stored in the gall bladder. It is released into the duodenum during digestion (Monte et al., 2009). The bile acids are the antibacterial component of bile; bile acids induce damage to the cell wall and DNA (Coleman et al., 1979; Bernstein et al., 1999; Prieto et al., 2004, 2006). Within the gall bladder, bile is found at a nearly neutral pH (7.5), while in the duodenum it is more acidic (pH 5.5) (White et al., 2015). Bile is more bactericidal at acidic pH than at a neutral pH, as indicated in a study that showed a decrease in survival in bile under pH 5.5 in comparison to a pH of 7.5 (Dowd et al., 2011). Many studies have been conducted to determine the global response of *L. monocytogenes* to bile encountered within the GI tract. For instance, the transcription factor *brtA*, which senses cholic acid and regulates efflux pumps (MdrM and MdrT) is involved in bile tolerance (Quillin et al., 2011). Bile salt hydrolases neutralize conjugated bile acids, thereby providing protection against the bactericidal properties of bile (Dowd et al., 2011). The *bilE* gene is also involved in detoxifying bile acids (Dowd et al., 2011).

In addition to changes in pH and bile, *L. monocytogenes* is also exposed to changes in oxygen concentrations. The duodenum is considered microaerophilic in nature, while the gall bladder is anaerobic (Zheng et al., 2015). Oxygen availability has been found to influence bile resistance. A proteomics study performed under anaerobic conditions in the presence of bile observed notable alterations in cell wall associated proteins, DNA repair proteins and oxidative stress response proteins. Under anaerobic conditions the *Listeria* adhesion protein has been observed to have a significant role in intestinal infection (Burkholder et al., 2009). Additionally, oxygen deprivation has been found to affect the survival of *L. monocytogenes in vitro* (Payne et al., 2013; Wright et al., 2016), as well as in cell cultures, guinea pigs (Bo Andersen et al., 2007), and gerbils (Harris et al., 2019). These studies highlight the importance of oxygen in regulation of virulence. However, it is not known what the transcriptomic response of *L. monocytogenes* is to conditions that mimic the GI tract under physiologically relevant anaerobic conditions. Therefore, the goal of this study was to determine the impact of oxygen on the transcriptomic response of *L. monocytogenes* to bile in conditions that mimic the duodenum (pH 5.5) and the gall bladder (pH 7.5).

RESULTS

Survival of *L. monocytogenes* in Conditions Mimicking Gastrointestinal Tract

Listeria monocytogenes exhibits slightly slower growth rates under anaerobic conditions (**Figures 1A** vs. **1B**). Bile also impacted the viability of *L. monocytogenes* strain F2365 differently under anaerobic conditions. Under neutral pH, bile did not have a significant impact on survival of *L. monocytogenes* strain F2365 under either aerobic (**Figure 1A**) or anaerobic conditions (**Figure 1B**).

At acidic pH in the presence of bile, which mimics the exposure to bile in the duodenum, the percentage of *L. monocytogenes* that survived significantly declined (**Figure 2A**; $p < 0.05$). This further demonstrates the increase in toxicity exhibited by bile when in acidic conditions. Survival also declined under anaerobic conditions in comparison to time 0 h (**Figure 2B**, $p < 0.05$). However, the decrease in viability was not as severe under anaerobic conditions (**Figure 2B**) in comparison to aerobic conditions (**Figure 2A**; $p < 0.05$). This indicates that anaerobic conditions improve the survival of *L. monocytogenes* to the toxic effects of bile.

Overall Changes in Transcript Levels in Response to Conditions Mimicking the Gastrointestinal Tract

As significant alterations in survival were observed following 1 h of bile exposure under acidic conditions, this time point was selected to compare the impact that oxygen had on the transcriptome. **Table 1** shows the overall changes in transcripts detected. Under anaerobic conditions, a total of 190 transcripts in media at pH 7.5 and 268 at pH of 5.5 were identified to be differentially expressed in comparison to aerobic conditions. In the presence of bile and absence of oxygen, 304 and 434 transcripts were differentially produced at pH 7.5 and 5.5, respectively. Under anaerobic conditions, upon exposure to bile, variations in the transcript levels of 200 genes were identified at pH 7.5 and 419 at pH 5.5. For all conditions tested, there were globally more transcripts identified to be up-regulated than down-regulated, except for acidic bile conditions under anaerobic growth.

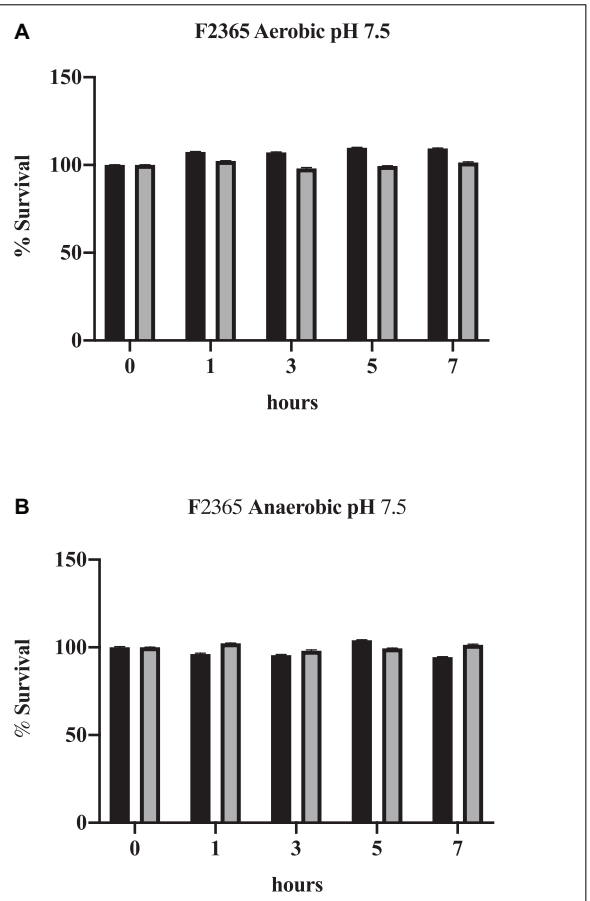

FIGURE 1 | Impact of oxygen on the survival of *L. monocytogenes* in conditions mimicking the gall bladder. F2365 was exposed to either aerobic **(A)** or anaerobic **(B)** conditions with 0% bile (black bars) or 1% bile (gray bars) at a pH of 7.5 and survival was measured by viable plate counts over 7 h. Data represent averages of three independent replicates. Error bars represent standard deviation from biological replicates.

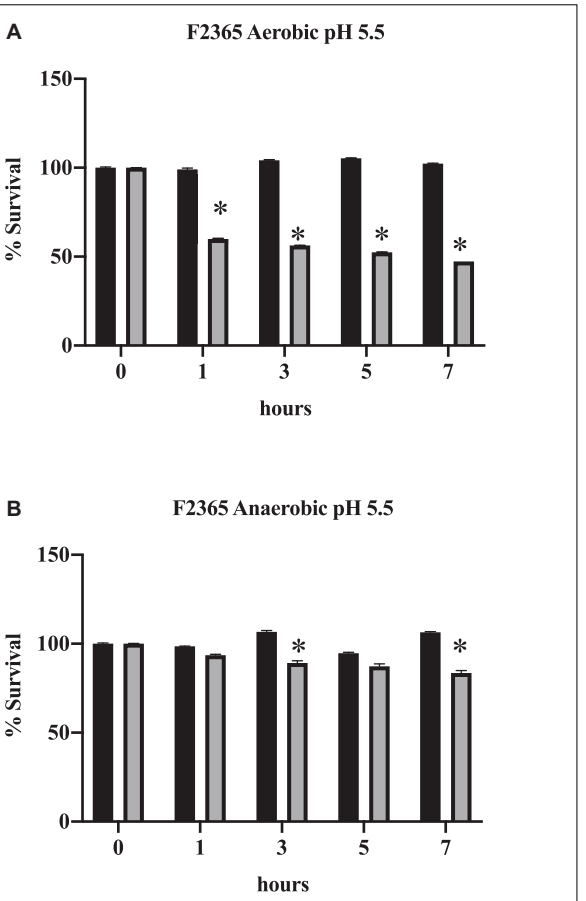

FIGURE 2 | Impact of oxygen on the survival of *L. monocytogenes* in conditions mimicking the duodenum. F2365 was exposed to either aerobic **(A)** or anaerobic conditions **(B)** with 0% bile (black bars) or 1% bile (gray bars) at a pH of 5.5 and survival was measured by viable plate counts over 7 h. Data represent averages of three independent replicates. Error bars represent standard deviation from biological replicates. * Indicates $p < 0.05$ in comparison to time 0.

Changes in Transcript Levels in Response to Anaerobic Conditions

Transcripts representative of five genes were found to be increased in expression levels under exposure to anaerobic conditions regardless of whether the cultivation was conducted under either neutral or acidic pH (**Table 2** and **Supplementary Figure 1**). These included genes involved in membrane transport, protein folding, and stress response. Of these transcripts the amino acid transporter (*LMOf2365_2333*) had nearly a 9-fold increase in levels at neutral pH in comparison to acidic pH. Transcripts representative of the *dnaJ* (*LMOf2365_1491*) and *dnaK* (*LMOf2365_1492*) genes, which encode for molecular chaperones and have roles in phagocytosis and protein homeostasis, were also increased under anaerobic conditions at both pH conditions tested. The transcript representative of the *cadA* (*LMOf2365_0672*) gene, which encodes for a heavy metal translocating P-type ATPase and is a component of the CadAC efflux cassette, was also increased 6.1-fold at pH 7.5 and 3.8 at pH 5.5 under oxygen depleted conditions (**Table 2**).

The transcript levels of 18 genes were decreased under anaerobic conditions regardless of the pH condition tested (**Table 3** and **Supplementary Figure 2**). Out of these eighteen transcripts, six were representative of uncharacterized hypothetical proteins; all of these had lower transcript levels under neutral conditions in comparison to acidic conditions. This could suggest that these hypothetical genes are regulated similarly. The remaining transcripts identified encoded for stress response, membrane associated protein, and metabolism protein (**Table 3**).

Changes in Transcript Levels in Response to Anaerobic Acidic Conditions

In acidic conditions, transcript levels of 140 genes were increased (**Table 4** and **Supplementary Figure 1**) and 104 were decreased under anaerobiosis (**Table 5**). Analyzing these transcripts up-regulated in response to acidic conditions under anaerobiosis

TABLE 1 | Total changes in transcript levels following exposure to bile at pH of 7.5 or 5.5 under either aerobic or anaerobic conditions.

	Aerobic vs. Anaerobic	Bile Aerobic vs. Bile Anaerobic	Anaerobic vs. Bile Anaerobic
pH 7.5	Total = 190	Total = 304	Total = 200
	Up = 125 Down = 65	Up = 207 Down = 97	Up = 131 Down = 69
pH 5.5	Total = 268	Total = 434	Total = 419
	Up = 147 Down = 121	Up = 213 Down = 221	Up = 264 Down = 155

TABLE 2 | Transcript levels increased in response to anaerobiosis at pH 7.5 or 5.5.

Gene ID	Gene product	Transcript fold changes	
	Membrane transport	***pH 7.5***	***pH 5.5***
cadA LMOf2365_0672	Cadmium translocating P-type ATPase	6.1	3.8
LMOf2365_2333	Amino acid antiporter	137.2	15.0
Protein folding			
dnaK LMOf2365_1492	Chaperone protein	5.3	8.6
dnaJ LMOf2365_1491	Chaperone protein	7.2	4.8
Stress response			
gadG LMOf2365_2405	Glutamate decarboxylase gamma	11.2	3.2

TABLE 3 | Transcript levels decreased in response to anaerobiosis at pH 7.5 or 5.5.

Gene ID	Gene product	Transcript fold changes	
		pH 7.5	**pH 5.5**
Membrane transport			
LMOf2365_2554	Sensor histidine kinase	−4.46	−12.1
Metabolism			
acpP LMOf2365_1834	Acyl carrier protein	−13.6	−5.3
LMOf2365_0511	Heme oxygenase (staphylobilin-producing)		
gcvT LMOf2365_1365	Glycine cleavage system T protein	−8.9	−4.7
LMOf2365_0585	Phosphoglycerate mutase family protein	−7.7	−3.6
Stress response			
LMOf2365_0544	Universal stress protein family	−5.9	−5.8
Hypothetical proteins			
LMOf2365_0964	Conserved hypothetical protein	−13.7	−5.9
LMOf2365_0511	Conserved hypothetical protein	−13.6	−5.3
LMOf2365_1087	Conserved hypothetical protein	−12.1	−3.9
LMOf2365_0808	Conserved hypothetical protein	−11.2	−3.1
LMOf2365_1179	Hypothetical protein	−8.3	−3.7
LMOf2365_2288	Conserved hypothetical protein	−6.3	−5.8

revealed that several biological pathways related to pathogenesis, stress response, membrane associated proteins, transcription factors and DNA repair mechanisms influenced the survival of *L. monocytogenes* (**Table 4**). Transcripts representative of genes involved in metabolism, transcription factor and pathogenesis were down-regulated (**Table 5**). Certain transcripts encoding for glycolytic enzymes increased under acidic anaerobic conditions as well (**Table 4**). These included the glyceraldehyde-3-phosphate dehydrogenase (5.4-fold increase), phosphoglycerate mutase (4.7-fold increase), and pyruvate kinase (6.7-fold increase).

Changes in Transcript Levels in Response to Bile Under Anaerobic Conditions

Transcripts representative of 53 genes were found to be up-regulated in response to exposure to bile under anaerobic conditions (**Table 6** and **Supplementary Figure 3**). Transcripts encoding for transcription regulators of virulence, antibiotic resistance, metabolism, and membrane associated proteins were also observed to increase in their levels of expression (**Table 6**). Transcripts representative of nine genes were down-regulated under anaerobic conditions in presence of bile at both pH 7.5 and 5.5 (**Table 7** and **Supplementary Figure 4**). Fold changes of the transcript levels of genes associated with metabolism, translation, pathogenesis, and transcription were down-regulated (**Table 7**).

Changes in Transcript Levels in Response to Bile Under Acidic and Anaerobic Conditions

Transcript levels of 210 genes were up-regulated in response to bile at acidic pH under anaerobic conditions (**Table 8** and **Supplementary Figure 3**). Transcripts encoding for transcription factors, metabolism, replication and repair, cell signaling, protein folding, and pathogenesis were also found to be up-regulated. Additionally, transcripts representing 146 genes were down-regulated under anaerobic conditions with acidic bile (**Table 9** and **Supplementary Figure 4**), with these being primarily associated with metabolism, membrane transport, replication and repair, pathogenesis, and transcription factors.

DISCUSSION

Anaerobiosis Improves Survival of *L. monocytogenes* in Conditions Mimicking the Gastrointestinal Tract

Survival of *L. monocytogenes* strain F2365 was analyzed under conditions mimicking the GI tract. This strain was chosen as it

TABLE 4 | Transcript levels increased for select genes in response to anaerobiosis at pH 5.5.

Gene ID	Gene product	Transcript fold changes
Metabolism		
hemL LMOf2365_1574	Glutamate-1-semialdehyde-2,1-aminomutase	3.1
nrdD LMOf2365_0299	Anaerobic ribonucleoside-triphosphate reductase	3.1
LMOf2365_1386	Phosphate acetyl/butyryltransferase family protein	3.1
panD LMOf2365_1929	Aspartate 1-decarboxylase	3.1
LMOf2365_0434	Polysaccharide deacetylase family protein	3.1
pepQ LMOf2365_1600	Proline dipeptidase	3.1
ldh-2 LMOf2365_1553	L-lactate dehydrogenase	3.2
LMOf2365_2670	N-acetylmuramoyl-L-alanine amidase, family 4	3.3
LMOf2365_1275	Hydrolase, alpha/beta fold family	3.3
LMOf2365_0372	Transcriptional regulator, DeoR family	3.4
LMOf2365_2200	Putative lactoylglutathione lyase	3.4
LMOf2365_0846	Pyruvate flavodoxin/ferredoxin oxidoreductase	3.4
LMOf2365_0277	Glycosyl hydrolase, family 1	3.7
asnB LMOf2365_1687	Asparagine synthase (glutamine-hydrolyzing)	3.8
pfl-1 LMOf2365_1425	Formate acetyltransferase	3.8
LMOf2365_2673	Orn/Lys/Arg decarboxylase	3.9
LMOf2365_0330	Threonine aldolase family protein	4.1
mvaS LMOf2365_1434	Hydroxymethylglutaryl-CoA synthase	4.2
LMOf2365_1633	Putative glutamyl-aminopeptidase	4.3
LMOf2365_1642	Dipeptidase	4.3
LMOf2365_0603	Glycosyl hydrolase, family 1	4.4
LMOf2365_0550	Glycosyl hydrolase, family 4	4.6
pnp LMOf2365_134	Polyribonucleotide nucleotidyltransferase	4.6
Gpm LMOf2365_2238	Phosphoglycerate mutase	4.7
LMOf2365_1226	Putative peptidase	5.2
LMOf2365_2528	Putative fructose-bisphosphate aldolase	5.3
gap LMOf2365_2432	Glyceraldehyde-3-phosphate dehydrogenase, type I	5.4
LMOf2365_1083	Inositol monophosphatase family protein	5.5
LMOf2365_2199	Metallo-beta-lactamase family protein	5.6
LMOf2365_1400	Putative acylphosphatase	5.7
LMOf2365_1299	4-hydroxybenzoyl-CoA thioesterase family protein	6.2
Pyk LMOf2365_1592	Pyruvate kinase	6.7
ldh-1 LMOf2365_0221	L-lactate dehydrogenase	7.5
pflA LMOf2365_1426	Pyruvate formate-lyase activating enzyme	7.6
galU LMOf2365_1099	UTP-glucose-1-phosphate uridylyltransferase	7.7
LMOf2365_0582	CBS domain protein	8.5
LMOf2365_2144	Nitroreductase family protein	9.3
LMOf2365_0802	Putative acyl-carrier protein phosphodiesterase	9.4
ald LMOf2365_1601	Alanine dehydrogenase	11.9
manA LMOf2365_2143	Mannose-6-phosphate isomerase, class I	13.6
LMOf2365_1608	Putative inorganic polyphosphate/ATP-NAD kinase	13.6
LMOf2365_2308	Aminopeptidase C	13.9
pfl-2 LMOf2365_1946	Formate acetyltransferase	40.3
murI LMOf2365_1246	Glutamate racemase	68
Transcription factors		
LMOf2365_2140	Transcriptional regulator, DeoR family	3.1
argR LMOf2365_1384	Arginine repressor	3.2
LMOf2365_1526	DNA-binding response regulator	4.1
LMOf2365_1907	Iron-dependent repressor family protein	4.3
LMOf2365_0755	Transcriptional regulator, PadR family	4.6
LMOf2365_0480	Putative transcriptional regulator	4.8
LMOf2365_1986	Transcriptional regulator, Fur family	4.8
LMOf2365_0814	Transcriptional regulator, MarR family	7.8
LMOf2365_1707	Peroxide operon transcriptional regulator	8.6
Pathogenesis		
LMOf2365_1812	Internalin family protein	5.4
hly LMOf2365_0213	Listeriolysin O	10.2
Motility		
LMOf2365_1723	Methyl-accepting chemotaxis protein	4.4
DNA repair		
topA LMOf2365_1293	DNA topoisomerase I	3.3
nth LMOf2365_1923	Endonuclease III	3.5
exoA LMOf2365_1807	Exodeoxyribonuclease	4.2
LMOf2365_1643	MutT/nudix family protein	4.4
ung-2 LMOf2365_1236	Uracil-DNA glycosylase	5.3
Stress response		
LMOf2365_1997	Putative tellurite resistance protein	3.1
LMOf2365_0783	Glyoxalase family protein	3.4
LMOf2365_0963	Peroxide resistance protein Dpr	3.5
LMOf2365_2735	General stress protein 26	5.1
LMOf2365_1121	Glyoxalase family protein	5.2
Protein folding		
groEL LMOf2365_2099	Chaperone protein GroEL	4.0
atpB LMOf2365_2508	ATP synthase F0, A subunit	4.1

is a serotype 4b strain, which represents the serotype of a large portion of outbreak strains. F2365 was isolated from one of the deadliest outbreaks of *L. monocytogenes* (Linnan et al., 1988). F2365 has been sequenced (Nelson et al., 2004) and has been extensively studied for genomic analyses (Chatterjee et al., 2006; Liu and Ream, 2008; Payne et al., 2013), making it an ideal strain to analyze transcriptomic responses.

TABLE 5 | Transcript levels decreased for select genes in response to anaerobiosis at pH 5.5.

Gene ID	Gene product	Transcript fold changes
Metabolism		
pheA LMOf2365_1555	Prephenate dehydratase	−18.8
LMOf2365_2263	Putative arsenate reductase	−14.8
LMOf2365_1556	GTP-binding protein, GTP1/OBG family	−13.4
LMOf2365_0148	Ser/Thr protein phosphatase family protein	−13.2
LMOf2365_2831	Sucrose phosphorylase	−9.3
LMOf2365_0128	Lipase	−8.9
cah LMOf2365_0827	Carbonic anhydrase	−8.9
LMOf2365_2647	Galactitol PTS system EIIA component	−8.5
tkt-3 LMOf2365_2640	Transketolase	−6.2
arcA LMOf2365_0052	Arginine deiminase	−6.1
LMOf2365_2643	Alcohol dehydrogenase, zinc-dependent	−5.7
qoxA LMOf2365_0016	Cytochrome aa3-600 menaquinol oxidase subunit II, Oxidative phosphorylation	−5.5
gabD LMOf2365_0935	Succinate-semialdehyde dehydrogenase	−5.4
LMOf2365_2364	Ferredoxin/flavodoxin—NADP+ reductase	−5.3
LMOf2365_0209	UDP-N-acetylglucosamine pyrophosphorylase	−4.9
guaB LMOf2365_2746	Inosine-5′-monophosphate dehydrogenase	−4.3
LMOf2365_0566	Putative N-carbamoyl-L-amino acid amidohydrolase	−4.1
ctaB LMOf2365_2088	Heme o synthase	−4.1
prs-1 LMOf2365_0210	Ribose-phosphate pyrophosphokinase	−3.9
LMOf2365_1048	Metallo-beta-lactamase family protein	−3.6
LMOf2365_2576	Acetamidase/formamidase family protein	−3.4
LMOf2365_2824	Glycosyl transferase, family 65	−3.0
Transcription Factors		
ada, LMOf2365_0093	AraC family transcriptional regulator	−9.4
LMOf2365_0127	Transcriptional regulator, AraC family	−7.2
purr LMOf2365_0203	Pur operon transcriptional repressor	−4.3
LMOf2365_1683	Phosphosugar-binding transcriptional regulator, RpiR family	−4.2
LMOf2365_0023	Transcriptional regulator, GntR family	−4.0
LMOf2365_2467	Phosphate transport system protein PhoU	−4.0
LMOf2365_2017	LacI family transcriptional regulator	−3.3
LMOf2365_2224	ArsC family protein, regulatory protein spx	−3.3
LMOf2365_1010	Transcriptional regulator, MarR family	−3.1
Membrane Transport		
LMOf2365_1428	MFS transporter, ACDE family, multidrug resistance protein	−7.9
LMOf2365_2542	Peptide/nickel transport system substrate-binding protein; bacterial extracellular solute-binding protein, family 5	−7.7
LMOf2365_2575	Putative Mg2+ transporter-C (MgtC) family protein	−5.4
LMOf2365_0759	Methyl-accepting chemotaxis protein	−4.2
LMOf2365_0267	Sugar ABC transporter, sugar-binding protein	−4.0
LMOf2365_0167	Peptide/nickel transport system substrate-binding protein	−3.9
LMOf2365_2351	Multicomponent Na+ :H+ antiporter subunit A	−3.3
LMOf2365_0876	Sugar ABC transporter, sugar-binding protein	−3.1
LMOf2365_2732	ATP-binding cassette, subfamily B, bacterial AbcA/BmrA	−3.1
Pathogenesis		
LMOf2365_0128	Lipase	−8.9
inlE LMOf2365_0283	Internalin E	−6.7
LMOf2365_2467	Phosphate transport system protein PhoU	−4.0

Bile is made in the liver, stored in the gall bladder, and released to the duodenum upon ingestion. The environment in the gall bladder is anaerobic and neutral pH, while the duodenum is acidic and microaerophilic (Zheng et al., 2015). The alterations in oxygen availability within the GI tract are essential to developing the redox relationship between microbes and host (He et al., 1999; Espey, 2013). Therefore, we tested how oxygen influenced the survival of *L. monocytogenes* under either acidic (mimicking the duodenum) or neutral (mimicking the gall bladder) bile conditions.

Since variations in transcript levels were observed due to alterations in oxygen availability, we wanted to determine which genes were commonly expressed under anaerobiosis. Transcript levels of five genes were found to be up-regulated under exposure to anaerobic conditions regardless of whether the cultivation was conducted under either neutral or acidic pH (**Table 2**), though there were differential expressions between the two conditions. Transcripts common to both conditions included two membrane transporters *LMOf2365_2333* and *cadA* (*LMOf2365_0672*), two chaperones, and the stress response related gene *gadG* (*LMOf2365_2405*). CadA has been previously shown to be involved in formation of biofilms at 25°C by *L. monocytogenes* (Parsons et al., 2017). CadA also has been implicated in having roles in virulence and pathogenesis (Parsons et al., 2017). Therefore, it is possible that CadA is involved in stress response mechanisms related to anaerobic survival and that the formation of biofilms may be a critical component to survival. Previous studies have also shown that various stressors

TABLE 6 | Transcript levels increased for select genes in response to anaerobiosis at pH of 7.5 and 5.5.

Gene ID	Gene product	Transcript fold changes	
	Transcription factors	***pH 7.5***	***pH 5.5***
LMOf2365_0641	Transcriptional regulator, MarR family	6.5	13.7
prfA LMOf2365_0211	Listeriolysin regulatory protein	11.5	3.7
LMOf2365_1986	Fur family transcriptional regulator, ferric uptake regulator	12.7	18.8
glnR LMOf2365_1316	Transcriptional repressor GlnR	13.6	13.9
Metabolism			
LMOf2365_2358	Thioesterase family protein	4.2	6.4
LMOf2365_0884	ATP-dependent RNA helicase DeaD	4.4	3.1
LMOf2365_1433	Acetyl-CoA acetyltransferase	4.5	6.6
LMOf2365_1729	Deoxynucleoside kinase family protein	4.6	10.5
LMOf2365_1660	Muramoyltetrapeptide carboxypeptidase	5.1	4.4
cysK LMOf2365_0234	Cysteine synthase A	6.1	6.2
LMOf2365_1038	Putative PTS system, glucose-specific, IIA component	6.3	4.4
LMOf2365_2371	NifU family protein	6.9	27.1
Cah LMOf2365_0827	Carbonic anhydrase	7.1	7.2
LMOf2365_1419	Acetyltransferase, GNAT family	7.3	3.7
trxB LMOf2365_2451	Selenocompound metabolism	8.7	5.0
glnA LMOf2365_1317	Glutamine synthetase, type I	9.9	3.3
LMOf2365_2364	Pyridine nucleotide-disulfide oxidoreductase family protein	10.1	5.1
LMOf2365_0861	Putative endoribonuclease L-PSP	10.6	4.2
LMOf2365_0391	Messenger RNA biogenesis	10.7	7.8
divIVA LMOf2365_2045	Cell division protein DivIVA	14.1	5.1
LMOf2365_0997	Acetyltransferase, GNAT family	14.5	7.1
alsS LMOf2365_2030	Acetolactate synthase	16.5	20.8
LMOf2365_0640	Flavodoxin-like fold domain protein	35.9	37.4
Membrane transport			
LMOf2365_0761	Putative membrane protein	4.0	6.0
LMOf2365_2229	Oligopeptide ABC transporter, oligopeptide-binding protein	4.3	3.6
LMOf2365_1443	Transporter, NRAMP family	5.7	6.3
LMOf2365_0168	Zinc ABC transporter, zinc-binding protein	6.9	52.5
LMOf2365_1435	Putative transporter	8.2	7.4
LMOf2365_1012	Membrane protein, TerC family	9.6	257.7
LMOf2365_2330	Putative membrane protein	18.9	46.3

TABLE 7 | Transcript levels decreased for select genes in response to anaerobiosis at pH 7.5 and 5.5.

Gene ID	Gene product	Transcript fold changes	
		pH 7.5	**pH 5.5**
Metabolism			
adhE LMOf2365_1656	Acetaldehyde dehydrogenase/alcohol dehydrogenase	−48.1	−71.2
LMOf2365_0250	Serine O-acetyltransferase	−5.8	−4.4
murE LMOf2365_2070	UDP-N-acetylmuramoyl-L-alanyl-D-glutamate–2,6-diaminopimelate ligase	−5.7	−4.5
Translation			
LMOf2365_2879	tRNA-Glu	−25.3	−4.8
LMOf2365_2913	tRNA Leu	−11.5	−4.1
hly LMOf2365_0213	Listeriolysin O	−70.0	−3.7
Transcription factors			
LMOf2365_2205	Sigma-54 dependent transcriptional regulator	−10.7	−5.5

(i.e., heat shock, nutrient limitation, acidic condition, etc.) cause an increase in the expression of chaperones (Wright et al., 2016). Indeed, the data showed an increase in the transcript levels of two chaperones (*dnaK* and *dnaJ*) under anaerobic conditions at both pH 7.5 and 5.5. Therefore, it is possible that *L. monocytogenes* uses molecular chaperones to combat anaerobic stress, which in

turn assists with phagocytosis. The *gadG* encodes for an amino acid antiporter that is part of the glutamate decarboxylase system, which is a defense mechanism up-regulated by *L. monocytogenes* under acid stress and anaerobiosis. This system alleviates the acidification of the cytoplasm by consuming a proton (Cotter et al., 2001; Jydegaard-Axelsen et al., 2004; Paudyal et al., 2020). The fact that this transcript was up-regulated in response to anaerobic conditions suggests that there may be overlapping functions of the GAD system in both acid resistance and anaerobiosis. The transcript level of the *LMOf2365_2333* gene was increased by nearly 9-fold in comparison to acidic pH. There is a possibility that this amino acid anti-transporter may function with *gadG* in response to bile. This should be further explored in future studies.

Transcript levels of eighteen genes were down-regulated under anaerobic conditions regardless of the pH, including histidine kinase, metabolic genes, a universal stress response gene, and genes coding for hypothetical proteins. As histidine kinases are involved in two-component systems, it is possible that suppression of this sensor is responsible for the response to oxygen availability. One of the metabolic genes, the phosphoglycerate mutase, has been shown in *Bacillus subtilis* to be responsible for the control of the two-component system required for sensing and responding to aerobic and anaerobic respiration (Nakano et al., 1999). The fact that the transcript level of this gene was down-regulated suggests that the accumulation of the product 1,3-bisphosphoglycerate, which is the intermediate in the reaction catalyzed by phosphoglycerate mutase, might impact the regulation of the histidine kinase *LMOf2365_2554*. The impact of this precursor on regulation of two-component systems needs to be explored in further detail. The transcript level of the gene *acpP* was also down-regulated. This gene product is involved in biosynthesis of fatty acids as a lipid transporter. This gene has been found to be differentially regulated under anaerobic conditions in many other bacteria, including *Escherichia coli* and *Neisseria gonorrhoeae* (Isabella and Clark, 2011). This indicates that the regulation of the fatty acid synthesis is necessary for the adaptability to anaerobiosis.

Differential Transcript Levels in Response to Anaerobic Acidic Conditions

An increase in the transcript levels of *nrdD* (*LMOf2365_0299*), which is an anaerobic ribonucleoside-triphosphate reductase that catalyzes the synthesis of dNTPs required for DNA replication, was observed under anaerobic conditions at acidic pH. NrdD is an essential enzyme required by *L. monocytogenes* and other GI pathogens, such as *E. coli*, to survive under anaerobic conditions (Garriga et al., 1996; Ofer et al., 2011). Since our study showed acidic conditions influence the up-regulation of this gene under anaerobic conditions, there is a possibility that this enzyme is involved in growth under acidic conditions. This may be required to stabilize the redox potential of the cell under acidic conditions. Ribonucleotide reductases have been explored as potential biomedical targets for bacterial infections (Torrents, 2014). Since the ribonucleotide reductase was up-regulated under anaerobic acidic conditions, it will be necessary for future studies to analyze the activity of antibacterial compounds under these conditions to effectively target the protein expressed.

Transcript levels of genes coding for a glycosyl hydrolases, which are involved in hydrolyzing the glycosidic linkages in sugars, were also up-regulated. Certain glycosyl hydrolases have been previously identified as virulence factors in gram positive pathogenic bacteria, including *Streptococcus pneumoniae* (Niu et al., 2013). Glycosyl hydrolase PssZ has been observed to degrade extracellular polymeric substance, thereby disrupting biofilm formation by *L. monocytogenes* (Wu et al., 2019). *L. monocytogenes*, which is an intracellular bacterium, may synthesize glycosyl hydrolases upon exposure to acidic pH under anaerobic conditions, which thereby hinders formation of biofilms and facilitates the bacterium's entry into the host cells.

One of the virulence factors of *L. monocytogenes* is metalloproteases. Few such proteases were identified to have an increase in transcript levels at pH 5.5 in anaerobic conditions, including the aminopeptidase (*LMOf2365_2308*) (**Table 4**). It has been shown that the bacterial burden of *L. monocytogenes* EGDe strain in host cells decreased significantly when the aminopeptidase T of family M29 was deleted (Cheng et al., 2015). Thus, at anaerobic conditions under acidic pH, aminopeptidases may be up-regulated and function as virulence factors.

GalU (*LMOf2365_1099*), UTP-glucose-1-phosphate uridyltransferase, which catalyzes cell wall teichoic acid glycosylation, had an increase in transcript levels under anaerobic conditions at pH 5.5 (**Table 4**; Kuenemann et al., 2018). *In silico* design of GalU inhibitors attenuated virulence of *L. monocytogenes*, proving GalU to be an instrumental part in virulence pathways (Kuenemann et al., 2018). Various transcription factors were up-regulated under anaerobic conditions at pH 5.5 (**Table 4**), including the *fur* regulator that controls virulence of various pathogenic bacteria. We also observed that transcripts coding for virulence genes, such as listeriolysin O and internalin family proteins, were also up-regulated under these conditions. The transcript level of a methyl accepting chemotaxis protein was also increased. In *L. monocytogenes* chemotaxis genes *cheA* and *cheY* have been shown to facilitate to adhesion and thereby invasion into the host epithelial cells. As *L. monocytogenes* is an intracellular pathogen, it may be possible that along with the CheA and CheY system, it is using the methyl accepting chemotaxis proteins to attach to epithelial cells under anaerobic conditions at pH 5.5 (Dons et al., 2004).

Internalins A and B are required by *L. monocytogenes* for facilitating entry inside host cells. Transcript levels for genes encoding internalin proteins were found to be up-regulated under the acidic environment in absence of oxygen. Interestingly, the transcript level of *inlE* (*LMOf2365_0283*), which is a gene coding for the secreted protein Internalin E, was decreased. Internalins A and B are involved in adhesion and invasion by *Listeria*, but Internalin E is not involved in invasion (Dramsi et al., 1997). This indicates anaerobiosis influences the invasive potential of *L. monocytogenes*. The impact of anaerobiosis on invasion has been shown *in vitro* and *in vivo*, but the exact

TABLE 8 | Transcript levels increased for select genes in response to bile in anaerobic conditions at pH 5.5.

Gene ID	Gene product	Transcript levels
Metabolism		
LMOf2365_0638	Rhodanese-like domain protein	3.4
LMOf2365_0686	Serine/threonine protein phosphatase family protein	4.1
mvaS LMOf2365_1434	Hydroxymethylglutaryl-CoA synthase	4.8
LMOf2365_1406	Putative pyrroline-5-carboxylate reductase	38
Pathogenesis		
inlE LMOf2365_0283	Internalin E	3.6
LMOf2365_0508	Putative antigen	4.4
LMOf2365_2725	CBS domain protein	5.2
hlY-III LMOf2365_1893	Hemolysin III	6.2
LMOf2365_0726	Flagellin	29.2
LMOf2365_1503	DNA-binding protein, ComEA family	130.5
Cell Signaling		
LMOf2365_0626	Cyclic nucleotide-binding protein	6.8
Protein Folding		
LMOf2365_1018	ATP-dependent Clp protease, ATP-binding subunitE	3.9
clpP LMOf2365_2441	ATP-dependent Clp protease, protease subunit	5.2
trx-1 LMOf2365_1242	Thioredoxin	6.2
clpP-1 LMOf2365_1146	ATP-dependent Clp protease, proteolytic subunit P	25.0
Membrane Transport		
LMOf2365_0153	Oligopeptide ABC transporter	3.0
LMOf2365_0288	Putative transporter	3.1
LMOf2365_2265	CBS domain protein	3.1
LMOf2365_0295	Competence protein ComEC/Rec2-related protein	3.3
LMOf2365_1088	Cell division protein, FtsW/RodA/SpoVE family	3.3
LMOf2365_1219	Putative membrane protein	3.4
acsA LMOf2365_2700	Acetyl-coenzyme A synthetase	3.6
LMOf2365_2554	Sensor histidine kinase	3.7
LMOf2365_2835	Major facilitator family transporter	3.7
LMOf2365_2647	PTS system, IIA component	3.8
zurM-2 LMOf2365_1465	Zinc ABC transporter, permease protein	4.0
LMOf2365_0622	Formate/nitrite transporter family protein	4.0
LMOf2365_1002	Drug resistance transporter, EmrB/QacA family	4.7
LMOf2365_0930	Putative membrane protein	5.0
LMOf2365_0967	Putative transporter	5.1
LMOf2365_0810	Putative membrane protein	5.6
LMOf2365_1721	Cation efflux family protein	6.4
LMOf2365_0588	Magnesium transporter, CorA family	6.5
LMOf2365_0701	ABC transporter, ATP-binding protein	7.1
lmrB-2 LMOf2365_2560	Lincomycin resistance protein LmrB	7.3
LMOf2365_1695	Putative laminin-binding surface protein	8.2
LMOf2365_2119	MATE efflux family protein	8.5
LMOf2365_2222	CoiA-like family protein	10.6
LMOf2365_0570	ABC transporter, substrate-binding protein	12.0
LMOf2365_0812	RarD protein	13.6
LMOf2365_0941	ABC transporter, ATP-binding protein	18.1
LMOf2365_1011	MATE efflux family protein	19.1
LMOf2365_0167	Bacterial extracellular solute-binding protein	20.4
LMOf2365_1502	Zinc-binding, ComEB family protein	21.8
LMOf2365_1428	Major facilitator family transporter	25.6
LMOf2365_1000	ABC transporter, ATP-binding protein	46.6
LMOf2365_0034	Putative membrane protein	60.2
Replication and Repair		
LMOf2365_0196	Deoxyribonuclease, TatD family	3.1
LMOf2365_1533	ATPase, AAA family domain protein	3.3
LMOf2365_1998	Putative DNA-damage-inducible protein P	4.2
LMOf2365_0949	Putative DNA-3-methyladenine glycosylase	4.7
rnhA LMOf2365_1909	Ribonuclease HI	4.9
LMOf2365_2784	Replication and repair	5.9
dbpA LMOf2365_1260	ATP-dependent RNA helicase DbpA	8.4
recA LMOf2365_1417	Recombination protein RecA	9.2
LMOf2365_0863	Excinuclease ABC subunit C domain protein	11.4
LMOf2365_2339	MutT/nudix family protein	11.6
LMOf2365_0849	Putative transposase OrfA, IS3 family	12.7
dnaG LMOf2365_1474	DNA primase	18.7
Transcription Factors		
LMOf2365_1427	Transcriptional regulator, PadR family	3.3
LMOf2365_1515	Transcription elongation factor GreA	3.4
nusG LMOf2365_0258	Transcription antitermination factor NusG	3.4
LMOf2365_2467	Phosphate transport system protein PhoU	3.4
LMOf2365_2223	MecA family protein	3.6
LMOf2365_0023	Transcriptional regulator, GntR family	3.6
LMOf2365_0576	Putative DNA-binding transcriptional regulator	3.6
LMOf2365_2337	Transcriptional regulator, DeoR family	3.7
ctsR LMOf2365_0241	Transcriptional regulator CtsR	3.8
LMOf2365_0119	Transcriptional regulator, ArsR family	4.0
LMOf2365_0446	Transcriptional regulator, LysR family	4.0
LMOf2365_2017	Transcriptional regulator, LacI family	4.1
LMOf2365_2841	Transcriptional regulator, AraC family	4.4
LMOf2365_1051	Transcriptional regulator, LacI family	4.4
LMOf2365_0906	Conserved hypothetical protein	4.8
LMOf2365_0794	ROK family protein	5.1
LMOf2365_2466	Transcriptional regulator, ArsR family	5.8
LMOf2365_2669	Transcriptional regulator, TetR family	5.8
LMOf2365_0266	Transcriptional regulator, DegA family	6.1
LMOf2365_0665	Rrf2 family protein	6.5
LMOf2365_0841	Transcriptional regulator, MerR family	7.7
LMOf2365_0394	Transcriptional regulator, DeoR family	9.5
LMOf2365_1894	DeoR family transcriptional regulator, catabolite repression regulator	11.5
LMOf2365_2224	ArsC family protein	11.7
LMOf2365_0940	PRD/PTS system IIA 2 domain protein	12.4
LMOf2365_2322	LysR family transcriptional regulator, regulator of the ytmI operon	13.1
LMOf2365_0435	DNA-binding protein	14.2
LMOf2365_2799	DNA-binding protein	14.7

(Continued)

TABLE 8 | (Continued)

Gene ID	Gene product	Transcript levels
LMOf2365_1010	Transcriptional regulator, MarR family	18.4
LMOf2365_2233	Transcriptional regulator, MarR family	19.1
LMOf2365_0755	Transcriptional regulator, PadR family	19.5
LMOf2365_0387	GntR family transcriptional regulator	25.7
LMOf2365_0326	DNA-binding protein	41.2

mechanism of such interplay has not been well characterized (Bo Andersen et al., 2007; Harris et al., 2019).

Differential Transcript Levels in Response to Bile Under Anaerobic Conditions

Previous studies have shown that following ingestion of *L. monocytogenes* into host systems, the *prfA* regulon is up-regulated (Scortti et al., 2007). *prfA*, the positive regulatory factor A, is a transcription factor that regulates major virulence factors of *L. monocytogenes*. *prfA* regulates listeriolysin O, phospholipase C and metalloproteases, all of which were up-regulated in anaerobiosis in presence of bile (**Table 6**). Following bile exposure, the transcript levels of the virulence regulator *prfA* were decreased (Boonmee et al., 2019); however these data show that under anaerobic conditions in presence of bile, *prfA* is up-regulated independent of pH. We have also observed that *L. monocytogenes* survives bile better under anaerobic conditions (**Figure 2**).

Previous transcriptomics studies in *L. monocytogenes* 10403S (Boonmee et al., 2019) have found that following exposure to bile, the house keeping sigma factor σ^A has a significant role in survival. *marR* [multiple antibiotic resistance regulator (*LMOf2365_0641*)] is a transcriptional regulator that was up-regulated in response to bile in anaerobic conditions regardless of the pH tested (**Table 6**). In pathogens such as *Salmonella* and *Staphylococcus*, *marR* homologs *slyA* and *sarZ* regulate virulence gene expression. *marR* homologs have also been found to regulate genes involved in stress response, degradation or efflux of harmful substances and metabolic pathways (Grove, 2013). Bile exposure under anaerobic environments may trigger the up-regulation of *marR* to export bile out of the bacterial cell, thereby contributing to the bile resistance of *L. monocytogenes* along with other factors. The role of *marR* in bile resistance needs to be further explored.

Glutamine synthetase catalyzes the condensation of ammonia and glutamate to form glutamine. The transcript level of the glutamine synthetase repressor, *glnR* (*LMOf2365_1316*) was increased following exposure to bile in anaerobic conditions. It is a central nitrogen metabolism regulator which is activated in presence of glutamine. When glutamine is in excess, GlnR represses the synthesis of glutamine synthetase (Kaspar et al., 2014). Another probable transcriptional regulator (*tnrA* or *codY*) represses glutamine synthetase and its activation have been found to be essential in replication *Listeria* intracellularly (Kaspar et al., 2014). Interestingly glutamine synthetase was also up-regulated

TABLE 9 | Transcript levels decreased for select genes in response to bile in anaerobic conditions at pH 5.5.

Gene ID	Gene name	Transcript levels
Metabolism		
LMOf2365_2610	Putative lipoprotein	−29.9
LMOf2365_0802	FMN-dependent NADH-azoreductase	−21.6
LMOf2365_1226	Putative peptidase	−18.2
LMOf2365_0565	6-phospho-beta-glucosidase	−18.2
pflA LMOf2365_1426	Pyruvate formate lyase activating enzyme	−11.1
LMOf2365_1975	Riboflavin transporter	−10.2
pyrH LMOf2365_1330	Uridylate kinase	−8.7
LMOf2365_1597	Bifunctional oligoribonuclease and PAP phosphatase NrnA	−8.5
LMOf2365_0277	Glycosyl hydrolase, family 1	−8.5
LMOf2365_0776	Hydrolase, alpha/beta fold family	−8.2
pfl-2 LMOf2365_1946	Formate C-acetyltransferase	−8.2
rplS LMOf2365_1814	Large subunit ribosomal protein L19	−7.7
pepQ LMOf2365_1600	Proline dipeptidase	−7.6
cadA LMOf2365_0672	Zn2+/Cd2+-exporting ATPase	−7.6
LMOf2365_2666	Cell division protein, FtsW/RodA/SpoVE family	−7.3
LMOf2365_0021	Glycosyl hydrolase, family 1	−6.9
LMOf2365_2146	Hydrogen peroxide-dependent heme synthase	−6.5
glmS LMOf2365_0762	Glutamine—fructose-6-phosphate transaminase	−6.3
LMOf2365_1093	N-acetylmuramoyl-L-alanine amidase	−6.3
LMOf2365_0057	Accessory gene regulator B	−5.9
LMOf2365_1386	Phosphate butyryltransferase	−5.7
thiI LMOf2365_1614	tRNA uracil 4-sulfurtransferase	−5.7
galU LMOf2365_1099	UTP–glucose-1-phosphate uridylyltransferase	−5.6
LMOf2365_1702	Methionine synthase/methylenetetrahydrofolate reductase (NADPH)	−5.6
LMOf2365_2609	FAD:protein FMN transferase	−5.6
eno LMOf2365_2428	Enolase	−5.5
LMOf2365_2670	N-acetylmuramoyl-L-alanine amidase, family 4	−5.3
fabI LMOf2365_0990	Enoyl-[acyl-carrier-protein] reductase I	−5.2
LMOf2365_1880	Copper chaperone; heavy metal binding protein	−5.1
LMOf2365_2711	PhnB protein	−5.1
LMOf2365_2673	Orn/Lys/Arg decarboxylase	−5.1
LMOf2365_1368	Rhodanese-like domain protein	−5.0
LMOf2365_2510	UDP-N-acetylglucosamine 2-epimerase	−4.8
mraY LMOf2365_2069	Phospho-N-acetylmuramoyl-pentapeptide-transferase	−4.7
purA LMOf2365_0065	Adenylosuccinate synthase	−4.7
ald LMOf2365_1601	Alanine dehydrogenase	−4.7
plcA LMOf2365_0212	1-phosphatidylinositol phosphodiesterase	−4.6
menE LMOf2365_1696	O-succinylbenzoate–CoA ligase	−4.6
murC LMOf2365_1627	UDP-N-acetylmuramate–alanine ligase	−4.5
LMOf2365_2743	Hydrolase, CocE/NonD family	−4.4
gpmA LMOf2365_2429	2,3-bisphosphoglycerate-independent phosphoglycerate mutase	−4.4
LMOf2365_0434	Peptidoglycan-N-acetylglucosamine deacetylase	−4.1

(Continued)

TABLE 9 | (Continued)

Gene ID	Gene name	Transcript levels
tmk LMOf2365_2672	Thymidylate kinase	−4.1
LMOf2365_1643	8-oxo-dGTP diphosphatase	−4.1
LMOf2365_2133	Pyridoxal 5′-phosphate synthase pdxS subunit	−3.9
pyk LMOf2365_1592	Pyruvate kinase	−3.9
alaS LMOf2365_1523	Alanyl-tRNA synthetase	−3.9
fhs LMOf2365_1906	Formate–tetrahydrofolate ligase	−3.9
LMOf2365_1033	N-acetyldiaminopimelate deacetylase	−3.8
LMOf2365_0872	D-alanine-D-alanine ligase	−3.8
LMOf2365_0987	Putative GTP pyrophosphokinase	−3.8
LMOf2365_1299	Acyl-CoA thioester hydrolase	−3.8
LMOf2365_1512	Peptidase, M3 family	−3.7
pfl-1 LMOf2365_1425	Formate C-acetyltransferase	−3.7
LMOf2365_2144	Nitroreductase family protein	−3.6
folA LMOf2365_1903	Dihydrofolate reductase	−3.6
LMOf2365_1371	Xaa-Pro aminopeptidase	−3.6
upp LMOf2365_2511	Uracil phosphoribosyltransferase	−3.5
uppS LMOf2365_133	Undecaprenyl diphosphate synthase	−3.5
LMOf2365_0239	Dihydrouridine synthase family protein	−3.5
LMOf2365_1633	Putative glutamyl-aminopeptidase	−3.4
LMOf2365_1476	[pyruvate, water dikinase]-phosphate phosphotransferase	−3.4
LMOf2365_0293	Acetyltransferase, GNAT family	−3.4
LMOf2365_1691	L-lactate dehydrogenase	−3.3
LMOf2365_0101	Oxidoreductase, aldo/keto reductase family	−−3.3
LMOf2365_1644	ADP-dependent NAD(P)H-hydrate dehydratase	−3.3
LMOf2365_0846	Pyruvate-ferredoxin/flavodoxin oxidoreductase	−3.3
LMOf2365_1915	Carboxypeptidase Taq	−3.3
hemE LMOf2365_2245	Uroporphyrinogen decarboxylase	−3.3
nrdD LMOf2365_0299	Ribonucleoside-triphosphate reductase	−3.3
sdhB LMOf2365_1841	L-serine dehydratase	−3.3
LMOf2365_2207	Oxidoreductase, short-chain dehydrogenase/reductase family	−3.2
LMOf2365_2514	L-threonylcarbamoyladenylate synthase	−3.2
pepT LMOf2365_1805	Tripeptide aminopeptidase	−3.1
LMOf2365_1048	Ribonuclease J	−3.1
mpl LMOf2365_0214	Zinc metalloproteinase	−3.1
LMOf2365_0488	Undecaprenyl diphosphate synthase	−3.1
LMOf2365_2308	Bleomycin hydrolase	−3.1
manA LMOf2365_2143	Mannose-6-phosphate isomerase, class I	−3.0
ftsX LMOf2365_2479	Cell division ABC transporter, permease protein FtsX	−3.0
gap LMOf2365_2432	Glyceraldehyde 3-phosphate dehydrogenase	−3.0
Pathogenesis		
plcB LMOf2365_0216	Phospholipase C	−10.0
LMOf2365_1812	Internalin family protein	−6.1
Replication and repair		
dnaE LMOf2365_1596	DNA polymerase III subunit alpha	−4.9
LMOf2365_1628	DNA segregation ATPase FtsK/SpoIIIE, S-DNA-T family	−4.3
ligA LMOf2365_1783	DNA ligase, NAD-dependent	−3.2
recG LMOf2365_1839	ATP-dependent DNA helicase RecG	−3.0
Transcription factor		
LMOf2365_2335	Transcriptional regulator, RofA family	−8.6
argR LMOf2365_1384	Arginine repressor	−4.4
LMOf2365_2715	Transcriptional regulator, MerR family	−3.4
LMOf2365_2780	DNA-binding protein	−3.2
Membrane transport		
LMOf2365_2388	D-methionine transport system substrate-binding protein	−9.1
LMOf2365_0606	Putative membrane protein	−8.4
Ffh LMOf2365_1828	Signal recognition particle subunit SRP54	−7.3
LMOf2365_2553	Putative ABC transport system permease protein	−6.3
ptsI LMOf2365_1024	Phosphoenolpyruvate-protein phosphotransferase	−5.9
LMOf2365_0803	D-serine/D-alanine/glycine transporter	−5.8
agrC LMOf2365_0059	Two-component system, LytTR family, sensor histidine kinase AgrC	−5.1
LMOf2365_0673	Putative membrane protein	−4.4
cydD LMOf2365_2695	ATP-binding cassette, subfamily C, bacterial CydC	−4.3
LMOf2365_1034	Moderate conductance mechanosensitive channel	−4.3
prf1 LMOf2365_2516	Peptide chain release factor 1	−4.2
ldh-1 LMOf2365_0221	L-lactate dehydrogenase	−4.2
LMOf2365_2148	ABC transporter, permease protein	−4.0
LMOf2365_1450	ABC transporter, ATP-binding protein	−3.8
LMOf2365_1994	ABC-2 type transport system ATP-binding protein	−3.8
LMOf2365_1264	Putative transporter	−3.3
LMOf2365_2323	Monovalent cation/hydrogen antiporter	−3.2
LMOf2365_0845	Na/Pi-cotransporter family protein	−3.2
LMOf2365_1091	Teichoic acid transport system permease protein	−3.1
LMOf2365_2844	YidC/Oxa1 family membrane protein insertase	−3.0
LMOf2365_0317	Putative membrane protein	−3.0
Translation		
tsf LMOf2365_1678	Elongation factor Ts	−11.4
rpsB LMOf2365_1679	Small subunit ribosomal protein S2	−5.4
valS LMOf2365_1573	Valyl-tRNA synthetase	−4.1
gatB MOf2365_1779	Aspartyl-tRNA(Asn)/glutamyl-tRNA(Gln) amidotransferase subunit B	−4.1
efp LMOf2365_1372	Translation elongation factor P	−3.4
thrS LMOf2365_1580	Threonyl-tRNA synthetase	−3.1
infA LMOf2365_2583	Translation initiation factor IF-1	−3.1

under the same conditions, which indicates the possibility of a feedback loop.

Metalloenzyme carbonic acid catalyzes hydration of carbon dioxide into bicarbonate and proton (Supuran, 2016). The infection cycle of *Legionella* has similarities with that of *L. monocytogenes*, such as invasion and escaping the phagosome. *Legionella* has been shown to evade the destruction by maintaining neutral pH (Supuran, 2016). One of the enzymes involved in regulating the pH is carbonic anhydrase; the transcript level of carbonic anhydrase increased under anaerobic

conditions in the presence of bile in *L. monocytogenes* (**Table 6**). This could indicate that environmental conditions mimicking parts of intestine can contribute to *Listeria's* pathogenic potential. Interestingly, the transcript level of this gene was down-regulated under acidic conditions (**Table 5**), suggesting that the influence of bile is important to the expression of this gene.

Transcript levels representative of an uncharacterized membrane protein *LMOf2365_1012* that belongs to the TerC family was up-regulated following exposure to bile in anaerobic conditions (**Table 6**). In *B. subtilis*, TerC has been found to confer manganese resistance (Paruthiyil et al., 2020). In *Streptococcus*, manganese homeostasis is linked to oxidative stress as well as virulence (Turner et al., 2015). It is possible that TerC is linked with manganese homeostasis and therefore virulence in the presence of bile under anaerobic conditions. Transcripts coding for several other membrane transporters were also increased in their levels under the anaerobic environment in response to bile. The zinc ABC transporter has been shown to have a role in virulence of *L. monocytogenes* in a mouse infection model (Corbett et al., 2012). Thus, bile exposure in absence of oxygen probably impacts uptake of zinc by the bacteria thereby impacting the virulence. NRAMP, which functions as a metal ion transporter on membranes, was up-regulated (Nevo and Nelson, 2006).

The transcript level of the oligopeptide ABC transporter, which is an oligopeptide binding protein that helps the bacteria survive intracellularly, was increased (Slamti and Lereclus, 2019). It is the substrate binding component or receptor of an ABC type oligopeptide transport system that binds extracellular peptides, relays it to the membrane component of the system and inside the bacterial cell afterward. Gram positive bacteria such as *Listeria*, *Streptococcus*, and *Enterococcus*, use peptides to sense and respond to environmental changes. The gene *oppA*, which encodes for an oligopeptide binding protein, has been found to be required for invasion (Borezee et al., 2000). Thus, the oligopeptide ABC transporter observed in our study could be responsible for intracellular survival of bacteria in presence of bile under anaerobic conditions.

Interestingly, there was a decrease in the transcript levels of *hly* (*LMOf2365_0213*), which encodes for listeriolysin O, at both pH 7.5 and 5.5 following exposure to bile under anaerobic conditions. This was different than what was observed under anaerobiosis at pH 5.5 alone, as *hly* (LMOf2365_0213) was up-regulated in these conditions (**Table 4**). This suggests that bile has an important role in regulating the invasiveness of *L. monocytogenes*. This correlates well with previous studies that have shown that *L. monocytogenes* remains extracellular in the gall bladder, which has high concentrations of bile (Hardy et al., 2004; Dowd et al., 2011).

Differential Transcript Levels in Response to Bile Under Acidic and Anaerobic Conditions

There was an increase in transcript levels for the myosin cross reactive antigen (McrA) (*LMOF2365_0508*; **Table 8**). Although its function in *L. monocytogenes* is yet unknown, in *Streptococcus pyogenes* McrA is a fatty acid double bond hydratase that adds water to double bonds of fatty acids. Upon deletion of this gene, decreased oleic acid resistance and reduced adherence and internalization in the host cell was observed in *S. pyogenes* (Volkov et al., 2010). Conditions encountered within the duodenum may directly or indirectly contribute to up-regulation of *mcrA*, which may regulate the pathogen's resistance to bile.

Internalin E and hemolysin III are both virulence factors responsible for internalization and invasion for *L. monocytogenes*. Both had an increase in transcript levels, indicating that bile exposure at acidic and anaerobic conditions, which mimics the duodenum, is conducive to the pathogenesis of the bacteria.

The transcript level of the LPXTG-motif cell wall anchor domain (*LMOF2365_1144*) was also up-regulated. In the *L. monocytogenes* EGDe strain, it has been shown that a LPXTG protein encoded by the *Listeria* mucin binding invasion A gene, or *lmiA*, has roles in promoting bacterial adhesion and entry into the host cell (Mariscotti et al., 2014). MucBP domain present in LPXTG was observed to bind to mucin. Thus, up-regulation of LPXTG gene under conditions mimicking the duodenum indicates that these conditions may facilitate invasion of host cells by the bacteria.

The level of transcripts representing flagellin also increased. It has been shown that flagellin helps in motility soon after ingestion *in vivo* (O'Neil and Marquis, 2006) and invasion (Dons et al., 2004). A previous study has also observed up-regulation of motility under exposure to bile at pH 5.5 (Guariglia-Oropeza et al., 2018). The fact that expression increased in conditions that would be encountered soon after ingestion suggests that the flagellin are important for the motility of the bacteria to the location in the GI tract where they will invade the intestinal lining.

The transcript level of the histidine kinase *LMOf2365_2554* was also up-regulated under conditions mimicking the duodenum. Histidine kinase is the signal receiver a two-component regulatory system. Its counterpart in the system is the response regulator (Chang and Stewart, 1998; Stock et al., 2000; West and Stock, 2001; Krell et al., 2010). Response regulators in *L. monocytogenes* have been proven to have roles in virulence and pathogenesis. Sensor histidine kinase, ChiS, regulates the chitin utilization pathway required by *Vibrio cholerae*, which is needed to survive in aquatic environments. Chourashi et al. (2016) observed that ChiS has an important role in adherence and intracellular survival of *V. cholerae* in HT-29 cell cultures. They also showed that the sensor histidine kinase ChiS was activated in the presence of intestinal mucin (Chourashi et al., 2016). In the case of *L. monocytogenes*, it could be possible that the conditions in the duodenum are favorable for activation of the sensor histidine kinase, which could in turn relay information that would result in the activation of transcription factors responsible for adhesion and invasion.

Transcript levels representative of replication and repair genes were also up-regulated. In *L. monocytogenes* strain EGDe, RecA has been shown to have roles in bile and acid resistance, as well as in adhesion and invasion to Caco-2 cell cultures (van der Veen and Abee, 2011). Our data indicate that in the pathogenic strain F2365, RecA has the similar role of bile and acid

resistance. In our study, we have also found that under anaerobic conditions (along with bile and acidic) the transcript level of *recA* changed, indicating absence of oxygen may have impact on activation of RecA.

The transcript level for a gene encoding for the transcriptional regulator *padR* was up-regulated (**Table 8**). In *L. monocytogenes* EGDe, LftR, which is a PadR like transcriptional regulator, has been shown to influence invasion of human host cells (Kaval et al., 2015). It is already known that *Listeria* uses internalin proteins for adhering and internalizing into the cell. Kaval et al. (2015) found that LftR, which is an uncharacterized protein, is required for invasion.

Transcript level of the gene encoding for *ctsR*, (LMOf2365_0241) a class III stress gene repressor that negatively regulates *clp*, was up-regulated under these conditions (**Table 8**). CtsR has been shown to be required for virulence in mice. PrfA which regulates many virulence genes of *L. monocytogenes* has been shown to down-regulate ClpC production (Karatzas et al., 2003). Although Karatzas et al. (2003) could not find any relationship between *clp* and *prfA*, there is still a possibility that there is a connection between the regulation of Clp by CtsR under anaerobic conditions in exposure to bile at acidic pH (Cui et al., 2018).

The transcript level of the transcription elongation factor *greA* (*LMOf2365_1515*) also increased under anaerobic conditions with acidic bile. GreA has been found to have roles in affecting functions of virulence gene expression in the pathogen *Francisella tularensis* subsp. Novicida (Cui et al., 2018). In *F. tularensis*, GreA was found to be required for invasion and intracellular growth of bacteria. Cui et al. (2018) also observed suppression of virulence of the *greA* mutant in mouse model. Transcriptomics analysis of the *greA* mutant revealed down-regulation of various genes responsible for virulence. Thus, with respect to our work, conditions in the duodenum are favorable for induction of the transcription elongation factor *greA*, which may in turn regulate genes responsible for invasion and multiplication of *L. monocytogenes*.

This study indicates that not only one stressor, but combinations of different stressors impact the transcription of various virulence genes. Transcriptomic and phenotypic studies in absence of these genes under mimicking physiological condition could give us an insight into this mechanism. A better understanding of how these biological processes help the survival of *L. monocytogenes* will lead us to understand how the physiological conditions contribute to the pathogenesis.

MATERIALS AND METHODS

Bacterial Strain and Culture Conditions

Listeria monocytogenes str. 4b F2365 was used for this study. Overnight cultures of *L. monocytogenes* str. 4b F2365 were grown at 37°C aerobically in Brain Heart Infusion (BHI) media at pH 7.5. Next day, inoculum (1:100) from the overnight culture was used to grow the cells to mid exponential phase in fresh BHI media (OD_{600} = 0.3 to 0.5) under either aerobic or anaerobic conditions in 5 mL aliquots. Anaerobic culture conditions were obtained using an incubator shaker set at 37°C inside a Coy Anaerobic Chamber with a gas mixture of 95% N_2 and 5% H_2 (Coy Laboratory Products, United States). Cells were then pelleted at 8000 × *g* at 23°C and resuspended in fresh BHI at a pH of either 7.5 or 5.5; pH was adjusted with either HCl or NaOH. For bile treated cells, mid exponential phase cells were resuspended in BHI at a pH of either 7.5 or 5.5 supplemented with 1% porcine bile extract (Sigma Aldrich, United States). Cells were then grown under either aerobic or anaerobic conditions at 37°C. This study had eight different conditions that mimicked parts of the GI tract. The conditions tested were: (1) aerobic at pH 5.5; (2) anaerobic at pH 5.5; (3) aerobic at pH 7.5; (4) anaerobic at pH 7.5; (5) aerobic at pH 5.5 with 1% porcine bile; (6) anaerobic at pH 5.5 with 1% porcine bile; (7) aerobic at pH 7.5 with 1% porcine bile; and (8) anaerobic at pH 7.5 with 1% porcine bile. For each time point during a 7 h incubation period, aliquots were serially diluted in phosphate buffered saline (PBS) and plated onto BHI agar plates. Plates were incubated overnight at 37°C prior to enumeration. Three independent replicates were performed in parallel for each individual condition tested.

RNA Extraction, Library Preparation and RNA Sequencing

To isolate the RNA for analysis of the transcript level expression, cells were collected after 1 h of incubation in the eight culture conditions described above. Three biological replicates were assayed. Briefly, 5 mL of culture was pelleted by centrifugation at 8,000 × *g* for 5 min at room temperature. Cell pellets were then treated with RNA Protect Bacterial Reagent (Qiagen, Germany). Total RNA was isolated using the RNeasy® Mini Kit (Qiagen, Germany) per manufacturer's instructions. The extracted RNA was quantitated using Qubit 3 Fluorometer (Invitrogen, United States) using the Qubit RNA BR assay kit (Thermo Fisher, United States). Extracted samples with values of A260/280 ∼ 2.0 were selected for sequencing. Illumina HiSeq™ 2000 paired-end 50 bp sequencer (PE50) was used. Ribosomal RNA was reduced with Epicentre RiboMinus kit (Illumina, United States) coupled with Directional RNA-Seq library prep with TruSeq indexes (Illumina, United States) per manufacturer's instructions.

Data Analysis

Differences in survival were determined using a student's *t*-test (Prism 8). Tophat-2.0.8.b (Trapnell et al., 2009) was used to align the RNA-Seq data to the reference genome, AE017262.2 *L. monocytogenes* str. 4b F2365. Transcript level calculation and FPKM normalization were performed using Cufflinks-2.1.1 (Trapnell et al., 2010). FPKM filtering cutoff of 1.0 was maintained to determine expressed transcripts. Differential transcript levels of the genes were determined using Cuffdiff (Trapnell et al., 2013). Differential transcript levels which had a greater than 3-fold expression and were statistically significant ($p < 0.01$ and $q < 0.01$) were subjected to Gene Ontology (GO) enrichment analysis using Blast2GO (Conesa et al., 2005). In this software, the up- and down-regulated transcripts were selected, and BLAST was performed against the *L. monocytogenes*

nucleotide database in NCBI. The BLAST results were then mapped and annotated.

DATA AVAILABILITY STATEMENT

SRA IDs of the submitted data: SRR13859772, SRR13859774, and SRR13859773: F2365 pH 5.5 Aerobic, SRR13859144, SRR13859143, and SRR13859142: F2365 pH 5.5 Anaerobic, SRR13859527, SRR13859526, and SRR13859525: F2365 pH 5.5+ Bile Anaerobic, SRR13859600, SRR13859599, and SRR13859598: F2365 pH 7.5+ Bile aerobic, SRR13858938, SRR13858937, and SRR13858936: F2365 pH 7.5+ Bile Anaerobic, SRR13858765, SRR13858767, and SRR13858766: F2365 pH 7.5 Anaerobic, SRR13853432, SRR13853433, and SRR13853431: F2365 pH 5.5+ Bile Aerobic, SRR13849951, SRR13849952, and SRR13849950: F2365 pH 7.5 aerobic.

AUTHOR CONTRIBUTIONS

JD: conceptualization, supervision, and project administration. MA, MD, JD, GS, and DC: methodology. GS and DC: software. GS, DC, and JD: validation and visualization. DC and JD: investigation and writing–review and editing. MA and GS: resources. DC: data curation and writing–original draft preparation. All authors have read and agreed to the published version of the manuscript.

FUNDING

This research was funded by the National Institutes of Health, Mississippi INBRE grant number P20GM103476 and MSU-COBRE grant number P20GM103646.

ACKNOWLEDGMENTS

We would like to extend our acknowledgment to Christopher Bryson and Trevor Perry for helping us with analyzing the data set.

SUPPLEMENTARY MATERIAL

The Supplementary Material for this article can be found online at: https://www.frontiersin.org/articles/10.3389/fmicb.2021.754748/full#supplementary-material

REFERENCES

Bernstein, C., Bernstein, H., Payne, C. M., Beard, S. E., and Schneider, J. (1999). Bile salt activation of stress response promoters in *Escherichia coli*. *Curr. Microbiol.* 39, 68–72. doi: 10.1007/s002849900420

Bo Andersen, J., Roldgaard, B. B., Christensen, B. B., and Licht, T. R. (2007). Oxygen restriction increases the infective potential of *Listeria monocytogenes* in vitro in Caco-2 cells and in vivo in guinea pigs. *BMC Microbiol.* 7:55. doi: 10.1186/1471-2180-7-55

Boonmee, A., Oliver, H. F., and Chaturongakul, S. (2019). *Listeria monocytogenes* sigma(A) is sufficient to survive gallbladder bile exposure. *Front. Microbiol.* 10:2070. doi: 10.3389/fmicb.2019.02070

Borezee, E., Pellegrini, E., and Berche, P. (2000). OppA of *Listeria monocytogenes*, an oligopeptide-binding protein required for bacterial growth at low temperature and involved in intracellular survival. *Infect. Immun.* 68, 7069–7077. doi: 10.1128/IAI.68.12.7069-7077.2000

Bowman, J. P., Hages, E., Nilsson, R. E., Kocharunchitt, C., and Ross, T. (2012). Investigation of the *Listeria monocytogenes* Scott A acid tolerance response and associated physiological and phenotypic features via whole proteome analysis. *J. Proteome Res.* 11, 2409–2426. doi: 10.1021/pr201137c

Burkholder, K. M., Kim, K. P., Mishra, K. K., Medina, S., Hahm, B. K., Kim, H., et al. (2009). Expression of LAP, a SecA2-dependent secretory protein, is induced under anaerobic environment. *Microbes Infect.* 11, 859–867. doi: 10.1016/j.micinf.2009.05.006

Chang, C., and Stewart, R. C. (1998). The two-component system. Regulation of diverse signaling pathways in prokaryotes and eukaryotes. *Plant Physiol.* 117, 723–731. doi: 10.1104/pp.117.3.723

Chatterjee, S. S., Hossain, H., Otten, S., Kuenne, C., Kuchmina, K., Machata, S., et al. (2006). Intracellular gene expression profile of *Listeria monocytogenes*. *Infect. Immun.* 74, 1323–1338. doi: 10.1128/IAI.74.2.1323-1338.2006

Cheng, C., Wang, X., Dong, Z., Shao, C., Yang, Y., Fang, W., et al. (2015). Aminopeptidase T of M29 family acts as a novel intracellular virulence factor for *Listeria monocytogenes* infection. *Sci. Rep.* 5:17370. doi: 10.1038/srep17370

Chourashi, R., Mondal, M., Sinha, R., Debnath, A., Das, S., Koley, H., et al. (2016). Role of a sensor histidine kinase ChiS of *Vibrio cholerae* in pathogenesis. *Int. J. Med. Microbiol.* 306, 657–665. doi: 10.1016/j.ijmm.2016.09.003

Coleman, R., Iqbal, S., Godfrey, P. P., and Billington, D. (1979). Membranes and bile formation. Composition of several mammalian biles and their membrane-damaging properties. *Biochem. J.* 178, 201–208. doi: 10.1042/bj1780201

Conesa, A., Gotz, S., Garcia-Gomez, J. M., Terol, J., Talon, M., and Robles, M. (2005). Blast2GO: a universal tool for annotation, visualization and analysis in functional genomics research. *Bioinformatics* 21, 3674–3676. doi: 10.1093/bioinformatics/bti610

Corbett, D., Wang, J., Schuler, S., Lopez-Castejon, G., Glenn, S., Brough, D., et al. (2012). Two zinc uptake systems contribute to the full virulence of *Listeria monocytogenes* during growth in vitro and in vivo. *Infect. Immun.* 80, 14–21. doi: 10.1128/IAI.05904-11

Cotter, P. D., Gahan, C. G., and Hill, C. (2001). A glutamate decarboxylase system protects *Listeria monocytogenes* in gastric fluid. *Mol. Microbiol.* 40, 465–475. doi: 10.1046/j.1365-2958.2001.02398.x

Cui, G., Wang, J., Qi, X., and Su, J. (2018). Transcription elongation factor GreA plays a key role in cellular invasion and virulence of *Francisella tularensis* subsp. novicida. *Sci. Rep.* 8:6895. doi: 10.1038/s41598-018-25271-5

Davis, M. J., Coote, P. J., and O'Byrne, C. P. (1996). Acid tolerance in *Listeria monocytogenes*: the adaptive acid tolerance response (ATR) and growth-phase-dependent acid resistance. *Microbiology* 142(Pt 10), 2975–2982. doi: 10.1099/13500872-142-10-2975

Dons, L., Eriksson, E., Jin, Y., Rottenberg, M. E., Kristensson, K., Larsen, C. N., et al. (2004). Role of flagellin and the two-component CheA/CheY system of *Listeria monocytogenes* in host cell invasion and virulence. *Infect. Immun.* 72, 3237–3244. doi: 10.1128/IAI.72.6.3237-3244.2004

Dowd, G. C., Joyce, S. A., Hill, C., and Gahan, C. G. (2011). Investigation of the mechanisms by which *Listeria monocytogenes* grows in porcine gallbladder bile. *Infect. Immun.* 79, 369–379. doi: 10.1128/IAI.00330-10

Dramsi, S., Dehoux, P., Lebrun, M., Goossens, P. L., and Cossart, P. (1997). Identification of four new members of the internalin multigene family of *Listeria monocytogenes* EGD. *Infect. Immun.* 65, 1615–1625. doi: 10.1128/iai.65.5.1615-1625.1997

Espey, M. G. (2013). Role of oxygen gradients in shaping redox relationships between the human intestine and its microbiota. *Free Radic. Biol. Med.* 55, 130–140. doi: 10.1016/j.freeradbiomed.2012.10.554

Garriga, X., Eliasson, R., Torrents, E., Jordan, A., Barbe, J., Gibert, I., et al. (1996). nrdD and nrdG genes are essential for strict anaerobic growth of *Escherichia*

coli. *Biochem. Biophys. Res. Commun.* 229, 189–192. doi: 10.1006/bbrc.1996.1778

Grove, A. (2013). MarR family transcription factors. *Curr. Biol.* 23, R142–R143. doi: 10.1016/j.cub.2013.01.013

Guariglia-Oropeza, V., Orsi, R. H., Guldimann, C., Wiedmann, M., and Boor, K. J. (2018). The *Listeria monocytogenes* bile stimulon under acidic conditions is characterized by strain-specific patterns and the upregulation of motility, cell wall modification functions, and the PrfA regulon. *Front. Microbiol.* 9:120. doi: 10.3389/fmicb.2018.00120

Hardy, J., Francis, K. P., DeBoer, M., Chu, P., Gibbs, K., and Contag, C. H. (2004). Extracellular replication of *Listeria monocytogenes* in the murine gall bladder. *Science* 303, 851–853. doi: 10.1126/science.1092712

Harris, J., Paul, O., Park, S. H., White, S. J., Budachetri, K., McClung, D. M., et al. (2019). Oxygen deprivation influences the survival of *Listeria monocytogenes* in gerbils. *Transl. Anim. Sci.* 3, 102–112. doi: 10.1093/tas/txy110

He, G., Shankar, R. A., Chzhan, M., Samouilov, A., Kuppusamy, P., and Zweier, J. L. (1999). Noninvasive measurement of anatomic structure and intraluminal oxygenation in the gastrointestinal tract of living mice with spatial and spectral EPR imaging. *Proc. Natl. Acad. Sci. U.S.A.* 96, 4586–4591. doi: 10.1073/pnas.96.8.4586

Isabella, V. M., and Clark, V. L. (2011). Identification of a conserved protein involved in anaerobic unsaturated fatty acid synthesis in *Neiserria gonorrhoeae*: implications for facultative and obligate anaerobes that lack FabA. *Mol. Microbiol.* 82, 489–501. doi: 10.1111/j.1365-2958.2011.07826.x

Jydegaard-Axelsen, A. M., Hoiby, P. E., Holmstrom, K., Russell, N., and Knochel, S. (2004). CO2- and anaerobiosis-induced changes in physiology and gene expression of different *Listeria monocytogenes* strains. *Appl. Environ. Microbiol.* 70, 4111–4117. doi: 10.1128/AEM.70.7.4111-4117.2004

Karatzas, K. A., Wouters, J. A., Gahan, C. G., Hill, C., Abee, T., and Bennik, M. H. (2003). The CtsR regulator of *Listeria monocytogenes* contains a variant glycine repeat region that affects piezotolerance, stress resistance, motility and virulence. *Mol. Microbiol.* 49, 1227–1238. doi: 10.1046/j.1365-2958.2003.03636.x

Kaspar, D., Auer, F., Schardt, J., Schindele, F., Ospina, A., Held, C., et al. (2014). Temperature- and nitrogen source-dependent regulation of GlnR target genes in *Listeria monocytogenes*. *FEMS Microbiol. Lett.* 355, 131–141. doi: 10.1111/1574-6968.12458

Kaval, K. G., Hahn, B., Tusamda, N., Albrecht, D., and Halbedel, S. (2015). The PadR-like transcriptional regulator LftR ensures efficient invasion of *Listeria monocytogenes* into human host cells. *Front. Microbiol.* 6:772. doi: 10.3389/fmicb.2015.00772

Krell, T., Lacal, J., Busch, A., Silva-Jimenez, H., Guazzaroni, M. E., and Ramos, J. L. (2010). Bacterial sensor kinases: diversity in the recognition of environmental signals. *Annu. Rev. Microbiol.* 64, 539–559. doi: 10.1146/annurev.micro.112408.134054

Kuenemann, M. A., Spears, P. A., Orndorff, P. E., and Fourches, D. (2018). In silico predicted glucose-1-phosphate uridylyltransferase (GalU) inhibitors block a key pathway required for *Listeria virulence*. *Mol. Inform.* 37:e1800004. doi: 10.1002/minf.201800004

Linnan, M. J., Mascola, L., Lou, X. D., Goulet, V., May, S., Salminen, C., et al. (1988). Epidemic listeriosis associated with Mexican-style cheese. *N. Engl. J. Med.* 319, 823–828. doi: 10.1056/NEJM198809293191303

Liu, Y., and Ream, A. (2008). Gene expression profiling of *Listeria monocytogenes* strain F2365 during growth in ultrahigh-temperature-processed skim milk. *Appl. Environ. Microbiol.* 74, 6859–6866. doi: 10.1128/AEM.00356-08

Mariscotti, J. F., Quereda, J. J., Garcia-Del Portillo, F., and Pucciarelli, M. G. (2014). The *Listeria monocytogenes* LPXTG surface protein Lmo1413 is an invasin with capacity to bind mucin. *Int. J. Med. Microbiol.* 304, 393–404. doi: 10.1016/j.ijmm.2014.01.003

Monte, M. J., Marin, J. J., Antelo, A., and Vazquez-Tato, J. (2009). Bile acids: chemistry, physiology, and pathophysiology. *World J. Gastroenterol.* 15, 804–816. doi: 10.3748/wjg.15.804

Nakano, M. M., Zhu, Y., Haga, K., Yoshikawa, H., Sonenshein, A. L., and Zuber, P. (1999). A mutation in the 3-phosphoglycerate kinase gene allows anaerobic growth of *Bacillus subtilis* in the absence of ResE kinase. *J. Bacteriol.* 181, 7087–7097. doi: 10.1128/JB.181.22.7087-7097.1999

Nelson, K. E., Fouts, D. E., Mongodin, E. F., Ravel, J., DeBoy, R. T., Kolonay, J. F., et al. (2004). Whole genome comparisons of serotype 4b and 1/2a strains of the food-borne pathogen *Listeria monocytogenes* reveal new insights into the core genome components of this species. *Nucleic Acids Res.* 32, 2386–2395. doi: 10.1093/nar/gkh562

Nevo, Y., and Nelson, N. (2006). The NRAMP family of metal-ion transporters. *Biochim. Biophys. Acta* 1763, 609–620. doi: 10.1016/j.bbamcr.2006.05.007

Niu, S., Luo, M., Tang, J., Zhou, H., Zhang, Y., Min, X., et al. (2013). Structural basis of the novel *S. pneumoniae* virulence factor, GHIP, a glycosyl hydrolase 25 participating in host-cell invasion. *PLoS One* 8:e68647. doi: 10.1371/journal.pone.0068647

Ofer, A., Kreft, J., Logan, D. T., Cohen, G., Borovok, I., and Aharonowitz, Y. (2011). Implications of the inability of *Listeria monocytogenes* EGD-e to grow anaerobically due to a deletion in the class III NrdD ribonucleotide reductase for its use as a model laboratory strain. *J. Bacteriol.* 193, 2931–2940. doi: 10.1128/JB.01405-10

O'Neil, H. S., and Marquis, H. (2006). *Listeria monocytogenes* flagella are used for motility, not as adhesins, to increase host cell invasion. *Infect. Immun.* 74, 6675–6681. doi: 10.1128/IAI.00886-06

Parsons, C., Lee, S., Jayeola, V., and Kathariou, S. (2017). Novel cadmium resistance determinant in *Listeria monocytogenes*. *Appl. Environ. Microbiol.* 83:e02580-16. doi: 10.1128/AEM.02580-16

Paruthiyil, S., Pinochet-Barros, A., Huang, X., and Helmann, J. D. (2020). *Bacillus subtilis* TerC family proteins help prevent manganese intoxication. *J. Bacteriol.* 202:e00624-19. doi: 10.1128/JB.00624-19

Paudyal, R., O'Byrne, C. P., and Karatzas, K. A. (2020). Amino acids other than glutamate affect the expression of the GAD system in *Listeria monocytogenes* enhancing acid resistance. *Food Microbiol.* 90:103481. doi: 10.1016/j.fm.2020.103481

Payne, A., Schmidt, T. B., Nanduri, B., Pendarvis, K., Pittman, J. R., Thornton, J. A., et al. (2013). Proteomic analysis of the response of *Listeria monocytogenes* to bile salts under anaerobic conditions. *J. Med. Microbiol.* 62(Pt 1), 25–35. doi: 10.1099/jmm.0.049742-0

Prieto, A. I., Ramos-Morales, F., and Casadesus, J. (2004). Bile-induced DNA damage in *Salmonella enterica*. *Genetics* 168, 1787–1794. doi: 10.1534/genetics.104.031062

Prieto, A. I., Ramos-Morales, F., and Casadesus, J. (2006). Repair of DNA damage induced by bile salts in *Salmonella enterica*. *Genetics* 174, 575–584. doi: 10.1534/genetics.106.060889

Quillin, S. J., Schwartz, K. T., and Leber, J. H. (2011). The novel *Listeria monocytogenes* bile sensor BrtA controls expression of the cholic acid efflux pump MdrT. *Mol. Microbiol.* 81, 129–142. doi: 10.1111/j.1365-2958.2011.07683.x

Scallan, E., Hoekstra, R. M., Angulo, F. J., Tauxe, R. V., Widdowson, M. A., Roy, S. L., et al. (2011). Foodborne illness acquired in the United States–major pathogens. *Emerg. Infect. Dis* 17, 7–15. doi: 10.3201/eid1701.P11101

Scortti, M., Monzo, H. J., Lacharme-Lora, L., Lewis, D. A., and Vazquez-Boland, J. A. (2007). The PrfA virulence regulon. *Microbes Infect.* 9, 1196–1207. doi: 10.1016/j.micinf.2007.05.007

Slamti, L., and Lereclus, D. (2019). The oligopeptide ABC-importers are essential communication channels in Gram-positive bacteria. *Res. Microbiol.* 170, 338–344. doi: 10.1016/j.resmic.2019.07.004

Sleator, R. D., and Hill, C. (2005). A novel role for the LisRK two-component regulatory system in listerial osmotolerance. *Clin. Microbiol. Infect.* 11, 599–601. doi: 10.1111/j.1469-0691.2005.01176.x

Stock, A. M., Robinson, V. L., and Goudreau, P. N. (2000). Two-component signal transduction. *Annu. Rev. Biochem.* 69, 183–215. doi: 10.1146/annurev.biochem.69.1.183

Supuran, C. T. (2016). *Legionella pneumophila* carbonic anhydrases: underexplored antibacterial drug targets. *Pathogens* 5:44. doi: 10.3390/pathogens5020044

Tessema, G. T., Moretro, T., Snipen, L., Heir, E., Holck, A., Naterstad, K., et al. (2012). Microarray-based transcriptome of *Listeria monocytogenes* adapted to sublethal concentrations of acetic acid, lactic acid, and hydrochloric acid. *Can. J. Microbiol.* 58, 1112–1123. doi: 10.1139/w2012-091

Thigpen, M. C., Whitney, C. G., Messonnier, N. E., Zell, E. R., Lynfield, R., Hadler, J. L., et al. (2011). Bacterial meningitis in the United States, 1998-2007. *N. Engl. J. Med.* 364, 2016–2025. doi: 10.1056/NEJMoa1005384

Torrents, E. (2014). Ribonucleotide reductases: essential enzymes for bacterial life. *Front. Cell Infect. Microbiol.* 4:52. doi: 10.3389/fcimb.2014.00052

Trapnell, C., Hendrickson, D. G., Sauvageau, M., Goff, L., Rinn, J. L., and Pachter, L. (2013). Differential analysis of gene regulation at transcript resolution with RNA-seq. *Nat. Biotechnol.* 31, 46–53. doi: 10.1038/nbt.2450

Trapnell, C., Pachter, L., and Salzberg, S. L. (2009). TopHat: discovering splice junctions with RNA-Seq. *Bioinformatics* 25, 1105–1111. doi: 10.1093/bioinformatics/btp120

Trapnell, C., Williams, B. A., Pertea, G., Mortazavi, A., Kwan, G., van Baren, M. J., et al. (2010). Transcript assembly and quantification by RNA-Seq reveals unannotated transcripts and isoform switching during cell differentiation. *Nat. Biotechnol.* 28, 511–515. doi: 10.1038/nbt.1621

Turner, A. G., Ong, C. L., Gillen, C. M., Davies, M. R., West, N. P., McEwan, A. G., et al. (2015). Manganese homeostasis in group A Streptococcus is critical for resistance to oxidative stress and virulence. *mBio* 6:e00278-15. doi: 10.1128/mBio.00278-15

van der Veen, S., and Abee, T. (2011). Contribution of *Listeria monocytogenes* RecA to acid and bile survival and invasion of human intestinal Caco-2 cells. *Int. J. Med. Microbiol.* 301, 334–340. doi: 10.1016/j.ijmm.2010.11.006

Volkov, A., Liavonchanka, A., Kamneva, O., Fiedler, T., Goebel, C., Kreikemeyer, B., et al. (2010). Myosin cross-reactive antigen of *Streptococcus pyogenes* M49 encodes a fatty acid double bond hydratase that plays a role in oleic acid detoxification and bacterial virulence. *J. Biol. Chem.* 285, 10353–10361. doi: 10.1074/jbc.M109.081851

West, A. H., and Stock, A. M. (2001). Histidine kinases and response regulator proteins in two-component signaling systems. *Trends Biochem. Sci.* 26, 369–376. doi: 10.1016/s0968-0004(01)01852-7

White, S. J., McClung, D. M., Wilson, J. G., Roberts, B. N., and Donaldson, J. R. (2015). Influence of pH on bile sensitivity amongst various strains of *Listeria monocytogenes* under aerobic and anaerobic conditions. *J. Med. Microbiol.* 64, 1287–1296. doi: 10.1099/jmm.0.000160

Wright, M. L., Pendarvis, K., Nanduri, B., Edelmann, M. J., Jenkins, H. N., Reddy, J. S., et al. (2016). The effect of oxygen on bile resistance in *Listeria monocytogenes*. *J. Proteomics Bioinform.* 9, 107–119. doi: 10.4172/jpb.1000396

Wu, H., Qiao, S., Li, D., Guo, L., Zhu, M., and Ma, L. Z. (2019). Crystal structure of the glycoside hydrolase PssZ from *Listeria monocytogenes*. *Acta Crystallogr. F Struct. Biol. Commun.* 75(Pt 7), 501–506. doi: 10.1107/S2053230X19008100

Zheng, L., Kelly, C. J., and Colgan, S. P. (2015). Physiologic hypoxia and oxygen homeostasis in the healthy intestine. A review in the theme: cellular responses to hypoxia. *Am. J. Physiol. Cell. Physiol.* 309, C350–C360. doi: 10.1152/ajpcell.00191.2015

Conflict of Interest: The authors declare that the research was conducted in the absence of any commercial or financial relationships that could be construed as a potential conflict of interest.

Publisher's Note: All claims expressed in this article are solely those of the authors and do not necessarily represent those of their affiliated organizations, or those of the publisher, the editors and the reviewers. Any product that may be evaluated in this article, or claim that may be made by its manufacturer, is not guaranteed or endorsed by the publisher.

frontiers in Microbiology

ORIGINAL RESEARCH
published: 11 November 2021
doi: 10.3389/fmicb.2021.736583

Functional Gene Identification and Corresponding Tolerant Mechanism of High Furfural-Tolerant *Zymomonas mobilis* Strain F211

Dongsheng Hu[1†], *Zhiquan Wang*[1,2†], *Mingxiong He*[3*] *and Yuanyuan Ma*[1,2*]

[1]*Department of Biochemical Engineering, School of Chemical Engineering and Technology, Tianjin University, Tianjin, China,* [2]*School of Marine Science and Technology, Tianjin University, Tianjin, China,* [3]*Biomass Energy Technology Research Centre, Key Laboratory of Development and Application of Rural Renewable Energy (Ministry of Agriculture and Rural Affairs), Biogas Institute of Ministry of Agriculture and Rural Affairs, Chengdu, China*

OPEN ACCESS

Edited by:
Peter Adrian Lund, University of Birmingham, United Kingdom

Reviewed by:
C. French, University of Edinburgh, United Kingdom
Jingwen Zhou, Jiangnan University, China

***Correspondence:**
Yuanyuan Ma
myy@tju.edu.cn
Mingxiong He
hemingxiong@caas.cn

[†]*These authors have contributed equally to this work*

Specialty section:
This article was submitted to Microbial Physiology and Metabolism, a section of the journal Frontiers in Microbiology

Received: *03 August 2021*
Accepted: *15 October 2021*
Published: *11 November 2021*

Citation:
Hu D, Wang Z, He M and Ma Y (2021) Functional Gene Identification and Corresponding Tolerant Mechanism of High Furfural-Tolerant Zymomonas mobilis Strain F211. Front. Microbiol. 12:736583. doi: 10.3389/fmicb.2021.736583

Furfural is a major inhibitor in lignocellulose hydrolysate for *Zymomonas mobilis*. A mutant F211 strain with high furfural tolerance was obtained from our previous study. Thus, its key tolerance mechanism was studied in the present study. The function of mutated genes in F211 was identified by functional complementation experiments, revealing that the improved furfural tolerance was resulted from the C493T mutation of the ZCP4_0270 gene promoting cell flocculation and the mutation (G1075A)/downregulation of ZCP4_0970. Comparative transcriptome analysis revealed 139 differentially expressed genes between F211 and the control, CP4, in response to furfural stress. In addition, the reliability of the RNA-Seq data was also confirmed. The potential tolerance mechanism was further demonstrated by functional identification of tolerance genes as follows: (I) some upregulated or downregulated genes increase the levels of NAD(P)H, which is involved in the reduction of furfural to less toxic furfuryl alcohol, thus accelerating the detoxification of furfural; (II) the mutated ZCP4_0270 and upregulated cellulose synthetase gene (ZCP4_0241 and ZCP4_0242) increased flocculation to resist furfural stress; (III) upregulated molecular chaperone genes promote protein synthesis and repair stress-damaged proteins; and (IV) transporter genes ZCP4_1623–1,625 and ZCP4_1702–1703 were downregulated, saving energy for cell growth. The furfural-tolerant mechanism and corresponding functional genes were revealed, which provides a theoretical basis for developing robust chassis strains for synthetic biology efforts.

Keywords: ***Zymomonas mobilis*, furfural, tolerance, RNA-Seq, functional investigation**

INTRODUCTION

Lignocellulosic biomass is an abundant renewable and sustainable resource used to produce biofuels and high-value chemicals (Yang et al., 2020). A major hindrance in converting lignocellulose to ethanol is the recalcitrance of biomass degradation, and pretreatment processes are thus required to release fermentable sugars (Moreno et al., 2015). Furan aldehyde (furfural and hydroxymethyl furfural), phenolic chlorine compounds, and organic acids are the major

inhibitors formed during the pretreatment process, which retards microbial fermentation and cellulose/hemicellulose hydrolysis (Yang et al., 2014). Therefore, breeding of inhibitor-tolerant strains and investigation of tolerance mechanisms have attracted a great deal of attention and providing strains and a theoretical basis for green bio-manufacturing (He et al., 2014; Pereira et al., 2020).

Zymomonas mobilis, a facultative anaerobic gram-negative bacterium that naturally produces ethanol, has excellent characteristics, such as a high specific rate of sugar uptake and high theoretical ethanol yield (Wang et al., 2018). It is also a promising chassis strain for the production of high value-added products from lignocellulosic biomass (He et al., 2014). *Zymomonas mobilis* detoxifies phenolic aldehydes to less toxic alcohols and exhibits stronger tolerance to phenolic acids than *Saccharomyces cerevisiae* (Gu et al., 2015). Nevertheless, aldehydes, especially furfural, tend to be more toxic to *Z. mobilis* than organic acids; therefore, the development of high furfural-tolerant *Z. mobilis* is crucial for the utilization of lignocellulose (Franden et al., 2009).

High furfural-tolerant *Z. mobilis* strains have been developed by directed evolution. For instance, ZMF3-3 (Shui et al., 2015) obtained by adaptive laboratory evolution (ALE) and ZM4-MF2 (Tan et al., 2015) developed from transcriptional engineering was able to tolerate 3 g/L furfural. In our previous study, the strain F211 (Huang et al., 2018), obtained through error-prone PCR-based whole genome shuffling, could tolerate up to 3.5 g/L of furfural. A rational design was also used to obtain furfural-tolerant strains. Overexpression of the ZMO1771 gene encoding alcohol dehydrogenase improved furfural tolerance by accelerating the reduction of furfural (Wang et al., 2017). Co-expression of ZMO1771 and *udhA* genes, encoding a transhydrogenase catalyzing the interconversion of NADH and NADPH, can maintain the balance between NAD(P)H/$NADP^+$, resulting in a more effective furfural tolerance (Wang et al., 2017).

Under furfural stress, the growth and survival of *Z. mobilis* were inhibited, and the specific production rate of ethanol was correspondingly reduced (Franden et al., 2009; Nouri et al., 2020). In addition, furfural also inhibits the synthesis of various proteins, causes DNA damage, and leads to the differential expression of genes involved in membrane and cell wall biogenesis, transcriptional regulators, and energy metabolism (He et al., 2012; Yang et al., 2020). *Zymomonas mobilis* may respond to stress in the following ways: (1) conversion of furfural to furfuryl alcohol reduces toxicity (Wang et al., 2017); (2) the genes related to macromolecule synthesis are upregulated to resist furfural stress (Miller et al., 2009; Yang et al., 2020); and (3) transcription factors regulate the expression of multiple genes in response to stress (He et al., 2012; Nouri et al., 2020). However, the defined roles of these corresponding genes are not yet known.

In summary, there is still a lack of comprehensive understanding of furfural tolerance. The high furfural tolerance mutant strain F211 was obtained in an earlier study, and single nucleotide polymorphisms (SNPs) between F211 and control strain CP4 were identified by genome resequencing of F211 (Huang et al., 2018); in this study, functional identification of the mutations and RNA-Seq was therefore performed to investigate the genotypic changes associated with furfural tolerance and reveal the molecular mechanism responsible for the improved furfural tolerance in F211.

MATERIALS AND METHODS

Bacterial Strain and Culture Conditions

The wild-type strain *Z. mobilis* CP4 was purchased from the China Center for Type Culture Collection (CCTTCC; Accession NO.CICC10232). F211 is a strain of *Z. mobilis* with high furfural tolerance obtained in the early stage of our laboratory (Huang et al., 2018). *Zymomonas mobilis* was cultured in Rich Medium (10 g/L yeast extract, 2 g/L KH_2PO_4, 20 g/L glucose, and different concentration of furfural as required) at 30°C without shaking.

Construction of Deletion and Overexpression Strains

Nine deletion strains (**Supplementary Table S1**) were constructed by homologous recombination as described in our previous study with some modification (Wang et al., 2013; Huang et al., 2018). The left and right homologous arm DNA fragments of the target gene were ligated to flank both sides of a chloramphenicol resistance gene, generating the homologous recombinant fragments (**Section 1.1 of Supplementary Materials and Methods**). The homologous recombinant fragments were ligated into the *Sph*I and *Sac*II sites of pUC19 to yield the plasmid pT-gene (**Supplementary Table S1**) by using the Gibson assembly (GA; Gibson et al., 2009). The target plasmids were then transformed into CP4 competent cells by electroporation (Ma et al., 2012). The target gene was replaced with the chloramphenicol resistance gene by homologous recombination using its native RecA recombinase (**Supplementary Figure S1**; Savvides et al., 2000; Huang et al., 2018). Transformants were screened on RM agar plates with 50 μg/ml chloramphenicol. Positive single colonies were confirmed by PCR using the appropriate geneGF/geneGR, geneGF/T-CM-R, and T-CM-F/geneGR (**Supplementary Table S2**) primer pairs (**Supplementary Materials and Methods**).

Overexpression vectors were constructed by ligating the target wild-type gene or its mutated gene into multiple clone sites of pEZ15Asp (pE)/pHW20a (pH) vector. The target genes were amplified from the genomes of CP4 and F211 using the primers gene OF/OR (**Supplementary Table S3**), and the P_{gap} promoter (Yang et al., 2019) was amplified from the genome of CP4 using the primers pgap-F/pgap-R (**Supplementary Table S3**). Then, the two fragments were fused by overlap-extension PCR using the primers pgap-F/gene-OR. The fusion fragment was inserted into the *Pst*I and *Eco*RI sites of pE/pH to yield the plasmid pE-gene/pH-gene by using the aforementioned GA (Gibson et al., 2009). Positive clones were further verified by DNA sequencing. The correctly sequenced recombinant plasmids were transformed into CP4 competent cells by electroporation.

The target plasmids were confirmed by PCR using the appropriate pEZ-F/pEZ-R (**Supplementary Table S3**) primer pairs.

Furfural Tolerance Assay

Strain was precultured in RM at 30°C to the late exponential stage, and the cultures were concentrated to an OD_{600} of 20 by centrifugation. The concentrated cells were inoculated into 100 ml RM medium containing 3.5 g/L furfural with an initial OD_{600} of 0.2, and the OD_{600} value was measured every 6 h to detect the growth of the cells for the evaluation of furfural tolerance. The degradation rate of furfural was calculated by the following formula:

$$\text{The degradation rate of furfural} = \frac{C_{initial} - C_{final}}{T}$$

where "T" indicated the fermentation time, and "$C_{initial}$" and "C_{final}" indicated "initial medium furfural concentration" and "final medium furfural concentration," respectively. All experiments were performed in triplicates, and statistical differences were analyzed using a one-way analysis of variance (ANOVA). $*p < 0.05$ was considered statistically significant, and $**p < 0.01$ was considered extremely significant.

Flocculation Measurement

Strains were cultured in RM medium containing 3 g/L furfural for 36 h, and 10 µl of the culture was taken to observe the flocculation under a light microscope (Olympus BX51, Japan). Five milliliter culture of each strain was collected and was shaken vigorously for 15 s and then rested for 5 min. Suspension of 1 ml was sampled from the upper section to measure OD_{600} and quantify the non-flocculating cells (*Cf*), and 1.2 units of cellulase (Novozymes, Denmark) was added to the remaining culture, which was incubated at 50°C for complete de-flocculation of the bacterial flocs to measure the concentration of total cells (Ct). The flocculation efficiency of *Z. mobilis* was calculated based on the formula:

$$R\% = \left(1 - \frac{Cf}{Ct}\right) \times 100$$ (Xia et al., 2018).

RNA-Seq Transcriptomic Analysis

Strain F211 and CP4 were cultured statically in RM medium with 3 g/L furfural. The cultures were collected by centrifugation when the OD_{600} reached 0.8–1.4, and the cells were washed with PBS buffer (pH = 7.4, 137 mM NaCl, 2.7 mM KCl, 10 mM $Na_2HPO_4{\cdot}12H_2O$, and 1.4 mM KH_2PO_4). The cells were collected by centrifugation and freeze in liquid nitrogen for 1 h. The samples were submitted to Novogene (China, Beijing) for RNA-Seq.

The integrity of the extracted RNA was tested using the Agilent Bioanalyzer 2,100 system (Agilent Technologies, CA, United States). cDNA library preparation and sequencing were conducted by the Novogene Technology Company in Beijing, China. The clean reads were obtained by sequencing and mapped to the *Z. mobilis* CP4 genome sequence (GenBank: CP006818.1) using Bowtie2-2.2.3. Differentially expressed genes (DEGs) between the two samples were identified using the DESeq package (1.20.0), and $|\log2(\text{FoldChange})| > 1$ and q-value < 0.005 were used as the threshold to identify significant differences in gene expression analysis of Gene Ontology (GO), which assigns genes into functional categories, was performed using the GO R packages. KOBAS software could perform KEGG enrichment analysis on differentially expressed genes to determine the metabolic pathways of genes.

Real-Time Quantitative Reverse Transcription PCR Analysis

The expression levels of 22 DEGs representing different functional categories were assessed by real-time quantitative reverse transcription PCR (qRT-PCR) to validate the reliability of the RNA-Seq data. The culture conditions of CP4 and F211 were the same as the RNA-Seq experiment. When the strains concentration reached $OD_{600} = 0.8–1.4$, about 10^8 cells were collected from each strain, and the cells are treated in liquid nitrogen for 5 min. Subsequently, the bacterial cells were ground in a mortar pre-cooled with liquid nitrogen, and the powder was transferred to 100 µl TE buffer (containing 400 µg/ml lysozyme), mixed, and placed at room temperature for 4 min to dissolve the cell wall. RNA was extracted with TRIzol reagent (Invitrogen, Carlsbad, CA, United States) according to the manufacturer's instructions.

DNase (RQ1 RNase-Free DNase, Promega, United States) was added to the RNA samples to remove genomic DNA. The PCR reaction with primer pair 16SrRNA-F/16SrRNA-R was performed on the total RNA in order to check for genomic DNA contamination. No product was observed, demonstrating that the sample had no genomic DNA contaminants and was suitable for qRT-PCR assay. Subsequently, cDNA was synthesized using iScript cDNA Synthesis Kit (Bio-Rad) with the purified total RNA of CP4 or F211 as a template following the manufacturer's instructions. Real-time qRT-PCR experiments were performed using CFX96 Real-Time System (Bio-Rad). Each reaction contained 2 µl of diluted (1/10) cDNA, Taq SYBR Green qPCR Premix (Yugong Biolabs Inc., Jiangsu, China) and the corresponding primer pairs (**Supplementary Table S4**). The 16S rRNA gene was used as a reference to normalize the qRT-PCR data. The expression level of each gene was calculated according to the 2(-Delta Delta C(T)) method (Livak and Schmittgen, 2001).

RESULTS AND DISCUSSION

Functional Identification of Mutated Genes in F211

Eleven SNPs (single nucleotide polymorphisms) were found in high furfural-tolerant F211 compared with the sequence (GenBank No. CP006818) of CP4 from Agricultural Research

Service Culture Collection (NRRL No. B-14023; Huang et al., 2018). The initial strain CP4 (CICC 10132) of F211 and the reference CP4 may have different SNPs. Therefore, in this study, except for the three synonymous mutated genes of ZCP4_0096, ZCP4_0593, and ZCP4_1887, seven missense mutated genes and one nonsense mutated gene of F211, along with the starting strain, CP4, were PCR-amplified and sequenced. F211 and CP4 shared consistent sequences of ZCP4_1431, ZCP4_1,616, ZCP4_0244, and ZCP4_0525. The ZCP4_1919, ZCP4_1419, and ZCP4_0270 genes in F211 carried missense mutations in G335A, C85T, and C493T, resulting in a substitution of V119I, G29S, and G165S, respectively. The mutation of ZCP4_0970 (1075G > A) converted a glutamine codon to a stop codon (Q359X), producing a truncated protein lacking 153 amino acids at the C-terminal end (**Table 1**). Therefore, these four genes were selected for functional studies related to furfural tolerance.

The deletion and overexpression strains of these genes were constructed to study furfural tolerance. In RM medium containing 3.5 g/L furfural, the deletion and overexpression strains of ZCP4_1419 and ZCP4_1919 genes did not show obvious growth differences (**Supplementary Figures S3A,B**), indicating that these two genes have no effect on furfural tolerance. The ZCP4_0970 gene encodes the TolC family protein of the bacterial type I secretion system, transporting proteins to the extracellular space coupled with ATP consumption (Delepelaire, 2004). The deletion strain Δ0970 (pE) showed a 13 and 7.6% increase in the maximum cell density and ethanol production, respectively, compared to the control CP4 (pE) (**Figures 1A,B**). In contrast, the overexpression strain CP4 (pE-W0970) had a 47 and 13.9% decrease in the maximum cell density and ethanol production, respectively, compared to the control CP4 (pE) (**Figures 1A,B**). The results showed that the downregulation of ZCP4_0970 can increase the furfural tolerance of strains, which indicates that the G1075A mutation in the ZCP4_0970 gene resulted in functional inactivation or attenuation, improving furfural tolerance.

Furfural destroys the tertiary structure of proteins and inhibits protein synthesis (He et al., 2012; Todhanakasem et al., 2014). Tolc inactivation leads to defects in the secretion system and the increase in ATP levels (Delepelaire, 2004), thereby providing more energy for cell growth and increasing furfural tolerance. Interesting, the deletion of the ZCP4_0970 gene destroys the efflux system, also yielding a reducing tetracycline resistance (Delepelaire, 2004; De Cristóbal et al., 2006), which causes the inability of transformants to grow on the tetracycline selection plates. And the original initial pHW20a plasmid containing tetracycline resistance gene (Dong et al., 2011) could not be transformed successfully into Δ0970 strain. So, the plasmid pEZ15Asp with an ampicillin resistance gene (Yang et al., 2016) was used as a starting vector for construction of wild-type and mutated ZCP4_0970 gene overexpression vectors.

ZCP4_0270 encodes a bifunctional protein with diguanylate cyclase (DGC)/phosphodiesterase (PDE), which synthesizes/degrades bis-(39–59)-cyclic dimeric guanosine monophosphate (c-di-GMP). The deletion strain Δ0270 (pH) and overexpression strain Δ0270 (pH-W0270) did not show significant growth differences compared to those of the control strains CP4 (pH) and Δ0270 (pE-W0270) (**Figures 1C,D**), indicating that deletion or overexpression of the native ZCP4_0270 gene did not affect furfural tolerance. The specific growth rate, degradation rate of furfural in the medium (0–48 h), and ethanol production of the mutated gene overexpression strain Δ0270 (pH-M0270) were 62, 8.3, and 38.5% higher than those of the control strain Δ0270 (pE-M0270) (**Figures 1C,D**), respectively, indicating that the C493T mutation of the ZCP4_0270 gene can promote the degradation of furfural, thereby improving furfural tolerance.

Flocculated yeast showed a higher tolerance to furfural than free yeast (Westman, 2014). The increased c-di-GMP, which is regulated by PDEs, can promote the flocculation of *Z. mobilis* (Tan et al., 2014). Therefore, the mutated ZCP4_0270 may improve furfural tolerance by promoting flocculation, and thus, the flocculation of F211 and Δ0270 (pH-M0270) was investigated. Flocculation was observed in both strains (**Figures 2A,C**), and the flocculation rates of F211 and Δ0270 (pH-M0270) were 600 and 470% higher than that of CP4, respectively (**Figure 2B**). The flocculation rate of the wild-type ZCP4_0270 gene overexpressing strain Δ0270 (pH-W0270) and the engineered strains of ZCP4_0970 and ZCP4_1419 were similar to those of the control CP4 (**Figure 2B**). These results show that the mutated ZCP4_0270 gene in F211 causes flocculation, resulting in an improved furfural tolerance.

TABLE 1 | Mutations identified in the F211 strain.

Gene	Function	Mutation	Effect
ZCP4_0270	Diguanylate cyclase/phosphodiesterase	C493T	G165S
ZCP4_0970	Type I secretion outer membrane protein, TolC family	G1075A	Q359X
ZCP4_1419	Surface lipoprotein	C85T	G29S
ZCP4_1919	A C-terminal OMP(outer membrane protein) domain	G355A	V119I

X, Termination codon.

Transcriptome Analysis of F211 and CP4 Under Furfural Stress

The bifunctional DGCs/PDEs encoded by the ZCP4_0270 gene can regulate the levels of the second messenger c-di-GMP, which coordinates diverse aspects of bacterial growth and behavior, including motility, virulence, biofilm formation, and cell cycle progression (Jenal et al., 2017). Therefore, enhanced tolerance by the mutated ZCP4_0270 also resulted in a change in the physiological, biochemical, and expression levels of some genes. Consequently, RNA-Seq was performed to analyze the transcriptome differences between F211 and CP4 under furfural stress and to explore the potential furfural tolerance mechanism.

A total of 139 DEGs were identified in F211 compared with the control, with 77 and 62 genes being upregulated and downregulated, respectively. The expression levels of the three missense genes in F211 did not change significantly, indicating

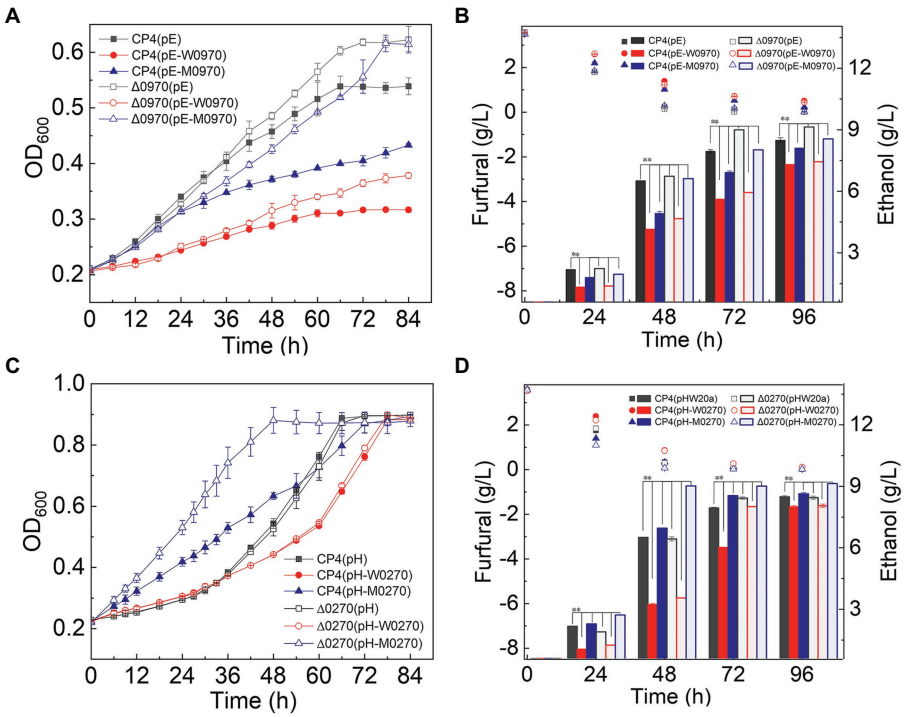

FIGURE 1 | Growth and fermentation of the functionally complementary strains of genes ZCP4_0270 and ZCP4_0970. Panel **(A)** and **(C)** indicated that the growth curves of engineered strains of ZCP4_0970 and ZCP4_0270 genes, respectively. The furfural (scatter plot) and ethanol (bar) concentration in RM medium of engineered strains of ZCP4_0970 and ZCP4_0270 genes were shown in Panel **(B)** and **(D)**, respectively.

that its enhanced tolerance was due to the changed protein function caused by the mutated ZCP4_0270 and ZCP4_0970 genes, rather than the changed transcript abundance. DEGs were subjected to GO enrichment analysis. The five GO clusters with the highest enrichment were as follows: "localization," "transport," "establishment of localization," "cofactor binding," and "response to stimulus" (**Supplementary Figure S4A**). The DEGs were enriched in 39 pathways, found using a Kyoto Encyclopedia of Genes and Genomes (KEGG) analysis, 27 of which were different from those previously reported (He et al., 2012; Yang et al., 2020). The significant KEGG terms were primarily associated with microbial metabolism in diverse environments, biosynthesis of secondary metabolites and antibiotics, bacterial chemotaxis, and sulfur metabolism (**Supplementary Figure S4B**).

We screened 22 DEGs representing different GO clusters from 139 DEGs (**Table 2**) for qRT-PCR verification. Based on the qRT-PCR results, the expression trends of these candidate genes were consistent with the RNA-Seq data (**Figure 3**). A comparison of the two methods indicated a high level of concordance ($R^2 = 0.7833$), indicating that the RNA-Seq data were reliable.

Furfural Tolerance Mechanism by Functional Analysis of DEGs

Increased Intracellular NAD(P)H Levels Resist Furfural Stress

The sulfur assimilation operon *CysJIH* (ZCP4_1208–1,210) and *CysGDNC* (ZCP4_1211–1,214) were significantly downregulated in F211 in response to furfural stress (**Table 2**). Deletion strains of these genes were engineered to investigate their furfural tolerance. The cell densities of the deletion strains ΔCysJI and ΔCysND were increased by 20 and 9% compared to those of CP4 (**Figure 5A**), respectively, showing that the deletion of these genes could improve the furfural tolerance. The enzymes encoded by *CysND* and *CysJI*(*G*) genes involved in cysteine synthesis coupled with ATP and NAD(P)H consumption (**Figure 4**; Miller et al., 2009; Takagi, 2019). And the conversion of NAD(P)H to $NAD(P)^+$ was coupled with reduction in furfural to furfuryl alcohol (Boopathy, 2009; Yi et al., 2015). The concentration of NADH of the ΔCysND and ΔCysJI was 35.7-fold and 44.6-fold higher than that of the control CP4 in RM without furfural (**Supplementary Figure S5A**), respectively, indicating that deletion of these genes can reduce NADH consumption. While the NADH/NAD^+ ratio was decreased by 49.5 and 34.5% for ΔCysND and ΔCysJI under furfural stress, respectively, compared with non-stress condition (**Supplementary Figure S5B**), demonstrating that the deletion strains consumed more NADH under furfural stress. Thereby, the downregulation of these genes could reduce the consumption of NADH, and the saved NADH may be used for the conversion of furfural to furfural alcohol, thus enhancing the detoxification of furfural. The damaged proteins and DNA were correspondingly reduced.

Interestingly, overexpression of the cysteine synthase operon *CysCNDG* (ZMO0003–0006) contributed to the production of cysteine, replenishing proteins damaged by furfural, thus improving the furfural tolerance of 8b (Miller et al., 2009;

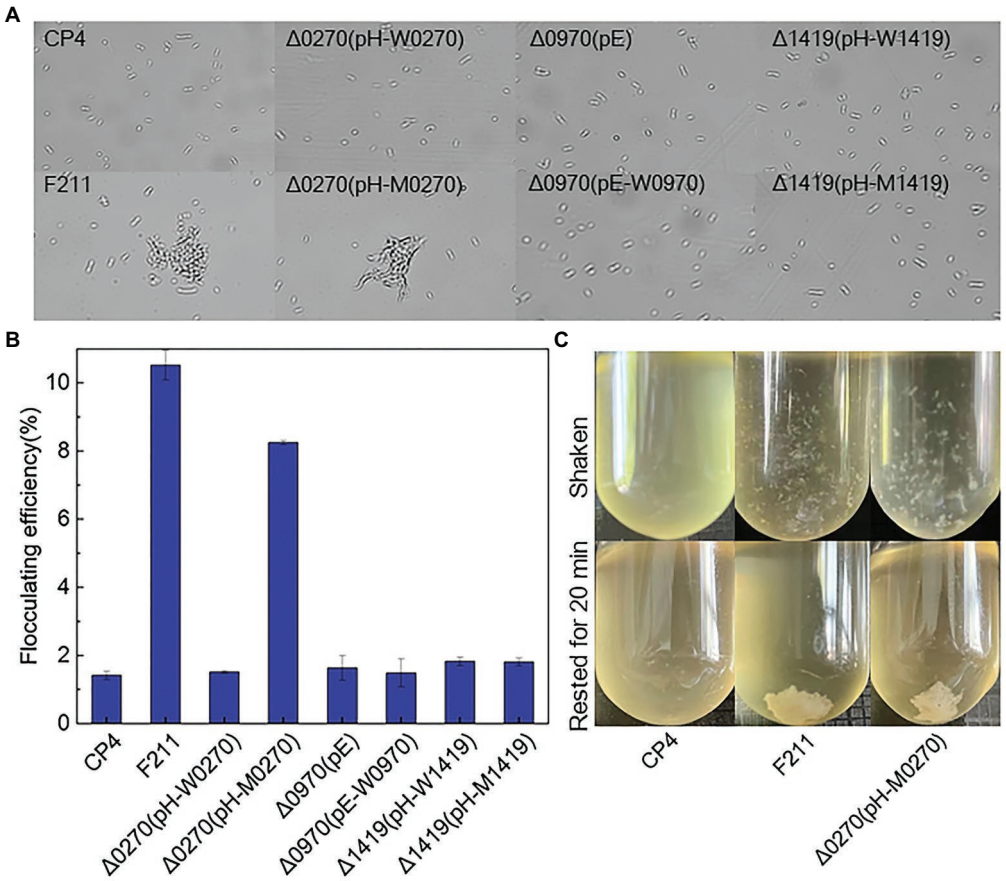

FIGURE 2 | Forces in *Zymomonas mobilis* flocculation. **(A)** Flocculent microscopic image of recombinant strains. **(B)** Flocculation rate. **(C)** Flocculation phenotype.

Yang et al., 2020). The destruction of sulfur assimilation pathway can reduce the synthesis of cysteine, a deficiency of amino acids for growth (Miller et al., 2009) and response stress. Therefore, the furfural tolerance characteristics of ΔCysJI and ΔCysND strain may be counteracted partially by the Cys deficiency. In our study, the downregulation of the *CysCNDG* operon in F211 may be caused by a mutation in the ZCP4_0270 gene, which regulates the content of c-di-GMP, causing physiological and biochemical changes such as cell flocculation (Tan et al., 2014).

The ZCP4_1,170 gene, encoding the efflux pump protein TauE, involved in efflux sulfite to the periplasmic space, is downregulated 3.0-fold under furfural stress. The overexpression and deletion strains of this gene were constructed to demonstrate their function. Compared with the control strain CP4 (pE), the cell density of the overexpression strain CP4 (pE-1,170) and deletion strain Δ1170 (pE) was increased and decreased by 21 and 22% (**Figure 5B**), respectively, showing that its upregulated expression improved furfural tolerance. Conversely, the expression of the ZCP4_1,170 gene is downregulated in furfural-tolerant F211 (**Table 2**), which results from feedback regulation by sulfate assimilation genes. The downregulation of *CysH* and *CysDNC* genes reduces sulfite synthesis and this may have corresponded with less TauE being needed; therefore, the genes were feedback downregulated.

The expression of the ZCP4_1,414 gene encoding succinate dehydrogenase was upregulated by 1.9-fold in F211 (**Table 2**). The enzyme catalyzes the conversion of succinic acid semialdehyde to succinate acid and concomitantly reduces $NAD(P)^+$ to NAD(P)H. The overexpression strains CP4 (pE-1,414) and Δ1414 (pE-1,414) of this gene showed a 24 and 11% increase (**Figure 5C**) in cell density compared with the control strains CP4 (pE) and Δ1414 (pE), indicating that its upregulation improved furfural tolerance. Furthermore, its upregulation can accelerate the regeneration of NAD(P)H and provide more reducing activity for furfural detoxification, thereby resulting in enhanced tolerance.

Responses of Molecular Chaperones and Stress Proteins to Furfural Stress

The ZCP4_0558 gene encoding a universal stress protein CsbD, molecular chaperone *yfdX* (ZCP4_0600), and *clpB* (ZCP4_1707), was significantly upregulated in F211 under furfural stress (**Table 2**). The overexpression and deletion strains of the ZCP4_0558 gene were constructed to study

TABLE 2 | The differentially expressed genes used for qRT-PCR verification.

Functional group and gene	Description	Log2 fold change in RNA-Seq	Log2 fold change in qRT-PCR
Transporter			
ZCP4_0708	MetI-like ABC transporter transmembrane protein	1.858	1.225
ZCP4_1,170	Anion permease, Sulfite exporter TauE/SafE	−2.986	−0.759
ZCP4_1331	Alginate export	−2.033	−0.554
ZCP4_1481	Aspartate-alanine antiporter	2.006	1.090
ZCP4_1624	Multidrug efflux pump subunit AcrB	−1.359	−1.147
ZCP4_1,625	Efflux transporter outer membrane factor lipoprotein, NodT family	−1.474	−0.310
ZCP4_1703	NodT family RND efflux system outer membrane lipoprotein	−1.665	−0.475
Stress related			
ZCP4_0558	General stress protein CsbD	2.138	0.424
ZCP4_0600	YfdX protein, putative chaperone	1.785	1.382
ZCP4_0601	OsmC family protein	1.701	1.062
ZCP4_1707	ATP-dependent chaperone ClpB	1.467	0.359
Metabolism			
ZCP4_1209	Sulfite reductase subunit beta, CysI	−1.414	−0.745
ZCP4_1212	Sulfate adenylyltransferase subunit 1, CysD	−2.331	−0.410
ZCP4_1213	Sulfate adenylyltransferase subunit 2, CysN	−1.842	−0.839
ZCP4_1,414	Succinate-semialdehyde dehydrogenase	1.945	0.761
ZCP4_1673	Acyltransferase of alpha/beta superfamily	2.836	1.629
Membrane related			
ZCP4_0241	Cellulose synthase operon C domain protein, BscC	1.670	0.635
ZCP4_0242	Cellulose synthase subunit B, BscB	1.035	1.341
ZCP4_0439	Squalene-hopene cyclase	−1.604	−0.108
ZCP4_0441	Squalene synthase HpnD	−1.367	−0.006
Regulator			
ZCP4_0221	AsnC family transcriptional regulator	1.109	0.943
ZCP4_0805	Transcriptional regulator	1.431	0.300

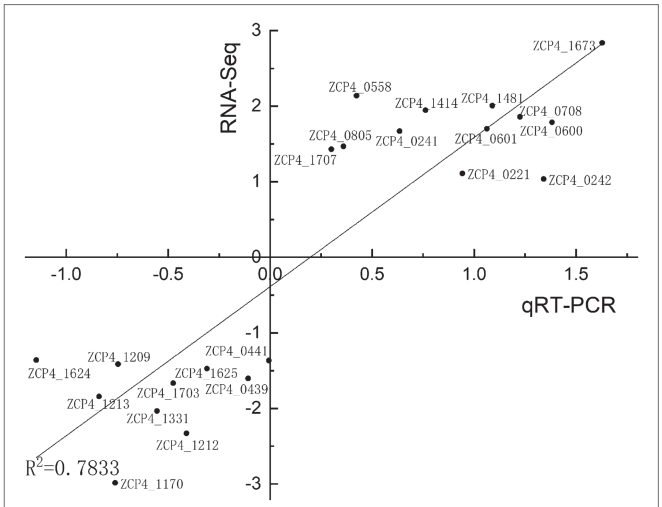

FIGURE 3 | Correlation between RNA-seq and qRT-PCR results for RNA-seq data verification. The gene expression ratios of RNA-seq and qRT-PCR data for the genes in **Table 2** were log transformed (base 2), and the RNA-seq log2 ratio values were plotted against the qRT-PCR log2 values.

the effect of its expression levels on furfural tolerance. The specific growth rate of the overexpression strain CP4 (pE-0558) and the deletion strain Δ0558 (pE) were increased and decreased by 27.6 and 9.5%, respectively, compared with the control strain CP4 (pE) (**Figure 5D**), indicating that its upregulation could improve furfural tolerance. The *csbD* from *Methylocystis* was upregulated under stress of starvation, high heat, and acid (Han et al., 2017). CsbD from *Bacillus coagulans* also showed upregulated expression in response to furfural stress (van der Pol et al., 2016). To our knowledge, this study provides the first evidence that its upregulation can improve the furfural tolerance of *Z. mobilis*. Chaperones play important roles in cell survival, and they can promote the folding of peptide chains and repair stress-damaged proteins, thus ensuring protein homeostasis in cells (Liu et al., 2016; Ghazaei, 2017). Furfural inhibits synthesis of various proteins and affects cell growth and survival (Franden et al., 2009; He et al., 2012). Therefore, the upregulated expression of molecular chaperones in F211 may promote protein synthesis, reduce damage to cells, and improve furfural tolerance.

Cell Flocculation

Two genes (ZCP4_0241 and ZCP4_0242) related to cellulose synthesis were upregulated in F211 (**Table 2**). The increased cellulose content on the cell surface contributes to cell flocculation (Jeon et al., 2012; Xia et al., 2018). The c-di-GMP, regulated by PDEs encoded by the ZCP_0270 gene, is an activator of cellulose synthesis (Xia et al., 2018); therefore, it may be because the mutated ZCP4_0270 gene may increase the activity of diguanylate cyclase, enhancing the content of c-di-GMP and activating cellulose synthesis, resulting in cell flocculation to resist stress. In addition, the chemotaxis (ZCP4_1147 and ZCP4_1150) and flagella (ZCP4_0645) genes were downregulated in F211 (**Supplementary Table S5**), which may reduce cell motility and facilitate cell flocculation, thus improving furfural tolerance (Jeon et al., 2012; Xia et al., 2018). A stronger flocculation ability was observed in F211 compared to CP4 (**Figure 2A**), demonstrating the potential furfural tolerance mechanism.

Reduce Energy Consumption of Efflux Pump

The ATP-binding cassette (ABC) transporter family (ZCP4_1623, ZCP4_1624, and ZCP4_1,625) genes and the resistance-nodulation-division (RND) family (ZCP4_1702 and ZCP4_1703) genes were downregulated in F211 (**Table 2**). They consume

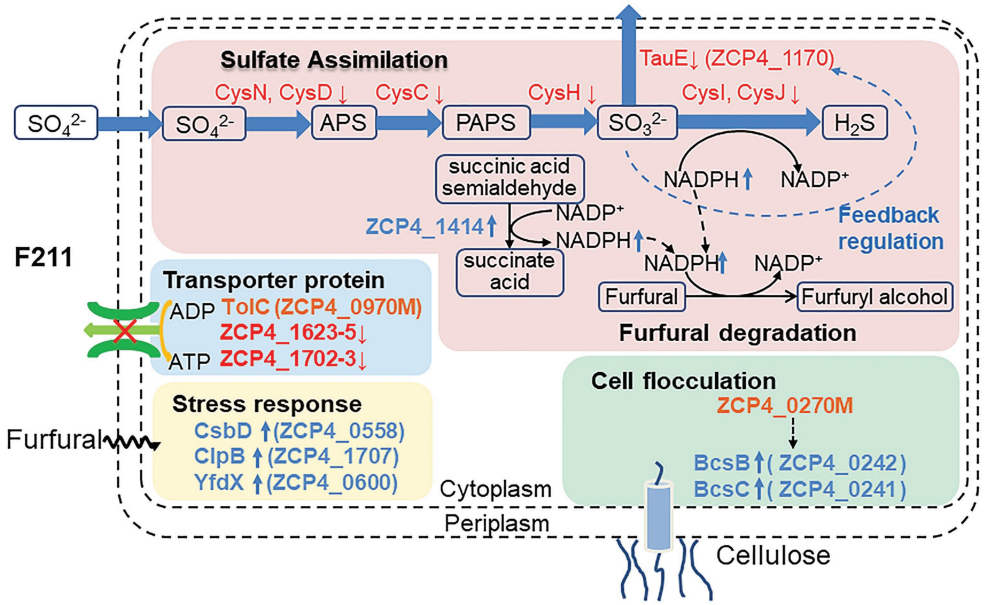

FIGURE 4 | Potential furfural tolerance mechanism of *Z. mobilis*.

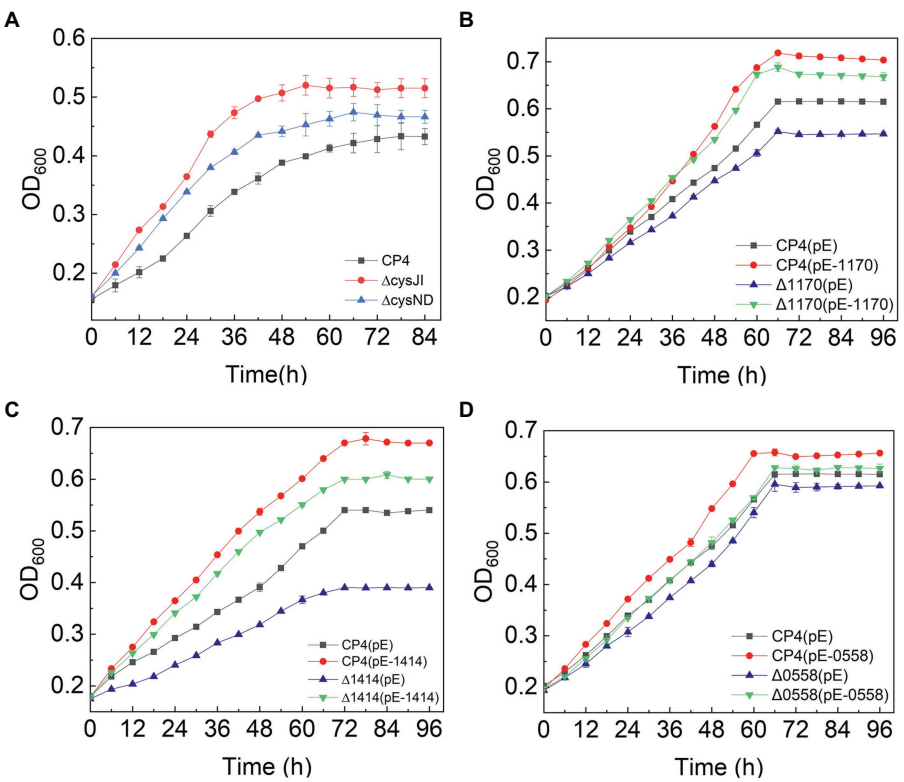

FIGURE 5 | Growth curves of engineered strains of *CysJI*, *CysND*, ZCP4_1,170, ZCP4_1,414, and ZCP4_0558 genes.

ATP to export lipids, amino acids, heavy metals, etc., to the outside of the cell (Saier and Paulsen, 2001). Deletion of an operon encoding the RND efflux system could improve the furfural tolerance of *Z. mobilis* ZM4 (Yang et al., 2020). The downregulation of these efflux pump genes may reduce the energy consumption of cells, providing more energy for cell

growth and increasing furfural tolerance. In future, corresponding functional verification experiment would be performed to consolidate the current discussion.

CONCLUSION

In conclusion, F211 resists furfural stress by accelerating the detoxification of furfural, improving cell flocculation, enhancing emergency response, and reducing energy consumption. This study lays the foundation for the rational design of high furfural tolerance strains, which would accelerate the industrialization process of lignocellulosic ethanol.

DATA AVAILABILITY STATEMENT

The RNA-seq datasets for this study can be found in the NCBI under accession number PRJNA743578.

AUTHOR CONTRIBUTIONS

YM conceived of the project, analyzed the data, supervised the study, and revised the manuscript. MH supervised the study and revised the manuscript. DH and ZW performed the experiments and drafted the manuscript. All authors contributed to the article and approved the submitted version.

FUNDING

This work was supported by the Tianjin Science & Technology Council (18JCYBJC24200), the National Natural Sciences Foundation of China (32070036), the Elite Program and Basic Research Program of Chinese Academy of Agricultural Sciences, and the Key Laboratory of Development and Application of Rural Renewable Energy, and the Ministry of Agriculture and Rural Affairs, China (2019003).

ACKNOWLEDGMENTS

We are thankful to Bo Wu for his very helpful advice on drafts of this paper.

SUPPLEMENTARY MATERIAL

The Supplementary Material for this article can be found online at: https://www.frontiersin.org/articles/10.3389/fmicb.2021.736583/full#supplementary-material

REFERENCES

Boopathy, R. (2009). Anaerobic biotransformation of furfural to furfuryl alcohol by a methanogenic archaebacterium. *Int. Biodeterior. Biodegradation* 63, 1070–1072. doi: 10.1016/j.ibiod.2009.09.011

De Cristóbal, R. E., Vincent, P. A., and Salomón, R. A. (2006). Multidrug resistance pump AcrAB-TolC is required for high-level, Tet(A)-mediated tetracycline resistance in *Escherichia coli*. *J. Antimicrob. Chemother.* 58, 31–36. doi: 10.1093/jac/dkl172

Delepelaire, P. (2004). Type I secretion in gram-negative bacteria. *Biochim. Biophys. Acta* 1694, 149–161. doi: 10.1016/j.bbamcr.2004.05.001

Dong, H., Bao, J., Ryu, D., and Zhong, J. (2011). Design and construction of improved new vectors for *Zymomonas mobilis* recombinants. *Biotechnol. Bioeng.* 108, 1616–1627. doi: 10.1002/bit.23106

Franden, M. A., Pienkos, P. T., and Zhang, M. (2009). Development of a high-throughput method to evaluate the impact of inhibitory compounds from lignocellulosic hydrolysates on the growth of *Zymomonas mobilis*. *J. Biotechnol.* 144, 259–267. doi: 10.1016/j.jbiotec.2009.08.006

Ghazaei, C. (2017). Molecular chaperones impacts in growth, metabolism, pathogenicity and production of virulence factors in bacterial pathogen. *Rev. Med. Microbiol.* 29:1. doi: 10.1097/MRM.0000000000000123

Gibson, D. G., Young, L., Chuang, R.-Y., Venter, J. C., Hutchison, C. A., and Smith, H. O. (2009). Enzymatic assembly of DNA molecules up to several hundred kilobases. *Nat. Methods* 6, 343–345. doi: 10.1038/nmeth.1318

Gu, H., Zhang, J., and Bao, J. (2015). High tolerance and physiological mechanism of Zymomonas mobilis to phenolic inhibitors in ethanol fermentation of corncob residue. *Biotechnol. Bioeng.* 112, 1770–1782. doi: 10.1002/bit.25603

Han, D., Link, H., and Liesack, W. (2017). Response of *Methylocystis* sp. strain SC2 to salt stress: physiology, global transcriptome, and amino acid profiles. *Appl. Environ. Microbiol.* 83, e00866–e00817. doi: 10.1128/AEM.00866-17

He, M. X., Wu, B., Qin, H., Ruan, Z. Y., Tan, F. R., Wang, J. L., et al. (2014). *Zymomonas mobilis*: a novel platform for future biorefineries. *Biotechnol. Biofuels* 7:101. doi: 10.1186/1754-6834-7-101

He, M.-X., Wu, B., Shui, Z.-X., Hu, Q.-C., Wang, W.-G., Tan, F.-R., et al. (2012). Transcriptome profiling of *Zymomonas mobilis* under furfural stress. *Appl. Microbiol. Biotechnol.* 95, 189–199. doi: 10.1007/s00253-012-4155-4

Huang, S., Xue, T., Wang, Z., Ma, Y., He, X., Hong, J., et al. (2018). Furfural-tolerant *Zymomonas mobilis* derived from error-prone PCR-based whole genome shuffling and their tolerant mechanism. *Appl. Microbiol. Biotechnol.* 102, 3337–3347. doi: 10.1007/s00253-018-8817-8

Jenal, U., Reinders, A., and Lori, C. (2017). Cyclic di-GMP: second messenger extraordinaire. *Nat. Rev. Microbiol.* 15, 271–284. doi: 10.1038/nrmicro.2016.190

Jeon, Y. J., Xun, Z., Su, P., and Rogers, P. L. (2012). Genome-wide transcriptomic analysis of a flocculent strain of *Zymomonas mobilis*. *Appl. Microbiol. Biotechnol.* 93, 2513–2518. doi: 10.1007/s00253-012-3948-9

Liu, Z., Meng, R., Zhao, X., Shi, C., Zhang, X., Zhang, Y., et al. (2016). Inhibition effect of tea tree oil on listeria monocytogenes growth and exotoxin proteins listeriolysin O and p60 secretion. *Lett. Appl. Microbiol.* 63, 450–457. doi: 10.1111/lam.12666

Livak, K. J., and Schmittgen, T. D. (2001). Analysis of relative gene expression data using real-time quantitative PCR and the 2(-Delta Delta C(T)) method. *Methods* 25, 402–408. doi: 10.1006/meth.2001.1262

Ma, Y., Dong, H., Zou, S., Hong, J., and Zhang, M. (2012). Comparison of glucose/xylose co-fermentation by recombinant *Zymomonas mobilis* under different genetic and environmental conditions. *Biotechnol. Lett.* 34, 1297–1304. doi: 10.1007/s10529-012-0897-4

Miller, E. N., Jarboe, L. R., Turner, P. C., Pharkya, P., Yomano, L. P., York, S. W., et al. (2009). Furfural inhibits growth by limiting sulfur assimilation in ethanologenic *Escherichia coli* strain LY180. *Appl. Environ. Microbiol.* 75, 6132–6141. doi: 10.1128/AEM.01187-09

Moreno, A. D., Ibarra, D., Alvira, P., Tomás-Pejó, E., and Ballesteros, M. (2015). A review of biological delignification and detoxification methods for lignocellulosic bioethanol production. *Crit. Rev. Biotechnol.* 35, 342–354. doi: 10.3109/07388551.2013.878896

Nouri, H., Moghimi, H., Marashi, S. A., and Elahi, E. (2020). Impact of hfq and sigE on the tolerance of Zymomonas mobilis ZM4 to furfural and acetic acid stresses. *PLoS One* 15:e0240330. doi: 10.1371/journal.pone.0240330

Pereira, R. A.-O. X., Mohamed, E. A.-O., Radi, M. A.-O., Herrgård, M. J., Feist, A. A.-O., Nielsen, J. A.-O., et al. (2020). Elucidating aromatic acid

tolerance at low pH in *Saccharomyces cerevisiae* using adaptive laboratory evolution. *Proc. Natl. Acad. Sci. U. S. A.* 117, 27954–27961. doi: 10.1073/pnas.2013044117

Saier, J. M. H., and Paulsen, I. T. (2001). Phylogeny of multidrug transporters. *Semin. Cell Dev. Biol.* 12, 205–213. doi: 10.1006/scdb.2000.0246

Savvides, A. L., Kallimanis, A., Varsaki, A., Koukkou, A. I., Drainas, C., Typas, M. A., et al. (2000). Simultaneous ethanol and bacterial ice nuclei production from sugar beet molasses by a *Zymomonas mobilis* CP4 mutant expressing the inaZ gene of pseudomonas syringae in continuous culture. *J. Appl. Microbiol.* 89, 1002–1008. doi: 10.1046/j.1365-2672.2000.01208.x

Shui, Z.-X., Qin, H., Wu, B., Ruan, Z.-Y., Wang, L.-S., Tan, F.-R., et al. (2015). Adaptive laboratory evolution of ethanologenic *Zymomonas mobilis* strain tolerant to furfural and acetic acid inhibitors. *Appl. Microbiol. Biotechnol.* 99, 5739–5748. doi: 10.1007/s00253-015-6616-z

Takagi, H. (2019). "L-cysteine metabolism found in *Saccharomyces cerevisiae* and *Ogataea parapolymorpha*," in *Non-conventional Yeasts: From Basic Research to Application*. ed. A. Sibirny (Cham: Springer International Publishing) 521–537.

Tan, F.-R., Dai, L.-C., Wu, B., Qin, H., Shui, Z.-X., Wang, J.-L., et al. (2015). Improving furfural tolerance of *Zymomonas mobilis* by rewiring a sigma factor RpoD protein. *Appl. Microbiol. Biotechnol.* 99, 5363–5371. doi: 10.1007/s00253-015-6577-2

Tan, H., West, J. A., Ramsay, J. P., Monson, R. E., Griffin, J. L., Toth, I. K., et al. (2014). Comprehensive overexpression analysis of cyclic-di-GMP signalling proteins in the phytopathogen *Pectobacterium atrosepticum* reveals diverse effects on motility and virulence phenotypes. *Microbiology* 160, 1427–1439. doi: 10.1099/mic.0.076828-0

Todhanakasem, T., Sangsutthiseree, A., Areerat, K., Young, G. M., and Thanonkeo, P. (2014). Biofilm production by *Zymomonas mobilis* enhances ethanol production and tolerance to toxic inhibitors from rice bran hydrolysate. *New Biotechnol.* 31, 451–459. doi: 10.1016/j.nbt.2014.06.002

van der Pol, E., Springer, J., Vriesendorp, B., Weusthuis, R., and Eggink, G. (2016). Precultivation of *Bacillus coagulans* DSM2314 in the presence of furfural decreases inhibitory effects of lignocellulosic by-products during L(+)-lactic acid fermentation. *Appl. Microbiol. Biotechnol.* 100, 10307–10319. doi: 10.1007/s00253-016-7725-z

Wang, X., Gao, Q., and Bao, J. (2017). Enhancement of furan aldehydes conversion in *Zymomonas mobilis* by elevating dehydrogenase activity and cofactor regeneration. *Biotechnol. Biofuels* 10:24. doi: 10.1186/s13068-017-0714-3

Wang, X., He, Q., Yang, Y., Wang, J., Haning, K., Hu, Y., et al. (2018). Advances and prospects in metabolic engineering of *Zymomonas mobilis*. *Metab. Eng.* 50, 57–73. doi: 10.1016/j.ymben.2018.04.001

Wang, C., Liu, C., Hong, J., Zhang, K., Ma, Y., Zou, S., et al. (2013). Unmarked insertional inactivation in the gfo gene improves growth and ethanol production by *Zymomonas mobilis* ZM4 in sucrose without formation of sorbitol as a by-product, but yields opposite effects in high glucose. *Biochem. Eng. J.* 72, 61–69. doi: 10.1016/j.bej.2012.12.020

Westman, J. (2014). Ethanol production from lignocellulose using high local cell density yeast cultures. Investigations of flocculating and encapsulated *Saccharomyces cerevisiae*. Dissertation. University of Borås.

Xia, J., Liu, C. G., Zhao, X. Q., Xiao, Y., Xia, X. X., and Bai, F. W. (2018). Contribution of cellulose synthesis, formation of fibrils and their entanglement to the self-flocculation of *Zymomonas mobilis*. *Biotechnol. Bioeng.* 115, 2714–2725. doi: 10.1002/bit.26806

Yang, S., Franden, M. A., Brown, S. D., Chou, Y. C., Pienkos, P. T., and Zhang, M. (2014). Insights into acetate toxicity in *Zymomonas mobilis* 8b using different substrates. *Biotechnol. Biofuels* 7:140. doi: 10.1186/s13068-014-0140-8

Yang, S., Franden, M. A., Wang, X., Chou, Y.-C., Hu, Y., Brown, S. D., et al. (2020). Transcriptomic profiles of *Zymomonas mobilis* 8b to furfural acute and long-term stress in both glucose and xylose conditions. *Front. Microbiol.* 11:13. doi: 10.3389/fmicb.2020.00013

Yang, S., Mohagheghi, A., Franden, M. A., Chou, Y. C., Chen, X., Dowe, N., et al. (2016). Metabolic engineering of Zymomonas mobilis for 2,3-butanediol production from lignocellulosic biomass sugars. *Biotechnol Biofuels* 9:189. doi: 10.1186/s13068-016-0606-y

Yang, Y., Shen, W., Huang, J., Li, R., Xiao, Y., Wei, H., et al. (2019). Prediction and characterization of promoters and ribosomal binding sites of *Zymomonas mobilis* in system biology era. *Biotechnol. Biofuels* 12:52. doi: 10.1186/s13068-019-1399-6

Yi, X., Gu, H., Gao, Q., Liu, Z. L., and Bao, J. (2015). Transcriptome analysis of *Zymomonas mobilis* ZM4 reveals mechanisms of tolerance and detoxification of phenolic aldehyde inhibitors from lignocellulose pretreatment. *Biotechnol. Biofuels* 8:153. doi: 10.1186/s13068-015-0333-9

Conflict of Interest: The authors declare that the research was conducted in the absence of any commercial or financial relationships that could be construed as a potential conflict of interest.

Publisher's Note: All claims expressed in this article are solely those of the authors and do not necessarily represent those of their affiliated organizations, or those of the publisher, the editors and the reviewers. Any product that may be evaluated in this article, or claim that may be made by its manufacturer, is not guaranteed or endorsed by the publisher.

frontiers in Microbiology

ORIGINAL RESEARCH
published: 07 December 2021
doi: 10.3389/fmicb.2021.792987

Experimental Treatment of Hazardous Ash Waste by Microbial Consortium *Aspergillus niger* and *Chlorella* sp.: Decrease of the Ni Content and Identification of Adsorption Sites by Fourier-Transform Infrared Spectroscopy

Alexandra Šimonovičová[1], Alžbeta Takáčová[2], Ivan Šimkovic[1] and Sanja Nosalj[1]*

[1] Department of Soil Science, Faculty of Natural Sciences, Comenius University, Bratislava, Slovakia, [2] Department of Environmental Ecology and Landscape Management, Comenius University, Bratislava, Slovakia

OPEN ACCESS

Edited by:
Jana Sedlakova-Kadukova, University of St. Cyril and Methodius, Slovakia

Reviewed by:
Izabela Michalak, Wrocław University of Science and Technology, Poland
Sandeep Panda, Süleyman Demirel University, Turkey

***Correspondence:**
Alexandra Šimonovičová
alexandra.simonovicova@uniba.sk

Specialty section:
This article was submitted to Microbiotechnology, a section of the journal Frontiers in Microbiology

Received: *11 October 2021*
Accepted: *17 November 2021*
Published: *07 December 2021*

Citation:
Šimonovičová A, Takáčová A, Šimkovic I and Nosalj S (2021) Experimental Treatment of Hazardous Ash Waste by Microbial Consortium Aspergillus niger and Chlorella sp.: Decrease of the Ni Content and Identification of Adsorption Sites by Fourier-Transform Infrared Spectroscopy. Front. Microbiol. 12:792987. doi: 10.3389/fmicb.2021.792987

Despite the negative impact on the environment, incineration is one of the most commonly used methods for dealing with waste. Besides emissions, the production of ash, which usually shows several negative properties, such as a higher content of hazardous elements or strongly alkaline pH, is problematic from an environmental viewpoint as well. The subject of our paper was the assessment of biosorption of Ni from ash material by a microbial consortium of *Chlorella* sp. and *Aspergillus niger*. The solid substrate represented a fraction of particles of size <0.63 mm with a Ni content of 417 mg kg^{-1}. We used a biomass consisting of two different organisms as the sorbent: a non-living algae culture of *Chlorella* sp. (an autotrophic organism) and the microscopic filamentous fungus *A. niger* (a heterotrophic organism) in the form of pellets. The experiments were conducted under static conditions as well as with the use of shaker (170 rpm) with different modifications: solid substrate, *Chlorella* sp. and pellets of *A. niger*; solid substrate and pellets of *A. niger*. The humidity-temperature conditions were also changed. Sorption took place under dry and also wet conditions (with distilled water in a volume of 30–50 ml), partially under laboratory conditions at a temperature of 25°C as well as in the exterior. The determination of the Ni content was done using inductively coupled plasma optical emission spectrometry (ICP-OES). The removal of Ni ranged from 13.61% efficiency (*Chlorella* sp., *A. niger* with the addition of 30 ml of distilled water, outdoors under static conditions after 48 h of the experiment) to 46.28% (*Chlorella* sp., *A. niger* with the addition of 30 ml of distilled water, on a shaker under laboratory conditions after 48 h of the experiment). For the purpose of analyzing the representation of functional groups in the microbial biomass and studying their interaction with the ash material, we used Fourier-transform infrared

(FTIR) spectroscopy. We observed that the amount of Ni adsorbed positively correlates with absorbance in the spectral bands where we detect the vibrations of several organic functional groups. These groups include hydroxyl, aliphatic, carbonyl, carboxyl and amide structural units. The observed correlations indicate that, aside from polar and negatively charged groups, aliphatic or aromatic structures may also be involved in sorption processes due to electrostatic attraction. The correlation between absorbance and the Ni content reached a maximum in amide II band ($r = 0.9$; $P < 0.001$), where vibrations of the C=O, C–N, and N–H groups are detected. The presented results suggest that the simultaneous use of both microorganisms in biosorption represents an effective method for reducing Ni content in a solid substrate, which may be useful as a partial process for waste disposal.

Keywords: microbial consortium, *Chlorella* sp., *Aspergillus niger*, nickel, FTIR spectroscopy, ash waste material

INTRODUCTION

In view of the relatively high consumption of natural resources and energy, finding alternative methods of obtaining renewable sources of raw materials or waste recycling has become a priority for every developed country (Markoš et al., 2010). Waste, along with the prevention of waste generation and recycling, is coming to the attention of the environmental policy of European Union Member States. The current policy of EU Member States stakes out three basic goals: (1) preventing waste generation, (2) supporting waste reuse by recycling, (3) recovering waste to reduce its impact on the environment (Directive 86/278/EEC, 1986; Directive 91/271/EEC, 1991; Directive 2000/76/EEC, 2000; Geffert and Geffertová, 2004; Geffert and Mojžišková, 2009).

With the rapid growth of industrialization worldwide, risk elements (cadmium, lead, nickel, cobalt, copper, zinc, and chromium) are being generated into wastewater. These are toxic and non-biodegradable pollutants with high toxicity even at very low concentrations. They accumulate in the food chain and are adsorbed in organisms, a result of which is serious health problems (Nebeská et al., 2018; Sathe et al., 2018; Kushwaha et al., 2019).

Removing heavy metals from wastewater through the individual steps of a wastewater treatment plant is insufficient, and these metals are subsequently accumulated in the treatment plant sludge. Wastewater treatment plants produce three types of sludge: primary sludge, excess activated sludge, and digested sludge. Primary sludge is generated by precipitation of insoluble substances and organic compounds, while excess activated sludge is a result of the subsequent biological treatment system (aerobic or anoxic-oxic) (Pinto et al., 2016). The primary sludge is taken from the settling tanks and mixed with the concentrated excess biological sludge. This mixed sludge is anaerobically treated in digesters. After anaerobic stabilization of the raw sludge, digested sludge is formed, which is less hazardous considering hygienic standards.

Sludge contains >95% water, so it must be drained before disposal. Although sludge is rich in nutrients, its application in agriculture is strictly regulated due to the presence of pollutants and pathogens. In this regard, its incineration is often a preferred method of recovery. The advantage of incinerating sludge is the processing of a large volume of waste, while the negative side of this process is the production of gas emissions and also solid waste–ash.

Sludge ash, as a waste material, often contains several risk elements, including mercury, arsenic, chromium, selenium, nickel, barium, and manganese. Besides alkaline pH, a characteristic attribute of ash is that the elements in it are present mainly in the form of oxides. Some of these oxides are characterized by significant solubility in water, which is associated with a higher risk of mobilization of selected elements. On the other hand, the properties of the ash can be exploited in uses with various added value, from low to technologically advanced applications, thus bringing substantial economic benefits. Ash is used, for example, for soil reclamation, in construction, in the ceramics industry, in catalysis processes, in the synthesis of zeolite and for precious metals regeneration (Dai et al., 2012; Li et al., 2018; Munir et al., 2018). However, as reported by Ukwattage et al. (2013), the direct application of ash for increasing the yield of crops due to the high content of micro- and macronutrients is limited due to its categorization as hazardous waste from a legislative point of view. Disposal of ash by solidification, which at present is used currently, is only a partial solution, because by changing ash into a stabilized form, a possible secondary raw material containing useful components is irreversibly lost.

Ash generated from a sludge incinerator offers high potential for heavy metal recycling (Reijnders, 2005). Several techniques have been tested to reduce contamination. The most common are: decomposition treatment with the addition of inorganic acids; phosphoric acid stabilization (Vavva et al., 2017), elution with nitric acid (HNO_3) (Wang Y. et al., 2015), application with diluted sulfuric acid (H_2SO_4) (Kashiwakura et al., 2010), washing with hydrochloric acid (HCl) (Weibel et al., 2018); using citric acid for stabilization (Wang H. et al., 2018), using chelating agents for electroplating processes (Chen et al., 2015), and using hydrothermal processes (Ullah et al., 2018).

The use of a biosorbents based on different types of biomass, including bacteria, fungi, algae, yeast, and aquatic plants, has been studied in the process of nickel biosorption. According to

Sari and Tuzen (2008) and Wang and Chen (2009), biosorption onto living or non-living biomass, can be a feasible method for metal removal, because it is efficient, minimizes secondary wastes and utilizes low-cost materials (Montazer-Rahmati et al., 2011). Algae are among the excellent sorbents due to their high relative binding capacity. Sorbents such as activated carbon and natural zeolite are more effective, and the results of sorption are comparable to the ion exchange processes that take place using resins. In case of algal biomass various structural units are involved in the adsorption including carboxyl, amino and hydroxyl groups in algal cell-wall polysaccharides, which can act as binding sites for metals (Guarín-Romero et al., 2019). There is evidence that phenomena of ion exchange, chelation, inorganic precipitation, or a combination thereof occur at the cell membrane of microorganisms (de Rome and Gadd, 1991; Tiemann et al., 1999; Deng et al., 2007).

In recent studies biosorption processes were often assessed with simultaneous use of various organisms in form of microbial consortia. The microscopic green algae *Chlorella* sp. and the microscopic filamentous fungus *Aspergillus niger* were applied in wastewater treatment (Nasir et al., 2019). Removal of cadmium by consortium of *A. niger* and *Chlorella vulgaris* (Bodin et al., 2017) and removal of arsenic by *Aspergillus oryzae* and *C. vulgaris* (Li et al., 2019) in wastewater treatment were confirmed. Raval et al. (2016) reviewed a variety of adsorbents for the removal of nickel(II) ions from wastewater using activated charcoal but also a biomass of the green algae *C. vulgaris*, brown algae, such as *Nizmuddinia zanardini, Sargassum glaucescens, Cystoseria indica,* and *Padina australis* and filamentous fungi, such as *A. niger* and *Rhizopus nigricans*. The species *Rhizopus stolonifer* proved to be effective in the removal of lead, cadmium, copper, and zinc from contaminated soil or a solid substrate (Fawzy et al., 2017), and *Mucor* sp. together with the microalgae *Chlorella* sp. have also been widely used in water treatment. The mycoalgae biofilm based processes, propounds the scope for exploring new avenues in the bio-production industry and bioremediation (Rajendran and Hu, 2016). The coagulation of microscopic algae and filamentous fungi in the form of pellets has many advantages (such as harvesting by simple filtration) and is also very advantageous economically because of the low costs (Alrubaie and Al-Shammari, 2018).

The aim of our work was to evaluate the use of a consortium of two different microorganisms–*Chlorella* sp. (autotrophic) and *A. niger* (heterotrophic)–as a tool for decreasing the nickel content in hazardous ash waste from an incinerator. Most of the work that has focused on the assessment of the biosorption of metals by a microbial biomass used only a single organism in the experiments conducted. In this work, we decided to use *A. niger* and *Chlorella* sp. at the same time for Ni(II) ions sorption by consortium biomass. We started with the assumption that if the adsorbent is formed by a mixture of biomass of both organisms, it will result in a greater diversity of its chemical composition, which may in the end lead to a larger amount of adsorbed Ni. In the framework of studying decrease of the nickel content, we focused on identifying the structural units of the biomass of the given microorganisms that Ni binds to during sorption. Similar to other studies, we also used FTIR spectroscopy for this purpose. In works with a similar focus, the authors typically interpreted changes in the spectrum of the biomass sample before and after its interaction with the hazardous element (Pradhan et al., 2007; D'Souza et al., 2008; Kang et al., 2011; Guarín-Romero et al., 2019). A change in the peak parameters usually helped to identify the functional groups bound in the biomass that are involved in the retention of the element. In this study we used slightly different approach. We identified the given functional groups on the basis of a correlation spectrum, where each value represents the Pearson correlation coefficient expressing the collinearity between the absorbance at a given wavelength and the adsorbed Ni content for a selected number of samples. We assume that in this way the main sorption sites of microbial biomass can be accurately identified.

MATERIALS AND METHODS

Ash Substrate for the Disposal of Waste (Nickel)

The ash intended for nickel decontamination comes from an industrial sludge incinerator (**Figure 1A**). The ash was analyzed on the basis of a requirement for landfill waste recovery (**Table 1**). The sample was taken as a so-called mixed sample, i.e. from ten partial point samples from a temporary storage site (a landfill), namely so that all properties of the waste are representative. The pre-treatment consisted of quartation, homogenization and subsequent fractionation through a fractional sieve (mesh size 0.63 mm).

Analysis of Metals in the Ash Substrate

The basis of the method is the measuring of the atomic emission by optical spectroscopy. After mineralization (decomposition of solid samples into an aqueous matrix), the samples are sucked using a peristaltic pump through a nebulizer into a misting chamber, where they are nebulized. The aerosol created is then carried into a plasma, where excitation of the atoms occurs. Characteristic atomic line spectra are then generated by high frequency inductively coupled plasma (ICP). The radiation emitted is decomposed using a spectrometer grid and the intensities of the lines are monitored by detectors.

The determination of metals for pre-treatment of the ash took place by extraction under a reflux condenser. The original homogenized sample was weighed in the amount of 0.3 g into a reaction vessel and 21 ml of HCl and 7 ml of HNO_3 were added.

The reaction vessels were left open until the initial reaction (foaming) took place. The mixture was covered with a watch glass and left to stand at room temperature for 16 h. The vessels were subsequently placed on a heater and the reflux condenser was installed. The temperature of the reaction mixture was slowly raised until reflux conditions were reached. This state was maintained for 2 h to ensure that the cooling zone is lower than one-third the height of the reflux condenser. The reaction mixture was then allowed to cool. The condenser was rinsed with 10 ml of 1 mol L^{-1} nitric acid in the reaction vessel. The mineralizate was then poured quantitatively through a filter paper

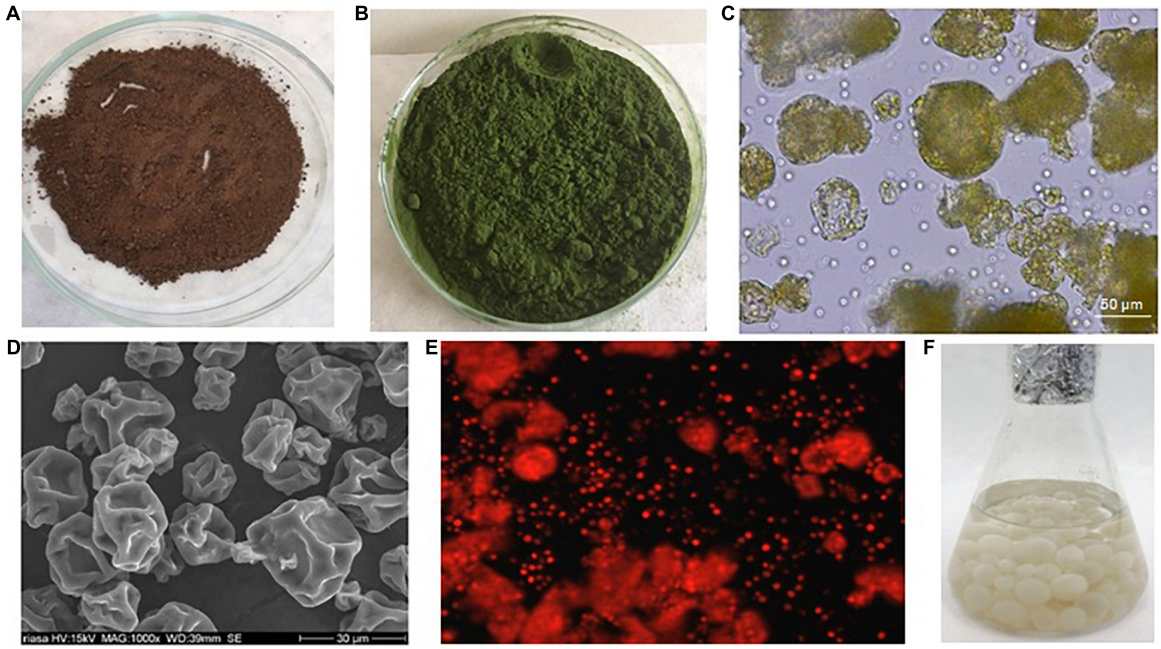

FIGURE 1 | (A) Treated ash substrate from the sludge incinerator. **(B)** Dry biomass of the green alga *Chlorella* sp. after pre-treatment. **(C)** Dry biomass of the green alga *Chlorella* sp. in a light microscope. **(D)** Dry biomass of the green alga *Chlorella* sp. in SEM. **(E)** Dry biomass of the green alga *Chlorella* sp. in a fluorescence microscope. **(F)** Pellets of *Aspergillus niger* after washing in distilled water.

TABLE 1 | Input values of ash from the sludge incinerator.

Parameter	Determined value	Unit of dry weight
Hg	0.02	mg kg^{-1}
As	41.0	mg kg^{-1}
Cd	7.64	mg kg^{-1}
Ni	417	mg kg^{-1}
Pb	146	mg kg^{-1}
PAU	<0.1	mg kg^{-1}
P	5.88	% (w/w)
S	1.22	% (w/w)
C	3.43	% (w/w)
H	0.36	% (w/w)
N	0.32	% (w/w)
NEL	<10.0	mg kg^{-1}
TOC	0.86	% (w/w)
dry mass	98.0	% (w/w)

PAU, polyaromatic hydrocarbons; NEL, non-polar extractables; TOC, total organic carbon.

into a 100 ml measuring cup, filled up to the mark and then poured into a 100 ml plastic storage container.

Green Algae *Chlorella* sp. as the Autotrophic Organism

The genus *Chlorella* sp. as a representative of algae ranks among the most numerous groups of green algae. In all the experiments an algal biomass of *Chlorella* sp. obtained from Institute of Microbiology of the Czech Academy of Sciences (Opatovický mlýn, Třeboň, Czechia), was used (**Figures 1B–D**). The dry biomass of algae was prepared by washing the biomass in deionized water and drying in an oven at 70°C for 24 h.

Microscopic Filamentous Fungus *Aspergillus niger* as the Heterotrophic Organism

A cosmopolitan strain of *A. niger* (**Figure 2A**) was isolated from Dystric Cambisol (contaminated and eroded) without vegetation. The chemical characteristics of the substrate showed an ultra-acidic soil reaction (pH 3.12), a very low amount of organic matter (%C_{ox} 0.49) and exceeded the value of aluminum (Al 727 mg kg^{-1}) (Šimonovičová et al., 2021).

Aspergillus niger fungal pellets were prepared in a 45 ml of SDB (Sabouraud Dextrose Broth Liquid Medium, Himedia, Mumbai, India) enriched with a 5 ml suspension of conidia from a pure culture of *A. niger*. Cultivation took place over 5 days at 25°C in 250 mL Erlenmeyer flasks, with stirring at 170 rpm (Unimax 2010 shaker, Heidolph, Germany) under laboratory condition at 25°C (**Figure 1F**). The *A. niger* fungal pellets formed very quickly, and after 5 days they were removed by filtration, washed with a large amount of distilled water and used in the experiments (**Figure 2B**).

Microscopy

The figures of the dry green algae biomass (**Figure 1C**), the filtered *A. niger* pellets (**Figures 2C–E**, **3B–E**), were made with a Canon IXUS 16.1 megapixel camera (Japan).

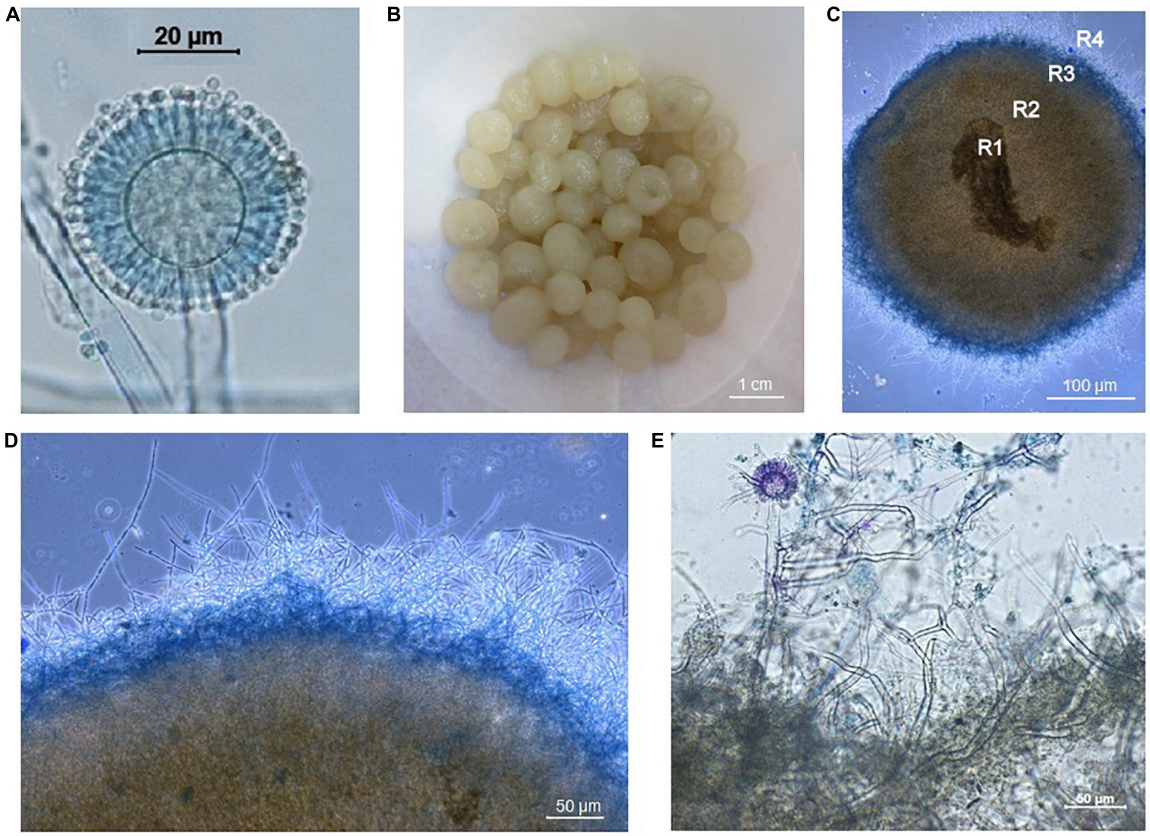

FIGURE 2 | (A) Conidial head of *Aspergillus niger* (conidiophore terminated by a vesicle with phialides and conidia). **(B)** *Aspergillus niger* pellets after washing and filtration. **(C)** *Aspergillus niger* pellets, which have four visible parts according to García-Reyes et al. (2017). R1 is the core of the pellet, R2 the hollow part, which may be around the core, R3 is the layer of fibers which may show signs of autolysis, R4 is the outer part of the pellet which appears to be fuzzy or hairy, the so-called "hairy region" and consists of viable fibers. **(D)** Detail of the "hairy region" of the pellet. **(E)** Detail of "hairy region" of the pellet with a conidiophore of *Aspergillus niger*.

The figures of the *Chlorella* sp. surface structure (**Figure 1D**) were observed under a JEOL JXA 840A Scan Electron Microscopy (SEM) (Japan).

The figures of the *A. niger* strain (**Figure 2A**), the *A. niger* pellets (**Figures 2C–E**), and the *A. niger* with *Chlorella* sp. pellets (**Figures 3B–E**) were observed under an Axio Scope A 1 Carl Zeiss Jena light microscope in a drop of lactic acid enriched with a cotton blue stain (0.01%).

Fluorescence Recording

Microscopic measurements [Microscope: AXIO–IMAGER A, CARL ZEISS (Germany), Filter set 02–excitation G 365, Beam splitter FT 396, Emission LP 420], chlorophyll in a metabolically inactive biomass (**Figure 1E**).

Fourier-Transform Infrared Spectroscopy

In the case of each sample, approximately 1 g of bulk material was pulverized into a fine powder in an agate mortar. After homogenization, the samples were dried at 60°C for 24 h. Before each measurement 2 mg (± <0.05 mg) of homogenized sample was thoroughly mixed with 200 mg of KBr and pressed into a small pellet. FTIR analysis was performed in transmission mode and the spectral data were expressed as absorbance values. Each spectrum was recorded in the mid-infrared region (from 4000 to 400 cm^{-1}) by averaging 128 scans, with a spectral resolution of 4 cm^{-1}. The analysis was performed using a NICOLET 6700 FTIR spectrometer and the OMNIC 8 software (Thermo Scientific). The FTIR spectra obtained were not corrected by any procedures, filters, or algorithms, such as smoothing, absorbance normalization, baseline corrections, etc.

Elemental Analysis (CHNSO)

Mass concentrations of C, H, N, and S were determined by combustion of the sample (app. 10 mg) in the atmosphere with elevated oxygen content and subsequent detection of liberated gases by the gas chromatography principle. The O content was measured similarly, but the sample was heated in an atmosphere of pure He, without the addition of a catalyst. The measurement was carried out by the elemental analyzer FLASH 2000 equipped with the Eager Xperience software (Thermo Scientific).

Organization of Experiments

All the experiments were organized according to **Table 2**. In all samples 3 g of ash were used. Dry biomass of *Chlorella* sp. in an

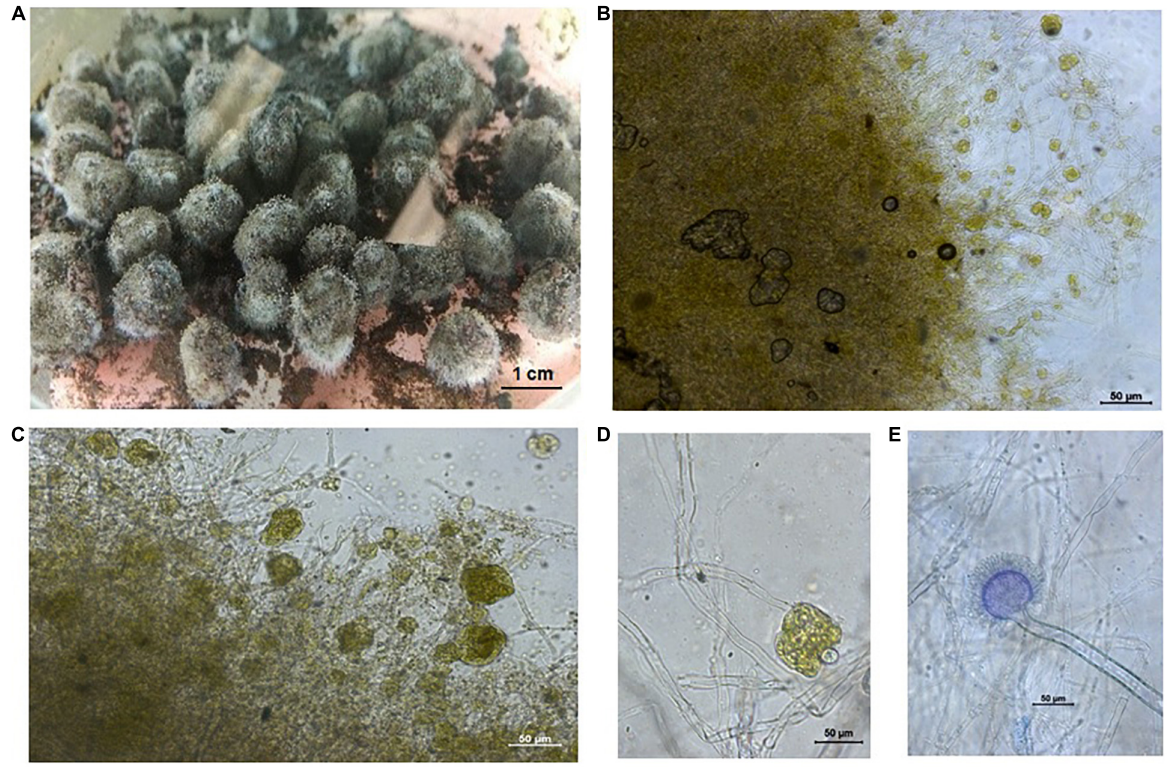

FIGURE 3 | (A) *Aspergillus niger* pellets after application to the ash substrate under laboratory conditions on a shaker and without addition of water. **(B)** Detail of the *Aspergillus niger* pellet with *Chlorella* sp. and with nickel particles. **(C,D)** Detail of the "hairy region" of the *Aspergillus niger* pellet with *Chlorella* sp.. **(E)** Detail of "hairy region" with the conidial head of *Aspergillus niger*.

TABLE 2 | Conditions of all experiments in laboratory or in the exterior.

Sample	Ash (3 g)	Pellets of *A. niger*	*Chlorella* sp. (1 g)	Distilled water	Shaker 170 rpm/min.	Laboratory exterior
1	+	+	–	30 ml	+	L
2	+	+	–	–	–	L
3	+	+	–	30 ml	+	L
4	+	+	–	–	–	L
5	+	+	+	30 ml	+	L
6	+	+	+	30 ml	+	L
7	+	+	+	–	–	L
8	+	+	+	–	–	L
9	+	+	+	30 ml	–	E
10	+	+	+	30 ml	–	E
11	+	+	+	–	–	E
12	+	+	+	–	–	E
13	+	+	+	–	+	L
14	+	+	+	–	–	E
15	+	+	+	50 ml	+	L

L, laboratory; E, exterior.

amount of 1 g was used only in samples 5–15. *A. niger* fungal pellets were also used in all samples. Distilled water in a volume of 30 ml was added to samples 1, 3, 5, 6, 9, 10, and a volume of 50 ml was added only to sample 15. Samples 1, 3, 5, 6, 13, and 15 were performed on a shaker, while all other samples were run under static conditions.

We chose the variability of individual samples within the experiments based on the different decontamination conditions both under natural conditions (exterior) and under laboratory conditions at a temperature of 25°C. The samples for analysis were taken at a defined time interval of 48 h. At the end of the experiments in the case with the addition of

distilled water, the suspension was separated from the solution by membrane filtration (Millipore, pore size 0.45 μm). The metal analysis of all samples was carried out on an emission spectrometer with inductance coupled plasma (ICP Profile Plus, Teledyne Leeman Labs, United States). All experiments were performed in duplicate.

RESULTS AND DISCUSSION

The Role of the Microbial Consortium in the Decrease of Ni Content

The input values of the ash from the sludge incinerator are documented in **Table 1**. The removal of Ni from the material ranged as follows: 13.61% (sample 10) < 17.25% (sample 3) < 18.58% (sample 9) < 19.68% (sample 4) < 22.49% (sample 12) < 28.37% (sample 11) < 30.95% (sample 8) < 34.56% (sample 7) < 37.90% (sample 6) < 44.01% (sample 15) < 46.28% (sample 5), as shown in **Figure 4**.

From the various experimental conditions, the combination of *A. niger* pellets and dry algal *Chlorella* sp. biomass, with the ash substrate moistened with 30 ml to 50 ml of distilled water, proved to be the most effective. The experiment ran on a shaker under laboratory conditions. During shaking, in addition to the even distribution of pellets with the ash substrate, the coagulation of pellets with the algal biomass also occurred (**Figures 3A–E**). The coagulates formed not only absorbed Ni on the surface but also bioleached in the presence of *A. niger* (samples 5, 6, and 15).

Under laboratory conditions, when only *A. niger* pellets were applied to the ash, we recorded a slightly higher efficiency under static conditions and without the addition of distilled water (sample 4) compared with the addition of 30 ml of distilled water on a shaker (sample 3). In the exteriors, experiments were conducted under static conditions, and in this case, too, we recorded lower values of Ni content reduction in the aqueous medium (samples 9 and 10) compared with the anhydrous environment (samples 11 and 12). The species *A. niger* is a known producer of many organic acids and secondary metabolites (Šimonovičová et al., 2020, 2021) which are used in bioleaching processes. It can be assumed that in the case of adding distilled water, the organic acids produced were diluted, which caused a slowing down/reduction of the bioleaching process from the solid substrate.

The absorption of Ni from the ash substrate occurs by means of several processes. When *A. niger* pellets are used alone, the process of bioleaching takes place. When a consortium of the microorganisms *Chlorella* sp. and *A. niger* were used, aside from the bioleaching, the efficiency is increased by involving the cell wall of green algae biomass. The cell wall of algae is made up of cellulose microfibrils, pectins, hemicelluloses, and proteins. These polymers form a complex network of pores and channels that influence the movement of substances in this space. But the surface negative charge of polymers can limit the movement of minerals as well as heavy metals by binding them. However, in general, the cell wall is permeable. The cytoplasmic membrane, as well as the vacuole membrane, represent a highly selective semipermeable barrier between the internal and external cell environment, and its role is to control the transfer of substances into and out of the cell to the surrounding space. It is only permeable for certain substances, for example, the molecules of some gases (O_2, CO_2, N_2) and for water, but less so for glycerol or ethanol. For substances that cannot pass freely into the cell through the cytoplasmic membrane, transmission is provided *via* pumps, transporters, and channels (which are membrane proteins), which are more or less specific for transport of the given substance.

For us, the so-called ABC carriers, which is a general term used for a large and diverse group of carriers, are of interest. ABC transporters on a tonoplast provide transport, for example, of heavy metals or herbicides into the vacuole as well as their sequestration. In an environment where different ions are present, competition often occurs between, for example, Ca^{2+} and other cations at the interaction site. Thus, instead of a "good cation," an unwanted ion, e.g., Cd or ion of another heavy metal, enters the cell. However, with damaged cells and a disrupted cell membrane system a loss of membrane semipermeability and uncontrolled movement of substances occurs. Microorganisms have the ability to accumulate many heavy metals and toxic elements (Pb, Ag, Pt, Pd, Au, Hg, Ga, Cd, Cu, Ni) from the external environment (Bulgariu and Bulgariu, 2020). Living and dead cells, the products of cell metabolism, extracellular polysaccharides and cell wall components all have the ability to receive and accumulate metals (Timková et al., 2018). The primary carrier surface of biosorption, however, is the cell wall of the biosorbent. The composition of the cell wall consists particularly of polymeric substances that are rich sources of various functional groups, by which the contaminants bind. The following groups can be included here: carboxyl (–COOH), hydroxyl (–OH), sulfhydryl (–SH), phosphate ($–PO_4^{3-}$), amino ($–NH_4^{+}$), and others (Gupta and Diwan, 2017).

The metabolically inactive, i.e., the dead culture of an algal biomass, can isolate metal ions and metal complexes from solution due to its unique chemical composition. When selecting metal-sorbent biomaterials, it is necessary to start from the factor of origin and thus resolve the issues of availability, quantity and potential demand (de Rome and Gadd, 1991; Tiemann et al., 1999). The advantage of applying dead biomass compared to a living one, i.e., an active biomass, is that the living biomass cells require the addition of a fermentation medium (which are costly), and the simultaneous addition of medium increases biological oxygen demand (BOD) and chemical oxygen demand (COD). Furthermore, dead biomass is not affected by the toxicity of metal ions and can be subjected to various chemical and physical pre-treatments to increase sorption. As a result, adsorbed metals can be easily obtained from the biomass by chemical or physical methods, which leads to repeated use of the biomass, thus reducing the costs of the process. Ash classified as hazardous waste is disposed of by several methods, such as heat treatment (e.g., sintering, melting and vitrification) (Park et al., 2005), the setting of cement (Bie et al., 2016), chemical stabilization (Nzihou and Sharrock, 2002; Wang F. H. et al., 2015), or extraction (Tang and Steenari, 2015; Wang W. et al., 2018). Other alternative methods for reducing hazardous substances in ash, which run with a lower energy load or better performance,

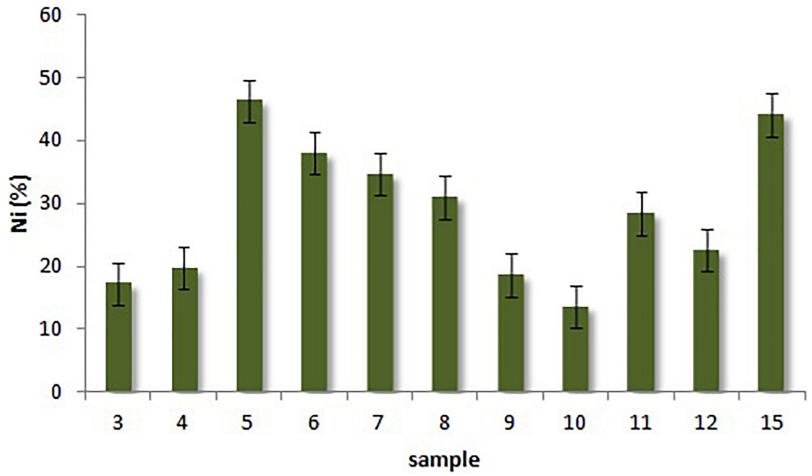

FIGURE 4 | Decrease of the nickel content in the ash from the sludge incinerator by the microbial consortium.

include hydrothermal treatment (Jin et al., 2013; Qiu et al., 2017, 2018) and mechanical-chemical treatment (Chen et al., 2019).

Fourier-Transform Infrared Spectra of *Chlorella* sp. and *Aspergillus niger* Biomass

There were several differences between the spectra of *Chlorella* sp. and *A. niger,* respectively, which are related to the different chemical composition of the two microorganisms. According to Johnson (1965), the main components building the mycelium of *Aspergillus* are carbohydrates (73–83%), with smaller portions of lipids (2–7%) and proteins (0.5–2.5%), while in the case of *Chlorella* sp., approximately 50% of the biomass is made up of proteins (Wild et al., 2019). Apart from proteins, *Chlorella* sp. Also contains a higher amount of lipids (∼18%) and a significantly lower concentration of carbohydrates (∼23%) in comparison to *A. niger* (Prabakaran et al., 2018). The results of FTIR spectroscopy were in general accordance with these differences. IR absorption in the *Chlorella* sp. spectrum may be associated mainly with amides and aliphatic structures, whereas the spectrum of *Aspergillus* showed more peaks characteristic for carbohydrates (polysaccharides). It should be noted that amide groups are not only a part of proteins but are also present in certain polysaccharides, such as chitin. In some cases, the amides bound in different structural units can be distinguished, as the vibrations of the respective functional groups manifest at different frequencies. The nitrogen content detected in the biomass was lower in the case of *A. niger* in comparison to *Chlorella* sp., and the same accounts for the N/C ratio (**Table 3**). This is associated with total amount of proteins in the biomass, which was probably lower in the case of *Aspergillus*.

There was a peak around 3280 cm^{-1} in the *A. niger* spectrum (**Figure 5A**) which was much less visible in the case of *Chlorella* sp. (**Figure 5B**). This absorption may be assigned to amines, which were detected in various fungal species and strains (Stüttgen et al., 1978; Karimi et al., 2019). Johnson (1965) reported that the cell wall of *A. niger* contains approximately 9–13% hexosamines. Amine and carboxylate groups were identified as major functional groups for metal biosorption in the *A. niger* biomass (Cai et al., 2016). This is in accordance with results presented here, as one of the peaks of the correlation spectrum reached a maximum at 3284 cm^{-1}, which lies within the amine frequency interval. Specifically, IR absorption around 3280 cm^{-1} is caused by the N–H stretching of secondary amines (Smith, 2019). However, this peak may also be associated with the amides bound in proteins (Forfang et al., 2017) or chitin (Rinaudo, 2006), as stretching vibrations of the N–H group and associated absorption around 3280 cm^{-1} are characteristic for both of these components. The peak with a maximum at 2143 cm^{-1} in the *A. niger* spectrum can be associated with isocyanides, which have been identified in various microorganisms, including *Aspergillus* species (Massarotti et al., 2021). According to Bittante and Cecchinato (2013), isocyanides show characteristic absorption between 2110 and 2165 cm^{-1}.

Another difference observed in the two spectra is the peak at 1602 cm^{-1}, which was absent in case of *Chlorella* sp. The absorption at frequencies around 1600 cm^{-1} is associated with vibrations of the aromatic ring and the presence of melanin pigments in the fungal biomass (Meenu and Xu, 2019). Information on the synthesis of various pigments by filamentous fungi, including *Aspergillus* species, were reviewed by Kalra et al. (2020). Significant differences between the spectra of *A. niger* and *Chlorella* sp. were detected in the regions of amide vibrations, particularly in the amide I and II spectral bands. This is related mainly to the differing overall protein content in the biomass of the two compared microorganisms, which was probably significantly higher in the case of *Chlorella* sp. Amide I and II bands are typically represented by two distinct peaks with maxima at around 1656 and 1547 cm^{-1}, respectively (Lorenz-Fonfria, 2020). These two peaks are very apparent in the *Chlorella* sp. spectrum, whereas they are less prominent in the case of *A. niger*. The absorption in each of the two amide bands is associated with the combination

TABLE 3 | Organic elemental composition (CHNSO) of biomass samples and solid substrate together with contents of adsorbed Ni.

Sample	C	H	N	S	O	SUM	C/N	Ni
			g kg^{-1}					mg kg^{-1}
1	402.80	62.71	56.62	2.76	398.23	923.11	7.11	–
2	390.76	60.95	57.34	1.44	400.88	911.37	6.82	–
3	57.73	6.43	6.10	1.55	136.56	208.36	9.47	55
4	109.10	13.46	13.28	5.39	165.31	306.53	8.22	62
5	175.74	24.72	27.50	5.72	207.08	440.75	6.39	147
6	135.43	15.88	22.05	2.08	151.86	327.30	6.14	120
7	118.31	13.80	18.83	1.22	146.53	298.68	6.28	110
8	149.87	18.44	23.94	5.71	174.13	372.08	6.26	98
9	160.58	19.61	24.29	–	166.40	370.88	6.61	59
10	167.06	20.80	27.09	2.15	168.08	385.18	6.17	43
11	165.54	22.98	26.74	–	192.37	407.63	6.19	24
12	168.97	23.33	27.29	5.08	190.74	415.40	6.19	71
13	452.89	66.08	75.23	3.78	340.55	938.53	6.02	–
14	506.22	64.74	62.63	–	320.15	953.75	8.08	–
15	231.55	30.56	38.80	2.72	217.88	521.52	5.97	140
Chlorella sp.	486.77	67.16	95.13	19.52	303.64	972.21	5.12	–

Samples 1–15 are assigned according to ***Table 2****.*

of vibrations of several functional groups. The amide I peak results from the stretching of the C=O and C–N groups, respectively, as well as N–H bending. Amide I absorption is primarily caused by the C=O stretching vibration of the amide group, with weaker contributions from the amide C–N stretching and the N–H bending. In the case of the amide II band, the absorption is caused mainly by N–H bending and C–N stretching (van Hoogmoed et al., 2003; Lorenz-Fonfria, 2020). However, due to the complex and variable structure of proteins, slightly differing frequencies are reported for the amide I and amide II bands when data from various sources are compared.

The spectra of *A. niger* and *Chlorella* sp. also exhibited different absorption patterns between 1470 and 1430 cm^{-1}. Whereas the spectrum of *Chlorella* sp. showed only one peak (1454 cm^{-1}) in the considered interval, the spectrum of *A. niger* showed a triplet of peaks, with maxima at 1469, 1450, and 1431 cm^{-1}, respectively. There are two adjacent bands in which the vibrations of aliphatic structures are detected: asymmetrical CH bending in the methyl group at 1470 cm^{-1} and methylene scissoring at 1465 cm^{-1} (Stuart, 2004). Other works report slightly different frequencies for these two bands. For example, Hollas (2004) associates the 1444 cm^{-1} frequency with asymmetric deformations of CH_3, while Haneef et al. (2017), who used fungal mycelia as a source of various fibrous materials, linked symmetric bending of CH_2 with the absorption around 1450 cm^{-1}. Although various authors who analyzed a fungal biomass associated the peaks between 1465 and 1450 cm^{-1} with the vibrations of the CH groups in lipids (Bhat, 2013; Lecellier et al., 2014; Haneef et al., 2017; Kosa et al., 2018), it is worth noting that the interval between 1500 and 1300 cm^{-1} is often termed as the "mixed" region. Besides lipids, vibrations of functional groups bound in polysaccharides, proteins and triterpene compounds may be detected in the considered interval (Meenu and Xu, 2019; Saif et al., 2021). The majority of absorption at 1430 cm^{-1} was probably caused by C–O–H bending in polysaccharides (Song et al., 2015; Meenu and Xu, 2019), but some contributions from the COO^- group in carboxylic acids cannot be ruled out (Max and Chapados, 2004; Stuart, 2004).

In the case of the *Chlorella* sp. spectrum there is a relatively broad peak at 1397 cm^{-1}, which can be associated with asymmetric stretching of COO^- (van Hoogmoed et al., 2003) and at the same time with the symmetric bending of CH in the CH_2 and CH_3 groups, respectively (D'Souza et al., 2008). A smaller peak at 1377 cm^{-1} can be assigned to symmetric bending of the aliphatic CH_3 (Kosa et al., 2018; Meenu and Xu, 2019). Haneef et al. (2017) associated the absorption around 1375 cm^{-1} with the CH bending of chitin molecules in the fungal mycelium. In our case, the peak was present only in the *A. niger* spectrum, which supports the assumption that it was caused by chitin. The relatively sharp absorption at 1312 cm^{-1} was probably caused by the C–O stretching of carboxylic acids (Meenu and Xu, 2019) and/or the asymmetric C–N–C stretching of aromatic amines (Stuart, 2004; Silverstein et al., 2005).

The peaks at 1250 (*A. niger*) and 1242 cm^{-1} (*Chlorella* sp.), respectively, can in both cases be linked to the amide III band, where the absorption is associated with CN stretching, NH bending and CO in-plane bending (López-Lorente and Mizaikoff, 2016). It is probable that the absorption in this region was also partially caused by asymmetric P=O stretching in nucleic acids (Haneef et al., 2017) and phospholipid substances (Kosa et al., 2018). From a comparison of the spectra it follows that the peak around 1250 cm^{-1} was more intense in the case of *Chlorella* sp. than in *A. niger*. This suggests that the absorption was caused mainly by proteins and also partially by phospholipids, as their portion in the biomass is higher in comparison to nucleic acids (especially in *Chlorella* sp.).

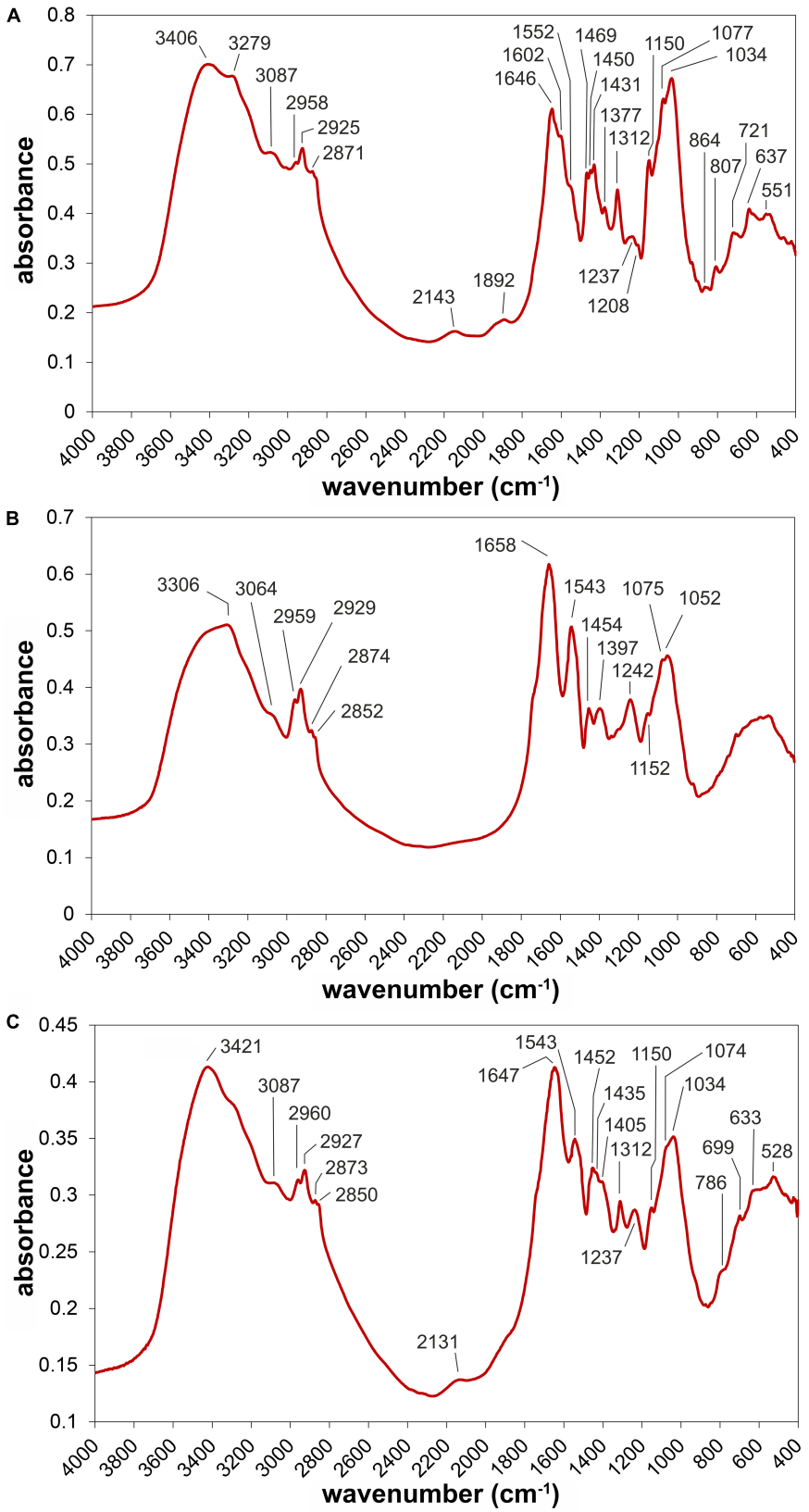

FIGURE 5 | FTIR spectra of *Aspergillus niger* biomass **(A)**, *Chlorella* sp. **(B)**, and the consortium of both microorganisms **(C)**, respectively.

The majority of the absorptions detected between 1200 and 900 cm^{-1} originate from the vibrations of carbohydrates. Specific functional groups and related frequencies include stretching vibrations of the COC (1150 cm^{-1}), CO (1075 cm^{-1}), and CC (1052 or 1034 cm^{-1}) groups (Bhat, 2013; Baeva et al., 2019). In addition to carbohydrates, the C–O stretching of alcohols and sulfoxides occur at 1053 and 1034 cm^{-1}, respectively (Rahman et al., 2014). However, the concentration of these substances in the biomass of both organisms is probably significantly lower in comparison to carbohydrates. Although the spectra of the *A. niger* and *Chlorella* sp. biomass were interpreted separately in this section, the adsorption experiments were carried out using the "mixture" of these two microorganisms. The spectrum of this this sample (without adsorbed Ni) is shown in **Figure 5C**.

Functional Groups Involved in the Adsorption of Ni

The interaction between the microbial biomass and the Ni substrate was assessed on the basis of a correlation spectrum. In the spectrum each value expresses the collinearity between the absorbance detected at certain wavelength and the amount of Ni retained by the sample. This approach enables better identification of the sorption sites in comparison to simple visual observation of the spectra. This follows from **Figure 6**, where the spectra are sorted according to the concentration of adsorbed Ni. It is hard to identify the change in absorbance or the shift in peak positions in the plotted spectra which would be related to concentration of Ni in the sample. Among the few visible changes in the spectra is the increase in absorbance between 1600 and 1400 cm^{-1}, which was at the same time accompanied by a higher amount of adsorbed Ni. In this regard, the correlation spectrum is more informative, as it indicates which functional groups are involved in the sorption of Ni.

The significance of the correlation ($P < 0.05$) was exceeded at frequencies characteristic for various organic groups (**Figure 7**). The first two peaks at the margin of the displayed spectral range, around 3284 and 3062 cm^{-1}, may be assigned to stretching vibrations of the NH group in amides (Parker, 1971; van Hoogmoed et al., 2003; Forfang et al., 2017). However, the origin of the 3284 cm^{-1} peak may also be associated with OH stretch due to the formation aquo-metal complexes (Zhang et al., 2021). The four adjacent peaks, within the 2960 and 2850 cm^{-1} interval, represent the different stretching vibrations of aliphatic CH groups, specifically: methyl symmetric CH stretching at 2960 cm^{-1}, methylene asymmetric CH stretching at 2930 cm^{-1}, methyl asymmetric CH stretching at 2870 cm^{-1}, and methylene symmetric C–H stretching at 2850 cm^{-1} (Stuart, 2004). A significant correlation between absorbance and the content of adsorbed Ni was also observed at 1695 and 1632 cm^{-1}, respectively. The more apparent peak at 1695 cm^{-1} is due to the stretching vibrations of the C=O group, which is a part of various organic structures, including carboxylic acids (COOH), amides (CONH) or esters (COOR). On the other hand, the smaller peak with a maximum around 1630 cm^{-1} probably represents the C=O stretching vibration of a dissociated COO^{-} group (Antisari et al., 2011; Kang et al., 2011).

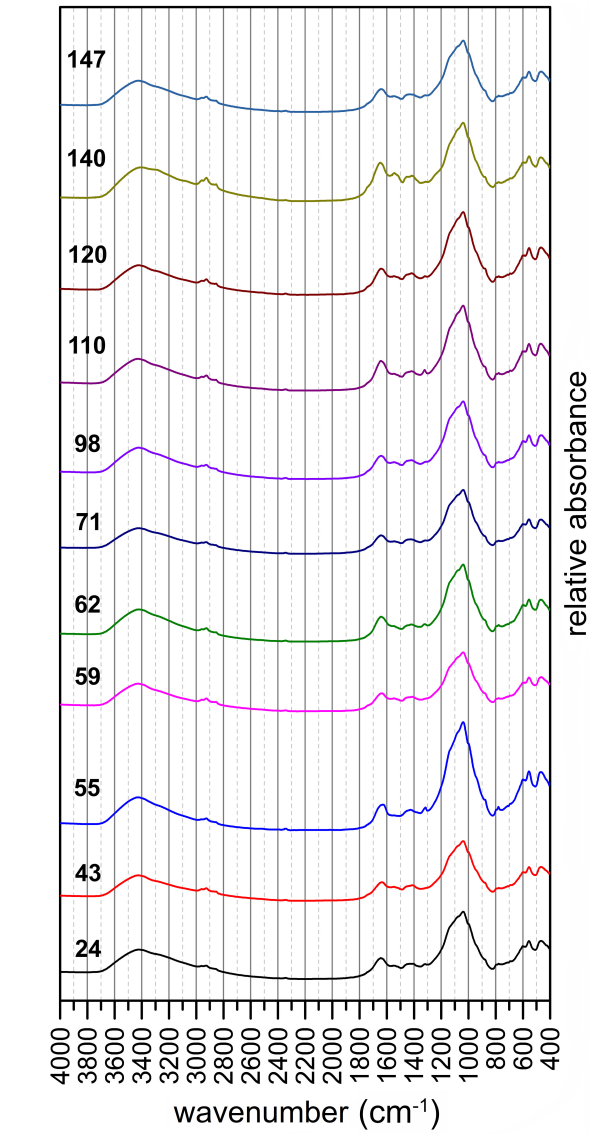

FIGURE 6 | FTIR spectra of *Chlorella* sp./*Aspergillus niger* pellets after the adsorption experiments (values on the left indicate the amount of adsorbed Ni).

The correlation between absorbance and the content of adsorbed Ni showed higher values in the amide I and II bands, which correspond with the intervals of 1710–1600 and 1580–1520 cm^{-1}, respectively (Lorenz-Fonfria, 2020). As was mentioned in the previous section, absorbance in amide I band is associated with the symmetric stretching of C=O and C–N together with N–H bending, whereas in case of the amide II band, the absorbance is indicative mainly of C–N stretching and N–H bending vibrations (Lecellier et al., 2014).

Although the correlation spectrum did not show peaks with maxima at 1650 or 1600 cm^{-1}, the *r* values at these wave numbers clearly exceeded the significance level ($P < 0.01$). The mentioned frequencies are associated with vibrations of aromatic carbon

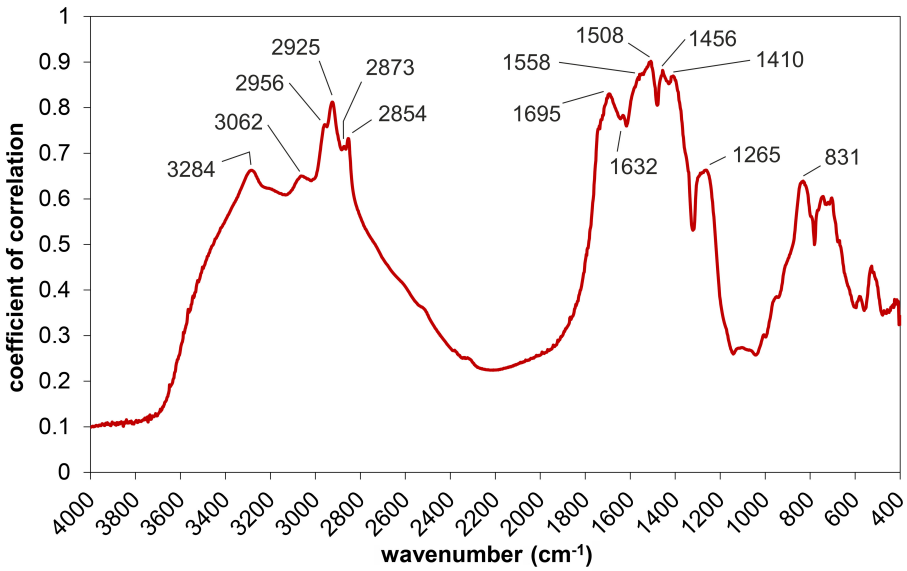

FIGURE 7 | Correlation spectrum expressing collinearity between the amount of adsorbed Ni and the absorbance detected in the mid-infrared region ($r > 0.6$ corresponds to the $P < 0.05$ significance level).

(Rahman et al., 2014; Meenu and Xu, 2019). Some amino acids (and their metabolites), which are synthesized by algae and other microorganisms, contain an aromatic ring in their structure (Żyszka-Haberecht et al., 2019). Aromatic structural units are also bound in various pigments, some of which (melanins) are present in fungal mycelium (Rahman et al., 2014). It cannot be ruled out that the mentioned substances contributed to the sorption of Ni by the microbial biomass.

A significant correlation between adsorbed Ni and absorbance was observed at 1558 and 1508 cm^{-1}, respectively. Both peaks are within the amide II interval, where IR absorption is caused by the combination of N–H bending and C–N stretching vibrations. In addition, the band around 1558 cm^{-1} was also associated with asymmetric stretching of the COO^- group of amino acids (Barth, 2000, 2007), carboxylic acids and their salts (Max and Chapados, 2004). This suggests that carboxyl groups can effectively contribute to Ni adsorption. The coefficient of correlation reached the highest value (0.9) at 1508 cm^{-1}. In a study of a similar nature, where the removal of Cd from water by cyanobacterial biomass was assessed, Bon et al. (2021) assigned the IR adsorption at 1510 cm^{-1} to N–H bending. Besides the mentioned C–N stretching and N–H bending, vibrations of aromatic carbon may be detected at frequencies around 1508 cm^{-1}, which means that various compounds containing an aromatic ring cause the absorption at the given wave number. In a number of works dealing with the composition of soil organic matter, the peak around 1510 cm^{-1} was associated with the stretching vibrations of aromatic carbon (Haberhauer and Gerzabek, 1999; Pietikäinen et al., 2000; Jiménez-González et al., 2019). Similar findings are reported in studies on the analysis of plant materials, where absorption at 1515 cm^{-1} indicates valence vibrations of aromatic C in phenolic compounds (Heredia-Guerrero et al., 2014). It is worth noting that Barth (2007) associated the band around 1510 cm^{-1} with the detection of amino acids containing an aromatic ring in their structure.

The correlation between absorbance and the content of adsorbed Ni also showed a maximum at 1456 cm^{-1}. This peak probably represents the bending of CH_2 groups in lipids, aliphatic structures (Mayers et al., 2013; Lecellier et al., 2014; Kosa et al., 2018), and polysaccharides (Meenu and Xu, 2019). The adjacent peak at 1410 cm^{-1} may be attributed to the asymmetric stretching of the COO^- group (van Hoogmoed et al., 2003). Even though the correlation culminating around 1265 cm^{-1} reached lower values in comparison to the IR bands mentioned above, the $P < 0.05$ significance threshold was exceeded. This band may be associated mainly with amide III vibrations, which consists of CN stretching, NH bending and CO in-plane bending (López-Lorente and Mizaikoff, 2016). Besides amides, IR absorption in this region is caused by asymmetric stretching of the P=O group in nucleic acids and phospholipids (Mayers et al., 2013; Lecellier et al., 2014; Kosa et al., 2018).

Absorption sites for Ni were found to provided mainly by amide, esters and lipidic structural units, whereas carbohydrates probably played a less important role in the sorption of Ni. This follows from the correlation between absorbance and the content of adsorbed Ni. In addition to the mentioned functional groups and structural moieties, it is also possible that other components of microbial biomass contributed to Ni adsorption, for example, amines or compounds containing an aromatic ring. On the other hand, the r values were mostly insignificant in the frequency interval characteristic for the vibrations of carbohydrates (between 1200 and 900 cm^{-1}). It should be noted that carbohydrates also cause absorption in a relatively broad region above 3000 cm^{-1}, where OH groups are detected. However, interpretation of the peaks between 3800 and 3000 cm^{-1} is often ambiguous, as the absorbance in this interval

is strongly affected by the water content in the sample. Although we dried all samples before FTIR measurements, it is difficult to prevent the absorption of water from the atmosphere by sample material, which proceeds quite rapidly.

The following section compares our findings with the results of other works assessing biosorption. Based on the peak position shift, Kang et al. (2011) and Guarín-Romero et al. (2019) both suggested that mainly OH and HN groups are involved in the metal uptake by the algal biomass. This is in general accordance with the results presented here, as we observed that the amount of adsorbed Ni and absorbance in bands of OH and NH vibrations show significant correlation. Rahman et al. (2014), who studied the adsorption of metal ions on the surface of *Trichoderma* presented similar findings. They found that the adsorption of metal caused changes in the FTIR spectra mainly in the 3800–3000 and 1600–1700 cm^{-1} intervals, where the vibrations of hydroxyl, carbonyl, carboxyl, and amide groups are detected, respectively. Besides the mentioned bands and functional groups, we also observed that other structural units may be involved in biosorption, which follows from the significant correlation of the 1600–1400 cm^{-1} interval. A substantial part of this region corresponds with the amide II band, but at lower wave numbers the vibrations of the other groups manifest, including CH and COO^- groups or an aromatic ring. Our observations are in relative accordance with the findings of Pradhan et al. (2007), who reported an increase of absorbance at 1550, 1538, and 1513 cm^{-1}, respectively, due to a change of the C=O stretching after Ni sorption on *Microcystis* capsules. We observed a significant correlation between absorbance detected at mentioned frequencies and the content of adsorbed Ni. The calculated r values were in this case above 0.87 ($P < 0.001$), and the correlation reached a maximum at 1508 cm^{-1}.

Although the value of the correlation coefficient and the peak positions indicate which functional groups are involved in the sorption of Ni, some aspects of this approach should be considered. A significant positive correlation between the content of adsorbed Ni and the absorbance detected at specific frequency does not prove that the group itself is directly involved in the sorption of Ni. Even if we exclude the overlapping of the respective spectral bands (which is a factor that is hard to eliminate), it is still possible that the considered functional group is part of a molecule that may be involved in the sorption process, but the group itself is not. In this study we observed a significant positive correlation in the case of IR bands associated with several functional groups, including OH, CH, COO^-, C=O, and NH groups, respectively. However, the presented FTIR results did not prove that all the mentioned groups were actively participating in the adsorption of Ni. It is possible that the structural units (or molecules) of the microbial biomass which were involved the adsorption of Ni contain the mentioned functional groups but that some of them (CH groups) did not participate in the adsorption. On the other hand, there are different adsorption mechanisms. Besides chemical bonding, which takes place between Ni cation and negatively charged functional groups (such as COO^-), weaker electrostatic attraction plays a role in biosorption, as well (Ren et al., 2021). In such a case, less reactive structural units, including non-polar CH groups, also take part in the retention of Ni. These factors probably contributed to the significant positive correlation that was observed between the content of adsorbed Ni and absorbance in the bands of CH vibrations (and possibly also vibrations of an aromatic ring).

CONCLUSION

This study showed that microbial consortium composed of algal biomass and fungi is capable of effectively reducing the Ni content in ash waste material. During the experiment, organic acids produced by *A. niger* disrupted the cell wall of the microalgae *Chlorella* sp.; the chloroplasts disintegrated and the chlorophyll concentration decreased, resulting in a change of color. Organic matter, which is a source of nutrients for *A. niger*, was released into the environment. In addition to the accumulation by the microscopic fungi (*A. niger*), biosorption mechanisms, such as ion exchange, microprecipitation and interaction of metal ions with functional groups of the algal culture surface of *Chlorella* sp., also took place concurrently. FTIR spectroscopy helped to identify the functional groups involved in the adsorption of Ni from the solid waste substrate by the *Chlorella* sp./*A. niger* biomass. These groups include hydroxyl, aliphatic, carbonyl, carboxyl, and amide structural units. The observed correlations between absorbance and adsorbed Ni content indicate that, in addition to polar (C=O) and negatively charged (COO^-) groups, aliphatic or aromatic structures may also be involved in sorption due to the weaker electrostatic attraction. The correlation between absorbance and Ni content reached a maximum in amide II band, where vibrations of the C=O, C–N, and N–H groups are detected. This suggests that during Ni adsorption, a significant portion of the adsorption sites is provided by the structural units of proteins in the biomass of *Chlorella* sp. and/or *A. niger*. It should be added that, despite the presented findings, it is relatively difficult to clearly identify the most important groups involved in adsorption based on the results of FTIR spectroscopy. This is partly due to the variable and complex structure of proteins. Another factor is the overlapping of the spectral bands in which the respective functional groups are detected. This also applies to the band of the highest correlation (1560–1500 cm^{-1}), where, besides the mentioned amide groups, vibrations of aromatic carbon may also be detected. Based on the observed correlations and results reported in previous works, it can be concluded that various organic structures are involved in the adsorption of heavy metal cations, and a strict attempt to identify "the most important" may lead to oversimplification of the true nature of the adsorption processes. Experiments carried out in this study demonstrate cost-effective application of microbial consortium in decontamination of waste ash material. The results suggest that proper combination of fungi and algae, as well as their simultaneos application may result in synergic mechanism of Ni adsorption. Lowering the concentration of risk element in the ash is important not only in the context of safe disposal, but also for purpose of recovery and separation of metals. This pertains

especially to Ni, which is widely used in the industry and up to date its recyclation has been limited.

DATA AVAILABILITY STATEMENT

The original contributions presented in the study are included in the article/**Supplementary Material**, further inquiries can be directed to the corresponding author.

AUTHOR CONTRIBUTIONS

AŠ: isolation of *Aspergillus niger* strain and preparation of fungal pellets. AT: work with *Chlorella* sp.. AŠ and AT: design and organization of the experiments. IŠ: FTIR analyses. SN: preparation of photo documentation. All authors prepared the manuscript, read, and agreed to the published version of the manuscript.

FUNDING

This research was funded by VEGA Projects No. 1/0194/21 and 1/0712/20, respectively.

SUPPLEMENTARY MATERIAL

The Supplementary Material for this article can be found online at: https://www.frontiersin.org/articles/10.3389/fmicb.2021.792987/full#supplementary-material

REFERENCES

Alrubaie, G., and Al-Shammari, R. H. H. (2018). Microalgae Chlorella vulgaris harvesting via copelletization with filamentous fungus. *Baghdad. Sci. J.* 15, 31–36. doi: 10.21123/bsj.2018.15.1.0031

Antisari, L. V., Marinari, S., Dell'Abate, M. T., Baffi, C., and Vianello, G. (2011). Plant cover and epipedon SOM stability as factors affecting brown soil profile development and microbial activity. *Geoderma* 161, 212–224. doi: 10.1016/j.geoderma.2010.12.021

Baeva, E., Bleha, R., Lavrova, E., Sushytskyi, L., Čopíková, J., Jablonsky, I., et al. (2019). Polysaccharides from basidiocarps of cultivating mushroom *Pleurotus ostreatus*: isolation and structural characterization. *Molecules* 24:2740. doi: 10.3390/molecules24152740

Barth, A. (2000). The infrared absorption of amino acid side chains. *Prog. Biophys. Mol. Biol.* 74, 141–173. doi: 10.1016/S0079-6107(00)00021-3

Barth, A. (2007). Infrared spectroscopy of proteins. *Biochim. Biophys. Acta* 1767, 1073–1101. doi: 10.1016/j.bbabio.2007.06.004

Bhat, R. (2013). Potential use of Fourier transform infrared spectroscopy for identification of molds capable of producing mycotoxins. *Int. J. Food Prop.* 16, 1819–1829. doi: 10.1080/10942912.2011.609629

Bie, R. S., Chen, P., Song, X. F., and Ji, X. Y. (2016). Characteristics of municipal solid waste incineration fly ash with cement solidification treatment. *J. Energy Inst.* 89, 704–712. doi: 10.1016/joei.2015.04.006

Bittante, G., and Cecchinato, A. (2013). Genetic analysis of the Fourier-transform infrared spectra of bovine milk with emphasis on individual wavelengths related to specific chemical bonds. *J. Dairy Sci.* 96, 5991–6006. doi: 10.3168/jds.2013-6583

Bodin, H., Asp, H., and Hultberg, M. (2017). Effects of biopellets composed of microaôlgae and fungi on cadmium present at environmentally relevant levels in water. *Int. J. Phytoremediation* 19, 500–504. doi: 10.1080/15226514.2016.1244170

Bon, I. C., Salvatierra, L. M., Lario, L. D., Morató, J., and Pérez, L. M. (2021). Prospects in cadmium-contaminated water management using free-living Cyanobacteria (*Oscillatoria* sp.). *Water* 13:542. doi: 10.3390/w13040542

Bulgariu, L., and Bulgariu, D. (2020). "Bioremediation of toxic heavy metals using marine algae biomass," in *Green Materials for Wastewater Treatment. Environmental Chemistry for a Sustainable World*, eds M. Naushad and E. Lichtfouse (Cham: Springer).

Cai, C. X., Xu, J., Deng, N. F., Dong, X. W., Tang, H., Liang, Y., et al. (2016). A novel approach of utilization of the fungal conidia biomass to remove heavy metals from the aqueous solution through immobilization. *Nat. Sci. Rep.* 6:36546. doi: 10.1038/srep36546

Chen, W., Jensen, P. E., Ottosen, L. M., and Kirkelund, G. M. (2015). Electrodialytic remediation of fly ash from co-combustion of wood and straw. *Electrochim. Acta* 181, 208–216. doi: 10.1016/j.electacta.2015.04.083

Chen, Z., Lu, S., Tang, M., Ding, J., Buekens, A., Yang, J., et al. (2019). Mechanical activation of fly ash from MSWI for utilization in cementitious materials. *Waste Manage.* 88, 182–190. doi: 10.1016/j.wasman.2019.03.045

Dai, S., Ren, D., Chou, C. L., Finkelman, R. B., Seredin, V. V., and Zhou, Y. (2012). Geochemistry of trace elements in Chinese coals: a review of abundances, genetic types, impacts on human health, and industrial utilization. *Int. J. Coal Geol.* 94, 3–21. doi: 10.1016/j.coal.2011.02.003

de Rome, L., and Gadd, G. M. (1991). Use of pelleted and immobilized yeast and fungal Biomass for heavy metal and radionuclide recovery. *J. Ind. Microbiol.* 7, 97–104. doi: 10.1007/bf01576071

Deng, L., Su, Y., Su, H., Wang, X., and Zhu, X. (2007). Sorption and desorption of lead(II) from wastewater by green algae *Cladophora fascicularis*. *J. Hazard. Mater.* 143, 220–225. doi: 10.1016/j.jhazmat.2006.09.009

Directive 2000/76/EEC (2000). *Official Journal of the European Communities*. Brussels: EU.

Directive 86/278/EEC (1986). *Official Journal of the European Communities*. Brussels: EU.

Directive 91/271/EEC (1991). *Official Journal of the European Communities*. Brussels: EU.

D'Souza, L., Devi, P., Shridhar, M. P. D., and Naik, C. G. (2008). Use of Fourier transform infrared (FTIR) spectroscopy to study cadmium-induced changes in Padina Tetrastromatica (Hauck). *Anal. Chem. Insights* 3, 135–143. doi: 10.4137/117739010800300001

Fawzy, E., Abdel-Motaal, F. F., and El-Zayat, S. A. (2017). Biosorption of heavy metals onto diferent eco-friendly substrates. *J. Bioremediat. Biodegrad.* 8, 3–7. doi: 10.4172/2155-6199.1000394

Forfang, K., Zimmermann, B., Kosa, G., Kohler, A., and Shapaval, V. (2017). FTIR Spectroscopy for evaluation and monitoring of lipid extraction efficiency for oleaginous fungi. *PLoS One* 12:e0170611. doi: 10.1371/journal.pone.0170611

García-Reyes, M., Beltrán-Hernández, R. I., Vázquez-Rodríguez, G. A., Coronel-Olivares, C., Medina-Mporeno, S. A., Juárez-Santillán, L. F., et al. (2017). Formation, morphology and biotechnological applications of filamentous fungal pellets: a review. *Rev. Mex. Ing. Quím.* 16, 703–720.

Geffert, A., and Geffertová, J. (2004). "Composition of pulp and paper sludges and possibilities of their use," in *Proceedings of the TOP 2004 Environmental Protection Technology*, (Slovakia: Slovak Univ. of Technol), 297–303.

Geffert, A., and Mojžišková, M. (eds) (2009). "Thermal insulation based on cellulose-paper sludge," in *Particulate matter in science, industry and the environment*, (Slovakia: Technical Univ., Fac. of Civil Engin.), 13–21.

Guarín-Romero, J. R., Rodríguez-Estupiñán, P., Giraldo, L., and Moreno-Piraján, J. C. (2019). Simple and competitive adsorption study of nickel(II) and chromium(III) on the surface of the brown algae *Durvillaea antarctica* biomass. *ACS Omega* 4, 18147–18158. doi: 10.1021/acsomega.9b02061

Gupta, P., and Diwan, B. (2017). Bacterial exopolysaccharide mediated heavy metal removal: a review on biosynthesis, mechanism and remediation strategies. *Biotechnol. Rep.* 13, 58–71. doi: 10.1016/j.btre.2016.12.006

Haberhauer, G., and Gerzabek, M. H. (1999). DRIFT and FTIR spectroscopy of forest soils: an approach to determine decomposition processes of forest litter. *Vibrational Spectrosc.* 19, 413–417. doi: 10.1016/S0924-2031(98)00046-0

Haneef, M., Ceseracciu, L., Canale, C., Bayer, I. S., Heredia-Guerrero, J. A., and Athanassiou, A. (2017). Advanced materials from fungal mycelium: fabrication and Tuning of physical properties. *Sci. Rep.* 7:41292. doi: 10.1038/srep41292

Heredia-Guerrero, J. A., Benítez, J. J., Domínguez, E., Bayer, I. S., Cingolani, R., Athanassiou, A., et al. (2014). Infrared and raman spectroscopic features of plant cuticles: a review. *Front. Plant Sci.* 5:305. doi: 10.3389/fpls.2014.00305

Hollas, M. J. (2004). *Modern Spectroscopy*, fourth Edn. Hoboken, NJ: John Wiley & Sons.

Jiménez-González, M. A., Álvarez, A. M., Carral, P., and Almendros, G. (2019). Chemometric assessment of soil organic matter storage and quality from humic acid infrared spectra. *Sci. Total Environ.* 685, 1160–1168. doi: 10.1016/j.scitotenv.2019.06.231

Jin, Y. Q., Ma, X. J., Jiang, X. G., Liu, H. M., Li, X. D., and Yan, J. H. (2013). Effects of hydrothermal treatment on the major heavy metals in fly ash from municipal solid waste incineration. *Energy Fuel* 27, 394–400. doi: 10.1021/ef3015525

Johnson, I. R. (1965). The composition of the cell wall of *Aspergillus niger*. *Biochem. J.* 96, 651–658. doi: 10.1042/bj0960651

Kalra, R., Conlan, X. A., and Goel, M. (2020). Fungi as a potential source of pigments: harnessing filamentous fungi. *Front. Chem.* 8:369. doi: 10.3389/fchem.2020.00369

Kang, O. L., Ramli, N., Said, M., Ahmad, M., Yasir, S. M., and Ariff, A. (2011). *Kappaphycus alvarezii* waste biomass: a potential biosorbent for chromium ions removal. *J. Environ. Sci.* 23, 918–922. doi: 10.1016/s1001-0742(10)60498-6

Karimi, S., Soofiani, N. M., Lundh, T., Mahboubi, A., Kiessling, A., and Taherzadeh, M. J. (2019). Evaluation of filamentous fungal biomass cultivated on vinasse as an alternative nutrient Source of fish feed: protein, lipid, and mineral composition. *Fermentation* 5:99. doi: 10.3390/fermentation5040099

Kashiwakura, S., Ohno, H., Matsubae-Yokoyama, K., Kumagai, Y., Kubo, H., and Nagasaka, T. (2010). Removal of arsenic in coal fly ash by acid washing process using dilute H2SO4 solvent. *J. Hazard Mater.* 181, 419–425. doi: 10.1016/j.jhazmat.2010.05.027

Kosa, G., Zimmermann, B., Kohler, A., Ekeberg, D., Afseth, N. K., Mounier, J., et al. (2018). High-throughput screening of Mucoromycota fungi for production of low- and high-value lipids. *Biotechnol. Biofuels* 11:66. doi: 10.1186/s13068-018-1070-7

Kushwaha, A., Rani, R., and Patra, J. K. (2019). Adsorption kinetics and molecular interactions of lead [Pb (II)] with natural clay and humic acid. *Int. J. Environ. Sci. Technol.* 17, 1325–1336. doi: 10.1007/s13762-019-02411-6

Lecellier, A., Mounier, J., Gaydou, V., Castrec, L., Barbier, G., Ablain, W., et al. (2014). Differentiation and identification of filamentous fungi by high-throughput FTIR spectroscopic analysis of mycelia. *Int. J. Food Microbiol.* 168–169, 32–41. doi: 10.1016/j.ijfoodmicro.2013.10.011

Li, B., Zhang, T., and Yang, Z. (2019). Immobilizing unicellular microalga on pellet-forming filamentous fungus: can this provide new insight into remediation of arsenic from contaminated water? *Bioresour. Technol.* 284, 231–239. doi: 10.1016/j.biortech.2019.03.128

Li, J., Zhuang, X., Querol, X., Font, O., and Moreno, N. (2018). A review on the applications of coal combustion products in China. *Int. Geol. Rev.* 60, 671–716. doi: 10.1080/00206814.2017.1309997

López-Lorente, Á I, and Mizaikoff, B. (2016). Mid-infrared spectroscopy for protein analysis: potential and challenges. *Anal. Bioanal. Chem.* 408, 2875–2889. doi: 10.1007/s00216-016-9375-5

Lorenz-Fonfria, V. A. (2020). Infrared difference spectroscopy of proteins: from bands to bonds. *Chem. Rev.* 120, 3466–3576. doi: 10.1021/acs.chemrev.9b00449

Markoš, J., Jelemenský, Ľ, and Gašparovič, L. (eds) (2010). "Biomass pyrolysis and gasification: basic characteristics of the process, and equipment," in *Biogas Production, Pyrolysis and Gasification - An Efficient Way of Utilizing Biomass as a Renewable Energy Source*, (Slovakia: Slovak Techn. Univ.), 36–48.

Massarotti, A., Brunelli, F., Aprile, S., Giustiniano, M., and Tron, G. C. (2021). Medicinal chemistry of isocyanides. *Chem. Rev.* 121, 10742–10788. doi: 10.1021/acs.chemrev.1c00143

Max, J. J., and Chapados, C. (2004). Infrared spectroscopy of aqueous carboxylic acids: comparison between different acids and their salts. *J. Phys. Chem. A* 108, 3324–3337. doi: 10.1021/jp036401t

Mayers, J. J., Flynn, K. J., and Shields, R. J. (2013). Rapid determination of bulk microalgal biochemical composition by Fourier-transform infrared spectroscopy. *Biores. Technol.* 148, 215–220. doi: 10.1016/j.biortech.2013.08.133

Meenu, M., and Xu, B. (2019). Application of vibrational spectroscopy for classification, authentication and quality analysis of mushroom: a concise review. *Food Chem.* 289, 545–557. doi: 10.1016/j.foodchem.2019.03.091

Montazer-Rahmati, M. M., Rabbani, P., Abdolali, A., and Keshtkar, A. R. (2011). Kinetics and equilibrium studies on biosorption of cadmium, lead, and nickel ions from aqueous solutions by intact and chemically modified brown algae. *J. Hazard. Mater.* 185, 401–407. doi: 10.1016/j.jhazmat.2010.09.047

Munir, M. A. M., Liu, G., Yousaf, B., Ali, M. U., Abbas, Q., and Ullah, H. (2018). Enrichment of Bi-Be-Mo-Cd-Pb-Nb-Ga, REEs and Y in the permian coals of the Huainan coalfield, Anhui, China. *Ore Geol. Rev.* 95, 431–455. doi: 10.1016/j.oregeorev.2018.02.037

Nasir, N. M., Yunos, F. H. M., Jusoh, H. H. W., Mohammad, A., Lam, S. S., and Jusoh, A. (2019). Subtopic: advances in water and wastewater treatment harvesting of *Chlorella* sp. microalgae using *Aspergillus niger* as bio-flocculant for aquaculture wastewater treatment. *J. Environ. Manag.* 249, 1–7. doi: 10.1016/j.jenvman.2019.109373

Nebeská, D., Trögl, J., Pidlisnyuk, V., Popelka, J., Dáňová, P. V., Ust'ak, S., et al. (2018). Effect of growing miscanthus x giganteus on soil microbial communities in post-military soil. *Sustainability* 10, 1–12. doi: 10.3390/su10114021

Nzihou, A., and Sharrock, P. (2002). Calcium phosphate stabilization of fly ash with chloride extraction. *Waste Manag.* 22, 235–239. doi: 10.1016/s0956-053x(01)00074-5

Park, K., Hyun, J., Maken, S., Jang, S., and Park, J. W. (2005). Vitrification of municipal solid waste incinerator fly ash using Brown's gas. *Energy Fuel* 19, 258–262. doi: 10.1021/ef049953z

Parker, F. S. (ed.) (1971). "Amides and amines," in *Applications of Infrared Spectroscopy in Biochemistry, Biology, and Medicine*, (Boston, MA: Springer).

Pietikäinen, J., Hiukka, R., and Fritze, H. (2000). Does short-term heating of forest humus change its properties as a substrate for microbes? *Soil Biol. Biochem.* 32, 277–288. doi: 10.1016/S0038-0717(99)00164-9

Pinto, N., Carvalho, A., Pacheco, J., and Duarte, E. (2016). Study of different ratios of primary and waste activated sludges to enhance the methane yield. *Water Environ. J.* 30, 203–210. doi: 10.1111/wej.12188

Prabakaran, G., Moovendhan, M., Arumugam, A., Matharasi, A., Dineshkumar, R., and Sampathkumar, P. (2018). Evaluation of chemical composition and in vitro antiinflammatory effect of marine microalgae *Chlorella vulgaris*. *Waste Biomass Valorization* 10, 3263–3270. doi: 10.1007/s12649-018-0370-2

Pradhan, S., Singh, S., and Rai, L. C. (2007). Characterization of various functional groups present in the capsule of Microcystis and study of their role in biosorption of Fe, Ni and Cr. *Biores. Technol.* 98, 595–601. doi: 10.1016/j.biortech.2006.02.041

Qiu, Q. L., Jiang, X. G., Chen, Z. L., Lu, S. Y., and Ni, M. J. (2017). Microwave-assisted hydrothermal treatment with soluble phosphate added for heavy metals solidification in MSWI Fly ash. *Energy Fuel* 31, 5222–5232. doi: 10.1021/acs.energyfuels.6b02516

Qiu, Q. L., Jiang, X. G., Lv, G. J., Chen, Z. L., Lu, S. Y., and Ni, M. J. (2018). Adsorption of heavy metal ions using zeolite materials of municipal solid waste incineration fly ash modified by microwave-assisted hydrothermal treatment. *Powder Technol.* 335, 156–163. doi: 10.1016/j.powtec.2018.05.003

Rahman, N. N. N. A., Shahadat, M., Won, C. A., and Omar, F. M. (2014). FTIR study and bioadsorption kinetics of bioadsorbent for the analysis of metal pollutants. *RSC Adv.* 4:58156. doi: 10.1039/C4RA05931J

Rajendran, A., and Hu, B. (2016). Mycoalgae biofilm: development of a novel platform technology using algae and fungal cultures. *Biotechnol. Biofuels* 9, 2–13. doi: 10.1186/s13068-016-0533-y

Raval, N. P., Shah, P. U., and Shah, N. K. (2016). Adsorptive removal of nickel(II) ions from aqueous environment: a review. *J. Environ. Manag.* 179, 1–20. doi: 10.1016/j.jenvman.2016.04.045

Reijnders, L. (2005). Disposal, uses and treatments of combustion ashes: a review. *Resour. Conserv. Recycle* 43, 313–336. doi: 10.1016/j.resconrec.2004.06.007

Ren, B., Zhao, L., Wang, Y., Song, X., Jin, Y., Ouyang, F., et al. (2021). Freezing/thawing pretreatment of dormant Aspergillus niger spores to increase the Cr(VI) adsorption capacity: process and mechanism. *RSC Adv.* 11:7704. doi: 10.1039/d0ra10198b

Rinaudo, M. (2006). Chitin and chitosan: properties and applications. *Prog. Polym. Sci.* 31, 603–632. doi: 10.1016/j.progpolymsci.2006.06.001

Saif, F. A., Yaseen, S. A., Alameen, A. S., Mane, S. B., and Undre, P. B. (2021). Identification and characterization of Aspergillus species of fruit rot fungi using microscopy, FT-IR, Raman and UV-Vis spectroscopy. *Spectrochim. Acta A Mol. Biomol. Spectrosc.* 246:119010. doi: 10.1016/j.saa.2020.119010

Sari, A., and Tuzen, M. (2008). Biosorption of Pb(II) and Cd(II) from aqueous solution using green alga (*Ulva lactuca*). *J. Hazard. Mater.* 152, 302–308. doi: 10.1016/j.jhazmat.2007.06.097

Sathe, S. S., Mahanta, C., and Mishra, P. (2018). Simultaneous influence of indigenous microorganism along with abiotic factors controlling arsenic mobilization in Brahmaputra flood plain, India. *J. Contam. Hydrol.* 213, 1–14. doi: 10.1016/j.jconhyd.2018.03.005

Silverstein, R. M., Webster, F. X., and Kiemle, D. J. (2005). *Spectrometric Identification of Organic Compounds*, Seventh Edn. Hoboken, NJ: John Wiley & Sons.

Šimonovičová, A., Kupka, D., Nosalj, S., Kraková, L., Drahovská, H., Bártová, Z., et al. (2020). Differences in metabolities production using the Biolog FF MicroplateTM system with anemphasis on some organic acids of *Aspergillus niger* wild type strains. *Biologia* 75, 1537–1546. doi: 10.2478/s11756-020-00521-y

Šimonovičová, A., Vojtková, H., Nosalj, S., Piecková, E., and Švehláková, H. (2021). *Aspergillus niger* environmental isolates and their specific diversity through metabolite profiling. *Front. Microbiol.* 12:658010. doi: 10.3389/fmicb.2021.658010

Smith, B. C. (2019). Organic nitrogen compounds III: secondary and tertiary amines. *Spectroscopy* 34, 22–26.

Song, Y., Zhang, J., Zhang, X., and Tan, T. (2015). The correlation between cellulose allomorphs (I and II) and conversion after removal of hemicellulose and lignin of lignocellulose. *Biores. Technol.* 193, 164–170. doi: 10.1016/j.biortech.2015.06.084

Stuart, B. (2004). *Infrared spectroscopy: Fundamentals and Applications*. Hoboken, NJ: John Wiley & Sons.

Stüttgen, G., Sya, R., and Dittmar, W. (1978). Determination of biogenous amines in fungus-cultures (*Candida albicans*, *Trichophyton mentagrophytes*, *Trichophyton rubrum* and *Microsporum canis*) by thin-layer chromatography and mass-spectrometry. *Mycoses Diagn. Ther. Prophylaxis Fungal Dis.* 21, 331–335. doi: 10.1111/j.1439-0507.1978.tb01578.x

Tang, J. F., and Steenari, B. M. (2015). Solvent extraction separation of copper and zinc from MSWI fly ash leachates. *Waste Manag.* 44, 147–154. doi: 10.1016/j.wasman.2015.07.028

Tiemann, K. J., Gardea-Torresdey, J. L., Gamez, G., Dokken, K., and Sias, S. (1999). Use of X-ray absorption spectroscopy and esterification to investigate chromium(III) and nickel(II) ligand in alfalfa biomass. *Environ. Sci. Technol.* 33, 150–154. doi: 10.1021/es9804722

Timková, I., Sedláková-Kaduková, J., and Pristaš, P. (2018). Biosorption and bioaccumulation abilities of Actinomycetes/Streptomycetes isolated from metal contaminated sites. *Separations* 5, 1–14. doi: 10.3390/separations5040054

Ukwattage, N., Ranjith, P. G., and Wang, S. (2013). Investigation of the potential of coal combustion fly ash for mineral sequestration of CO2 by accelerated carbonation. *Energy* 52, 230–236. doi: 10.1016/j.energy.2012.12.048

Ullah, H., Liu, G., Yousaf, B., Ali, M. U., Abbas, Q., Zhou, C., et al. (2018). Hydrothermal dewatering of low-rank coals: influence on the properties and combustion characteristics of the solid products. *Energy* 158, 1192–1203. doi: 10.1016/j.energy.2018.06.052

van Hoogmoed, C. G., Busscher, H. J., and de Vos, P. (2003). Fourier transform infrared spectroscopy studies of alginate–PLL capsules with varying compositions. *J. Biomed. Mater. Res.* 67, 172–178. doi: 10.1002/jbm.a.10086

Vavva, C., Voutsas, E., and Magoulas, K. (2017). Process development for chemical stabilization of fly ash from municipal solid waste incineration. *Chem. Eng. Res. Des.* 125, 57–71. doi: 10.1016/j.cherd.2017.06.021

Wang, F. H., Zhang, F., Chen, Y. J., Gao, J., and Zhao, B. (2015). A comparative study on the heavy metal solidification/stabilization performance of four chemical solidifying agents in municipal solid waste incineration fly ash. *J. Hazard Mater.* 300, 451–458. doi: 10.1016/j.jhazmat.2015.07.037

Wang, H., Fan, X., Wang, Y. N., Li, W., Sun, Y., Zhan, M., et al. (2018). Comparative leaching of six toxic metals from raw and chemically stabilized MSWI fly ash using citric acid. *J. Environ. Manag.* 208, 15–23. doi: 10.1016/j.jenvman.2017.11.071

Wang, J., and Chen, C. (2009). Biosorbents for heavy metals removal and their future. *Biotechnol. Adv.* 27, 195–226. doi: 10.1016/j.biotechadv.2008.11.002

Wang, W., Gao, X., Li, T., Cheng, S., Yang, H., and Qiao, Y. (2018). Stabilization of heavy metals in fly ashes from municipal solid waste incineration via wet milling. *Fuel* 216, 153–159. doi: 10.1016/j.fuel.2017.11.045

Wang, Y., Pan, Y., Zhang, L., Yue, Y., Zhou, J., Xu, Y., et al. (2015). Can washing pretreatment eliminate the health risk of municipal solid waste incineration fly ash reuse? *Ecotoxicol. Environ. Saf.* 111, 177–184. doi: 10.1016/j.ecoenv.2014.09.030

Weibel, G., Eggenberger, U., Kulik, D. A., Hummel, W., Schlumberger, S., Klink, W., et al. (2018). Extraction of heavy metals from MSWI fly ash using hydrochloric acid and sodium chloride solution. *Waste Manag.* 76, 457–471. doi: 10.1016/j.wasman.2018.03.022

Wild, K. J., Trautmann, A., Katzenmeyer, M., Steingaß, H., Posten, C., and Rodehutscord, M. (2019). Chemical composition and nutritional characteristics for ruminants of the microalgae *Chlorella vulgaris* obtained using different cultivation conditions. *Algal Res.* 38:101385. doi: 10.1016/j.algal.2018.101385

Zhang, F., Ou, X., Chen, S., Ran, C., and Quan, X. (2021). Competitive adsorption and desorption of copper and lead in some soil of North China. *Front. Environ. Sci. Eng.* 6:484. doi: 10.1007/s11783-012-0423-x

Żyszka-Haberecht, B., Niemczyk, E., and Lipok, J. (2019). Metabolic relation of cyanobacteria to aromatic compounds. *Appl. Microbiol. Biotechnol.* 103, 1167–1178. doi: 10.1007/s00253-018-9568-2

Conflict of Interest: The authors declare that the research was conducted in the absence of any commercial or financial relationships that could be construed as a potential conflict of interest.

Publisher's Note: All claims expressed in this article are solely those of the authors and do not necessarily represent those of their affiliated organizations, or those of the publisher, the editors and the reviewers. Any product that may be evaluated in this article, or claim that may be made by its manufacturer, is not guaranteed or endorsed by the publisher.

frontiers in Microbiology

ORIGINAL RESEARCH
published: 13 December 2021
doi: 10.3389/fmicb.2021.794535

Comparative Genome-Wide Transcriptome Analysis of *Brucella suis* and *Brucella microti* Under Acid Stress at pH 4.5: Cold Shock Protein CspA and Dps Are Associated With Acid Resistance of *B. microti*

Jorge A. de la Garza-García[1†], Safia Ouahrani-Bettache[1†], Sébastien Lyonnais[2], Erika Ornelas-Eusebio[3], Luca Freddi[1‡], Sascha Al Dahouk[4], Alessandra Occhialini[1] and Stephan Köhler[1]*

[1] Institut de Recherche en Infectiologie de Montpellier (IRIM), CNRS, University Montpellier, INSERM, Montpellier, France, [2] CEMIPAI, CNRS, University Montpellier, Montpellier, France, [3] Unité des Zoonoses Bactériennes and Unité d'Epidémiologie, Laboratoire de Santé Animale, ANSES, University Paris-Est, Maisons-Alfort, France, [4] German Federal Institute for Risk Assessment, Berlin, Germany

OPEN ACCESS

Edited by:
Peter Adrian Lund,
University of Birmingham,
United Kingdom

Reviewed by:
Wanderson Marques da Silva,
Consejo Nacional de Investigaciones Científicas y Técnicas (CONICET), Argentina
Sébastien Bontemps-Gallo,
Institut Pasteur de Lille, France

***Correspondence:**
Stephan Köhler
stephan.kohler@irim.cnrs.fr

[†] These authors have contributed equally to this work

[‡] **Present address:**
Luca Freddi
Unité des Zoonoses Bactériennes,
ANSES, Maisons-Alfort, France

Specialty section:
This article was submitted to Microbial Physiology and Metabolism, a section of the journal Frontiers in Microbiology

Received: 13 October 2021
Accepted: 12 November 2021
Published: 13 December 2021

Citation:
de la Garza-García JA, Ouahrani-Bettache S, Lyonnais S, Ornelas-Eusebio E, Freddi L, Al Dahouk S, Occhialini A and Köhler S (2021) Comparative Genome-Wide Transcriptome Analysis of Brucella suis and Brucella microti Under Acid Stress at pH 4.5: Cold Shock Protein CspA and Dps Are Associated With Acid Resistance of B. microti. Front. Microbiol. 12:794535. doi: 10.3389/fmicb.2021.794535

Brucellae are facultative intracellular coccobacilli causing brucellosis, one of the most widespread bacterial zoonosis affecting wildlife animals, livestock and humans. The genus *Brucella* comprises classical and atypical species, such as *Brucella suis* and *Brucella microti*, respectively. The latter is characterized by increased metabolic activity, fast growth rates, and extreme acid resistance at pH 2.5, suggesting an advantage for environmental survival. In addition, *B. microti* is more acid-tolerant than *B. suis* at the intermediate pH of 4.5. This acid-resistant phenotype of *B. microti* may have major implications for fitness in soil, food products and macrophages. Our study focused on the identification and characterization of acid resistance determinants of *B. suis* and *B. microti* in Gerhardt's minimal medium at pH 4.5 and 7.0 for 20 min and 2 h by comparative RNA-Seq-based transcriptome analysis, validated by RT-qPCR. Results yielded a common core response in both species with a total of 150 differentially expressed genes, and acidic pH-dependent genes regulated specifically in each species. The identified core response mechanisms comprise proton neutralization or extrusion from the cytosol, participating in maintaining physiological intracellular pH values. Differential expression of 441 genes revealed species-specific mechanisms in *B. microti* with rapid physiological adaptation to acid stress, anticipating potential damage to cellular components and critical energy conditions. Acid stress-induced genes encoding cold shock protein CspA, pseudogene in *B. suis*, and stress protein Dps were associated with survival of *B. microti* at pH 4.5. *B. suis* response with 284 specifically regulated genes suggested increased acid stress-mediated protein misfolding or damaging, triggering the set-up of repair strategies countering the

consequences rather than the origin of acid stress and leading to subsequent loss of viability. In conclusion, our work supports the hypothesis that increased acid stress resistance of *B. microti* is based on selective pressure for the maintenance of functionality of critical genes, and on specific differential gene expression, resulting in rapid adaptation.

Keywords: *Brucella*, acid stress, cold shock protein, Dps, transcriptome

INTRODUCTION

Brucellae are facultative intracellular coccobacilli causing brucellosis, a widespread bacterial zoonosis, infecting wildlife animals, livestock and humans. Transmission routes of *Brucella* spp. to humans include aerosols, direct contact with infected animals, and most frequently, ingestion of contaminated and unpasteurized dairy products (Pappas et al., 2005). *Brucella abortus*, *Brucella melitensis*, and *Brucella suis* are the most relevant species for human infections (Pappas et al., 2005).

After their uptake by the host cell, brucellae establish a specific intracellular niche, the *Brucella*-containing vacuole (BCV), in which the bacteria survive and replicate (Celli, 2019). This vacuole undergoes endosomal maturation during the early phase of infection, interacting rapidly with early and late endosomes as well as lysosomes, resulting in transient acidification to a pH of 4-4.5 (Porte et al., 1999). This acidification is crucial for intracellular replication and induction of the major virulence factor of *Brucella* spp., the type IV secretion system VirB (O'Callaghan et al., 1999; Porte et al., 1999; Boschiroli et al., 2002; Köhler et al., 2002).

In the past, the protein profile of *B. melitensis* in response to an intermediate acid stress at pH 5.5 has been studied by two-dimensional polyacrylamide gel electrophoresis (Teixeira-Gomes et al., 2000). Two chaperones have been reported to be involved in acid stress resistance: ClpB of *B. suis* (Ekaza et al., 2001) and HdeA, regulated by the RNA-binding protein Hfq (Valderas et al., 2005). The importance of the latter was confirmed by microarray-based transcriptome analysis and by the impact of Hfq-inactivation on stress resistance and intracellular survival of *B. melitensis* (Cui et al., 2013). The transcriptional regulator OtpR was described to be important for tolerance to acid stress in *B. melitensis*, and RNA-Seq whole transcriptome analysis under these conditions showed that OtpR regulates genes mainly involved in bacterial metabolism, but also virulence factors such as *virB* and other transcriptional regulators, predicted to be controlled by OtpR-mediated sRNA expression (Vishnu et al., 2017). More recently, two RNA-Seq transcriptome analyses were performed to study the global gene expression profile of *B. melitensis* 16M in adaptation to pH 4.4: The first study identified a two-component system regulator essential for acid resistance, intramacrophagic and *in vivo* survival of the pathogen (Liu et al., 2016). However, experimental conditions were not clearly described, since both minimal and complex medium were mentioned for acid stress, and bacterial mRNAs were supposedly purified using oligo (dT) beads. The second study focused on the comparison of normal and acid pH gene expression profiles in the 16M wild-type and the Rev1 vaccine strain, providing possible explanations for the attenuated virulence of the latter. In the 16M strain, 773 genes were differentially expressed, encoding predominantly transmembrane transporters, oxido-reductase activities and nucleoside triphosphate biosynthetic processes (Salmon-Divon et al., 2019).

All twelve recognized *Brucella* species, including zoonotic species, share highly conserved genomes and are classified on the basis of their host preference, pathogenicity, and phenotypic and biochemical characteristics. New and atypical species and strains, such as *Brucella microti* isolated from common vole, *Brucella inopinata* from humans (Scholz et al., 2008b, 2010; Tiller et al., 2010), and strains isolated from non-mammal hosts (Soler-Llorens et al., 2016; Al Dahouk et al., 2017; Eisenberg et al., 2017), have been described over the last 15 years. Most of them, isolated from hitherto unknown wildlife hosts and the environment, are characterized by increased metabolic activity and faster growth rates than the classical species, suggesting an advantage for environmental survival (Al Dahouk et al., 2017) and raising the question whether they may be transmitted from these reservoirs to livestock and humans in brucellosis-free areas.

Brucella microti has been isolated in Central Europe from soil and wildlife (Scholz et al., 2008a, 2009; Ronai et al., 2015). Phylogenetically, this species is closer to those pathogenic for human and livestock than to the group of newly described atypical species/strains comprising *B. inopinata* and strains from Australian rodents (Wattam et al., 2014). Its replication rate in murine and human macrophage cells is higher than that of classical species, and *B. microti* is the first *Brucella* species described to be lethal in mice (Jiménez De Bagüés et al., 2010). This lethal phenotype depends on the type IV secretion system VirB (Hanna et al., 2011) and, as we reported lately, on a smooth LPS with an intact O-polysaccharide (Ouahrani-Bettache et al., 2019). In contrast, at sub-lethal doses, *B. microti* is rapidly cleared from infected mice, never gives rise to chronic infection and confers protection.

New and atypical species, and also those isolated from marine mammals, but not classical ones, are characterized by the presence of two functional acid resistance systems conferring extreme acid resistance *in vitro* at pH 2.5 in the presence of glutamate or glutamine: the glutamate decarboxylase (Gad)- and the glutaminase-dependent system AR2_Q (Damiano et al., 2015; Freddi et al., 2017). In *B. microti*, the Gad system was also shown to play an important role in oral murine infection (Occhialini et al., 2012). In classical species, urease has been described to contribute to acid resistance at very low pH, and most *Brucella* strains show urease activity. Analysis of genome sequences revealed the existence of two urease gene clusters, *ure1* and *ure2*. However, the function of *ure2* is not clear, and *ure1*

appears to play the principal role in *in vitro* acid resistance at pH 2.0 and in murine infection *via* the oral route (Bandara et al., 2007; Sangari et al., 2007).

In addition to the observed extreme acid resistance, our previous results had shown that *B. microti* was more acid-tolerant than *B. suis* in a synthetic minimal medium at pH 4.5 (Jiménez De Bagüés et al., 2010), mimicking the acidity encountered by *Brucella* in the host cell phago(lyso)some, or possibly in particular soil environments (Scholz et al., 2008a). The lack of transient intramacrophagic mortality of *B. microti* at 7 h post infection, as opposed to the fate of *B. suis*, might also be linked to its increased acid-resistance (Jiménez De Bagüés et al., 2010). Despite highly conserved genome sequences with an overall identity of 99.8% and not more than 130 genes inactivated in either of the two species but intact in the other (Audic et al., 2009), these two species, which represent an appropriate model for classical versus atypical *Brucella* spp. comparisons, are phenotypically distinct and obviously developed species-specific responses to acid stress. Consequently, the more acid-resistant phenotype of *B. microti* may have major implications for fitness and virulence, both in soil and in the host.

To better understand the molecular mechanisms leading to acid resistance of *B. microti* at pH 4.5, we identified and characterized common and species-specific acid resistance determinants by comparative RNA-Seq-based transcriptome analysis of bacteria exposed to pH 4.5 and 7.0 in minimal medium. Our starting hypothesis was, that the gene expression patterns of the two species may differ under the conditions chosen, and that the observed phenotypic difference in acid resistance between *B. suis* and *B. microti* might be due to specific mutations, and/or to differential gene expression. Our analysis revealed at least two genes of *B. microti* with increased expression under acid stress and associated with better survival in minimal medium at pH 4.5, one of which was inactive in *B. suis* due to frameshift mutation.

MATERIALS AND METHODS

Bacterial Strains and Culture Conditions

Brucella suis 1330 (ATCC 23444) and *B. microti* CCM4915, as well as derived mutant strains, were grown in Tryptic Soy broth (TSB) at 37°C under BSL-3 conditions. *Escherichia coli* DH5α, used for cloning and plasmid production, was cultured in Lysogeny Broth (LB). For selection of strains carrying antibiotic resistance genes, kanamycin, ampicillin, and chloramphenicol were added to a final concentration of 50 μg/ml each, when needed.

Growth and survival assays for *B. suis* and *B. microti* strains were performed using Gerhardt's Minimal Medium (GMM) supplemented with vitamins (Hanna et al., 2013), and with ammonium sulfate (1 g/l) replacing glutamic acid, at the appropriate pH values. For stress survival assays, stationary phase pre-cultures of *Brucella* strains were centrifuged, washed once in PBS and resuspended in twice the volume of GMM pH 4.5. 150 μl of the dilutions were transferred to 1350 μl of the corresponding medium and incubated at 37°C with shaking (160 rpm). To assess bacterial viability at different time points, serial dilutions were plated onto Tryptic Soy agar and colony forming units (CFU) were determined. Experiments were done at least three times in triplicates. The low-pH assay for RNA-Seq analysis was performed as follows: Pre-cultures of *B. microti* CCM 4915 and *B. suis* 1330 were grown overnight to stationary phase and diluted each in 40 ml TSB to reach an OD of 0.8 after 15 h of culture. Cultures were dispatched to 4 tubes with 10 ml each, centrifuged, and the pellets resuspended in 20 ml of GMM pH 4.5 or GMM pH 7.0 for the control conditions (2 tubes per strain and pH), pre-heated to 37°C. For each species and pH, the tubes were incubated at 37°C for 20 or 120 min. To preserve specific expression profiles, cultures were inactivated by the addition of 1/10 volume of a 30% phenol/ethanol solution and vigorous mixing, followed by centrifugation and storage of the bacterial pellets at −80°C.

RNA Isolation and RNA-Seq

The total RNA of *Brucella* was isolated using the mirVana RNA Isolation Kit (Ambion), according to the manufacturer's instructions. Each sample was treated with RNase-free DNase (Ambion) and tested by Polymerase Chain Reaction (PCR) for possible residual DNA contamination. When necessary, samples were treated again with DNase, prior to Agilent Bioanalyzer 2000 quality analysis of the RNA samples. rRNA depletion using the RiboZero Kit, generation of the cDNA libraries, and deep-sequencing was performed by Eurofins Genomics (formerly GATC, Germany) using an Illumina^{TM} Hi-Seq 2500 platform and in-house protocols. The 51-bp reads were single-end, with a total yield of 34-64 million reads for the four *B. suis* samples and 38-62 million reads for the four *B. microti* samples.

RNA-Seq Analysis

The CRAC software (Philippe et al., 2013) was used to strand-specifically map the reads to the reference genomes of *B. suis* 1330 (NC_004310.3 and NC_004311.2 for chromosomes I and II, respectively) and *B. microti* CCM 4915 (NC_013119.1 and NC_013118.1 for chromosomes I and II, respectively), and to filter out multi-aligned reads. 96-98% of the total mapped reads of all samples were single-aligned reads to the corresponding reference genomes, except for *B. suis* at pH 7/20 min (61%), and only these reads were kept for further analysis. Following mapping, the read counts for each gene were determined with the "featureCounts" software (Liao et al., 2014). Based on the CRAC output, normalization and differential gene expression analysis for the two different pH-conditions in each species were performed with DESeq (Anders and Huber, 2010), calculating the ratios of normalized reads at pH 4.5/normalized reads at pH 7.0, and the corresponding log2-values of the fold-changes, for each species and time point (20 min or 2 h). A threshold of $\geq$1.5 or $\leq$−1.5 was fixed for the log2-fold change. The sequencing reads from this study were deposited in the SRA database (NCBI) under the accession number PRJNA644280.

The genes selected on the base of the $\geq$ 1.5/$\leq$ −1.5 log2-fold change threshold were classified by assigning the predicted

proteins to their respective Cluster of Orthologous Groups (COG), using the Genoscope MicroScope platform from the French Sequencing Center[1] (Vallenet et al., 2020), and according to *B. suis* 1330 and *B. microti* CCM 4915 operons predicted in the Database of prokaryotic OpeRons (DOOR) (Mao et al., 2009). In addition, a search for genes reported as virulence-associated was performed using the Pathogen-Host Interaction Data Integration and Analysis System (PHIDIAS) – Virulence Factors (Victors)[2] (Sayers et al., 2019), as well as on the Virulence Factor DataBase (VFDB)[3] (Liu et al., 2019). The mapping tool available at the Pathosystems Resource Integration Center (PATRIC)[4] allowed the screening for possible clusters in the expression profiles. The metabolic pathway assessment was performed using the Kyoto Encyclopedia of Genes and Genomes (KEGG) Pathway Database.[5]

Quantitative Reverse Transcriptase Polymerase Chain Reaction

To validate RNA-seq results, 95 differentially expressed candidate genes were selected and their expression changes at the pH-values and time points chosen were confirmed by Quantitative Reverse Transcriptase PCR (RT-qPCR). Primers were designed with the Primer3 software (**Supplementary Table 1**). Complementary DNA (cDNA) was obtained by reverse transcription of 1μg of total RNA in a final reaction volume of 20 μl, containing 4 μl SuperScript VILO Master Mix, at 42°C for 90 min. The working sample of cDNA was diluted 1:20 (2.5 ng/μl). RT-qPCRs were performed in triplicate per sample and experimental condition, using a Light Cycler^{TM} 480 qPCR machine (Roche) and SYBR Green I Master (Roche) in a final volume of 1.5 μl per reaction. The reference gene for 16S-rRNA (*rrs*) was amplified in parallel for normalization. 396-wells microplates were prepared with the assistance of an Echo 525 Liquid Handler (Labcyte Inc.) at the Montpellier GenomiX (MGX) Platform. For each gene tested, the mean calculated threshold cycles (Ct) were averaged and normalized to the Ct of the 16S-rRNA gene used for reference. Calculation of the fold change using the ΔΔCt method was based on the normalized Ct (Hanna et al., 2011).

Construction and Complementation of *Brucella* Mutant Strains

Mutant strains of *B. microti* were constructed by target gene deletion and replacement with a kanamycin resistance cassette obtained from pUC4K (Amersham Biosciences). Briefly, a fragment containing 2 homology regions at the 5'- and 3'-ends of the gene of interest was generated by overlap extension PCR (Heckman and Pease, 2007). This fragment was cloned into pGEM-T Easy (Promega; non-replicative in *Brucella*) and amplified in *E. coli* DH5α prior to insertion of the kanamycin resistance cassette into the unique restriction site *Stu*I and introduction into *Brucella* by electroporation, as described previously (Köhler et al., 1996). To select for allelic exchange mutants, Kan^R colonies were checked for sensitivity to ampicillin. Allelic exchange in Kan^R/Amp^S clones was validated by PCR. Homologous complementation of *B. microti* mutants was achieved by transformation with the replicative *E. coli-Brucella* shuttle vector pBBR1-MCS (Kovach et al., 1994) carrying the intact sequences of the genes of interest. For *B. suis* 1330, pBBR1-AMP, containing a *bla* gene conferring resistance to ampicillin and replacing the chloramphenicol resistance marker of pBBR1-MCS by insertion into the *Nco*I-*Aat*II restriction sites, was used. DNA-fragments were obtained by PCR amplification using *Pfx* high fidelity DNA polymerase (Life Technologies) with primers containing restriction sites *Kpn*I/*Sac*I, followed by insertion into pBBR1-MCS. Primers used for gene deletion and complementation of *Brucella* strains are listed in **Supplementary Table 2**.

Infection of J774-Murine Macrophage-Like Cells

Experiments were performed in triplicate as described previously, using J774A.1 murine macrophage-like cells at a multiplicity of infection of 20 bacteria per cell (Burkhardt et al., 2005). At defined time points, cells were lysed in 0.2% Triton X-100, and viable intracellular bacteria were determined after plating serial dilutions of lysates on TS agar and incubation for 3 days at 37°C.

Atomic Force Microscopy

Tryptic Soy broth (TSB) cultures of *B. microti* were treated following the protocol described for acid stress assays and incubation in GMM for 6 h at pH 4.5 or pH 7.0. 1.5 ml of cultures were centrifuged, and the pellets washed with 0.22 μm-filtered PBS, prior to resuspension in 1 ml of 2.5% glutaraldehyde and incubation for 1 h. Fixed bacteria were washed with filtered PBS and resuspended in 150 μl. For Atomic Force Microscopy (AFM), FluoroDish^{TM} cell culture dishes (World Precision Instruments, United Kingdom) were coated overnight at 4°C with 0.1% poly-L-lysine, washed with PBS, air dried and stored at 4°C. Bacteria were diluted 20-fold in filtered PBS and added to the functionalized dish. Topographic imaging in PBS at 20°C was performed on a NanoWizard IV AFM (JPK-Bruker) using a force-curve-based imaging mode (QI mode), with qp-BioAC cantilevers (Nanosensors, mean cantilever spring constant $k_{cant} = 0.09$ N/m). The applied force was kept at 300 pN, and a constant approach/retract speed of 80 μm/s (z range of 800 nm). Images were flattened with a polynomial/histogram line-fit with the AFM software.

Statistical Analysis

Data from stress assays and infections were analyzed with the Student's *t*-test, using Graph Pad Prism and Sigma Plot software. Data were expressed as means of at least three independent experiments with standard deviations. Differences were considered statistically significant when P-values were < 0.05.

[1]https://www.genoscope.cns.fr/agc/microscope/mage/viewer.php
[2]http://www.phidias.us/victors/index.php
[3]http://www.mgc.ac.cn/VFs/main.htm
[4]https://www.patricbrc.org/
[5]https://www.genome.jp/kegg/pathway.html

RESULTS AND DISCUSSION

Increased Resistance of *Brucella microti* to Intermediate Acid Stress at pH 4.5 *in vitro*

Our group previously described that *B. microti* was more resistant to pH 4.5 in minimal medium than *B. suis* (Jiménez De Bagüés et al., 2010). To further explore this observation, comparative analyses of survival or growth rates of both species were performed in rich (TS) and minimal medium (GMM) at different pH values and time points (**Figure 1**). Whereas survival of *B. suis* and *B. microti* decreased in GMM at pH 4.5 and 5.0, with a significantly more rapid decline for *B. suis*, growth was observed for *B. microti* at the same pH values in complex TS broth. Growth of *B. suis* started at pH 5.0 in TS medium, and both species grew in GMM and TS broth at pH 5.5 (**Figure 1**). These results confirmed a better global adaptation of *B. microti* to intermediate acid stress at pH 4.0-5.0 than of the classical human pathogen *B. suis*, especially when coupled with a nutrient-poor environment.

Transcriptome Analysis of Differential Gene Expression in *Brucella suis* 1330 and *Brucella microti* at pH 4.5 and pH 7.0 Reveals Common and Species-Specific Adaptation Profiles

Common and species-specific gene expression profiles of *B. suis* and *B. microti* during acid stress at pH 4.5 were obtained by RNA-Seq and analyzed following exposure of both species to pH 4.5 and pH 7.0 in GMM for 20 and 120 min, mimicking very early, possibly critical stages of adaptation to an acidified host cell vacuole during infection or to out-of-the-host environments such as fermented food products or acid soils. In contrast, previous transcriptome analyses of *Brucella* spp. at pH 4.4 generally focused on later time points, reflecting adaptation to an advanced stage of acidified endosomal BCV (Liu et al., 2016; Salmon-Divon et al., 2019).

Our results yielded a total of 935 and 1092 genes identified as being differentially regulated in *B. suis* and *B. microti*, respectively, at both time points (30–34% of the *Brucella* genome), applying as criterion a > 1.5 or <-1.5 log2-fold change to the ratio of the pH 4.5/pH 7.0 expression values. From these genes, 651 were commonly induced or repressed during acid stress, with 150 being significantly regulated in both species and at both time points, hereafter called "core genes" (**Supplementary Table 3**). Regarding the species-specific responses, only 284 genes (9% of the genome) were specifically regulated in *B. suis*, as opposed to 441 genes (14% of the genome) in *B. microti* (**Supplementary Table 3**). Whereas the distribution between conditions of the number of differentially expressed genes with higher rates of expression either at pH 4.5 or at pH 7 was similar in each species, the number of genes differentially regulated at 120 min and at both time points was clearly higher in *B. microti* (**Figure 2**).

Genomic distribution of the genes differentially expressed at pH 4.5 and pH 7.0 did not reveal any clustering and was homogeneous in both species (not shown).

Quantitative Reverse Transcriptase Polymerase Chain Reaction Validates RNA-Seq Analysis

Reliability of the transcriptome analysis was assessed by RT-qPCR-based quantification of the RNAs from 95 representative genes. These genes were selected according to the following criteria: bacterial species; time points (20 or 120 min); COG groups; operon organization; annotated functions; log2-fold change ratios (significantly higher expression at pH 4.5 or 7.0). Expression of the genes was assessed with technical triplicates, using the 16S rRNA-gene as reference (constant expression rates under all conditions). RT-qPCR results were compared to those obtained by RNA-Seq, and correlations for each of the 4 experimental conditions are shown in **Figure 3**. Gene expression profiles identified by RNA-Seq were considered as validated, when expression rates determined by both approaches matched for one of the three conditions included in the analysis: significantly higher or lower expression at pH 4.5 than at pH 7, or non-significant differences in expression. The validation rates for the four experimental conditions chosen ranged from 70-90%, confirming the soundness of the RNA-Seq data (**Supplementary Table 4**).

As RT-qPCR was carried out with 7% of the total number of genes identified by RNA-Seq, a much larger sampling than that performed in other RNA-Seq studies described in the literature, the obtained validation rates were considered as solid for analysis of the RNA-Seq results, confirming the robustness of the experimental design and of the quantification procedures applied, in accordance with literature reports (Fang and Cui, 2011).

Deciphering of Global *Brucella suis* and *Brucella microti* Transcription Profiles Contributes to the Understanding of the Increased Survival of *Brucella microti* at pH 4.5 *in vitro*

Core Genes

Of the 150 significantly regulated "core genes," 108 genes were more expressed at pH 4.5, 38 at pH 7, and four in an opposite manner in both species (**Figure 4A**). The first group comprised genes encoding the following factors involved in energy production: F_1F_0-ATP synthase, cytochrome oxidases and NADH-quinone oxidoreductase (**Supplementary Table 3**). The activation of the F_1F_0-ATPase/ATP-synthase has been reported under acid conditions in bacterial species such as *E. coli* (Sun et al., 2012) and *Listeria monocytogenes* (Cotter et al., 2000). In our study, the induction of three of the F_1F_0-ATPase/ATP-synthase genes was observed: *atpG*, *atpD*, and *atpC*, the latter encoding the subunit participating in proton translocation. *atpC* activation in *Brucella* fits with previous reports in other bacteria, where its activity is presumed to act directly as a mechanism for intracellular proton extrusion,

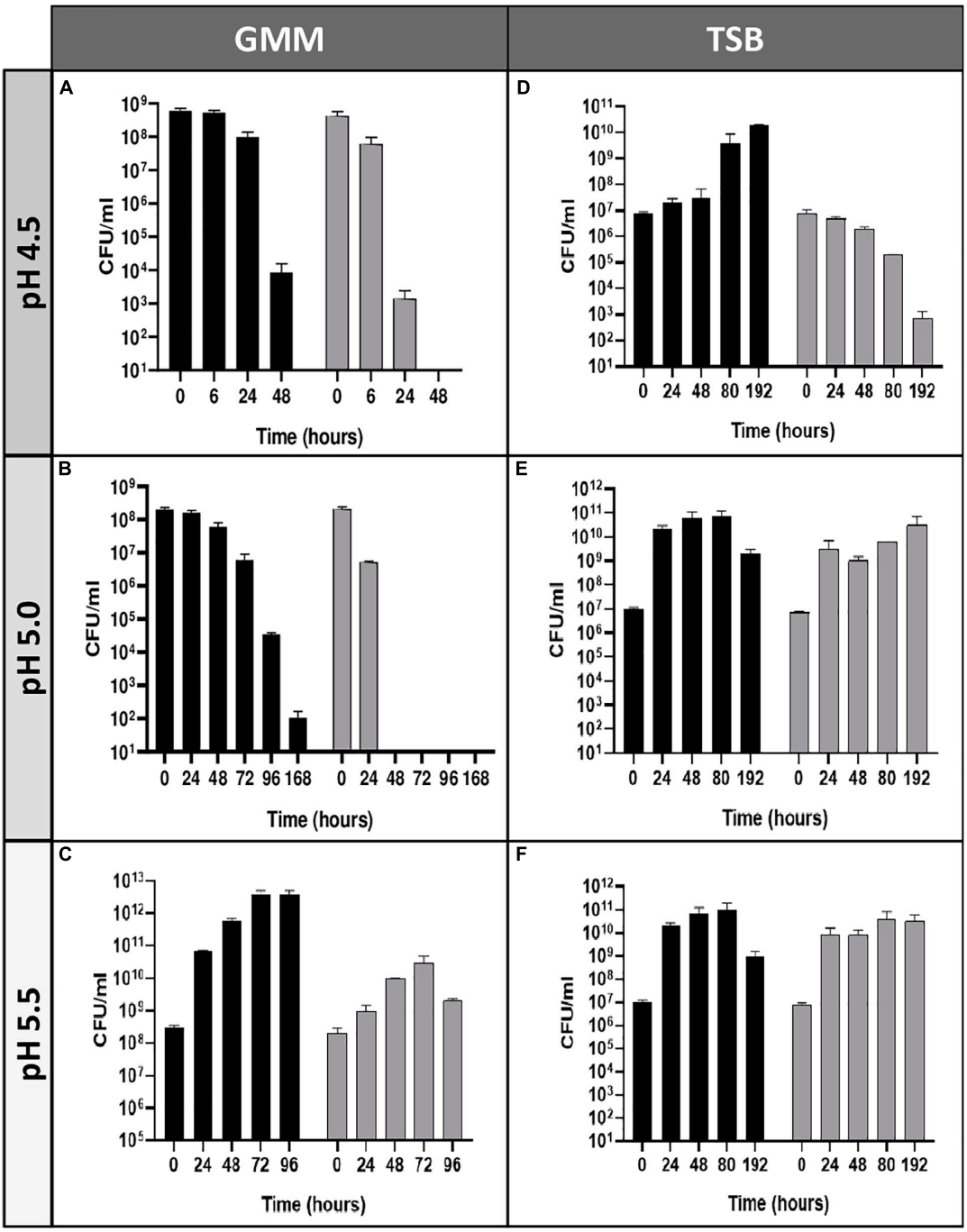

FIGURE 1 | Survival and replication of *B. microti* and *B. suis* in minimal or complex medium at pH 4.5–5.5. Viability of *B. microti* (black bars) and *B. suis* (gray bars) in modified Gerhardt's Minimal Medium **(A–C)** or Tryptic Soy broth **(D–F)** adjusted to pH 4.5, 5.0, and 5.5 was determined at different time points. Values are shown as means of 3 experiments ± standard deviations (SD).

consuming ATP (Lund et al., 2014). However, due to the dual function of this machinery acting also as an ATP-synthase, it can generate ATP using an inward-directed proton-motive force, suggesting that the enzyme may also play a role in the production of the energy required for the activities of ATP-dependent proteases, chaperones or transporters involved in diverse acid resistance and repair mechanisms (Lund et al., 2014). In *E. coli*, the ATP production capacity was reported to be essential for acid resistance (Sun et al., 2011). Likewise, increase in intracellular ATP concentration during rapid environmental shifts such as a switch from neutral pH to pH 3.5, has been reported in *E. coli*, *Pseudomonas putida* and *Bacillus subtilis* (Albert and Brown, 2015). The potential importance of an alternating ATPase/ATP-synthase activity is evidenced by its

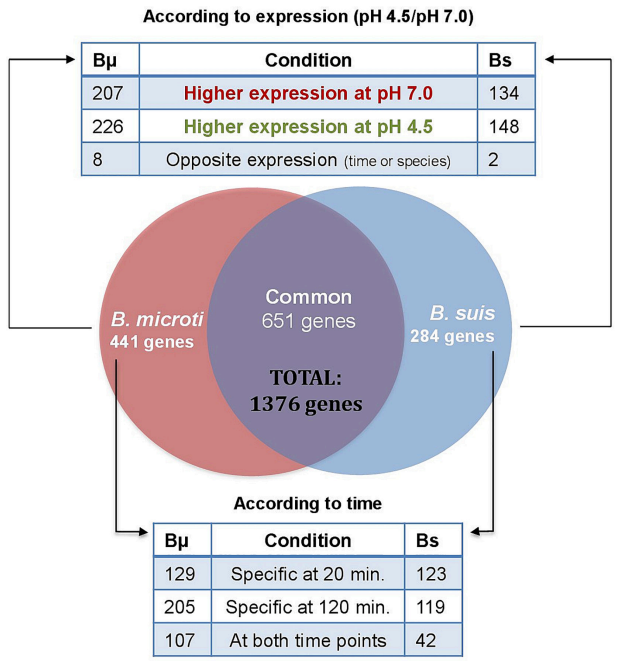

FIGURE 2 | Distribution of differentially expressed genes in *B. microti* and *B. suis*. Numbers of genes differentially expressed in both species at pH 4.5/pH 7 were determined either according to the rates of expression at both pH-values (upper panel), or according to the time points where differential expression was significant (lower panel). Bμ: *B. microti*; Bs: *B. suis*.

activation under acid and alkaline stress in *E. coli*, demonstrating its versatile role in bacterial pH homeostasis (Maurer et al., 2005). However, the mechanisms remain to be elucidated, and deepening the understanding of the ATPase/ATP-synthase role in *Brucella* may contribute to a better comprehension of acid resistance and physiology.

The induction of cytochrome oxidase genes, mainly *cco* encoding the cytochrome cbb_3 oxidase, was in line with acid stress resistance, as cytochrome oxidases catalyze the reduction of O_2 to water, acting thereby as a proton-pump (Pitcher and Watmough, 2004). In addition to the also acid-dependent expression of the NADH-ubiquinone oxidoreductase complex I (*nuoEFHIKLMN*), the major respiratory chain complex, the cbb_3 oxidase may act as a complementary system in the export of protons. In agreement with these findings, genes encoding the Ccm complex (*ccmDEFGHI*) involved in cytochrome *c* biogenesis, and the FnrN transcriptional regulator (BMI_I653/BR0654) were also induced. FnrN is known to regulate the cytochrome cbb_3 oxidase through an oxygen sensing mechanism (Loisel-Meyer et al., 2005), and expression was increased in both species at pH 4.5 after 20 min Moreover, the cytochrome cbb_3 oxidase as well as FnrN have been linked to bacterial persistence in the host, as inactivation of their genes in *B. suis* results in strong attenuation in murine infection during the chronic phase (Jiménez De Bagüés et al., 2007). A relationship between the aerobic/anaerobic metabolism of *Brucella* and its within-the-host life is known, with interplays between different cytochromes (Loisel-Meyer et al., 2005; Jiménez De Bagüés et al., 2007; Abdou et al., 2013). According to our results, the acid pH signal may also play a role in these crosstalks, possibly acting as a trigger for certain respiratory and metabolic changes.

While an active ATP-synthase generates translocation of protons from the periplasm to the cytosol, these proton-pumping mechanisms contribute to pH homeostasis under acid stress conditions, exporting protons to the external medium. Additionally, the cytochrome cbb_3 oxidase is tightly linked to the initiation of denitrification processes, which are activated during microaerophilic and anoxic conditions and allow the bacteria to use nitrogen oxides as electron acceptors under these conditions. Interestingly, the cytochrome *bd* ubiquinol oxidase genes *cydDAB*, related to the denitrification process in *B. suis* since their lack impairs nitrite utilization (Jiménez De Bagüés et al., 2007), were also more expressed at pH 4.5.

It must be taken into consideration that the acidic environment created in the experimental model used in this study leads to a potential drop of the dissolved oxygen concentration, due to the reaction of hydrogen ions with oxygen. This phenomenon most likely explains the activation of systems associated to microaerophilic conditions, such as cytochrome cbb_3 oxidase and denitrification, during exposure to acid stress.

The increased expression of two genes encoding outer membrane proteins (Omp) was also part of the common response in GMM at pH 4.5: the gene coding for an OmpW family small outer membrane protein whose function remains unknown but is predicted to be a porin, and *omp31*, encoding one of the major Omp in *Brucella* more expressed at pH 4.5 under three of the four conditions (Cloeckaert et al., 2002) (**Supplementary Table 3**). The OmpW family proteins form eight-stranded beta-barrels with a hydrophobic channel, possibly for small-molecule transport across the membrane. They have been related to resistance to environmental stress and to phagocytosis in *E. coli* (Wu et al., 2013). Omp31 has also been linked to resistance to diverse stress types (e.g., peroxide, polymyxin) and it participates in intracellular survival (Verdiguel-Fernandez et al., 2017). As a transmembrane protein, it is in direct contact with the extracellular acidic environment, which may lead to rapid protonation and possible denaturation, followed by loss of function of Omp31. Considering the importance of these proteins in stress resistance, the increased expression of their genes at pH 4.5 might reflect a compensatory mechanism to renew the acid-denatured molecules, thus maintaining their outer membrane functions; these may involve charge balancing, osmoregulation and transport. Genes of other Omps such as OmpF and OmpC are also induced and play an important role in survival under acid stress (Sato et al., 2000). The closed state of OmpC is induced and stabilized when the cytoplasmic pH drops and acid stimulation reaches the Omps from the periplasmic space (Liu and Delcour, 1998). Moreover, polyamines such as cadaverine and putrescine, released under acid stress by the action of lysine and ornithine decarboxylases, respectively, also contribute to closure of the outer membrane porins, reducing general permeability of the membrane (Samartzidou et al., 2003). Hence, maintenance of the porins' closed state can contribute to protection against internalization of hydrogen ions.

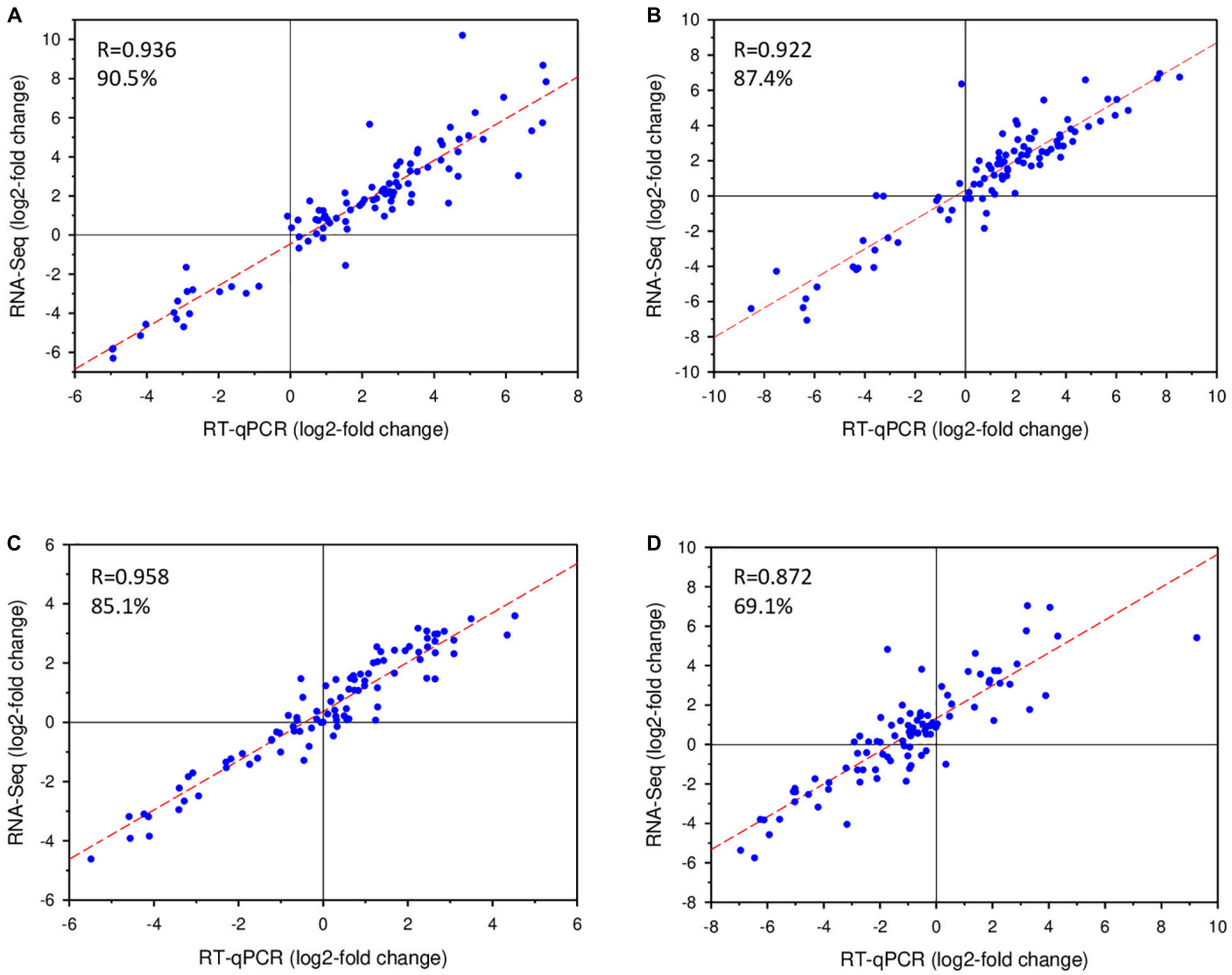

FIGURE 3 | Validation of RNA-Seq data by RT-qPCR. Log2-values of fold-changes of gene expression at pH 4.5 and pH 7.0 detected by RNA-Seq were plotted against RT-qPCR data. Rates of validation are indicated as percentages in the graphs. **(A)** *B. microti*, 20 min; **(B)** *B. microti*, 120 min; **(C)** *B. suis*, 20 min; **(D)** *B. suis*, 120 min.

Interestingly, genes of both major pathways of histidine metabolism were found to be more expressed in both species during acid stress: the histidine biosynthesis pathway, encoded by the *his* operon with *hisA*, *hisF*, and *hisI* (core gene), and the histidine degradation pathway, encoded by the *hut* operon with *hutI*, *H*, *G*, *J*. Based on the log2-fold change ratios, the expression rates of the *hut* operon were higher in *B. suis*, reaching values >4.0. Each pathway has different biological implications and both are tightly regulated. Biosynthesis of histidine provides carbon, nitrogen and energy sources, whereas acid resistance mechanisms are linked to degradation of histidine, generating ammonia and glutamate, the latter also playing a role in osmotic regulation. The *hut* system is regulated by diverse stimuli such as histidine or urocanate availability and nitrogen-limiting conditions, and controlled by the Ntr system. Despite nitrogen abundance, *ntrB* and *ntrC* showed increased expression at low pH in both species, which may be explained by the potential role of Ntr in ammonia supply for other pathways, such as glutamate synthesis and polyamine metabolism. The increased expression of the histidine utilization pathway genes therefore reflected a potential adaptation to low-nutrient conditions, as well as an attempt to provide molecules participating in the regulation of the internal pH. The increased expression of genes involved in the L-histidine biosynthetic pathway may contribute to purine biosynthesis, since both pathways share common steps. This is in agreement with increased expression of purine biosynthesis genes under acid stress, observed specifically in *B. suis* and discussed later. Due to its capacity to function as a major proton donor or acceptor, histidine plays a central role at crossroads of diverse cellular functions in bacteria, from purine and nucleotide synthesis to signal transduction, and histidine decarboxylation has been described in acid adaption (Trip et al., 2012).

Another highlight among the group of core genes with an increased rate of expression at pH 4.5 in both species were the genes encoding urease, a well-known actor in acid resistance, where hydrolization of urea by urease yields CO_2

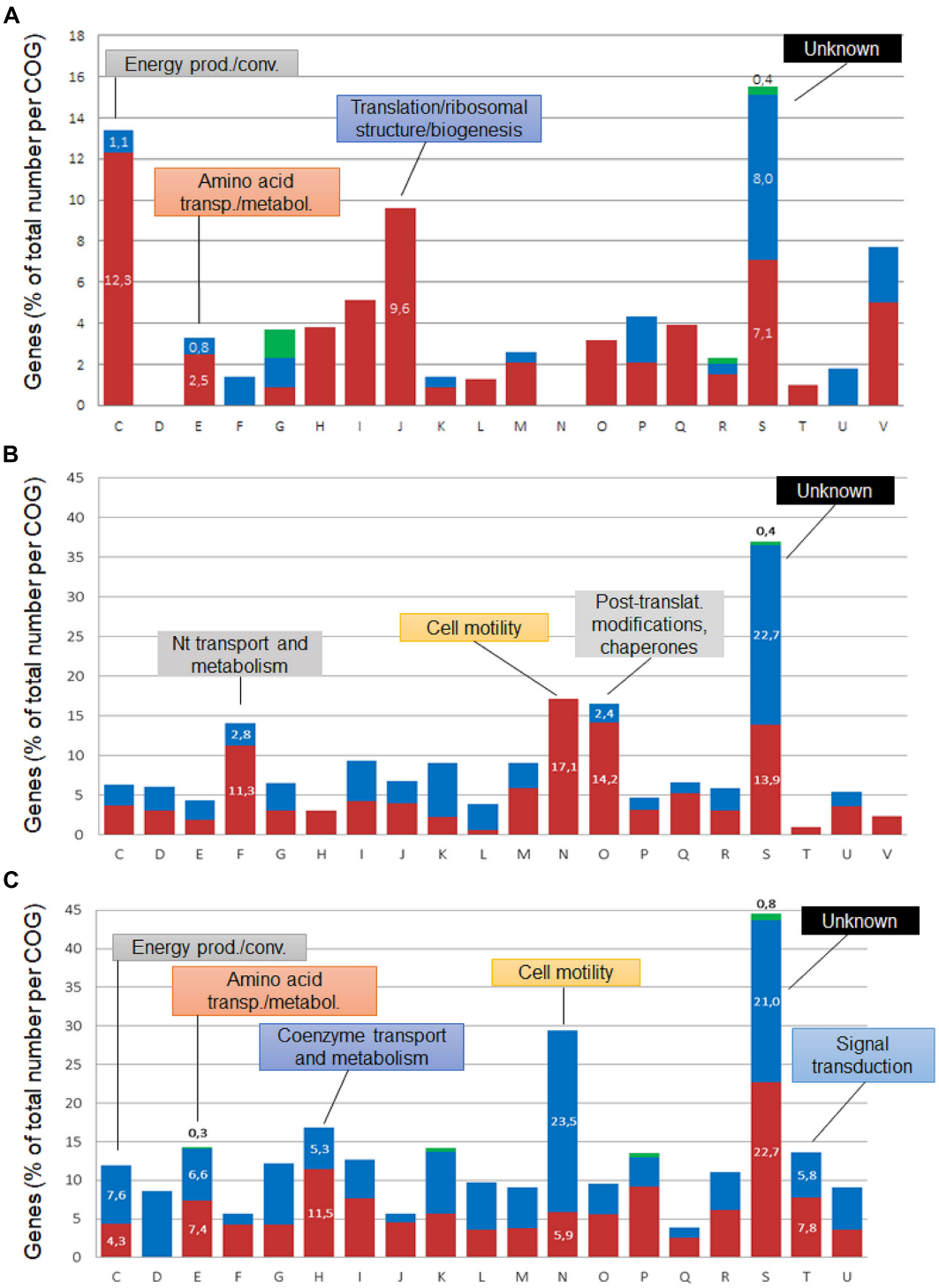

FIGURE 4 | COG classification of *Brucella* genes regulated at pH 4.5. The differentially expressed core genes **(A)** and those specific to *B. suis* **(B)** and *B. microti* **(C)** cumulated for both 20 and 120 min were classified into Clusters of Orthologous Groups, and their percentages were determined with respect to the total number of genes affiliated to each group. Blue sections of the bars represent genes with higher expression at pH 7, red sections genes with higher expression at pH 4.5, and green sections correspond to genes with opposite expression over time. COGs: C: Energy production/conversion; D: Cell cycle control, cell division; E: amino acid transport/metabolism; F: Nucleotide transport/metabolism; G: Carbohydrate transport/metabolism; H: Coenzyme transport/metabolism; I: Lipid transport/metabolism; J: Translation/ribosomal structure/biogenesis; K: Transcription; L: Replication, recombination/repair; M: Cell wall/membrane/envelope biogenesis; N: Cell motility; O: Posttranslational modification/protein turnover/chaperones; P: Inorganic ion transport/metabolism; Q: Secondary metabolites synthesis/transport/catabolism; R: General function prediction; S: Function unknown; T: Signal transduction; U: Intracellular trafficking, secretion/vesicular transport; V: Defense mechanisms.

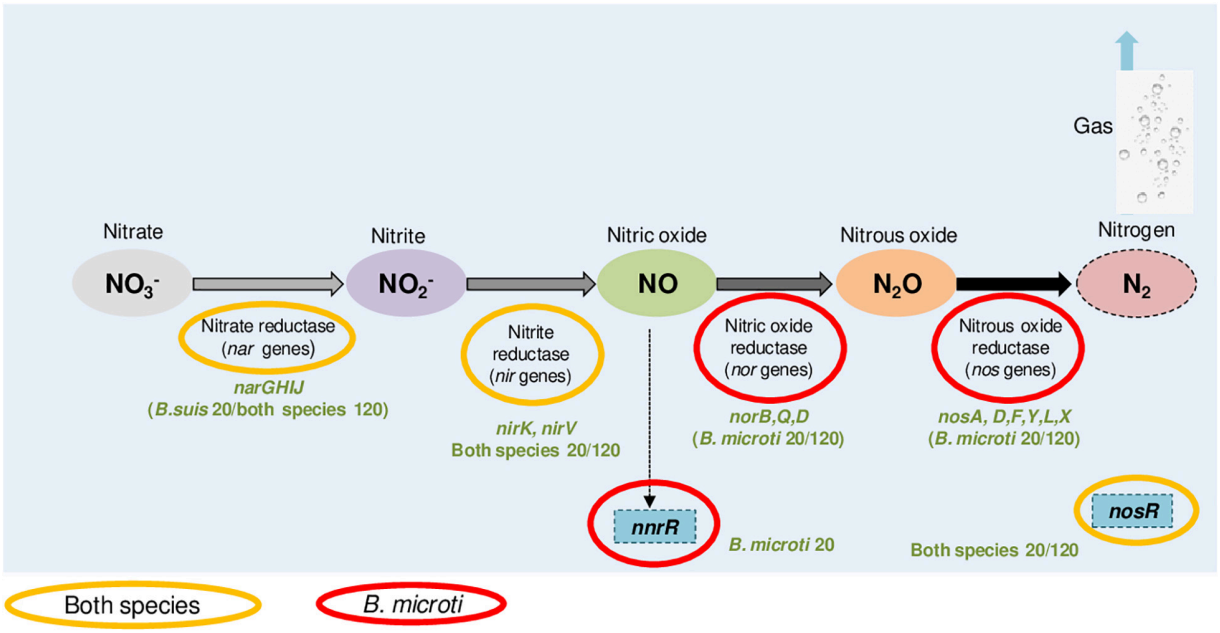

FIGURE 5 | *B. microti* and *B. suis* genes of the denitrification pathway with increased expression at pH 4.5. Color codes indicate the species and the experimental time points (20 or 120 min) for each of the genes identified as being more expressed at pH 4.5 than at pH 7.

and ammonia, which counteracts the acid pH by protonation (Sangari et al., 2007; Lund et al., 2014). However, the genes for the accessory proteins participating in the maturation process of the urease (*ureE*, *ureF*, and *ureG*) were expressed differentially only in *B. suis*, suggesting an increased activity in this species (**Supplementary Table 3**). In the absence of urea in the medium, ammonium sulfate as well as glutamate, glutamine, arginine and their derivatives may feed the system and are possible NH^{4+}-sources for the urea cycle. In line with this strategy is the activation of the *hut* operon, which encodes factors involved in degradation of histidine to yield ammonia and glutamate (Bender, 2012). The activation of the *hut* operon may also explain the lack of induction of the T4SS at these early time points of acid stress: *hut* operon repressor HutC is a positive regulator of the expression of the *virB* operon (Sieira et al., 2010). Hence, as long as the *hut* operon remains active, expression of the *virB* operon cannot be supported by the action of HutC.

A total of 38 core genes showed higher expression at pH 7.0 (**Supplementary Table 3**). Some of these genes encode key enzymes involved in gluconeogenesis: phosphoenolpyruvate carboxykinase (*pckA*), fructose-1,6-bisphosphatase (*fbp*), and fructose-1,6-bisphosphate aldolase (*fbaA*). A possible explanation for this metabolic down-regulation at pH 4.5 could be the favoring of other metabolic pathways such as the pentose phosphate pathway, the major pathway of hexose and pentose catabolism in most *Brucella* species. Moreover, in *B. microti* the genes encoding fructose 1,6-biphosphatase II, (*glpX*) participating in gluconeogenesis, and malic enzyme, catalyzing the conversion of malic acid to pyruvate with production of NADPH and linking glycolysis and gluconeogenesis with the tricarboxylic acid cycle, were also less expressed (**Supplementary Table 3**; *B. microti*-specific genes). The lower expression of these genes at pH 4.5 further reduced the gluconeogenic pathway during acid stress. Interestingly, the gene encoding malic enzyme is annotated as pseudogene in *B. suis*, resulting in modifications of the so-called phosphoenolpyruvate (PEP)-pyruvate-oxaloacetate node that regulates the major carbon metabolic pathways, but also in the possible loss of a pathway allowing generation of the key metabolic cofactor NADPH. In addition, of the four core genes showing opposite regulation in the two species, three encode sugar transporters.

Brucella microti- and *Brucella suis*-Specific Acid-Responsive Genes

In addition to the acid-responsive core genes, each species possessed a specific set of genes whose expression was modified by the acid stress. The genes specific to each species at 20 and 120 min were classified into Clusters of Orthologous Groups (COG) to predict possible functions, and their percentages were determined with respect to the total number of genes affiliated to each group (**Figures 4B,C**). Group S was the most abundant, but several groups with known functions were also identified as harboring an important number of acid stress-dependent factors (**Figures 4B,C**): C (energy production and conversion); E (amino acid transport and metabolism), F (nucleotide transport and metabolism); H (coenzyme transport and metabolism); N (cell motility); O (post-translational modification, protein turnover and chaperones).

Brucella microti-Specific Acid-Responsive Genes

The analysis of the *B. microti*-specific acid stress response gave some important clues on the adaptation of the pathogen to

these harsh environmental conditions (**Supplementary Table 3**). A remarkable feature was the increased expression at pH 4.5 of the genes encoding RNA polymerase sigma factors sigma 24 (*rpoE*) and sigma 32 (*rpoH2*), in accordance with previous reports where *rpoE* activates *rpoH2* (Roncarati and Scarlato, 2017). This strengthened the hypothesis of a species-specific processing of the acid stress signals in *Brucella*, with a possibly earlier response in *B. microti*. The *B. microti*-specific increased expression of a two-component response regulator-encoding gene (BMI_I1679), annotated in some *Brucella* species as PhyR, was in line with the increased expression of *rpoE*: Both are central elements of the general stress response in alpha-proteobacteria and have been described as required in *B. abortus* for *in vitro* stress survival and chronic murine infection (Kim et al., 2013). Moreover, *rpoE* has been reported to be expressed consecutively to envelope damage detected by sensing of misfolded Omps, and both factors are involved in maintaining the integrity of periplasmic and outer membrane components (Raivio and Silhavy, 2001). In *B. melitensis*, RpoE1 also acts as repressor of the flagellar genes (Ferooz et al., 2011). Hence, increased expression of the corresponding gene at pH 4.5 exclusively in *B. microti* may explain the lack of activation of flagellar genes in the atypical species during acid stress, whereas flagellar genes are more expressed in *B. suis* (see below).

Another particular feature of the specific *B. microti* response to acid stress was the strong activation of nitrogen metabolism genes, especially the denitrification pathways (**Supplementary Table 5**), with 19 members one of the strongest sets of positively regulated genes at pH 4.5. This observation was in agreement with the increased expression at pH 4.5 of the cbb_3 cytochrome oxidase components, linked to denitrification and induced by low oxygen concentrations and by exposure to reactive nitrogen species and nitrite. Despite the fact that the genes encoding nitrate reductase Nar and nitrite reductase Nir, catalyzing the first two steps of denitrification, were more expressed at pH 4.5 in both species, acid-induced expression of *nor* and *nos*, encoding nitric oxide and nitrous oxide reductases, was specific to *B. microti* (**Figure 5**). As a consequence, *B. microti* avoided the possible accumulation of harmful NO, which may, in contrast, affect *B. suis*. This evidence suggested a differential regulation of the denitrification pathways under acid stress, and hence a species-specific control of the anaerobic/microaerobic respiration. Specific activation of *nor* and *nos* operons is likely to be based on the pH-mediated decrease of dissolved oxygen in acid medium, suggesting that *B. microti* may have a faster adaptive response under acid-induced low oxygen conditions. Interestingly, the *Brucella nar* operon is also induced during the stringent response, constituting another overlapping factor in multiple stress responses (Hanna et al., 2013), and the denitrification pathway has been related to *Brucella* virulence in mice and intracellular resistance to NO (Haine et al., 2006; Loisel-Meyer et al., 2006).

Furthermore, acid-dependent regulation of genes involved in methionine metabolism was significantly different between both pathogens: The acid-induction of four genes (*ahcY*, *metH*, *metF* and *sahR*) involved in the S-adenosylmethionine (SAM)-S-adenosylhomocysteine (SAH) cycle suggested a higher methylation activity in *B. microti*, since SAM, a nucleoside generated from methionine, is a coenzyme for methyltransferases (**Supplementary Table 6**). It is also required for the synthesis of polyamines, quorum sensing molecules and production of vitamins, demonstrating the important role of SAM in bacterial metabolism. This enhanced activity of the SahR regulon may also be related to the higher expression of the genes *bioA* and *bioB*, coding for biotin-ligase and dethiobiotin synthase, respectively, and to the induction of the cobalamin (B12) synthesis pathway (precorrin-2 methyltransferase, *cbiG*, *cbiQ*, *cobN* and cobalamin synthesis proteins) in *B. microti* (**Supplementary Table 3**). Increased DNA-methylation activity *via* SAM impacts regulation of gene expression, conservation of genome integrity and cell cycle regulation, and SAM has also been associated to riboswitch-dependent genetic regulation (Batey, 2011). An active methionine metabolism in *B. microti* may be related to a higher rate of transcriptional/translational activity, but also points out differences to *B. suis* concerning regulation of the sulfur metabolism, which most likely participates in redox homeostasis through biosynthesis of thiol antioxidants such as glutathione, cysteine, and homocysteine, also required during acid stress.

Overall, 4–7% of the putative protein-encoding genes in *Brucella* genomes are pseudogenes. Pseudogenization can lead to many phenotypical differences and play an important role in *Brucella* host specificity and virulence (Chain et al., 2005). Interestingly, expression of 15 genes reported as being pseudogenes exclusively in *B. suis* was influenced by acid stress in *B. microti* (**Supplementary Table 7**): genes encoding choline dehydrogenase (BMI_I1654), cold-shock protein CspA and D-lactate dehydrogenase Dld were of main interest. The choline dehydrogenase is an enzyme linked to osmoprotection, catalyzing the glycine betaine synthesis from choline oxidation. Glycine betaine has been reported to protect also from heat shock, acting as a protein stabilizer and contributing to protein renaturation (Caldas et al., 1999). Other osmoregulation mechanisms are also coordinately activated in *B. microti*, such as glycine betaine/L-proline ABC transporters, while the gene encoding the mechanosensitive channel MscL, undergoing conformational change under membrane stretching, is repressed in *B. microti*, possibly due to ion permeability when the channel is open (**Supplementary Table 3**). Due to the intricate regulation of osmotic and acid stress responses, characterized by the overlapping functions of molecules involved in both responses such as K^+, glutamate and other osmolytes, pH-regulating mechanisms can have an impact on osmotic pressure through membrane permeability changes, denaturation of proteins and generation of metabolites such as ammonia, urea, GABA, etc. These variations, possibly resulting in osmotic imbalance, may activate the adequate systems to cope with this additional stress.

The identification of certain pseudogenes in *B. suis* may also give some clues about metabolic and physiologic differences between both *Brucella* species, looking at the examples of the genes encoding thioredoxin reductase and D-lactate dehydrogenase Dld (**Supplementary Table 7**). Thioredoxin reductase, whose expression was downregulated at pH

4.5 in *B. microti*, is involved in ribonucleotide reduction. Hence, its lack in *B. suis* may imply the use of alternative pathways to produce deoxyribonucleotides. The D-lactate dehydrogenase (Dld), activated by *B. microti* early at pH 4.5 but downregulated later, may play a role in electron transfer during anaerobic conditions. The loss of the D-lactate dehydrogenase expression in *B. suis* in addition to less efficient denitrification suggests a better adaptation of *B. microti* to anaerobic or microaerophilic conditions. Interestingly, in opposition to the situation observed in *B. suis* with 15 pseudogenes which were acid-stress regulated in *B. microti*, none of the acid stress-regulated genes found in *B. suis* were pseudogenes in *B. microti*, despite the fact that a total of 79 pseudogenes are present in *B. microti* versus 109 pseudogenes in *B. suis* (NCBI Genome database; Audic et al., 2009). It is conceivable that the loss of certain genes during host-adaptation impairs *B. suis* acid stress resistance, when compared to the more ancestral and free-living species *B. microti*. These results therefore give additional evidence that gene mutations shape the physiology of *Brucella* species.

In our study, genes encoding the type IV secretion system components were not characterized by increased rates of expression under acid conditions (**Supplementary Table 3**), which was unexpected, since acid stimulation and nutrient-poor medium are known to trigger *virB* expression (Boschiroli et al., 2002). *virB1* and *virB6* were significantly less expressed at pH 4.5 in *B. microti* at both time points, while *virB7* was less expressed under acid conditions in *B. suis* at 20 min The low ratios of transcription at pH 4.5 *versus* pH 7.0 may be explained by the fact that the *virB* operon is induced at pH 4.5 at later time points only.

Interestingly, three genes corresponding to cold shock proteins (*csp*), including *cspA*, showed higher expression at pH 4.5 in *B. microti*, two of them specifically. In line with the described cold shock responses (Zhang et al., 2018), two helicases and a VacB/RNAse II exoribonuclease, possibly the RNAse R described to act with CspA, also presented increased expression (**Supplementary Table 8**). In addition, the *B. melitensis* homolog of the *csp* gene BMI_I1528 was reported to play an important role in *Brucella* virulence and stress adaptation (Wang et al., 2014).

The sulfur mobilization (*suf*) operon, considered as essential in *Brucella* (Sternon et al., 2018), was also more expressed in *B. microti* at pH 4.5. It is required for the assembly of Fe-S clusters, acting as cofactors in diverse metabolic reactions, as electron carriers in redox reactions, and in gene regulation and DNA repair and replication. It is activated during iron limitation or oxidative stress (Blahut et al., 2020). Due to protonation and denaturation induced by acid stress, Fe-S cluster-containing proteins as well as DNA are likely to be damaged, explaining the increased expression under acid conditions of the *suf* operon in *B. microti* (**Supplementary Table 9**). Moreover, the ATPase function of SufC may also have a role as a proton pump in acid stress, suggesting different ways for the Fe-S clusters in the bacteria to cope with redox state disturbances. Under acid stress, expression profiles of *B. microti* and *B. suis* were different for iron and sulfur acquisition pathways, including higher expression in *B. microti* of genes coding for certain iron transporters, sulfur-containing amino acid metabolism and the ferritin-like protein Dps.

Brucella suis-Specific Acid-Responsive Genes

The identification of different groups of genes specifically regulated in *B. suis* sheds light not only on the mechanisms this pathogen has set up to respond to acid stress, but also on the physiological alterations the species may be exposed to. The higher rates of expression at pH 4.5 of genes participating in purine biosynthesis (*purE*, *purH*, *purC*, *purL*), peptidoglycan biosynthesis (*nagB*, *mraY*, *murE*, *murD*, *murF*) and lipid A biosynthesis (*lpxL*) suggested increased levels of structural damages of the DNA, cell wall and outer membrane, when comparing to the expression rates of the same sets of genes in *B. microti*, and could be a clue to the observed reduced survival of *B. suis in vitro* at pH 4.5 (**Supplementary Table 3**).

DNA damage, known to be one of the harmful effects of acid stress profoundly altering normal cell physiology, is mediated by DNA depurination, with rates increasing as the pH decreases (Raja et al., 1991). Increased expression of the purine biosynthesis operon *pur* may therefore contribute to generate nucleotides for the repair of damaged DNA. In line with this observation was the increased expression of genes at pH 4.5 in *B. suis* encoding the ribonucleotide-diphosphate reductase (RNR), involved in the synthesis of deoxyribonucleotides from ribonucleotides required for DNA synthesis during replication or repair processes (Torrents, 2014). Under our experimental conditions, *B. suis* increased the expression of the genes encoding the RNR subunits alpha (*nrdE*) and beta (*nrdF*) at pH 4.5, whereas *B. microti* showed a higher rate of expression of these genes at pH 7.0 (**Supplementary Table 3**). Since this system plays an essential role, its operon must be tightly regulated to ensure correct RNR concentrations and balanced dNTP levels (Torrents, 2014), a fact that adds to the biological relevance regarding different expression levels observed in both *Brucella* species. In the absence of growth of *Brucella* in minimal medium at pH 4.5, increased expression of *nrdE* and *nrdF* suggested an active DNA-repairing process in *B. suis*, as a response to increased sensitivity to acid stress at pH 4.5.

Genes involved in the peptidoglycan-recycling pathway and in peptidoglycan (PG) synthesis also showed increased expression specifically in *B. suis* at pH 4.5, among which *nagB*, encoding glucosamine-fructose-6-phosphate aminotransferase, and genes encoding the three main ATP-dependent amino acid ligases MurD, MurE, MurF and phospho-N-acetylmuramoyl-pentapeptide transferase (MraY) (**Supplementary Table 3**). The potential acid-related damage to PG in *B. suis* may affect bacterial physiology and hamper *Brucella* survival. PG plays a crucial role in maintaining bacterial shape and turgor pressure while allowing nutrient transport. In addition, the movement of the bacterial cytoskeleton-like elements has been shown to be tightly interdependent with PG synthesis, which is also regulated by lipoproteins anchored to the inner layer of the outer membrane, suggesting that PG synthesis is governed by internal and external signaling (Typas et al., 2011). These links may give clues about possible envelope rearrangements during acid stress, when the outer membrane is damaged by high H^+-concentrations. The

stronger expression of purine and peptidoglycan biosynthesis genes at acid pH in *B. suis* was consistent with studies performed in *E. coli* (Shayanfar et al., 2018), suggesting their participation in a general acid-stress response in certain Gram-negative bacteria. In the outer membrane, acid pH induces loss of stabilization of LPS as a consequence of increased phosphorylation of lipid A (Li et al., 2020). Therefore, the increased expression of *lpxL* encoding lauroyl acyltransferase and participating in lipid A biosynthesis may represent, alongside with PG and purine synthesis, an attempt to maintain cellular integrity during acid stress in *B. suis*.

Furthermore, a significant increase in expression of *entC* encoding isochorismate synthase was observed at pH 4.5 in *B. suis* (**Supplementary Table 3**). This enzyme participates in the 2,3-dihydroxybenzoic acid siderophore synthesis pathway, catalyzing the conversion of chorismate to isochorismate and it is responsive to environmental iron availability. The increased expression of a gene of the enterobactin operon suggested an important need for iron in *B. suis* during acid stress, which can be explained by the fact that iron is an essential cofactor for the assembly of Fe-S cluster proteins and ribonucleotide reductases.

The increased expression of the erythritol metabolism-related genes under acidic conditions only in *B. suis* is remarkable, since this sugar alcohol is a major substrate in brucellae. Erythritol feeds the pentose phosphate pathway and is considered as one of the determinants for the tissue tropism of *Brucella* toward the host's reproductive tract (Barbier et al., 2014). In addition, genes *eryB* and *eryC* are necessary for intramacrophagic growth (Köhler et al., 2002). This acid pH-mediated differential expression of *ery* genes may reflect specific metabolic adaptation and mechanisms of regulation, possibly having an impact on the within-the-host life of *Brucella*.

Function-Based Expression Analysis, Independent of Species-Specificities

The identification of acid-dependent genes encoding factors interacting with the bacterial envelope added information on the strategies the pathogen has set up to create an efficient barrier against adverse effects of low pH. Some of these genes have already been presented above. To assess the possibility of an eventual acid stress-induced activation of repair processes in the outer membrane, a survey of acid stress-regulated genes potentially associated to such processes was carried out with the threshold-selected 1376 genes. Eleven of them encoded factors involved in LPS or outer membrane proteins biosynthesis (**Supplementary Table 10**). The modulation of outer membrane compound synthesis may have significant impacts on bacterial survival at acid pH and on infection biology. The LPS, major component of the outer membrane, is well-recognized to be crucial for host-pathogen interactions, and microorganisms adapt the LPS structure in response to the environmental conditions, including acid stress (Li et al., 2020). Regarding the outer membrane proteins and their function as permeable channels as well as their role in sensing, the increased expression of Omp31-1, Omp31-2 and the OmpW family protein may be an indicator of additional repair mechanisms in both species.

Remarkably, in *B. suis* the acid stress induced, at the early time point of analysis, an almost species-specific, significant increase in the expression of 14 genes belonging to the flagellar machinery (**Supplementary Table 11**). A heatmap of the expression profiles of the genes assigned to COG N for both *B. suis* and *B. microti* is shown in **Supplementary Figure 1A**, giving a comparative overview of differential expression of functionally related genes for all experimental conditions applied. Most genes encoding flagella components showed a significantly higher expression at pH 7.0 in *B. microti* at 120 min, whereas a transient trend for increased expression at pH 4.5 was observed for the same genes in *B. suis* at 20 min. *Brucella* species normally do not display a motile phenotype, with the exception of *B. melitensis* and bullfrog and Pac-Man frog isolates, where a flagellum was reported (Fretin et al., 2005; Soler-Llorens et al., 2016; Al Dahouk et al., 2017). The biological function of these genes in *Brucella* is still unknown, however, the bacterial flagellum contains a transmembrane Type III secretion system, including the ATPase encoded by *fliI*, evolutionarily related to the F_1F_0-ATPase. This suggested that this apparatus or part of it may function as an additional proton-pump under acid stress in *B. suis*.

In addition, 17 genes encoding proteins of the classical heat shock response showed higher expression at acid pH (**Supplementary Table 12**). Ten of these were specifically more expressed in *B. suis*, suggesting that the classical pathogen was activating more chaperone- and protease-dependent mechanisms of protein degradation or re-folding. Increased expression of the genes encoding the chaperone pairs DnaK/J and GroEL strongly suggested that acid stress-mediated protein misfolding or damaging occurred in a more significant way in *B. suis* than in *B. microti*. Genes encoding heat shock-induced proteases, important in degradation of aggregated or denatured proteins and in the removal of potentially toxic degradation products, also showed an increased expression under acid stress in *B. suis*. In bacteria, Lon is the major protease participating in degradation of misfolded proteins under stress conditions, but as a player in the protein quality-control system, it also degrades proteins under physiological conditions. Exemplified by ClpB, DnaK, and DnaJ, proteases can also assist chaperones unfolding and renaturing protein aggregates. Other genes more expressed at pH 4.5 encode the ATP-dependent protease Hsl forming a proteasome-like degradation complex (**Supplementary Table 12**). Presented as a heatmap, the divergence between *B. suis* and *B. microti* in acid-dependent regulation of these COG O-associated genes encoding factors involved in posttranslational modification, protein turnover and chaperones, was evident: At 120 min, 11 of the 47 differentially expressed genes were regulated in an opposite manner in the two pathogens, with a clear domination of higher expression at pH 4.5 in *B. suis*, whereas the majority of the genes more expressed at pH 7.0 were found in *B. microti* (**Supplementary Figure 1B**). General increase of expression of genes involved in protein turnover and in chaperone biosynthesis at low pH in *B. suis* gave rise to the speculation that under these conditions, this pathogen was more exposed to harmful protein denaturation than *B. microti*. Increased expression of certain heat shock factors (GroEL, DnaK) during acid stress has been previously reported for *Brucella* (Köhler et al., 1996; Teixeira-Gomes et al., 2000). Remarkably, expression of heat-shock response sigma factor-encoding *rpoH* and *rpoE* genes was

not increased under acid conditions in *B. suis*, while *B. microti* showed an increase already during early exposure (see above). Our results showed that the acid stress-induced response in *B. suis* has the traits of a marked heat shock response, with several factors shared by the responses to different stress types: DnaK, related to heat and hyperosmotic stress; HslO, known to be redox-regulated and to participate, together with LbpA, in oxidative and heat stress; Lon, involved in the heat-shock response and in drug resistance processes. These findings are in agreement with a previous report on the induction of a heat shock-like response by *pmf* dissipation in *E. coli* (Gage and Neidhardt, 1993), fitting also with the hypothesis of increased envelope damage in *B. suis* at pH 4.5.

Furthermore, RNA-Seq results revealed that transport functions of *Brucella* were highly impacted by acid stress, and species-dependent specificities of transport activities may influence acid stress responses. A total of 180 genes encoding transporters had an altered expression profile under acidic conditions. Among those, a vast majority of 154 genes were found to be associated to ABC-transporters, with more than 50% of them affected, and 142 out of the 180 genes belonged to 71 predicted operons (**Supplementary Table 13**). 67 genes were significantly regulated in *B. microti* only. Interestingly, a general tendency of increased expression of genes encoding branched-chain amino acid transporters was observed in *B. microti* at pH 4.5 after 120 min of exposure. Similarly, 3 genes of a glycine betaine/L-proline transport system described for *Brucella*, as well as a sulfate ABC transporter and the permease component of a taurine transporter, were more expressed in *B. microti* under these conditions (Jenner et al., 2009). The activation of the glycine betaine/L-proline system reflected a potential need for these osmolytes, since pH homeostasis is interconnected with osmoregulation and the redox state of the cell: H^+ extrusion has to be compensated to maintain osmotic and redox homeostasis. Higher expression of sulfate and taurine transporters suggested a more active sulfur metabolism in *B. microti* during acid stress. Taurine, an amino acid-like organosulfonate, is an osmolyte that also participates in osmoregulation. ABC transporters have been associated with diverse physiological processes from DNA-repair to gene regulation, and are related to virulence (Jenner et al., 2009). 10 of the identified ABC transporter-encoding genes are listed in the PHIDIAS Victors database as virulence-associated. Finally, the general induction of ATP hydrolysis-based transporters might contribute to bacterial pH homeostasis through proton expulsion by the ATPase components of these systems. In some cases, when the transported molecule is an osmolyte or compatible solute (sugars, polyols, amino acids), the process may result in a double win situation for the cell, expelling protons and importing a neutral molecule.

Eighty-one genes encoding transcriptional regulators and two-component systems (TCS) were identified as being differentially regulated in the two *Brucella* species (**Supplementary Table 14**). A lower expression of most transcriptional regulators was observed under acid stress with only 26 genes being more expressed at pH 4.5, of which 13 were specifically regulated in *B. microti*, 4 in *B. suis* and 9 in both species. The most represented regulator families were GntR and AsnC, followed by AraC, ArsR, MarR, and LysR. In addition, *betI* (BMI_I553/BR0554) was more expressed in *B. suis* but less expressed in *B. microti* after 120 min. BetI is a repressor of the glycine betaine synthesis pathway and of a choline transporter.[6] This difference may reflect species-specific osmoregulation, with an increase of glycine betaine synthesis and transport in *B. microti* (see above). The genes with higher expression under acid conditions in *B. suis* encoded members of the DeoR, GntR and AsnC families. In *Brucella*, DeoR and GntR regulators are linked to host-pathogen interactions, but also involved in sugar metabolism and control of carbon and amino acid metabolism, or fatty and organic acids concentrations. In *B. microti*, genes coding for transcriptional regulators with increased expression under acid stress belonged to the ArsR, AsnC, IclR, LysR, OmpR and Ros/Muc families. The homologs of the *B. microti* Ros/MucR transcriptional regulator (BMI_I569) have been associated with virulence in *B. melitensis* and *B. abortus*, since their inactivation impairs intracellular growth and results in strong attenuation (Caswell et al., 2013). Despite the fact that these data must be interpreted with caution, because most of these regulators belong to large families with a wide array of possible functions in interconnected networks, such a difference between *B. suis* and *B. microti* in transcriptional regulation goes well with an earlier activation of virulence mechanisms in *B. microti*. Among the TCS, we identified two pairs of candidates with increased expression at pH 4.5 (**Supplementary Table 14**): BMI_II225/BMI_II226, the latter being a pseudogene in *B. suis*; BMI_I1535/BMI_I1537 at 120 min in *B. microti* only, encoding OmpR/EnvZ originally described as a porin regulator, controlling the outer membrane proteins OmpF and OmpC linked to acid stress response. In *Salmonella* and *E. coli*, OmpR/EnvZ participate in sensing of environmental signals such as osmotic and acid stress, and the intracellular acidification promoted by OmpR is necessary for T3SS expression (Chakraborty and Kenney, 2018). The genes BMI_II231 and BMI_II615, encoding potential TCS members with GGDEF-domains related to diguanylate cyclase- and phosphodiesterase-mediated biosynthesis and degradation, respectively, of the bacterial second messenger c-di-GMP, were acid pH-induced in *B. microti*, possibly indicating species-specific activation of the c-di-GMP second messenger functions linked to virulence, stringent response, motility, proteolysis, cell cycle and cell-cell communication (Römling et al., 2013). The complex functions of transcriptional regulators identified here necessitate specific transcriptomic studies to deepen knowledge on their biological roles under these environmental conditions.

Virulence-Related, Acid-Stress Responsive Genes

Several acid-responsive genes of *Brucella* have been previously reported as virulence-related, according to PHIDIAS Victors and VFBP databases. In our work, 69 virulence genes listed in these databases were identified as acid-stress responsive (**Supplementary Table 15**), out of 159 virulence-associated genes reported for *B. suis*. From the 69 genes, 28 were

[6]https://www.uniprot.org/uniprot/Q2YMS6

regulated in both species, 19 and 22 specifically in *B. suis* and *B. microti*, respectively. Altogether, 25 of the virulence-related genes were down-regulated, while 39 were more expressed under acid conditions, and 5 showed up- or down-regulation, depending on time-points or species. Species-specifically regulated virulence genes with increased expression under acid conditions were more numerous in *B. suis* (14/19) than in *B. microti* (10/22), indicating specific gene expression signatures, possibly in the species' interactions with the host cell. The most represented COGs were the groups E (amino acid transport/metabolism), C (energy production/conversion) and G (carbohydrate transport/metabolism). As an example of genes listed in both databases, *rfbD* encodes the LPS O-antigen export system permease. It was more expressed at pH 4.5 in *B. microti*, suggesting that *B. microti* may preserve structural integrity of the envelope by activation of specific repair mechanisms, while *B. suis* engages into a larger response involving chaperones, proteases and potential DNA-repairing mechanisms.

Recently, Salmon-Divon et al. reported 773 *B. melitensis* 16M genes differentially expressed (fold change $\geq$ 2) between normal and low-pH conditions in TS broth at pH 4.4 after 4 h of incubation. Despite the differences in experimental conditions, 25 of these genes were also identified in our analysis as being differentially expressed simultaneously for both *B. suis* and *B. microti* (fold change $\geq$ 2.8), including 15 that were upregulated and 10 that were downregulated under acid-pH conditions. Another 12 and 6 genes were identified as being specifically regulated in *B. suis* and *B. microti*, respectively (**Supplementary Table 16**). The common induction of genes of the respiratory chain points out the importance of this system comprising proton pumps which maintain physiological conditions in the cytosol of *Brucella* species. Other highly conserved mechanisms of acid protection were induction of histidine degradation *via hut* genes generating protective ammonia and glutamate, and increased expression of urease-associated genes.

Selection of Acid Stress-Induced *Brucella* Genes and Evaluation of Their Participation in Acid Stress Resistance at pH 4.5 and in Intramacrophagic Survival

Based on their predicted biological functions, their acid stress-induced expression rates, and their potential relationship to virulence or acid resistance mechanisms, 16 genes were selected for inactivation by homologous recombination (**Table 1**). All mutants were constructed in *B. microti*, aiming at the identification of factors contributing to the increased acid resistance of this atypical species versus *B. suis*, and then tested for *in vitro* acid stress resistance in minimal medium at pH 4.5 and for intracellular growth in J774 murine macrophages. Fourteen of the mutants, affected in the genes BMI_I1066, BMI_II893, BMI_I1677, BMI_II226, BMI_II385, BMI_II460, BMI_II847, BMI_I1652, BMI_I1679, BMI_I733, BMI_I686, BMI_II580, BMI_II225, and BMI_II898, did not show any reduction in survival as compared to the wild-type strain in minimal medium at pH 4.5 over an incubation period of 24 h (not shown). In the J774 murine macrophage infection model, characterized by transient acidification to pH 4–4.5 during the first phase of *Brucella* infection (Porte et al., 1999), none of the 16 mutants showed attenuation, and intracellular survival and replication profiles were identical to that of the wild-type strain for all time points [data not shown; (Jiménez De Bagüés et al., 2010)]. In addition, mutants in genes BMI_I426 and BMI_I2170 were also studied in human monocyte-derived macrophages from peripheral blood mononuclear cells, and intracellular replication profiles were identical to those in J774 cells (not shown).

TABLE 1 | Genes selected for mutation in *Brucella microti*.

Gene ID (*Bs*/*Bμ*)	Function/Protein	Deletion (nt/total)
BR1061/BMI_I1066	Zn-containing alcohol dehydrogenase	766/984
BR0423/BMI_I426	Cold Shock Protein CspA (Pseudogene in Bs)	159/210
BRA0899/BMI_II893	Ornithine cyclodeaminase ArcB	890/1077
BR1655/BMI_I1677	Sensor histidine kinase	705/936
BRA0229/BMI_II226	Two-component response regulator (Pseudogene in Bs)	481/669
BRA0388/BMI_II385	Heme-thiolate monooxygenase	1006/1164
BRA0463/BMI_II460	HlyD family secretion protein	634/945
BRA0853/BMI_II847	Hypothetical protein (putative permease of DMT family)	246/420
BR1634/BMI_I1652	Hypothetical protein (T4SS effector VceA)	197/318
BR1657/BMI_I1679	Two-component response regulator	694/795
BR0735/BMI_I733	Hypothetical protein (TIR domain-containing protein; T4SS effector BtpB)	731/834
BR0691/BMI_I686	Hypothetical protein (T4SS effector BspB)	193/255
BRA0586/BMI_II580	Hypothetical protein (virulence protein VirJ)	1014/1161
BR2149/BMI_I2170	DNA starvation/stationary phase protection protein Dps	389/498
BRA0228/BMI_II225	Sensor histidine kinase	1132/1341
BRA0904/BMI_II898	RNA-binding S1 domain-containing protein/Transcriptional accessory protein	2238/2304

Bs: B. suis.
Bμ: B. microti.
nt: nucleotides.

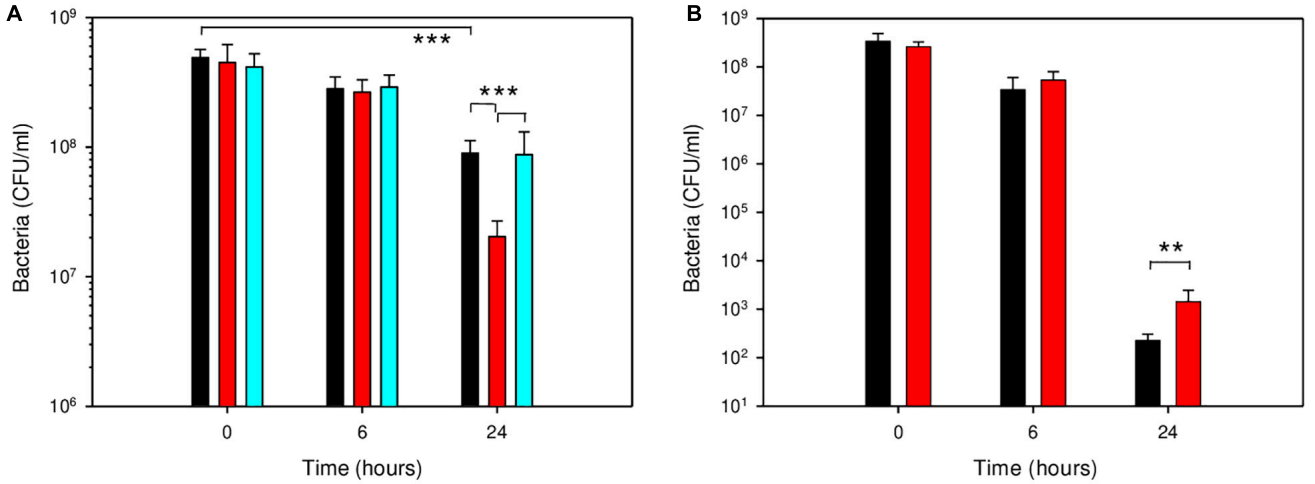

FIGURE 6 | Participation of CspA in survival of *B. microti* **(A)** and *B. suis* **(B)** in GMM at pH 4.5. Survival of *B. microti* wild-type strain (black bars), *B. microti* Δ*cspA* (red bars), *B. microti* Δ*cspA* complemented with pBBR1-*cspA* (cyan bars), and of *B. suis* wild-type with pBBR1-AMP (black bars) or complemented with pBBR1-AMP-*cspA* (red bars) containing functional *cspA* of *B. microti*. Values are shown as means of 7 experiments ± SD. **: $P < 0.01$; ***: $P < 0.001$.

Cold Shock Protein A and DNA-Binding Protein From Starved Cells Contribute to *Brucella microti* Acid Resistance at pH 4.5

In contrast to the 14 mutants described above, inactivation of genes BMI_I426 and BMI_I2170 significantly affected *B. microti* mutant survival in the *in vitro* acid stress model at pH 4.5. BMI_I426 encodes the cold shock protein CspA, previously studied in *E. coli* (Jiang et al., 1997), and BMI_I2170 codes for the "DNA-binding protein from starved cells" (Dps), also called DNA starvation/stationary phase protection protein, a nucleoid-associated protein (NAP) that participates in the arrangement of the bacterial chromosome (Calhoun and Kwon, 2011). Both *cspA* and *dps* have been originally related to other types of stress and can now be associated to acid stress response in *B. microti*.

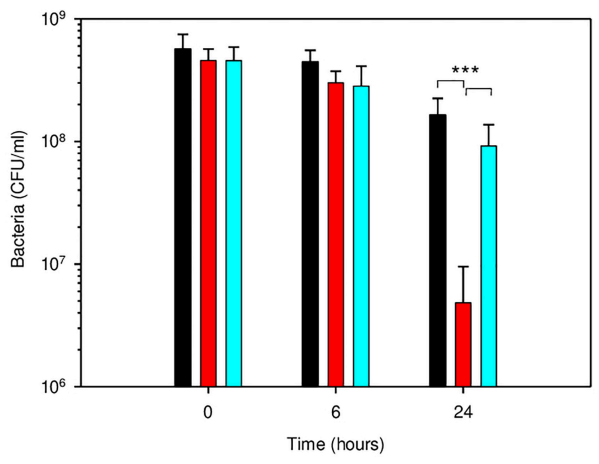

FIGURE 7 | Participation of Dps in survival of *B. microti* in GMM at pH 4.5. Survival of *B. microti* wild-type strain (black bars), *B. microti* Δ*dps* (red bars), and of *B. microti* Δ*dps* complemented with pBBR1-*dps* (cyan bars). Values are shown as means of 6 experiments ± SD. ***: $P < 0.005$.

The CSP are multifunctional, highly conserved, RNA-/DNA-binding small proteins of 65–70 amino acids in size, whose expression is mainly induced by temperature decrease. The cold shock domain contains 2 nucleic acid-binding motifs, directly interacting with DNA or RNA. Despite their designation, CSP are present under physiological conditions and, as other stress-related proteins, have been linked to osmotic, oxidative, starvation and acid stress (Keto-Timonen et al., 2016). The *B. microti cspA* gene was identified as a promising candidate in resistance to pH 4.5 because of its higher expression under acid conditions at both time points with a RNA-Seq-based log2-fold change > 3.0, and its pseudogene character in *B. suis* due to a frameshift mutation.

Deletion of *cspA* in *B. microti* reduced its survival in GMM at pH 4.5 approximately 4.5-fold at 24 h (**Figure 6A**). No effect was noticeable at the earlier time point of 6 h, explaining the lack of phenotype in the macrophage model of infection. Complementation of the *B. microti* Δ*cspA* strain with the native gene cloned in vector pBBR1MCS restored a level of resistance not significantly different from that of the wild-type, confirming a role of CspA in acid stress resistance at pH 4.5. To investigate if the pseudogene character of *cspA* in *B. suis* 1330 was related to the increased acid sensitivity of the classical species after 24 h at pH 4.5, *B. suis* was complemented with the intact gene from *B. microti* on the replicative plasmid pBBR1-AMP, and survival was compared to that of the wild-type. Survival of *B. suis* expressing *cspA* of *B. microti* was more than 6-fold increased ($P < 0.01$) at pH 4.5 after 24 h (**Figure 6B**). Although this gain of viability under these environmental conditions correlated well with the degree of loss of survival of the *B. microti* Δ*cspA* mutant strain as compared to the wild-type, general impact on survival of both species remained limited: CspA is obviously only one factor

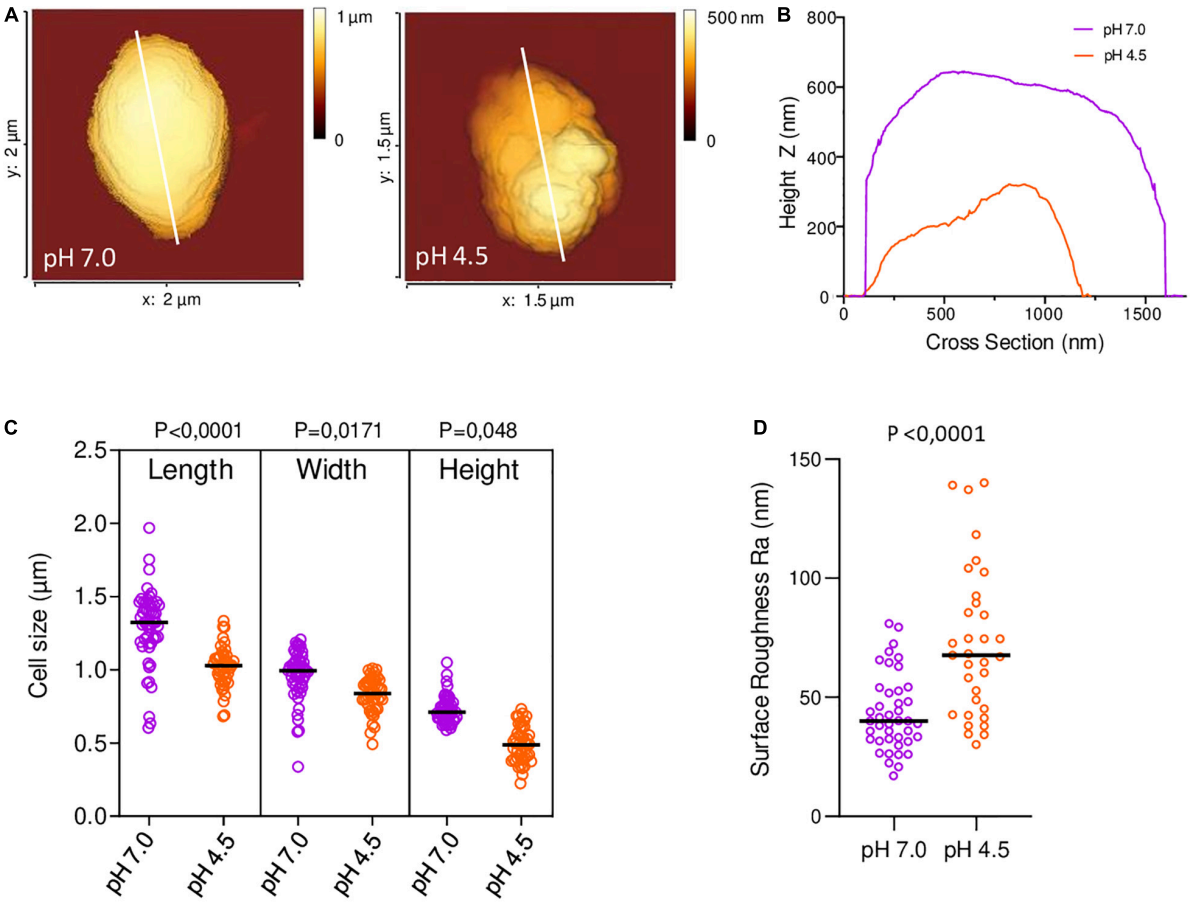

FIGURE 8 | Morphological characterization of *B. microti* CCM4915 in GMM pH 7.0 and pH 4.5 by Atomic Force Microscopy (AFM). **(A)** AFM topographic images of *B. microti* at both pH values. **(B)** Topographical profile plots measured along the longitudinal axis of the cells, indicated by solid lines in **(A)**. **(C)** Length, width and height measurements of bacteria at pH 7.0 ($n = 46$) and pH 4.5 ($n = 53$). **(D)** Average roughness R_a of the bacteria at pH 7.0 ($n = 42$) and pH 4.5 ($n = 33$), based on recorded surface roughness. Cell height analysis was carried out using the height (measured) channel of the QI mode, which corresponds to the height at 80% of the setpoint force determined on the reference force-distance curve. Height was calculated as the topographical maximal central height on each cell using the section tool of the analysis software. The average roughness (Ra) was calculated on the z channel values using a 400 × 400 nm area for each cell. Statistical differences were analyzed by *t*-test and yielded P values < 0.05, as indicated for panels **(C)** and **(D)**.

amongst others in acid resistance of *B. microti*. As expected, the causes of increased survival of *B. microti* observed in GMM at pH 4.5 are multifactorial, involving genes inactive in *B. suis* as described above and, most likely, genes differentially regulated in both species.

Besides CspA, the nucleoid-associated protein Dps played an important role in *B. microti* acid resistance. In *E. coli*, it participates in resistance to oxidative, UV, γ-radiation, metal ion toxicity and acid stress, and variations of nucleoid conformation have an important influence on bacterial physiology (Calhoun and Kwon, 2011). *Brucella microti dps* (BMI_I2170) was chosen for mutagenesis because of the potential biological roles of the encoded protein and its specific, higher differential expression at both time points, with a RNA-Seq-based log2-fold change > 2.0, validated by RT-qPCR (**Supplementary Table 4**). At 24 h, inactivation of *dps* in *B. microti* resulted in a strong reduction of survival in GMM at pH 4.5, with an approximately 34-fold decrease in the number of viable bacteria, when compared to *B. microti* wild-type (**Figure 7**). Complementation of the *B. microti* Δ*dps* mutant with the intact *dps* gene expressed in plasmid pBBR1MCS restored wild-type survival, confirming Dps participation in acid stress resistance at pH 4.5. As for the Δ*cspA* mutant, no effect was measurable after 6 h of exposure to pH 4.5 (**Figure 7**).

The Dps protein has three intrinsic properties that determine its important physiological roles: DNA-binding, resulting in DNA compaction and crystallization; iron sequestration; and ferroxidase activity, responsible for resistance to oxidative stress and protecting the DNA against ROIs. These properties play a central role in iron and hydrogen peroxide detoxification and in acid resistance. As the pH drops, interactions of Dps with DNA may become stronger, and this ability to aggregate DNA at acid pH, results in increased protection (Jeong et al., 2008). In *B. suis*, concentration of Dps increases under extreme nutrient starvation (Al Dahouk et al., 2013), evidencing together with the here-described results the important role of Dps in

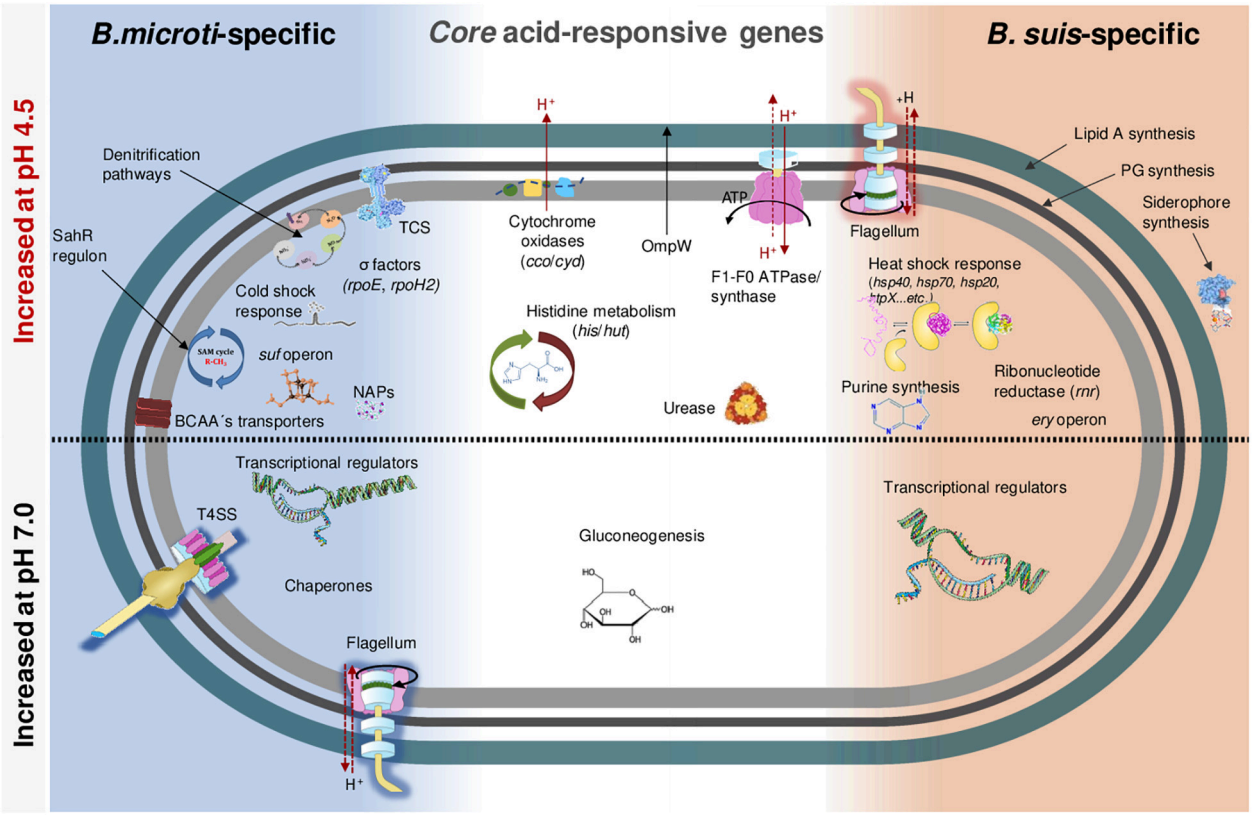

FIGURE 9 | Schematic representation of the highlighted common and species-specific responses for both *Brucella* species. For the experimental time points chosen, genes with higher expression at pH 4.5 are shown in the upper half, those with higher expression at pH 7 in the lower half of the scheme.

countering harmful environmental conditions. Moreover, *dps* expression is reported to be controlled by RpoE (Kim et al., 2014), fitting to the *B. microti*-specific increased transcription of sigma factors in our RNA-Seq study. Dps has also been detected in culture supernatants and in outer membrane vesicles (OMVs) produced by *Brucella*, alongside with other oxidative stress-related factors (Avila-Calderon et al., 2012; Lee et al., 2014), of which GroES also showed higher expression in *B. microti* at pH 4.5. This may suggest potential extracellular and pathogenesis-related functions, since both culture supernatants and OMVs have been reported to induce cytotoxic and immunogenic responses in infection models. Therefore, a possible role of Dps in pathogenesis of *Brucella* cannot be excluded and further studies would be of interest, as Dps has been linked to virulence in other pathogens (Martinez-Sanguiné et al., 2021).

In conclusion, the involvement of CspA and Dps in acid stress resistance in GMM at pH 4.5 after 24 h of exposure and the lack of phenotype in a cellular model of infection indicated that these genes may play a role in resistance of the atypical species *B. microti* to out-of-the-host conditions, such as strongly acidified soils. The lack of CspA in *B. suis* due to pseudogenization contributed to increased acid sensitivity *in vitro* but did not affect the capacity of intracellular replication of the pathogen, confirming that this gene has become dispensable in the course of adaptation to the host organism.

As mentioned earlier, neither Δ*cspA* nor Δ*dps* of *B. microti* showed phenotypes different from that of the wild-type strain in the J774 murine macrophage model of infection. A likely explanation is, that the duration of exposure to pH 4.5 in the BCV lasts only for a few hours, too short for an impact on viability of the mutant strain. Redundancy of gene functions and/or of acid stress-protective systems is also conceivable. An additional factor to be taken into consideration resides in the differences between the *in vitro* acid stress models and the intramacrophagic vacuole. GMM at pH 4.5 mimics the low nutrient and acidic environment of the phagocytic vacuole, but variability of certain parameters such as oxygen and metal ion concentrations is not considered. During the maturation process of the *Brucella* vacuole, it is likely that adaptation to acid stress is a dynamic process with variable expression profiles corresponding to the momentary conditions, and our data reflect the initial stage of this response, prone to change over time.

Brucella Cell Morphology Is Affected by Acidic pH 4.5 in Gerhardt's Minimal Medium

The impact of GMM pH 4.5 on *Brucella* cell morphology has been studied for *B. microti* using atomic force microscopy (AFM).

At acidic pH, bacteria are significantly shorter and "flatter" than at pH 7, resulting in volume reduction (**Figure 8**). In addition, cell surface roughness is considerably increased at low pH, indicating potential acid-mediated damage on proteins and/or LPS (**Figure 8**). Bacterial shape is dependent on peptidoglycan and on the bacterial cytoskeleton, whereby cellular localization of components of the latter is controlled by the membrane potential (Jones et al., 2001; Strahl and Hamoen, 2010). As a consequence, acid stress, altering this potential, may induce the morphological changes observed. Furthermore, due to the interconnection of osmoregulation and pH homeostasis, a sudden modification in one of the systems may create an imbalance, affecting also the other and possibly bacterial morphology.

GENERAL CONCLUSION

An overview of major results presented above is given in **Figure 9**, which illustrates the highlighted common and species-specific responses for both *Brucella* species.

Most central elements in the core response to pH 4.5 during the early phase of acid stress are the increased rates of expression of genes for cytochrome oxidases, the F_1F_0-ATPase/ATP-synthase, and the histidine metabolism together with the urease system. These systems have in common proton neutralization or extrusion from the cytosol, maintaining physiological intracellular pH values. In addition, species-specific mechanisms were identified that resulted in the conclusion that both species faced acid stress in distinct ways. At pH 4.5, *B. microti* increased expression of: (1) key elements of the general stress response; (2) genes of all denitrification steps, favoring rapid adaptation to acid-induced low oxygen conditions; (3) methionine metabolism genes, involved in DNA-methylation and in sulfur metabolism participating in redox homeostasis through biosynthesis of thiol antioxidants; (4) genes involved in Fe-S-cluster assembly, countering redox-state disturbance; (5) cold shock proteins, possibly acting as RNA chaperones; (6) nucleoid-associated protein Dps, playing a protective role in stress resistance by increased DNA aggregation. Altogether, these observations revealed rapid physiological adaptation of *B. microti* to acid stress, anticipating potential damage to cellular components and critical energy conditions.

On the other hand, at pH 4.5, *B. suis* increased expression of genes participating in: (1) purine and ribonucleotide-diphosphate reductase, (2) peptidoglycan, and (3) lipid A biosynthesis, indirectly suggesting increased levels of structural damages of the DNA, cell wall and outer membrane; (4) erythritol metabolism, possibly reflecting specific metabolic adaptation to the within-the-host life; (5) siderophore biosynthesis, indicating an important need for iron during acid stress; (6) flagella assembly, potentially contributing to proton export; (7) heat shock response, suggesting significantly increased acid stress-mediated protein misfolding or damaging in *B. suis*. The classical species therefore set up an array of repair strategies aiming at countering the symptoms rather than the origins of acid stress, resulting in subsequent loss of viability.

Remarkable was the identification of 15 acid stress-induced genes, all pseudogenes exclusively in *B. suis*. This loss of functionality during the host adaptation process most likely participated in reduced *B. suis* acid stress resistance when compared to the more ancestral and free-living species *B. microti*, as confirmed for the cold shock protein CspA. Dps, on the other hand, is an example for a factor whose pH-dependent regulation of expression in *B. microti* coincides with increased resistance of this species to pH 4.5. *B. microti* mutants with reduced survival at pH 4.5 in GMM showed a phenotype only after more than 6 h of exposure, explaining why none of the mutants tested were affected in the macrophage, where the duration of BCV acidification is limited. This observation was also coherent with the host adaptation-related accumulation of pseudogenes in *B. suis*, not impacting intracellular survival.

In conclusion, our work supported the hypothesis that increased acid stress resistance of *B. microti* was based on selective pressure for the maintenance of functionality of critical genes, and on specific differential gene expression, resulting in rapid adaptation.

DATA AVAILABILITY STATEMENT

The datasets presented in this study can be found in online repositories. The names of the repository/repositories and accession number(s) can be found below: https://www.ncbi.nlm.nih.gov/, PRJNA644280.

AUTHOR CONTRIBUTIONS

SK, AO, and SA designed the study. JG-G, SO-B, SL, EO-E, LF, SK, and AO carried out the experiments and/or performed analysis of the data. SK, AO, JG-G, and SA were involved in drafting the manuscript. All authors read and approved the final manuscript.

FUNDING

This work was supported by grants n° 1329-485 and 1329-562 from the German Federal Institute for Risk Assessment. LF and JG-G were recipients of a doctoral fellowship from the foundation Infectiopôle Sud, JG-G also of a doctoral fellowship from the Conacyt/Mexico.

ACKNOWLEDGMENTS

We are grateful to A. R. Wattam for matching *Brucella* locus tags between species, and G. Jiménez-Dominguez for participation in heatmap construction. We thank P. Bouhours and M. Abrantes for technical assistance in solution and media preparation, and A. Roux and A. Trausch in constructing plasmids in *E. coli*.

We are grateful to V. Jubier-Maurin, D. de Biase, A. Blanc-Potard, and S. Gaudriault for helpful discussions, and acknowledge the Bio2M bioinformatics and bio-markers platform of the CHU Montpellier (T. Commes and A. Boureux) for support in bioinformatics analysis.

SUPPLEMENTARY MATERIAL

The Supplementary Material for this article can be found online at: https://www.frontiersin.org/articles/10.3389/fmicb.2021.794535/full#supplementary-material

REFERENCES

Abdou, E., Deredjian, A., Jimenez De Bagues, M. P., Köhler, S., and Jubier-Maurin, V. (2013). RegA, the regulator of the two-component system RegB/RegA of *Brucella suis*, is a controller of both oxidative respiration and denitrification required for chronic infection in mice. *Infect. Immun.* 81, 2053–2061. doi: 10.1128/IAI.00063-13

Al Dahouk, S., Jubier-Maurin, V., Neubauer, H., and Köhler, S. (2013). Quantitative analysis of the *Brucella suis* proteome reveals metabolic adaptation to long-term nutrient starvation. *BMC Microbiol.* 13:199. doi: 10.1186/1471-2180-13-199

Al Dahouk, S., Köhler, S., Occhialini, A., Jiménez De Bagüés, M. P., Hammerl, J. A., Eisenberg, T., et al. (2017). *Brucella* spp. of amphibians comprise genomically diverse motile strains competent for replication in macrophages and survival in mammalian hosts. *Sci. Rep.* 7:44420. doi: 10.1038/srep44420

Albert, L. S., and Brown, D. G. (2015). Variation in bacterial ATP concentration during rapid changes in extracellular pH and implications for the activity of attached bacteria. *Colloids Surf. B Biointerfaces* 132, 111–116. doi: 10.1016/j.colsurfb.2015.05.020

Anders, S., and Huber, W. (2010). Differential expression analysis for sequence count data. *Genome Biol.* 11:R106. doi: 10.1186/gb-2010-11-10-r106

Audic, S., Lescot, M., Claverie, J. M., and Scholz, H. C. (2009). *Brucella microti*: the genome sequence of an emerging pathogen. *BMC Genomics* 10:352. doi: 10.1186/1471-2164-10-352

Avila-Calderon, E. D., Lopez-Merino, A., Jain, N., Peralta, H., Lopez-Villegas, E. O., Sriranganathan, N., et al. (2012). Characterization of outer membrane vesicles from *Brucella melitensis* and protection induced in mice. *Clin. Dev. Immunol.* 2012:352493. doi: 10.1155/2012/352493

Bandara, A. B., Contreras, A., Contreras-Rodriguez, A., Martins, A. M., Dobrean, V., Poff-Reichow, S., et al. (2007). *Brucella suis* urease encoded by *ure1* but not *ure2* is necessary for intestinal infection of BALB/c mice. *BMC Microbiol.* 7:57. doi: 10.1186/1471-2180-7-57

Barbier, T., Collard, F., Zuniga-Ripa, A., Moriyon, I., Godard, T., Becker, J., et al. (2014). Erythritol feeds the pentose phosphate pathway *via* three new isomerases leading to D-erythrose-4-phosphate in *Brucella*. *Proc. Natl. Acad. Sci. U.S.A.* 111, 17815–17820. doi: 10.1073/pnas.1414622111

Batey, R. T. (2011). Recognition of S-adenosylmethionine by riboswitches. *Wiley Interdiscip. Rev. RNA* 2, 299–311. doi: 10.1002/wrna.63

Bender, R. A. (2012). Regulation of the histidine utilization (hut) system in bacteria. *Microbiol. Mol. Biol. Rev.* 76, 565–584. doi: 10.1128/MMBR.00014-12

Blahut, M., Sanchez, E., Fisher, C. E., and Outten, F. W. (2020). Fe-S cluster biogenesis by the bacterial Suf pathway. *Biochim. Biophys. Acta Mol. Cell. Res.* 1867:118829. doi: 10.1016/j.bbamcr.2020.118829

Boschiroli, M. L., Ouahrani-Bettache, S., Foulongne, V., Michaux-Charachon, S., Bourg, G., Allardet-Servent, A., et al. (2002). The *Brucella suis virB* operon is induced intracellularly in macrophages. *Proc. Natl. Acad. Sci. U.S.A.* 99, 1544–1549. doi: 10.1073/pnas.032514299

Burkhardt, S., Jiménez De Bagüés, M. P., Liautard, J. P., and Köhler, S. (2005). Analysis of the behavior of *eryC* mutants of *Brucella suis* attenuated in macrophages. *Infect. Immun.* 73, 6782–6790. doi: 10.1128/IAI.73.10.6782-6790.2005

Caldas, T., Demont-Caulet, N., Ghazi, A., and Richarme, G. (1999). Thermoprotection by glycine betaine and choline. *Microbiology* 145(Pt. 9), 2543–2548. doi: 10.1099/00221287-145-9-2543

Calhoun, L. N., and Kwon, Y. M. (2011). Structure, function and regulation of the DNA-binding protein Dps and its role in acid and oxidative stress resistance in *Escherichia coli*: a review. *J. Appl. Microbiol.* 110, 375–386. doi: 10.1111/j.1365-2672.2010.04890.x

Caswell, C. C., Elhassanny, A. E., Planchin, E. E., Roux, C. M., Weeks-Gorospe, J. N., Ficht, T. A., et al. (2013). Diverse genetic regulon of the virulence-associated transcriptional regulator MucR in *Brucella abortus* 2308. *Infect. Immun.* 81, 1040–1051. doi: 10.1128/IAI.01097-12

Celli, J. (2019). The intracellular life cycle of *Brucella* spp. *Microbiol. Spectr.* 7, BAI–0006–2019. doi: 10.1128/microbiolspec.BAI-0006-2019

Chain, P. S., Comerci, D. J., Tolmasky, M. E., Larimer, F. W., Malfatti, S. A., Vergez, L. M., et al. (2005). Whole-genome analyses of speciation events in pathogenic Brucellae. *Infect. Immun.* 73, 8353–8361. doi: 10.1128/IAI.73.12.8353-8361.2005

Chakraborty, S., and Kenney, L. J. (2018). A new role of OmpR in acid and osmotic stress in *Salmonella* and *E. coli*. *Front. Microbiol.* 9:2656. doi: 10.3389/fmicb.2018.02656

Cloeckaert, A., Vizcaino, N., Paquet, J. Y., Bowden, R. A., and Elzer, P. H. (2002). Major outer membrane proteins of *Brucella* spp.: past, present and future. *Vet. Microbiol.* 90, 229–247. doi: 10.1016/s0378-1135(02)00211-0

Cotter, P. D., Gahan, C. G., and Hill, C. (2000). Analysis of the role of the *Listeria monocytogenes* F0F1 -AtPase operon in the acid tolerance response. *Int. J. Food Microbiol.* 60, 137–146. doi: 10.1016/s0168-1605(00)00305-6

Cui, M., Wang, T., Xu, J., Ke, Y., Du, X., Yuan, X., et al. (2013). Impact of Hfq on global gene expression and intracellular survival in *Brucella melitensis*. *PLoS One* 8:e71933. doi: 10.1371/journal.pone.0071933

Damiano, M. A., Bastianelli, D., Al Dahouk, S., Köhler, S., Cloeckaert, A., De Biase, D., et al. (2015). Glutamate decarboxylase-dependent acid resistance in *Brucella* spp.: distribution and contribution to fitness under extremely acidic conditions. *Appl. Environ. Microbiol.* 81, 578–586. doi: 10.1128/AEM.02928-14

Eisenberg, T., Risse, K., Schauerte, N., Geiger, C., Blom, J., and Scholz, H. C. (2017). Isolation of a novel 'atypical' *Brucella* strain from a bluespotted ribbontail ray (Taeniura lymma). *Antonie Van Leeuwenhoek* 110, 221–234. doi: 10.1007/s10482-016-0792-4

Ekaza, E., Teyssier, J., Ouahrani-Bettache, S., Liautard, J. P., and Köhler, S. (2001). Characterization of *Brucella suis clpB* and *clpAB* mutants and participation of the genes in stress responses. *J. Bacteriol.* 183, 2677–2681. doi: 10.1128/JB.183.8.2677-2681.2001

Fang, Z., and Cui, X. (2011). Design and validation issues in RNA-seq experiments. *Brief. Bioinform.* 12, 280–287. doi: 10.1093/bib/bbr004

Ferooz, J., Lemaire, J., Delory, M., De Bolle, X., and Letesson, J. J. (2011). RpoE1, an extracytoplasmic function sigma factor, is a repressor of the flagellar system in *Brucella melitensis*. *Microbiology* 157, 1263–1268. doi: 10.1099/mic.0.044875-0

Freddi, L., Damiano, M. A., Chaloin, L., Pennacchietti, E., Al Dahouk, S., Köhler, S., et al. (2017). The glutaminase-dependent system confers extreme acid resistance to new species and atypical strains of *Brucella*. *Front. Microbiol.* 8:2236. doi: 10.3389/fmicb.2017.02236

Fretin, D., Fauconnier, A., Köhler, S., Halling, S., Leonard, S., Nijskens, C., et al. (2005). The sheathed flagellum of *Brucella melitensis* is involved in persistence in a murine model of infection. *Cell. Microbiol.* 7, 687–698. doi: 10.1111/j.1462-5822.2005.00502.x

Gage, D. J., and Neidhardt, F. C. (1993). Adaptation of *Escherichia coli* to the uncoupler of oxidative phosphorylation 2,4-dinitrophenol. *J. Bacteriol.* 175, 7105–7108. doi: 10.1128/jb.175.21.7105-7108.1993

Haine, V., Dozot, M., Dornand, J., Letesson, J. J., and De Bolle, X. (2006). NnrA is required for full virulence and regulates several *Brucella melitensis* denitrification genes. *J. Bacteriol.* 188, 1615–1619. doi: 10.1128/JB.188.4.1615-1619.2006

Hanna, N., Jiménez De Bagüés, M. P., Ouahrani-Bettache, S., El Yakhlifi, Z., Köhler, S., and Occhialini, A. (2011). The *virB* operon is essential for lethality of *Brucella microti* in the Balb/c murine model of infection. *J. Infect. Dis.* 203, 1129–1135. doi: 10.1093/infdis/jiq163

Hanna, N., Ouahrani-Bettache, S., Drake, K. L., Adams, L. G., Köhler, S., and Occhialini, A. (2013). Global Rsh-dependent transcription profile of *Brucella suis* during stringent response unravels adaptation to nutrient starvation and

cross-talk with other stress responses. *BMC Genomics* 14:459. doi: 10.1186/1471-2164-14-459

Heckman, K. L., and Pease, L. R. (2007). Gene splicing and mutagenesis by PCR-driven overlap extension. *Nat. Protoc.* 2, 924–932. doi: 10.1038/nprot.2007.132

Jenner, D. C., Dassa, E., Whatmore, A. M., and Atkins, H. S. (2009). ATP-binding cassette systems of *Brucella*. *Comp. Funct. Genomics* 2009:354649. doi: 10.1155/2009/354649

Jeong, K. C., Hung, K. F., Baumler, D. J., Byrd, J. J., and Kaspar, C. W. (2008). Acid stress damage of DNA is prevented by Dps binding in *Escherichia coli* O157:H7. *BMC Microbiol.* 8:181. doi: 10.1186/1471-2180-8-181

Jiang, W., Hou, Y., and Inouye, M. (1997). CspA, the major cold-shock protein of *Escherichia coli*, is an RNA chaperone. *J. Biol. Chem.* 272, 196–202. doi: 10.1074/jbc.272.1.196

Jiménez De Bagüés, M. P., Loisel-Meyer, S., Liautard, J. P., and Jubier-Maurin, V. (2007). Different roles of the two high-oxygen-affinity terminal oxidases of *Brucella suis*: cytochrome c oxidase, but not ubiquinol oxidase, is required for persistence in mice. *Infect. Immun.* 75, 531–535. doi: 10.1128/IAI.01185-06

Jiménez De Bagüés, M. P., Ouahrani-Bettache, S., Quintana, J. F., Mitjana, O., Hanna, N., Bessoles, S., et al. (2010). The new species *Brucella microti* replicates in macrophages and causes death in murine models of infection. *J. Infect. Dis.* 202, 3–10. doi: 10.1086/653084

Jones, L. J., Carballido-Lopez, R., and Errington, J. (2001). Control of cell shape in bacteria: helical, actin-like filaments in *Bacillus subtilis*. *Cell* 104, 913–922. doi: 10.1016/s0092-8674(01)00287-2

Keto-Timonen, R., Hietala, N., Palonen, E., Hakakorpi, A., Lindstrom, M., and Korkeala, H. (2016). Cold shock proteins: a minireview with special emphasis on Csp-family of Enteropathogenic *Yersinia*. *Front. Microbiol.* 7:1151. doi: 10.3389/fmicb.2016.01151

Kim, H. S., Caswell, C. C., Foreman, R., Roop, R. M. II, and Crosson, S. (2013). The *Brucella abortus* general stress response system regulates chronic mammalian infection and is controlled by phosphorylation and proteolysis. *J. Biol. Chem.* 288, 13906–13916. doi: 10.1074/jbc.M113.459305

Kim, H. S., Willett, J. W., Jain-Gupta, N., Fiebig, A., and Crosson, S. (2014). The *Brucella abortus* virulence regulator, LovhK, is a sensor kinase in the general stress response signalling pathway. *Mol. Microbiol.* 94, 913–925. doi: 10.1111/mmi.12809

Köhler, S., Foulongne, V., Ouahrani-Bettache, S., Bourg, G., Teyssier, J., Ramuz, M., et al. (2002). The analysis of the intramacrophagic virulome of *Brucella suis* deciphers the environment encountered by the pathogen inside the macrophage host cell. *Proc. Natl. Acad. Sci. U.S.A.* 99, 15711–15716. doi: 10.1073/pnas.232454299

Köhler, S., Teyssier, J., Cloeckaert, A., Rouot, B., and Liautard, J. P. (1996). Participation of the molecular chaperone DnaK in intracellular growth of *Brucella suis* within U937-derived phagocytes. *Mol. Microbiol.* 20, 701–712. doi: 10.1111/j.1365-2958.1996.tb02510.x

Kovach, M. E., Phillips, R. W., Elzer, P. H., Roop, R. M. II, and Peterson, K. M. (1994). pBBR1MCS: a broad-host-range cloning vector. *Biotechniques* 16, 800–802.

Lee, J. J., Lim, J. J., Kim, D. G., Simborio, H. L., Kim, D. H., Reyes, A. W., et al. (2014). Characterization of culture supernatant proteins from *Brucella abortus* and its protection effects against murine brucellosis. *Comp. Immunol. Microbiol. Infect. Dis.* 37, 221–228. doi: 10.1016/j.cimid.2014.06.001

Li, Z., Jiang, B., Zhang, X., Yang, Y., Hardwidge, P. R., Ren, W., et al. (2020). The role of bacterial cell envelope structures in acid stress resistance in *E. coli*. *Appl. Microbiol. Biotechnol.* 104, 2911–2921. doi: 10.1007/s00253-020-10453-x

Liao, Y., Smyth, G. K., and Shi, W. (2014). FeatureCounts: an efficient general purpose program for assigning sequence reads to genomic features. *Bioinformatics* 30, 923–930. doi: 10.1093/bioinformatics/btt656

Liu, B., Zheng, D., Jin, Q., Chen, L., and Yang, J. (2019). VFDB 2019: a comparative pathogenomic platform with an interactive web interface. *Nucleic Acids Res.* 47, D687–D692. doi: 10.1093/nar/gky1080

Liu, N., and Delcour, A. H. (1998). Inhibitory effect of acidic pH on OmpC porin: wild-type and mutant studies. *FEBS Lett.* 434, 160–164. doi: 10.1016/s0014-5793(98)00975-2

Liu, Q., Liu, X., Yan, F., He, Y., Wei, J., Zhang, Y., et al. (2016). Comparative transcriptome analysis of *Brucella melitensis* in an acidic environment: identification of the two-component response regulator involved in the acid resistance and virulence of *Brucella*. *Microb. Pathog.* 91, 92–98. doi: 10.1016/j.micpath.2015.11.007

Loisel-Meyer, S., Jiménez de Bagüés, M. P., Basseres, E., Dornand, J., Köhler, S., Liautard, J. P., et al. (2006). Requirement of *norD* for *Brucella suis* virulence in a murine model of *in vitro* and *in vivo* infection. *Infect. Immun.* 74, 1973–1976. doi: 10.1128/IAI.74.3.1973-1976.2006

Loisel-Meyer, S., Jiménez de Bagüés, M. P., Köhler, S., Liautard, J. P., and Jubier-Maurin, V. (2005). Differential use of the two high-oxygen-affinity terminal oxidases of *Brucella suis* for *in vitro* and intramacrophagic multiplication. *Infect. Immun.* 73, 7768–7771. doi: 10.1128/IAI.73.11.7768-7771.2005

Lund, P., Tramonti, A., and De Biase, D. (2014). Coping with low pH: molecular strategies in neutralophilic bacteria. *FEMS Microbiol. Rev.* 38, 1091–1125. doi: 10.1111/1574-6976.12076

Mao, F., Dam, P., Chou, J., Olman, V., and Xu, Y. (2009). DOOR: a database for prokaryotic operons. *Nucleic Acids Res.* 37, D459–D463. doi: 10.1093/nar/gkn757

Martinez-Sanguiné, A. Y., D'alessandro, B., Langleib, M., Traglia, G. M., Monaco, A., Duran, R., et al. (2021). *Salmonella enterica* serovars dublin and enteritidis comparative proteomics reveals differential expression of proteins involved in stress resistance, virulence, and anaerobic metabolism. *Infect. Immun.* 89, e606–e620. doi: 10.1128/IAI.00606-20

Maurer, L. M., Yohannes, E., Bondurant, S. S., Radmacher, M., and Slonczewski, J. L. (2005). pH regulates genes for flagellar motility, catabolism, and oxidative stress in *Escherichia coli* K-12. *J. Bacteriol.* 187, 304–319. doi: 10.1128/JB.187.1.304-319.2005

O'Callaghan, D., Cazevieille, C., Allardet-Servent, A., Boschiroli, M. L., Bourg, G., Foulongne, V., et al. (1999). A homologue of the *Agrobacterium tumefaciens* VirB and *Bordetella pertussis* Ptl type IV secretion systems is essential for intracellular survival of *Brucella suis*. *Mol. Microbiol.* 33, 1210–1220. doi: 10.1046/j.1365-2958.1999.01569.x

Occhialini, A., Jiménez de Bagüés, M. P., Saadeh, B., Bastianelli, D., Hanna, N., De Biase, D., et al. (2012). The glutamic acid decarboxylase system of the new species *Brucella microti* contributes to its acid resistance and to oral infection of mice. *J. Infect. Dis.* 206, 1424–1432. doi: 10.1093/infdis/jis522

Ouahrani-Bettache, S., Jiménez de Bagüés, M. P., de la Garza, J., Freddi, L., Bueso, J. P., Lyonnais, S., et al. (2019). Lethality of *Brucella microti* in a murine model of infection depends on the *wbkE* gene involved in O-polysaccharide synthesis. *Virulence* 10, 868–878. doi: 10.1080/21505594.2019.1682762

Pappas, G., Akritidis, N., Bosilkovski, M., and Tsianos, E. (2005). Brucellosis. *N. Engl. J. Med.* 352, 2325–2336. doi: 10.1056/NEJMra050570

Philippe, N., Salson, M., Commes, T., and Rivals, E. (2013). CRAC: an integrated approach to the analysis of RNA-seq reads. *Genome Biol.* 14:R30. doi: 10.1186/gb-2013-14-3-r30

Pitcher, R. S., and Watmough, N. J. (2004). The bacterial cytochrome *cbb3* oxidases. *Biochim. Biophys. Acta* 1655, 388–399. doi: 10.1016/j.bbabio.2003.09.017

Porte, F., Liautard, J. P., and Köhler, S. (1999). Early acidification of phagosomes containing *Brucella suis* is essential for intracellular survival in murine macrophages. *Infect. Immun.* 67, 4041–4047. doi: 10.1128/IAI.67.8.4041-4047.1999

Raivio, T. L., and Silhavy, T. J. (2001). Periplasmic stress and ECF sigma factors. *Annu. Rev. Microbiol.* 55, 591–624. doi: 10.1146/annurev.micro.55.1.591

Raja, N., Goodson, M., Smith, D. G., and Rowbury, R. J. (1991). Decreased DNA damage by acid and increased repair of acid-damaged DNA in acid-habituated *Escherichia coli*. *J. Appl. Bacteriol.* 70, 507–511. doi: 10.1111/j.1365-2672.1991.tb02748.x

Römling, U., Galperin, M. Y., and Gomelsky, M. (2013). Cyclic di-GMP: the first 25 years of a universal bacterial second messenger. *Microbiol. Mol. Biol. Rev.* 77, 1–52. doi: 10.1128/MMBR.00043-12

Ronai, Z., Kreizinger, Z., Dan, A., Drees, K., Foster, J. T., Banyai, K., et al. (2015). First isolation and characterization of *Brucella microti* from wild boar. *BMC Vet. Res.* 11:147. doi: 10.1186/s12917-015-0456-z

Roncarati, D., and Scarlato, V. (2017). Regulation of heat-shock genes in bacteria: from signal sensing to gene expression output. *FEMS Microbiol. Rev.* 41, 549–574. doi: 10.1093/femsre/fux015

Salmon-Divon, M., Zahavi, T., and Kornspan, D. (2019). Transcriptomic analysis of the *Brucella melitensis* Rev.1 vaccine strain in an acidic environment: insights into virulence attenuation. *Front. Microbiol.* 10:250. doi: 10.3389/fmicb.2019.00250

Samartzidou, H., Mehrazin, M., Xu, Z., Benedik, M. J., and Delcour, A. H. (2003). Cadaverine inhibition of porin plays a role in cell survival at acidic pH. *J. Bacteriol.* 185, 13–19. doi: 10.1128/JB.185.1.13-19.2003

Sangari, F. J., Seoane, A., Rodriguez, M. C., Aguero, J., and Garcia Lobo, J. M. (2007). Characterization of the urease operon of *Brucella abortus* and assessment of its role in virulence of the bacterium. *Infect. Immun.* 75, 774–780. doi: 10.1128/IAI.01244-06

Sato, M., Machida, K., Arikado, E., Saito, H., Kakegawa, T., and Kobayashi, H. (2000). Expression of outer membrane proteins in *Escherichia coli* growing at acid pH. *Appl. Environ. Microbiol.* 66, 943–947. doi: 10.1128/AEM.66.3.943-947.2000

Sayers, S., Li, L., Ong, E., Deng, S., Fu, G., Lin, Y., et al. (2019). Victors: a web-based knowledge base of virulence factors in human and animal pathogens. *Nucleic Acids Res.* 47, D693–D700. doi: 10.1093/nar/gky999

Scholz, H. C., Hofer, E., Vergnaud, G., Le Fleche, P., Whatmore, A. M., Al Dahouk, S., et al. (2009). Isolation of *Brucella microti* from mandibular lymph nodes of red foxes, *Vulpes vulpes*, in lower Austria. *Vector Borne Zoonotic Dis.* 9, 153–156. doi: 10.1089/vbz.2008.0036

Scholz, H. C., Hubalek, Z., Nesvadbova, J., Tomaso, H., Vergnaud, G., Le Fleche, P., et al. (2008a). Isolation of *Brucella microti* from soil. *Emerg. Infect. Dis.* 14, 1316–1317. doi: 10.3201/eid1408.080286

Scholz, H. C., Hubalek, Z., Sedlacek, I., Vergnaud, G., Tomaso, H., Al Dahouk, S., et al. (2008b). Brucella microti sp. nov., isolated from the common vole *Microtus arvalis*. *Int. J. Syst. Evol. Microbiol.* 58, 375–382. doi: 10.1099/ijs.0.65356-0

Scholz, H. C., Nöckler, K., Göllner, C., Bahn, P., Vergnaud, G., Tomaso, H., et al. (2010). *Brucella inopinata* sp. nov., isolated from a breast implant infection. *Int. J. Syst. Evol. Microbiol.* 60, 801–808.

Shayanfar, S., Broumand, A., and Pillai, S. D. (2018). Acid stress induces differential accumulation of metabolites in *Escherichia coli* O26:H11. *J. Appl. Microbiol.* doi: 10.1111/jam.14081 Online ahead of print.

Sieira, R., Arocena, G. M., Bukata, L., Comerci, D. J., and Ugalde, R. A. (2010). Metabolic control of virulence genes in *Brucella abortus*: HutC coordinates *virB* expression and the histidine utilization pathway by direct binding to both promoters. *J. Bacteriol.* 192, 217–224. doi: 10.1128/JB.01124-09

Soler-Llorens, P. F., Quance, C. R., Lawhon, S. D., Stuber, T. P., Edwards, J. F., Ficht, T. A., et al. (2016). A *Brucella* spp. isolate from a Pac-Man frog (*Ceratophrys ornata*) reveals characteristics departing from classical brucellae. *Front. Cell. Infect. Microbiol.* 6:116. doi: 10.3389/fcimb.2016.00116

Sternon, J. F., Godessart, P., Gonçalves de Freitas, R., Van der Henst, M., Poncin, K., Francis, N., et al. (2018). Transposon sequencing of *Brucella abortus* uncovers essential genes for growth *in vitro* and inside macrophages. *Infect. Immun.* 86:e00312–18. doi: 10.1128/IAI.00312-18

Strahl, H., and Hamoen, L. W. (2010). Membrane potential is important for bacterial cell division. *Proc. Natl. Acad. Sci. U.S.A.* 107, 12281–12286. doi: 10.1073/pnas.1005485107

Sun, Y., Fukamachi, T., Saito, H., and Kobayashi, H. (2011). ATP requirement for acidic resistance in *Escherichia coli*. *J. Bacteriol.* 193, 3072–3077. doi: 10.1128/JB.00091-11

Sun, Y., Fukamachi, T., Saito, H., and Kobayashi, H. (2012). Respiration and the F(1)Fo-ATPase enhance survival under acidic conditions in *Escherichia coli*. *PLoS One* 7:e52577. doi: 10.1371/journal.pone.0052577

Teixeira-Gomes, A. P., Cloeckaert, A., and Zygmunt, M. S. (2000). Characterization of heat, oxidative, and acid stress responses in *Brucella melitensis*. *Infect. Immun.* 68, 2954–2961. doi: 10.1128/IAI.68.5.2954-2961.2000

Tiller, R. V., Gee, J. E., Lonsway, D. R., Gribble, S., Bell, S. C., Jennison, A. V., et al. (2010). Identification of an unusual *Brucella* strain (BO2) from a lung biopsy in a 52 year-old patient with chronic destructive pneumonia. *BMC Microbiol.* 10:23. doi: 10.1186/1471-2180-10-23

Torrents, E. (2014). Ribonucleotide reductases: essential enzymes for bacterial life. *Front. Cell. Infect. Microbiol.* 4:52. doi: 10.3389/fcimb.2014.00052

Trip, H., Mulder, N. L., and Lolkema, J. S. (2012). Improved acid stress survival of *Lactococcus lactis* expressing the histidine decarboxylation pathway of *Streptococcus thermophilus* CHCC1524. *J. Biol. Chem.* 287, 11195–11204. doi: 10.1074/jbc.M111.330704

Typas, A., Banzhaf, M., Gross, C. A., and Vollmer, W. (2011). From the regulation of peptidoglycan synthesis to bacterial growth and morphology. *Nat. Rev. Microbiol.* 10, 123–136. doi: 10.1038/nrmicro2677

Valderas, M. W., Alcantara, R. B., Baumgartner, J. E., Bellaire, B. H., Robertson, G. T., Ng, W. L., et al. (2005). Role of HdeA in acid resistance and virulence in *Brucella abortus* 2308. *Vet. Microbiol.* 107, 307–312. doi: 10.1016/j.vetmic.2005.01.018

Vallenet, D., Calteau, A., Dubois, M., Amours, P., Bazin, A., Beuvin, M., et al. (2020). MicroScope: an integrated platform for the annotation and exploration of microbial gene functions through genomic, pangenomic and metabolic comparative analysis. *Nucleic Acids Res.* 48, D579–D589. doi: 10.1093/nar/gkz926

Verdiguel-Fernandez, L., Oropeza-Navarro, R., Basurto-Alcantara, F. J., Castaneda-Ramirez, A., and Verdugo-Rodriguez, A. (2017). Omp31 plays an important role on outer membrane properties and intracellular survival of *Brucella melitensis* in murine macrophages and HeLa cells. *Arch. Microbiol.* 199, 971–978. doi: 10.1007/s00203-017-1360-7

Vishnu, U. S., Sankarasubramanian, J., Gunasekaran, P., and Rajendhran, J. (2017). Identification of OtpR regulated sRNAs in *Brucella melitensis* expressed under acidic stress and their roles in pathogenesis and metabolism. *Comp. Immunol. Microbiol. Infect. Dis.* 50, 40–47. doi: 10.1016/j.cimid.2016.11.007

Wang, Z., Wang, S., and Wu, Q. (2014). Cold shock protein A plays an important role in the stress adaptation and virulence of *Brucella melitensis*. *FEMS Microbiol. Lett.* 354, 27–36. doi: 10.1111/1574-6968.12430

Wattam, A. R., Foster, J. T., Mane, S. P., Beckstrom-Sternberg, S. M., Beckstrom-Sternberg, J. M., Dickerman, A. W., et al. (2014). Comparative phylogenomics and evolution of the Brucellae reveal a path to virulence. *J. Bacteriol.* 196, 920–930. doi: 10.1128/JB.01091-13

Wu, X. B., Tian, L. H., Zou, H. J., Wang, C. Y., Yu, Z. Q., Tang, C. H., et al. (2013). Outer membrane protein OmpW of *Escherichia coli* is required for resistance to phagocytosis. *Res. Microbiol.* 164, 848–855. doi: 10.1016/j.resmic.2013.06.008

Zhang, Y., Burkhardt, D. H., Rouskin, S., Li, G. W., Weissman, J. S., and Gross, C. A. (2018). A stress response that monitors and regulates mRNA structure is central to cold shock adaptation. *Mol. Cell.* 70, 274–286.e7. doi: 10.1016/j.molcel.2018.02.035

Conflict of Interest: The authors declare that the research was conducted in the absence of any commercial or financial relationships that could be construed as a potential conflict of interest.

Publisher's Note: All claims expressed in this article are solely those of the authors and do not necessarily represent those of their affiliated organizations, or those of the publisher, the editors and the reviewers. Any product that may be evaluated in this article, or claim that may be made by its manufacturer, is not guaranteed or endorsed by the publisher.

frontiers in Microbiology

ORIGINAL RESEARCH
published: 07 January 2022
doi: 10.3389/fmicb.2021.802169

Real-Time Monitoring of the Yeast Intracellular State During Bioprocesses With a Toolbox of Biosensors

Luca Torello Pianale[1†], Peter Rugbjerg[1,2†] and Lisbeth Olsson[1†]*

[1] Industrial Biotechnology Division, Department of Biology and Biological Engineering, Chalmers University of Technology, Gothenburg, Sweden, [2] Enduro Genetics ApS, Copenhagen, Denmark

OPEN ACCESS

Edited by:
Nuno Pereira Mira,
University of Lisbon, Portugal

Reviewed by:
Soo Rin Kim,
Kyungpook National University, South Korea
Rodrigo Ledesma-Amaro,
Imperial College London, United Kingdom

***Correspondence:**
Lisbeth Olsson
lisbeth.olsson@chalmers.se

†ORCID:
Luca Torello Pianale
orcid.org/0000-0001-7673-0059
Peter Rugbjerg
orcid.org/0000-0003-2561-5063
Lisbeth Olsson
orcid.org/0000-0002-0827-5442

Specialty section:
This article was submitted to Microbial Physiology and Metabolism, a section of the journal Frontiers in Microbiology

Received: 26 October 2021
Accepted: 16 December 2021
Published: 07 January 2022

Citation:
Torello Pianale L, Rugbjerg P and Olsson L (2022) Real-Time Monitoring of the Yeast Intracellular State During Bioprocesses With a Toolbox of Biosensors. Front. Microbiol. 12:802169. doi: 10.3389/fmicb.2021.802169

Industrial fermentation processes strive for high robustness to ensure optimal and consistent performance. Medium components, fermentation products, and physical perturbations may cause stress and lower performance. Cellular stress elicits a range of responses, whose extracellular manifestations have been extensively studied; whereas intracellular aspects remain poorly known due to lack of tools for real-time monitoring. Genetically encoded biosensors have emerged as promising tools and have been used to improve microbial productivity and tolerance toward industrially relevant stresses. Here, fluorescent biosensors able to sense the yeast intracellular environment (pH, ATP levels, oxidative stress, glycolytic flux, and ribosome production) were implemented into a versatile and easy-to-use toolbox. Marker-free and efficient genome integration at a conserved site on chromosome X of *Saccharomyces cerevisiae* strains and a commercial *Saccharomyces boulardii* strain was developed. Moreover, multiple biosensors were used to simultaneously monitor different intracellular parameters in a single cell. Even when combined together, the biosensors did not significantly affect key physiological parameters, such as specific growth rate and product yields. Activation and response of each biosensor and their interconnection were assessed using an advanced micro-cultivation system. Finally, the toolbox was used to screen cell behavior in a synthetic lignocellulosic hydrolysate that mimicked harsh industrial substrates, revealing differences in the oxidative stress response between laboratory (CEN.PK113-7D) and industrial (Ethanol Red) *S. cerevisiae* strains. In summary, the toolbox will allow both the exploration of yeast diversity and physiological responses in natural and complex industrial conditions, as well as the possibility to monitor production processes.

Keywords: fluorescence, stress, ATP concentration, oxidative stress, intracellular pH (pHi), glycolytic flux, ribosome production

INTRODUCTION

Industrial fermentation processes use microorganisms as cell factories to convert a given substrate to valuable products (Demain, 2000). However, complex substrates (e.g., lignocellulosic hydrolysates), product inhibition (e.g., ethanol), and other perturbations (e.g., inhibitors or physical constrains) are stressful for the cells, leading to suboptimal production (Deparis et al., 2017).

Although efforts have been made to develop microbial strains more tolerant to the stressors present during different fermentation processes (Swinnen et al., 2017; Ko et al., 2020; Liu et al., 2020), achieving this at industrial scale remains a challenge (Wehrs et al., 2019). Because controlled laboratory conditions cannot fully mimic industrial settings, new strains tend to perform poorly upon scaling up (Wehrs et al., 2019). Moreover, while the extracellular environment and phenotypic characteristics of microorganisms (e.g., titers, rates, and yields) are easily analyzed online or via real-time sampling, little is known about the microbes' intracellular and metabolic responses in these complex environments. This discrepancy in information comes from the lack of tools to monitor parameters, such as intracellular pH, ATP concentration, and oxidative stress. Understanding the cellular responses and linking them to specific environmental conditions would lead to more robust strains and consistent production processes.

Genetically encoded fluorescent biosensors are promising tools for evaluating the intracellular environment, as they can sense compounds or conditions inside the cell, and thus track the ensuing response (Carpenter et al., 2018). They have already been used both to improve microbial production (Raman et al., 2014), such as in the case of muconic and octanoic acids (Leavitt et al., 2017; Wang et al., 2020; Baumann et al., 2021), and tolerance to industrially relevant stresses (Alvarez-Gonzalez and Dixon, 2019). However, some constraints limited the application of biosensors in real-time strain or process diagnostics. For example, acidic environments, often found in bioprocesses, should be taken into account when choosing a fluorescent protein as pH affects the fluorescence output (Shinoda et al., 2018). Combining multiple fluorescent proteins in the same cell is hampered by overlap of excitation/emission spectra (Botman et al., 2019). Tagging up to four different proteins in separate organelles with four distinct fluorescent probes was shown not to cause spectral overlap or organelle malfunction (Higuchi-Sanabria et al., 2016). A more recent study confirmed the possibility of tagging multiple proteins in different organelles with non-overlapping fluorescent probes, although it led to some protein disfunctions (Zhu et al., 2019). In *Escherichia coli*, efforts have been made to develop a platform for real-time detection of metabolites using fluorescent proteins (Rogers et al., 2015). However, testing and monitoring the physiological performance of yeasts with biosensors remain uncommon for the risk of affecting productivity, particularly if multiple biosensors are combined in the same cell.

Saccharomyces cerevisiae is one of the most studied and used microorganisms in the laboratory and bioindustry (Kampranis and Makris, 2012). Owing to its wide range of applications, industrial strains of *S. cerevisiae* have been developed to address specific requirements, such as higher ethanol or biomass production (Parapouli et al., 2020). Moreover, *S. cerevisiae* strains with interesting features for industrial purposes are being isolated from natural habitats (da Conceição et al., 2015; Liti, 2015). In spite of this wide diversity, only an accurate assessment of cell physiology and the intracellular environment will reveal the mechanisms responsible for greater tolerance and robustness and, hence, drive a more targeted, faster, and cost-effective development of industrial strains (Molinet and Cubillos, 2020).

The present study aimed to select various genetically encoded fluorescent biosensors capable of sensing key intracellular parameters (e.g., pH, ATP concentration, ribosome production, oxidative stress, and glycolytic flux) and implement them in a toolbox for real-time monitoring of yeast strains (**Figure 1** and **Table 1**). Owing to its easy and versatile build-transform-assess workflow (**Figure 1B**), this toolbox could facilitate the exploration of yeast metabolism during industrial processes and help monitor production. First, we demonstrated that the toolbox could be integrated in the genome by an easy, efficient, and marker-free method, compatible with different *S. cerevisiae* strains. Second, we showed that the selected biosensors did not affect key yeast performance indicators of growth and metabolism, thus proving reliable monitoring of the intracellular state. Third, we demonstrated the simultaneous function of multiple biosensors in the same cell by using non-overlapping fluorescence spectra. Finally, we applied the toolbox for real-time monitoring under stressful conditions mimicking industrial fermentation and demonstrated that different *S. cerevisiae* strains elicited different stress responses.

MATERIALS AND METHODS

Strains and Media Composition

All yeast strains used in this study are listed in **Table 2**. The *S. cerevisiae* strains bearing fluorescent biosensors were constructed from the laboratory strain CEN.PK113-7D (MATa URA3 HIS3 LEU2 TRP1 MAL2-8c SUC2) (Entian and Kötter, 2007) and the commercial bioethanol-producing strain Ethanol Red (Société Industrielle Lesaffre, Division Leaf). Chemically competent *E. coli* DH5α were used for plasmid construction and selection (Seidman and Struhl, 1998).

For transformation and for curing the Cas9-bearing plasmid used in genome integration, yeast strains were grown in YPD medium (10 g/L yeast extract, 20 g/L peptone, and 20 g/L glucose, plus 15 g/L agar for plates), supplemented with 200 mg/L G418 sulfate when required. For flask and BioLector I (M2p-labs GmbH) screening, synthetic defined minimal Verduyn ("Delft") medium adjusted to pH 5 was used. The medium contained 20 g/L glucose, 5 g/L $(NH_4)_2SO_4$, 3 g/L KH_2PO_4, 1 g/L $MgSO_4 \cdot 7H_2O$, 20.4 g/L K-phthalate, 1 mL/L trace metal solution, and 1 mL/L vitamin solution (trace metals and vitamin solution compositions are listed in **Supplementary Table 1**).

When assessing oxidative stress and intracellular pH under specific stressors typically released during pre-treatment of lignocellulosic hydrolysates, acetic acid (4.5 or 6 g/L), furfural (1 or 3 g/L), vanillin (0.5 g/L), or xylose (20 or 40 g/L) were added to Delft medium.

To mimic wheat-straw hydrolysate, a second-generation bioethanol production substrate, a selection of key compounds at specific concentrations was added to Delft medium (**Table 3**) and pH was adjusted to 5. To serve as growth substrate, this synthetic wheat-straw hydrolysate (SWSH) was diluted at 50 and 80% using Delft medium without any carbon source.

Competent *E. coli* DH5α were grown in LB medium (10 g/L bacto-tryptone, 5 g/L yeast extract, and 10 g/L NaCl, plus 15 g/L

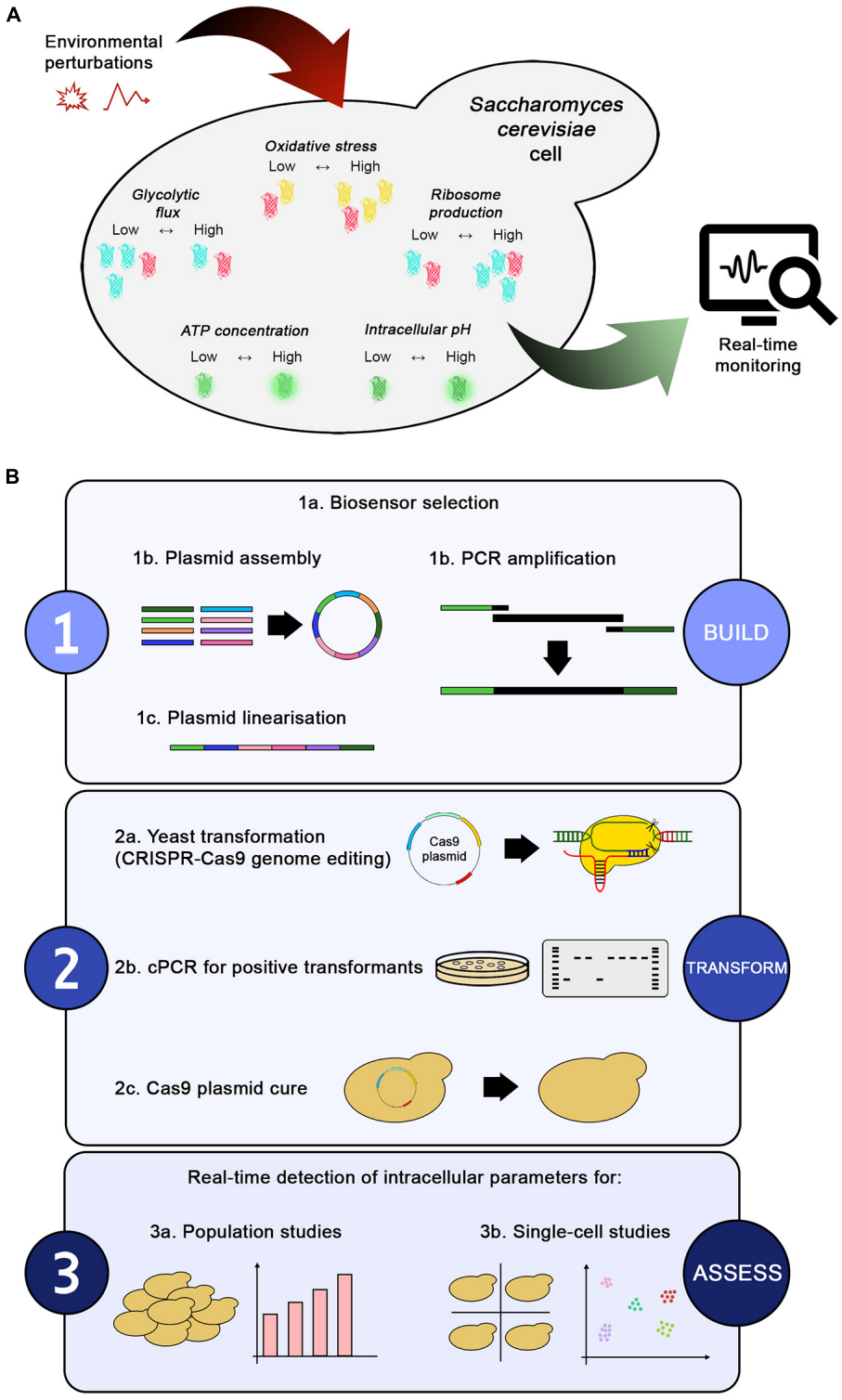

FIGURE 1 | Toolbox overview and workflow. **(A)** Environmental perturbations in a bioprocess directly affect the intracellular environment of a yeast cell. The biosensors present in the toolbox enable real-time monitoring of changes in intracellular parameters, such as glycolytic flux (with GlyRNA), oxidative stress (with OxPro), ribosome production (with RibPro), intracellular pH (with sfpHluorin), and ATP concentration (with QUEEN-2m). **(B)** The workflow for generating the toolbox can be summarized in three steps: (1) building the desired biosensor, (2) transforming yeast, and (3) assessing the biosensors' output under different conditions. Once selected, the biosensors can be assembled into plasmids or amplified by PCR to obtain marker-free constructs used for genome integration via CRISPR-Cas9 editing technology. Positive transformants are confirmed by colony PCR, followed by curing of the Cas9 plasmid to remove the selection markers. Finally, the new strains can be used for population or single-cell studies. Alternative plasmid assembly or genome integration methods can be easily fitted in the workflow.

TABLE 1 | Summary of biosensors in the toolbox.

Biosensor	Intracellular parameter	Detection of	Fluorescent protein (s)	Optimal λex (nm)	Optimal λem (nm)	References
QUEEN-2m	ATP concentration	ATP	QUEEN-2m	410 and 480	520	Takaine et al., 2019
sfpHluorin	Intracellular pH	pH	SfpHluorin	390 and 470	512	Reifenrath and Boles, 2018
GlyRNA	Glycolytic flux	Fructose-bisphosphate	mTurquoise2	436	488	Ortega et al., 2021
			mCherry*	587	610	
OxPro	Oxidative stress response	YAP1 activation	YmYPET	516	526	Zhang et al., 2016
			mCherry*	587	610	
RibPro	Ribosome production	RPL13A production	mTurquoise2	436	488	Janssens and Veenhoff, 2016
			mCherry*	587	610	

*List of the biosensors included in the toolbox and characterization of the fluorescent proteins used in this study. *Refers to a fluorescent protein used for normalization, not for the detection of the intracellular parameter.*

TABLE 2 | Yeast strains.

Strain	Description	References
CEN.PK113-7D*	Haploid laboratory strain	Entian and Kötter, 2007
S288C*	Haploid laboratory strain	Mortimer and Johnston, 1986
Ethanol red*	Diploid industrial strain	Société industrielle lesaffre, division leaf
Red star*	Industrial strain	Red star yeast company, LLC
Thermosacc*	Industrial strain	Lallemand biofuels and distilled spirits, United States
PE-2*	Diploid industrial strain	Fermentec, brazil
CCUG 53310*	Industrial strain	Purwadi et al., 2007
LARS*	Industrial strain	Our laboratory collection
X218-1A*	Haploid wild-type strain	Raschke et al., 1973
LBCM1001*, 1003*, 1008*, 1013*, 1014, 1017*, 1030*, 1037*, 1046*, 1067*, 1079*, 1095*, 1097*, 1099*, 1103*, 1106*, 1109*	Wild-type isolates from LBCM collection, which includes 138 strains isolated from cachaça distilleries located in Brazil	da Conceição et al., 2015
Saccharomyces boulardii CNCM I-745	Commercial probiotic strain, purchased from PRECOSA (Biocodex, France)	Moré and Swidsinski, 2015
Saccharomyces bayanus FM361	Wild-type strain	Cliften et al., 2001
Saccharomyces castellii FM476	Wild-type strain	Cliften et al., 2001
Saccharomyces kluyveri FM479	Wild-type strain	Cliften et al., 2001
Saccharomyces kudriavzevii FM527	Wild-type strain	Cliften et al., 2001
Saccharomyces mikatae FM356	Wild-type strain	Cliften et al., 2001
Zygosaccharomyces bailii CBS 1170	Wild-type strain	Suh et al., 2013
Candida intermedia CBS 2044	Wild-type strain	Pham et al., 2011
Kluyveromyces marxianus NCYC 179	Industrial strain	Steele and Miller, 1974

*Yeast strains used in this study. *Refers to Saccharomyces cerevisiae strains.*

agar for plates) with the required antibiotic (ampicillin 100 mg/L or neomycin 50 mg/L). Plates were incubated at 30°C, and liquid cultures at 30°C and 220 rpm, in order to limit the possibility of recombination events when repeated regions were presents in the plasmids.

Cloning, Yeast Transformation, and Gene Amplification

Cloning

Plasmids used for genome integration and bearing either the CRISPR-Cas9 system or single/pairs of biosensors were generated using the MoClo Modular Cloning System Plasmid Kit (Lee et al., 2015). Constructs not included in the kit, such as promoters or coding sequences, were ordered from Twist Bioscience[1] and contained suitable flanking restriction sites that could be excised with Eco31I and Esp3I. Alternatively, they were amplified by PCR and inserted in the entry vector pYTK001 (**Supplementary Table 2**; Lee et al., 2015). The complete list of plasmids generated in this study is provided in **Supplementary Table 3**.

Plasmid assembly was carried out by mixing 50 ng of each desired plasmid, 1 μL T4 Ligase Buffer 10 × (Thermo Fisher Scientific), 0.5 μL T4 DNA Ligase (Thermo Fisher Scientific), 0.5 μL FastDigest Esp3I or FastDigest Eco31I (Thermo Fisher Scientific), 0.5 μL dithiothreitol 20 mM (if needed), and MilliQ-H_2O up to 10 μL. Reactions proceeded as follows: 4 min at 37°C, 40 cycles of 1 min at 37°C, 2 min at 16°C, 4 min at 37°C, and final 10 min at 65°C. Next, 5 μL of the assembly reaction was used to transform competent *E. coli* DH5α, which were plated on LB agar with suitable antibiotics. White colonies were then verified by colony PCR. The correct clones were

[1] www.twistbioscience.com

TABLE 3 | Composition of synthetic wheat-straw hydrolysate.

Compounds	g/L	References
Mannose	1	López-Abelairas et al., 2013
Glucose	68.8	van Dijk et al., 2019
Xylose	36.4	van Dijk et al., 2019
Arabinose	4	Baroi et al., 2015
Galactose	0.6	López-Abelairas et al., 2013
Acetic acid	4.7	van Dijk et al., 2019
Formic acid	1.2	van Dijk et al., 2019
Levulinic acid	–	van Dijk et al., 2019
Furfural	3	van Dijk et al., 2019
5-(Hydroxymethyl)furfural	0.6	van Dijk et al., 2019
Vanillin	0.03	Almeida et al., 2007

The amounts refer to 100% medium.

cultured overnight in suitable LB medium and the target plasmid was purified using the GeneJET Plasmid Miniprep Kit (Thermo Fisher Scientific).

Yeast Transformation

Genome integration in yeast was performed using the LiAc/salmon sperm carrier DNA/polyethylene glycol method (Gietz, 2014) and CRISPR/Cas9 for improved integration efficiency (Akhmetov et al., 2018). The backbone Cas9 plasmid was YN2_1_Cas9_exp, developed in a previous study in our lab (Cámara et al., 2020), in which suitable single guide RNA (sgRNA) was inserted to target the desired sequences (**Supplementary Table 3**).

The sgRNA-targeting regions were identified using CRISPR-ERA (Liu et al., 2015), Yeast CRISPRi (Smith et al., 2016), and CHOPCHOP (Labun et al., 2019). The following parameters were checked: (i) an ATAC-seq value close to 1; (ii) a nucleosome presence value close to 0; (iii) absence of poly-N and off-targets; (iv) CG content between 40 and 60; and (v) presence of the sgRNA in multiple databases. Single-stranded (forward and reverse) oligonucleotides for sgRNAs were ordered from Eurofins and contained sticky ends suitable for assembly in the YN2_1_Cas9_exp vector (**Supplementary Table 4**). Double-stranded oligonucleotides were generated by combining 20 μL of each single-stranded oligonucleotide (100 μM) and 10 μL 5 × T4 Ligase Buffer. The mixture was incubated at 98°C for 5 min to denature the oligonucleotides, followed by a gradual decrease of 1°C/30 s over 86 cycles to allow for oligonucleotide annealing.

To insert the sgRNA target sequence in the plasmid, YN2_1_Cas9_exp (∼1 μg) and the annealed sgRNA sequence (0.5 μL of the above reaction) underwent the same MoClo steps as described in section "Cloning" using FastDigest Esp3I.

Prior to transformation in yeast, plasmids harboring the donor DNA were linearized with FastDigest NotI (Thermo Fisher Scientific) for 2 h at 37°C, followed by 5 min at 80°C for enzyme inactivation. For each restriction reaction (20 μL), the following reagents were used: 2 μL 10 × FastDigest Buffer, 1 μL FastDigest NotI, 1 μL Fast AP (Thermo Fisher Scientific), ∼1.5 μg of the desired plasmid, and MilliQ-H_2O up to 20 μL. The restriction reaction was then mixed with 500 ng of suitable Cas9 plasmid (YN2_1_LT58 or YN2_1_LT84), 5 μL salmon sperm DNA (10 mg/mL), and MilliQ-H_2O up to 75 μL, and used for subsequent yeast transformation. In the case of RPL13A tagging, plasmid pYTK032 bearing mTurquoise2 (Lee et al., 2015) was used as template for PCR amplification of the donor DNA using oligos LT174_F and LT174_R. In this case, 1 μg of purified PCR product was used in the transformation mixture.

Transformation was carried out as described previously (Gietz, 2014), with an 18-min heat-shock. Cells were plated on YPD + G418 plates and incubated for 3 days at 30°C. Colonies were then verified by colony PCR using oligos LT183_F and LT183_R for integration at the X2 site, or LT87 and LT88 for RPL13A tagging (**Supplementary Table 4**). Positive clones were re-streaked twice on YPD plates with no antibiotic to cure the Cas9 plasmid.

To test genome integration efficiency, the linearized plasmid LT1_33 (pTEFmut8-mCherry) was used as donor DNA. Ten colonies from each strain were tested by colony PCR using oligos LT183_F and LT183_R.

PCR and Sequencing

The PCR oligos used in the present study are listed in **Supplementary Table 4**. All PCR and colony PCR products were amplified as instructed by the manufacturer. Phusion High-Fidelity DNA Polymerase (Thermo Fisher Scientific) was used in 50-μL reactions to amplify constructs to be used for cloning the plasmids or the X2 site to be sent for sequencing (colony PCR). Phire Hot Start II DNA Polymerase (Thermo Fisher Scientific) was used in 20-μL reactions to verify either successful cloning in bacteria or genome integration in yeast. When performing colony PCR, a small lump of cells from the selected colony was diluted in 20 μL MilliQ-H_2O, microwaved for 5 min at 800 W (yeast colonies only), and 1 μL of the solution was used as template. The PCR products were run on 1% agarose gels, with 0.5 × TAE buffer, and at 80 mV for 40 min. GeneRuler 1 kb DNA Ladder (Thermo Fisher Scientific) was used to estimate product length. When required, PCR products were purified using the GeneJET PCR Purification Kit (Thermo Fisher Scientific).

The X2 fragment from various strains was amplified with oligos LT185_F and LT185_R and sent for sequencing to Macrogen.[2] Sequences were then aligned for comparison.

Cultivation Conditions and Analytical Methods

Cultivation in Flasks and High-Performance Liquid Chromatography

For strain characterization, a two-step preculture was employed. Specifically, cells were inoculated from a cyostock in 5 mL Delft medium and grown in a 50-mL tube for 24 h. Then, 100 μL were re-inoculated into 10 mL Delft medium and incubated in 100-mL baffled flasks for 16 h. The characterization was performed in 500-mL screw-top shake flasks (Duran), with a one-way valve for CO_2 release and a swabable valve for sterile sampling connected to the cap (Eppendorf). The working volume was 150 mL, initial optical density at 600 nm (OD_{600}) was 0.1, rotation was 140 rpm, and temperature was set to 30°C. N_2 was flushed for 10 s after cell inoculation to create

[2]https://dna.macrogen-europe.com

a microaerobic environment. OD_{600} was measured every 2 h using 1-mL samples. Additional 1-mL samples were taken at 0, 12, and 15 h for yields determination and were centrifuged at 4,000 rpm for 5 min. The supernatant was filtered through 0.2-μm nylon membrane filters (VWR) and extracellular metabolites (glucose, ethanol, acetic acid, and glycerol) were analyzed using a high-performance liquid chromatography system equipped with a refractive index detector (Jasco) and a Rezex ROA-Organic Acid H^+ column (Phenomenex). Separation was carried out at a flow rate of 0.8 mL/min, 80°C, and using 5 mM H_2SO_4 as eluent. The pellet was used for cell dry weight determination upon resuspension in 1 mL distilled water and filtration through a pre-dried and weighed 0.45-μm polyether sulfone membrane (Sartorius). The membrane was dried for 24 h at 70°C and the weight checked again.

Biomass, ethanol, acetic acid, and glycerol yields were expressed in $g/g_{glucose}$, and calculated using Equation 1:

$$Yield_{Compound} = \frac{[Compound]_{t12\ or\ t15} - [Compound]_{t0}}{[Glucose]_{t0} - [Glucose]_{t12\ or\ t15}} \quad (1)$$

Where $t0$ refers to the sample taken at 0 h, $t12$ at 12 h, and $t15$ at 15 h from the start of the screening. The specific growth rate was computed by calculating the linear regression of the natural logarithm of the OD_{600} value between 4 and 10 h (at least 4 time points).

Cultivation in the BioLector I

Yeast cells from a cryo-stock were inoculated the day prior the screening in 5 mL Delft medium and grown overnight at 30°C in 50-mL tubes. Cells were then inoculated in a suitable medium to a final volume of 200 μL using CELLSTAR black clear-bottom 96-well microtiter plates (Greiner bio-one) and sealed with AeraSeal films (Sigma-Aldrich). Initial OD_{600} was 0.2 for wells containing SWSHs and 0.1 for all other samples. The temperature was set to 30°C with 85% humidity, shaker frequency was 900 rpm, and cycle time was 30 min. Filter properties are described in section "BioLector I Filters and Analysis" and **Supplementary Table 5**. All cultivation conditions were investigated in triplicates.

Intracellular pH Calibration

Parental yeast strains and those bearing sfpHluorin were taken from a cryo-stock and grown overnight in Delft medium. In the morning, cells were re-inoculated at an OD_{600} of 0.4 in 100-mL baffled flasks containing 15 mL Delft medium and grown at 30°C and 200 rpm. A fresh 10 × digitonin stock solution (10 mg/mL in MilliQ-H_2O) was prepared by mixing at 70°C until a clear solution was obtained. Upon reaching an OD_{600} of ∼1, 10 mL of culture was harvested and centrifuged for 3 min at 3,000 rpm. The cell pellet was washed once with phosphate-buffered saline (PBS) at pH 5, resuspended in 10 mL PBS (pH 7.4) containing 100 μg/mL digitonin, and incubated for 10 min at room temperature with shaking at low rpm. Cells were then centrifuged, washed once with PBS (pH 7.4), and resuspended in PBS (pH 7.4) to an OD_{600} of 20. Cells were added to citric acid/Na_2HPO_4 buffer, whose pH ranged from 4.5 to 8, to a final OD_{600} of 0.5 and in a final volume of 200 μL. Fluorescence was measured in a BioLector I using CELLSTAR black clear-bottom 96-well microtiter plates. Measurements were taken 30 min after the addition of cells. Fluorescence was plotted against pH and calibration curves were generated.

BioLector I Filters and Analysis

The emission/excitation filters used in this study are summarized in **Supplementary Table 5**. At each time point, background fluorescence from the parental strain was subtracted from the fluorescence signal of strains bearing a biosensor. The signals from OxPro (ymYPET), GlyRNA (mTurquoise2), and RPL13A-mTurquoise2 (mTurquoise2) biosensors were normalized to the mCherry fluorescence of the pTEFmut8-mCherry construct. Instead, for QUEEN-2m and sfpHluorin, the ratio between the filters E-OP-341 and E-OP-304 was computed. In all cases, samples were analyzed in triplicates, and the mean and standard deviation among replicates were computed after calculating the ratio. When selecting the fluorescent proteins, we considered the following aspects: spectrum overlap, brightness, monomeric structure, and pKa < 5. Further details can be found in section 1.1 of **Supplementary Material**.

Statistical Analysis

Pairwise comparisons were carried out in R (R Core Team, 2020), using unpaired Student's *t*-test. Statistical significance was defined as follows: $^{ns}p > 0.05$; $^{*}p \leq 0.05$; $^{**}p \leq 0.01$, and $^{***}p \leq 0.001$.

Deposition to Addgene

Plasmids will be available from the Addgene repository[3] using IDs (177705-177712) or by contacting the corresponding author.

RESULTS

Five Biosensors Are Selected to Monitor the Yeast Intracellular Status During Stress

Five biosensors already proven to function in yeast and capable of detecting key intracellular parameters were selected from the literature (**Figure 1A**, **Table 1**, and **Supplementary Table 5**). They included ratiometric biosensors (pH and ATP concentration) and intensiometric biosensors (ribosome production, oxidative stress, and glycolytic flux), also selected on the need to match different fluorescent spectra if combined.

ATP is a crucial molecule in the energetic balance of the cell and exploring its fluctuations over time would reveal the energy fluxes associated with stress responses. Therefore, QUEEN-2m was selected as biosensor for this parameter (Yaginuma et al., 2014; Takaine et al., 2019). QUEEN-2m is biosensor based on a circularly permutated GFP, whose fluorescent intensity changes upon binding of ATP.

The intracellular pH biosensor sfpHluorin (Reifenrath and Boles, 2018) represents an improved version of the more

[3]https://www.addgene.org

commonly used pHluorin (Nygård et al., 2014). Owing to its greater pH stability, it is more suitable for industrial applications, as the elevated amount of weak acids in those substrates leads to acidification of the cytosol (Guldfeldt and Arneborg, 1998).

Furaldehydes and phenolic compounds in lignocellulosic biomass are often associated with redox imbalance because their detoxification requires NAD(P)H as a cofactor (Deparis et al., 2017; Liu, 2018). OxPro (Oxidative stress Probe) was selected as an oxidative stress sensor (Zhang et al., 2016). This biosensor is based on a synthetic promoter driving the expression of a fluorescent protein dependent by the activation of the transcription factor YAP1, the main oxidative stress mediator in yeast (Estruch, 2000). This construct formed part of a circuit capable of regenerating NADPH when the cell required it (Zhang et al., 2016).

In many fermentation processes, end products are synthesized starting from sugars (Francois et al., 2020; Maicas, 2020; Sharma et al., 2020). GlyRNA (Glycolytic RNA probe) was selected as an aptameric sensor for glycolytic flux, because degradation of its mRNA is sensible to the intracellular concentration of fructose-bisphosphate (Ortega et al., 2021). Given that the sensor's response decreases with an increasing concentration of fructose-bisphosphate, a negative peak denotes maximum glycolytic flux.

Lastly, ribosomes have been suggested to control the lifespan of cells and might improve tolerance to growth inhibitors (Steffen et al., 2008; Gonskikh and Polacek, 2017). Therefore, to monitor ribosome production, RPL13A, one of the proteins in the 60S ribosomal subunit, was tagged with a fluorescent protein as done previously to correlate lifespan and ribosome levels (Janssens and Veenhoff, 2016). This biosensor, referred to as RibPro (Ribosome Probe), with the tagging of the endogenous RPL13A with a fluorescent protein, offered two important advantages. First, it avoided the need to introduce an additional tagged copy of the same gene, which might have led to unwanted overexpression. Second, it allowed a more accurate readout, as using the promoter activity of a ribosomal protein might have overlooked post-transcriptional regulation of the corresponding mRNA (Roy et al., 2020).

In the case of intensiometric biosensors GlyRNA, OxPro, and RibPro, a constitutively expressed fluorescent reporter (constructed in plasmid LT1_33_pTEFmut8-mCherry) was added to normalize the biosensor output; thus ensuring reliable readouts and minimizing the effect of population heterogeneity (see section 1.2 of the **Supplementary Material**). As both QUEEN-2m and sfpHluorin are ratiometric probes, they did not require this addition.

The Highly Efficient X2 Integration Site Is Conserved in *Saccharomyces cerevisiae* Strains

The proposed biosensor toolbox offers a simple and marker-free integration method that allows: (1) easy investigation of multiple yeast strains, (2) the possibility to avoid selection markers, and (3) stable expression of the fluorescent biosensors. In *S. cerevisiae*, the HO site is a common target for genome integration of a desired construct/pathway as it does not affect growth (Baganz et al., 1997). To allow use of the toolbox even in strains with HO-integrated constructs/pathways, we explored the possibility of integrating the biosensors in another site. Fourteen other safe-to-use sites offering elevated and stable expression have been described in *S. cerevisiae* (Mikkelsen et al., 2012). One of the most used ones is the X2 site on chromosome X. Owing to its location between two essential genes, GCD14 and CCT7, we hypothesized that this site could be conserved across yeast species and genera. Therefore, the presence of the X2 site was checked by colony PCR in laboratory, industrial, and wild-type *S. cerevisiae* strains, as well as in other *Saccharomyces* and non-*Saccharomyces* strains (**Table 2**). The X2 site was present in all 28 *S. cerevisiae* strains and *Saccharomyces boulardii* CNCM I-745, which shares 95% genome homology with *S. cerevisiae* (Khatri et al., 2017), but was absent from the remaining eight yeasts tested (**Figure 2A**). The sequence of the locus was blasted in NCBI to confirm that the missing band was not caused by primer mismatch. Given the above result and the dominant role of *S. cerevisiae* in bioindustry (Kampranis and Makris, 2012), this site seemed a good candidate for genome integration and for exploring the diversity within this genus.

CRISPR-Cas9 editing technology has been shown to improve genome integration efficiency (Akhmetov et al., 2018). Therefore, we used the construct LT1_33_pTEFmut8-mCherry to test genome integration efficiency in 13 of the 29 X2-positive strains. First, we designed a sgRNA (oligos LT58) targeting the region of interest and inserted it in a Cas9-expressing vector (final plasmid YN2_1_LT58_X2site, Addgene ID: 177705). Integration efficiency was > 80% for all laboratory and industrial strains tested, but between 60 and 80% for several Brazilian wild-type strains (**Figure 2B**). However, strains LBCM1037 and LBCM1106 showed no integration success even after repeating the transformation procedure 3 times. To determine the cause of such low efficiency, the X2 site was sequenced in the 13 strains harboring it (**Supplementary Figure 1**). The sequence for 12 of the 13 strains was very similar to that of CEN.PK113-7D; whereas the sequence of LBCM1106 was substantially different, including in the target sgRNA region. Therefore, optimization of the sgRNA sequence might be sufficient to improve integration efficiency. Prior any integration into a yeast strain not presented in this study, assessment of the presence of the X2 site should be performed. In addition, the presence of conserved single nucleotide polymorphisms and deletions in the three different yeast types (laboratory, industrial, and wild-type) pointed to possible similarities between strains (**Supplementary Figure 1**).

Genome-Integrated Biosensors Do Not Affect the Central Metabolism of Yeast

To test the biosensors in the toolbox, we decided to continue the experiments using *S. cerevisiae* CEN.PK113-7D and Ethanol Red, as representatives of laboratory and industrial strains, respectively. All biosensors were first constructed as plasmids using the MoClo Modular Cloning System Plasmid Kit (Lee et al., 2015). No yeast selection markers were necessary as a dummy sequence containing STOP codons in different shift-frames was employed instead (oligos LT179_F and LT179_R). Then,

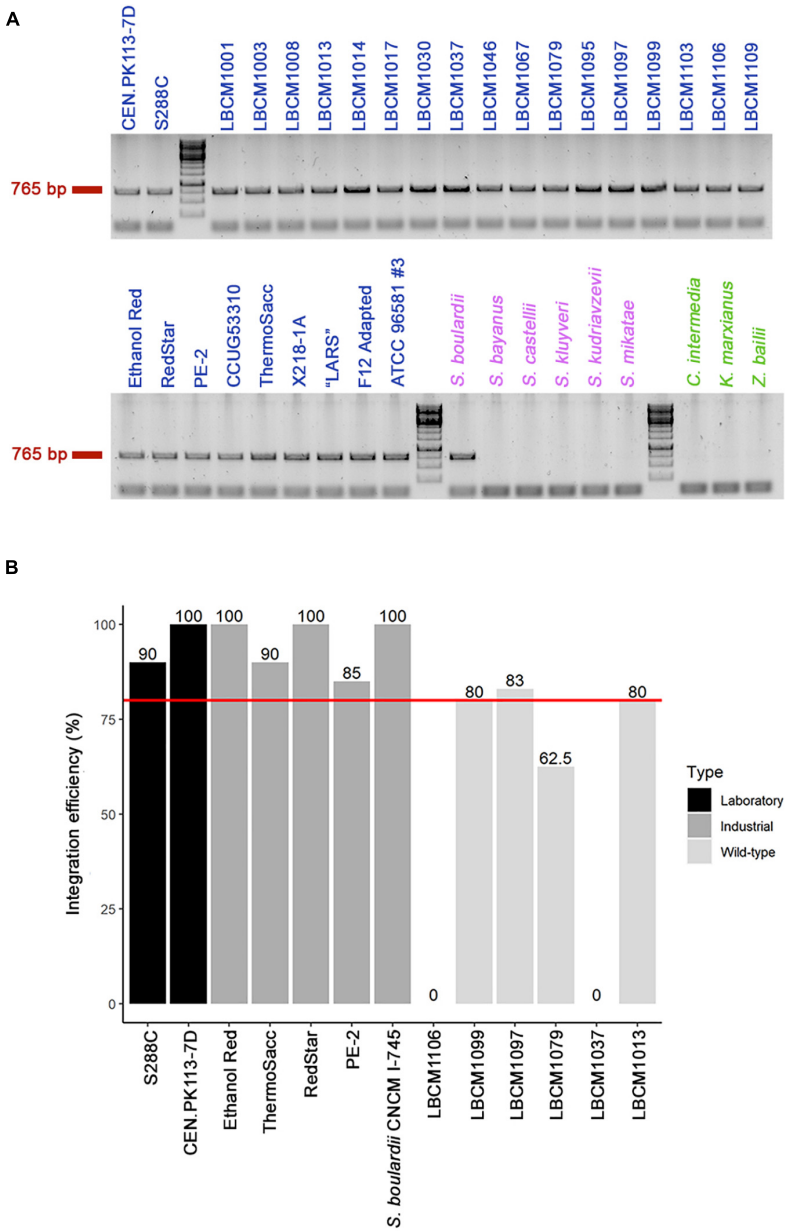

FIGURE 2 | Presence of the X2 site and genome integration efficiency. **(A)** Presence of the conserved X2 site (band at 765 bp) was verified by colony PCR in multiple yeast strains, including 28 *Saccharomyces cerevisiae* (blue), six other *Saccharomyces* (violet), and three non-*Saccharomyces* (green) strains (see **Table 2** for a full list of yeast strains). **(B)** Assessment of genome integration efficiency in 13 of the 29 *Saccharomyces* (28 *S. cerevisiae* and 1 *S. boulardii*) strains that harbored the X2 site was carried out using CRISPR-Cas9 genome editing technology. The red line represents 80% integration efficiency and the value for each strain is reported above the bar.

after linearization, yeasts were transformed using CRISPR-Cas9 genome editing technology. Cells bearing the Cas9 plasmid were selected on medium containing G418, as it was assumed that they had most likely integrated the linearized donor DNA with the desired biosensor (see **Supplementary Table 3** for a list of constructs). After selection of the correct clones by colony PCR, the Cas9 plasmid was cured to obtain the marker-free strains.

As the selected biosensors would monitor the intracellular environment, their presence should not cause any significant alteration in cellular metabolism. CEN.PK113-7D strains bearing single biosensors were cultured anaerobically in 500-mL flasks in Delft medium (minimal defined synthetic medium) to quantify their growth performance. Neither the growth curves (**Figure 3A**) nor the maximum specific growth rates (**Table 4**) of strains bearing single biosensors showed any significant difference with respect to the parental strain. The same trend was observed also for the yields of key metabolites at the beginning of incubation and during stationary phase; only the acetic acid

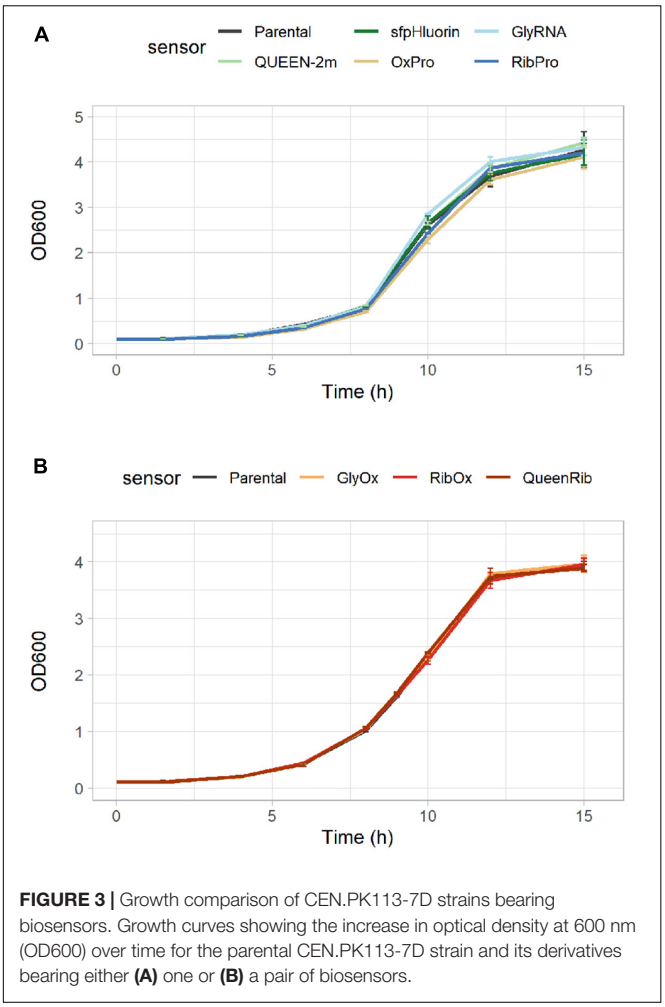

FIGURE 3 | Growth comparison of CEN.PK113-7D strains bearing biosensors. Growth curves showing the increase in optical density at 600 nm (OD600) over time for the parental CEN.PK113-7D strain and its derivatives bearing either **(A)** one or **(B)** a pair of biosensors.

yield of the strain carrying sfpHluorin differed from that in the parental strain (**Table 4**).

To allow detection of several intracellular parameters simultaneously, multiple biosensors were integrated in the same cell. Again, neither the growth curves (**Figure 3B**) nor the performance parameters of strains bearing multiple biosensors (GlyOx, RibOx, and QueenRib) differed from those of the parental CEN.PK113-7D strain (**Table 5**). Overall, the selected biosensors did not affect yeast growth and could reliably convey the cells' physiological state during different growth conditions.

Combining Biosensors in Different Carbon Sources Gives a Reliable Fluorescence Output

Simultaneous detection of multiple intracellular parameters could point to correlations among them. To this end, we combined pairs of biosensors with non-overlapping spectral properties in the same cell and assessed their fluorescent signal. As in the case of singular biosensors, paired biosensors were all introduced into the X2 site, together with the normalization construct. The GlyRNA-OxPro (GlyOx) combination allowed simultaneous detection of oxidative stress and glycolytic flux

TABLE 4 | Physiological rates and yields of yeast strains harboring singular biosensors.

CEN.PK113-7D strain	Specific growth rate (h^{-1})	Biomass yield (g/g)		Ethanol yield (g/g)		Glycerol yield (g/g)		Acetic acid yield (g/g)	
		12 h	15 h	12 h	15 h	12 h	15 h	12 h	15 h
Parental	0.379 ± 0.000	0.090 ± 0.015	0.088 ± 0.008	0.388 ± 0.008	0.387 ± 0.006	0.167 ± 0.027	0.167 ± 0.03	0.018 ± 0.002	0.019 ± 0.000
QUEEN-2m	0.382 ± 0.002^{ns}	0.098 ± 0.006^{ns}	0.083 ± 0.004^{ns}	0.393 ± 0.011^{ns}	0.38 ± 0.009^{ns}	0.150 ± 0.020^{ns}	0.149 ± 0.019^{ns}	0.019 ± 0.001^{ns}	0.020 ± 0.001^{ns}
sfpHluorin	0.372 ± 0.014^{ns}	0.102 ± 0.005^{ns}	0.091 ± 0.006^{ns}	0.384 ± 0.012^{ns}	0.374 ± 0.011^{ns}	0.157 ± 0.026^{ns}	0.157 ± 0.027^{ns}	0.017 ± 0.001^{ns}	0.018 ± 0.000*
GlyRNA	0.379 ± 0.009^{ns}	0.093 ± 0.008^{ns}	0.085 ± 0.002^{ns}	0.392 ± 0.013^{ns}	0.380 ± 0.009^{ns}	0.163 ± 0.015^{ns}	0.162 ± 0.021^{ns}	0.016 ± 0.001^{ns}	0.020 ± 0.001^{ns}
OxPro	0.360 ± 0.033^{ns}	0.088 ± 0.003^{ns}	0.087 ± 0.006^{ns}	0.389 ± 0.012^{ns}	0.378 ± 0.009^{ns}	0.147 ± 0.021^{ns}	0.144 ± 0.022^{ns}	0.018 ± 0.001^{ns}	0.019 ± 0.001^{ns}
RibPro	0.375 ± 0.011^{ns}	0.094 ± 0.007^{ns}	0.087 ± 0.004^{ns}	0.39 ± 0.01^{ns}	0.380 ± 0.012^{ns}	0.148 ± 0.025^{ns}	0.147 ± 0.024^{ns}	0.017 ± 0.001^{ns}	0.019 ± 0.001^{ns}

$^{ns}p > 0.05$; $^{*}p \leq 0.05$.

TABLE 5 | Physiological rates and yields of yeast strains harboring multiple biosensors.

CEN.PK113-7D Strain	Specific growth rate (h^{-1})	Biomass yield (g/g)		Ethanol yield (g/g)		Glycerol yield (g/g)		Acetic acid yield (g/g)	
		12 h	15 h	12 h	15 h	12 h	15 h	12 h	15 h
Parental	0.418 ± 0.006	0.121 ± 0.006	0.125 ± 0.002	0.387 ± 0.002	0.376 ± 0.003	0.056 ± 0.002	0.055 ± 0.002	0.011 ± 0.000	0.015 ± 0.001
GlyOx	0.414 ± 0.005^{ns}	0.120 ± 0.004^{ns}	0.125 ± 0.003^{ns}	0.387 ± 0.001^{ns}	0.372 ± 0.002^{ns}	0.054 ± 0.001^{ns}	0.053 ± 0.001^{ns}	0.011 ± 0.000^{ns}	0.016 ± 0.000^{ns}
RibOx	0.405 ± 0.003^{ns}	0.123 ± 0.004^{ns}	0.127 ± 0.003^{ns}	0.390 ± 0.000^{ns}	0.375 ± 0.002^{ns}	0.052 ± 0.001^{ns}	0.052 ± 0.001^{ns}	0.011 ± 0.000^{ns}	0.016 ± 0.001^{ns}
QueenRib	0.420 ± 0.011^{ns}	0.116 ± 0.002^{ns}	0.126 ± 0.002^{ns}	0.387 ± 0.001^{ns}	0.374 ± 0.002^{ns}	0.056 ± 0.002^{ns}	0.056 ± 0.002^{ns}	0.011 ± 0.000^{ns}	0.016 ± 0.001^{ns}

$^{ns}p > 0.05$.

(LT2_14_GlyOx as plasmid for integration, **Supplementary Table 3**); whereas the RibPro-OxPro (RibOx) pair allowed simultaneous detection of ribosome production and oxidative stress (RPL13A-mTuquoise2 Tag plus LT2_7_OxPro as plasmid for integration, **Supplementary Table 3**). The cells carrying either single or paired biosensors were grown on two distinct carbon sources, glucose and ethanol, to determine if different metabolic pathways affected the fluorescent response (**Figure 4** and **Supplementary Figure 2**). Under aerobic batch conditions, *S. cerevisiae* consumes all the glucose through glycolysis and fermentation, converting it into ethanol. Once glucose is exhausted, ethanol can be used as an alternative carbon source through the tricarboxylic acid cycle (Pfeiffer and Morley, 2014). If ethanol is used as the sole carbon source, only the tricarboxylic acid cycle is activated.

During growth on glucose, the signal from the GlyRNA biosensor was low in exponential phase, but increased as the glucose was exhausted (**Figure 4A** and **Supplementary Figures 2A,B**). In contrast, when grown solely on ethanol, the GlyRNA signal increased from the start, indicating no active glycolytic flux (**Figure 4A** and **Supplementary Figures 2A,B**). Oxidative stress fluctuated over time in glucose-grown cells, with a minor increase of OxPro biosensor fluorescence during the diauxic shift (**Figure 4B** and **Supplementary Figures 2C,D**); whereas ethanol resulted in a continuous decrease (**Figure 4B** and **Supplementary Figures 2C,D**). The same trend was observed for ribosome production (**Figure 4C** and **Supplementary Figures 2E,F**). The bump in RibPro fluorescence detected during the diauxic shift can be explained by the switch from a fermentative to a respiratory metabolism, which coincides with more protein synthesis. For the same reason, activation of the tricarboxylic acid cycle during the diauxic shift coincides with an increased release of reactive oxygen species (Balaban et al., 2005), which yeast cells need to acclimate to. In the case of ethanol-grown cells, this adaptation is missing, and the trends are comparable with the second growth on ethanol of glucose-grown cells.

Overall, we showed that the fluorescent outputs from both single (**Figures 4A–C**) and combined (**Figures 4D–F**) biosensors displayed comparable trends (**Supplementary Figure 2**). Considering that the use of these biosensors should be qualitative and for the comparison of trends, we confirm a reliable readout from the strains with combined biosensors.

Tight Regulation Between ATP Production and Intracellular pH

ATP production and intracellular pH are two key indicators of the state and activity of cells. To study the correlation between them, CEN.PK113-7D strains bearing sfpHluorin and QUEEN-2m were cultured in Delft medium and spiked or not with 2-deoxy-D-glucose (2DG, final concentration of 0.5 g/L) at 6 h to inhibit the glycolytic flux, ATP production, and exponential growth (**Figure 5A**) (Ortega et al., 2020). At 30 h, the medium in spiked and non-spiked cultures was replaced with fresh Delft medium (**Figure 5A**). The QUEEN-2m biosensor revealed that ATP was produced when cells grew exponentially on either

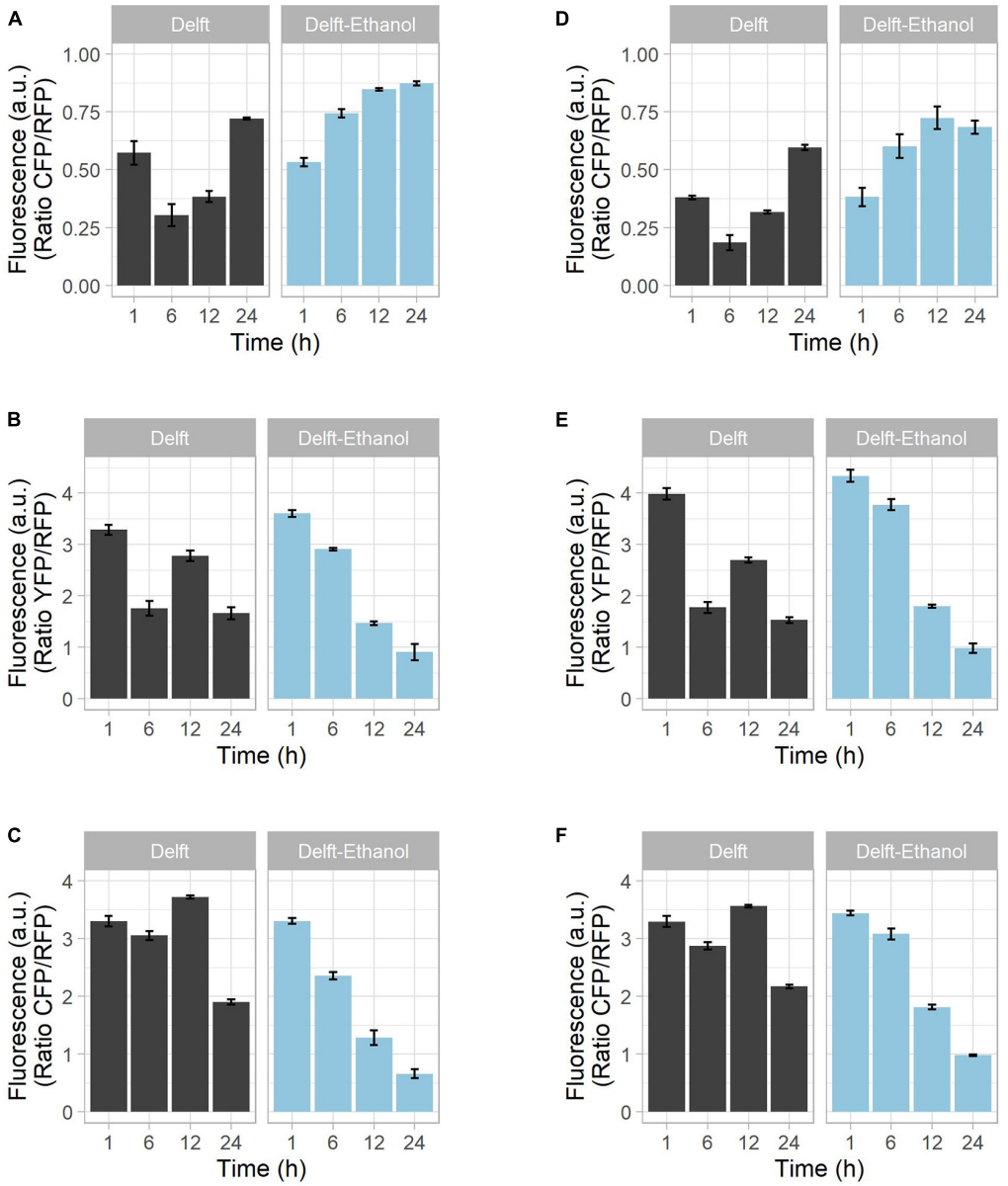

FIGURE 4 | Growth of strains on different carbon sources and biosensor combination. CEN.PK113-7D strains bearing biosensors were grown in synthetic minimal Delft medium containing either 20 g/L glucose (black bars) or 20 g/L ethanol (blue bars) as sole carbon source. Mutants with **(A–C)** a single biosensor or **(D–F)** pairs of biosensors were tested to determine the reliability of the fluorescence output. The tested intracellular parameters included **(A,D)** glycolytic flux (via GlyRNA and GlyOx), **(B,E)** oxidative stress (via OxPro and GlyOX), and **(C,F)** ribosome production (via RibPro and RibOx). Using glucose as carbon source, the time points denote lag phase (1 h), exponential phase (6 h), diauxic shift (12 h), and stationary phase (24 h). With growth on ethanol, time points denote lag phase (1–12 h) and active growth (24 h).

glucose (6 h) or ethanol (18 h) (**Figures 5A,B**). At the same time, the sfpHluorin biosensor revealed that intracellular pH was maintained between 6 and 6.5 during growth, but dropped below 6 when ATP was no longer produced (12 and 30 h) (**Figure 5C**). Eventually, if glucose was added during stationary phase (36 h), new ATP was produced and pH stabilized around 6 again (**Figures 5B,C**).

When 2-deoxy-D-glucose was added to the medium at 6 h, ATP production decreased, and intracellular pH dropped below 5 (time points 12–30 h) (**Figures 5B,C**). Upon medium replacement at 30 h, both ATP production and intracellular pH were restored (**Figures 5B,C**). This finding highlights the link between intracellular pH and ATP production. Intracellular pH regulation needs high amounts of ATP to power membrane pumps. Hence, in the absence or limitation of ATP, pH regulation cannot function properly and intracellular acidification ensues, as confirmed by a decrease in cytoplasmic pH following inactivation of an ATP-driven proton pump (Isom et al., 2018).

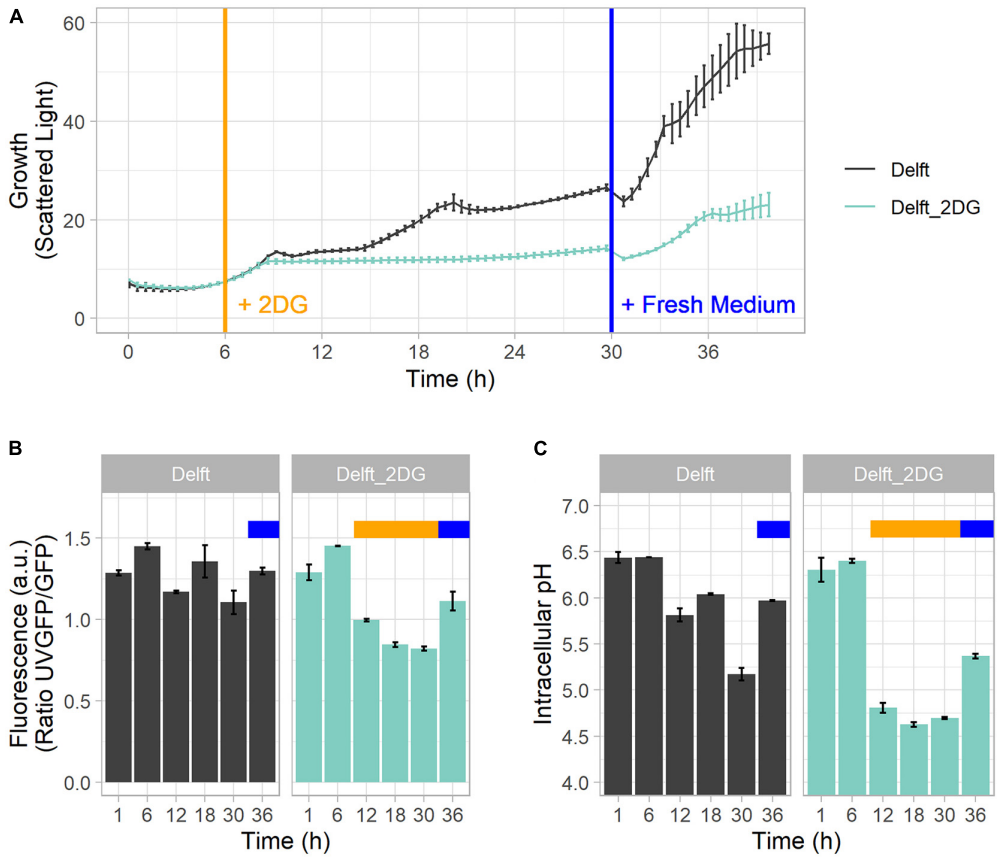

FIGURE 5 | Mutual connection between ATP and intracellular pH. **(A)** Growth curve profile of CEN.PK113-7D in Delft medium and Delft medium spiked at 6 h (orange line) with 2-deoxy-D-glucose (2DG) to stop growth and ATP production by glycolysis. In both conditions, medium was replaced at 30 h with fresh Delft medium (blue line). **(B)** ATP concentration detected with sfpHluorin. **(C)** Intracellular pH detected with QUEEN-2m. In Delft medium, the time points denote lag phase (1 h), first exponential phase (6 h), diauxic shift (12 h), second growth on ethanol (18 h), stationary phase (30 h), and growth after additional glucose supplementation (36 h). The orange bar denotes the presence of 2DG in the medium; the blue bar denotes replacement with fresh medium.

Activation of the Oxidative Stress Response and Correlation With Intracellular pH in the Presence of Stressors

Oxidative stress is very common in industrial bioethanol production plants due to the elevated amount of furaldehydes and phenolics released from the degradation of sugars and lignin (Sjulander and Kikas, 2020). Moreover, substrate pre-treatments release also weak acids (affecting the intracellular pH) and sugars (Deparis et al., 2017). To investigate changes in intracellular pH (using sfpHluorin) and activation of the oxidative stress response (using OxPro) under industrial-type settings, cells were subjected to four individual stressors commonly found in lignocellulosic hydrolysates, namely acids, phenolics, furaldehydes, and sugars (**Figure 6** and **Supplementary Figures 3, 4**).

Acetic acid is a common and abundant weak acid in lignocellulosic hydrolysates, where it is generally found in its protonated form (Cunha et al., 2019). Upon diffusing into the cell, it releases a proton, acidifying the cytosol (Ullah et al., 2012). When cultured in acetic acid at 4.5 and 6 g/L, the cells did not show any activation of the stress response (**Figure 6A** and **Supplementary Figures 3A, 4A**). Intracellular pH remained stable until the end of exponential phase (**Supplementary Figures 3B, 4B**), but dropped thereafter more than with any of the other stressors tested (**Figure 6B**), probably due to an ATP shortage (see section "Tight Regulation Between ATP Production and Intracellular pH"). Note that acetic acid (pKa = 4.75) increase its inhibitory effect on growth as the pH in the medium (Pampulha and Loureiro-Dias, 1989).

Furfural and vanillin are known for causing a redox imbalance due to NAD(P)H depletion (Liu, 2018). Indeed, furfural elicited a strong oxidative stress response (**Figure 6A**), especially in lag phase (**Supplementary Figures 3C, 4C**). The timing of the response can be explained by the need for yeast cells to detoxify the medium prior to starting exponential growth (Liu, 2018). In contrast, vanillin did not activate the oxidative stress response (**Figure 6A**) and intracellular pH remained constant (pH 5) during the entire period (**Supplementary Figures 3D, 4D**).

Finally, xylose, which cannot be metabolized by any of the two strains, was used to induce osmotic stress, a common event with lignocellulosic substrates (Deparis et al., 2017). The oxidative

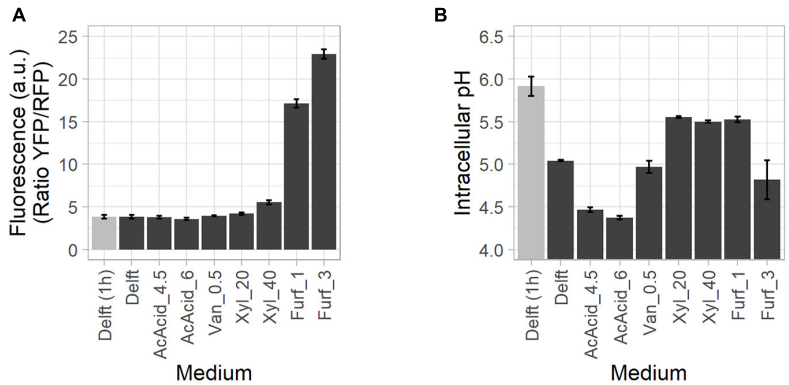

FIGURE 6 | Oxidative stress activation and drop in intracellular pH during growth in the presence of lignocellulosic inhibitors. CEN.PK113-7D cells were grown in the presence of lignocellulose-derived stressors, including acetic acid (AcAcid) at 4.5 and 6 g/L, vanillin (Van), xylose (Xyl) at 20 and 40 g/L, and furfural (Furf) at 1 and 3 g/L. **(A)** Oxidative stress response activation (highest values, in black) assessed with the OxPro biosensor. **(B)** Intracellular pH (lowest values, in black) assessed with the sfpHluorin biosensor. "Delft (1 h)" (in gray) refers to the parameter at 1 h after the onset of screening.

stress response showed moderate activation during exponential growth (**Figure 6A** and **Supplementary Figures 3E, 4E**) while intracellular pH was stable over the growth period (**Figure 6B** and **Supplementary Figures 3F, 4F**).

Capturing and Correlating Physiological Responses in an Industrial Setup

To demonstrate application of the toolbox under typically harsh industrial settings (Deparis et al., 2017), the biosensor-containing strains were tested in synthetic wheat straw hydrolysate (SWSH). Wheat straw is an abundant residue of low commercial value (Talebnia et al., 2010). SWSH was tested in aerobic conditions at 50 and 80% of total compound concentration (**Table 3**) to assess dose-dependent effects. Both laboratory (CEN.PK113-7D) and industrial (Ethanol Red) *S. cerevisiae* were used to highlight differences and similarities in the stress response. SWSH was expected to cause elevated oxidative stress and pronounced redox imbalance due its high furfural, 5-(hydroxymethyl) furfural, and vanillin content (Liu, 2018). At the same time, its production of fermentable (e.g., glucose, mannose, and galactose) and non-fermentable (e.g., xylose and arabinose) sugars was expected to cause moderate osmotic stress (Wang et al., 2013).

As highlighted in previous experiments, intracellular pH and ATP were strictly interconnected in both CEN.PK113-7D and Ethanol Red cells (**Figure 7**). Intracellular pH remained stable if ATP was produced from hexoses or ethanol (**Figures 7A,B**), but its baseline was seen to decrease with increasing harshness of the medium (**Figures 7C,D**). Ribosome production (detected with RibOx) remained generally stable in CEN.PK113-7D in both Delft medium and different types of SWSH (**Figure 8A**). Instead, ribosomes of Ethanol Red cells grown in SWSHs became more abundant during exponential phase, peaked at the diauxic shift, and started to decline thereafter (**Figure 8B**). Even though SWSH50 and SWSH80 were similar, ribosomes remained more numerous in cells grown on SWSH80, probably due to a prolonged diauxic shift, which extended beyond 36 h. The glycolytic flux (detected with GlyOx) in CEN.PK113-7D rose sharply during exponential phase but came to a halt at the beginning of the diauxic shift (**Figure 8C**). In Ethanol Red, the glycolytic flux rose slowly during exponential phase, started declining during the diauxic shift, and stabilized in stationary phase (note that in SWSH80, the diauxic shift was not over at 36 h) (**Figure 8D**). Lastly, the oxidative stress pattern (monitored with GlyOx) differed between the two strains. In CEN.PK113-7D grown in SWSH80, oxidative stress peaked first in lag phase, then decreased, peaked again upon diauxic shift, and stabilized in stationary phase (**Figure 8E**). Oxidative stress in Ethanol Red, instead, kept increasing over time, peaked in exponential phase, and stabilized thereafter at a higher level with respect to the control condition (**Figure 8F**). These differences seen between the two strains might rely on the fact that being an industrial strain, Ethanol Red's stress response is more adapted to face industrial conditions, while laboratory CEN.PK113-7D is not.

DISCUSSION

Bioindustries are constantly on the lookout for more robust and efficient microbial strains. On-line monitoring of physicochemical parameters in bioreactors (e.g., gas exit, pH, oxygen levels, and pressure) and analytical methods for quantifying various compounds already allow for performance estimations. However, tools capable of providing real-time information about the cell physiological or metabolic status are still inadequate. Their development would offer new insights on yeast physiology, thereby improving cell factories and providing new means for monitoring and controlling such processes. To this end, biosensors capable of detecting changing parameters in real time, represent a key resource (Alvarez-Gonzalez and Dixon, 2019).

In this study, we combined five genetically encoded fluorescent biosensors, monitoring intracellular ATP, pH, oxidative stress, ribosome production, and glycolytic flux, into a toolbox. All constructs were created using the MoClo Modular Cloning System Plasmid Kit (Lee et al., 2015), which

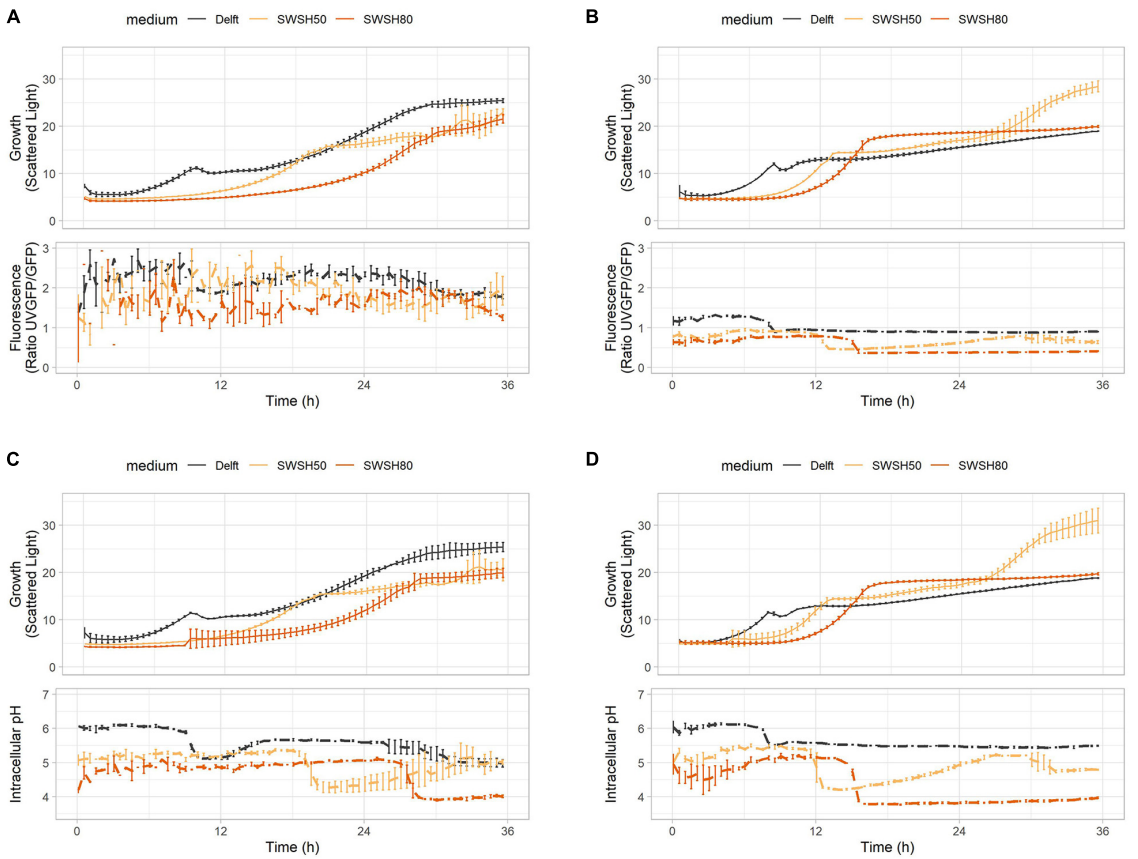

FIGURE 7 | ATP production and intracellular pH during growth in synthetic wheat-straw hydrolysate (SWSH). **(A,B)** Growth curves and ATP concentration for **(A)** CEN.PK113-7D and **(B)** Ethanol Red strains harboring the QUEEN-2m biosensor. **(C,D)** Growth curves and intracellular pH for **(C)** CEN.PK113-7D and **(D)** Ethanol Red strains harboring the sfpHluorin biosensor. Cells were grown in Delft medium (black line), SWSH diluted at 50% with Delft medium (SWSH50; orange line), and SWSH diluted at 80% with Delft medium (SWSH80; red line).

allows for easy implementation of new biosensors (i.e., sensing other parameters) and adjustment of already existing ones (e.g., replacement of fluorescent proteins). A safe-to-use site situated on chromosome X was chosen for genome integration (Mikkelsen et al., 2012), which appeared to be conserved in all tested *S. cerevisiae* strains plus a commercial *S. boulardii* strain (**Figure 2**). For integration, an efficient and marker-free workflow using CRISPR-Cas9 genome editing technology was designed. Such an approach will favor the exploration of natural diversity in *S. cerevisiae* strains collected from nature, whose features might be of interest to the industrial sector. Indeed, the genetic and phenotypic variation in industrial strains has been shown to be low and the implementation of new improved genetic stocks might be the next step for bioindustries (Molinet and Cubillos, 2020). Moreover, we proved that the presence of these biosensors inside the cell did not affect the specific growth rate and yields of key intracellular metabolites (**Tables 4**, **5**), allowing to use the system for quantitative and real-time monitoring.

By combining distinct biosensors in the same cell, we investigated possible correlations between different intracellular parameters. For example, we showed a tight connection between ATP concentration and intracellular pH, as well as followed simultaneously the oxidative stress response and variations in intracellular pH of cells grown in the presence of lignocellulose-specific stressors. Using SWSH-containing medium to mimic industrial conditions, we highlighted how the laboratory CEN.PK113-7D and industrial Ethanol Red *S. cerevisiae* strains responded differently to oxidative stress. In the laboratory strain, the response peaked during lag phase and then decreased over time; whereas in the industrial strain, the peak was seen during exponential growth. Therefore, this toolbox proves to be an instrument to study strain-specific and time-resolved differences in physiological responses. Implementing such multi-sensing tool together with high-throughput technology enables the parallel investigation of the intracellular status in known or newly identified candidate microorganisms. This approach would guide strain characterization ahead of more detailed high-resolution omics studies.

Some limitations of the toolbox remain unsolved. One is the impossibility to combine more than two biosensors in the same cell due to emission/excitation spectral overlap. If single-cell analysis such as flow cytometry is performed, one solution would be the co-culture of strains harboring different biosensor combinations to create a fluorescent footprint. For

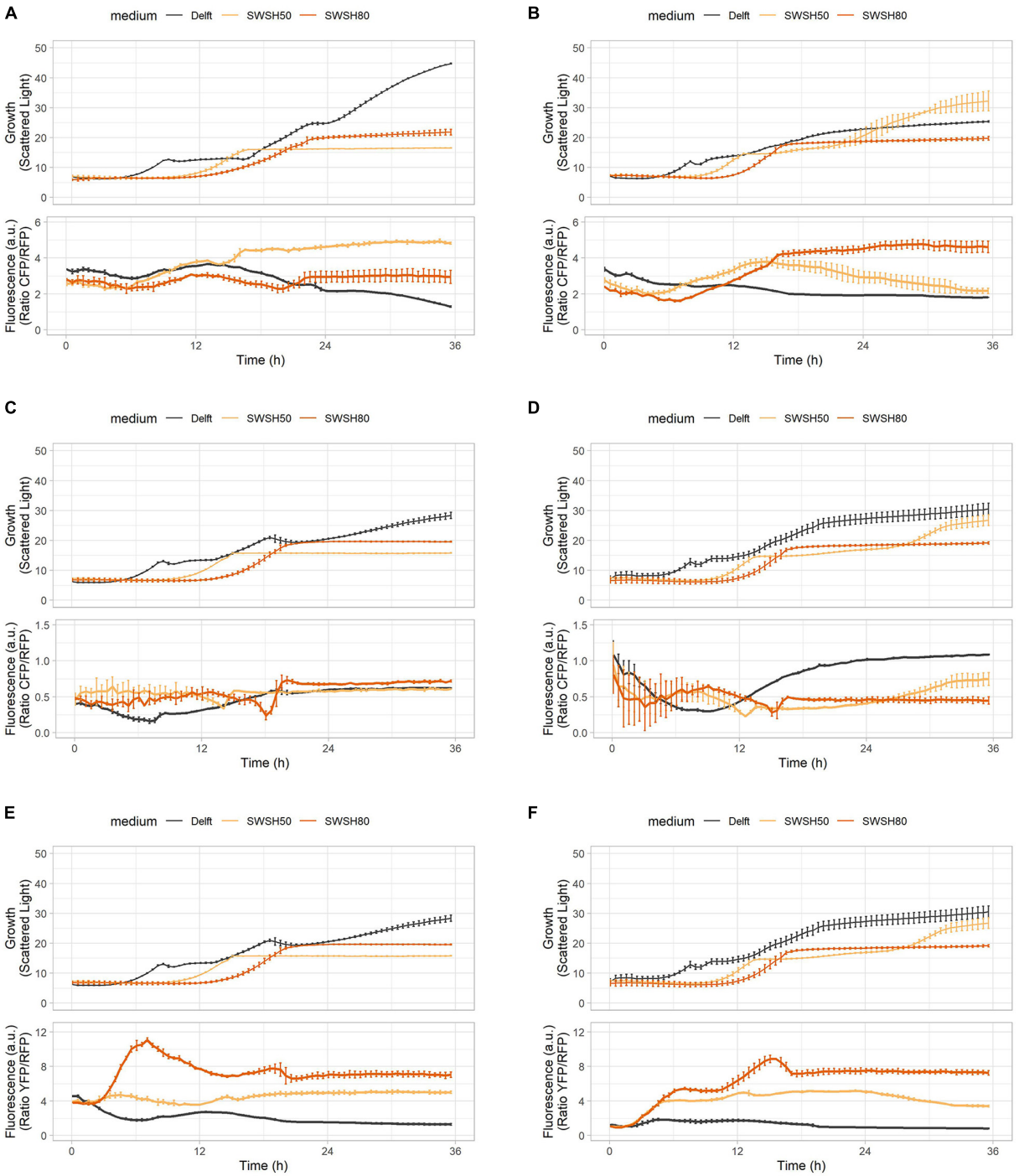

FIGURE 8 | Oxidative stress, ribosome production, and glycolytic flux during growth in synthetic wheat-straw hydrolysate (SWSH). **(A,B)** Growth curves and ribosome production for **(A)** CEN.PK113-7D and **(B)** Ethanol Red strains harboring the RibOx biosensor. **(C,D)** Growth curves and glycolytic flux for **(C)** CEN.PK113-7D and **(D)** Ethanol Red strains harboring the GlyOx biosensor. **(E,F)** Growth curves and oxidative stress for **(E)** CEN.PK113-7D and **(F)** Ethanol Red strains harboring the GlyOx biosensor. Cells were grown in Delft medium (black line), SWSH diluted at 50% with Delft medium (SWSH50; orange line), and SWSH diluted at 80% with Delft medium (SWSH80; red line).

example, by co-culturing strains carrying either sfpHluorin, RibPro or GlyOx, it is possible to first filter mCherry^{-} cells (sfpHluorin) from mCherry^{+} cells (GlyOx and RibPro). Then, among the mCherry^{+} subpopulation, ymYPET^{-} cells (RibPro) can be separated from ymYPET^{+} cells (GlyOx). This strategy would enable the simultaneous detection of

multiple intracellular parameters in the same bioreactor using flow-cytometry. Importantly, as the performance of different strains is not affected by the biosensor, co-culture does not lead to any bias. Real-time monitoring is attractive, but although some high-throughput instruments (such as the BioLector I) allow for detection of growth and fluorescence in real time, such measurements are not implemented in industrial bioreactors. Sampling of cells during the process is still possible, but additional fluorescence-detecting instrumentation, such as a fluorescent microscope or a flow cytometer, as well as subsequent analysis are necessary. Although this problem affects laboratory-scale yeast studies only in a limited way, it can be a stumbling block for industrial applications, where on-line measurements are common for process monitoring and control.

Although only examples and applications of the toolbox in population studies were presented, normalization to an additional fluorescent protein (see section 1.2 of the **Supplementary Material**) enables better single-cell analysis, an area of increasing interest in research and application. For instance, this toolbox could shed a light on unresolved and peculiar phenomena happening in industrial processes, such as the drop in productivity during certain high-gravity fermentations (Koppram et al., 2012) or near-zero growth (Boender et al., 2011; Vos et al., 2016). Moreover, the physicochemical gradients formed during large-volume fermentation processes cause the emergence of subpopulations within the cultures (Wehrs et al., 2019). Even within the same bulk population, different cells might behave differently and possess different characteristics (Heins and Weuster-Botz, 2018). These phenomena are referred to as population heterogeneity (Heins and Weuster-Botz, 2018). For example, flow cytometry studies have highlighted how cells at different growth stages and exposed to a varying external pH, have different intracellular pH and form subpopulations (Valli et al., 2005). Another single-cell study unveiled the increased tolerance to lignocellulosic inhibitors of cell populations harvested in early-stationary phase (Narayanan et al., 2017). Bioreactor subpopulations have been studied thanks to the use of propidium iodide and a fluorescent reporter expressed under the promoter of the ribosomal gene RPL22A, whose transcription has shown to be correlated with cell growth (Carlquist et al., 2012; Delvigne et al., 2015). Microfluidic devices and product biosensors revealed different production phases and subpopulations during *L*-valine generation in bacteria (Mustafi et al., 2014). The study focused on the subpopulations arising during bioprocesses can be the key to improve consistency of existing bioprocesses, understand and implement new robustness features, and direct the next generation of cell factories.

The here presented toolbox offers two main opportunities. First, it allows for the investigation and the acquisition of a deeper knowledge on the intracellular state of cells during bioprocesses. Second, it has the potential to be a tool for monitor of industrial bioproduction processes, especially when coupled with biosensors able to detect the desired product (Marsafari et al., 2020; Zhang and Shi, 2021). The easy implementations into the toolbox of newly developed or already-existing biosensors able to sense additional intracellular parameters of interest would further promote the comprehension of microbial behaviors in such processes. For instance, a recently developed biosensor able to detect the unfolded protein response might be useful in the development of the new generation of yeast expressing heterologous proteins (Peng et al., 2021). The design of the YAP1-based biosensor for oxidative stress has been improved and showed potential applications also in the probiotic yeast *S. boulardii* (Dacquay and McMillen, 2021). Acid stress resulting from acids in the substrates and/or products used in bioindustries can be sensed with HAA1-based or acid-responsive-promoter-based biosensors and used for screening new acetic-acid-producing strains (Hahne et al., 2021; Mormino et al., 2021). New condition-specific biosensors can be developed thanks to the use of yeast native promoters (Xiong et al., 2018). Therefore, future studies using biosensors should focus both on the single-cell aspect and on the performance comparison of industrially relevant and newly isolated strains in different substrates and conditions to point out robustness features.

DATA AVAILABILITY STATEMENT

The datasets presented in this study can be found in online repositories. The names of the repository/repositories and accession number(s) can be found below: https://www.addgene.org, 177705–177712.

AUTHOR CONTRIBUTIONS

LT performed the experiments and wrote the manuscript. LO and PR supervised and contributed for the discussion of the collected data. All authors conceived the study and contributed for the correction of the manuscript prior submission.

FUNDING

The present study was supported by the Novo Nordisk Foundation grant DISTINGUISHED INVESTIGATOR 2019—Research within biotechnology-based synthesis and production (Grant No. 0055044).

ACKNOWLEDGMENTS

The *S. cerevisiae* Ethanol Red strain was kindly provided by Société Industrielle Lesaffre, Division Leaf. We thank Cecilia Trivellin for help with the synthetic hydrolysate composition and Prof. Matthias Heinemann for fruitful discussions.

SUPPLEMENTARY MATERIAL

The Supplementary Material for this article can be found online at: https://www.frontiersin.org/articles/10.3389/fmicb.2021.802169/full#supplementary-material

REFERENCES

Akhmetov, A., Laurent, J., Gollihar, J., Gardner, E., Garge, R., Ellington, A., et al. (2018). Single-step precision genome editing in yeast using CRISPR-Cas9. *Bio Protoc.* 8:2765.

Almeida, J. R., Modig, T., Petersson, A., Hähn-Hägerdal, B., Lidén, G., and Gorwa-Grauslund, M. F. (2007). Increased tolerance and conversion of inhibitors in lignocellulosic hydrolysates by *Saccharomyces cerevisiae*. *J. Chem. Technol. Biotechnol.* 82, 340–349.

Alvarez-Gonzalez, G., and Dixon, N. (2019). Genetically encoded biosensors for lignocellulose valorization. *Biotechnol. Biofuels* 121, 1–14. doi: 10.1186/s13068-019-1585-6

Baganz, F., Hayes, A., Marren, D., Gardner, D. C. J., and Oliver, S. G. (1997). Suitability of replacement markers for functional analysis studies in *Saccharomyces cerevisiae*. *Yeast* 13, 1563–1573. doi: 10.1002/(SICI)1097-0061(199712)13:16<1563::AID-YEA240>3.0.CO;2-6

Balaban, R. S., Nemoto, S., and Finkel, T. (2005). Mitochondria, oxidants, and aging. *Cell* 120, 483–495. doi: 10.1016/j.cell.2005.02.001

Baroi, G. N., Skiadas, I. V., Westermann, P., and Gavala, H. N. (2015). Continuous fermentation of wheat straw hydrolysate by *Clostridium tyrobutyricum* with in-situ acids removal. *Waste Biomass Valorization* 63, 317–326. doi: 10.1007/s12649-015-9348-5

Baumann, L., Bruder, S., Kabisch, J., Boles, E., and Oreb, M. (2021). High-Throughput screening of an octanoic acid producer strain library enables detection of new targets for increasing titers in *Saccharomyces cerevisiae*. *ACS Synth. Biol.* 10, 1077–1086. doi: 10.1021/acssynbio.0c00600

Boender, L. G. M., van Maris, A. J. A., de Hulster, E. A. F., Almering, M. J. H., van der Klei, I. J., Veenhuis, M., et al. (2011). Cellular responses of *Saccharomyces cerevisiae* at near-zero growth rates: transcriptome analysis of anaerobic retentostat cultures. *FEMS Yeast Res.* 11, 603–620. doi: 10.1111/j.1567-1364.2011.00750.x

Botman, D., de Groot, D. H., Schmidt, P., Goedhart, J., and Teusink, B. (2019). In vivo characterisation of fluorescent proteins in budding yeast. *Sci. Rep* 9:2234. doi: 10.1038/s41598-019-38913-z

Cámara, E., Lenitz, I., and Nygård, Y. (2020). A CRISPR activation and interference toolkit for industrial *Saccharomyces cerevisiae* strain KE6-12. *Sci. Rep*. 10:14605. doi: 10.1038/s41598-020-71648-w

Carlquist, M., Fernandes, R. L., Helmark, S., Heins, A. L., Lundin, L., Sørensen, S. J., et al. (2012). Physiological heterogeneities in microbial populations and implications for physical stress tolerance. *Microb. Cell Fact.* 11:94. doi: 10.1186/1475-2859-11-94

Carpenter, A. C., Paulsen, I. T., and Williams, T. C. (2018). Blueprints for biosensors: design, limitations, and applications. *Genes (Basel).* 9:375. doi: 10.3390/genes9080375

Cliften, P. F., Hillier, L. W., Fulton, L., Graves, T., Miner, T., Gish, W. R., et al. (2001). Surveying *Saccharomyces* genomes to identify functional elements by comparative DNA sequence analysis. *Genome Res.* 11, 1175–1186. doi: 10.1101/gr.182901

Cunha, J. T., Romaní, A., Costa, C. E., Sá-Correia, I., and Domingues, L. (2019). Molecular and physiological basis of *Saccharomyces cerevisiae* tolerance to adverse lignocellulose-based process conditions. *Appl. Microbiol. Biotechnol.* 103, 159–175. doi: 10.1007/s00253-018-9478-3

da Conceição, L. E. F. R., Saraiva, M. A. F., Diniz, R. H. S., Oliveira, J., Barbosa, G. D., Alvarez, F., et al. (2015). Biotechnological potential of yeast isolates from cachaça: the Brazilian spirit. *J. Ind. Microbiol. Biotechnol.* 42, 237–246. doi: 10.1007/s10295-014-1528-y

Dacquay, L. C., and McMillen, D. R. (2021). Improving the design of an oxidative stress sensing biosensor in yeast. *FEMS Yeast Res.* 21:25. doi: 10.1093/femsyr/foab025

Delvigne, F., Baert, J., Gofflot, S., Lejeune, A., Telek, S., Johanson, T., et al. (2015). Dynamic single-cell analysis of *Saccharomyces cerevisiae* under process perturbation: comparison of different methods for monitoring the intensity of population heterogeneity. *J. Chem. Technol. Biotechnol.* 90, 314–323.

Demain, A. L. (2000). Microbial biotechnology. *Trends Biotechnol.* 18, 26–31.

Deparis, Q., Claes, A., Foulquié-Moreno, M. R., and Thevelein, J. M. (2017). Engineering tolerance to industrially relevant stress factors in yeast cell factories. *FEMS Yeast Res.* 17:fox036. doi: 10.1093/femsyr/fox036

Entian, K. D., and Kötter, P. (2007). 25 yeast genetic strain and plasmid collections. *Methods Microbiol.* 36, 629–666.

Estruch, F. (2000). Stress-controlled transcription factors, stress-induced genes and stress tolerance in budding yeast. *FEMS Microbiol. Rev.* 24, 469–486. doi: 10.1111/j.1574-6976.2000.tb00551.x

Francois, J. M., Alkim, C., and Morin, N. (2020). Engineering microbial pathways for production of bio-based chemicals from lignocellulosic sugars: current status and perspectives. *Biotechnol. Biofuels* 131, 1–23. doi: 10.1186/s13068-020-01744-6

Gietz, R. D. (2014). Yeast transformation by the LiAc/SS carrier DNA/PEG method. *Methods Mol. Biol.* 313, 107–120.

Gonskikh, Y., and Polacek, N. (2017). Alterations of the translation apparatus during aging and stress response. *Mech. Ageing Dev.* 168, 30–36. doi: 10.1016/j.mad.2017.04.003

Guldfeldt, L. U., and Arneborg, N. (1998). Measurement of the effects of acetic acid and extracellular ph on intracellular ph of nonfermenting, individual *Saccharomyces cerevisiae* cells by fluorescence microscopy. *Appl. Environ. Microbiol.* 64:530. doi: 10.1128/AEM.64.2.530-534.1998

Hahne, K., Rödel, G., and Ostermann, K. (2021). A fluorescence-based yeast sensor for monitoring acetic acid. *Eng. Life Sci.* 21, 303–313. doi: 10.1002/elsc.202000006

Heins, A. L., and Weuster-Botz, D. (2018). Population heterogeneity in microbial bioprocesses: origin, analysis, mechanisms, and future perspectives. *Bioprocess Biosyst. Eng.* 41, 889–916. doi: 10.1007/s00449-018-1922-3

Higuchi-Sanabria, R., Garcia, E. J., Tomoiaga, D., Munteanu, E. L., Feinstein, P., and Pon, L. A. (2016). Characterization of fluorescent proteins for three- and four-color live-cell imaging in *S. cerevisiae*. *PLoS One* 11:e0146120. doi: 10.1371/journal.pone.0146120

Isom, D. G., Page, S. C., Collins, L. B., Kapolka, N. J., Taghon, G. J., and Dohlman, H. G. (2018). Coordinated regulation of intracellular pH by two glucose-sensing pathways in yeast. *J. Biol. Chem.* 293, 2318–2329. doi: 10.1074/jbc.RA117.000422

Janssens, G. E., and Veenhoff, L. M. (2016). The natural variation in lifespans of single yeast cells is related to variation in cell size, ribosomal protein, and division time. *PLoS One* 11:e0167394. doi: 10.1371/journal.pone.0167394

Kampranis, S. C., and Makris, A. M. (2012). Developing A yeast cell factory for the production of Terpenoids. *Comput. Struct. Biotechnol. J.* 3:e201210006. doi: 10.5936/csbj.201210006

Khatri, I., Tomar, R., Ganesan, K., Prasad, G. S., and Subramanian, S. (2017). Complete genome sequence and comparative genomics of the probiotic yeast *Saccharomyces boulardii*. *Sci. Rep*. 71:371. doi: 10.1038/s41598-017-00414-2

Ko, J. K., Enkh-Amgalan, T., Gong, G., Um, Y., and Lee, S.-M. (2020). Improved bioconversion of lignocellulosic biomass by *Saccharomyces cerevisiae* engineered for tolerance to acetic acid. *GCB Bioenergy* 12, 90–100. doi: 10.1111/gcbb.12656

Koppram, R., Albers, E., and Olsson, L. (2012). Evolutionary engineering strategies to enhance tolerance of xylose utilizing recombinant yeast to inhibitors derived from spruce biomass. *Biotechnol. Biofuels* 51, 1–12. doi: 10.1186/1754-6834-5-32

Labun, K., Montague, T. G., Krause, M., Torres Cleuren, Y. N., Tjeldnes, H., and Valen, E. (2019). CHOPCHOP v3: expanding the CRISPR web toolbox beyond genome editing. *Nucleic Acids Res.* 47, W171–W174. doi: 10.1093/nar/gkz365

Leavitt, J. M., Wagner, J. M., Tu, C. C., Tong, A., Liu, Y., and Alper, H. S. (2017). Biosensor-Enabled directed evolution to improve muconic acid production in *Saccharomyces cerevisiae*. *Biotechnol. J.* 12:687, doi: 10.1002/biot.201600687

Lee, M. E., DeLoache, W. C., Cervantes, B., and Dueber, J. E. (2015). A highly characterized yeast toolkit for modular, multipart assembly. *ACS Synth. Biol.* 4, 975–986. doi: 10.1021/sb500366v

Liti, G. (2015). The fascinating and secret wild life of the budding yeast S. cerevisiae. *Elife* 4:e05835. doi: 10.7554/eLife.05835

Liu, C.-G., Li, K., Li, K.-Y., Sakdaronnarong, C., Mehmood, M. A., Zhao, X.-Q., et al. (2020). Intracellular redox perturbation in *Saccharomyces cerevisiae* improved furfural tolerance and enhanced cellulosic bioethanol production. *Front. Bioeng. Biotechnol.* 8:615. doi: 10.3389/fbioe.2020.00615

Liu, H., Wei, Z., Dominguez, A., Li, Y., Wang, X., and Qi, L. S. (2015). CRISPR-ERA: a comprehensive design tool for CRISPR-mediated gene editing, repression and activation. *Bioinformatics* 31, 3676–3678. doi: 10.1093/bioinformatics/btv423

Liu, Z. L. L. (2018). Understanding the tolerance of the industrial yeast *Saccharomyces cerevisiae* against a major class of toxic aldehyde compounds. *Appl. Microbiol. Biotechnol.* 102, 5369–5390. doi: 10.1007/s00253-018-8993-6

López-Abelairas, M., Lu-Chau, T. A., and Lema, J. M. (2013). Fermentation of Biologically pretreated wheat straw for ethanol production: comparison of fermentative microorganisms and process configurations. *Appl. Biochem. Biotechnol.* 1708, 1838–1852. doi: 10.1007/s12010-013-0318-8

Maicas, S. (2020). The role of yeasts in fermentation processes. *Microorganisms* 8, 1–8.

Marsafari, M., Ma, J., Koffas, M., and Xu, P. (2020). Genetically-encoded biosensors for analyzing and controlling cellular process in yeast. *Curr. Opin. Biotechnol.* 64, 175–182. doi: 10.1016/j.copbio.2020.04.006

Mikkelsen, M. D., Buron, L. D., Salomonsen, B., Olsen, C. E., Hansen, B. G., Mortensen, U. H., et al. (2012). Microbial production of indolylglucosinolate through engineering of a multi-gene pathway in a versatile yeast expression platform. *Metab. Eng.* 14, 104–111.

Molinet, J., and Cubillos, F. A. (2020). Wild yeast for the future: exploring the use of wild strains for wine and beer fermentation. *Front. Genet.* 11:1281. doi: 10.3389/fgene.2020.589350

Moré, M. I., and Swidsinski, A. (2015). *Saccharomyces boulardii* CNCM I-745 supports regeneration of the intestinal microbiota after diarrheic dysbiosis-a review. *Clin. Exp. Gastroenterol.* 8:237. doi: 10.2147/CEG.S85574

Mormino, M., Siewers, V., and Nygård, Y. (2021). Development of an Haa1-based biosensor for acetic acid sensing in *Saccharomyces cerevisiae*. *FEMS Yeast Res.* 21:49. doi: 10.1093/femsyr/foab049

Mortimer, R. K., and Johnston, J. R. (1986). Genealogy of principal strains of the yeast genetic stock center. *Genetics* 113:35. doi: 10.1093/genetics/113.1.35

Mustafi, N., Grünberger, A., Mahr, R., Helfrich, S., Nöh, K., Blombach, B., et al. (2014). Application of a genetically encoded biosensor for live cell imaging of l-valine production in pyruvate dehydrogenase complex-deficient Corynebacterium glutamicum Strains. *PLoS One* 9:e85731. doi: 10.1371/journal.pone.0085731

Narayanan, V., Schelin, J., Gorwa-Grauslund, M., van Niel, E. W., and Carlquist, M. (2017). Increased lignocellulosic inhibitor tolerance of *Saccharomyces cerevisiae* cell populations in early stationary phase. *Biotechnol. Biofuels* 101:114. doi: 10.1186/s13068-017-0794-0

Nygård, Y., Maaheimo, H., Mojzita, D., Toivari, M., Wiebe, M., Resnekov, O., et al. (2014). Single cell and in vivo analyses elucidate the effect of xylC lactonase during production of D-xylonate in *Saccharomyces cerevisiae*. *Metab. Eng.* 25, 238–247. doi: 10.1016/j.ymben.2014.07.005

Ortega, A. D., Takhaveev, V., Bonsing-Vedelaar, S., Long, Y., Mestre-Farràs, N., Incarnato, D., et al. (2020). A synthetic RNA-based biosensor for fructose-1,6-bisphosphate that reports glycolytic flux. *bioRxiv* [Preprint]. doi: 10.1101/2020.10.11.335109

Ortega, A. D., Takhaveev, V., Vedelaar, S. R., Long, Y., Mestre-Farràs, N., Incarnato, D., et al. (2021). A synthetic RNA-based biosensor for fructose-1,6-bisphosphate that reports glycolytic flux. *Cell Chem. Biol.* 28, 1554.e8–1568.e8. doi: 10.1016/j.chembiol.2021.04.006

Pampulha, M. E., and Loureiro-Dias, M. C. (1989). Combined effect of acetic acid, pH and ethanol on intracellular pH of fermenting yeast. *Appl. Microbiol. Biotechnol.* 315, 547–550.

Parapouli, M., Vasileiadis, A., Afendra, A.-S., and Hatziloukas, E. (2020). *Saccharomyces cerevisiae* and its industrial applications. *AIMS Microbiol.* 6:1. doi: 10.3934/microbiol.2020001

Peng, K., Kroukamp, H., Pretorius, I. S., and Paulsen, I. T. (2021). Yeast synthetic minimal biosensors for evaluating protein production. *ACS Synth. Biol.* 10, 1640–1650. doi: 10.1021/acssynbio.0c00633

Pfeiffer, T., and Morley, A. (2014). An evolutionary perspective on the Crabtree effect. *Front. Mol. Biosci.* 1:17. doi: 10.3389/fmolb.2014.00017

Pham, T., Wimalasena, T., Box, W. G., Koivuranta, K., Storgårds, E., Smart, K. A., et al. (2011). Evaluation of ITS PCR and RFLP for differentiation and identification of brewing yeast and brewery 'wild' yeast contaminants. *J. Inst. Brewing.* 117:556. doi: 10.1002/j.2050-0416.2011.tb00504.x

Purwadi, R., Brandberg, T., and Taherzadeh, M. J. (2007). A possible industrial solution to ferment lignocellulosic hydrolyzate to ethanol: continuous cultivation with flocculating yeast. *Int. J. Mol. Sci.* 8, 920–932. doi: 10.3390/i8090920

R Core Team (2020). *R: A Language and Environment for Statistical Computing*.

Raman, S., Rogers, J. K., Taylor, N. D., and Church, G. M. (2014). Evolution-guided optimization of biosynthetic pathways. *Proc. Natl. Acad. Sci. U.S.A.* 111, 17803–17808. doi: 10.1073/pnas.1409523111

Raschke, W. C., Kern, K. A., Antalis, C., and Ballou, C. E. (1973). Genetic control of yeast mannan structure: isolation and characterization of mannan mutants. *J. Biol. Chem.* 248, 4660–4666. doi: 10.1016/s0021-9258(19)43714-9

Reifenrath, M., and Boles, E. (2018). A superfolder variant of pH-sensitive pHluorin for in vivo pH measurements in the endoplasmic reticulum. *Sci. Rep.* 8:11985. doi: 10.1038/s41598-018-30367-z

Rogers, J. K., Guzman, C. D., Taylor, N. D., Raman, S., Anderson, K., and Church, G. M. (2015). Synthetic biosensors for precise gene control and real-time monitoring of metabolites. *Nucleic Acids Res.* 43, 7648–7660. doi: 10.1093/nar/gkv616

Roy, B., Granas, D., Bragg, F., Cher, J. A. Y., White, M. A., and Stormo, G. D. (2020). Autoregulation of yeast ribosomal proteins discovered by efficient search for feedback regulation. *Commun. Biol.* 31, 1–9. doi: 10.1038/s42003-020-01494-z

Seidman, C. E., and Struhl, K. (1998). Introduction of plasmid DNA into cells. *Curr. Protoc. Neurosci.* 13, A.4D.1–A.4D.2. doi: 10.1002/0471140864.psa04ds13

Sharma, R., Garg, P., Kumar, P., Bhatia, S. K., and Kulshrestha, S. (2020). Microbial fermentation and its role in quality improvement of fermented foods. *Ferment* 6, 106–106. doi: 10.1007/s00253-013-5146-9

Shinoda, H., Shannon, M., and Nagai, T. (2018). Fluorescent proteins for investigating biological events in acidic environments. *Int. J. Mol. Sci.* 19:1548. doi: 10.3390/ijms19061548

Sjulander, N., and Kikas, T. (2020). Origin, impact and control of lignocellulosic inhibitors in bioethanol production-a review. *Energies* 13:4751. doi: 10.3390/en13184751

Smith, J. D., Suresh, S., Schlecht, U., Wu, M., Wagih, O., Peltz, G., et al. (2016). Quantitative CRISPR interference screens in yeast identify chemical-genetic interactions and new rules for guide RNA design. *Genome Biol.* 17:45. doi: 10.1186/s13059-016-0900-9

Steele, S. D., and Miller, J. J. (1974). Pseudomycelium development and sporulation in *Saccharomyces fragilis*. *Can. J. Microbiol.* 20, 265–267. doi: 10.1139/m74-042

Steffen, K. K., MacKay, V. L., Kerr, E. O., Tsuchiya, M., Hu, D., Fox, L. A., et al. (2008). Yeast lifespan extension by depletion of 60S ribosomal subunits is mediated by Gcn4. *Cell* 133:292. doi: 10.1016/j.cell.2008.02.037

Suh, S. O., Gujjari, P., Beres, C., Beck, B., and Zhou, J. (2013). Proposal of *Zygosaccharomyces parabailii sp. nov.* and *Zygosaccharomyces pseudobailii sp. nov.*, novel species closely related to *Zygosaccharomyces bailii*. *Int. J. Syst. Evol. Microbiol.* 63, 1922–1929. doi: 10.1099/ijs.0.048058-0

Swinnen, S., Henriques, S. F., Shrestha, R., Ho, P. W., Sá-Correia, I., and Nevoigt, E. (2017). Improvement of yeast tolerance to acetic acid through Haa1 transcription factor engineering: towards the underlying mechanisms. *Microb. Cell Fact.* 16:7.

Takaine, M., Ueno, M., Kitamura, K., Imamura, H., and Yoshida, S. (2019). Reliable imaging of ATP in living budding and fission yeast. *J. Cell Sci.* 132:jcs230649. doi: 10.1242/jcs.230649

Talebnia, F., Karakashev, D., and Angelidaki, I. (2010). Production of bioethanol from wheat straw: an overview on pretreatment, hydrolysis and fermentation. *Bioresour. Technol.* 101, 4744–4753. doi: 10.1016/j.biortech.2009.11.080

Ullah, A., Orij, R., Brul, S., and Smits, G. J. (2012). Quantitative analysis of the modes of growth inhibition by weak organic acids in *Saccharomyces cerevisiae*. *Appl. Environ. Microbiol.* 78, 8377–8387. doi: 10.1128/AEM.02126-12

Valli, M., Sauer, M., Branduardi, P., Borth, N., Porro, D., and Mattanovich, D. (2005). Intracellular pH distribution in *Saccharomyces cerevisiae* cell populations, analyzed by flow cytometry. *Appl. Environ. Microbiol.* 71, 1515–1521. doi: 10.1128/AEM.71.3.1515-1521.2005

van Dijk, M., Erdei, B., Galbe, M., Nygård, Y., and Olsson, L. (2019). Strain-dependent variance in short-term adaptation effects of two xylose-fermenting strains of *Saccharomyces cerevisiae*. *Bioresour. Technol.* 292:121922. doi: 10.1016/j.biortech.2019.121922

Vos, T., Hakkaart, X. D. V., de Hulster, E. A. F., van Maris, A. J. A., Pronk, J. T., and Daran-Lapujade, P. (2016). Maintenance-energy requirements and robustness of Saccharomyces cerevisiae at aerobic near-zero specific growth rates. *Microb. Cell Fact.* 151, 1–20. doi: 10.1186/s12934-016-0501-z

Wang, G., Øzmerih, S., Guerreiro, R., Meireles, A. C., Carolas, A., Milne, N., et al. (2020). Improvement of cis, cis-muconic acid production in *Saccharomyces*

cerevisiae through biosensor-aided genome engineering. *ACS Synth. Biol.* 9, 634–646. doi: 10.1021/acssynbio.9b00477

Wang, L., Zhao, X.-Q., Xue, C., and Bai, F.-W. (2013). Impact of osmotic stress and ethanol inhibition in yeast cells on process oscillation associated with continuous very-high-gravity ethanol fermentation. *Biotechnol. Biofuels* 61, 1–10. doi: 10.1186/1754-6834-6-133

Wehrs, M., Tanjore, D., Eng, T., Lievense, J., Pray, T. R., and Mukhopadhyay, A. (2019). Engineering robust production microbes for large-scale cultivation. *Trends Microbiol.* 27, 524–537. doi: 10.1016/j.tim.2019.01.006

Xiong, L., Zeng, Y., Tang, R. Q., Alper, H. S., Bai, F. W., and Zhao, X. Q. (2018). Condition-specific promoter activities in *Saccharomyces cerevisiae*. *Microb. Cell Fact.* 17:58. doi: 10.1186/s12934-018-0899-6

Yaginuma, H., Kawai, S., Tabata, K. V., Tomiyama, K., Kakizuka, A., Komatsuzaki, T., et al. (2014). Diversity in ATP concentrations in a single bacterial cell population revealed by quantitative single-cell imaging. *Sci. Rep.* 4:6522. doi: 10.1038/srep06522

Zhang, J., Sonnenschein, N., Pihl, T. P. B., Pedersen, K. R., Jensen, M. K., and Keasling, J. D. (2016). Engineering an NADPH/NADP+ Redox Biosensor in Yeast. *ACS Synth. Biol.* 5, 1546–1556. doi: 10.1021/acssynbio.6b00135

Zhang, Y., and Shi, S. (2021). Transcription factor-based biosensor for dynamic control in yeast for natural product synthesis. *Front. Bioeng. Biotechnol.* 9:635265. doi: 10.3389/fbioe.2021.635265

Zhu, J., Zhang, Z.-T., Tang, S.-W., Zhao, B.-S., Li, H., Song, J.-Z., et al. (2019). A validated set of fluorescent-protein-based markers for major organelles in yeast (*Saccharomyces cerevisiae*). *MBio* 10:e01691–e01719. doi: 10.1128/mBio.01691-19

Conflict of Interest: PR has financial interests in Enduro Genetics ApS.

The remaining authors declare that the research was conducted in the absence of any commercial or financial relationships that could be construed as a potential conflict of interest.

Publisher's Note: All claims expressed in this article are solely those of the authors and do not necessarily represent those of their affiliated organizations, or those of the publisher, the editors and the reviewers. Any product that may be evaluated in this article, or claim that may be made by its manufacturer, is not guaranteed or endorsed by the publisher.

frontiers in Microbiology

ORIGINAL RESEARCH
published: 17 January 2022
doi: 10.3389/fmicb.2021.803307

Use of Transposon Directed Insertion-Site Sequencing to Probe the Antibacterial Mechanism of a Model Honey on *E. coli* K-12

*Maria Masoura[1,2], Mathew T. Milner[2], Tim W. Overton[1], Konstantinos Gkatzionis[1,3] and Peter A. Lund[2]**

[1] School of Chemical Engineering, University of Birmingham, Birmingham, United Kingdom, [2] Institute of Microbiology and Infection (IMI), University of Birmingham, Birmingham, United Kingdom, [3] Department of Food Science and Nutrition, School of the Environment, University of the Aegean, Lemnos, Greece

OPEN ACCESS

Edited by:
Patrick Eichenberger, New York University, United States

Reviewed by:
Juraj Majtan, Independent Researcher, Bratislava, Slovakia
Elizabeth Harry, University of Technology Sydney, Australia

***Correspondence:**
Peter A. Lund
p.a.lund@bham.ac.uk

Specialty section:
This article was submitted to Microbial Physiology and Metabolism, a section of the journal Frontiers in Microbiology

Received: *27 October 2021*
Accepted: *19 November 2021*
Published: *17 January 2022*

Citation:
Masoura M, Milner MT, Overton TW, Gkatzionis K and Lund PA (2022) Use of Transposon Directed Insertion-Site Sequencing to Probe the Antibacterial Mechanism of a Model Honey on E. coli K-12. Front. Microbiol. 12:803307. doi: 10.3389/fmicb.2021.803307

Antimicrobial resistance is an ever-growing health concern worldwide that has created renewed interest in the use of traditional anti-microbial treatments, including honey. However, understanding the underlying mechanism of the anti-microbial action of honey has been hampered due to the complexity of its composition. High throughput genetic tools could assist in understanding this mechanism. In this study, the anti-bacterial mechanism of a model honey, made of sugars, hydrogen peroxide, and gluconic acid, was investigated using genome-wide transposon mutagenesis combined with high-throughput sequencing (TraDIS), with the strain *Escherichia coli* K-12 MG1655 as the target organism. We identified a number of genes which when mutated caused a severe loss of fitness when cells were exposed to the model honey. These genes encode membrane proteins including those involved in uptake of essential molecules, and components of the electron transport chain. They are enriched for pathways involved in intracellular homeostasis and redox activity. Genes involved in assembly and activity of formate dehydrogenase O (FDH-O) were of particular note. The phenotypes of mutants in a subset of the genes identified were confirmed by phenotypic screening of deletion strains. We also found some genes which when mutated led to enhanced resistance to treatment with the model honey. This study identifies potential synergies between the main honey stressors and provides insights into the global antibacterial mechanism of this natural product.

Keywords: TraDIS, genome wide mutagenesis, flow cytometry, antimicrobial, mechanism, model, honey

INTRODUCTION

The use of honey to treat infections dates back several millennia, and with the growing global threat of AMR, natural products such as honey are being explored as alternatives to antibiotics. Although the antimicrobial activity of various honeys has been extensively studied, to date the mechanisms by which honey acts are still not fully understood (Albaridi, 2019). The high variability of honey

composition makes it difficult to draw general conclusions about mechanisms, and it is likely that the effects of honey arise from synergistic interactions between several different components (Brudzynski and Sjaarda, 2021). A fuller understanding of the antibacterial mechanism of honey would be helpful in promoting the acceptance of this product as an alternative form of antimicrobial treatment and could also enable the development of standardized model honeys and medicinal honey formulations.

Regardless of the physicochemical variability between different honeys, enzymatic conversion of glucose to gluconate and hydrogen peroxide (H_2O_2) is believed to have a major role in the antimicrobial activity of honey (Brudzynski et al., 2017; Brudzynski, 2020; Masoura et al., 2020). This is mediated upon honey dilution by the bee-derived enzyme glucose oxidase (GOx). Both gluconic acid and H_2O_2 act as antibacterial/antifungal agents (Bucekova et al., 2014). Other phytochemical components (e.g., antimicrobial peptides, polyphenols, transition metals etc.), and acidity, all of which vary depending on the floral source of the nectar, can enhance the antimicrobial strength of different honeys (Sindi et al., 2019). The autooxidation of polyphenols in the presence of transition metals such as Fe (II) and Cu (I) can further enhance the production of H_2O_2. Also, a high correlation was found between honey color, polyphenols and/or total flavonoids, minerals and the acidity of honey. The binding of metal and protein to polyphenols increases in acidic conditions. Polyphenols can be involved in binding of proteins, carbohydrates, and lipids of bacterial cell membranes, which then exerts antibiofilm forming activity and inhibition of bacterial growth (Sindi et al., 2019). Thus, darker honeys (e.g., from buckwheat pollen), which are usually more abundant in polyphenol content, demonstrate higher antimicrobial activity. These honeys also usually result in a higher concentration of H_2O_2 upon dilution, which increases the generation of hydroxyl radicals (Bucekova et al., 2018; Brudzynski, 2020).

The damage caused by different kinds of model honey including model honeys has been further studied using a range of methods including microscopy (TEM, SEM), flow cytometry (FC), and screening of single gene knockouts. TEM micrographs showed enlargement of both Gram-negative and Gram-positive bacteria which might be due to partial disruption or degradation of the cell wall, which in turn could lead to the formation of spheroplasts, cell lysis and cytoplasmic leakage (Nishio et al., 2016). Two types of H_2O_2-producing acacia honeys were reported to significantly reduce the viability of *H. influenzae* (Newby et al., 2018) and enterohemorrhagic *Escherichia coli* O157:H7 biofilm (Lee et al., 2011). Transcriptome analysis, in the second of these studies, showed that exposure to polyfloral, clover, and acacia honey significantly repressed the expression of curli, quorum sensing and virulence genes in *E. coli* O157:H7 (in *E. coli* phylogroup E). A separate study using qPCR of selected genes in exponential-growing *E. coli* Crooks ATCC 8739 (which like *E. coli* K-12 is in phylogroup A) exposed to clover, citrus, and marjoram honey gave similar results, showing particularly strong down-regulation of *tnaA*, the gene for indole biosynthesis; indole plays a signaling role in biofilm formation (Wasfi et al., 2016). SEM and FC showed that exposure of *E. coli* ATCC 14948 (also in phylogroup A) to natural multifloral unpasteurized honey disrupted the cell wall and caused filamentation, filament lysis, formation of spheroplasts and eventually cell lysis (Brudzynski and Sjaarda, 2014). These findings were recently confirmed in our study which also revealed that H_2O_2-producing honey compromises membrane polarity and integrity, an effect which is caused by the synergy of oxidative, acid and osmotic stress. We also identified significantly greater sensitivity to model honey (composed of sugars, gluconic acid, and H_2O_2) of catalase mutants (i.e., Δ*katE* and Δ*katG*) (Masoura et al., 2020). Transcriptome analysis of the effects of manuka honey on *Pseudomonas aeruginosa* showed synergies between different components, with effects on genes involved with the SOS response, oxidative damage, and maintenance of the proton motive force, among others (Bouzo et al., 2020).

Gene knockout screening is a useful tool to identify molecular targets of antimicrobials of known composition, but is challenging in the case of honey, due to its complexity in composition and the synergies between honey innate components that exert antibacterial activity. The use of a chemically defined model honey should allow to clarify the roles of the most abundant antimicrobial components and the interactions between them. We wished to understand the contribution of different genes to the overall ability of a given organism to survive a sub-lethal exposure to model honey, as this could aid in identifying which proteins and cellular pathways are the targets of the H_2O_2-producing honey. Here, we applied transposon directed insertion-site sequencing (TraDIS) to identify the genes with a role in resistance or susceptibility of *E. coli* K-12 MG1655 to stress caused by a model honey, as described in our previous work (Masoura et al., 2020). This model honey imposes the three main stressors (sugars, gluconic acid, and H_2O_2), involved in the Gox reaction and which are thought to be key components of the antibacterial activity of H_2O_2-producing honey. TraDIS involves the sequencing of high-density transposon libraries using next generation sequencing (NGS) to identify the location and relative frequencies of every insertion within a transposon library. This can then be used to determine the relative contribution to fitness of each gene before and after bacterial growth in the presence of specific stressors (Hayes, 2003; Langridge et al., 2009). The term "fitness" in this context is a measure of how well a cell competes with others to survive and reproduce in the presence of a given stress. Enrichment of strains containing insertions in that gene would indicate that deletion of that gene confers a fitness advantage to the population, while reduction would show that loss of function of this gene makes the strain less fit.

In this study, a transposon library was used to identify features important in the fitness of *E. coli* K-12 exposed to model honey. By this approach, we identified the genes in which transposon insertions caused a significant and time-dependent advantage (increase of fitness) or disadvantage (decrease of fitness) to *E. coli* post-exposure to model honey. Data were tested by construction and analysis of single knockout mutants. As a result of our analysis of these, we discuss pathways that may be of particular importance in understanding the impact of H_2O_2-producing honeys on *E. coli*.

MATERIALS AND METHODS

Model Honey

The model honey was prepared by dissolving fructose (2.24 M), glucose (1.85 M), maltose (0.219 M) and sucrose (0.04 M) (all purchased from Sigma-Aldrich, United Kingdom) in deionized sterile water at 37°C as described previously (Bogdanov, 1997). Stock solutions of gluconic acid and H_2O_2 (Sigma-Aldrich, United Kingdom) were prepared in deionized sterile water and were added, at the appropriate concentrations, immediately before the start of the assay. The H_2O_2 stock contained stabilizer, which in theory could affect data interpretation, but we expect its effects if any to be small. The compositions of the model honey stocks (A and B) used in this study are presented in **Table 1**. The pH of model honeys (A; pH 4.1, B; pH 3.8) was measured using a Mettler Toledo pH meter (Mettler-Toledo Ltd., United Kingdom). The effects of model honeys were always assayed following dilution with an equal volume of bacterial cell culture.

Construction of Transposon Library

E. coli K-12 strain MG1655 was used for the construction of a transposon library. Briefly, 200 μL of *E. coli* K-12 MG1655 ultracompetent cells were transformed with 0.2 μL of EZ-Tn5^{TM} < KAN-2 > Tnp Transposome^{TM} (Kit; Lucigen, Cambridge, United Kingdom) and electroporated. Once electroporated, cells were recovered in SOC media (2% tryptone, 0.5% yeast extract, 10 mM NaCl, 2.5 mM KCl, 10 mM $MgCl_2$, 10 mM $MgSO_4$, and 20 mM glucose, all purchased from Sigma-Aldrich., United Kingdom) for 2 h at 37°C, plated onto LBA plates containing 30 μg/mL Kanamycin to achieve single colonies, and incubated overnight at 37°C. For a full library, the process was repeated 10 times with mutants being pooled and then stored using 10% glycerol at −80°C. Overall, a total of 450,581 unique insertion sites were identified corresponding to an average insertion every 10.3 bp.

Single MG1655 Mutants

A total of 11 genes that were either significant enriched (*ompR*, *wecA*, *wecC*, *wecG*) or depleted (*fdoH*, *fdhD*, *moaA*, *moaB*, *moaC*, *gor*, and *prc*) in the TraDIS dataset (see **Supplementary Table 3**) were selected for validation experiments, and these genes were deleted from MG1655 using P1 transduction from the Keio library (Baba et al., 2006) into *E. coli* K-12 MG1655. All mutants were validated using PCR with appropriate gene-specific primers (**Supplementary Table 4**), as described previously in Thomason et al. (2007).

Optimization Experiment for Antibacterial Assay

Overnight bacterial cultures were diluted in 5 mL Luria broth (LB) (10 g/L tryptone; 5 g/L yeast extract; 10 g/L NaCl; Sigma, United Kingdom) to a starting OD_{600} of 0.05 and incubated until the $OD_{600\ nm}$ reached 0.5 McFarland Standard (approx. 1.5×10^8 CFU/mL). Before use, cells were pelleted (3900 g for 3 min in an Eppendorf centrifuge 5810), washed twice (pelleted, supernatant poured off, and cells resuspended with an equal volume of PBS), and resuspended again in PBS (BR0014, Oxoid Ltd., United Kingdom) to a final absorbance at 600 nm of 0.5. Resuspended cultures (100 μL) were mixed with equal volume (100 μL) of model honeys (Model A and Model B; **Table 1**) or PBS (as a negative control) and incubated at 22°C. Samples were taken at 30, 60, 90, and 120 min post-treatment and washed in PBS. After removing the PBS, each pellet was resuspended in 200 μL of LB, this inoculum was then transferred into 50 mL LB and incubated with shaking (150 rpm) at 37°C. Two hours post-incubation, each sample was washed twice and resuspended in equal volume of PBS. The antibacterial activity of the model honey was determined using total viable counts (TVC) and flow cytometry (FC).

Flow Cytometry

A BD Accuri C6 flow cytometer (Becton Dickinson Biosciences, Oxford, United Kingdom) was used for FC analysis. For analysis of membrane permeability, samples were stained directly with 4 μg/mL Propidium iodide (PI) (Sigma, United Kingdom) and incubated at room temperature in the dark for 10 min. Untreated bacteria and bacteria treated with 3 M H_2O_2 for 30 min, served as "healthy" and "dead or membrane compromised" controls, respectively. For all assays, samples were excited using a 488 nm solid-state laser. PI fluorescence was detected using 670 LP filters. 25,000 data points were collected at a maximum rate of 2,500 events/sec and the data were analyzed using CFlow (BD) software.

Treatment of the Transposon Library With Model Honey

For the transposon library, 10 μL of the library (∼2.4×10^9 cells) were inoculated in 50 mL LB at a starting OD_{600} ∼0.05 and grown overnight at 37°C with shaking (150 rpm). 500 μL of the activated library was then inoculated into 50 mL of fresh LB and incubated until the OD_{600} reached 0.5 McFarland Standard. Before use, cells were pelleted (3,900 g for 3 min in an Eppendorf Centrifuge 5810), washed twice, resuspended in PBS (BR0014, Oxoid Ltd., United Kingdom) to a final absorbance of 1 OD_{600}. 1 mL of the activated library was mixed with 1 mL model honey (model

TABLE 1 | Composition of the model honeys.

Model honey	Sugars (w/v%)/gluconic acid (v/v %)/H_2O_2 (v/v %)	Fructose (M)	Glucose (M)	Maltose (M)	Sucrose (M)	Glu. acid (mM)	H_2O_2 (mM)
A	30%/0.14%/0.006%	0.8	0.66	0.07	0.014	9	2
B	30%/0.14%/0.009%	0.8	0.66	0.07	0.014	9	3

B) or 1 mL PBS (negative control). Samples were incubated for 30 or 90 min. Following this, samples were then subjected to 2 h outgrowth in fresh LB (as was described in optimization experiment). The biological replicate samples are referred in the text as TL30 (TL30_1, TL30_2), TL90 (TL90_1, TL90_2), and TL0 (TL0_1, TL0_2).

DNA Extraction and Transposon Directed Insertion-Site Sequencing

Genomic DNA was isolated from all samples using a RTP® Bacteria DNA Mini Kit according to the manufacturer's specifications (Protocol 2: Isolation of DNA from bacteria pellets (1×10^9 bacteria cells), STRATEC Molecular GmbH, Berlin). DNA was quantified using the Qubit™ dsDNA HS Assay kit (Invitrogen). 1 μg of gDNA was then fragmented using a bioruptor® plus (Diagenode). NEB Next Ultra I kit (New England Biolabs, United Kingdom) was used to repair the ends of the fragmented DNA and to ligate an adaptor to the ends of the newly prepared DNA fragments. Following adaptor ligation, a PCR step was used to enrich the transposon junction fragments, using a custom forward primer annealed to the transposon end and a reverse primer annealed to the ligated adaptor. The second PCR step prepared DNA for sequencing through the addition of Illumina-specific flow cell adaptor sequences and custom inline index barcodes of variable length in the forward primers. The purpose of this was to increase indexing capacity while staggering the introduction of the transposon sequence, which increases base diversity during sequencing. Samples were sequenced using Illumina MiSeq 150 cycle v3 cartridges, aiming for an optimal cluster density of 900 clusters per mm^2.

Bioinformatics Analysis: Sequencing Analysis and Prediction of Gene Essentiality

Sequencing analysis was performed using custom scripts as described in Goodall et al. (2018). Read counts associated with transposon insertions were checked for any inline index barcode. Independently processed samples and short sequence reads were removed, and the data were then combined to increase the coverage resulting in 4,423,778 transposon-tagged reads which resulted in 450,581 unique insertion sites identified in the library. Insertion index scores were generated by dividing the number of unique insertions per gene by the gene length. Using this insertion index score, essential genes were identified using the procedure described in Goodall et al. (2018). This essential genome was then excluded from further analysis. For all remaining genes, relative fitness score (defined as $\log_2$-fold changes in read counts between the treated and control samples) were calculated using EdgeR within the ESSENTIALS package. Genes that showed a $\log_2$-fold change >1 or <-1 and an adjusted p-value of 0.005, after a Bonferroni correction was performed, were selected for further analysis (Zomer et al., 2012). Adjusted p-values and $\log_2$-fold changes for all genes for both T30 and T90 are shown in **Supplementary Table 1**.

Gene Ontology Terms and Pathway Enrichment Analysis

The GO annotation of genes with a significant TraDIS score as defined above was done using the DAVID Bioinformatics Resources 6.7 and Gene Ontology Consortium Bioinformatics data bases (Ashburner et al., 2000). Any Biological Pathway that showed an enrichment for specific GO terms in the gene set with a p-value ≤ 0.005 was considered to be significantly enriched.

Validation Experiments

Validation experiments involved testing the susceptibility of single knockout mutants to model honey and measuring relative selection rates against a *lacZ* derivative of MG1655. Susceptibility of the mutants was tested post-exposure to model honey B for 24 h as described above. Following overnight growth, strains were grown to the exponential phase (OD_{600} 0.5), washed twice in PBS and the OD_{600} was adjusted to 1. Each strain was combined with the *E. coli* Lac^- in a 1:1 ratio and was mixed with an equal volume (1 mL) of model honey B. Thirty (30) and ninety (90) min post-treatment with model honey, the cell pellet was harvested by centrifugation at 4,000 × *g* for 3 min and was resuspended in equal volume of PBS (2 mL). A 100 μL sample of the honey-treated samples (t30 and t90, respectively) and the control (cells kept in PBS) were plated on MacConkey Lactose agar and incubated overnight at 37°C, after which numbers of each strain were scored visually. As a measure of fitness, selection rate Lenski et al. (1991) was calculated for each experiment:

$$Selection\ rate\ (r) = \ln\left(\frac{R_t}{R_0}\right) - \ln\left(\frac{V_t}{V_0}\right)$$

Where r is defined as the relative competitive index, R (mutant) and V (WT) represent the two competing populations, 0 is the colony counts at timepoint zero (control) and t is the colony counts at timepoint 30 or 90 min, respectively.

RESULTS

Optimization Step: Composition of Model Honey and Transposon Library Treatment

We used two model honeys with different concentrations of H_2O_2 to define one that caused logarithmic reduction without completely eradicating the bacterial population. These were model honey A and B, composed of 30% sugars, 8.6 mM gluconic acid, and 2 mM or 3 mM H_2O_2, respectively (**Table 1**). The bacterial viability was determined by colony counts and the phenotypic changes upon honey treatment were examined by flow cytometry (FC) using propidium iodide (PI), a DNA intercalating dye used as an indicator of cell membrane damage as it only enters cells with disrupted membranes (Nebe-von-Caron et al., 2000).

Within 90 min of treatment, model honey B (3 mM H_2O_2) caused almost 3 logs reduction while model honey A (2 mM H_2O_2) caused 1 log reduction, as assessed by viable counts (**Figure 1A**). FC showed that both model honeys affected cell

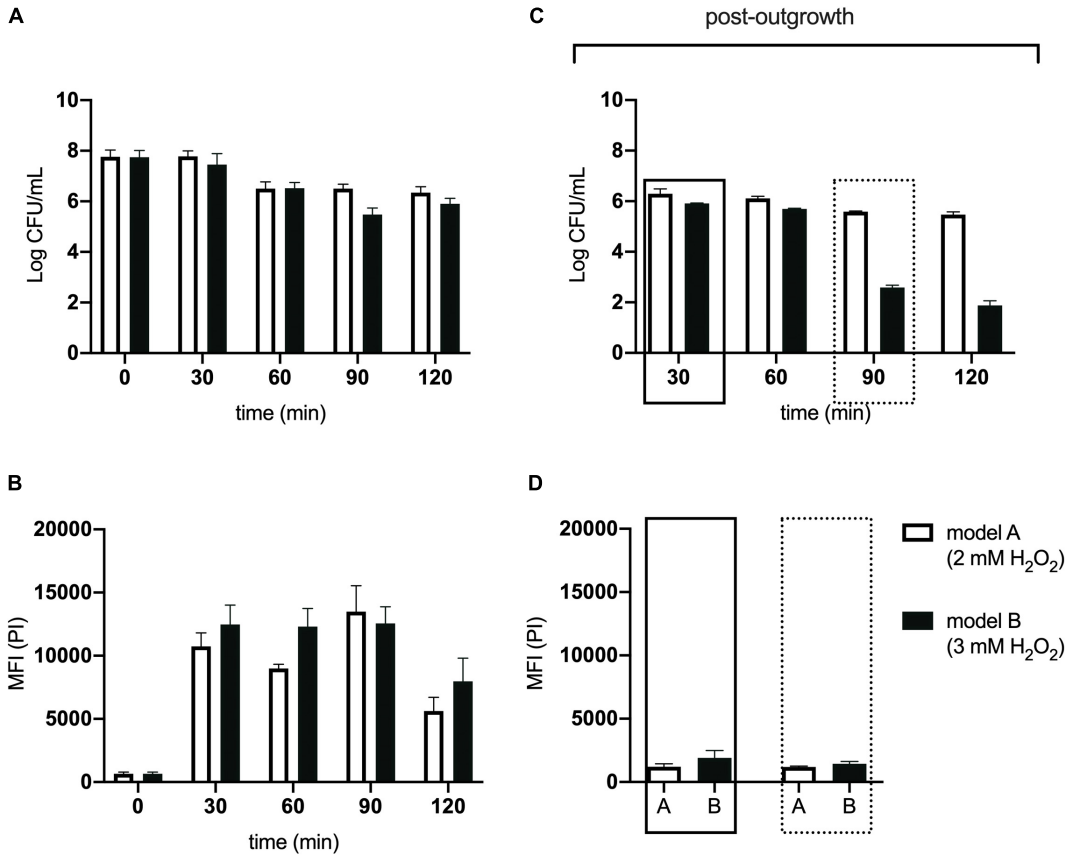

FIGURE 1 | Antibacterial effect of model honeys on *E. coli*. Colony counts, showing the cell survival **(A)**, and mean fluorescence intensity (MFI) of PI, showing the extent of cell wall damage **(B)**, are plotted for 30, 60, 90, and 120 min post-exposure to honey model honey A (plain bars) and B (black bars). Colony counts **(C)** show the survival of the four treated populations after 2 h outgrowth in LB and the MFI of PI **(D)** of 30 min- and 90 min-treated population post- 2 h outgrowth in fresh LB. Error bars show standard deviations, (n = 3; biological replicates).

membrane integrity within a few minutes of treatment. Cells exposed to model honey B showed consistently enhanced PI fluorescence, while in the case of cells exposed to model honey A, mean PI fluorescence intensity (MFI) also increased but fluctuated more during the 2 h of treatment (**Figure 1B**). This variation may be due to the bacterial catalase activity which degrades the H_2O_2 and to self-repair mechanisms that protect membrane integrity (Seaver and Imlay, 2001).

Following the treatment with model honeys, an outgrowth step was introduced as described by Phan et al. (2013). This step allowed the growth of all cells which had survived honey treatment and ensured that the cultures yielded enough genomic DNA (gDNA) for TraDIS sequencing. **Figure 1C** shows that the effect of both model honeys was time- and dose- dependent, with cfu dropping with longer exposure to honey (more slowly for treatment with model honey A). This may be due to a combination of irreversible cell injury/death and an extended lag phase caused by the stress (Hamill et al., 2020). Therefore, only intact and moderately injured cells are expected to grow in LB medium during the outgrowth step. FC showed that within the 2 h outgrowth, the surviving bacterial cells repaired their membranes, with the fluorescence of PI consequently decreasing compared to levels seen directly after treatment with model honey A and B (compare **Figure 1D** with **Figure 1B**).

Exposure and Sequencing of Transposon Insertion Library to Model Honey

For these experiments we used a TraDIS library constructed in-house in the model *E. coli* K-12 strain MG1655. The distribution of insertion sites in this library covers the full genome with high frequency (**Figure 2**). Based on the results above, this library was exposed to model honey B (30% sugars, 8.6 mM gluconic acid, and 3 mM H_2O_2) for 30 and 90 min, followed in each case by 2 h outgrowth in LB. Given that *E. coli* quickly degrades H_2O_2, we hoped that the comparison of bacterial responses between these two time intervals (30 and 90 min) could give some insight into the synergy between honey components when H_2O_2 is more abundant (30 min) and when it is mostly degraded (90 min). The experiment was done twice, together with duplicate controls where the resuspended library was kept in phosphate-buffered saline (PBS) for equal times (30 and 90 min) without being treated with the model honey. The samples were labeled TL30_1, TL30_2, TL90_1, and TL90_2 for the 30- and 90-min time points of the two experiments, respectively, and two control samples

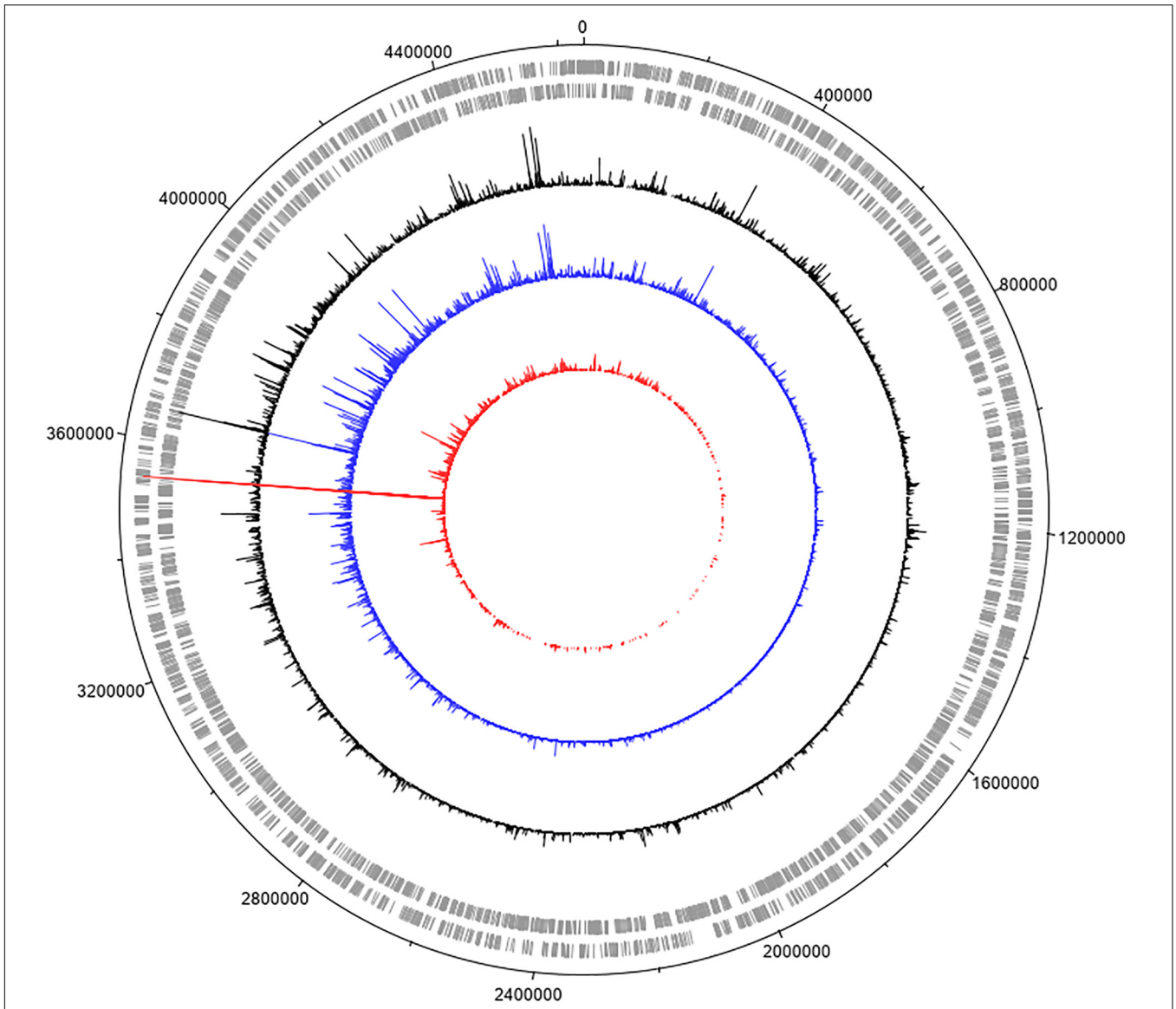

FIGURE 2 | Genome-wide transposon insertion sites mapped to *E. coli* strain MG1655 in the TraDIS library. Frequency and location of transposon junction sequences from a mini-Tn*5* transposon library in strain MG1655, mapped to the MG1655 genome (CP009273.1). The outermost track marks the MG1655 genome in base pairs starting at the annotation origin. The next two inner tracks correspond to sense and antisense CDS, respectively. The innermost circles correspond to the frequency and location of transposons mapped to the MG1655 genome. The circles represent the initial MG1655 transposon library (black), and the library after 30 min (blue) and 90 min (red) exposure to model honey. The figure was created using DNAPlotter.

were labeled TL0_1 and TL0_2. Reproducibility of the biological replicates was very high, as shown by a value of R^2 (Pearson correlation) between 0.97 and 0.98 (**Figure 3**).

Identification of Conditionally Essential Genes

Transposon directed insertion-site sequencing data were analyzed by the ESSENTIALS pipeline (Zomer et al., 2012). The main output of ESSENTIALS is the $\log_2$-fold change ($\log_2$FC) of insertion counts between the treated and control samples, calculated by the EdgeR internal package (Robinson et al., 2010), and an adjusted *P*-value for each gene showing the level of significance of the measured $\log_2$FC. **Figure 4** shows the $\log_2$FC for the whole bacterial genome following exposure to model honey for 30 and 90 min (TL30 and TL90), with genes ranked from smallest to largest $\log_2$FC. We took a $\log_2$FC of >1 or <-1 and an adjusted *P*-value of 0.005 to generate lists of genes where transposon insertion had a significant effect on strain fitness upon exposure to model honey.

Using this approach, we identified 42 (at TL30) and 41 (at TL90) genes where transposon insertion had a significant effect on strain fitness. Twenty-six of these were common between the two conditions (30 and 90 min) tested (listed in **Table 2**).

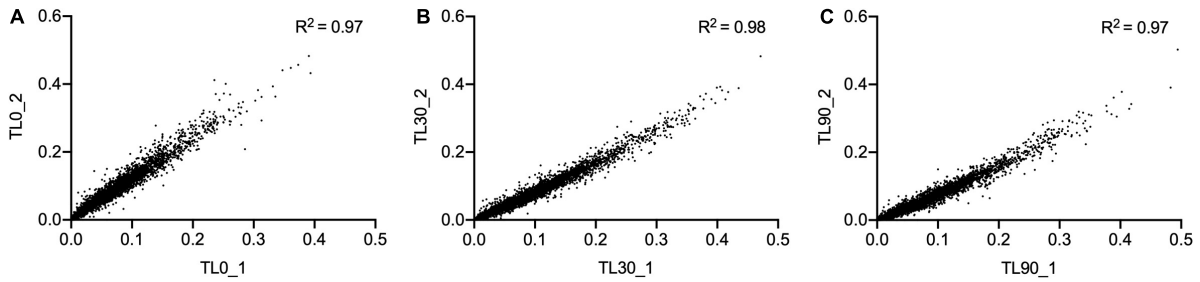

FIGURE 3 | Replicates of TraDIS samples are highly correlated. Gene insertion index scores for all non-essential genes are shown for the two biological replicates of the control (input) transposon library **(A)**, and after selection in model honey for **(B)** 30 min (TL30_1, TL30_2) and **(C)** 90 min (TL90_1, TL90_2), followed by 2 h outgrowth in LB in both cases.

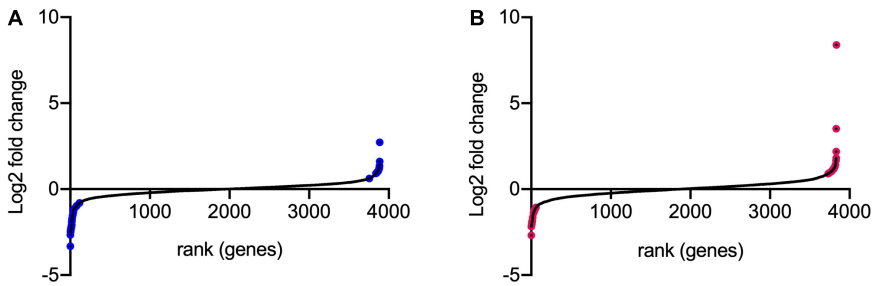

FIGURE 4 | Log_2FC of transposon insertion frequency for all non-essential genes. The log_2FC for each non-essential gene was calculated for **(A)** 30 min stress/control and **(B)** 90 min stress/control. Log_2FC values were then ranked from lowest to highest. Genes colored in blue and pink are those with logFC >1 or <−1 and with adjusted *p*-values < 0.005.

A further 16 mutants showed a significant effect at 30 min but not at 90 min (**Supplementary Table 2**), and 15 had a significant effect at 90 min but not at 30 min (**Supplementary Table 3**). The identification of mutants with a role in fitness when exposed to model honey at 90 min only may be explained by their effect being time-dependent and relatively slow, but it is harder to explain why some mutants might have an effect at 30 min but not at 90 min. This point is considered further in the section "Discussion."

Gene Ontology Analysis of Transposon Directed Insertion-Site Sequencing Data

In order to gain preliminary insight into the possible function of genes identified in the TraDIS analysis, we undertook a basic gene ontology analysis of selected TraDIS data. Specifically, we analyzed genes where insertions caused a significant loss of fitness at both the 30- and 90-min time points (with significance defined as above), looking at the biological processes that were enriched in the genes represented in the lists. The annotation analysis was conducted in terms of their biological pathway. The results (shown in **Figure 5**) suggests that selenocysteine, Mo cofactor biosynthesis and the activity of formate dehydrogenases (FDHs) were the most significantly affected pathways upon exposure to model honey. The roles of these genes, plus other genes in the significant lists, and the possible explanations of their effects on fitness in honey treated cells, are considered in the section "Discussion."

Validation of Transposon Directed Insertion-Site Sequencing Data

Having identified genes whose inactivation has an impact on the fitness of honey-treated cells, we attempted to validate a representative selection of these by creating deletions of the appropriate genes and testing their effects on bacterial fitness relative to wild type when exposed to model honey B, as used for the TraDIS experiment. As described in section "Materials and Methods," we used assays that measured relative rates of killing in mixtures of the wild type strain with individual knockout strains (having marked the wild type with a *lacZ* mutation for ease of screening on MacConkey-lactose plates; control experiments confirmed this mutation had no effect on strain fitness). We also directly measured the sensitivity of the individual mutants to model honey B. Deletions of eleven of the genes were engineered by P1 transduction from the Keio library (Baba et al., 2006), selecting for kanamycin resistance, as described in Materials and Methods. All deletions were verified using PCR. **Figure 6** shows the fitness of these eleven deletion mutants relative to the wild type strain with the *lacZ* marker gene. The relative rate of killing is equivalent to the selection rate and was calculated as described in Lenski et al. (1991).

In the case of genes where transposon insertion caused a significant decrease in fitness in the TraDIS experiment, loss of strain fitness was also generally seen when these genes were deleted (**Figure 6A**). Deletions of *moaA, moaB, fdhD, gor* and *prc* showed agreement with the TraDIS data, showing significantly

TABLE 2 | Genes that when mutated had a significant loss or gain of fitness at both 30 and 90 min following model honey challenge as identified by TraDIS.

Gene	Description	Operon structure	30' (significant)		90' (significant)	
			Log2 score	Adj. *p*-value	Log2 score	Adj. *p*-value
Genes whose deletion caused loss of fitness on exposure to model honey						
prc	Periplasmic tail-specific protease	*proQ-prc*	−3.323	1.13×10^{-27}	−2.180	7.70×10^{-13}
moeB	Molybdopterin-synthase adenylyltransferase	*moeAB*	−2.501	4.26×10^{-23}	−1.646	0.0011
moaA	Molybdopterin biosynthesis: GTP 3′,8-cyclase	*moaABCDE*	−2.419	3.54×10^{-15}	−1.288	0.0037
fdoH	Formate dehydrogenase O β subunit (FeS containing)	*fdoGHI-fdhE*	−2.393	6.72×10^{-20}	−1.888	5.10×10^{-09}
selB	Selenoprotein synthesis: Selenocysteine-specific elongation factor	*selAB*	−2.360	4.13×10^{-24}	−1.901	8.01×10^{-12}
selA	Selenoprotein synthesis: L-seryl-tRNA (Sec) selenium transferase	*selAB*	−2.274	5.02×10^{-18}	−2.136	1.51×10^{-09}
fdoI	Formate dehydrogenase O γ subunit (cytochrome b_{556})	*fdoGHI-fdhE*	−2.269	4.04×10^{-11}	−1.889	4.39×10^{-05}
atpD	ATP synthase β subunit	*atpABCDEFGH*	−2.257	3.99×10^{-11}	−1.837	0.0003
yohD	Inner membrane protein	*yohD*	−2.245	2.25×10^{-07}	−1.957	0.0017
fdhE	Formate dehydrogenase formation protein	*fdoGHI-fdhE*	−2.128	1.16×10^{-11}	−2.047	2.15×10^{-06}
fdhD	Sulphurtransferase for molybdenum cofactor sulphuration	*fdhD*	−2.103	4.48×10^{-12}	−1.869	7.38×10^{-06}
fdoG	Formate dehydrogenase O α subunit (MGD-containing, selenoprotein)	*fdoGHI-fdhE*	−2.070	1.26×10^{-25}	−2.035	1.85×10^{-15}
selD	Selenoprotein synthesis: Selenide, water dikinase	*selD-topB*	−1.931	1.45×10^{-06}	−2.685	5.57×10^{-09}
moeA	MoCo biosynthesis: Molybdopterin molybdenumtransferase	*moeAB*	−1.467	6.25×10^{-09}	−1.200	0.0009
glnG	DNA-binding transcriptional regulator NtrC	*glnALG*	−1.215	8.43×10^{-05}	−1.391	3.41×10^{-05}
fetA	Iron export ABC transporter *fetAB*	*fetAB*	−1.149	0.0002	−1.172	5.61×10^{-05}
fetB	Iron export ABC transporter *fetAB*	*fetAB*	−0.961	0.0026	−1.061	0.0041
Genes whose deletion caused gain of fitness on exposure to model honey						
rep	ATP-dependent DNA helicase	*rep*	0.913	0.0002	1.263	6.97×10^{-10}
acnB	Aconitate hydratase B	*acnB*	0.940	0.0023	1.182	1.39×10^{-05}
wecC (rffD)	ECA biosynthesis: UDP-N-acetyl-D-mannosamine dehydrogenase	*wecA-wzzE-wecBC-rffGHC-wecE-wzxE-wecF-wxyE-wecG*	0.947	5.14×10^{-05}	1.212	6.58×10^{-06}
envZ	EnvZ/OmrR Two-component signal transduction system	*ompR-envZ*	1.030	7.95×10^{-06}	3.522	1.70×10^{-44}
wecB (rffE)	ECA biosynthesis: UDP-N-acetylglucosamine 2-epimerase	*wecA-wzzE-wecBC-rffGHC-wecE-wzxE-wecF-wxyE-wecG*	1.035	2.23×10^{-12}	1.335	1.11×10^{-11}
wecG (rffM)	ECA biosynthesis: UDP-N-acetyl-D-mannosaminuronic acid transferase	*wecA-wzzE-wecBC-rffGHC-wecE-wzxE-wecF-wxyE-wecG*	1.044	1.59×10^{-05}	1.203	6.74×10^{-05}
wecA (rfe)	ECA biosynthesis: UDP-N-acetylglucosamine—undecaprenyl-phosphate N-acetylglucosaminephosphotransferase	*wecA-wzzE-wecBC-rffGHC-wecE-wzxE-wecF-wxyE-wecG*	1.045	8.17×10^{-07}	1.092	0.0002
tolA	Tol-Pal system protein	*ybgC-tolQRA*	1.148	0.0031	1.174	0.0009
ompR	EnvZ/OmrR Two-component signal transduction system	*ompR-envZ*	1.613	6.99×10^{-12}	8.392	5.06×10^{-134}

The genes are ranked according to the log_2FC. Operon structures are from Ecocyc.org.

reduced fitness relative to the wild-type after 90 min of exposure to honey. The *prc* mutant, in particular, was very rapidly eliminated in these experiments, with zero viable colonies being seen after 30 and 90 min of exposure to honey; it also showed the largest log_2-fold decrease in the TraDIS data. Deletion of other genes also showed an impact on fitness though not always with an identical pattern to the TraDIS data. Deletion of *fdhD* was significant at both times in TraDIS, but only at 90 min in the competition experiment. Interestingly, deletion of *gor* was only just significant at 30 min and not at all at 90 min in the TraDIS experiment but had a significant impact on fitness only at the 90 min time point in the competition experiment. Conversely, *fdoH* was clearly significant at both time points in the TraDIS experiment, but only a slight and non-significant decline in fitness was seen in the competition experiment when this gene was deleted. Also, TraDIS showed that the loss of function both *moaA* and *moaB* was more significant at 30 min compared to 90 min, while the competition experiments showed the alternative with both mutants having a higher loss of fitness at 90 min compared with 30 min.

The agreement between competition and TraDIS experiments was less clear for genes where transposon insertion caused a gain

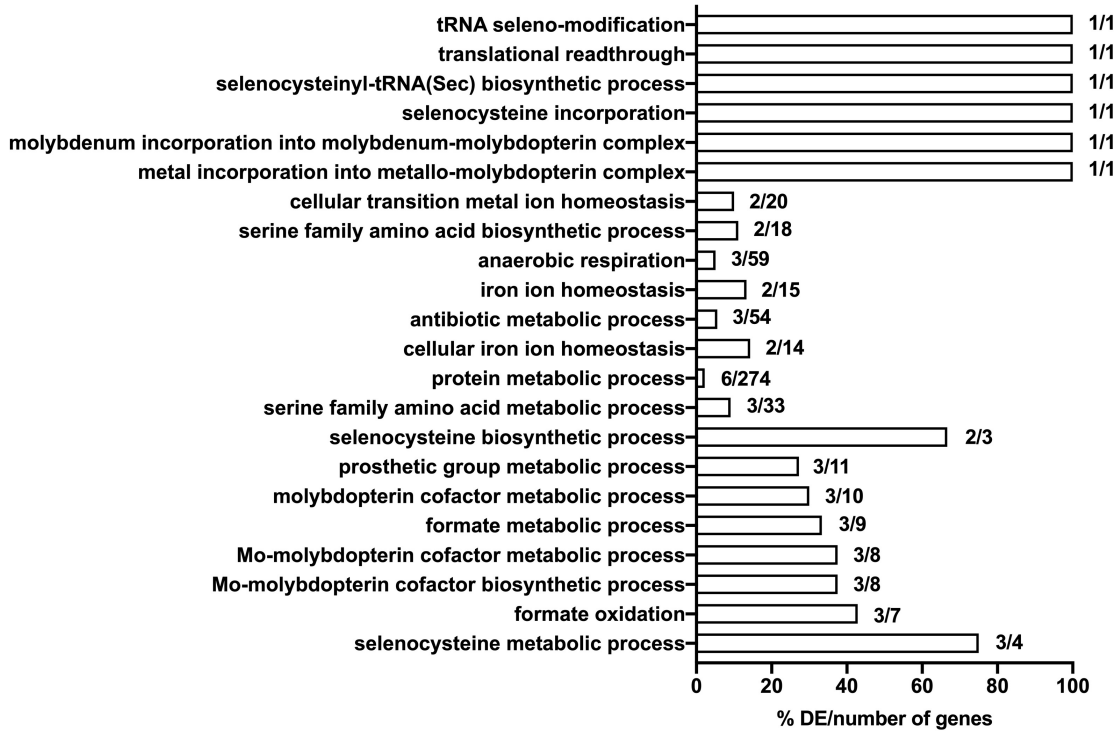

FIGURE 5 | Significantly enriched gene ontology (GO) terms for the seventeen mutants that show significant loss of fitness following 30- and 90-min exposure to model honey. Genes included in the analysis were these whose corresponding mutants had a logFC >1 or <−1 with adjusted *p*-values < 0.005. Comparisons were made using the number of genes associated with each term in the gene set versus the total number of genes associated with each term in the (*E. coli* MG1655) genome. The respective percentage is given in *x* axis.

of fitness in the TraDIS. Transposon inserts in *ompR* showed the most significant increase in relative fitness in the TraDIS experiments, particularly at 90 min. However, in the competition experiments, the *ompR* deletion strain showed a slight but non-significant decline in fitness relative to wild-type (**Figure 6B**). Moreover, inserts in the *wecA*, *wecB*, *wecC,* and *wecG* genes all caused slightly increased fitness in the TraDIS experiments, but deletion of these genes caused significant loss of fitness relative to wild type in the competition experiments. Because of the discrepancies seen with some of the mutants, a separate measurement was done of the susceptibility of each of the mutants to 24 h exposure to model honey (B), as an independent way to evaluate the impact of loss of function of these genes on strain fitness. To define the severity of a phenotype, thresholds were set to cluster the mutants into three groups; (a) "weak" for mutants showing less than 2 logs reduction, (b) "intermediate" for those showing 3–4 logs reduction and (c) "strong" those with higher than 5 logs reduction. **Figure 7** shows that Δ*fdhD*, Δ*gor,* and Δ*prc* were the most susceptible strains to model honey. In agreement with both TraDIS and the competition assay, Δ*prc* demonstrated a strong loss of fitness phenotype followed by Δ*gor* and Δ*fdhD* which both had intermediate phenotypes. The rest of the mutants (Δ*moaA*, Δ*moaB*, Δ*moaC,* and Δf*doH*) had an intermediate phenotype apart from Δ*ompR* and Δ*wecC*, both of which were more resistant than the wild type, although this was only statistically significant in the case of the Δ*ompR* strain.

Overall, most of the phenotypes observed in these experiments agreed with TraDIS analysis. Thus, *prc*, *gor,* and *fdhD* are the genes which under the conditions of our experiment are most important to enable the bacteria to resist the effects of the model honey, while loss of *ompR* led to better survival than the wild type in the presence of model honey.

DISCUSSION

Our aim in this study was to identify genes in *E. coli* which, when their function was lost, caused a significant change in the ability of the organism to survive exposure to a model honey. Our choice of model honey was based on previous work showing that dilution of honey to 30–50% of its initial concentration led to H_2O_2 concentrations between 0.04 and 4 mM, and gluconic acid concentrations between 8.6 and 60 mM (Manyi-Loh et al., 2011; Bucekova et al., 2018). Identification of these genes should provide insights into the role of particular pathways in surviving the stress caused by the model honey, which in turn can give further information about the mechanisms by which honey causes cell damage and death (**Figure 8**). *E. coli* K-12 MG1655 was used for the experiments described here and in our earlier study because of the large amount of available prior knowledge of gene function in this organism; subsequent work on clinical isolates and other bacterial species

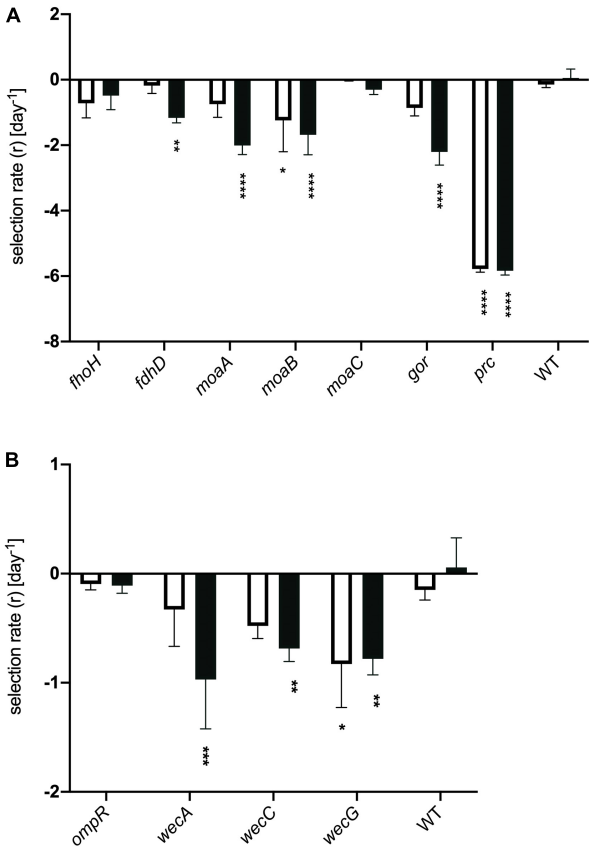

FIGURE 6 | Selection rates for strains deleted for individual genes. Genes classified in the TraDIS dataset as having **(A)** negative fitness or **(B)** positive fitness when containing transposon insertions. Strains were mixed with represented their wild type parent (*E. coli* MG1655, marked with a *lacZ* mutation) in model honey for 30 min (plain bar) or 90 min (black bar), before plating on MacConkey lactose to determine relative survival rates. The WT control shows the data for MG1655 *lacZ* mixed with MG1655 LacZ$^+$. Data were analyzed using two-way ANOVA: asterisks show significance levels of Sidak's multiple comparisons test (****$p \leq 0.0001$, ***$p \leq 0.0005$, **$p \leq 0.005$, *$p \leq 0.05$); all bars without asterisks are not significant ($p > 0.05$). Error bars represent the average ± SD ($n = 3$; independent biological replicates).

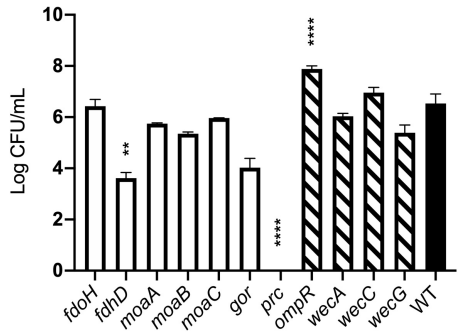

FIGURE 7 | Effect of model honey B on strains deleted for individual genes. Strains containing deletions of genes previously identified as "loss of fitness" (plain bars) and "gain of fitness" (hatched bars) were treated with model honey B for 24 h before plating to measure survival. ****$p \leq 0.0001$, **$p \leq 0.005$. The graph shows average ± standard deviation ($n = 3$; biological replicates).

will be needed to see the extent to which our findings can be generalized. Here, we consider those genes that caused a loss of fitness when disrupted, where data from single gene knockouts agreed with data from the TraDIS experiments. We then briefly consider the smaller number of genes where disruption caused a gain of fitness relative to the wild type strain, although with these genes, data from the two assay methods were not always consistent.

Mutation of seventeen genes caused a significant loss of fitness at both time points in the treatment with model honey (*fetB* is included although it is fractionally below the cut-off for impact on fitness at 30 min). Of these, eleven are involved directly or indirectly in formate oxidation, encoding formate dehydrogenase O (FDH-O; *fdoGHI*), or proteins involved in providing FDH-O with its molybdenum-containing cofactor (molybdenumtransferases; *moeAB*, molybdenum cofactor; *moaA*, and the *fdhED* genes), or proteins involved in selenocysteine biosynthesis (*selABD*). Selenocysteine is an amino acid present in the three formate dehydrogenases. GO term analysis of this list confirms that pathways affecting selenocysteine biosynthesis, Mo cofactor biosynthesis and the activity of formate dehydrogenases (FDHs) were the most significantly enriched pathways where mutation caused loss of fitness on exposure to model honey.

In *E. coli*, FDH-O is one of three formate dehydrogenases (FDH-N, FDH-O, and FDH-H) that have a role in formate oxidation. All contain selenocysteine (sec), moco (molybdenum cofactor), iron-sulfur (4Fe-4S) clusters, and require the FdhE and (with the exception of FDH-N) FdhD proteins for maturation (Lüke et al., 2008). The products of four *sel* genes (*selABCD*) have been identified as prerequisites for the biosynthesis and incorporation of sec into selenoproteins. Strains carrying mutations in *selD*, *selA*, and *selB* all significantly lost fitness upon honey treatment which suggests that one or more selenoproteins are important for bacterial survival under the tested conditions, the most likely candidate being FDH-O itself as it is the only selenoprotein also encoded by members of the list of significant genes. Molybdenum, an essential transition metal in biological systems, is involved in redox activities and has a key role in PMF generation (Leimkühler, 2014). Most of the terminal reductases that take electrons from FDH-O are also molybdoproteins (NarGHI, NarZYV, TorAC, DmsABC). The *moa* and *moe* operons encode proteins that are directly involved in the biosynthesis of moco (Coughlan, 1983). The deletion of genes involved in molybdoprotein synthesis increased the susceptibility of *E. coli* toward HAP (6-N-hydroxylaminopurine) and chlorate due to the reduced reductase activity which caused an imbalance in the PMF (Kozmin and Schaaper, 2013) and destruction of membrane polarity and integrity (Riondet et al., 1999). Again, their appearance in the list of significant genes is likely be due to their role in FDH-O function.

During formate oxidation, FDH-O donates electrons to the quinone pool and can contribute to the proton motive force

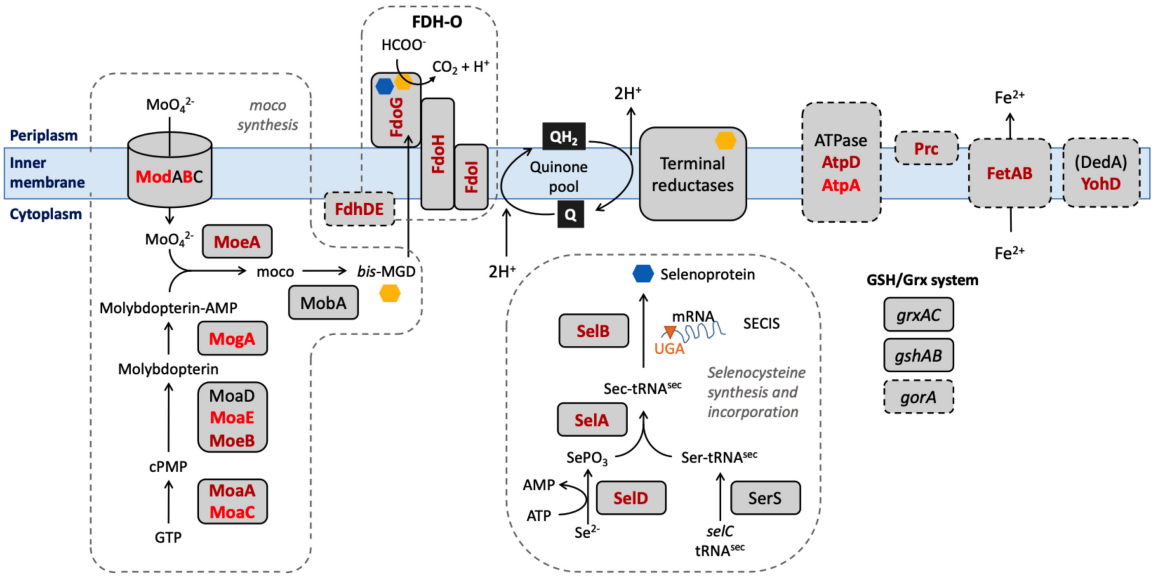

FIGURE 8 | Selected biological pathways where the "loss of fitness" genes are involved. Dashed boxes include biological pathways and genes which were shown to be significantly affected after the exposure to honey. Mo cofactor and selenocysteine, being incorporated into the 3 FDHs after the biosynthesis, are denoted by yellow and blue polygons, respectively. Genes found in both lists are shown in dark red; genes found only in the TL30 list are shown in light red.

(PMF) in a redox loop with nitrate reduction under anaerobic conditions (Abaibou et al., 1995). The role of FDH-O in anaerobic growth is well studied, but its role in aerobic growth is less well understood, despite the fact that it is produced constitutively under aerobic conditions. Recent observations suggest that it has a role in survival of stress caused by ROS. Over-production of the electron transfer sub-units of FDH-O (*fdoH* and *fdoI*) causes an increase in resistance in stationary phase to menadione, a redox cycling agent that generates H_2O_2 and superoxide (Iwadate et al., 2017). This activity does not require the formate dehydrogenase activity *per se*, so its connection with our finding that mutation of gene encoding the α sub-unit of FDH-O (*fdoG*) also causes sensitivity to model honey is not clear. A study using Tnseq (closely related to TraDIS) showed that strains carrying mutations in seven of the genes that we detected (*fdhE*, *fdhD*, *fdoH*, *fdoG*, *selA*, *selB*, and *moaA*) showed enhanced resistance to killing by mammalian peptidoglycan recognition proteins (PGRPs) (Kashyap et al., 2020). The authors propose this may arise because in wild type cells treated with PGRP, FDH-O is activated, leading to an increased flow of electrons into the respiratory chain and generation of damaging hydrogen peroxide by cytochrome *bd*, which is functioning incorrectly due to the action of the PGRPs. This hypothesis in turn suggests a possible model for this part of our current findings. Cytochrome *bd* is itself an effective quinol peroxidase, reducing hydrogen peroxide to water and using ubiquinol as an electron donor, and has been proposed to be an important scavenger of exogenous hydrogen peroxide (Al-Attar et al., 2016). Ubiquinol can be generated by FDH-O catalyzed oxidation of formate (Hartwig et al., 2015). Therefore, one of the routes that *E. coli* can potentially use to defend itself against the hydrogen peroxide generated in model honey is via the ubiquinol-dependent peroxidase activity of cytochrome *bd*, and this would be reduced if FDH-O were absent or inactive, consistent with our TraDIS data. The genes for the other membrane located formate dehydrogenases (FDH-N) showed no evidence of loss of fitness when mutated in the TraDIS experiment, consistent with the fact that FDH-O is expressed aerobically but FDH-N is not (Abaibou et al., 1995). We note that cytochrome *bd* is itself essential under the conditions of our experiment, so would not generate a TraDIS signal.

A plausible hypothesis for the roles of the *fetAB* genes, which were significant at both time points, is also suggested by their known functions. FetAB is a membrane transporter that exports Fe^{2+} from cells, and deletion of *fetA* or *fetB* results in increased sensitivity to H_2O_2, presumably because increased intracellular Fe^{2+} favors the Fenton reaction that leads to disproportionation of hydrogen peroxide and the production of damaging ROS (Nicolaou et al., 2013). The fact that mutation of these genes also causes increased sensitivity to model honey in our experiments suggests that the production of ROS by the Fenton reaction is a key factor in the antibacterial effect of honey.

Roles for the remaining genes in the list based on their known functions are more speculative. The *prc* gene is of particular interest, as both TraDIS and analysis of the Δ*prc* strain showed strains lacking Prc were extremely susceptible to treatment with honey. Prc is a periplasmic protease which cleaves the C-termini of several proteins, and its loss causes a range of effects including increased outer membrane permeability, periplasmic protein leakage, and sensitivity to several antibiotics (Hara et al., 1991; Seoane et al., 1992; Deng et al., 2014). In extraintestinal pathogenic *E. coli*, *prc* mutants are attenuated in a mouse model of urinary tract infections (Huang et al., 2020), where deletion of *prc* has been implicated in perturbation of the cell envelope and induction of the Rcs and σ^E regulons. These

examples show that Prc has an important extra-cytoplasmic role, but the pleiotropic nature of the mutant makes it difficult to propose a specific mechanism for its role in the context of honey treatment. The strength of the phenotype suggests this would repay further study. The *yohD* gene has not been much studied but is a member of the DedA family of proteins that have a role in membrane homeostasis, with mutants showing phenotypes such as cell division defects, altered membrane lipid composition, loss of PMF and increased envelop-related stress responses. For this reason, DedA proteins have been studied as a potential drug target (Doerrler et al., 2013). *E. coli* has eight DedA proteins (YghB, YqjA, YabI, DedA, YdjX, YdjZ, YqaA, and YohD) but other than YohD, none of these showed any significant change in the TraDIS data, and further study of the role of this particular DedA protein in protecting against honey would therefore be of interest. The *atpD* gene encodes a sub-unit of the F_1 component of the F_0F_1-ATPase; the other two non-essential sub-units (*atpA* and *atpG*) also showed loss of fitness though not all below the stringent $p < 0.005$ cut-off we have applied here. Loss of function of this complex will both reduce ATP levels in cells, with a negative effect on ATP-requiring processes, and also may prevent the ATP-driven efflux of protons which is used in some organisms, possibly including *E. coli*, as a defense against acidification (Sun et al., 2012). As model honey (which has a pH of 3.8) contains gluconic acid which has a pKa of 3.86, 50% of the gluconic acid will be in the non-ionized state and could easily cross the bacterial inner membrane, where it will ionize in the bacterial cytoplasm, potentially causing acid stress, although we did not see evidence for loss of fitness caused by mutations in any of the known acid response genes. The *glnG* gene (also known as *ntrC*) is part of the NtrBC two component system which responds to nitrogen limitation in *E. coli* (Jiang and Ninfa, 1999). Intriguingly, *glnL* (*ntrB*) also caused loss of fitness when mutated, as did *rpoN*, the gene for the sigma-54 sub-unit of RNA polymerase, which is needed for the expression of many NtrC-regulated genes, although neither of these genes were significant enough to be included in our lists. For now, the reason why these genes show a TraDIS signal remains unclear, as *E. coli* at exponential phase in LB is not expected to be nitrogen-limited.

Of the mutations causing significant loss of fitness in the TraDIS data at 30 min only, several are in genes involved in moco biosynthesis (*moaC*, *moaE*, *modB,* and *mogA*) and also show loss of fitness at 90 min, though not at significant levels. This may reflect higher variability in the TraDIS values for these genes in the 90 min dataset and is consistent with the central importance of the FDH-O-ubiquinone-cytochrome *bd* pathway proposed above. The *atpA* gene, another non-essential component of the F1 ATPase complex, is also in this category, consistent with the proposed role of this complex in reducing intracellular proton concentration. The *gntR* gene also shows significant loss of fitness at 30 min and evidence of loss of fitness at 90 min. The GntR protein regulates both gluconate metabolism and the import of gluconate, and the negative fitness seen with loss of this gene may be caused by depression of the gluconate I and II import systems which would cause even more stress due to high cytoplasmic gluconate concentration (Rodionov et al., 2000). Of the remaining genes in the list, polyphosphate kinase (*ppk*) has been identified as having a role in resistance to H_2O_2 and heat shock (Crooke et al., 1994). The *Salmonella* Typhimurium *mrp* homolog, *apbC*, is thought to have a role in FeS center metabolism (Skovran et al., 2004) so is potentially involved in maintenance of redox enzymes. Glutathione reductase (*gor*) reduces oxidized glutathione (Lu and Holmgren, 2014) thus can be implicated in repair of oxygen-mediated damage. We suggest that all these genes may represent response mechanisms especially important in the short term after exposure to model honey; further studies on individual mutants will be needed to test this.

Only four genes showed a significant loss of fitness in the TraDIS data at 90 min but not 30, and these were only marginally significant compared to most of the genes that lost fitness at both time points, showing that most of the fitness effects detected by TraDIS occur during the early stages of exposure to model honey. Gluconate is degraded in *E. coli* by conversion into 6-phosphonogluconate which is then fed into the pentose phosphate pathway by the activity of 6-phosphogluconate dehydrogenase, encoded by *gnd*, so the deleterious effect of mutations in this gene may be caused by limitation the cell's ability to metabolize the gluconate component of model honey. The reasons for the other phenotypes for mutants in this list are not clear.

There were some surprises at genes that did not meet our significance criteria. For example, neither *katE* nor *katG*, two genes that we had previously shown to cause increased sensitivity to model honey appeared in the significant gene lists, although *katE* only narrowly missed inclusion in the 90-min list. This may reflect a difference in the assay methods: in a TraDIS experiment, the overwhelming majority of strains in the population will be wild type for these two genes, so the rare loss of function mutants may benefit from the activity of the majority of strains carrying these wild type genes in the population. We also looked at the fitness of *tnaA* mutants, as this gene has been reported to be very strongly down-regulated on exposure to honey (Lee et al., 2011; Wasfi et al., 2016), but there was no fitness defect associated with these mutants under our conditions. The loss of OxyR, the regulator which controls the expression of genes to combat oxidative stress, had a small deleterious fitness effect at both time points which again was not significant enough to be included in our list, consistent with the view that the effects of hydrogen peroxide are not the only cause of the impact of model honey.

Finally, we turn to the phenomenon of genes whose loss of function caused gain of fitness in the TraDIS experiments. The data here are less clear as the measurements of relative killing rates using the mixed populations, and sensitivity of individual mutants, did not always correlate with the TraDIS data, so these may be phenotypes which are only observed when the mutants are present as a very small proportion of the population. We are currently investigating this in more detail.

The appearance of three genes from the *wec* operon in this list, together with *tolA*, was particularly intriguing. This operon (*wecABCG*) encodes some of the proteins required for synthesis and translocation of the Enterobacterial Common Antigen (ECA) (Danese et al., 1998). ECA mutants are viable but have an elongated and swollen cell morphology, suggestive

of an altered cell envelope. In *E. coli*, mutants of the ECA synthesis pathway have an activated Rcs phosphorelay system that is required for inducible acid resistance in *E. coli* (Johnson et al., 2011; Castelli and Véscovi, 2011). Rcs is also activated by mutants of the Tol-Pal system which has a role in maintaining lipid homeostasis in the outer membrane (Clavel et al., 1996; Shrivastava et al., 2017). It has been shown that Tol mutants show enhanced sensitivity to vancomycin, and this is rescued by mutants in the *wec* operon (Jiang et al., 2020). Thus, the fact that both *tolA* and *wec* mutants show enhanced resistance to model honey could be directly related to the defect in ECA biosynthesis or to the induction of the Rcs phosphorelay, and this will repay further investigation.

The most striking example of genes which, when mutated, caused increased fitness in the presence of model honey were *ompR* and *envZ*. Together, these encode a two-component system which has important roles in response to several stresses, including osmotic stress and low pH. Generally, this is due to the phosphorylated form of OmpR which is an activator, but non-canonical behavior that does not require phosphorylation is also important (Kenney and Anand, 2020). Why should loss of function of these genes lead to a significant enhancement in resistance to model honey, particularly in TraDIS experiments but much less so when looking at single mutants? The EnvZ-OmpR two-component system regulates bacterial response to acid and osmotic stress, and its activity affects the acidification of the cytoplasm via repression of the *cadA*, *cadBC,* and *speF* genes (Stincone et al., 2011; Quinn et al., 2014; Chakraborty et al., 2017; Chakraborty and Kenney, 2018). For instance, on exposure to pH 5.6, the *E. coli* cytoplasm was shown to acidify from pH 7.13 to 6.55 in an OmpR-dependent manner, due to repression of the *cadA* and *cadBC* genes by OmpR. High osmolarity was also shown to result in acidification of the cytoplasm (to pH 6.75), but by a different pathway: repression *speF*, encoding ornithine decarboxylase, by OmpR. OmpR requires contact with EnvZ, but not phosphorylation, for this regulation to occur. An *ompR* mutant retained a neutral cytoplasmic pH in response to both pH 5.6 and osmotic stresses. Although the decrease in cytoplasmic pH seen in acid or osmotic stress by Chakraborty et al. is likely to be advantageous in surviving a single stress, it may be that the combination of stresses delivered by model honey means that maintaining a neutral cytoplasmic pH (as would occur in an *ompR* or *envZ* mutant) improves resistance to one or more components in model honey. This would explain the apparent fitness advantage of mutants in these genes that was seen in the TraDIS data. However, other effects such as the impact of *envZ* and *ompR* mutants on the expression of OM porins, that are needed for the passive diffusion of small hydrophilic molecules such as β-lactams and fluoroquinolones, (Ceccarelli and Ruggerone, 2008), cannot be ruled out.

Some genes showed increased fitness in the TraDIS data at 30 min only or 90 min only, though many of these effects were relatively small. At 30 min, *ymjC* had the strongest apparent advantage; however, no reads corresponding to this gene were found in the 90 min dataset. The *ymjC* gene is small (138 base pairs) and hence has very few inserts, which makes it more susceptible to variation due to stochastic effects alone in a TraDIS population, so this data must be interpreted cautiously. Similarly, knockout of eleven genes significantly increased fitness at 90 min post-challenge but not at 30 min (**Supplementary Table 2**), though some of these levels were again marginal. Most of these genes have previously been linked to stress responses and four are involved or implicated in envelope integrity. The first of these, the small RNA *mgrR*, regulates lipopolysaccharide remodeling and plays a role in ROS response (Klein and Raina, 2015). However, TraDIS data for this small gene (98 base pairs) has to be interpreted with caution for the same reasons given for *ymjC* above. Of the other genes, PlsX is involved in phospholipid biosynthesis (overexpression of *plsX* resulted in increased tolerance to the solvent styrene (Machas et al., 2021), suggesting a strengthening of the membrane against some stresses); the porin OmpC has a role in response to envelope stress such as salt, ethanol and SDS (Choi and Lee, 2019); and finally MepS (Spr) remodels the peptidoglycan; a *mepS* deletion prevents growth at high temperatures (42°C) on nutrient agar (Singh et al., 2015). The reasons why mutations in these genes appear to cause improved resistance to the effects of 90 min exposure to model honey are not clear, although it is likely to be related to the importance of the bacterial envelope. Compromising envelope integrity is likely to be associated with sensitivity to components in model honey, consistent with our results above and in Masoura et al., 2020, but some alterations to the envelope may improve resistance.

In addition, three regulators caused fitness improvement at 90 min when mutated. ComR regulates copper acquisition (Rademacher and Masepohl, 2012). ComR regulates expression of *bhsA*, which is also upregulated in the presence of styrene (Machas et al., 2021). Knockout of *qseC* (encoding a sensor kinase involved in motility regulation) increases sensitivity to several cations (Zhou et al., 2003). The oxygen-sensing diguanylate kinase DosC regulates biofilm formation; its expression is upregulated in stationary phase in an RpoS-dependent manner (Weber et al., 2006). Finally, three poorly characterized genes are implicated in resistance to diverse stressors: *yciF* is upregulated under osmotic stress (Weber et al., 2006); overexpression of *yejG* increases resistance to some antibiotics (Soo et al., 2011) and *yejG* is upregulated in response to citral (Chueca et al., 2017); *ydcT*, encoding a putative ABC transporter, is implicated in triclosan resistance (Zheng et al., 2001). Thus, in all cases these genes are involved in different aspects of stress resistance, but we currently do not have simple explanations for why mutations in them can enhance fitness under our experimental conditions. Overall, these data suggest that the pathways that allow adaptation to model honey overlap many other stress responses in *E. coli*.

We have thus used a range of physiological and molecular approaches to characterize the mechanism of action of a defined model honey. Even though the honey has only three chemical components, its deleterious effects on *E. coli* appears to be mediated through multiple pathways and mechanisms, consistent with synergies between these components. We specifically propose the involvement of cytochrome *bd* in detoxification of the hydrogen peroxide which is produced when the honey is activated, but many other pathways are

also clearly involved. Our model honey represents a baseline for understanding the anti-microbial mechanism in H_2O_2-producing honeys. The method we describe here can be extended by adding other important components (such as polyphenols) to model honey and looking at the additional impacts of this, and by using clinically important isolates as target organisms in such experiments. Ultimately, this research should provide understanding that may improve the modification of natural honey into bio-engineered formulations with medicinal use.

DATA AVAILABILITY STATEMENT

The original contributions presented in the study are included in the article/**Supplementary Material**, further inquiries can be directed to the corresponding author/s.

AUTHOR CONTRIBUTIONS

MM, TO, PL, and KG conceived and designed the experiments. MM executed the experiments and together with MTM performed the TraDIS experiment. MTM analyzed the TraDIS data and Gene Ontology. MM wrote the manuscript. TO, MTM, PL, and KG critically reviewed the manuscript. PL acted as the primary supervisor of this work. All authors have read and approved the manuscript.

FUNDING

MM and MTM were funded by the Midlands Integrative Biosciences Training Partnership and a Doctoral Training Program funded by the Biotechnology and Biological Sciences Research Council, United Kingdom. MTM is currently supported by a grant (RPG-2020-252) from the Leverhulme Trust.

SUPPLEMENTARY MATERIAL

The Supplementary Material for this article can be found online at: https://www.frontiersin.org/articles/10.3389/fmicb.2021.803307/full#supplementary-material

REFERENCES

Abaibou, H., Pommier, J., Benoit, S., Giordano, G., and Mandrand-Berthelot, M. A. (1995). Expression and characterization of the *Escherichia coli* fdo locus and a possible physiological role for aerobic formate dehydrogenase. *J. Bacteriol.* 177, 7141–7149. doi: 10.1128/jb.177.24.7141-7149.1995

Al-Attar, S., Yu, Y., Pinkse, M., Hoeser, J., Friedrich, T., Bald, D., et al. (2016). Cytochrome bd displays significant quinol peroxidase activity. *Sci. Rep.* 6:27631. doi: 10.1038/srep27631

Albaridi, N. A. (2019). Antibacterial potency of honey. *Int. J. Microbiol.* 2019:2464507. doi: 10.1155/2019/2464507

Ashburner, M., Ball, C. A., Blake, J. A., Botstein, D., Butler, H., Cherry, J. M., et al. (2000). Gene ontology: tool for the unification of biology. The gene ontology consortium. *Nat. Genet.* 25, 25–29. doi: 10.1038/75556

Baba, T., Ara, T., Hasegawa, M., Takai, Y., Okumura, Y., Baba, M., et al. (2006). Construction of *Escherichia coli* K-12 in-frame, single-gene knockout mutants: the Keio collection. *Mol. Syst. Biol.* 2:2006.0008. doi: 10.1038/msb4100050

Bouzo, D., Cokcetin, N. N., Li, L., Ballerin, G., Bottomley, A. L., Lazenby, J., et al. (2020). Characterizing the mechanism of action of an ancient antimicrobial, manuka honey, against *Pseudomonas aeruginosa* Using modern transcriptomics. *mSystems* 5, e106–e120. doi: 10.1128/mSystems.00106-20

Bogdanov, S. (1997). Nature and origin of the antibacterial substances in honey. *LWT - Food Sci. Technol.* 30, 48–753. doi: 10.1006/fstl.1997.0259

Brudzynski, K. (2020). A current perspective on hydrogen peroxide production in honey. A review. *Food Chem.* 332:127229. doi: 10.1016/j.foodchem.2020.127229

Brudzynski, K., and Sjaarda, C. (2014). Antibacterial compounds of Canadian honeys target bacterial cell wall inducing phenotype changes, growth inhibition and cell lysis that resemble action of β-lactam antibiotics. *PLoS One* 9:e106967. doi: 10.1371/journal.pone.0106967

Brudzynski, K., and Sjaarda, C. P. (2021). Colloidal structure of honey and its influence on antibacterial activity. *Compr. Rev. Food Sci. Food Saf.* 20, 2063–2080. doi: 10.1111/1541-4337.12720

Brudzynski, K., Miotto, D., Kim, L., Sjaarda, C., Maldonado-Alvarez, L., and Fukś, H. (2017). Active macromolecules of honey form colloidal particles essential for honey antibacterial activity and hydrogen peroxide production. *Sci. Rep.* 7:7637. doi: 10.1038/s41598-017-08072-0

Bucekova, M., Buriova, M., Pekarik, L., Majtan, V., and Majtan, J. (2018). Phytochemicals-mediated production of hydrogen peroxide is crucial for high antibacterial activity of honeydew honey. *Sci. Rep.* 8:9061. doi: 10.1038/s41598-018-27449-3

Bucekova, M., Valachova, I., Kohutova, L., Prochazka, E., Klaudiny, J., and Majtan, J. (2014). Honeybee glucose oxidase–its expression in honeybee workers and comparative analyses of its content and H2O2-mediated antibacterial activity in natural honeys. *Naturwissenschaften* 101, 661–670. doi: 10.1007/s00114-014-1205-z

Castelli, M. E., and Véscovi, E. G. (2011). The Rcs signal transduction pathway is triggered by enterobacterial common antigen structure alterations in *Serratia marcescens*. *J. Bacteriol.* 193, 63–74. doi: 10.1128/JB.00839-10

Ceccarelli, M., and Ruggerone, P. (2008). Physical insights into permeation of and resistance to antibiotics in bacteria. *Curr. Drug Targets* 9, 779–788. doi: 10.2174/138945008785747770

Chakraborty, S., and Kenney, L. J. (2018). A new role of OmpR in acid and osmotic stress in *Salmonella* and *E. coli*. *Front. Microbiol.* 9:2656. doi: 10.3389/fmicb.2018.02656

Chakraborty, S., Winardhi, R. S., Morgan, L. K., Yan, J., and Kenney, L. J. (2017). Non-canonical activation of OmpR drives acid and osmotic stress responses in single bacterial cells. *Nat. Commun.* 8:1587. doi: 10.1038/s41467-017-02030-0

Choi, U., and Lee, C. R. (2019). Distinct roles of outer membrane porins in antibiotic resistance and membrane integrity in *Escherichia coli*. *Front. Microbiol.* 10:953. doi: 10.3389/fmicb.2019.00953

Chueca, B., Pérez-Sáez, E., Pagán, R., and García-Gonzalo, D. (2017). Global transcriptional response of *Escherichia coli* MG1655 cells exposed to the oxygenated monoterpenes citral and carvacrol. *Int. J. Food Microbiol.* 257, 49–57. doi: 10.1016/j.ijfoodmicro.2017.06.002

Clavel, T., Lazzaroni, J. C., Vianney, A., and Portalier, R. (1996). Expression of the tolQRA genes of *Escherichia coli* K-12 is controlled by the RcsC sensor protein involved in capsule synthesis. *Mol. Microbiol.* 19, 19–25. doi: 10.1046/j.1365-2958.1996.343880.x

Coughlan, M. P. (1983). The role of molybdenum in human biology. *J. Inherit. Metab. Dis.* 6 Suppl 1, 70–77. doi: 10.1007/BF01811327

Crooke, E., Akiyama, M., Rao, N. N., and Kornberg, A. (1994). Genetically altered levels of inorganic polyphosphate in *Escherichia coli*. *J. Biol. Chem.* 269, 6290–6295. doi: 10.1016/s0021-9258(17)37370-2

Danese, P. N., Oliver, G. R., Barr, K., Bowman, G. D., Rick, P. D., and Silhavy, T. J. (1998). Accumulation of the enterobacterial common antigen lipid II biosynthetic intermediate stimulates degP transcription in *Escherichia coli*. *J. Bacteriol.* 180, 5875–5884. doi: 10.1128/JB.180.22.5875-5884.1998

Deng, C. Y., Deng, A. H., Sun, S. T., Wang, L., Wu, J., Wu, Y., et al. (2014). The periplasmic PDZ domain-containing protein Prc modulates full virulence, envelops stress responses, and directly interacts with dipeptidyl peptidase of

Xanthomonas oryzae pv. oryzae. *Mol. Plant Microbe Interact.* 27, 101–112. doi: 10.1094/MPMI-08-13-0234-R

Doerrler, W. T., Sikdar, R., Kumar, S., and Boughner, L. A. (2013). New functions for the ancient DedA membrane protein family. *J. Bacteriol.* 195, 3–11. doi: 10.1128/JB.01006-12

Goodall, E., Robinson, A., Johnston, I. G., Jabbari, S., Turner, K. A., Cunningham, A. F., et al. (2018). The essential genome of *Escherichia coli* K-12. *mBio* 9:e02096–17. doi: 10.1128/mBio.02096-17

Hamill, P. G., Stevenson, A., McMullan, P. E., Williams, J. P., Lewis, A., Sudharsan, S., et al. (2020). Microbial lag phase can be indicative of, or independent from, cellular stress. *Sci. Rep.* 10:5948. doi: 10.1038/s41598-020-62552-4

Hara, H., Yamamoto, Y., Higashitani, A., Suzuki, H., and Nishimura, Y. (1991). Cloning, mapping, and characterization of the *Escherichia coli* prc gene, which is involved in C-terminal processing of penicillin-binding protein 3. *J. Bacteriol.* 173, 4799–4813. doi: 10.1128/jb.173.15.4799-4813.1991

Hartwig, S., Pinske, C., and Sawers, R. G. (2015). Chromogenic assessment of the three molybdo-selenoprotein formate dehydrogenases in *Escherichia coli*. *Biochem. Biophys. Rep.* 1, 62–67. doi: 10.1016/j.bbrep.2015.03.006

Hayes, F. (2003). Transposon-based strategies for microbial functional genomics and proteomics. *Annu. Rev. Genet.* 37, 3–29. doi: 10.1146/annurev.genet.37.110801.142807

Huang, W. C., Lin, C. Y., Hashimoto, M., Wu, J. J., Wang, M. C., Lin, W. H., et al. (2020). The role of the bacterial protease Prc in the uropathogenesis of extraintestinal pathogenic *Escherichia coli*. *J. Biomed. Sci.* 27:14. doi: 10.1186/s12929-019-0605-y

Iwadate, Y., Funabasama, N., and Kato, J. I. (2017). Involvement of formate dehydrogenases in stationary phase oxidative stress tolerance in *Escherichia coli*. *FEMS Microbiol. Lett.* 364, 1–8. doi: 10.1093/femsle/fnx193

Jiang, P., and Ninfa, A. J. (1999). Regulation of autophosphorylation of *Escherichia coli* nitrogen regulator II by the PII signal transduction protein. *J. Bacteriol.* 181, 1906–1911. doi: 10.1128/JB.181.6.1906-1911.1999

Jiang, X., Tan, W. B., Shrivastava, R., Seow, D., Chen, S. L., Guan, X. L., et al. (2020). Mutations in enterobacterial common antigen biosynthesis restore outer membrane barrier function in *Escherichia coli* tol-pal mutants. *Mol. Microbiol.* 114, 991–1005. doi: 10.1111/mmi.14590

Johnson, M. D., Burton, N. A., Gutiérrez, B., Painter, K., and Lund, P. A. (2011). RcsB is required for inducible acid resistance in *Escherichia coli* and acts at gadE-dependent and -independent promoters. *J. Bacteriol.* 193, 3653–3656. doi: 10.1128/JB.05040-11

Kashyap, D. R., Kowalczyk, D. A., Shan, Y., Yang, C. K., Gupta, D., and Dziarski, R. (2020). Formate dehydrogenase, ubiquinone, and cytochrome bd-I are required for peptidoglycan recognition protein-induced oxidative stress and killing in *Escherichia coli*. *Sci. Rep.* 10:1993. doi: 10.1038/s41598-020-58302-1

Kenney, L. J., and Anand, G. S. (2020). EnvZ/OmpR two-component signaling: an archetype system that can function noncanonically. *EcoSal Plus* 9, 1–47. doi: 10.1128/ecosalplus.ESP-0001-2019

Klein, G., and Raina, S. (2015). Regulated Control of the Assembly and Diversity of LPS by Noncoding sRNAs. *BioMed Res. Int.* 2015:153561. doi: 10.1155/2015/153561

Kozmin, S. G., and Schaaper, R. M. (2013). Genetic characterization of moaB mutants of *Escherichia coli*. *Res. Microbiol.* 164, 689–694. doi: 10.1016/j.resmic.2013.05.001

Langridge, G. C., Phan, M. D., Turner, D. J., Perkins, T. T., Parts, L., Haase, J., et al. (2009). Simultaneous assay of every *Salmonella Typhi* gene using one million transposon mutants. *Genome Res.* 19, 2308–2316. doi: 10.1101/gr.097097.109

Lee, J. H., Park, J. H., Kim, J. A., Neupane, G. P., Cho, M. H., Lee, C. S., et al. (2011). Low concentrations of honey reduce biofilm formation, quorum sensing, and virulence in *Escherichia coli* O157:H7. *Biofouling* 27, 1095–1104. doi: 10.1080/08927014.2011.633704

Leimkühler, S. (2014). The biosynthesis of the molybdenum cofactor in *Escherichia coli* and its connection to FeS cluster assembly and the thiolation of tRNA. *Adv. Biol.* 29, 1–29. doi: 10.1155/2014/808569

Lenski, R. E., Rose, M. R., Simpson, S. C., and Tadler, S. C. (1991). Long-term experimental evolution in *Escherichia coli*. I. Adaptation and divergence during 2,000 generations. *Am. Nat.* 138, 1315–1341. doi: 10.1086/285289

Lu, J., and Holmgren, A. (2014). The thioredoxin antioxidant system. *Free Rad. Biol. Med.* 66, 75–87. doi: 10.1016/j.freeradbiomed.2013.07.036

Lüke, I., Butland, G., Moore, K., Buchanan, G., Lyall, V., Fairhurst, S. A., et al. (2008). Biosynthesis of the respiratory formate dehydrogenases from Escherichia coli: characterization of the FdhE protein. *Arch. Microbiol.* 190, 685–696. doi: 10.1007/s00203-008-0420-4

Machas, M., Kurgan, G., Abed, O. A., Shapiro, A., Wang, X., and Nielsen, D. (2021). Characterizing *Escherichia coli*'s transcriptional response to different styrene exposure modes reveals novel toxicity and tolerance insights. *J. Ind. Microbiol. Biotechnol.* 48:kuab019. doi: 10.1093/jimb/kuab019

Manyi-Loh, C. E., Clarke, A. M., and Ndip, N. (2011). An overview of honey: therapeutic properties and contribution in nutrition and human health. *Afr. J. Microbiol. Res.* 5, 844–852.

Masoura, M., Passaretti, P., Overton, T. W., Lund, P. A., and Gkatzionis, K. (2020). Use of a model to understand the synergies underlying the antibacterial mechanism of H2O2-producing honeys. *Sci. Rep.* 10:17692. doi: 10.1038/s41598-020-74937-6

Nebe-von-Caron, G., Stephens, P. J., Hewitt, C. J., Powell, J. R., and Badley, R. A. (2000). Analysis of bacterial function by multi-colour fluorescence flow cytometry and single cell sorting. *J. Microbiol. Methods* 42, 97–114. doi: 10.1016/s0167-7012(00)00181-0

Newby, R. S., Dryden, M., Allan, R. N., and Salib, R. J. (2018). Antimicrobial activity of a novel bioengineered honey against non-typeable *Haemophilus influenzae* biofilms: an in vitro study. *J. Clin. Pathol.* 71, 554–558. doi: 10.1136/jclinpath-2017-204901

Nicolaou, S. A., Fast, A. G., Nakamaru-Ogiso, E., and Papoutsakis, E. T. (2013). Overexpression of fetA (ybbL) and fetB (ybbM), encoding an iron exporter, enhances resistance to oxidative stress in *Escherichia coli*. *Appl. Environ. Microbiol.* 79, 7210–7219. doi: 10.1128/AEM.02322-13

Nishio, E. K., Ribeiro, J. M., Oliveira, A. G., Andrade, C. G., Proni, E. A., Kobayashi, R. K., et al. (2016). Antibacterial synergic effect of honey from two stingless bees: *Scaptotrigona bipunctata Lepeletier*, 1836, and *S. postica Latreille*, 1807. *Sci. Rep.* 6:21641. doi: 10.1038/srep21641

Phan, M. D., Peters, K. M., Sarkar, S., Lukowski, S. W., Allsopp, L. P., Gomes Moriel, D., et al. (2013). The serum resistome of a globally disseminated multidrug resistant uropathogenic *Escherichia coli* clone. *PLoS Genet.* 9:e1003834. doi: 10.1371/journal.pgen.1003834

Quinn, H. J., Cameron, A. D., and Dorman, C. J. (2014). Bacterial regulon evolution: distinct responses and roles for the identical OmpR proteins of *Salmonella Typhimurium* and *Escherichia coli* in the acid stress response. *PLoS Genet.* 10:e1004215. doi: 10.1371/journal.pgen.1004215

Rademacher, C., and Masepohl, B. (2012). Copper-responsive gene regulation in bacteria. *Microbiology (Reading, England)* 158(Pt 10), 2451–2464. doi: 10.1099/mic.0.058487-0

Riondet, C., Cachon, R., Waché, Y., Alcaraz, G., and Diviès, C. (1999). Changes in the proton-motive force in *Escherichia coli* in response to external oxidoreduction potential. *Eur. J. Biochem.* 262, 595–599. doi: 10.1046/j.1432-1327.1999.00429.x

Robinson, M. D., McCarthy, D. J., and Smyth, G. K. (2010). edgeR: a Bioconductor package for differential expression analysis of digital gene expression data. *Bioinformatics* 26, 139–140. doi: 10.1093/bioinformatics/btp616

Rodionov, D. A., Mironov, A. A., Rakhmaninova, A. B., and Gelfand, M. S. (2000). Transcriptional regulation of transport and utilization systems for hexuronides, hexuronates and hexonates in gamma purple bacteria. *Mol. Microbiol.* 38, 673–683. doi: 10.1046/j.1365-2958.2000.02115.x

Seaver, L. C., and Imlay, J. A. (2001). Hydrogen peroxide fluxes and compartmentalization inside growing *Escherichia coli*. *J. Bacteriol.* 183, 7182–7189. doi: 10.1128/JB.183.24.7182-7189.2001

Seoane, A., Sabbaj, A., McMurry, L. M., and Levy, S. B. (1992). Multiple antibiotic susceptibility associated with inactivation of the prc gene. *J. Bacteriol.* 174, 7844–7847. doi: 10.1128/jb.174.23.7844-7847.1992

Shrivastava, R., Jiang, X., and Chng, S. S. (2017). Outer membrane lipid homeostasis via retrograde phospholipid transport in *Escherichia coli*. *Mol. Microbiol.* 106, 395–408. doi: 10.1111/mmi.13772

Sindi, A., Chawn, M., Hernandez, M. E., Green, K., Islam, M. K., Locher, C., et al. (2019). Anti-biofilm effects and characterisation of the hydrogen peroxide activity of a range of Western Australian honeys compared to Manuka and multifloral honeys. *Sci. Rep.* 9:17666. doi: 10.1038/s41598-019-54217-8

Singh, S. K., Parveen, S., SaiSree, L., and Reddy, M. (2015). Regulated proteolysis of a cross-link-specific peptidoglycan hydrolase contributes to bacterial morphogenesis. *Proc. Natl. Acad. Sci. U.S.A.* 112, 10956–10961. doi: 10.1073/pnas.1507760112

Skovran, E., Lauhon, C. T., and Downs, D. M. (2004). Lack of YggX results in chronic oxidative stress and uncovers subtle defects in Fe-S cluster metabolism in *Salmonella enterica*. *J. Bacteriol.* 186, 7626–7634. doi: 10.1128/JB.186.22.7626-7634.2004

Soo, V. W., Hanson-Manful, P., and Patrick, W. M. (2011). Artificial gene amplification reveals an abundance of promiscuous resistance determinants in *Escherichia coli*. *Proc. Natl. Acad. Sci. U.S.A.* 108, 1484–1489. doi: 10.1073/pnas.1012108108

Stincone, A., Daudi, N., Rahman, A. S., Antczak, P., Henderson, I., Cole, J., et al. (2011). A systems biology approach sheds new light on *Escherichia coli* acid resistance. *Nucleic Acids Res.* 39, 7512–7528. doi: 10.1093/nar/gkr338

Sun, Y., Fukamachi, T., Saito, H., and Kobayashi, H. (2012). Respiration and the F1Fo-ATPase enhance survival under acidic conditions in *Escherichia coli*. *PLoS One* 7:e52577. doi: 10.1371/journal.pone.0052577

Thomason, L. C., Costantino, N., and Court, D. L. (2007). *E. coli* genome manipulation by P1 transduction. *Curr. Protoc. Mol. Biol.* 1, 1–17 doi: 10.1002/0471142727.mb0117s79

Wasfi, R., Elkhatib, W. F., and Khairalla, A. S. (2016). Effects of selected egyptian honeys on the cellular ultrastructure and the gene expression profile of *Escherichia coli*. *PLoS One* 11:e0150984. doi: 10.1371/journal.pone.0150984

Weber, H., Pesavento, C., Possling, A., Tischendorf, G., and Hengge, R. (2006). Cyclic-di-GMP-mediated signalling within the sigma network of *Escherichia coli*. *Mol. Microbiol.* 62, 1014–1034. doi: 10.1111/j.1365-2958.2006.05440.x

Zheng, M., Wang, X., Templeton, L. J., Smulski, D. R., LaRossa, R. A., and Storz, G. (2001). DNA microarray-mediated transcriptional profiling of the *Escherichia coli* response to hydrogen peroxide. *J. Bacteriol.* 183, 4562–4570. doi: 10.1128/JB.183.15.4562-4570.2001

Zhou, L., Lei, X. H., Bochner, B. R., and Wanner, B. L. (2003). Phenotype microarray analysis of *Escherichia coli* K-12 mutants with deletions of all two-component systems. *J. Bacteriol.* 185, 4956–4972. doi: 10.1128/JB.185.16.4956-4972.2003

Zomer, A., Burghout, P., Bootsma, H. J., Hermans, P. W., and van Hijum, S. A. (2012). ESSENTIALS: software for rapid analysis of high throughput transposon insertion sequencing data. *PLoS One* 7:e43012. doi: 10.1371/journal.pone.0043012

Conflict of Interest: The authors declare that the research was conducted in the absence of any commercial or financial relationships that could be construed as a potential conflict of interest.

Publisher's Note: All claims expressed in this article are solely those of the authors and do not necessarily represent those of their affiliated organizations, or those of the publisher, the editors and the reviewers. Any product that may be evaluated in this article, or claim that may be made by its manufacturer, is not guaranteed or endorsed by the publisher.

frontiers in Microbiology

REVIEW
published: 20 January 2022
doi: 10.3389/fmicb.2021.738470

Landscape of Stress Response and Virulence Genes Among *Listeria monocytogenes* Strains

Brankica Z. Lakicevic[1], Heidy M. W. den Besten[2] and Daniela De Biase[3]*

[1] Institute of Meat Hygiene and Technology, Belgrade, Serbia, [2] Food Microbiology, Wageningen University and Research, Wageningen, Netherlands, [3] Department of Medico-Surgical Sciences and Biotechnologies, Sapienza University of Rome, Latina, Italy

The pathogenic microorganism *Listeria monocytogenes* is ubiquitous and responsible for listeriosis, a disease with a high mortality rate in susceptible people. It can persist in different habitats, including the farm environment, the food production environments, and in foods. This pathogen can grow under challenging conditions, such as low pH, low temperatures, and high salt concentrations. However, *L. monocytogenes* has a high degree of strain divergence regarding virulence potential, environmental adaption, and stress response. This review seeks to provide the reader with an up-to-date overview of clonal and serotype-specific differences among *L. monocytogenes* strains. Emphasis on the genes and genomic islands responsible for virulence and resistance to environmental stresses is given to explain the complex adaptation among *L. monocytogenes* strains. Moreover, we highlight the use of advanced diagnostic technologies, such as whole-genome sequencing, to fine-tune quantitative microbiological risk assessment for better control of listeriosis.

Keywords: *L. monocytogenes*, stress genes, genomic islands, diversity, lineages, clonal complexes, low pH, persistence

OPEN ACCESS

Edited by:
Arun K. Bhunia,
Purdue University, United States

Reviewed by:
Beatrix Stessl,
University of Veterinary Medicine Vienna, Austria
Trond Møretrø,
Norwegian Institute of Food, Fisheries and Aquaculture Research (Nofima), Norway

****Correspondence:***
Brankica Z. Lakicevic
brankica.lakicevic@inmes.rs

Specialty section:
This article was submitted to Food Microbiology, a section of the journal Frontiers in Microbiology

Received: *08 July 2021*
Accepted: *30 November 2021*
Published: *20 January 2022*

Citation:
Lakicevic BZ, Den Besten HMW and De Biase D (2022) Landscape of Stress Response and Virulence Genes Among Listeria monocytogenes Strains. Front. Microbiol. 12:738470. doi: 10.3389/fmicb.2021.738470

INTRODUCTION

Listeria monocytogenes is a Gram-positive, facultative anaerobe, non-spore-forming, and psychro- and salt-tolerant organism. It is also a facultative intracellular pathogen, both for humans and animals. In susceptible people, including immunocompromised persons, infants, pregnant women, and older people, it can cause clinical manifestations with high mortality rates (Desai et al., 2019; Kayode et al., 2019; Schlech, 2019). Cases of human listeriosis often can be traced back to food products contaminated during production, on which the microorganism grows to high numbers. Special concern is in particular given to ready-to-eat (RTE) products, such as salads, deli meat, or smoked salmon, because these are consumed without a further heating step (Leong et al., 2015; EFSA Panel on Biological Hazards [Efsa Biohaz Panel]et al., 2018). Given the ubiquitous distribution of this microorganism, its transmission into food-processing facilities occurs either *via* raw materials or *via* equipment and employees. Once introduced in the facilities, several factors have been suggested to contribute to the ability of a strain to establish long-lasting colonization (Holch et al., 2013; Leong et al., 2014; Lakicevic and Nastasijevic, 2017; Stoller et al., 2019). Some authors hypothesized that a particular feature that makes the control of *L. monocytogenes* difficult in the processing environment is its capacity to survive or even to grow in different stressful conditions and to form biofilms (Gandhi and Chikindas, 2007; Ferreira et al., 2014; Gahan and Hill, 2014; Ariza-Miguel et al., 2015). The fast ability of *L. monocytogenes* to

colonize food-processing facilities and the formation of persisters of some *L. monocytogenes* strains in various niches along the food chain have been described (Berrang et al., 2010; Leong et al., 2014; Bolocan et al., 2016). This suggests that persister cells provide reservoirs for contamination, ultimately increasing the likelihood of infecting humans. An alternative hypothesis is that there are no strains of *L. monocytogenes* with unique attributes but hard-to-reach areas (also known as harborage sites) in food industry environments and equipment where *L. monocytogenes* can reside (Carpentier and Cerf, 2011). Furthermore, tolerance to sanitizers and disinfectants such as benzalkonium chloride (BC) was observed in *L. monocytogenes* isolates from food-processing environments. This tolerance may be attributed to subinhibitory concentrations of a disinfectant, which are caused by insufficient cleaning and improper sanitation, thus probably contributing to biofilm formation and leading to *Listeria* persistence (Martínez-Suárez et al., 2016). The same authors have hypothesized that these subinhibitory concentrations cause the expression of stress response genes leading to a reduction in cell permeability to these compounds. These genetic traits include resistance genes such as the *qacH* gene of transposon Tn*6188* and the resistance cassette *bcrABC* (Elhanafi et al., 2010; Müller et al., 2013, 2014; Zuber et al., 2019), described in *Persistence mechanisms*. Moreover, it is crucial to identify the interactions between stress response and virulence and to know how this microorganism survives, adapts to adverse conditions, and triggers genes involved in virulence or promoting persistence. This would help to explain the observed inverse correlation between strains with a higher prevalence of genes involved in BC tolerance, as well as other stress-related genes, amongst hypovirulent (i.e., low virulence) lineage II strains (Quereda et al., 2021). All this knowledge may contribute to the development of new intervention strategies for better control of the level of *L. monocytogenes* in the food chain.

LISTERIA MONOCYTOGENES DIVERSITY AND HETEROGENEITY OF THE VIRULENCE DETERMINANTS

L. monocytogenes evolves slowly but has been characterized by a significant level of diversity (Ragon et al., 2008; Orsi et al., 2011). It can be grouped into four major evolutionary lineages indicated by the roman numbers from I to IV, by 14 lineage-related serotypes and more than 170 clonal complexes (CCs),[1] geographically and temporally widespread, as defined by multilocus sequence typing, and whole-genome phylogenetic analysis (Doumith et al., 2004; Orsi et al., 2011; Haase et al., 2014; Doijad et al., 2015; Chen et al., 2016; Moura et al., 2016; Bergholz et al., 2018). It belongs to the genus that currently includes 26 recognized species, of which notably 20 have been described since 2009 (Graves et al., 2010; Leclercq et al., 2010, 2019; Bertsch et al., 2013; Lang Halter et al., 2013; den Bakker et al., 2014; Weller et al., 2015; Doijad et al., 2018; Nuñez-Montero et al., 2018; Quereda et al., 2020; Carlin et al., 2021). Lineage I of *L. monocytogenes* encompasses serotypes 1/2b, 3b, 4b, 4d, 4e, and 7, lineage II includes serotypes 1/2a, 1/2c, 3a, 3c, and 4h, lineage III comprises serotypes 4a, atypical 4b, and 4c, whereas lineage IV encompasses serotypes 4a and 4c (Seeliger and Hohne, 1979; Ragon et al., 2008; Maury et al., 2016; Painset et al., 2019; Yin et al., 2019).

Previous studies have found that some hypervirulent clones such as CC1, CC2, CC4, and CC6 (all of lineage I and predominant in Western countries) were strongly associated with listeriosis, whereas hypovirulent clones, including CC8, CC9, CC101, CC121, and CC204 (lineage II), were strongly associated with food product contamination but less with human infections, in part due to loss-of-function mutations in virulence genes (Fagerlund et al., 2016; Maury et al., 2016, 2019). In accordance with that, all CC2 isolates carried a full-length *inlA* gene (see later), whereas CC9 and CC121 presented a premature stop codon mutation in this gene that correlated with reduced virulence (Gelbíčová et al., 2015; Guidi et al., 2021). Maury et al. (2019) demonstrated that differences in product associations among clones might be attributed to adaptation differences between clones in distinct ecological niches and/or different food product contamination routes during processing. They showed that CC1 was more representative for dairy products, whereas hypovirulent clones, mainly CC9 and CC121, were strongly associated with meat and fish products and produced more biofilm in the presence of low BC concentrations. Hypervirulent strains of *L. monocytogenes* sequence type (ST) 6 have been associated with outbreaks, including an outbreak linked to frozen vegetables in five countries in Europe during 2015–2018, an outbreak associated with contaminated meat pâté in Switzerland during 2016, listeriosis outbreak that occurred in South Africa during 2017–2018 with a 27% mortality rate, and the largest outbreak of listeriosis in Germany linked to blood sausages in 2018–2019 (Althaus et al., 2017; EFSA and ECDC, 2018; Halbedel et al., 2020; Thomas et al., 2020). More recently, an outbreak of listeriosis was caused by the persistence of *L. monocytogenes* serotype 4b ST6 (lineage I) in a cheese-processing facility in Switzerland (Nüesch-Inderbinen et al., 2021).

To cause listeriosis in humans and animals, important genes must be present in *L. monocytogenes* genome and expressed under the appropriate conditions. The *inlAB* locus and the pathogenicity islands LIPI-1, LIPI-3, and LIPI-4 encode such key virulence factors (Gelbíčová et al., 2015; Maury et al., 2016; Quereda et al., 2018). In particular, *inlA* and *inlB* code for internalin A (InlA) and internalin B (InlB) that bind the host cell receptors E-cadherin and Met, respectively. The transcriptional regulator positive regulator factor A (PrfA) controls the expression of both *inlAB* and LIPI-1 (Quereda et al., 2018).

LIPI-1, present in all *L. monocytogenes*, is found between the genes *prs* and *orfX*, is 9-kb long, and consists of six genes, i.e., *prfA*, *plcA*, *hly*, *mpl*, *actA*, and *plcB* (Dussurget, 2008). Notably, *Listeria innocua*, a non-pathogenic *Listeria* species, lacks both LIPI-1 and *inlAB* genes; however, LIPI-1 and *inlA*, functional both *in vivo* and *in vitro*, are present in rare, natural, atypical *L. innocua* species (Johnson et al., 2004; Volokhov et al., 2007; den Bakker et al., 2010; Moreno et al., 2012; Moura et al., 2019). This suggested that *L. monocytogenes* and *L. innocua* likely evolved from a common ancestor where the virulence loci LIPI-1 and *inlAB* were both present (Volokhov et al., 2007).

[1] http://bigsdb.pasteur.fr/listeria

L. innocua FSL J1-023 is one such aberrant strain, described as a rare, natural, non-pathogenic, hemolytic-positive, rhamnose and xylose fermentation-negative strain; its genome sequence is the reference one for linking horizontal gene transfer and recombination as drivers in the evolution of *Listeria* pathogenicity (Johnson et al., 2004; Lakicevic et al., 2014). Notably, all *L. innocua* genomes lack other internalins (i.e., *inlCEFGHJKP*), and this suggested that, unlike *inlAB*, the former genes were not present in the common ancestor and acquired at a later stage by *L. monocytogenes* (Moura et al., 2019).

As for LIPI-2, this pathogenicity island was discovered in *Listeria ivanovii*, a species pathogenic for feedstocks, mostly ovines and bovines, and humans, though rarely (Guillet et al., 2010). Originally, it was described as a LIPI specific to *L. ivanovii.* It encompasses the *smcL* gene coding for sphingomyelinase (involved in phagosome disruption) and 10 genes coding for proteins of the internalin family (Domínguez-Bernal et al., 2006). However, recent studies showed that *L. monocytogenes* isolates, belonging to a new sub-lineage of the major lineage II with hypervirulent features (SL626/CC33, serovar 4 h), contain a truncated LIPI-2, i.e., carrying only *smcL* and two internalins genes, namely *i-inlF* and *i-inlE*, likely acquired by transposon-mediated horizontal gene transfer from *L. ivanovii* (Yin et al., 2019; Feng et al., 2020).

LIPI-3 is an additional sub-lineage pathogenicity island encoding listeriolysin S (LLS), a bacteriocin. LLS (coded by *llsA*), a hemolytic toxin secreted by *L. monocytogenes*, is present only in a subset of isolates from lineage I epidemic strains that specifically secrete it in the gut (Quereda et al., 2017). Notably, Quereda et al. (2016) demonstrated that in an orally infected mouse model, *L. monocytogenes lls* mutants exhibited reduced bacterial load in the intestinal content at 6 h post-infection as compared with the wild-type strain, and the differences were also evident at 24 and 48 h post-infection and correlated with the reduced number of intracellular bacteria. Moreover, the same authors showed that the presence of *L. monocytogenes*-produced LLS in the intestine of the infected mice caused a significant decrease in the occurrence of different bacterial genera, such as *Alloprevotella*, *Allobaculum*, and *Streptococcus*. These results, for the first time, provided evidence that LLS plays an important role in the interaction with other species in the gut microbiota. In a study conducted by Matle et al. (2020), LIPI-3 was detected in isolates of which the majority were from lineage I, i.e., CC1, CC2, CC3, and CC228. Also, Roedel et al. (2019) found LIPI-3 in *L. monocytogenes* isolates belonging to CC1, CC3, CC4, CC6, and CC288. Tavares et al. (2020) described single-nucleotide polymorphism (SNP) of eight LIPI-3 genes (*llsAGHXBYDP*) of the four different STs (ST1, ST3, ST218, and ST288) compared with reference strain F2365 (lineage I). The authors revealed that LIPI-3 genes are well conserved in ST1 (serogroup IVb), whereas a number of SNPs were identified in ST3 (serogroup IIb), ST218 (serogroup IVb-v1), and ST288 (serogroup IIb). Within the LIPI-3 island, *llsX* is the only gene that is highly conserved among different LIPI-3-positive *L. monocytogenes* CC (**Figure 1**) and even in atypical hemolytic *L. innocua* (**Figure 1**). However, under acid stress conditions, only reference strain F2365 (4b) presented expression of *llsX* comparable with ST3 and ST288 (serogroup IIb, lineage I) strains, which points to acidic pH as an important environmental trigger (Clayton et al., 2014).

LIPI-4 pathogenic island is a cluster of six genes encoding a putative cellobiose family phosphotransferase system and shown to confer hypervirulence by enhancing invasion of the CNS and placenta (Maury et al., 2016). It is only found in some isolates of lineage I, i.e., CC2, CC4, and CC87 (Maury et al., 2016; Chen et al., 2018, 2020; Hilliard et al., 2018; Painset et al., 2019; Roedel et al., 2019; Matle et al., 2020; Zhang et al., 2020). It is known that CC2 has a worldwide distribution, whereas CC4 and CC87 are the most prevalent clones in France and China (Maury et al., 2016; Zhang et al., 2020). The latter CC was also responsible for two outbreaks in Guipúzcoa (Northern Spain) in 2013 and 2014 (Pérez-Trallero et al., 2014; Wang et al., 2019). In addition to LIPI-4, all CC87 strains contained a novel type II restriction–modification system with unknown significance (Wang et al., 2019).

Anaerobiosis represents an important trigger for virulence determinants because, in the gastrointestinal tract, the oxygen level gradually decreases and favors facultative anaerobic microorganisms such as *L. monocytogenes* (Horn and Bhunia, 2018). Indeed, Müller-Herbst et al. (2014) detected 28 non-essential genes that were upregulated only anaerobically, of which a subset were virulence-related genes, e.g., *inlB* and *Listeria* adhesion protein that is essential for full virulence (Burkholder et al., 2009). A complementary screening of an insertion mutant library of *L. monocytogenes* demonstrated that F_1F_0-ATPase (see *FoF1-ATPase, Glutamate decarboxylase, and Arginine and Agmatine deiminases*) is essential for anaerobic proliferation of *L. monocytogenes* (Müller-Herbst et al., 2014). Anaerobiosis also induced an acid tolerance response (Sewell et al., 2015), providing *L. monocytogenes* robustness to survive the stomach acidity and transit to the intestine. According to that, some CCs are more tolerant to low pH and colonize better the intestinal lumen (also known as host-associated hypervirulent clones) than those of hypovirulent CCs (Hingston et al., 2017; Maury et al., 2019).

All this information highlight that hypervirulent clones (CC1, CC2, CC4, and CC6) greatly connect with clinical cases, are predominantly found in lineage I, colonize better in the intestine lumen, cause listeriosis in a healthy host, and are strongly associated with dairy products. On the contrary, hypovirulent clones (e.g., CC9 and CC121), greatly connected with food and food-related isolates, are predominantly found in lineage II, causing listeriosis in immunocompromised patients, and are strongly associated with meat and fish products. All lineages of *L. monocytogenes* possess highly conserved LIPI-1 and *inlA/B* locus, which fits with the fact that the majority of hypovirulent clones and other lineage II isolates present truncated InlA, leading to virulence attenuation. Furthermore, comparative genomics analysis between hypo- and hypervirulent clones have uncovered the specific virulence clusters such as LIPI-3 (present approximately in 50% of lineage I strains) and LIPI-4. Regardless of these facts, the regulatory authorities consider all strains of *L. monocytogenes* to be equally pathogenic (Vázquez-Boland et al., 2020; Quereda et al., 2021), whereas the food safety risk attributed to different subgroups differ (Chen et al., 2006).

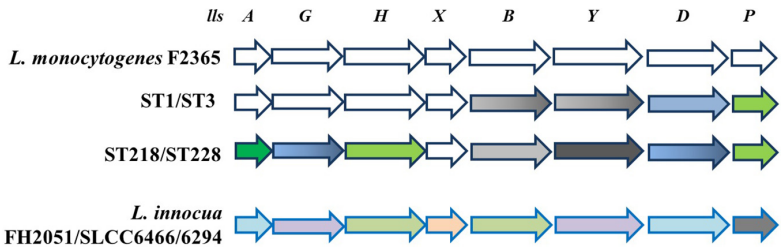

FIGURE 1 | Schematic representation of LIPI-3 pathogenicity island. In *L. monocytogenes* reference strain F2365 and different STs, all LIPI-3 genes display SNPs, except *llsX*, which is strongly conserved. SNPs are shown as follows: 0—white; 1—gray; 2—green; 4—dark green; 10–17—blue; 18—black. When color is shaded, SNPs are present only in one of two ST indicated. Bottom line shows that LIPI-3 is also present in some strains of *L. innocua*, where sequence identity with *L. monocytogenes* reference strain F2365 ranges from 91% (*llsP,* gray) to 95% (*llsY* and *llsG*, violet), 97% (*llsX,* pink), 98% (*llsA* and *llsD,* light blue), and 99% (*llsH* and *llsB,* light green) (adapted from Clayton et al., 2014; Tavares et al., 2020).

LISTERIA MONOCYTOGENES AND STRESS RESISTANCE GENES

The resistance to environmental stresses such as acidic environment, nisin, bile acids, and high osmolarity is conferred to *L. monocytogenes* by stress resistance determinants located on the Stress Survival Islet 1 (SSI-1), whereas stress resistance determinants to alkaline and oxidative stresses are located on the SSI-2 (Hein et al., 2011; Guidi et al., 2021).

Generally, uncovering the resistance mechanisms to stressful conditions in food matrices and the environment is regarded as important to contribute to the development of novel and efficient measures to prevent contamination through the whole food chain continuum and control the growth of *L. monocytogenes* during food storage (Bucur et al., 2018).

Stress Survival Islets 1 and 2

SSI-1, a five-gene stress survival islet [*lmo0444*, *lmo0445*, *lmo0446* (*pva*), *lmo0447* (*gadD1*), and *lmo0448* (*gadT1*)], has an equal distribution in human clinical isolates and in strains isolated from food and food-processing environments (Ryan et al., 2010). The presence of SSI-1, as well as the ability to form biofilms, correlated with the persistence of *L.monocytogenes* strains (Keeney et al., 2018). Notably, the strongest biofilms were formed by strains from serotype 1/2b, such as CC3 and CC5, the majority of which contained SSI-1, whereas serotype 4b (such as CC2 and CC6), most of which do not contain SSI-1, formed the weakest biofilms (Keeney et al., 2018).

According to Harter et al. (2017), SSI-2, consisting of the genes *lin0464* and *lin0465*, encoding a putative transcriptional regulator and an intracellular PfpI protease, respectively, is predominantly found in the hypovirulent strains of *L. monocytogenes* ST121. SSI-2 contributes to survival upon oxidative and alkaline stress conditions, thus potentially favoring *L. monocytogenes* adaptation and persistence in the food-processing environments. Notably, in addition to SSI-2, the genome of *L. monocytogenes* ST121 possesses plasmids and the transposon Tn*6188*, which were hypothesized to be responsible for supporting its survival in food-processing environments (Müller et al., 2014; Schmitz-Esser et al., 2015; Pasquali et al., 2018). SSI-2 occasionally is found in other *L. monocytogenes* strains, such as ST1033 (CC1, serotype 4b).

Interestingly, SSI-2-positive strains were detected in *L. monocytogenes* lineage I, lineage III, and also in *L. innocua* but with a slightly shorter islet harboring only 1,947 bp (Harter et al., 2017). Phylogenetic analysis indicated that *L. innocua* SSI-2 shares the highest similarity with those of *L. monocytogenes* strains ST13 and CC193 that belong to lineage II (i.e., all food isolates) (Harter et al., 2017).

F_oF_1-ATPase, Glutamate Decarboxylase, and Arginine and Agmatine Deiminases

Notably, SSI-1 contains *gadD1* and *gadT1*, which are among the genes protecting from acid stress. Indeed, the ability to tolerate a low pH environment is an important feature of *L. monocytogenes* because it allows survival in acidic environments encountered in the gastrointestinal tract of the host, in the macrophage phagosome, and in natural and food-processing environments (Gahan and Hill, 2014; Lund et al., 2014; Arcari et al., 2020; Lund et al., 2020). *L. monocytogenes* harbors membrane-associated systems and intracellular systems to resist acidic environments and to control intracellular pH. Several mechanisms, schematically depicted in **Figure 2**, are known to maintain intracellular pH (pH_i) to values compatible with *L. monocytogenes* vitality. These include the F_0F_1-ATPase, the glutamate decarboxylase (GAD) system, and the arginine and agmatine deiminases (ADI and AgDI, respectively) (Cotter et al., 2000; Feehily et al., 2014; Cheng et al., 2017). The F_0F_1-ATPase, a multi-subunit enzyme system, is involved in the acid tolerance response initiation upon mild acidic pH stress. The GAD system, on the other hand, can affect survival under mild acid stress but also under harsher acidic conditions (Karatzas et al., 2012). Notably, the GAD system is also activated under low oxygen availability, typically encountered by *L. monocytogenes* when exposed to food packaging atmosphere (Francis et al., 2007; Sewell et al., 2015). The system consists of three homologous glutamate decarboxylases, namely GadD1, GadD2, and GadD3, and of the cognate glutamate/GABA antiporters GadT1 and GadT2 (**Figure 2**). The decarboxylases and the antiporters are encoded by the relevant genes at three distinct genetic loci. Four genes are organized in the following operons: *gadD1T1*

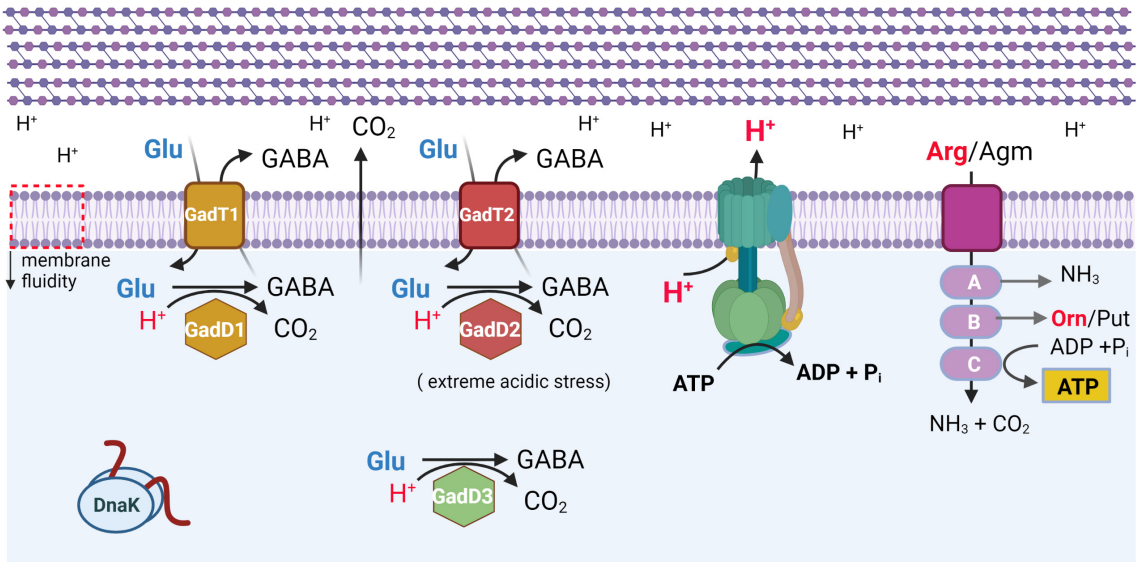

FIGURE 2 | Schematic representation of most effective systems protecting *L. monocytogenes* from acidic stress. All systems are activated under mild acidic stress, with GadD2T2 system mostly effective under extreme acidic stress (adapted from Lund et al., 2020). F_0F_1-ATPase is shown in blue-green. ArgD/AguD transporter is shown in purple. A, ArcA (arginine), AguA1 (agmatine) deiminase; B, ArcB/AguB carbamoyl-transferase; C, ArcC/AguC carbamate kinase. GadT1 and GadT2 refer to glutamate (Glu)/GABA antiporters. GadD1, GadD2, and GadD3 are glutamate decarboxylase isoforms. Orn, ornithine. Put, putrescine. DnaK, chaperone. All membrane proteins are localized in lipid bilayer of plasma membrane, which also undergoes a decrease in membrane fluidity (downward pointing arrow, on leftmost side). Multilayered peptidoglycan of cell wall is schematically represented above plasma membrane. Created with BioRender.com.

and *gadT2D2*, whereas the *gadD3* gene, the fifth gene, is an independent unit (Cotter et al., 2005). In particular, the *gadD1T1* operon enhances growth under mildly acidic conditions (see also *Stress survival islets 1 and 2*), whereas *gadT2D2* plays an important role in conferring survival under extremely acidic conditions (Cotter et al., 2001, 2005). The *gadD3* gene, positively regulated by the stationary-phase sigma factor σ^B, in addition to being part of the GAD system, was shown to be involved in nisin resistance (Begley et al., 2010). According to Chen et al. (2012), *gadD2* and *gadD3* are present in all *L. monocytogenes* strains, whereas *gadD1* is present in only 36.6% of the strains, including all those belonging to serovar 1/2c, and 68.5% of the strains of serovar 1/2a. Notably, only a small fraction of the strains of *L. monocytogenes* serovar 1/2b and lineage III strains (including J2-071 and HCC23) possess the *gadD1* gene. Furthermore, the *gadD1T1* operon is absent in most serotype 4 *L. monocytogenes* clinical strains (Cotter et al., 2005).

Paudyal et al. (2020) have shown that casamino acids, peptone, and tryptone are major GAD system activators resulting in upregulation of the transcription of *gadD2*. Furthermore, Paudyal et al. (2018) demonstrated that maleic acid inhibits the GAD of *L. monocytogenes* significantly, enhancing its sensitivity to acidic conditions, and thus, together with the ability to remove biofilms, maleic acid has been proposed to make a good candidate for disinfection regimes.

Moreover, Boura et al. (2020) recently showed a secondary novel role of the GAD system in protection against oxidative stress. The authors hypothesized that under oxidative stress GABA, instead of being exported by the transporter (**Figure 2**), is transferred to the GABA shunt enzymes that provide NADPH to contrast oxidative stress and allow to bypass two missing steps in the TCA cycle. They also suggested that this knowledge could find application in food hurdle technology to eliminate *L. monocytogenes*.

In addition to the GAD system, also the ADI system can be activated in response to low pH. This latter system consists of three enzymatic activities, namely arginine deiminase, ornithine carbamoyl-transferase, and carbamate kinase, encoded by the *arcA*, *arcB,* and *arcC* genes, respectively (Cheng et al., 2017). Through these enzymatic activities, arginine is converted to ornithine, CO_2, and ammonia, with concomitant production of adenosine triphosphate (**Figure 2**). It was previously reported that this gene cluster is present in lineage I and lineage II but absent from lineage III and non-pathogenic *L. innocua* and *Listeria welshimeri* (Ryan et al., 2009). However, Deng et al. (2010) showed that the ADI gene cluster is also highly conserved in lineage IIIB.

The AgDI pathway is a less known system of acid stress tolerance in *L. monocytogenes*. AgDI converts agmatine into putrescine, ammonia, and CO_2 and produces adenosine triphosphate (Chen J. et al., 2011; Soares and Knuckley, 2016). Cheng et al. (2013) found that *L. monocytogenes* harbors two putative AgDIs (*aguA1* and *aguA2*), but only AguA1 functionally participates in the AgDI pathway and mediates acid tolerance in *L. monocytogenes*.

Also, the thiamine uptake system, encoded by the *thiT* gene (formerly *lmo1429*), was shown to be required for full acid tolerance in *L. monocytogenes* (Madeo et al., 2012). According to the authors' findings, a *thiT* mutant strain resulted in significantly higher acid sensitivity than the control strain. It was suggested

that the acid sensitivity is due to the lack of thiamine that does not allow the reaction of acetolactate synthase to occur, and therefore, acetoin synthesis, which involves proton consumption, is impaired (Madeo et al., 2012).

When different *L. monocytogenes* strains are exposed to acidic environments, the acid tolerance displayed varies significantly, and this might contribute to the observed strains' differences in robustness and pathogenicity (Conte et al., 2000). The virulent reference strains *L. monocytogenes* EGD-e (1/2a, lineage II), 850658 (4a, lineage III), and 10403S (1/2a, lineage II) were more resistant to acidic stress than the avirulent M7 (4a, lineage III), which showed a defect in maintaining pH_i homeostasis (Cheng et al., 2015). Despite the observations mentioned, EGD-e cannot export GABA and relies exclusively on GadD3, whereas strain 10403S relies upon GadD2 (Feehily et al., 2014). This suggested that the GAD system in the commonly used reference strains originated from separate lines of evolution. Strain-specific patterns of acid resistance are also recognizable in other datasets (Ramalheira et al., 2010).

σ^B Regulon

The sigma factor of RNA polymerase, responsive to general stress, namely σ^B, plays an important role in *L. monocytogenes*, both in the adaptation to different stress conditions and in virulence. As shown by many studies conducted using the lineage II reference strains (mainly the 10403S as mentioned earlier and EGD-e), σ^B regulates approximately 300 genes important for virulence and responses to stresses (Severino et al., 2007; Hain et al., 2008; Raengpradub et al., 2008). Also, the literature review revealed that the σ^B regulon played a significant role in the resistance of *L. monocytogenes* strains belonging to lineages I, II, and IIIB and a limited role in the resistance of the *L. monocytogenes* lineage IIIA strain to acid and oxidative stresses (Oliver et al., 2010; Liu et al., 2019). Similarly, σ^B plays a significant role in resistance to acid and salt stresses also in *L. innocua* (Raengpradub et al., 2008).

A systematic review of the σ^B regulon in *L. monocytogenes* identifies several regulon members that include genes involved, or putatively involved, in stress response: osmotic (18 genes), oxidative (14 genes), acid (12 genes), antibiotic (6 genes), bile (3 genes), and others (24 genes) (Liu et al., 2019). However, σ^B is not the only alternative sigma factor that has been shown to play a role in the stress tolerance of *L. monocytogenes*. Other alternative sigma factors, including σ^C (previously implicated in nisin response), σ^H, and σ^L (RpoN), also regulate transcription of genes important for virulence and response to various stress and growth conditions (Glaser et al., 2001; Chaturongakul et al., 2011). Some of the genes needed in the stress responses of *L. monocytogenes* are regulated by more than one sigma factor. Overlaps have been reported between σ^B and σ^H, σ^B and σ^L, and σ^C and σ^B regulons (Chaturongakul et al., 2011). Notably, the regulation of SSI-2 (see *Stress survival islets 1 and 2*) is independent of the σ^B, but σ^H or σ^L could be involved (Harter et al., 2017). Interestingly, of the 51 genes classified in the "virulence" group of the σ^B regulon, 23 were also classified in the "stress response" group and 4 in the "metabolism" group (Liu et al., 2019). The genes that belonged both to the "virulence" and "stress response" groups included those required for survival and multiplication under host-imposed stress conditions such as acidic pH and bile acids in the gastrointestinal tract of the host and those contrasting oxidative stress in the mammalian host phagosome. These observations reinforced the hypothesis that stress response and virulence are strongly associated. Among the 24 genes of the σ^B regulon that belong only to the "virulence" group, there is the gene coding for the PrfA, located in LIPI-1 (see *L. monocytogenes diversity and heterogeneity of the virulence determinants*), which can be transcribed from multiple promoters, regulated by σ^B, σ^A, and PrfA itself (De Las Heras et al., 2011).

Resistance to Nisin and Envelope Remodeling

Natural antimicrobials, such as nisin (which belongs to the class I bacteriocins), sakacins, pediocin PA-1, plantaricin BM-1, and leucocin A (which belong to the class II bacteriocins), can be used to control *L. monocytogenes* on RTE foods (Ferreira and Lund, 1996; Nilsson et al., 1997; Franklin et al., 2004; Trinetta et al., 2010; Woraprayote et al., 2013; Ortiz et al., 2014; Balay et al., 2017; Xie et al., 2018). However, nisin is the only bacteriocin approved as a preserving additive in food. It should be highlighted that RTE foods add up further stress to *L. monocytogenes* when these foods are exposed to cold stress, organic acid stress, and osmotic stress, and some of these environmental stresses may affect bacteriocin resistance, e.g., nisin resistance increases if *L. monocytogenes* is preexposed to acid stress (van Schaik et al., 1999; Bonnet and Montville, 2005).

VirR, the response regulator of the VirRS two-component system, with a role in defense against cell envelope stress (Mandin et al., 2005), is directly controlling nisin resistance. In this specific case, instead of the receptor histidine kinase VirS, an ABC-transporter encoded by *virAB* seems to be responsible for sensing the stressor (Grubaugh et al., 2018). VirR mediates nisin and other cell envelope stress resistance by regulating the *dltABCD* operon (Kang et al., 2015), which modifies lipoteichoic acids (Abachin et al., 2002). In addition to VirR, the two-component systems LiaRS and LisRK were shown to be involved in resistance to nisin (Cotter et al., 2002; Collins et al., 2012; Bergholz et al., 2013; Nikparvar et al., 2021). In particular, these two-component systems regulate the expression of *anrAB*, *dltABCD*, *lmo2229*, *mprF*, and *telA* (Abachin et al., 2002; Gravesen et al., 2004; Thedieck et al., 2006; Collins et al., 2010a,b, 2012). With the exception of the latter, all the listed genes have an assigned role in the biosynthesis/metabolism of components of the membrane and the cell wall. Using a laboratory cheese model, temperature and pH were shown to be among the environmental conditions that affected the sensitivity of *L. monocytogenes* to nisin, the efficacy of which was stronger when the cheese was stored at low temperatures and prepared at pH close to neutrality (i.e., pH 6 and 6.5), due to the activity of *dltA* and *mprF* (Henderson et al., 2020).

The resistance to nisin varies among the various lineages, with lineage II strains being more tolerant than lineage I strains. These differences extended to serotype and CC levels. For example, serotypes 1/2a and 1/2c were more tolerant than serotype 1/2b, whereas serotype 4b showed the least tolerance to nisin, as also supported by studies showing that serotype 1/2a and 4b strains were more tolerant and sensitive to nisin, respectively

(Buncic et al., 2001; Katla et al., 2003; Szendy et al., 2019; Wambui et al., 2020). Comparing clonal types, Wambui et al. (2020) concluded that CC7 (lineage II, 1/2a) strains displayed the highest nisin resistance, whereas CC2 (lineage I, 4b) and CC3 (lineage I, 1/2b) strains showed the lowest nisin resistance levels, similar to previous observations (Malekmohammadi et al., 2017). In addition, among CCs belonging to lineage II serotype 1/2a, CC155 was the most nisin tolerant, whereas CC14, CC199, and CC403 (lineage II, serotype 1/2a) had increased nisin sensitivity. Differences in the ability to respond to stress among the *L. monocytogenes* genotypes are probably linked to differences in the expression of proteins associated with the membrane, such as the penicillin-binding proteins coded by the *lmo0441*, *lmo0540*, *lmo1892* genes, and *lmo2229* as mentioned earlier, as well as the gene coding for σ^B, all of which were reported to be more expressed in lineage II than lineage I (Gravesen et al., 2004; Begley et al., 2006; Severino et al., 2007).

PERSISTENCE MECHANISMS

In food factories, sanitizer tolerance or resistance and an enhanced ability to form biofilms have been suggested as typical strain characteristics contributing to persistence (Norwood and Gilmour, 1999; Aase et al., 2000; Lundén et al., 2000, 2003; Borucki et al., 2003; Heir et al., 2004; Pan et al., 2006; Lourenço et al., 2009). However, the exact mechanisms behind persistence are not fully understood. Difficulties in eradicating *L. monocytogenes* contamination in food-processing settings may be conferred by the BC tolerance that some strains harbor and which provides an advantage for survival under stress and in food-processing settings, allowing the bacteria to persist in the environment (Mullapudi et al., 2008). A recent publication by Guérin et al. (2021) reported the capacity of *L. monocytogenes* strains to adapt to biocides, in particular ammonium quaternary compounds (commonly known as quats or QACs), and proposed the possible link between this adaptation and the selection of resistance regarding the fluoroquinolone antibiotic ciprofloxacin. This link was investigated also by others (Martínez-Suárez et al., 2016; Kode et al., 2021). The current hypothesis is that dilution in the environment and biodegradation give rise to QAC concentration gradients, which means that microorganisms (including *L. monocytogenes*) become frequently exposed to sub-inhibitory concentrations of QACs (Martínez-Suárez et al., 2016). Indeed, Møretrø et al. (2017) measured and found residues of QACs after sanitation in meat- and salmon-processing plants in Norway and suggested that this may result in a growth advantage for *L. monocytogenes* harboring the QAC resistance genes (i.e., *qacH* and *bcrABC*; see later). Therefore, the low-level resistance to QACs in *L. monocytogenes* has been proposed to be a contributing factor to its environmental adaptation and persistence. This may explain why the minimal inhibitory concentration of QAC tolerant strains way below user concentrations of QAC may still be of practical relevance. More studies are needed to confirm this hypothesis. Another study conducted by Castro et al. (2021) demonstrated that mobile genetic elements (MGEs) support the persistence of *L. monocytogenes* on dairy farms and may be spread through the food industry. It is believed that MGEs are pivotal in increasing the antimicrobial resistance of *L. monocytogenes* strains. MGEs can be exchanged between *Listeria* and other species leading to the creation of novel resistance phenotypes (Matereke and Okoh, 2020; Castro et al., 2021).

Several BC tolerance determinants have been identified in *L. monocytogenes*, including BC efflux pumps *qacH* (Tn*6188*), *bcrABC*, and *emrE*, which are located on MGEs and mostly present in lineage II isolates, i.e., CC9, CC13, CC14, CC31, and CC121 (Dutta et al., 2013; Müller et al., 2013, 2014; Ebner et al., 2015; Kovacevic et al., 2015; Maury et al., 2016; Ortiz et al., 2016; Zuber et al., 2019). Additional BC tolerance genes have been identified, such as *emrC*, identified on a plasmid in some ST6 isolates, *qacA* and *qacC*, which are both located on plasmids, and multidrug resistance *Listeria mdrL* (*lmo1409*), negatively regulated by *ladR* (*lmo1408*) (Xu et al., 2014; Kremer et al., 2017; Jiang et al., 2019). Literature data on the presence of resistance genes are sometimes contradictory and not always related to all strains of a particular *L. monocytogenes* CC. For example, Hurley et al. (2019) and Chen et al. (2020) did not find *emrC* in ST6, as previously described by Kremer et al. (2017) in ST6.

Several very recent investigations showed that gene *qacH* can occasionally be present in some different CC primarily of serotype 1/2a (CC8, CC20, CC31, CC101, and CC121) but also in serotypes 4b (CC2) and 1/2c (CC9) (Ebner et al., 2015; Meier et al., 2017; Horlbog et al., 2018; Roedel et al., 2019; Stoller et al., 2019; Zuber et al., 2019; Wieczorek et al., 2020; Gelbicova et al., 2021; Guidi et al., 2021; Palaiodimou et al., 2021; Pérez-Baltar et al., 2021). In general, Cherifi et al. (2018) recommended that only one genetic determinant should not be taken into consideration when strain persistence is investigated.

The *bcrABC* cassette was first described by Elhanafi et al. (2010) and isolated from *L. monocytogenes* strains associated with the 1998–1999 listeriosis outbreak in the United States caused by hotdog contamination. It consists of a TetR family transcriptional regulator (*bcrA*) and two small multidrug resistance genes (*bcrB* and *bcrC*). This cassette is located in the pLM80 plasmid, but a chromosomal location was also reported. The occurrence of the *bcrABC* cassette in non-pathogenic species of *Listeria*, such as *L. innocua* and *L. welshimeri*, suggests that these species may be the reservoirs of BC and other resistance determinants that are transferred to *L. monocytogenes* by conjugation (Katharios-Lanwermeyer et al., 2012). The *bcrABC* cassette was significantly associated with *L. monocytogenes* isolates belonging to CC321, CC155, CC204, and CC199 but can be present in other CCs such as ST14, CC288, ST9, ST121, CC5, *L. welshimeri*, and *L. innocua* (Meier et al., 2017; Møretrø et al., 2017; Pasquali et al., 2018; Chen et al., 2020; Naditz, 2020; Cooper et al., 2021; Gelbicova et al., 2021; Palaiodimou et al., 2021).

Another putative efflux pump gene responsible for increased tolerance to QACs is the *emrE* gene. This gene is located on a mobile genomic island LGI1 and was found in one clone (CC8) that includes strains implicated in the 2008 deli meat outbreak in Canada (Kovacevic et al., 2015). Meier et al. (2017) concluded that the *emrE* is associated with a serotype 1/2a (CC8) and seems to be limited to sublineage 8 strains. The expression of *emrE* was

found to be upregulated in the presence of BC, demonstrating that *emrE*-harboring strains are likely to adapt in food-processing environments better (Kovacevic et al., 2015).

The link between BC resistance and cadmium (Cd) resistance in *Listeria* spp. strains has been reported in several studies (Mullapudi et al., 2008; Ratani et al., 2012; Korsak and Szuplewska, 2016). In particular, in *L. monocytogenes* strains, five Cd resistance determinants (*cadAC* efflux systems) were identified (Chmielowska et al., 2021). The *cadA1* gene is located on the transposon Tn*5422* and often plasmid-borne, and predominates (as operon *cadA1C1*) in CC3, CC8, and CC121 (Lebrun et al., 1994; Gelbicova et al., 2021). Also, the *cadA2* gene is usually found on plasmids and is typically accompanied by the *bcrABC* cassette (Kuenne et al., 2010; Dutta et al., 2013). As for the genes *cadA3*, *cadA4* (also involved in biofilm formation), and *cadA5*, their location is typically on chromosomes, as part of integrative conjugative elements and genomic islands (LGI2 and LGI2-1), respectively (Kuenne et al., 2013; Lee et al., 2017; Parsons et al., 2017, 2019). Notably, LGI2, in addition to carrying *cadA4*, also carries a cassette for resistance to arsenic, which encompasses the *arsR1D2R2A2B1B2* operon and the upstream *arsA1D1* (Kuenne et al., 2013). The arsenic resistance is primarily associated with *L. monocytogenes* strains belonging to 4b serotype, particularly CC1, CC2, and CC4 hypervirulent clonal clones (Lee et al., 2017). On the contrary, Cd resistance typically is found in *L. monocytogenes* strains belonging to serotypes 1/2a and 1/2b, from food and food-processing environments (Mullapudi et al., 2008; Ratani et al., 2012). In addition, a specific association with lineages was found, namely *cadA1C1* cassette with lineage II and *cadA2C2* cassette with lineage I. On the other hand, strains containing both *cadA1* and *cadA2* were more frequent in lineage I than in lineage II (Mullapudi et al., 2010).

As said at the beginning of this section, the enhanced ability to form a biofilm that is hard to remove mechanically and less sensitive to sanitizers was proposed as a mechanism for persistence, given that the biofilm provides a clear advantage for surviving in food-processing or retail environments. However, other studies have not found a clear link between the biofilm-forming ability of some isolates and their persistence, and differences in the experimental setup and in the strains used have been ascribed as the reasons for the observed different results (Djordjevic et al., 2002; Holch et al., 2013; Kadam et al., 2013; Lee et al., 2019). Although some authors reported a correlation between lineages and biofilm-forming ability, with lineage II strains presenting higher levels of biofilm production, other results did not support these findings (Norwood and Gilmour, 2001; Djordjevic et al., 2002; Borucki et al., 2003; Di Bonaventura et al., 2008; Takahashi et al., 2009; Combrouse et al., 2013; Bai et al., 2021). Maury et al. (2019) found that hypovirulent genotypes, CC121 and CC9, were more efficient in biofilm production than hypervirulent clones (such as lineage I clones: CC1, CC2, CC4, and CC6) under sub-lethal concentrations of BC, implying that lineage II hypovirulent clones were associated with persistence features. Also, Pérez-Baltar et al. (2021) found that CC121 strains are strong biofilm formers, and some harbored the transposon Tn*6188*, related to increased tolerance to QACs. Interestingly, the *lmo0435* homolog biofilm-associated protein, BapL, putative peptidoglycan bound protein involved in biofilm formation, but not essential, is truncated in ST121 strains, which belong to CC121 (Jordan et al., 2008; Schmitz-Esser et al., 2015). Some authors suggested that CC8 strains possess a strong capacity for biofilm formation, which may support persistence within food production environments and subsequent contamination of foods (Verghese et al., 2011; Zuber et al., 2019). A study done in Canada by Upham et al. (2019) found that the formation of biofilms is associated with serotype 1/2a isolates in lineage II, as well as the presence of SSI-1. SSI-1, rare in clinical isolates, has been shown to be associated with a survival advantage in the environment, thus supporting the link between SSI-1 and persistence in *L. monocytogenes* (Hilliard et al., 2018). Furthermore, SSI-1 was strongly correlated with biofilm formation and a truncation (stop codon) in *inlA* (Franciosa et al., 2009; Keeney et al., 2018). More recent findings confirmed the influence of SSI-1 and a truncated *inlA* in increased biofilm levels in *L. monocytogenes* (Ciccio et al., 2019).

Regarding niche preference, reasons why the so-called persistent isolates are recurrently isolated in the same food-processing premises over long periods remain elusive. Persistent isolates could belong to specific STs particularly well adapted to the environmental conditions of the food manufacturing environment (Knudsen et al., 2017). It is, however, difficult to pinpoint adaptive traits directly correlated to persistence.

Notably, intra-genotype variation was observed in some CCs, suggesting that minor genetic variants within a genotype may impact biofilm phenotype (Lee et al., 2019; Zuber et al., 2019). Nevertheless, it should be pointed out that next to genetic determinants, biofilm formation is influenced by factors such as temperature, nutrient availability, and biofilm formation maturity (de Oliveira et al., 2010; Barbosa et al., 2013; Kadam et al., 2013). The limitation of most biofilm studies is that they have been done in monocultures, which may not be most relevant, as this bacterium is not alone in the food industry. Therefore, research on multispecies community might be more suitable to gain better insights into interactions among different species within the biofilms and the formation of the biofilm itself.

OPPORTUNITIES OF WHOLE-GENOME SEQUENCING FOR QUANTITATIVE MICROBIOLOGICAL RISK ASSESSMENTS

Whole-genome sequencing (WGS) of strains that have been isolated from different ecological niches has become more and more standard practice and demonstrates to be powerful in outbreak investigations at national and international levels (ECDC, 2019). These outbreak investigations rely on cross-sectorial cooperation between epidemiologists, microbiologists, and bioinformaticians to link clinical isolates to outbreak isolates. The availability of WGS data gives new opportunities to explain intraspecific variability and to find genetic biomarkers that predict microbial behavior. Multilocus sequence typing and whole-genome phylogenetic analyses demonstrated that pathogenic subtypes vary in their virulence and association with food (*L. monocytogenes diversity and*

heterogeneity of the virulence determinants), and this intraspecific variability is relevant for risk assessments in general and, more specifically, also for quantitative microbiological risk assessments (QMRA). A QMRA is a structured and quantitative process for determining the risk associated with microbiological hazards in a food (CAC, 1999). The basic steps of a QMRA include hazard identification, exposure assessment, hazard characterization, and risk characterization, and this formalized approach has been adopted by regulators globally and is also used by industry. Various QMRA studies have been performed for different product/pathogen combinations (e.g., FDA/CFSAN and USDA/FSIS, 2003; Tirloni et al., 2018; EFSA, 2019) aiming to characterize and quantify the risk of a pathogen associated with a product (category). In these studies, the exposure assessment and hazard characterization steps of QMRAs are performed for a pathogenic species as a whole. The current advances in the field of omics technology give opportunities to make use of the greater understanding of intraspecific variability based on various recently published bioinformatics tools (Brul et al., 2012; Den Besten et al., 2018; Haddad et al., 2018; Rantsiou et al., 2018; Fritsch et al., 2019; Njage et al., 2020). Instead of considering all-hazard strains of a species as equally likely to cause disease or equally likely to survive the food chain, WGS data could give support to rank subtypes with respect to their virulence potential (Chen Y. et al., 2011; Collineau et al., 2019) or to groups subtypes with respect to their differences in robustness or fitness to reach the consumer stage (Den Besten et al., 2018). The QMRA input distributions can be tailored to each subgroup accordingly, making it possible to fine-tune the QMRA output. The studies of Chen Y. et al. (2011) and Fritsch et al. (2018) illustrate the potential to refine QMRA studies when considering pheno-genotype associations for specific properties of *L. monocytogenes*. The authors described the variability of *L. monocytogenes*' growth characteristics more accurately using two different distributions for the minimum temperature of growth (T_{min}). For risk characterization, three different groups of virulence were considered according to the CCs, making use of reported differences in clinical frequencies of different CCs (Maury et al., 2016, see also *L. monocytogenes diversity and heterogeneity of the virulence determinants*). The QMRA output showed that CCs that are contributing the most to consumer exposure were not those that contributed the most to listeriosis cases. Chen Y. et al. (2011) followed a similar approach for the hazard characterization step where they attributed different dose-response models for *L. monocytogenes* subtypes with genes encoding a full-length and a truncated InlA, respectively. These examples of fine-tuning a QMRA highlight the potential impact of implementing genomic data in QMRA. This field is still young and relies on high efforts to phenotypically characterize strain variability. Grouping of strains with shared characteristics is only possible when subgroups of strains have different phenotypes. This pushes the need to characterize various aspects of strains, such as fitness and stress robustness, because these details are needed to quantitatively describe intraspecific variability in the exposure assessment part of a QMRA. Also, it is important to note that routine collection of WGS data is more standardized across regulatory and public health agencies and more limited in surveillance by industry (Jagadeesan et al., 2019; Cohn et al., 2021), and this introduces a bias in isolate characterization, whereas representative WGS data from food and human isolates

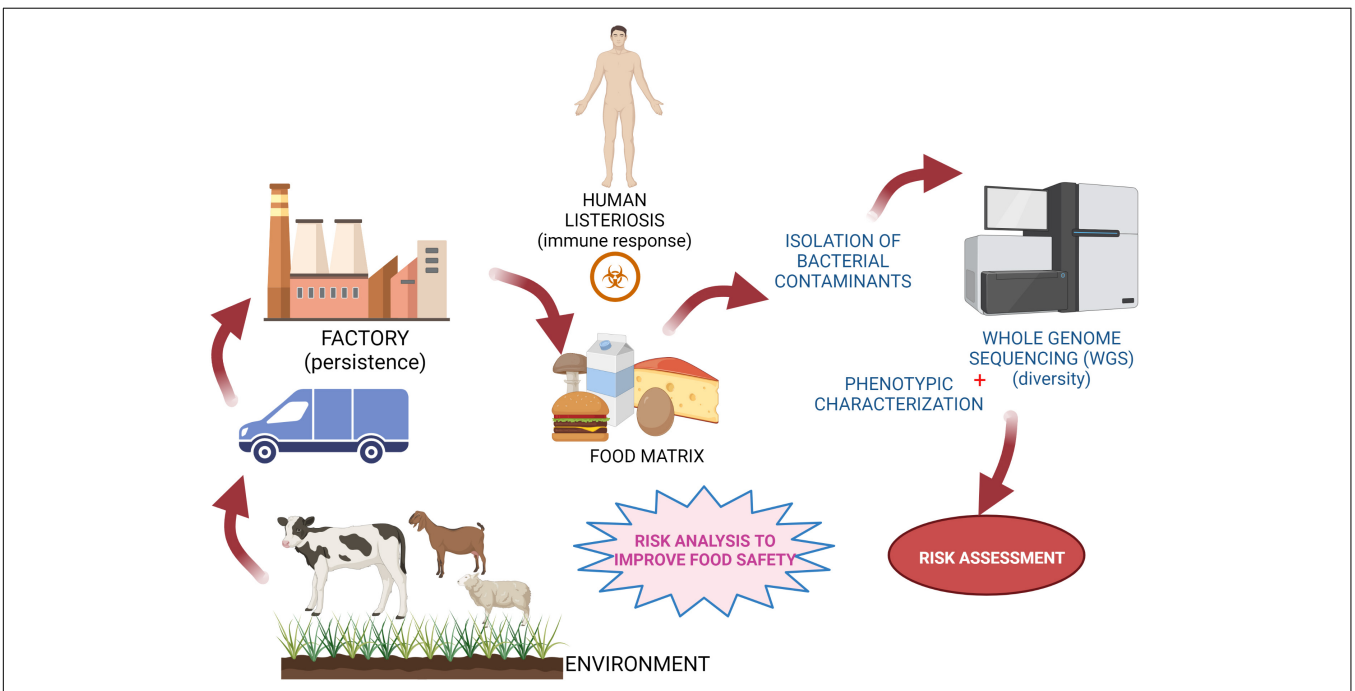

FIGURE 3 | Schematic representation of risk control strategies. Experimental concept to assess risk and monitor diversity among *L. monocytogenes* strains for prevention/control of food chain contamination. Created with BioRender.com.

are critical to assess the likelihood of subtypes to cause disease. When these challenges are recognized and taken up, it will open avenues to make use of pheno-genotype associations in the next generation of QMRA and to incorporate subtype-specific assessment of public health significance in food control strategies and regulations.

CONCLUSION AND FUTURE PERSPECTIVES

The notorious foodborne pathogen *L. monocytogenes* is ubiquitous in nature and can be found in soil, in the farm environment, in the food production environment, and in food products (**Figure 3**) (Kallipolitis et al., 2020). As highlighted in this review, there is a high degree of strain divergence regarding virulence potential, environmental adaption, and stress response. In addition, persistent *L. monocytogenes* subtypes have the ability to survive and persist for months and even years in food-processing environments and to keep contaminating food products. It is, however, difficult to correlate adaptive traits directly to persistence. Hence, pheno-genotype association studies are promising approaches to increase our mechanistic understanding of how this pathogen survives along the food chain and infects the human host. Notably, most published studies do not assess the presence/absence of specific genes (or sets of genes) in all currently known *L. monocytogenes* lineages, CCs/sequence types. Hence, experimental and holistic approaches based on WGS and environmental studies may play a role in determining the distribution and diversity of *Listeria* species. The use of advanced diagnostic technologies such as WGS can open avenues to fine-tune risk assessments, which is of great importance in the prevention and control of both animal and human listeriosis (Den Besten et al., 2018; Rantsiou et al., 2018). Successful implementation and use of WGS needs, however, an appropriate and functioning infrastructure and resources (Grace, 2015), i.e., functional control and an already established surveillance system to collect isolates and metadata from clinical, food, and environmental samples (EFSA, 2008; FAO, 2016). This will support an unbiased assessment of the likelihood of subtypes to be present in food and to cause disease to come to risk-based interventions at the intraspecific level.

AUTHOR CONTRIBUTIONS

All authors listed have made a substantial, direct, and intellectual contribution to the work, and approved it for publication.

FUNDING

This work was funded through the COST Action "Understanding and exploiting the impacts of low pH on microorganisms" (EuroMicropH) CA18113. BL visited the DD laboratory as the recipient of a Short-Term Scientific Mission grant supported by the COST Action CA18113 EuroMicropH (https://euromicroph.eu/stsm/).

REFERENCES

Aase, B., Sundheim, G., Langsrud, S., and Rørvik, L. M. (2000). Occurrence of and a possible mechanism for resistance to a quaternary ammonium compound in *Listeria monocytogenes*. *Int. J. Food Microbiol.* 62, 57–63. doi: 10.1016/s0168-1605(00)00357-3

Abachin, E., Poyart, C., Pellegrini, E., Milohanic, E., Fiedler, F., Berche, P., et al. (2002). Formation of D-alanyl-lipoteichoic acid is required for adhesion and virulence of *Listeria monocytogenes*. *Mol. Microbiol.* 43, 1–14. doi: 10.1046/j.1365-2958.2002.02723.x

Althaus, D., Jermini, M., Giannini, P., Martinetti, G., Reinholz, D., Nüesch-Inderbinen, M., et al. (2017). Local outbreak of *Listeria monocytogenes* serotype 4b sequence type 6 due to contaminated meat pâté. *Foodborne Pathog. Dis.* 14, 219–222. doi: 10.1089/fpd.2016.2232

Arcari, T., Feger, M. L., Guerreiro, D. N., Wu, J., and O'Byrne, C. P. (2020). Comparative review of the responses of *Listeria monocytogenes* and *Escherichia coli* to low pH stress. *Genes (Basel)* 11:1330. doi: 10.3390/genes11111330

Ariza-Miguel, J., Fernandez-Natal, M. I., Soriano, F., Hernandez, M., Stessl, B., and Rodríguez Lazaro, D. (2015). Molecular epidemiology of invasive listeriosis due to *Listeria monocytogenes* in a Spanish hospital over a nine-year study period, 2006-2014. *BioMed Res. Int.* 2015:191409. doi: 10.1155/2015/191409

Bai, X., Liu, D., Xu, L., Tenguria, S., Drolia, R., Gallina, N. L. F., et al. (2021). Biofilm-isolated *Listeria monocytogenes* exhibits reduced systemic dissemination at the early (12–24 h) stage of infection in a mouse model. *NPJ Biofilms Microbiomes* 7:18. doi: 10.1038/s41522-021-00189-5

Balay, D. R., Dangeti, R. V., Kaur, K., and McMullen, L. M. (2017). Purification of leucocin A for use on wieners to inhibit *Listeria monocytogenes* in the presence of spoilage organisms. *Int. J. Food Microbiol.* 255, 25–31.

Barbosa, J., Borges, S., Camilo, R., Magalhães, R., Ferreira, V., Santos, I., et al. (2013). Biofilm formation among clinical and food isolates of *Listeria monocytogenes*. *Int. J. Microbiol.* 2013:524975. doi: 10.1155/2013/524975

Begley, M., Cotter, P. D., Hill, C., and Ross, R. P. (2010). Glutamate decarboxylase-mediated nisin resistance in *Listeria monocytogenes*. *Appl. Environ. Microbiol.* 76, 6541–6546. doi: 10.1128/aem.00203-10

Begley, M., Hill, C., and Ross, R. P. (2006). Tolerance of *Listeria monocytogenes* to cell envelope-acting antimicrobial agents is dependent on SigB. *Appl. Environ. Microbiol.* 72, 2231–2234. doi: 10.1128/AEM.72.3.2231-2234.2006

Bergholz, T. M., Shah, M. K., Burall, L. S., Rakic-Martinez, M., and Datta, A. R. (2018). Genomic and phenotypic diversity of *Listeria monocytogenes* clonal complexes associated with human listeriosis. *Appl. Microbiol. Biotechnol.* 102, 3475–3485. doi: 10.1007/s00253-018-8852-5

Bergholz, T. M., Tang, S., Wiedmann, M., and Boor, K. J. (2013). Nisin resistance of *Listeria monocytogenes* is increased by exposure to salt stress and is mediated via LiaR. *Appl. Environ. Microbiol.* 79, 5682–5688. doi: 10.1128/AEM.01797-13

Berrang, M. E., Meinersmann, R. J., Frank, J. F., and Ladely, S. R. (2010). Colonization of a newly constructed commercial chicken further processing plant with *Listeria monocytogenes*. *J. Food Prot.* 73, 286–291. doi: 10.4315/0362-028X-73.2.286

Bertsch, D., Rau, J., Eugster, M. R., Haug, M. C., Lawson, P. A., Lacroix, C., et al. (2013). *Listeria fleischmannii* sp. nov., isolated from cheese. *Int. J. Syst. Evol. Microbiol.* 63, 526–532.

Bolocan, A. S., Nicolau, A. I., Álvarez-Ordóñez, A., Borda, D., Oniciuc, E. A., Stessl, B., et al. (2016). Dynamics of *Listeria monocytogenes* colonisation in a newly-opened meat processing facility. *Meat Sci.* 113, 26–34. doi: 10.1016/j.meatsci.2015.10.016

Bonnet, M., and Montville, T. J. (2005). Acid-tolerant *Listeria monocytogenes* persist in a model food system fermented with nisin-producing bacteria. *Lett. Appl. Microbiol.* 40, 237–242. doi: 10.1111/j.1472-765X.2005.01661.x

Borucki, M. K., Peppin, J. D., White, D., Loge, F., and Call, D. R. (2003). Variation in biofilm formation among strains of *Listeria monocytogenes*. *Appl. Environ. Microbiol.* 69, 7336–7342. doi: 10.1128/AEM.69.12.7336-7342.2003

Boura, M., Brensone, D., and Karatzas, K. A. G. (2020). A novel role for the glutamate decarboxylase system in *Listeria monocytogenes*; protection against oxidative stress. *Food Microbiol.* 85:103284. doi: 10.1016/j.fm.2019.103284

Brul, S., Bassett, J., Cook, P., Kathariou, S., McClure, P., Jasti, P. R., et al. (2012). 'Omics' technologies in quantitative microbial risk assessment. *Trends Food Sci. Technol.* 27, 12–24.

Bucur, F. I, Grigore-Gurgu, L., Crauwels, P., Riedel, C. U., and Nicolau, A. I (2018). Resistance of *Listeria monocytogenes* to stress conditions encountered in food and food processing environments. *Front. Microbiol.* 9:2700. doi: 10.3389/fmicb.2018.02700

Buncic, S., Avery, S. M., Rocourt, J., and Dimitrijevic, M. (2001). Can food-related environmental factors induce different behaviour in two key serovars, 4b and 1/2a, of *Listeria monocytogenes*? *Int. J. Food Microbiol.* 65, 201–212. doi: 10.1016/s0168-1605(00)00524-9

Burkholder, K. M., Kim, K.-P., Mishra, K. K., Medina, S., Hahm, B.-K., Kim, H., et al. (2009). Expression of LAP, a SecA2-dependent secretory protein, is induced under anaerobic environment. *Microbes Infect.* 11, 859–867. doi: 10.1016/j.micinf.2009.05.006

CAC (1999). "Principles and guidelines for the conduct of a microbiological risk assessment. 1999," in *Proccedings of the Joint FAO/WHO Food Standards Programme, CAC/GL-30, Rome (1999)* (Rome).

Carlin, C. R., Liao, J., Weller, D., Guo, X., Orsi, R., and Wiedmann, M. (2021). *Listeria cossartiae* sp. nov. *Listeria immobilis* sp. nov., *Listeria portnoyi* sp. nov. and *Listeria rustica* sp. nov., isolated from agricultural water and natural environments. *Int. J. Syst. Evol. Microbiol.* 71:004795. doi: 10.1099/ijsem.0.004795

Carpentier, B., and Cerf, O. (2011). Review–persistence of *Listeria monocytogenes* in food industry equipment and premises. *Int. J. Food Microbiol.* 145, 1–8. doi: 10.1016/j.ijfoodmicro.2011.01.005

Castro, H., Douillard, F. P., Korkeala, H., and Lindström, M. (2021). Mobile elements harboring heavy metal and bacitracin resistance genes are common among *Listeria monocytogenes* strains persisting on dairy farms. *mSphere* 6:00383-21. doi: 10.1128/mSphere.00383-21

Chaturongakul, S., Raengpradub, S., Palmer, M. E., Bergholz, T. M., Orsi, R. H., Hu, Y., et al. (2011). Transcriptomic and phenotypic analyses identify coregulated, overlapping regulons among PrfA, CtsR, HrcA, and the alternative sigma factors σB, σC, σH, and σL in *Listeria monocytogenes*. *Appl. Environ. Microbiol.* 7, 187–200. doi: 10.1128/AEM.00952-10

Chen, J., Cheng, C., Xia, Y., Zhao, H., Fang, C., Shan, Y., et al. (2011). Lmo0036, an ornithine and putrescine carbamoyltransferase in *Listeria monocytogenes*, participates in arginine deiminase and agmatine deiminase pathways and mediates acid tolerance. *Microbiology* 157, 3150–3161. doi: 10.1099/mic.0.049619-0

Chen, J., Fang, C., Zheng, T., Zhu, N., Bei, Y., and Fang, W. (2012). Genomic presence of gadD1 glutamate decarboxylase correlates with the organization of ascB-dapE internalin cluster in *Listeria monocytogenes*. *Foodborne Pathog. Dis.* 9, 175–178. doi: 10.1089/fpd.2011.1022

Chen, M., Cheng, J., Wu, Q., Zhang, J., Chen, Y., Zeng, H., et al. (2018). Prevalence, potential virulence, and genetic diversity of *Listeria monocytogenes* isolates from edible mushrooms in chinese markets. *Front Microbiol.* 9:1711. doi: 10.3389/fmicb.2018.01711

Chen, Y., Chen, Y., Pouillot, R., Dennis, S., Xian, Z., Luchansky, J. B., et al. (2020). Genetic Diversity and profiles of genes associated with virulence and stress resistance among isolates from the 2010-2013 interagency market basket survey. *PLos One* 15:e0231393. doi: 10.1371/journal.pone.0231393

Chen, Y., Gonzalez-Escalona, N., Hammack, T. S., Allard, M. W., Strain, E. A., and Brown, E. W. (2016). Core genome multilocus sequence typing for identification of globally distributed clonal groups and differentiation of outbreak strains of *Listeria monocytogenes*. *Appl. Environ. Microbiol.* 282, 6258–6672. doi: 10.1128/AEM.01532-16

Chen, Y., Ross, W. H., Gray, M. J., Wiedmann, M., Whiting, R. C., and Scott, V. N. (2006). Attributing risk to *Listeria monocytogenes* subgroups: dose response in relation to genetic lineages. *J. Food Prot.* 69, 335–344. doi: 10.4315/0362-028x-69.2.335

Chen, Y., Ross, W. H., Whiting, R. C., Van Stelten, A., Nightingale, K. K., Wiedmann, M., et al. (2011). Variation in *Listeria monocytogenes* dose responses in relation to subtypes encoding a full-length or truncated internalin A. *Appl. Environ. Microbiol.* 77, 1171–1180. doi: 10.1128/AEM.01564-10

Cheng, C., Chen, J., Fang, C., Xia, Y., Shan, Y., Liu, Y., et al. (2013). *Listeria monocytogenes* aguA1, but Not aguA2, encodes a functional agmatine deiminase. *J. Biol. Chem.* 288, 26606–26615. doi: 10.1074/jbc.M113.477380

Cheng, C., Dong, Z., Han, X., Sun, J., Wang, H., Jiang, L., et al. (2017). *Listeria monocytogenes* 10403S arginine repressor ArgR finely tunes arginine metabolism regulation under acidic conditions. *Front. Microbiol.* 8:145. doi: 10.3389/fmicb.2017.00145

Cheng, C., Yang, Y., Dong, Z., Wang, X., Fang, C., Yang, M., et al. (2015). *Listeria monocytogenes* varies among strains to maintain intracellular pH homeostasis under stresses by different acids as analyzed by a high-throughput microplate-based fluorometry. *Front. Microbiol.* 6:15. doi: 10.3389/fmicb.2015.00015

Cherifi, T., Carrillo, C., Lambert, D., Miniaï, I., Quessy, S., Larivière-Gauthier, G., et al. (2018). Genomic characterization of *Listeria monocytogenes* isolates reveals that their persistence in a pig slaughterhouse is linked to the presence of benzalkonium chloride resistance genes. *BMC Microbiol.* 18:220. doi: 10.1186/s12866-018-1363-9

Chmielowska, C., Korsak, D., Szuplewska, M., Grzelecka, M., Maćkiw, E., Stasiak, M., et al. (2021). Benzalkonium chloride and heavy metal resistance profiles of *Listeria monocytogenes* strains isolated from fish, fish products and food-producing factories in Poland. *Food Microbiol.* 98:103756. doi: 10.1016/j.fm.2021.103756

Ciccio, P. D., Chiesa, F., Rubiola, S., and Civera, T. (2019). "Genetic determinants associated with biofilm formation of *Listeria monocytogenes* from food and food processing environment," in *Proceedings of the 33rd EFFoST International Conference Sustainable Food Systems-Performing by Connecting*, (Rotterdam).

Clayton, E. M., Daly, K. M., Guinane, C. M., Hill, C., Cotter, P. D., and Ross, P. R. (2014). Atypical *Listeria innocua* strains possess an intact LIPI-3. *BMC Microbiol.* 14:58. doi: 10.1186/1471-2180-14-58

Cohn, A. R., Cheng, R. A., Orsi, R. H., and Wiedmann, M. (2021). Moving past species classifications for risk-based approaches to food safety: *Salmonella* as a case study. *Front. Sustain. Food Syst.* 5:652132. doi: 10.3389/fsufs.2021.652132

Collineau, L., Boerlin, P., Carson, C. A., Chapman, B., Fazil, A., Hetman, B., et al. (2019). Integrating whole-genome sequencing data into quantitative risk assessment of foodborne antimicrobial resistance: a review of opportunities and challenges. *Front. Microbiol.* 10:1107. doi: 10.3389/fmicb.2019.01107

Collins, B., Curtis, N., Cotter, P. D., Hill, C., and Ross, R. P. (2010a). The ABC transporter AnrAB contributes to the innate resistance of *Listeria monocytogenes* to nisin, bacitracin, and various β-lactam antibiotics. *Antimicrob. Agents Chemother.* 54, 4416–4423. doi: 10.1128/AAC.00503-10

Collins, B., Guinane, C. M., Cotter, P. D., Hill, C., and Ross, P. R. (2012). Assessing the contributions of the lias histidine kinase to the innate resistance of *Listeria monocytogenes* to nisin, cephalosporins, and disinfectants. *Appl. Environ. Microbiol.* 78, 2923–2929. doi: 10.1128/AEM.07402-11

Collins, B., Joyce, S., Hill, C., Cotter, P. D., and Ross, R. P. (2010b). TelA contributes to the innate resistance of *Listeria monocytogenes* to nisin and other cell wall-acting antibiotics. *Antimicrob. Agents Chemother.* 54, 4658–4663. doi: 10.1128/AAC.00290-10

Combrouse, T., Sadovskaya, I., Faille, C., Kol, O., Guérardel, Y., and Midelet-Bourdin, G. (2013). Quantification of the extracellular matrix of the *Listeria monocytogenes* biofilms of different phylogenic lineages with optimization of culture conditions. *J. Appl. Microbiol.* 114, 1120–1131. doi: 10.1111/jam.12127

Conte, M. P., Petrone, G., Di Biase, A. M., Ammendolia, M. G., Superti, F., and Seganti, L. (2000). Acid tolerance in *Listeria monocytogenes* influences invasiveness of enterocyte-like cells and macrophage-like cells. *Microb. Pathog.* 29, 137–144. doi: 10.1006/mpat.2000.0379

Cooper, A. L., Carrillo, C. D., Deschênes, M., and Blais, B. W. (2021). Genomic markers for quaternary ammonium compound resistance as a persistence indicator for *Listeria monocytogenes* contamination in food manufacturing environments. *J. Food Prot.* 84, 389–398. doi: 10.4315/JFP-20-328

Cotter, P. D., Gahan, C. G. M., and Hill, C. (2000). Analysis of the role of the *Listeria monocytogenes*F0F1-ATPase operon in the acid tolerance response. *Int. J. Food Microbiol.* 60, 137–146. doi: 10.1016/S0168-1605(00)00305-6

Cotter, P. D., Gahan, C. G. M., and Hill, C. (2001). A glutamate decarboxylase system protects *Listeria monocytogenes* in gastric fluid. *Mol. Microbiol.* 40, 465–475. doi: 10.1046/j.1365-2958.2001.02398.x

Cotter, P. D., Guinane, C. M., and Hill, C. (2002). The LisRK signal transduction system determines the sensitivity of *Listeria monocytogenes* to nisin and

cephalosporins. *Antimicrob. Agents Chemother.* 46, 2784–2790. doi: 10.1128/AAC.46.9.2784-2790.2002

Cotter, P. D., Ryan, S., Gahan, C. G. M., and Hill, C. (2005). Presence of GadD1 glutamate decarboxylase in selected *Listeria monocytogenes* strains is associated with an ability to grow at low pH. *Appl. Environ. Microbiol.* 71, 2832–2839. doi: 10.1128/AEM.71.6.2832

De Las Heras, A., Cain, R. J., Bielecka, M. K., and Vazquez-Boland, J. A. (2011). Regulation of Listeria virulence: prfa master and commander. *Curr. Opin. Microbiol.* 14, 118–127. doi: 10.1016/j.mib.2011.01.005

de Oliveira, M. M., Brugnera, D. F., Alves, E., and Piccoli, R. H. (2010). Biofilm formation by *Listeria monocytogenes* on stainless steel surface and biotransfer potential. *Braz. J. Microbiol.* 41, 97–106. doi: 10.1590/S1517-838220100001000016

den Bakker, H. C., Cummings, C. A., Ferreira, V., Vatta, P., Orsi, R. H., Degoricija, L., et al. (2010). Comparative genomics of the bacterial genus *Listeria*: genome evolution is characterized by limited gene acquisition and limited gene loss. *BMC Genom.* 11:688. doi: 10.1186/1471-2164-11-688

den Bakker, H. C., Warchocki, S., Wright, E. M., Allred, A. F., Ahlstrom, C., Manuel, C. S., et al. (2014). *Listeria floridensis* sp. nov., *Listeria aquatica* sp. nov., *Listeria cornellensis* sp. nov., *Listeria riparia* sp. nov. and *Listeria grandensis* sp. nov., from agricultural and natural environments. *Int. J. Syst. Evol. Microbiol.* 64, 1882–1889.

Den Besten, H. M. W., Amézquita, A., Bover-Cid, S., Dagnas, S., Ellouze, M., Guillou, S., et al. (2018). Next generationof microbiological risk assessment: potential of omics data for exposure assessment. *Int. J. Food Microbiol.* 287, 18–27.

Deng, X., Phillippy, A. M., Li, Z., Salzberg, S. L., and Zhang, W. (2010). Probing the pan-genome of *Listeria monocytogenes*: new insights into intraspecific niche expansion and genomic diversification. *BMC Genom.* 11:500. doi: 10.1186/1471-2164-11-500

Desai, A. N., Anyoha, A., Madoff, L. C., and Lassmann, B. (2019). Changing epidemiology of *Listeria monocytogenes* outbreaks, sporadic cases, and recalls globally: a review of ProMED reports from 1996 to 2018. *Int. J. Infect. Dis.* 84, 48–53. doi: 10.1016/j.ijid.2019.04.021

Di Bonaventura, G., Piccolomini, R., Paludi, D., D'Orio, V., Vergara, A., Conter, M., et al. (2008). Influence of temperature on biofilm formation by *Listeria monocytogenes* on various food-contact surfaces: relationship with motility and cell surface hydrophobicity. *J. Appl. Microbiol.* 104, 1552–1561. doi: 10.1111/j.1365-2672.2007.03688.x

Djordjevic, D., Wiedmann, M., and McLandsborough, L. A. (2002). Microtiter plate assay for assessment of *Listeria monocytogenes* biofilm formation. *Appl. Environ. Microbiol.* 68, 2950–2958. doi: 10.1128/aem.68.6.2950-2958.2002

Doijad, S., Weigel, M., Barbuddhe, S., Blom, J., Goesmann, A., Hain, T., et al. (2015). Phylogenomic grouping of *Listeria monocytogenes*. *Can. J. Microbiol.* 61, 637–646. doi: 10.1139/cjm-2015-0281

Doijad, S. P., Poharkar, K. V., Kale, S. B., Kerkar, S., Kalorey, D. R., Kurkure, N. V., et al. (2018). *Listeria goaensis* sp. nov. *Int. J. Syst. Evol. Microbiol.* 68, 3285–3291. doi: 10.1099/ijsem.0.002980

Domínguez-Bernal, G., Müller-Altrock, S., González-Zorn, B., Scortti, M., Herrmann, P., Monzó, H. J., et al. (2006). A spontaneous genomic deletion in *Listeria ivanovii* identifies LIPI-2, a species-specific pathogenicity island encoding sphingomyelinase and numerous internalins. *Mol. Microbiol.* 59, 415–432. doi: 10.1111/j.1365-2958.2005.04955.x

Doumith, M., Cazalet, C., Simoes, N., Frangeul, L., Jacquet, C., Kunst, F., et al. (2004). New aspects regarding evolution and virulence of *Listeria monocytogenes* revealed by comparative genomics and DNA arrays. *Infect. Immun.* 72, 1072–1083. doi: 10.1128/IAI.72.2.1072-1083.2004

Dussurget, O. (2008). New insights into determinants of *Listeria monocytogenes* virulence. *Int. Rev. Cell Mol. Biol.* 270, 1–38. doi: 10.1016/S1937-6448(08)01401-9

Dutta, V., Elhanafi, D., and Kathariou, S. (2013). Conservation and distribution of the benzalkonium chloride resistance cassette bcrABC in *Listeria monocytogenes*. *Appl. Environ. Microbiol.* 79, 6067–6074. doi: 10.1128/AEM.01751-13

Ebner, R., Althaus, S. R., Brisse, D., Maury, S., and Tasara, M. T. (2015). Phenotypic and genotypic characteristics of *Listeria monocytogenes* strains isolated during 2011–2014 from different food matrices in Switzerland. *Food Control* 57, 321–326. doi: 10.1016/j.foodcont.2015.04.030

ECDC (2019). *ECDC Strategic Framework for the Integration of Molecular and Genomic Typing into European Surveillance and Multi-Country Outbreak Investigations - 2019-2021. Stockholm:ECDC; 2019*. Solna Municipality: ECDC.

EFSA (2008). Working Group on Developing Harmonised Schemes for Monitoring Antimicrobial Resistance in Zoonotic Agents. Harmonised monitoring of antimicrobial resistance in *Salmonella* and Campylobacter isolates from food animals in the European Union. *Clin. Microbiol. Infect.* 14, 522–533.

EFSA (2019). Quantitative risk assessment of *Listeria monocytogenes* in a traditional RTE product. *EFSA J.* 17:e170906. doi: 10.2903/j.efsa.2019.e170906

EFSA and ECDC (2018). Multi-country outbreak of *Listeria monocytogenes* serogroup IVb, multi-locus sequence type 6, infections probably linked to frozen corn. *EFSA Support Publ.* 15:1402E.

EFSA Panel on Biological Hazards [Efsa Biohaz Panel] Ricci, A., Allende, A., Bolton, D., Chemaly, M., Davies, R., et al. (2018). *Listeria monocytogenes* contamination of ready-to-eat foods and the risk for human health in the EU. *EFSA J.* 16:5134. doi: 10.2903/j.efsa.2018.5134

Elhanafi, D., Dutta, V., and Kathariou, S. (2010). Genetic characterization of plasmid-associated benzalkonium chloride resistance determinants in a *Listeria monocytogenes* strain from the 1998-1999 outbreak. *Appl. Environ. Microbiol.* 76, 8231–8238. doi: 10.1128/AEM.02056-10

Fagerlund, A., Langsrud, S., Schirmer, B. C. T., Møretrø, T., and Heir, E. (2016). Genome analysis of *Listeria monocytogenes* sequence type 8 strains persisting in salmon and poultry processing environments and comparison with related strains. *PLoS One.* 11:e0151117. doi: 10.1371/journal.pone.0151117

FAO (2016). *Applications of Whole Genome Sequencing (WGS) in Food Safety Management. Technical Background Paper, Draft Version 6: 11 April 2016*. Rome: FAO.

FDA/CFSAN and USDA/FSIS (2003). *Quantitative Assessment of Relative Risk to Public Health From Foodborne Listeria monocytogenes* Among Selected Categories of Ready-to-Eat Foods. Silver Spring, MD: FDA.

Feehily, C., Finnerty, A., Casey, P. G., Hill, C., Gahan, C. G. M., O'Byrne, C. P., et al. (2014). Divergent evolution of the activity and regulation of the glutamate decarboxylase systems in *Listeria monocytogenes* EGD-e and 10403S: roles in virulence and acid tolerance. *PLoS One* 9:e112649. doi: 10.1371/journal.pone.0112649

Feng, Y., Yao, H., Chen, S., Sun, X., Yin, Y., and Jiao, X. (2020). Rapid detection of hypervirulent serovar 4h *Listeria monocytogenes* by multiplex PCR. *Front. Microbiol.* 11:1309. doi: 10.3389/fmicb.2020.01309

Ferreira, M. A., and Lund, B. M. (1996). The effect of nisin on *Listeria monocytogenes* in culture medium and long-life cottage cheese. *Lett. Appl. Microbiol.* 22, 433–438. doi: 10.1111/j.1472-765x.1996.tb01197.x

Ferreira, V., Wiedmann, M., Teixeira, P., and Stasiewicz, M. J. (2014). *Listeria monocytogenes* persistence in food-associated environments: epidemiology, strain characteristics, and implications for public health. *J. Food Prot.* 77, 150–170. doi: 10.4315/0362-028X.JFP-13-150

Franciosa, G., Maugliani, A., Scalfaro, C., Floridi, F., and Aureli, P. (2009). Expression of internalin A and biofilm formation among *Listeria monocytogenes* clinical isolates. *Int. J. Immunopathol. Pharmacol.* 22, 183–193. doi: 10.1177/039463200902200121

Francis, G. A., Scollard, J., Meally, A., Bolton, D. J., Gahan, C. G. M., Cotter, P. D., et al. (2007). The glutamate decarboxylase acid resistance mechanism affects survival of *Listeria monocytogenes*LO28 in modified atmosphere-packaged foods. *J. Appl. Microbiol.* 103, 2316–2324. doi: 10.1111/j.1365-2672.2007.03466.x

Franklin, N. B., Cooksey, K. D., and Getty, K. J. (2004). Inhibition of *Listeria monocytogenes* on the surface of individually packaged hot dogs with a packaging film coating containing nisin. *J. Food Prot.* 67, 480–485. doi: 10.4315/0362-028x-67.3.480

Fritsch, L., Felten, A., Palma, F., Mariet, J.-F., Radomski, N., Mistou, M.-Y., et al. (2019). Insights from genome-wide approaches to identify variants associated to phenotypes at pan-genome scale: application to *L. monocytogenes*' ability to grow in cold conditions. *Int. J. Food Microbiol.* 291, 181–188. doi: 10.1016/j.ijfoodmicro.2018.11.028

Fritsch, L., Guillier, L., and Augustin, J. C. (2018). Next generation quantitative microbiological risk assessment: refinement of the cold smoked salmon-related listeriosis risk model by integrating genomic data. *Microb. Risk Anal.* 10, 20–27.

Gahan, C. G., and Hill, C. (2014). *Listeria monocytogenes*: survival and adaptation in the gastrointestinal tract. *Front. Cell. Infect. Microbiol.* 4:9. doi: 10.3389/fcimb.2014.00009

Gandhi, M., and Chikindas, M. L. (2007). Listeria: a foodborne pathogen that knows how to survive. *Int. J. Food Microbiol.* 113, 1–15. doi: 10.1016/j.ijfoodmicro.2006.07.008

Gelbicova, T., Florianova, M., Hluchanova, L., Kalova, A., Korena, K., Strakova, N., et al. (2021). Comparative analysis of genetic determinants encoding cadmium, arsenic, and benzalkonium chloride resistance in *Listeria monocytogenes* of human, food, and environmental origin. *Front. Microbiol.* 11:599882. doi: 10.3389/fmicb.2020.599882

Gelbíčová, T., Kolácková, I., Pantucek, R., and Karpíšková, R. (2015). A novel mutation leading to a premature stop codon in inlA of *Listeria monocytogenes* isolated from neonatal listeriosis. *New Microbiol.* 38, 293–296.

Glaser, P., Frangeul, L., Buchrieser, C., Rusniok, C., Amend, A., Baquero, F., et al. (2001). Comparative genomics of *Listeria* species. *Science* 294, 849–852. doi: 10.1126/science.1063447

Grace, D. (2015). Food safety in low and middle income countries. *Int. J. Environ. Res. Public Health* 12, 10490–10507. doi: 10.3390/ijerph120910490

Graves, L. M., Helsel, L. O., Steigerwalt, A. G., Morey, R. E., Daneshvar, M. I., Roof, S. E., et al. (2010). *Listeria marthii* sp. nov., isolated from the natural environment, Finger Lakes National Forest. *Int. J. Syst. Evol. Microbiol.* 60, 1280–1288.

Gravesen, A., Kallipolitis, B., Holmstrøm, K., Høiby, P. E., Ramnath, M., and Knøchel, S. (2004). pbp2229-mediated nisin resistance mechanism in *Listeria monocytogenes* confers cross-protection to class IIa bacteriocins and affects virulence gene expression. *Appl. Environ. Microbiol.* 70, 1669–1679. doi: 10.1128/AEM.70.3.1669

Grubaugh, D., Regeimbal, J. M., Ghosh, P., Zhou, Y., Lauer, P., Dubensky, T. W., et al. (2018). The VirAB ABC transporter is required for VirR regulation of *Listeria monocytogenes* virulence and resistance to nisin. *Infect. Immun.* 86, e901–e917. doi: 10.1128/IAI.00901-17

Guérin, A., Bridier, A., Le Grandois, P., Sévellec, Y., Palma, F., Félix, B., et al. (2021). Exposure to quaternary ammonium compounds selects resistance to ciprofloxacin in *Listeria monocytogenes*. *Pathogens* 10:220. doi: 10.3390/pathogens10020220

Guidi, F., Orsini, M., Chiaverini, A., Centorame, P., Acciari, V. A., Salini, R., et al. (2021). Hypo - and hyper-virulent *Listeria monocytogenes* clones persisting in two different food processing plants of central Italy. *Microorganisms* 9:376.

Guillet, C., Join-Lambert, O., Le Monnier, A., Leclercq, A., Mechaï, F., Mamzer-Bruneel, M. F., et al. (2010). Human listeriosis caused by *Listeria ivanovii*. *Emerg. Infect. Dis.* 16, 136–138. doi: 10.3201/eid1601.091155

Haase, J. K., Didelot, X., Lecuit, M., Korkeala, H., Group, LmMS, et al. (2014). The ubiquitous nature of *Listeria monocytogenes* clones: a large-scale multilocus sequence typing study. *Environ. Microbiol.* 16, 405–416. doi: 10.1111/1462-2920.12342

Haddad, N., Johnson, N., Kathariou, S., Métris, A., Phister, T., Pielaat, A., et al. (2018). Next generation microbiological risk assessment-Potential of omics data for hazard characterisation. *Int. J. Food Microbiol.* 287, 28–39.

Hain, T., Hossain, H., Chatterjee, S. S., Machata, S., Volk, U., Wagner, S., et al. (2008). Temporal transcriptomic analysis of the *Listeria monocytogenes* EGD-e sigmaB regulon. *BMC Microbiol.* 8:20. doi: 10.1186/1471-2180-8-20

Halbedel, S., Wilking, H., Holzer, A., Kleta, S., Fischer, M. A., Lüth, S., et al. (2020). Large nationwide outbreak of invasive listeriosis associated with blood sausage, Germany, 2018-2019. *Emerg. Infect. Dis.* 26, 1456–1464. doi: 10.3201/eid2607.200225

Harter, E., Wagner, E. M., Zaiser, A., Halecker, S., Wagner, M., and Rychli, K. (2017). Stress survival islet 2, predominantly present in *Listeria monocytogenes* strains of sequence type 121, is involved in the alkaline and oxidative stress responses. *Appl. Environ. Microbiol.* 83:e00827-17. doi: 10.1128/AEM.00827-17

Hein, I., Klinger, S., Dooms, M., Flekna, G., Stess, B., Leclercq, A., et al. (2011). Stress survival islet 1 (SSI-1) survey in *Listeria monocytogenes* reveals an insert common to Listeria innocua in Sequence Type 121 *L. monocytogenes* strains. *Appl. Environ. Microbiol.* 77, 2169–2173. doi: 10.1128/AEM.02159-10

Heir, E., Lindstedt, B.-A., Røtterud, O.-J., Vardund, T., Kapperud, G., and Nesbakken, T. (2004). Molecular epidemiology and disinfectant susceptibility of *Listeria monocytogenes* from meat processing plants and human infections. *Int. J. Food Microbiol.* 96, 85–96. doi: 10.1016/j.ijfoodmicro.2004.03.014

Henderson, L. O., Erazo Flores, B. J., Skeens, J., Kent, D., Murphy, S. I., Wiedmann, M., et al. (2020). Nevertheless, she resisted - Role of the environment on *Listeria monocytogenes* sensitivity to nisin treatment in a laboratory cheese model. *Front. Microbiol.* 11:635. doi: 10.3389/fmicb.2020.00635

Hilliard, A., Leong, D., Callaghan, A. O., Culligan, E. P., Morgan, C. A., Delappe, N., et al. (2018). Genomic characterization of *Listeria monocytogenes* isolates associated with clinical listeriosis and the food production environment in Ireland. *Genes* 9:171. doi: 10.3390/genes9030171

Hingston, P., Chen, J., Dhillon, B. K., Laing, C., Bertelli, C., Gannon, V., et al. (2017). Genotypes associated with *Listeria monocytogenes* isolates displaying impaired or enhanced tolerances to cold, salt, acid, or desiccation stress. *Front. Microbiol.* 8:369. doi: 10.3389/fmicb.2017.00369

Holch, A., Webb, K., Lukjancenko, O., Ussery, D., Rosenthal, B. M., and Gram, L. (2013). Genome sequencing identifies two nearly unchanged strains of persistent *Listeria monocytogenes* isolated at two different fish processing plants sampled 6 years apart. *Appl. Environ. Microbiol.* 79, 2944–2951. doi: 10.1128/AEM.03715-12

Horlbog, J. A., Kent, D., Stephan, R., and Guldimann, C. (2018). Surviving host- and food relevant stresses: phenotype of *L. monocytogenes* strains isolated from food and clinical sources. *Sci. Rep.* 8:12931. doi: 10.1038/s41598-018-30723-z

Horn, N., and Bhunia, A. K. (2018). Food-associated stress primes foodborne pathogens for the gastrointestinal phase of infection. *Front. Microbiol.* 9:1962. doi: 10.3389/fmicb.2018.01962

Hurley, D., Luque-Sastre, L., Parker, C. T., Huynh, S., Eshwar, A. K., Nguyen, S. V., et al. (2019). Whole-genome sequencing-based characterization of 100 *Listeria monocytogenes* isolates collected from food processing environments over a four-year period. *mSphere* 4:e00252-19. doi: 10.1128/mSphere.00252-19

Jagadeesan, B., Gerner Smidt, P., Allard, M. W., Leuillet, S., Winkler, A., Xiao, Y., et al. (2019). The use of next generation sequencing for improving food safety: translation into practice. *Food Microbiol.* 79, 96–115. doi: 10.1016/j.fm.2018.11.005

Jiang, X., Yu, T., Xu, Y., Wang, H., Korkeala, H., and Shi, L. (2019). MdrL, a major facilitator superfamily efflux pump of *Listeria monocytogenes* involved in tolerance to benzalkonium chloride. *Appl. Microbiol. Biotechnol.* 103, 1339–1350. doi: 10.1007/s00253-018-9551-y

Johnson, J., Jinneman, K., Stelma, G., Smith, B. G., Lye, D., Messer, J., et al. (2004). Natural atypical Listeria innocua strains with *Listeria monocytogenes* pathogenicity island 1 genes. *Appl. Environ. Microbiol.* 70, 4256–4266. doi: 10.1128/AEM.70.7.4256-4266.2004

Jordan, S. J., Perni, S., Glenn, S., Fernandes, I., Barbosa, M., Sol, M., et al. (2008). *Listeria monocytogenes* biofilm-associated protein (BapL) may contribute to surface attachment of *L. monocytogenes*but is absent from many field isolates. *Appl. Environ. Microbiol.* 74, 5451–5456. doi: 10.1128/AEM.02419-07

Kadam, S. R., Den Besten, H. M. W., van der Veen, S., Zwietering, M. H., Moezelaar, R., and Abee, T. (2013). Diversity assessment of *Listeria monocytogenes* biofilm formation: impact of growth condition, serotype and strain origin. *Int. J. Food Microbiol.* 165, 259–264. doi: 10.1016/j.ijfoodmicro.2013.05.025

Kallipolitis, B., Gahan, C. G. M., and Piveteau, P. (2020). Factors contributing to *Listeria monocytogenes* transmission and impact on food safety. *Curr. Opin.Food Sci.* 36, 9–17.

Kang, J., Wiedmann, M., Boor, K. J., and Bergholz, T. M. (2015). VirR-mediated resistance of *Listeria monocytogenes* against food antimicrobials and cross-protection induced by exposure to organic acid salts. *Appl. Environ. Microbiol.* 81, 4553–4562. doi: 10.1128/AEM.00648-15

Karatzas, K. A. G., Suur, L., and O'Byrne, C. P. (2012). Characterization of the intracellular glutamate decarboxylase system: analysis of its function, transcription, and role in the acid resistance of various strains of *Listeria monocytogenes*. *Appl. Environ. Microbiol.* 78, 3571–3579. doi: 10.1128/AEM.00227-12

Katharios-Lanwermeyer, S., Rakic-Martinez, M., Elhanafi, D., Ratani, S., Tiedje, J. M., and Kathariou, S. (2012). Coselection of cadmium and benzalkonium chloride resistance in conjugative transfers from nonpathogenic *Listeria* spp. to other *Listeriae*. *Appl. Environ. Microbiol.* 78, 7549–7556. doi: 10.1128/AEM.02245-12

Katla, T., Naterstad, K., Vancanneyt, M., Swings, J., and Axelsson, L. (2003). Differences in susceptibility of *Listeria monocytogenes* strains to sakacin P, sakacin A, pediocin PA-1, and nisin. *Appl. Environ. Microbiol.* 69, 4431–4437. doi: 10.1128/AEM.69.8.4431-4437.2003

Kayode, A. J., Igbinosa, E. O., and Okoh, A. I. (2019). Overview of listeriosis in the Southern African hemisphere-review. *J. Food Saf.* 40:e12732. doi: 10.1111/jfs.12732

Keeney, K., Trmcic, A., Zhu, Z., Delaquis, P., and Wang, S. (2018). Stress survival islet 1 contributes to serotype-specific differences in biofilm formation in *Listeria monocytogenes*. *Lett. Appl. Microbiol.* 67, 530–536. doi: 10.1111/lam.13072

Knudsen, G. M., Nielsen, J. B., Marvig, R. L., Ng, Y., Worning, P., Westh, H., et al. (2017). Genome-wide-analyses of *Listeria monocytogenes* from food-processing plants reveal clonal diversity and date the emergence of persisting sequence types. *Environ. Microbiol. Rep.* 9, 428–440. doi: 10.1111/1758-2229.12552

Kode, D., Nannapaneni, R., Bansal, M., Chang, S., Cheng, W. H., Sharma, C. S., et al. (2021). Low-level tolerance to fluoroquinolone antibiotic ciprofloxacin in QAC-adapted subpopulations of *Listeria monocytogenes*. *Microorganisms* 9:1052. doi: 10.3390/microorganisms9051052

Korsak, D., and Szuplewska, M. (2016). Characterization of nonpathogenic Listeria species isolated from food and food processing environment. *Int. J. Food Microbiol.* 238, 274–280. doi: 10.1016/j.ijfoodmicro.2016.08.032

Kovacevic, J., Ziegler, J., Wałecka-Zacharska, E., Reimer, A., Kitts, D. D., and Gilmour, M. W. (2015). Tolerance of *Listeria monocytogenes* to quaternary ammonium sanitizers is mediated by a novel efflux pump encoded by emrE. *Appl. Environ. Microbiol.* 82, 939–953. doi: 10.1128/AEM.03741-15

Kremer, P. H., Lees, J. A., Koopmans, M. M., Ferwerda, B., Arends, A. W., Feller, M. M., et al. (2017). Benzalkonium tolerance genes and outcome in *Listeria monocytogenes* meningitis. *Clin. Microbiol. Infect.* 23, 265.e1–265.e7. doi: 10.1016/j.cmi.2016.12.008

Kuenne, C., Billion, A., Mraheil, M. A., Strittmatter, A., Daniel, R., Goesmann, A., et al. (2013). Reassessment of the *Listeria monocytogenes* pan-genome reveals dynamic integration hotspots and mobile genetic elements as major components of the accessory genome. *BMC Genom.* 14:47. doi: 10.1186/1471-2164-14-47

Kuenne, C., Voget, S., Pischimarov, J., Oehm, S., Goesmann, A., Daniel, R., et al. (2010). Comparative analysis of plasmids in the genus *Listeria*. *PLoS One* 5:e12511. doi: 10.1371/journal.pone.0012511

Lakicevic, B., Buncic, O., Katic, V., Lepsanovic, Z., Petrovic, L., Jankovic, V., et al. (2014). Detection of *Listeria* spp. during production and ripening of Petrovská klobása. *Acta Vet.* 64, 367–377. doi: 10.2478/acve-2014-0035

Lakicevic, B., and Nastasijevic, I. (2017). *Listeria monocytogenes* in retail establishments: contamination routes and control strategies. *Food Rev. Int.* 33, 247–269. doi: 10.1080/87559129.2016.1175017

Lang Halter, E., Neuhaus, K., and Scherer, S. (2013). *Listeria weihenstephanensis* sp. nov., isolated from the water plant *Lemna trisulca* taken from a freshwater pond. *Int. J. Syst. Evol. Microbiol.* 63, 641–647.

Lebrun, M., Audurier, A., and Cossart, P. (1994). Plasmid-borne cadmium resistance genes in *Listeria monocytogenes* are present on Tn5422, a novel transposon closely related to Tn917. *J. Bacteriol.* 176, 3049–3061.

Leclercq, A., Clermont, D., Bizet, C., Grimont, P. A., Le Fleche-Mateos, A., Roche, S. M., et al. (2010). *Listeria rocourtiae* sp. nov. *Int. J. Syst. Evol. Microbiol.* 60, 2210–2214. doi: 10.1099/ijs.0.017376-0

Leclercq, A., Moura, A., Vales, G., Tessaud-Rita, N., Aguilhon, C., and Lecuit, M. (2019). *Listeria thailandensis* sp. nov. *Int. J. Syst. Evol. Microbiol.* 69, 74–81. doi: 10.1099/ijsem.0.003097

Lee, B.-H., Cole, S., Badel-Berchoux, S., Guillier, L., Felix, B., Krezdorn, N., et al. (2019). Biofilm formation of *Listeria monocytogenes* strains under food processing environments and pan-genome-wide association study. *Front. Microbiol.* 10:2698. doi: 10.3389/fmicb.2019.02698

Lee, S., Ward, T. J., Jima, D. D., Parsons, C., and Kathariou, S. (2017). The arsenic resistanceassociated *Listeria* genomic island LGI2 exhibits sequence and integration site diversity and a propensity for three *Listeria monocytogenes* clones with enhanced virulence. *Appl. Environ. Microbiol.* 83: e01189-17. doi: 10.1128/AEM.01189-17

Leong, D., Alvarez-Ordóñez, A., and Jordan, K. (2014). Monitoring occurrence and persistence of *Listeria monocytogenes* in foods and food processing environments in the Republic of Ireland. *Front. Microbiol.* 5:436. doi: 10.3389/fmicb.2014.00436

Leong, D., Alvarez-Ordóñez, A., Zaouali, S., and Jordan, K. (2015). Examination of *Listeria monocytogenes* in seafood processing facilities and smoked salmon in the Republic of Ireland. *J. Food Prot.* 78, 2184–2190. doi: 10.4315/0362-028X.JFP-15-233

Liu, Y., Orsi, R. H., Gaballa, A., Wiedmann, M., Boor, K. J., and Guariglia Oropeza, V. (2019). Systematic review of the *Listeria monocytogenes* σB regulon supports a role in stress response, virulence and metabolism. *Future Microbiol.* 14, 801–828. doi: 10.2217/fmb-2019-0072

Lourenço, A., Neves, E., and Brito, L. (2009). Susceptibility of *Listeria monocytogenes* from traditional cheese-dairies to in-use sanitizers. *Food Control* 20, 585–589. doi: 10.1016/j.foodcont.2008.08.009

Lund, P., Tramonti, A., and De Biase, D. (2014). Coping with low pH: molecular strategies in neutralophilic bacteria. *FEMS* 38, 1091–1125. doi: 10.1111/1574-6976.12076

Lund, P. A., De Biase, D., Liran, O., Scheler, O., Mira, N. P., Cetecioglu, Z., et al. (2020). Understanding how microorganisms respond to acid pH is central to their control and successful exploitation. *Front. Microbiol.* 11:556140. doi: 10.3389/fmicb.2020.556140

Lundén, J., Autio, T., Markkula, A., Hellström, S., and Korkeala, H. (2003). Adaptive and cross-adaptive responses of persistent and non-persistent *Listeria monocytogenes* strains to disinfectants. *Int. J. Food Microbiol.* 82, 265–272. doi: 10.1016/s0168-1605(02)00312-4

Lundén, J. M., Miettinen, M. K., Autio, T. J., and Korkeala, H. J. (2000). Persistent *Listeria monocytogenes* strains show enhanced adherence to food contact surface after short contact times. *J. Food Prot.* 63, 1204–1207. doi: 10.4315/0362-028X-63.9.1204

Madeo, M., O'Riordan, N., Fuchs, T. M., Utratna, M., Karatzas, K. A., and O'Byrne, C. P. (2012). Thiamine plays a critical role in the acid tolerance of *Listeria monocytogenes*. *FEMS Microbiol. Lett.* 326, 137–143. doi: 10.1111/j.1574-6968.2011.02442.x

Malekmohammadi, S., Kodjovi, K. K., Sherwood, J., and Bergholz, T. M. (2017). Genetic and environmental factors influence *Listeria monocytogenes* nisin resistance. *J. Appl. Microbiol.* 123, 262–270. doi: 10.1111/jam.13479

Mandin, P., Fsihi, H., Dussurget, O., Vergassola, M., Milohanic, E., Toledo-Arana, A., et al. (2005). VirR, a response regulator critical for *Listeria monocytogenes* virulence. *Mol. Microbiol.* 57, 1367–1380. doi: 10.1111/j.1365-2958.2005.04776.x

Martínez-Suárez, J. V., Ortiz, S., and López-Alonso, V. (2016). Potential impact of the resistance to quaternary ammonium disinfectants on the persistence of *Listeria monocytogenes* in food processing environments. *Front. Microbiol.* 7:638. doi: 10.3389/fmicb.2016.00638

Matereke, L. T., and Okoh, A. I. (2020). *Listeria monocytogenes* virulence, antimicrobial, resistance and environmental persistence: a review. *Pathogens* 9:528. doi: 10.3390/pathogens9070528

Matle, I., Mafuna, T., Madoroba, E., Mbatha, K. R., Magwedere, K., and Pierneef, R. (2020). Population structure of non-ST6 *Listeria monocytogene* isolated in the red meat and poultry value chain in South Africa. *Microorganisms* 8:1152. doi: 10.3390/microorganisms8081152

Maury, M. M., Bracq-Dieye, H., Huang, L., Vales, G., Lavina, M., Thouvenot, P., et al. (2019). Hypervirulent *L. monocytogenes* clones' adaption to mammalian gut accounts for their association with dairy products. *Nat. Commun.* 10:2488. doi: 10.1038/s41467-019-10380-0

Maury, M. M., Tsai, Y. H., Charlier, C., Touchon, M., Chenal-Francisque, V., Leclercq, A., et al. (2016). Uncovering *Listeria monocytogenes* hypervirulence by harnessing its biodiversity. *Nat. Genet.* 8, 308–313. doi: 10.1038/ng.3501

Meier, A. B., Guldimann, C., Markkula, A., Pöntinen, A., Korkeala, H., and Tasara, T. (2017). Comparative phenotypic and genotypic analysis of Swiss and Finnish *Listeria monocytogenes* isolates with respect to benzalkonium chloride resistance. *Front. Microbiol.* 8:397. doi: 10.3389/fmicb.2017.00397

Moreno, L. Z., Paixão, R., Gobbi, D. D., Raimundo, D. C., Ferreira, T. P., Hofer, E., et al. (2012). Characterization of atypical Listeria innocua isolated from swine slaughterhouses and meat markets. *Res. Microbiol.* 163, 268–271. doi: 10.1016/j.resmic.2012.02.004

Møretrø, T., Schirmer, B. C. T., Heir, E., Fagerlund, A., Hjemli, P., and Langsrud, S. (2017). Tolerance to quaternary ammonium compound disinfectants may enhance growth of *Listeria monocytogenes* in the food industry. *Int. J. Food Microbiol.* 241, 215–224. doi: 10.1016/j.ijfoodmicro.2016.10.025

Moura, A., Criscuolo, A., Pouseele, H., Maury, M. M., Leclercq, A., Tarr, C., et al. (2016). Whole genome based population biology and epidemiological surveillance of *Listeria monocytogenes*. *Nat. Microbiol.* 2:16185. doi: 10.1038/nmicrobiol.2016.185

Moura, A., Disson, O., Lavina, M., Thouvenot, P., Huang, L., Leclercq, A., et al. (2019). Atypical hemolytic Listeria innocua isolates are virulent, albeit less than

Listeria monocytogenes. *Infect. Immun.* 87:e00758-18. doi: 10.1128/IAI.00758-18

Mullapudi, S., Siletzky, R. M., and Kathariou, S. (2008). Heavy-metal and benzalkonium chloride resistance of *Listeria monocytogenes* isolates from the environment of turkey-processing plants. *Appl. Environ. Microbiol.* 74, 1464–1468. doi: 10.1128/AEM.02426-07

Mullapudi, S., Siletzky, R. M., and Kathariou, S. (2010). Diverse cadmium resistance determinants in *Listeria monocytogenes* isolates from the turkey processing plant environment. *Appl. Environ. Microbiol.* 76, 627–630.

Müller, A., Rychli, K., Muhterem-Uyar, M., Zaiser, A., Stessl, B., Guinane, C. M., et al. (2013). Tn6188 – a novel transposon in *Listeria monocytogenes* responsible for tolerance to benzalkonium chloride. *PLoS One* 8:e76835. doi: 10.1371/journal.pone.0076835

Müller, A., Rychli, K., Zaiser, A., Wieser, C., Wagner, M., and Schmitz-Esser, S. (2014). The *Listeria monocytogenes* transposon Tn6188 provides increased tolerance to various quaternary ammonium compounds and ethidium bromide. *FEMS Microbiol. Lett.* 361, 166–173. doi: 10.1111/1574-6968.12626

Müller-Herbst, S., Wüstner, S., Mühlig, A., Eder, D., Fuchs, T. M., Held, C., et al. (2014). Identification of genes essential for anaerobic growth of *Listeria monocytogenes*. *Microbiology* 160, 752–765. doi: 10.1099/mic.0.075242-0

Naditz, A. (2020). *A Comparative Analysis of Listeria monocytogenes* Plasmids: Presence, Contribution to Stress and Conservation. Graduate Theses and Dissertations. Ames, IA: Iowa State University.

Nikparvar, B., Andreevskaya, M., Duru, I. C., Bucur, F. I., Grigore-Gurgu, L., Borda, D., et al. (2021). Analysis of temporal gene regulation of *Listeria monocytogenes* revealed distinct regulatory response modes after exposure to high pressure processing. *BMC Genom.* 22:266. doi: 10.1186/s12864-021-07461-0

Nilsson, L., Huss, H. H., and Gram, L. (1997). Inhibition of *Listeria monocytogenes* on cold-smoked salmon by nisin and carbon dioxide atmosphere. *Int. J. Food Microbiol.* 38, 217–227. doi: 10.1016/s0168-1605(97)00111-6

Njage, P. M. K., Leekitcharoenphon, P., Hansen, L. T., Hendriksen, R. S., Faes, C., Aerts, M., et al. (2020). Quantitative microbial risk assessment based on whole genome sequencing data: case of *Listeria monocytogenes*. *Microorganisms* 8:1772. doi: 10.3390/microorganisms8111772

Norwood, D. E., and Gilmour, A. (1999). Adherence of *Listeria monocytogenes* strains to stainless steel coupons. *J. Appl. Microbiol.* 86, 576–582. doi: 10.1046/j.1365-2672.1999.00694.x

Norwood, D. E., and Gilmour, A. (2001). The differential adherence capabilities of two *Listeria monocytogenes* strains in monoculture and multispecies biofilms as a function of temperature. *Lett. Appl. Microbiol.* 33, 320–324. doi: 10.1046/j.1472-765x.2001.01004.x

Nüesch-Inderbinen, M., Bloemberg, G. V., Müller, A., Stevens, M., Cernela, N., Kollöffel, B., et al. (2021). *Listeriosis* caused by persistence of *Listeria monocytogenes* serotype 4b sequence type 6 in cheese production environment. *Emerg. Infect. Dis.* 27, 284–288. doi: 10.3201/eid2701.203266

Nuñez-Montero, K., Leclercq, A., Moura, A., Vales, G., Peraza, J., Pizarro-Cerda, J., et al. (2018). *Listeria costaricensis* sp. nov. *Int. J. Syst. Evol. Microbiol.* 68, 844–850. doi: 10.1099/ijsem.0.002596

Oliver, H. F., Orsi, R. H., Wiedmann, M., and Boor, K. J. (2010). *Listeria monocytogenes*sigmaB has a small core regulon and a conserved role in virulence but makes differential contributions to stress tolerance across a diverse collection of strains. *Appl. Environ. Microbiol.* 76, 4216–4232. doi: 10.1128/AEM.00031-10

Orsi, R. H., den Bakker, H. C., and Wiedmann, M. (2011). *Listeria monocytogenes* lineages: genomics, evolution, ecology, and phenotypic characteristics. *Int. J. Med. Microbiol.* 301, 79–96. doi: 10.1016/j.ijmm.2010.05.002

Ortiz, S., López, V., Garriga, M., and Martínez-Suárez. (2014). Antilisterial effect of two bioprotective cultures in a model system of Iberian chorizo fermentation. *Int. J. Food Sci. Technol.* 49, 753–758. doi: 10.1111/ijfs.12362

Ortiz, S., Lopez-Alonso, V., Rodriguez, P., and Martinez-Suarez, J. V. (2016). The connection between persistent, disinfectant-resistant *Listeria monocytogenes* strains from two geographically separate Iberian pork processing plants: evidence from comparative genome analysis. *Appl. Environ. Microbiol.* 82, 308–317. doi: 10.1128/AEM.02824-15

Painset, A., Björkman, J. T., Kiil, K., Guillier, L., Mariet, J. F., Félix, B., et al. (2019). LiSEQ - whole genome sequencing of a cross - sectional survey of *Listeria monocytogenes* in ready-to-eat foods and human clinical cases in Europe. *Microb. Genom.* 5:e000257. doi: 10.1099/mgen.0.000257

Palaiodimou, L., Fanning, S., and Fox, E. M. (2021). Genomic insights into persistence of Listeria species in the food processing environment. *J. Appl. Microbiol.* 131, 2082–2094. doi: 10.1111/jam.15089

Pan, Y., Breidt, F., and Kathariou, S. (2006). Resistance of *Listeria monocytogenes* biofilms to sanitizing agents in a simulated food processing environment. *Appl. Environ. Microbiol.* 72, 7711–7717. doi: 10.1128/AEM.01065-06

Parsons, C., Lee, S., Jayeola, V., and Kathariou, S. (2017). Novel cadmium resistance determinant in *Listeria monocytogenes*. *Appl. Environ. Microbiol.* 83:e02580-16. doi: 10.1128/AEM.02580-16

Parsons, C., Lee, S., and Kathariou, S. (2019). Heavy metal resistance determinants of the foodborne pathogen *Listeria monocytogenes*. *Genes* 10:11. doi: 10.3390/genes10010011

Pasquali, F., Palma, F., Guillier, L., Lucchi, A., De Cesare, A., and Manfreda, G. (2018). *Listeria monocytogenes* sequence types 121 and 14 repeatedly isolated within one year of sampling in a rabbit meat processing plant: persistence and ecophysiology. *Front. Microbiol.* 9:596. doi: 10.3389/fmicb.2018.00596

Paudyal, R., Barnes, C. P., and Karatzas, K. A. (2018). A novel approach in acidic disinfection through inhibition of acid resistance 2 mechanisms; maleic acid-mediated inhibition of glutamate decarboxylase activity 3 enhances acid sensitivity of *Listeria monocytogenes*. *Food Microbiol.* 69, 96–104. doi: 10.1016/j.fm.2017.07.013

Paudyal, R., O'Byrne, R. H., and Karatzas, K. A. (2020). Amino acids other than glutamate affect the expression of the GAD system in *Listeria monocytogenes* enhancing acid resistance. *Food Microbiol.* 90:103481. doi: 10.1016/j.fm.2020.103481

Pérez-Baltar, A., Pérez-Boto, D., Medina, M., and Montiel, R. (2021). Genomic diversity and characterization of *Listeria monocytogenes* from dry-cured ham processing plants. *Food Microbiol.* 99:103779. doi: 10.1016/j.fm.2021.103779

Pérez-Trallero, E., Zigorraga, C., Artieda, J., Alkorta, M., and Marimón, J. M. (2014). Two outbreaks of *Listeria monocytogenes* infection, Northern Spain. *Emerg. Infect. Dis* 20, 2155–2157. doi: 10.3201/eid2012.140993

Quereda, J. J., Andersson, C., Cossart, P., Johansson, J., and Pizarro-Cerda, J. (2018). Role in virulence of phospholipases, listeriolysin O and listeriolysin S from epidemic *Listeria monocytogenes* using the chicken embryo infection model. *Vet. Res.* 49:13. doi: 10.1186/s13567-017-0496-4

Quereda, J. J., Dussurget, O., Nahori, M. A., Ghozlane, A., Volant, S., Dillies, M. A., et al. (2016). Bacteriocin from epidemic Lis*t*eria strains alters the host intestinal microbiota to favor infection. *Proc. Natl. Acad. Sci. U.S.A.* 113, 5706–5711. doi: 10.1073/pnas.1523899113

Quereda, J. J., Leclercq, A., Moura, A., Vales, G., Gomez-Martin, A., Garcia-Munoz, A., et al. (2020). *Listeria valentina* sp. nov., isolated from a water trough and the faeces of healthy sheep. *Int. J. Syst. Evol. Microbiol.* 70, 5868–5879. doi: 10.1099/ijsem.0.004494

Quereda, J. J., Meza-Torres, J., Cossart, P., and Pizarro-Cerdá, J. (2017). *Listeriolysin S*: a bacteriocin from epidemic *Listeria monocytogenes* strains that targets the gut microbiota. *Gut Microb.* 8, 384–391. doi: 10.1080/19490976.2017.1290759

Quereda, J. J., Morón-García, A., Palacios-Gorba, C., Dessaux, C., García-del Portillo, F., Graciela Pucciarelli, M., et al. (2021). Pathogenicity and virulence of *Listeria monocytogenes*: a trip from environmental to medical microbiology. *Virulence* 12, 2509–2545. doi: 10.1080/21505594.2021.1975526

Raengpradub, S., Wiedmann, M., and Boor, K. J. (2008). Comparative analysis of the sigma B-dependent stress responses in *Listeria monocytogenes* and *Listeria innocua* strains exposed to selected stress conditions. *Appl. Environ. Microbiol.* 74, 158–171. doi: 10.1128/AEM.00951-07

Ragon, M., Wirth, T., Hollandt, F., Lavenir, R., Lecuit, M., Le Monnier, A., et al. (2008). A new perspective on *Listeria monocytogenes* evolution. *PLoS Pathog.* 4:e1000146. doi: 10.1371/journal.ppat.1000146

Ramalheira, R., Almeida, M., Azeredo, J., Brandão, T. R., Almeida, G., Silva, J., et al. (2010). Survival of clinical and food isolates of *Listeria monocytogenes* through simulated gastrointestinal tract conditions. *Foodborne Pathog. Dis.* 7, 121–128. doi: 10.1089/fpd.2009.0319

Rantsiou, K., Kathariou, S., Winkler, A., Skandamis, P., Saint-Cyr, M. J., Rouzeau-Szynalski, K., et al. (2018). Next generation microbiological risk assessment: opportunities of whole genome sequencing (WGS) for foodborne pathogen surveillance, source tracking and risk assessment. *Int. J. Food Microbiol.* 287, 3–9.

Ratani, S. S., Siletzky, R. M., Dutta, V., Yildirim, S., Osborne, J. A., Lin, W., et al. (2012). Heavy metal and disinfectant resistance of *Listeria monocytogenes* from

foods and food processing plants. *Appl. Environ. Microbiol.* 78, 6938–6945. doi: 10.1128/AEM.01553-12

Roedel, A., Dieckmann, R., Brendebach, H., Hammerl, J. A., Kleta, S., Noll, M., et al. (2019). Biocide-tolerant *Listeria monocytogenes* isolates from German food production plants do not show cross-resistance to clinically relevant antibiotics. *Appl. Environ. Microbiol.* 85:e01253-19. doi: 10.1128/AEM.01253-19

Ryan, S., Begley, M., Gahan, C. G., and Hill, C. (2009). Molecular characterization of the arginine deiminase system in *Listeria monocytogenes*: regulation and role in acid tolerance. *Environ. Microbiol.* 11, 432–445. doi: 10.1111/j.1462-2920.2008.01782.x

Ryan, S., Begley, M., Hill, C., and Gahan, C. G. M. (2010). A five-gene stress survival islet (SSI-1) that contributes to the growth of *Listeria monocytogenes* in suboptimal conditions. *J. Appl. Microbiol.* 109, 984–995. doi: 10.1111/j.1365-2672.2010.04726.x

Schlech, W. (2019). Epidemiology and clinical manifestations of *Listeria monocytogenes* infection. *Microbiol. Spectr.* 7, 1–12. doi: 10.1128/9781683670131.ch50

Schmitz-Esser, S., Müller, A., Stessl, B., and Wagner, M. (2015). Genomes of sequence type 121 *Listeria monocytogenes* strains harbor highly conserved plasmids and prophages. *Front. Microbiol.* 6:380. doi: 10.3389/fmicb.2015.00380

Seeliger, H. P. R., and Hohne, K. (1979). Serotyping of *Listeria monocytogenes* and related species. *Methods Microbiol.* 13, 31–49.

Severino, P., Dussurget, O., Vêncio, R. Z., Dumas, E., Garrido, P., Padilla, G., et al. (2007). Comparative transcriptome analysis of *Listeria monocytogenes* strains of the two major lineages reveals differences in virulence, cell wall, and stress response. *Appl. Environ. Microbiol.* 73, 6078–6088. doi: 10.1128/AEM.02730-06

Sewell, D., Allen, S. C. H., and Phillips, C. A. (2015). Oxygen limitation induces acid tolerance and impacts simulated gastro-intestinal transit in *Listeria monocytogenes* J0161. *Gut Pathog.* 7, 1–5. doi: 10.1186/s13099-015-0058-0

Soares, C. A., and Knuckley, B. (2016). Mechanistic studies of the agmatine deiminase from *Listeria monocytogenes*. *Biochem. J.* 473, 1553–1561. doi: 10.1042/BCJ20160221

Stoller, A., Stevens, M., Stephan, R., and Guldimann, C. (2019). Characteristics of *Listeria monocytogenes* strains persisting in a meat processing facility over a 4-year period. *Pathogens* 8:32. doi: 10.3390/pathogens8010032

Szendy, M., Kalkhof, S., Bittrich, S., Kaiser, F., Leberecht, C., Labudde, D., et al. (2019). Structural change in GadD2 of *Listeria monocytogenes* field isolates supports nisin resistance. *Int. J. Food Microbiol.* 305:108240. doi: 10.1016/j.ijfoodmicro.2019.108240

Takahashi, H., Miya, S., Igarashi, K., Suda, T., Kuramoto, S., and Kimura, B. (2009). Biofilm formation ability of *Listeria monocytogenes* isolates from raw ready-to-eat seafood. *J. Food Prot.* 72, 1476–1480. doi: 10.4315/0362-028X-72.7.1476

Tavares, R. M., Silva, D. A. L. D., Camargo, A. C., Yamatogi, R. S., and Nero, L. A. (2020). Interference of the acid stress on the expression of llsX by *Listeria monocytogenes* pathogenic island 3 (LIPI-3) variants. *Food Res. Int.* 132:109063. doi: 10.1016/j.foodres.2020.109063

Thedieck, K., Hain, T., Mohamed, W., Tindall, B. J., Nimtz, M., Chakraborty, T., et al. (2006). The MprF protein is required for lysinylation of phospholipids in listerial membranes and confers resistance to cationic antimicrobial peptides (CAMPs) on *Listeria monocytogenes*. *Mol. Microbiol.* 62, 1325–1339. doi: 10.1111/j.1365-2958.2006.05452.x

Thomas, J., Govender, N., McCarthy, K. M., Erasmus, L. K., Doyle, T. J., Allam, M., et al. (2020). Outbreak of listeriosis in South Africa associated with processed meat. *N. Engl. J. Med.* 382, 632–643. doi: 10.1056/NEJMoa1907462

Tirloni, E., Stella, S., de Knegt, L. V., Gandolfi, G., Bernardi, C., and Nauta, M. J. (2018). A quantitative microbial risk assessment model for *Listeria monocytogenes* in RTE sandwiches. *Microb. Risk Anal.* 9, 11–21.

Trinetta, V., Floros, J. D., and Cutter, C. N. (2010). Sakacin a-containing pullulan film: an active packaging system to control epidemic clones of *Listeria monocytogenes* in ready-to-eat foods. *J. Food Saf.* 30, 366–381. doi: 10.1111/j.1745-4565.2010.00213.x

Upham, J., Chen, S., Boutilier, E., Hodges, L., Eisebraun, M., Croxen, M. A., et al. (2019). Potential ad hoc markers of persistence and virulence in Canadian *Listeria monocytogenes* food and clinical isolates. *J. Food Prot.* 82, 1909–1921. doi: 10.4315/0362-028X.JFP-19-028

van Schaik, W., Gahan, C. G., and Hill, C. (1999). Acid-adapted *Listeria monocytogenes* displays enhanced tolerance against the lantibiotics nisin and lacticin 3147. *J. Food Prot.* 62, 536–539. doi: 10.4315/0362-028x-62.5.536

Vázquez-Boland, J. A., Wagner, M., and Scortti, M. (2020). Why are some *Listeria monocytogenes* genotypes more likely to cause invasive (brain, placental) infection? *mBio* 11:e03126-20. doi: 10.1128/mBio.03126-20

Verghese, B., Lok, M., Wen, J., Alessandria, V., Chen, Y., Kathariou, S., et al. (2011). comK prophage junction fragments as markers for *Listeria monocytogenes* genotypes unique to individual meat and poultry processing plants and a model for rapid niche-specific adaptation, biofilm formation, and persistence. *Appl. Environ. Microbiol.* 77, 3279–3292. doi: 10.1128/AEM.00546-11

Volokhov, D. V., Duperrier, S., Neverov, A. A., George, J., Buchrieser, C., and Hitchins, A. D. (2007). The presence of the internalin gene in natural atypically hemolytic Listeria innocua strains suggests descent from *L. monocytogenes*. *Appl. Environ. Microbiol.* 73, 1928–1939. doi: 10.1128/AEM.01796-06

Wambui, J., Eshwar, A. K., Aalto-Araneda, M., Pöntinen, A., Stevens, M. J. A., Njage, P. M. K., et al. (2020). The analysis of field strains isolated from food, animal and clinical sources uncovers natural mutations in *Listeria monocytogenes* nisin resistance genes. *Front. Microbiol.* 6:549531. doi: 10.3389/fmicb.2020.549531

Wang, Y., Luo, L., Li, O., Wang, H., Wang, Y., Sun, H., et al. (2019). Genomic dissection of the most prevalent *Listeria monocytogenes* clone, sequence type ST87, in China. *BMC Genom.* 20:1014. doi: 10.1186/s12864-019-6399-1

Weller, D., Andrus, A., Wiedmann, M., and den Bakker, H. C. (2015). Listeria booriae sp. nov. and Listeria newyorkensis sp. nov., from food processing environments in the USA. *Int. J. Syst. Evol. Microbiol.* 65, 286–292. doi: 10.1099/ijs.0.070839-0

Wieczorek, K., Bomba, A., and Osek, J. (2020). Whole-genome sequencing-based characterization of *Listeria monocytogenes* from fish and fish production environments in Poland. *Int. J. Mol. Sci.* 21:9419. doi: 10.3390/ijms21249419

Woraprayote, W., Kingcha, Y., Amonphanpokin, P., Kruenate, J., Zendo, T., Sonomoto, K., et al. (2013). Anti-listeria activity of poly(lactic acid)/sawdust particle biocomposite film impregnated with pediocin PA-1/AcH and its use in raw sliced pork. *Int. J. Food Microbiol.* 167, 229–235. doi: 10.1016/j.ijfoodmicro.2013.09.009

Xie, Y., Zhang, M., Gao, X., Shao, Y., Liu, H., Jin, J., et al. (2018). Development and antimicrobial application of plantaricin BM-1 incorporating a PVDC film on fresh pork meat during cold storage. *J. Appl. Microbiol.* 125, 1108–1116. doi: 10.1111/jam.13912

Xu, D., Li, Y., Zahid, M. S., Yamasaki, S., Shi, L., Li, J. R., et al. (2014). Benzalkonium chloride and heavy-metal tolerance in *Listeria monocytogenes* from retail foods. *Int. J. Food Microbiol.* 190, 24–30. doi: 10.1016/j.ijfoodmicro.2014.08.017

Yin, Y., Yao, H., Doijad, S., Kong, S., Shen, Y., Cai, X., et al. (2019). A hybrid sub-lineage of *Listeria monocytogenes* comprising hypervirulent isolates. *Nat. Commun.* 10:4283. doi: 10.1038/s41467-019-12072-1

Zhang, H., Chen, W., Wang, J., Xu, B., Liu, H., Dong, Q., et al. (2020). 10-year molecular surveillance of *Listeria monocytogenes* using whole-genome sequencing in Shanghai. *China, 2009-2019. Front. Microbiol.* 11:551020. doi: 10.3389/fmicb.2020.551020

Zuber, I., Lakicevic, B., Pietzka, A., Milanov, D., Djordjevic, V., Karabasil, N., et al. (2019). Molecular characterization of *Listeria monocytogenes* isolates from a small-scale meat processor in Montenegro 2011-2014. *Food Microbiol.* 79, 116–122. doi: 10.1016/j.fm.2018.12.005

Conflict of Interest: The authors declare that the research was conducted in the absence of any commercial or financial relationships that could be construed as a potential conflict of interest.

frontiers in Microbiology

ORIGINAL RESEARCH
published: 03 February 2022
doi: 10.3389/fmicb.2022.792755

Isolation, Identification and Characterization of Two Kinds of Deep-Sea Bacterial Lipopeptides Against Foodborne Pathogens

*Yanjun Gu[1], Rikuan Zheng[2,3,4], Chaomin Sun[2,3,4] and Shimei Wu[1]**

[1] College of Life Sciences, Qingdao University, Qingdao, China, [2] CAS and Shandong Province Key Laboratory of Experimental Marine Biology, Institute of Oceanology, Chinese Academy of Sciences, Qingdao, China, [3] Laboratory for Marine Biology and Biotechnology, Qingdao National Laboratory for Marine Science and Technology, Qingdao, China, [4] Center of Ocean Mega-Science, Chinese Academy of Sciences, Qingdao, China

OPEN ACCESS

Edited by:
Jana Sedlakova-Kadukova, University of St. Cyril and Methodius, Slovakia

Reviewed by:
Kui Zhu, China Agricultural University, China
Tao Wei, South China Agricultural University, China

***Correspondence:**
Shimei Wu
shimeiwu2016@126.com

Specialty section:
This article was submitted to Food Microbiology, a section of the journal Frontiers in Microbiology

Received: *11 October 2021*
Accepted: *13 January 2022*
Published: *03 February 2022*

Citation:
Gu Y, Zheng R, Sun C and Wu S (2022) Isolation, Identification and Characterization of Two Kinds of Deep-Sea Bacterial Lipopeptides Against Foodborne Pathogens. Front. Microbiol. 13:792755. doi: 10.3389/fmicb.2022.792755

Under multiple stresses of deep sea, many microorganisms have evolved potentials to produce different metabolites to cope with the stresses they face. In this study, we isolated a bacterial strain *Bacillus* sp. YJ17 from the deep-sea cold seep. Compared with commercial food preservative nisin, it showed broad and strong antibacterial activities against foodborne pathogens, including multiple resistant bacteria *Pseudomonas aeruginosa* PAO1 and methicillin-resistant *Staphylococcus aureus* (MRSA). The active agents were purified by reversed-phase high performance liquid chromatography (RP-HPLC). Analysis of high-energy collision induced dissociation mass spectrometry (HCD-MS) showed that the two active agents belong to family of fengycin and surfactin, and based on results of tandem mass spectrometry (HCD-MS/MS), the amino acid sequence of purified fengycin and surfactin might be Glu-Orn-Tyr-Thr-Glu-Val-Pro-Gln-Tyr-Ile and Glu-Leu/Ile-Leu/Ile-Leu/Ile-Val-Asp-Leu/Ile, respectively. Since the purified fengycin and surfactin exhibited strong inhibition against *P. aeruginosa* PAO1 and MRSA respectively, the inhibition mechanisms of fengycin against *P. aeruginosa* PAO1 and surfactin against MRSA were investigated by electron microscopy. After treatment with purified fengycin, the morphology of *P. aeruginosa* PAO1 became abnormal and aggregated together, and obvious cytoplasmic leakage was observed. After treatment with purified surfactin, the MRSA cells clustered together, and cell surface became rough and jagged. Further study showed that reactive oxygen species (ROS) accumulation and cell membrane damage occurred in *P. aeruginosa* PAO1 and MRSA after treated with fengycin and surfactin, respectively. Furthermore, typical ROS scavenging enzymes catalase (CAT) and superoxide dismutase (SOD) were also significantly reduced in *P. aeruginosa* PAO1 and MRSA after treated with fengycin and surfactin, respectively. Therefore, the inhibition mechanisms of fengycin against *P. aeruginosa* PAO1 and

surfactin against MRSA are closely related with accumulation of ROS, which might be due to the decreased activity of CAT and SOD after treated with fengycin and surfactin, respectively. Overall, our study provides good candidates from the deep-sea environment to deal with foodborne pathogens, especially multidrug-resistant bacteria.

Keywords: *Bacillus*, deep-sea, lipopeptides, foodborne pathogens, fengycin, surfactin

INTRODUCTION

Under multiple stresses in the environment, microorganisms have evolved different mechanisms in order to survive, such as secreting diverse secondary metabolites to compete with other organisms for nutrients or living space (Williams et al., 1989). Members of the genus *Bacillus* have been described as potential biological control agents for their ability to produce various bioactive substances, such as lipopeptides, polyketides, and volatile metabolites (Caulier et al., 2019; Jiao et al., 2021). Lipopeptides have been widely studied because of their various biological activities, such as anti-bacterial, anti-fungal, anti-tumor and anti-virus activities (Meena and Kanwar, 2015; Zhao et al., 2017; Meena et al., 2019). According to amino acid sequences and fatty acid branches, lipopeptides can be classified into three families: iturin, surfactin, and fengycin (Romero et al., 2007; Yang et al., 2015). Iturin is composed of heptapeptide containing β-amino fatty acids (Zhou et al., 2020). Surfactin is formed by a C_{12}-C_{16} β-hydroxy fatty acid linked to heptapeptide (Bonmatin et al., 1995). Fengycin is connected by a β-hydroxyl fatty acid and a decapeptide, forming a circular lactone ring like surfactin (Yang et al., 2015; Zhang and Sun, 2018).

Listeria monocytogenes, Salmonella choleraesuis, Staphylococcus aureus and *Pseudomonas aeruginosa* are common foodborne pathogens, which often cause serious foodborne diseases and have become a global public health problem (Zarei et al., 2014; Patra and Baek, 2017; Yasmin et al., 2017). However, the overuse of antibiotics, especially different kinds of antibiotics, has led to the increase of multidrug resistant bacteria and the accelerated spread of antibiotic resistance genes (Bjerketorp et al., 2021). Many studies have shown that lipopeptides produced by *Bacillus* have effective antibacterial activity against resistant bacterial strains (Gudina et al., 2016; Zhao et al., 2018). Due to their specific amphiphilic structure, the antibacterial mechanisms of lipopeptides are different from conventional antibiotics, mainly by destroying the integrity of microbial cell membrane or cell wall, forming holes in the membrane, allowing the leakage of cell contents and killing cells, so as to show lower drug resistance (Banat et al., 2010; Yount and Yeaman, 2013; Patel et al., 2015; Ben Ayed et al., 2017). In addition, lipopeptides have the excellent characteristics of low toxicity, biodegradability, environmental friendliness and tolerance to extreme environmental conditions (Cameotra and Makkar, 2004), which confer lipopeptides the promising potential utilization value in food health, biological prevention and medical treatment.

In this study, a marine bacterium *Bacillus* sp. YJ17 was isolated from the cold spring of the South China Sea, which exhibited broad antibacterial activity against common foodborne pathogens, and two corresponding active agents were purified. The structures of the purified active agents were analyzed by tandem mass spectrometry, and the antibacterial mechanisms were also investigated in details.

MATERIALS AND METHODS

Stain Isolation, Culture Conditions and Strain Identification

The sediments used in this experiment were collected from the cold seep in the South China Sea (119°17′05.3940″E, 22°06′58.7264″N) at a depth of about 1,173 m in June 2020. The sediments were separated from the above samples after serial dilution with sterile seawater and incubated in 2216E agar medium (5 g tryptone, 1 g yeast paste, 15 g agar, 1,000 ml filtered seawater, pH adjusted to 7.4–7.6) at 28°C. For screening of strains with antibacterial activity, indicator bacteria were incubated in LB agar medium (10 g tryptone, 5 g yeast extract, 10 g NaCl, 15 g agar, pH adjusted to 7.0) and Trypticase Soy Broth (TSB) agar medium (17 g tryptone, 3 g Plant peptone, 5 g NaCl, 2.5g K_2HPO_4, 2.5 g glucose, 15 g agar, pH adjusted to 7.1–7.5) at 28°C.

For the identification of the isolated strain, the corresponding 16S ribosomal DNA (rDNA) was amplified using universal forward primer 27F (AGAGTTTGATCCTGGCTCAG) and reverse primer 1492R (TACGGCTACCTTGTTCGACTT). The high-fidelity PCR enzyme KOD One ^{TM} was used in this process. The PCR products were mixed with 6 × loading buffer (Qingdao, Tsingke) and the bands were separated by one-percent agarose gel electrophoresis, and the corresponding fragments were recovered by the gel recovery kit and sequenced by company (Qingdao, Tsingke). The obtained sequences were compared with 16S rDNA sequences in NCBI database[1] using the BLAST algorithm. Phylogenetic trees were constructed by MEGA-X to determine its species information.

Screening of Strains With Antimicrobial Activity

Pseudomonas aeruginosa PAO1, methicillin-resistant *Staphylococcus aureus* (MRSA), *Salmonella choleraesuis* and *Listeria monocytogenes* are known to be foodborne pathogens and used as indicator strains to screen marine bacteria with high antimicrobial activity. The assay for antimicrobial activity of the isolated strains was performed as previously described (Fan et al., 2017). Briefly, to prepare the screening plate, the overnight broth culture of the foodborne pathogens was added to 50–60°C LB medium, then mixed well and poured into the

[1]http://www.ncbi.nlm.nih.gov/BLAST/

plate. To screen the strain with antibacterial activity, the isolated marine strains were inoculated in screening plate, and incubated at 28°C for 48 h. If the isolated strain can secrete substances with antimicrobial activity against the indicator bacteria, an inhibition zone will be observed around the colony of the isolated strain. To further detect the antimicrobial activity of the strain with inhibition zone, the strain was inoculated into LB medium, and incubated at 28°C for 48 with a shaking speed of 150 rpm, then the supernatant was collected and the antimicrobial activity was detected against the indicator strains.

Isolation and Purification of Antimicrobial Agents From *Bacillus* sp. YJ17

To purify the antimicrobial agents produced by *Bacillus* sp. YJ17, overnight cultures of *Bacillus* sp. YJ17 were inoculated in 250 ml conical flasks containing 100 ml LB liquid medium and incubated at 28°C for 48 h with a shaking speed of 150 rpm. The fermentation broth was centrifuged at 8,000 × *g* for 10 min at 4°C, and the cell free supernatant was precipitated by adjusting the pH to 2.5 with 6 N HCl, which was stored overnight at 4°C. The precipitate was obtained by centrifugation, then washed with 50 ml of distilled water, air-dried, and suspended in 100% methanol. The crude methanol extract was filtered through a 0.22 μm nylon membrane and injected into a reverse high performance liquid chromatography (RP-HPLC) (Agilent 1260) with an Eclipse XDB-C_{18} column (5 μm, 250 × 4.6 mm, Agilent) for further purification. Mobile phase A was water and methanol (30:70, vol/vol), and mobile phase B was 100% methanol, and elution was carried out at a flow rate of 2 ml/min under the following conditions: 0–45 min, 0% B to 100% B, then 45–60 min, 100% B. Monitoring was performed using a 210 nm UV detector, and the elution products of each peak were collected manually to detect their inhibitory activity against the indicator bacteria.

Mass Spectrometry Analysis of Antimicrobial Agents

To obtain molecular mass information of antimicrobial agents, high-energy collisional dissociation (HCD) of active elution fractions was performed using linear ion trap Orbitrap spectrometer (LTQ Orbitrap XL; Thermo Fisher, United States), a well-established mass spectrometric cleavage technique that produces more fragments and higher quality mass spectra to enhance identification (Wang et al., 2020). The m/z values were measured from 150 to 2,000. HCD-MS-MS was used to analyze the fragment ions and further determine the structure of the antimicrobial agent. The following conditions were used for data acquisition: electrospray ion source (ESI); 3 KV spray voltage; dry gas was nitrogen, pressure was kept at 0.05 mpa; ion transfer capillary temperature was 275°C; HCD collision gas was helium, anion mode detection; collision energy was 45–60 ev. Then, Xcalibur2.1 was used to analyze the results.

Activity Assay of Purified Antimicrobial Agents Against Foodborne Pathogens

To determine the antimicrobial activity of the purified antimicrobial agents, growth inhibition tests were performed against Gram-negative and Gram-positive foodborne pathogens according to the previously described method with some modifications (Medeot et al., 2017). Antibacterial activity assay plates were prepared as described in "Screening of Strains with Antimicrobial Activity" above. The bacteria used were: MRSA, *S. choleraesuis*, *L. monocytogenes*, *P. aeruginosa* PAO1, *Pseudomonas oryzihabitans*, *Vibrio vulnificus*, *Bacillus cereus* and *Escherichia coli*. Purified fengycin and surfactin were prepared in methanol at final concentration of 1 mg/ml, and crude methanol extract (1 mg/ml) and nisin (1 mg/ml) were prepared simultaneously. In addition, the supernatant of *Bacillus* sp. YJ17 was filtered through a 0.22 μm microporous membrane and the inhibition assay was performed. The same amount of sterile water, LB medium and methanol was used as a negative control.

Ultrastructural and Morphological Observation of Indicator Strain After Treated With Purified Antimicrobial Agents

The effects of antimicrobial agents on foodborne pathogens *P. aeruginosa* PAO1 and MRSA were investigated by scanning electron microscopy (SEM) and transmission electron microscopy (TEM). This experiment was conducted in 24-well plates, which was added 50 μl of antimicrobial agent at a final concentration of 200 μg/ml and 1 ml LB broth inoculated with 1% overnight culture of indicator strain, then incubated in shaker at 28°C 150 rpm for 18 h. The suspension was centrifuged at 3,000 rpm for 15 min and the supernatant was aspirated off, and the precipitate was fixed by slowly adding pre-cooled 2.5% glutaraldehyde along the wall of the tube. Fixed cells were washed three times with 0.1 M phosphate buffer solution (PBS), eluted with ethanol gradient and other steps, and then observed by SEM (S-3400N; Hitachi, Tokyo, Japan) and TEM (HT7700; Hitachi, Tokyo, Japan), respectively. The same treatment was performed on the control group, with methanol instead of the antimicrobial agent. Three replicates were conducted in this assay.

Detection of Reactive Oxygen Species Levels and Cell Integrity of Indicator Strain After Treated With Purified Antimicrobial Agents

In order to detect reactive oxygen species (ROS) levels and cell integrity of the indicator bacteria after treated with purified antimicrobial agents, when *P. aeruginosa* PAO1 and MRSA grow to the OD_{600} of 0.3, fengycin and surfactin were added to *P. aeruginosa* PAO1 and MRSA at the final concentration of 200 μg/ml, respectively, and incubated at 28°C for 4 h. After incubation, 2′,7′-dichlorofluorescein diacetate ($DCFH_2$-DA; Sigma-Aldrich) dye was added and incubated for 30 min under dark conditions, then the cells were observed under a fluorescent microscope with a filter (488 nm/525 nm). Similarly, to detect the cell integrity, *P. aeruginosa* PAO1 and MRSA were treated with the same concentration of fengycin or surfactin, then stained with propidium iodide (PI) dye for 30 min under dark conditions and observed under fluorescent microscope with a

535 nm/615 nm filter. The same treatment was performed on the control group, with methanol instead of the fengycin or surfactin.

Studies on the Intracellular Catalase and Superoxide Dismutase Activities of Indicator Strain

The effects of purified fengycin and surfactin on the activity catalase (CAT) and superoxide dismutase (SOD) in *P. aeruginosa* PAO1 and MRSA cells were assayed with corresponding assay kits (Solarbo, Beijing, China). *P. aeruginosa* PAO1 and MRSA were treated with purified fengycin or surfactin at the concentration of 0 and 200 μg/ml respectively, then incubated overnight at 28°C at a speed of 150 rpm. To obtain the total protein, the bacterial cells were collected and ultrasonicated in corresponding extraction solution, then centrifuged at 8,000 *g* for 10 min under 4°C, and the supernatant was placed on ice for testing. For CAT enzyme activity determination, 1 ml of CAT assay solution and 35 μl of supernatant were added to a 1 ml quartz cuvette and mixed for 5 s, then the absorbance was measured at 240 nm immediately, after reacted for 1 min, the absorbance was measured again, then the activity of CAT was calculated according to the absorbance at 240 nm. One CAT unit was defined as the relative degradation amount of 1 μmol of H_2O_2 by 1 mg of protein in one minute. For SOD activity determination, 90 μl of supernatant was added to corresponding SOD assay solution, while 90 μl distilled water was added in the control group, then incubated at 37°C for 30 min, and the absorbance was measured at 560 nm. The SOD activity was calculated according to the absorbance at 560 nm. One SOD unit was defined as enzyme activity which inhibit formation rate of blue formazan at 50% by 1 mg of protein. The absorbance was detected with a microplate reader (Infinite M200 Pro; Tecan, Switzerland).

RESULTS

Screening and Identification of Antimicrobial Strains

In order to obtain strains that might produce antimicrobial agents, about 300 strains of deep-sea marine bacteria were isolated and purified from cold spring sediments in the South China Sea, and their inhibitory activities against common foodborne pathogens were detected on screening plates. For the strains with antimicrobial activities, their fermentation broth was further measured to quantify their antibacterial activity. Among them, strain YJ17 showed significant inhibitory activity against detected foodborne pathogens. As shown in **Table 1**, the supernatant of strain YJ17 showed inhibition circle diameters of 6.5, 13.53, 3.22, and 24.17 mm against *P. aeruginosa* PAO1, MRSA, *S. choleraesuis* and *L. monocytogenes*, respectively. The 16S rDNA sequence of strain YJ17 was sequenced and deposited into NCBI database under accession number OK067785, which exhibited high homology with *B. velezensis* strain CBMB205 (99.93%) and *B. velezensis* strain FZB42 (99.45%) in NCBI database. The phylogenetic tree was constructed by the neighbor-joining algorithm, which showed that *B. velezensis* and *B. siamensis* are the most closely related neighbors to strain YJ17 (**Figure 1**). Therefore, strain YJ17 was designated as *Bacillus* sp. strain YJ17.

Isolation and Purification of Antimicrobial Agents Produced by *Bacillus* sp. YJ17

To obtain agents with antibacterial activity from *Bacillus* sp. YJ17, the fermentation broth was purified by acid precipitation, methanol extraction and RP-HPLC. In the final purification step, eight different fractions with antibacterial activity from the crude extract were purified by RP-HPLC with the elution time at 36.6, 37.6, 38.5, 39.4, 44.2, 46.1, 46.4, and 47.2 min, respectively (**Figure 2A**). Among them, the strongest inhibitory activity was observed in the fractions with elution time of 39.4 min (peak 4) and elution time of 46.4 min (peak 7), which were designed as eluent 39.4 and eluent 46.4, respectively. Therefore, these two antimicrobial active fractions were further purified and analyzed in the next steps (**Figures 2B,C**).

Mass Spectrometry Analysis of Purified Antimicrobial Agents

To determine the molecular mass of purified active agents, the purified fractions of eluent 39.4 and eluent 46.4 were analyzed by

TABLE 1 | Inhibition spectrum of purified fengycin and surfactin.

Indicator strains	Inhibition zone (mm)				
	Supernatant (100 μl)	Methanol extract (1 mg/ml)	Fengycin (1 mg/ml)	Surfactin (1 mg/ml)	Nisin (1 mg/ml)
MRSA	13.53 ± 0.66	16.53 ± 0.43	5.56 ± 1.48	9.48 ± 0.87	–
L. monocytogenes	24.17 ± 1.04	17.17 ± 0.29	16.83 ± 0.28	–	–
S. choleraesuis	3.22 ± 0.25	2.27 ± 0.75	2.16 ± 0.25	–	–
P. aeruginosa	6.5 ± 0.5	5.77 ± 0.25	6.96 ± 0.50	–	–
P. oryzihabitans	21.33 ± 1.04	15.44 ± 1.01	16.17 ± 0.76	3.83 ± 0.76	–
V. vulnificus	4.66 ± 0.57	4.15 ± 0.21	2.11 ± 0.11	1.28 ± 0.26	–
B. cereus	12.07 ± 0.90	13.2 ± 1.04	7.06 ± 0.40	2.97 ± 0.50	–
E. coli	12.5 ± 1.32	5.83 ± 0.28	6.83 ± 1.04	–	–

–, no inhibition zone.

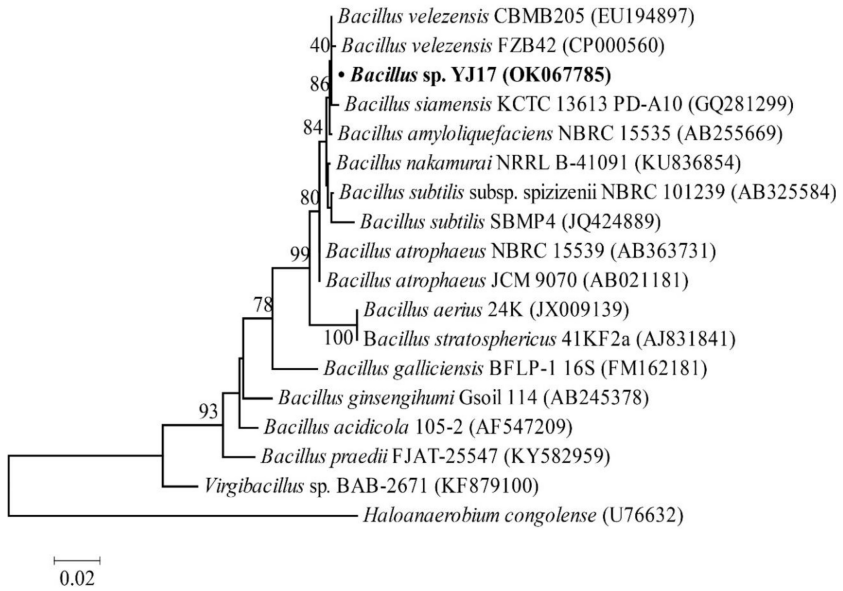

FIGURE 1 | Neighbor-joining phylogenetic tree based on 16S rDNA gene sequences (1,000 bootstrap replicates).

HCD-MS (**Figure 3**). For the active fraction of eluent 39.4, two peaks at m/z values of 753.43 and 1505.86 were detected, which correspond to the doubly protonated molecular ion $[M + 2H]^{2+}$ and the singly protonated molecular ion $[M + H]^{+}$, respectively. Combined with our purification procedure and previous reports on fengycin, most of them were detected at m/z values of 1463.80, 1477.81, 1491.83, 1505.84, and 1519.86 (Monaci et al., 2016), eluent 39.4 was presumed to belong to the category of fengycin. For the active fraction of eluent 46.4, a singly protonated ion $[M + H]^{+}$ at m/z 1022.68 and a sodium cationized ion $[M + Na]^{+}$ at m/z 1044.66 were detected, respectively. Based on previously reported for the surfactin, which showed typical m/z values at 999.64, 1008.65, 1022.67, 1036.68, and 1050.70 (Yang et al., 2015; Monaci et al., 2016), eluent 46.4 was presumed to belong to the category of surfactin. Therefore, the two antimicrobial agents produced by *Bacillus* sp. YJ17 belonged to lipopeptide type of fengycin and surfactin.

HCD-MS-MS Analysis of Purified Antimicrobial Agents

In order to figure out the primary peptide sequences of eluent 39.4 and eluent 46.4, the purified fractions were further analyzed by HCD-MS-MS. For the active fraction of eluent 39.4 (**Figure 4A**), typical y ion fragments m/z 1108.57 and m/z 994.49 were detected, which were due to the breakage at Glu-Orn and Orn-Tyr bonds, resulting in the loss of ion fragments in the N terminal fatty acid-Glu and fatty acid-Glu-Orn. And this loss of ionic fragments usually results in the formation of specific nine peptide (Orn-Tyr-Thr-Glu-Val-Pro-Gln-Tyr-Ile) and octapeptide (Tyr-Thr-Glu-Val-Pro-Gln-Tyr-Ile). Ion fragments 226.12, 389.18, and 502.26 were also detected, which indicates the peptide sequence might be Pro-Gln-Tyr-Ile starting from the N terminus in order, which are formed by the breakage of the Val-Pro bond of a specific octapeptide ring ion. So, the amino acid sequence of fengycin might be Glu-Orn-Tyr-Thr-Glu-Val-Pro-Gln-Tyr-Ile (**Figure 4B**). It is noteworthy that the analytical results are consistent with previously report about C_{17}-fengycin B (Liu and Sun, 2021). Therefore, it can be inferred that the eluent 39.4 is C_{17}-fengycin B.

For the active fraction of eluent 46.4, the b and y ion fragments were shown in **Figure 4C**. The detectable b ion fragments in order from the N terminus are 909.59(b_7), 794.56(b_6), 695.49(b_5), 582.41 (b_4), 469.33 (b_3), 356.24 (b_2), and 227.18 (b_1), while the given value of $[M + H]^{+}$ is 1022.68, and the differences between these two values in order is consistent with Leu/Ile, Asp, Val, Leu/Ile, Leu/Ile, Leu/Ile and Glu fragment ions. Starting from the C terminus, the detectable y ion fragments are in the order of 667.50 (y_6), 554.42 (y_5), 441.27 (y_4), 328.19 (y_3) and 229.12 (y_2), and the difference between them exactly coincide with Leu/Ile, Leu/Ile, Leu/Ile, Val ion fragments. The results were identical to the analysis of b ion fragments above. Therefore, it was tentatively concluded that the primary amino acid sequence of eluent 46.4 was β-OH fatty acid-Glu-Leu/Ile-Leu/Ile-Leu/Ile-Val-Asp-Leu/Ile as shown in **Figure 4D**, which was different from that of previously reported surfactins (Zhao et al., 2017, 2018).

In vitro Antimicrobial Activity of Purified Fengycin and Surfactin

In order to further clarify the activities of antimicrobial agents produced by *Bacillus* sp. YJ17, the supernatant, crude methanol extract and purified fengycin and surfactin were measured against common foodborne pathogens. As showed in **Table 1**, fengycin exhibited inhibition activity against all detected foodborne pathogens, and the most sensitive pathogen to fengycin was *L. monocytogenes*, while surfactin only showed strong antibacterial activity against MRSA. Furthermore, the

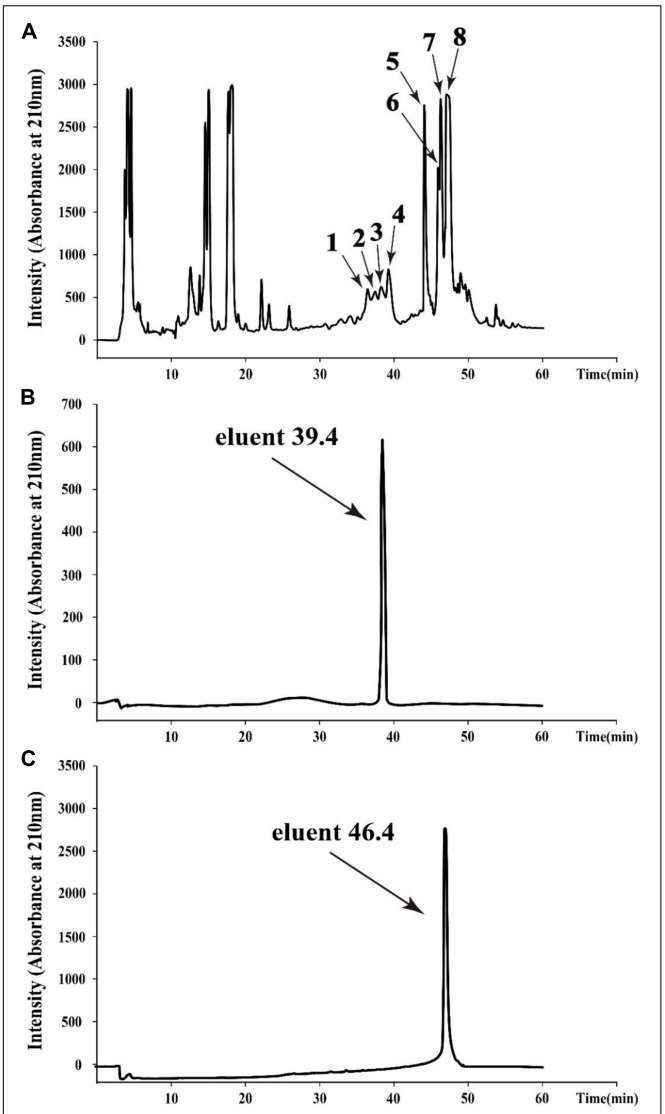

FIGURE 2 | HPLC chromatogram of the antimicrobial agents produced by *Bacillus* sp. YJ17 **(A)** and further purified antimicrobial fractions of eluent 39.4 **(B)** and eluent 46.4 **(C)**.

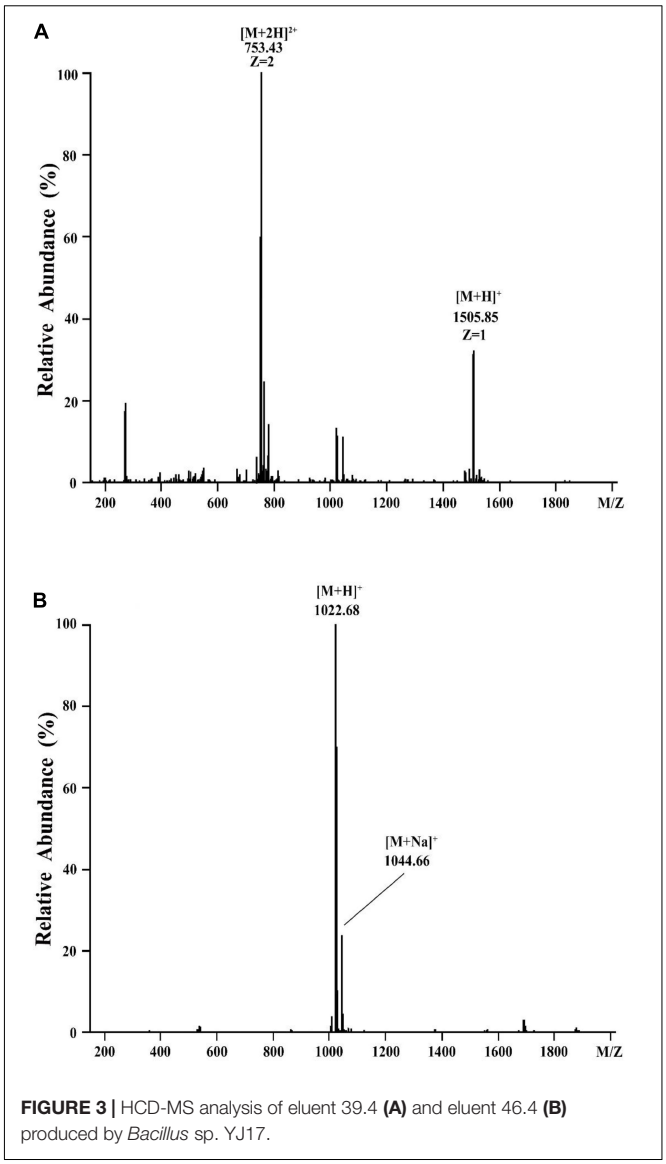

FIGURE 3 | HCD-MS analysis of eluent 39.4 **(A)** and eluent 46.4 **(B)** produced by *Bacillus* sp. YJ17.

purified surfactin exhibited stronger antimicrobial activity against MRSA than purified fengycin did. Combining the results of the supernatant and crude methanol extracts, fengycin and surfactin maintained the main antibacterial activity of *Bacillus* sp. YJ17. Furthermore, compared with commercial food preservative nisin, fengycin and surfactin showed unique advantages in inhibiting the growth of pathogenic bacteria with broader inhibitory spectrum.

Ultrastructural and Morphological Changes Caused by Purified Fengycin and Surfactin

Considering that the control of infections caused by *P. aeruginosa* and MRSA is increasingly difficult due to their inherent or acquired resistance mechanisms (Kaur and Chate, 2015; Pang et al., 2019), the antimicrobial mechanisms of purified fengycin against *P. aeruginosa* PAO1 and purified surfactin against MRSA were investigated by SEM and TEM. As shown in **Figure 5A**, the images of *P. aeruginosa* cells without fengycin treatment showed a smooth and intact cell surface with neat edges and clear contours, and it was in uniform short rod shape without abnormal morphology under SEM (**Figure 5Aa**). The morphology of *P. aeruginosa* cells showed abnormal and aggregated together after being treated by fengycin (**Figure 5Ab**). The results from TEM showed that the *P. aeruginosa* cells in the control group had tightly bound cell walls and intact cytoplasm (**Figure 5Ac**). On the contrary, after being treated with fengycin, the surface of the cell wall was uneven with ruptures, and the material inside the cell was sparse, indicating that the cytoplasm was severely leaked or even all outflowed (**Figure 5Ad**). These results indicated that fengycin exerted its

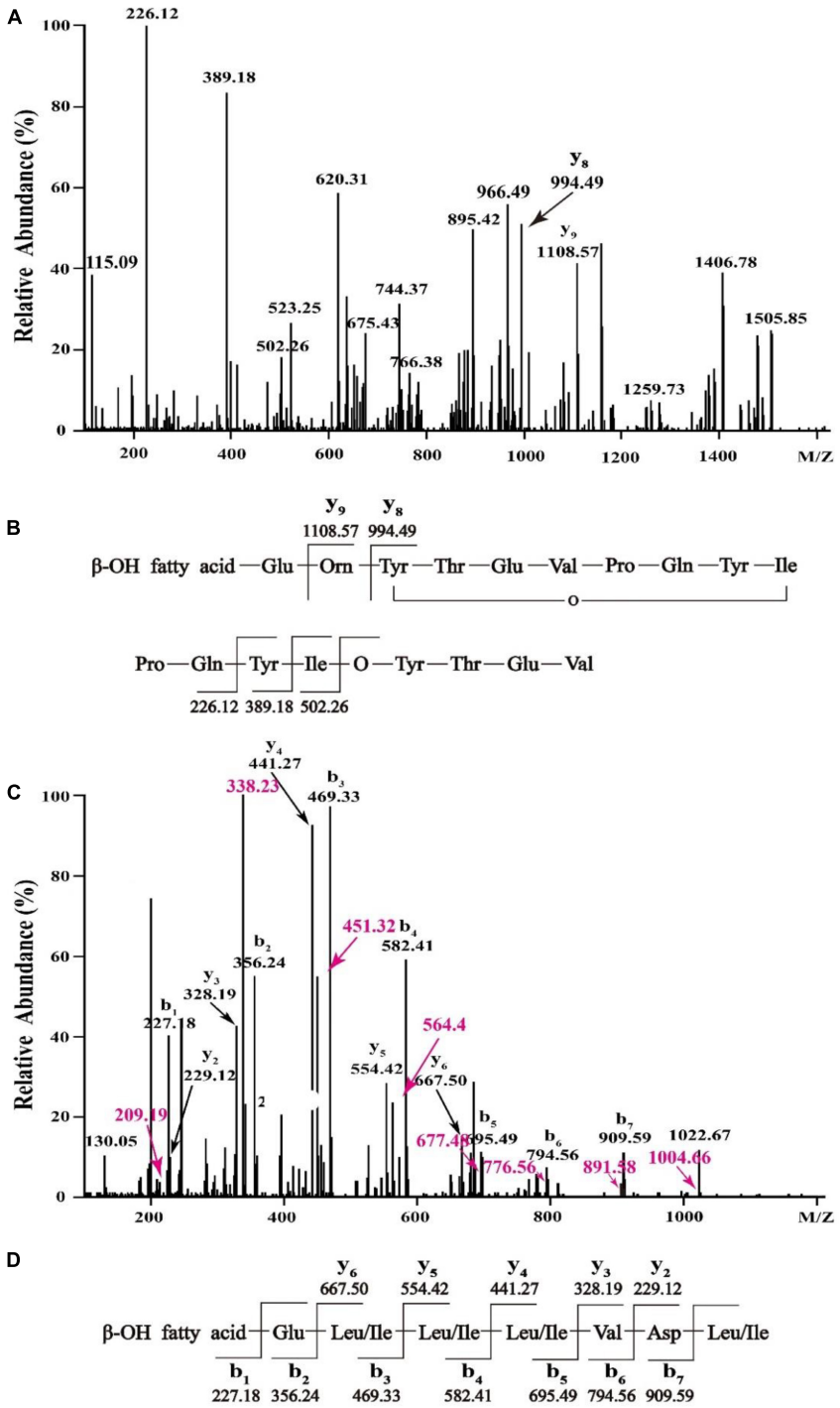

FIGURE 4 | HCD-MS-MS analysis of eluent 39.4 **(A,B)** and eluent 46.4 **(C,D)** produced by *Bacillus* sp. YJ17.

antibacterial activity against *P. aeruginosa* by causing severe damage to the cell membrane and cell wall, thus leading to cytoplasmic leakage and cell death.

Similarly, under SEM, the morphology of MRSA cells without surfactin treatment looked healthy and intact, and there was no phenomenon of multiple bacteria contracted together, while the cells clustered together after being treated with surfactin (**Figures 5Ba,b**). Under TEM, the MRSA cells in the control group had clear edges and uniform cytoplasm (**Figure 5Bc**), while the cells became rough and jagged surfaces, and increased abnormal cells clustered together after treated with surfactin (**Figure 5Bd**).

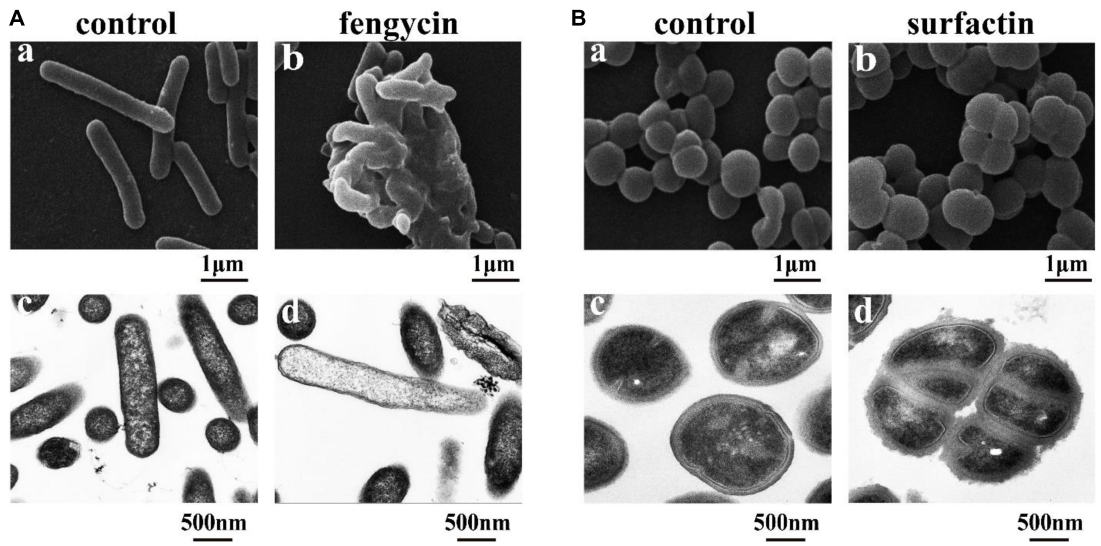

FIGURE 5 | Effects of the purified fengycin and surfactin on morphology and ultrastructure of bacteria. **(A)** Effects of fengycin on the morphology and ultrastructure of *P. aeruginosa* PAO1 cells observed by SEM (a,b) and TEM (c,d). **(B)** Effects of surfactin on the morphology and ultrastructure of MRSA cells observed by SEM (a,b) and TEM (c,d). The bacterial cells in the control group were treated with the same amount of methanol, and the bacterial cells in the test group were treated with 200 μg/ml of the antimicrobial agents.

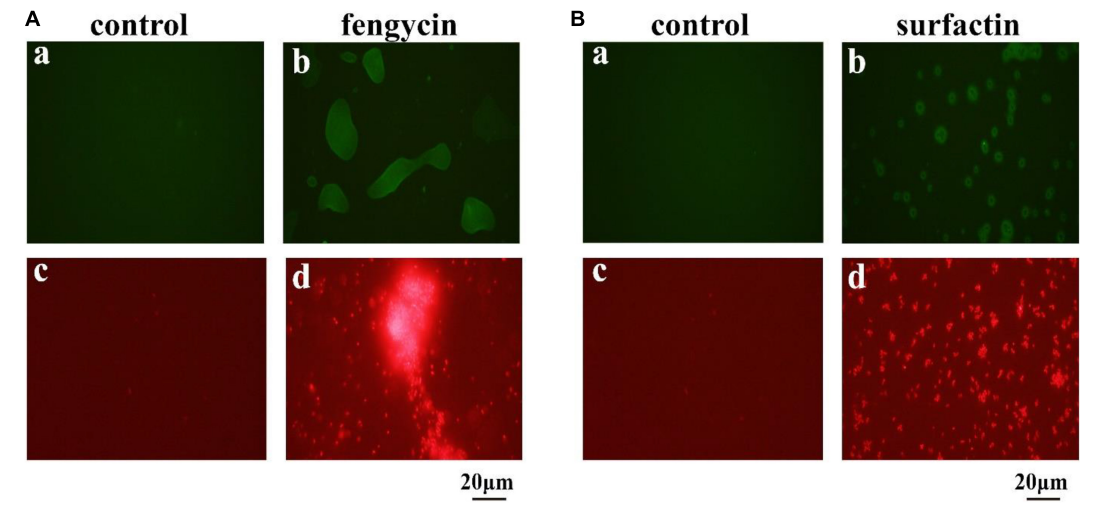

FIGURE 6 | Effect of purified antimicrobial agents on ROS levels and cell integrity of *P. aeruginosa* PAO1 and MRSA under fluorescence microscopy. **(A)** Effects of fengycin on ROS accumulation (a,b) and cell membrane damage (c,d) of *P. aeruginosa* PAO1. **(B)** Effects of surfactin on ROS accumulation (a,b) and cell membrane damage (c,d) of MRSA cells. The bacterial cells in the test group were treated with the antimicrobial agents at the final concentration of 200 μg/ml, that were dissolved in methanol, and the bacterial cells in the control group were treated with the same amount of methanol.

Accumulation of Reactive Oxygen Species and Cell Membrane Damage of the Indicator Bacteria Caused by Fengycin and Surfactin

The killing effect of several antimicrobial agents has been reported to be associated with a surge of intracellular ROS (Zhao and Drlica, 2014). Since fengycin and surfactin can cause severe inhibition to bacteria, in order to investigate whether ROS is involved in this process, ROS level was detected using the fluorescent probe $DCFH_2$-DA. As shown in **Figure 6**, *P. aeruginosa* PAO1 and MRSA cells exhibited obvious green fluorescence after treatment with fengycin and surfactin, respectively (**Figures 6Ab,Bb**), while untreated control cells showed almost no green fluorescence (**Figures 6Aa,Ba**). The result suggests that ROS accumulation was induced in *P. aeruginosa* PAO1 and MRSA after treatment with fengycin and surfactin, respectively.

Propidium iodide can enter cells to emit red fluorescence if cell membrane is damaged and can be used as an indicator

of the presence of dead cells. To further clarify whether the cell membrane of *P. aeruginosa* PAO1 and MRSA was damaged by fengycin and surfactin respectively, corresponding cells were stained by propidium iodide dye after treatment with fengycin or surfactin. As shown in **Figure 6**, *P. aeruginosa* PAO1 exhibited strong red fluorescence after treatment with fengycin (**Figure 6Ad**), and MRSA cells also showed strong red fluorescence after treatment with surfactin (**Figure 6Bd**), while the control group had almost no red fluorescence (**Figures 6Ac,Bc**). Therefore, the purified fengycin and surfactin caused the cell membrane damage of *P. aeruginosa* PAO1 and MRSA respectively, thus leading to cell death.

Catalase and Superoxide Dismutase Activities in Indicator Bacteria

To further verify whether the ROS accumulation caused by fengycin and surfactin was related to the expression level of ROS scavenging enzymes, enzyme activities of CAT and SOD in *P. aeruginosa* PAO1 and MRSA were detected after treatment with fengycin and surfactin, respctively. The CAT activity in *P. aeruginosa* PAO1 cells was 164.80 U/mg prot after treated with 200 μg/ml of fengycin, which was far lower than that of cells treated with 0 μg/ml of fengycin (787.81 U/mg prot) (**Figure 7Aa**). Similarly, the CAT enzyme activity of MRSA cells was 231.09 U/mg prot after treated with 200 μg/ml of surfactin, which was also significantly reduced compared with the cells treated with 0 μg/ml of surfactin (777.93 U/mg prot) (**Figure 7Ba**). In addition, the SOD activities in *P. aeruginosa* PAO1 and MRSA were also strongly affected by purified fengyicn and surfactin. The SOD activity was 23.50 U/mg prot in *P. aeruginosa* PAO1 and 22.83 U/mg prot in MRSA after treatment with 200 μg/ml of fengycin and surfactin, respectively, while the SOD activities were as high as 61.44 U/mg prot and 56.02 U/mg prot when cells treated with 0 μg/ml of fengycin and surfactin (**Figures 7Ab,Bb**). Therefore, the activities of CAT and SOD in *P. aeruginosa* PAO1 and MRSA were dramatically reduced by fengycin and surfactin, respectively.

DISCUSSION

Foodborne pathogens, especially the multi-drug resistant pathogens, often cause human diseases and even lead to death (Tack et al., 2020). *Bacillus* has been generally recognized as a bio-control agent that can be safely applied in the food industry

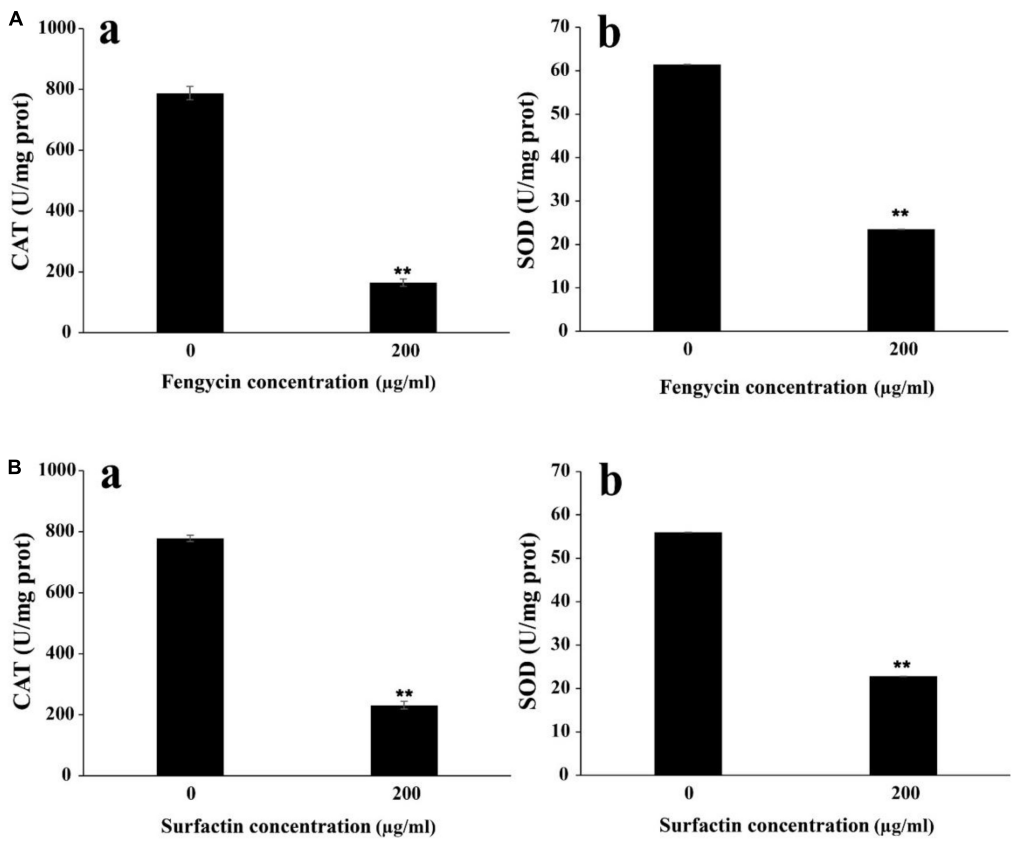

FIGURE 7 | Effect of purified fengycin and surfactin on the activities of ROS scavenging enzymes CAT and SOD in *P. aeruginosa* PAO1 and MRSA. **(A)** Effect of fengycin on the activity of ROS scavenging enzymes CAT (a) and SOD (b) in *P. aeruginosa* PAO1. **(B)** Effect of surfactin on the activity of ROS scavenging enzymes CAT (a) and SOD (b) in MRSA. The error bars indicated the standard error of the mean. To denote the statistical difference between the control and treated sets, *P* values were calculated using ANOVA. $^{**}P < 0.01$.

(Torres et al., 2015; Lastochkina et al., 2019), and lipopeptides produced by *Bacillus* have a well-recognized potential in controlling pathogens (Gudina et al., 2016). Normally, surfactins have been widely studied for antibacterial and their antitumor activity (Zhao et al., 2018), and the reports about fengycins have been mainly restricted to their antifungal effects (Kulimushi et al., 2017; Zhang and Sun, 2018; Jiao et al., 2021), while the effects of fengycins on bacterial cells have rarely been reported in the literature (Medeot et al., 2020).

In our study, a marine strain *Bacillus* sp. YJ17 showed antimicrobial activities against common foodborne pathogens, and three different types of lipopeptides were isolated and purified: iturin, fengycin and surfactin. Of these, iturin did not exhibit inhibitory activity against the indicator bacteria and therefore was not investigated further. Fengycin produced by this strain exhibited strong antimicrobial activity against *P. aeruginosa* PAO1, MRSA, *S. choleraesuis*, and *L. monocytogenes*, while surfactin produced by this strain showed obvious inhibition effect against MRSA. Furthermore, compared with commercial food preservative nisin, fengycin and surfactin produced by *Bacillus* sp. YJ17 showed broad and strong antibacterial activities against foodborne pathogens. Therefore, lipopeptides produced by *Bacillus* sp. YJ17 have the potential to be used as biological preservatives in the food industry and can be used as a substitute for chemical synthetic preservatives.

High concentrations of ROS have been reported to oxidize DNA, proteins and carbohydrates in organisms, leading to cell membrane damage or cell death (Rodriguez and Redman, 2005; Trachootham et al., 2009). In our study, a process accompanied by ROS accumulation and cell membrane damage was observed after the indicator bacteria were treated with fengycin or surfactin, which indicated that the ROS accumulation induced by fengycin or surfactin is an important factor leading to cell death. In addition, the activities of two typical ROS scavenging enzymes, CAT and SOD, were significantly reduced after the indicator bacteria were treated with fengycin or surfactin. Therefore, the ROS accumulation in the indicator bacteria after treated with fengycin or surfactin may due to the decreased expression of ROS scavenging enzymes, which weakens the ability to neutralize ROS and leads to the accumulation of ROS. Collectively, the cell death of indicator bacteria is closely related with the activity decrease of ROS scavenging enzymes and increase of ROS accumulation.

Altogether, both the crude extract and purified fengycin and surfactin from *Bacillus* sp. YJ17 showed strong antibacterial activity against a variety of food-borne pathogenic and spoilage bacteria, heralding their future potential in food preservative industry.

DATA AVAILABILITY STATEMENT

The original contributions presented in the study are publicly available. This data can be found here: National Center for Biotechnology Information (NCBI) database under accession number OK067785.

AUTHOR CONTRIBUTIONS

YG and SW conceived the study and designed the experiments. YG conducted the experiments and wrote the manuscript draft. RZ helped to conduct the experiment. CS and SW corrected the manuscript. All authors have read and approved the manuscript.

FUNDING

This work was financially supported by the Shandong Provincial Natural Science Foundation (ZR2021ZD28), National Key R&D Program of China (Grant No. 2018YFC0310800), and the Taishan Young Scholar Program of Shandong Province (tsqn20161051) for CS, was also funded by National Natural Science Foundation of China (No. 31600035) for SW.

REFERENCES

Banat, I. M., Franzetti, A., Gandolfi, I., Bestetti, G., Martinotti, M. G., Fracchia, L., et al. (2010). Microbial biosurfactants production, applications and future potential. *Appl. Microbiol. Biotechnol.* 87, 427–444. doi: 10.1007/s00253-010-2589-0

Ben Ayed, H., Hmidet, N., Bechet, M., Jacques, P., and Nasri, M. (2017). Identification and natural functions of cyclic lipopeptides from *Bacillus amyloliquefaciens* An6. *Eng. Life Sci.* 17, 536–544. doi: 10.1002/elsc.201600050

Bjerketorp, J., Levenfors, J. J., Nord, C., Guss, B., Oberg, B., and Broberg, A. (2021). Selective isolation of multidrug-resistant pedobacter spp., producers of novel antibacterial peptides. *Front. Microbiol.* 12:642829. doi: 10.3389/fmicb.2021.642829

Bonmatin, J. M., Labbe, H., Grangemard, I., Peypoux, F., Mageтdana, R., Ptak, M., et al. (1995). Production, isolation and characterization of [Leu^4]- and [Ile^4] surfactins from *Bacillus subtilis*. *Lett. Pept. Sci.* 2, 41–47. doi: 10.1007/Bf00122922

Cameotra, S. S., and Makkar, R. S. (2004). Recent applications of biosurfactants as biological and immunological molecules. *Curr. Opin. Microbiol.* 7, 262–266. doi: 10.1016/j.mib.2004.04.006

Caulier, S., Nannan, C., Gillis, A., Licciardi, F., Bragard, C., and Mahillon, J. (2019). Overview of the antimicrobial compounds produced by members of the *Bacillus subtilis* group. *Front. Microbiol.* 10:302. doi: 10.3389/fmicb.2019.00302

Fan, H. Y., Zhang, Z. W., Li, Y., Zhang, X., Duan, Y. M., and Wang, Q. (2017). Biocontrol of bacterial fruit blotch by *Bacillus subtilis* 9407 *via* surfactin-mediated antibacterial activity and colonization. *Front. Microbiol.* 8:1973. doi: 10.3389/fmicb.2017.01973

Gudina, E. J., Teixeira, J. A., and Rodrigues, L. R. (2016). Biosurfactants produced by marine microorganisms with therapeutic applications. *Mar. Drugs* 14:38. doi: 10.3390/md14020038

Jiao, R., Cai, Y. Z., He, P. F., Munir, S., Li, X. Y., Wu, Y. X., et al. (2021). *Bacillus amyloliquefaciens* YN201732 produces lipopeptides with promising biocontrol activity against fungal pathogen erysiphe cichoracearum. *Front. Cell. Infect. Microbiol.* 11:598999. doi: 10.3389/fcimb.2021.598999

Kaur, D. C., and Chate, S. S. (2015). Study of antibiotic resistance pattern in methicillin resistant *Staphylococcus aureus* with special reference to newer antibiotic. *J. Glob. Infect. Dis.* 7, 78–84. doi: 10.4103/0974-777X.157245

Kulimushi, P. Z., Arias, A. A., Franzil, L., Steels, S., and Ongena, M. (2017). Stimulation of fengycin-type antifungal lipopeptides in *Bacillus amyloliquefaciens* in the Presence of the maize fungal pathogen *Rhizomucor variabilis*. *Front. Microbiol.* 8:850. doi: 10.3389/fmicb.2017.00850

Lastochkina, O., Seifikalhor, M., Aliniaeifard, S., Baymiev, A., Pusenkova, L., Garipova, S., et al. (2019). *Bacillus* spp.: efficient biotic strategy to control postharvest diseases of fruits and vegetables. *Plants* 8:97. doi: 10.3390/plants8040097

Liu, W., and Sun, C. (2021). C_{17}-fengycin B, produced by deep-sea-derived *Bacillus subtilis*, possessing a strong antifungal activity against *Fusarium solani*. *J. Ocean. Limnol.* 39, 1938–1947. doi: 10.1007/s00343-020-0215-2

Medeot, D. B., Bertorello-Cuenca, M., Liaudat, J. P., Alvarez, F., Flores-Caceres, M. L., and Jofre, E. (2017). Improvement of biomass and cyclic lipopeptides production in *Bacillus amyloliquefaciens* MEP218 by modifying carbon and nitrogen sources and ratios of the culture media. *Biol. Control* 115, 119–128. doi: 10.1016/j.biocontrol.2017.10.002

Medeot, D. B., Fernandez, M., Morales, G. M., and Jofre, E. (2020). Fengycins from *Bacillus amyloliquefaciens* MEP_218 exhibit antibacterial activity by producing alterations on the cell surface of the pathogens *xanthomonas axonopodis* pv. *vesicatoria* and *Pseudomonas aeruginosa* PA01. *Front. Microbiol.* 10:3107. doi: 10.3389/fmicb.2019.03107

Meena, K. R., and Kanwar, S. S. (2015). Lipopeptides as the antifungal and antibacterial agents: applications in food safety and therapeutics. *Biomed Res. Int.* 2015:473050. doi: 10.1155/2015/473050

Meena, K. R., Sharma, A., and Kanwar, S. S. (2019). Antitumoral and antimicrobial activity of surfactin extracted from *Bacillus subtilis* KLP2015. *Int. J. Pept. Res. Ther.* 26, 423–433. doi: 10.1007/s10989-019-09848-w

Monaci, L., Quintieri, L., Caputo, L., Visconti, A., and Baruzzi, F. (2016). Rapid profiling of antimicrobial compounds characterising *B. subtilis* TR50 cell-free filtrate by high-performance liquid chromatography coupled to high-resolution Orbitrap^{TM} mass spectrometry. *Rapid Commun. Mass Spectrom.* 30, 45–53. doi: 10.1002/rcm.7408

Pang, Z., Raudonis, R., Glick, B. R., Lin, T. J., and Cheng, Z. Y. (2019). Antibiotic resistance in *Pseudomonas aeruginosa*: mechanisms and alternative therapeutic strategies. *Biotechnol. Adv.* 37, 177–192. doi: 10.1016/j.biotechadv.2018.11.013

Patel, S., Ahmed, S., and Eswari, J. S. (2015). Therapeutic cyclic lipopeptides mining from microbes: latest strides and hurdles. *World J. Microbiol. Biotechnol.* 31, 1177–1193. doi: 10.1007/s11274-015-1880-8

Patra, J. K., and Baek, K. H. (2017). Antibacterial activity and synergistic antibacterial potential of biosynthesized silver nanoparticles against foodborne pathogenic bacteria along with its anticandidal and antioxidant effects. *Front. Microbiol.* 8:167. doi: 10.3389/fmicb.2017.00167

Rodriguez, R., and Redman, R. (2005). Balancing the generation and elimination of reactive oxygen species. *Proc. Natl. Acad. Sci. U. S. A.* 102, 3175–3176. doi: 10.1073/pnas.0500367102

Romero, D., De Vicente, A., Rakotoaly, R. H., Dufour, S. E., Veening, J. W., Arrebola, E., et al. (2007). The iturin and fengycin families of lipopeptides are key factors in antagonism of *Bacillus subtilis* toward *Podosphaera fusca*. *Mol. Plant Microbe Interact.* 20, 430–440. doi: 10.1094/Mpmi-20-4-0430

Tack, D. M., Ray, L., Griffin, P. M., Cieslak, P. R., Dunn, J., Rissman, T., et al. (2020). Preliminary incidence and trends of infections with pathogens transmitted commonly through food - foodborne diseases active surveillance network, 10 U.S. sites, 2016-2019. *MMWR Morb. Mortal. Wkly. Rep.* 69, 509–514. doi: 10.15585/mmwr.mm6917a1

Torres, M. J., Petroselli, G., Daz, M., Erra-Balsells, R., and Audisio, M. C. (2015). *Bacillus subtilis subsp subtilis* CBMDC3f with antimicrobial activity against Gram-positive foodborne pathogenic bacteria: UV-MALDI-TOF MS analysis of its bioactive compounds. *World J. Microbiol. Biotechnol.* 31, 929–940. doi: 10.1007/s11274-015-1847-9

Trachootham, D., Alexandre, J., and Huang, P. (2009). Targeting cancer cells by ROS-mediated mechanisms: a radical therapeutic approach? *Nat. Rev. Drug Discov.* 8, 579–591. doi: 10.1038/nrd2803

Wang, L., Nwosu, C., Gao, Y. F., and Zhu, M. M. (2020). Signature ions triggered electron-transfer/higher-energy collisional dissociation (EThcD) for specific and confident glycation site mapping in therapeutic proteins. *J. Am. Soc. Mass Spectr.* 31, 473–478. doi: 10.1021/jasms.9b00101

Williams, D. H., Stone, M. J., Hauck, P. R., and Rahman, S. K. (1989). Why are secondary metabolites (Natural-Products) biosynthesized. *J. Nat. Prod.* 52, 1189–1208. doi: 10.1021/np50066a001

Yang, H., Li, X., Li, X., Yu, H. M., and Shen, Z. Y. (2015). Identification of lipopeptide isoforms by MALDI-TOF-MS/MS based on the simultaneous purification of iturin, fengycin, and surfactin by RP-HPLC. *Anal. Bioanal. Chem.* 407, 2529–2542. doi: 10.1007/s00216-015-8486-8

Yasmin, N., Hameed, S., Javed, R., Ahmed, S., and Imran, M. (2017). Inactivation of foodborne pathogens on food packaging and in cow milk by exposure to a Nd:YAG laser. *Can. J. Phys.* 95, 662–669. doi: 10.1139/cjp-2016-0676

Yount, N. Y., and Yeaman, M. R. (2013). Peptide antimicrobials: cell wall as a bacterial target. *Ann. N. Y. Acad. Sci.* 1277, 127–138. doi: 10.1111/nyas.12005

Zarei, M., Jamnejad, A., and Khajehali, E. (2014). Antibacterial effect of silver nanoparticles against four foodborne pathogens. *Jundishapur J. Microbiol.* 7:e8720. doi: 10.5812/jjm.8720

Zhang, L. L., and Sun, C. M. (2018). Fengycins, cyclic lipopeptides from marine *Bacillus subtilis* strains, kill the plant-pathogenic fungus magnaporthe grisea by inducing reactive oxygen species production and chromatin condensation. *Appl. Environ. Microbiol.* 84, e00445–18. doi: 10.1128/AEM.00445-18

Zhao, H. B., Shao, D. Y., Jiang, C. M., Shi, J. L., Li, Q., Huang, Q. S., et al. (2017). Biological activity of lipopeptides from *Bacillus*. *Appl. Microbiol. Biotechnol.* 101, 5951–5960. doi: 10.1007/s00253-017-8396-0

Zhao, P. C., Xue, Y., Gao, W. N., Li, J. H., Zu, X. Y., Fu, D. L., et al. (2018). *Bacillaceae*-derived peptide antibiotics since 2000. *Peptides* 101, 10–16. doi: 10.1016/j.peptides.2017.12.018

Zhao, X. L., and Drlica, K. (2014). Reactive oxygen species and the bacterial response to lethal stress. *Curr. Opin. Microbiol.* 21, 1–6. doi: 10.1016/j.mib.2014.06.008

Zhou, S. N., Liu, G., Zheng, R. K., Sun, C. M., and Wu, S. M. (2020). Structural and functional Insights into Iturin W, a novel lipopeptide produced by the deep-sea Bacterium *Bacillus* sp. strain wsm-1. *Appl. Environ. Microbiol.* 86, e01597–20. doi: 10.1128/AEM.01597-20

Conflict of Interest: The authors declare that the research was conducted in the absence of any commercial or financial relationships that could be construed as a potential conflict of interest.

Publisher's Note: All claims expressed in this article are solely those of the authors and do not necessarily represent those of their affiliated organizations, or those of the publisher, the editors and the reviewers. Any product that may be evaluated in this article, or claim that may be made by its manufacturer, is not guaranteed or endorsed by the publisher.

frontiers in Microbiology

ORIGINAL RESEARCH
published: 24 February 2022
doi: 10.3389/fmicb.2022.822864

Physiological and Molecular Characterization of an Oxidative Stress-Resistant *Saccharomyces cerevisiae* Strain Obtained by Evolutionary Engineering

*Nazlı Kocaefe-Özşen[1,2‡], Bahtiyar Yilmaz[1,2†‡], Ceren Alkım[1,2†], Mevlüt Arslan[1,2†], Alican Topaloğlu[1,2], Halil İbrahim Kısakesen[1,2], Erdinç Gülsev[1,2] and Z. Petek Çakar[1,2]**

[1] Department of Molecular Biology and Genetics, Istanbul Technical University, Istanbul, Turkey, [2] Dr. Orhan Öcalgiray Molecular Biology, Biotechnology and Genetics Research Center (ITU-MOBGAM), Istanbul Technical University, Istanbul, Turkey

Oxidative stress is a major stress type observed in yeast bioprocesses, resulting in a decrease in yeast growth, viability, and productivity. Thus, robust yeast strains with increased resistance to oxidative stress are in highly demand by the industry. In addition, oxidative stress is also associated with aging and age-related complex conditions such as cancer and neurodegenerative diseases. *Saccharomyces cerevisiae*, as a model eukaryote, has been used to study these complex eukaryotic processes. However, the molecular mechanisms underlying oxidative stress responses and resistance are unclear. In this study, we have employed evolutionary engineering (also known as adaptive laboratory evolution – ALE) strategies to obtain an oxidative stress-resistant and genetically stable *S. cerevisiae* strain. Comparative physiological, transcriptomic, and genomic analyses of the evolved strain were then performed with respect to the reference strain. The results show that the oxidative stress-resistant evolved strain was also cross-resistant against other types of stressors, including heat, freeze-thaw, ethanol, cobalt, iron, and salt. It was also found to have higher levels of trehalose and glycogen production. Further, comparative transcriptomic analysis showed an upregulation of many genes associated with the stress response, transport, carbohydrate, lipid and cofactor metabolic processes, protein phosphorylation, cell wall organization, and biogenesis. Genes that were downregulated included those related to ribosome and RNA processing, nuclear transport, tRNA, and cell cycle. Whole genome re-sequencing analysis of the evolved strain identified mutations in genes related to the stress response, cell wall organization, carbohydrate metabolism/transport, which are in line with the physiological and transcriptomic results, and may give insight toward the complex molecular mechanisms of oxidative stress resistance.

Keywords: oxidative stress, reactive oxygen species, evolutionary engineering, stress resistance, heat preconditioning, *Saccharomyces cerevisiae*, adaptive laboratory evolution, genomic variants

OPEN ACCESS

Edited by:
Peter Adrian Lund, University of Birmingham, United Kingdom

Reviewed by:
Agustin Aranda, University of Valencia, Spain
Akira Nishimura, Nara Institute of Science and Technology (NAIST), Japan

****Correspondence:***
Z. Petek Çakar
cakarp@itu.edu.tr

†Present address:
Bahtiyar Yilmaz, Maurice Müller Laboratories, Department for Biomedical Research, University of Bern, Bern, Switzerland; Department of Visceral Surgery and Medicine, Bern University Hospital, University of Bern, Bern, Switzerland
Ceren Alkım, Toulouse Biotechnology Institute, CNRS, INRA, INSA, Toulouse, France; Toulouse White Biotechnology (TWB, UMS INRA/INSA/CNRS), NAPA CENTER Bat B, Ramonville Saint-Agnes, France
Mevlüt Arslan, Department of Genetics, Faculty of Veterinary Medicine, Van Yüzüncü Yıl University, Van, Turkey

‡These authors have contributed equally to this work

Specialty section:
This article was submitted to Microbial Physiology and Metabolism, a section of the journal Frontiers in Microbiology

Received: *26 November 2021*
Accepted: *02 February 2022*
Published: *24 February 2022*

INTRODUCTION

In all aerobic organisms, the generation of reactive oxygen species (ROS), as side products of cellular metabolism, including hydrogen peroxide (H_2O_2), the hydroxyl radical (.OH), or superoxide anions (O_2^-) by reduction of molecular oxygen is an inevitable aspect of life (Jamieson, 1992; Izawa et al., 1995; Bayliak et al., 2017). All living organisms including microbes, plants and other multicellular organisms use signal transduction mechanisms to sense and respond to different forms of environmental stress (Hong et al., 2013). As plants are sedentary organisms and possess photosynthetic systems, they cannot move to find optimal conditions and consequently, they produce a lot of ROS. They balance the overoxidation and overreduction with short term and long-term mechanisms, including enzymatic systems (Lushchak, 2011). In mammalian systems, about 90% of the ATP is generated *via* oxidative phosphorylation and is the primary source of ROS in cells (Candas and Li, 2014). An increasing body of evidence indicates that oxidative stress participates in the pathogenesis of many diseases including cardiovascular disease (Förstermann, 2008), cancer (Reuter et al., 2010), neurodegenerative disorders (Li et al., 2013), and inflammatory bowel diseases (Lih-Brody et al., 1996; Sokol et al., 2017). When antioxidant defenses are overwhelmed and unable to counteract ROS, the resulting oxidative stress (Finkel and Holbrook, 2000; Finkel, 2005) can damage nucleic acids, oxidize amino acids, as well as co-factors of proteins, and disturb cellular homeostasis (Imlay, 2015).

Reactive oxygen species are also specifically generated in host phagocytes as microbicidal molecules and in non-phagocytic cells they have important roles in fertilization, thyroid hormone synthesis and cell signaling (Görlach et al., 2015). These products of oxygen metabolism may have damaging effects on an organism, in essence, due to oxidation of essential cellular components. Steady-state formation of pro-oxidant free radicals is normally balanced by a similar rate of breakdown by antioxidants (Finkel and Holbrook, 2000; Finkel, 2005). Although imperfectly coupled aerobic respiration is the main source of ROS, they can also be generated by peroxisomal β-oxidation of fatty acids, microsomal cytochrome P450 metabolism of xenobiotic compounds, stimulation of phagocytic NADP-oxidase by pathogens or lipopolysaccharides, and tissue specific enzymes. In an inflammatory condition, the host cannot maintain anaerobic conditions in the gut, consequently leading to reductions in microbiota-derived fermentation products such as short-chain fatty acids (SCFAs) produced by obligate anaerobic bacteria in the colon: these are important to promote the maturation and expansion of regulatory T (T_{reg}) cells (Espey, 2013; Faber and Bäumler, 2014; Byndloss et al., 2017). The amount of oxygen diffusion into the gut lumen is limited by epithelial metabolism and thus, obligate anaerobic bacteria are able to continue short chain fatty acid production in the intestinal lumen. In contrast, inflammation leads to the loss of butyrate, which disrupts metabolic signaling in intestinal epithelial cells and this promotes nitrate in the lumen *via* nitric oxidase induction and also disables β-oxidation in epithelial cells that would otherwise control the oxygen levels in the colon (Byndloss et al., 2017; Rivera-Chávez et al., 2017). ROS, that plays a critical role in host-microbe interactions, may lead to cellular oxidative damage that makes host tissues more susceptible to oxidant-induced damage.

Antioxidant mechanisms provide an evolutionary advantage to cells to control ROS production and its deleterious effects. There have been numerous studies characterizing the response mechanism of living organisms to oxidative stress, which has been mostly studied in the prokaryotes *Escherichia coli* and *Salmonella typhimurium*. Many proteins and their corresponding genes in bacterial defense systems against oxidative stress have been identified (Storz et al., 1990). As a eukaryotic model organism, *Saccharomyces cerevisiae* has been useful to study the response to endogenous and exogenous oxidative stress. It possesses several enzymatic and non-enzymatic ROS detoxifying enzymes, such as cytochrome *c* peroxidase, superoxide dismutase (SOD), glutathione (GSH) peroxidase, catalase (CAT), glutaredoxin and peroxiredoxin to protect cellular compartments and maintain a cellular redox state (Jamieson, 1998; Charizanis et al., 1999; Park et al., 2000; Grant, 2001).

The heat stress response, a protective transcriptional program activation against heat stress, includes the reprogramming of an important part of the transcriptome. Environmental Stress Response (ESR) genes, involved in metabolism, oxidant defense, and growth control, are induced by the heat shock (Davidson et al., 1996). There is an important overlap between the gene expression programs against different stress factors. This phenomenon is named "cross-protection." Treatment with one stress enhances tolerance to a subsequent stressor of a different nature; e.g., heat shock induces tolerance to oxidants or osmotic shock. Specifically, genes that are regulated by the transcription factors Msn2/4, most of which exhibit a common gene expression profile in response to various stressors, suggest a general, rather than a stress-specific response. Nowadays, heat stress and oxidative stress responses are better understood. The focus now is on the products generated by the stress response and their roles in stress tolerance and adaptation. Although the expression of the genes related to stress response have been studied, the precise signaling mechanism that triggers this reaction remains unclear (Morano et al., 2012).

The definition of heat stress is a rise in temperature beyond a threshold level for a period sufficient to cause irreversible damage within a few minutes to cellular compartments on the host as a consequence of extensive protein denaturation and aggregation, and loss of membrane integrity (Wahid, 2007; Allakhverdiev et al., 2008). Oxidative stress is directly linked to heat stress and when it occurs simultaneously with heat exposure, it can manifest in all parts of the body. Upon heat stress, ROS and NADPH oxidase levels in different cellular compartments such as chloroplasts, mitochondria and peroxisomes increase as a by-product in various aerobic metabolic pathways, and the antioxidant enzyme activities are down-regulated (Morimoto, 1998). In a chronic heat stress condition, downsizing of mitochondrial metabolic oxidative capacity, up-regulation of uncoupling proteins, a clear reduction in antioxidant enzyme activities, and depletion of antioxidant reserves occur, as the

main reasons for the reduced tolerance to oxidative stress and tissue damage.

The very first step of induction of heat stress appears to be an increase in cellular energy expenditure and later, enhanced mitochondrial transportation and β-oxidation of fatty acids. To cope with the enhanced energy expenditure within cells and mitochondrial biogenesis, the production of reducing equivalents and the enzymatic activity of subunits of respiratory chain complexes are increased. Increased mitochondrial energy generation is intrinsically associated with an increase in ROS (Mujahid et al., 2005; Yang et al., 2010). Defense mechanisms against oxidative and heat stress conditions share a common player. Induced protection for heat stress tolerance has been suggested to be correlated with the appearance of heat shock proteins which is also induced by H_2O_2, UV radiation, sodium arsenite and cadmium, all common oxidative stress inducers in mammalian systems. In mammals, HO-1 (heme oxygenase – 1) can also be induced, which are protective against these stress conditions (Steels et al., 1992). In contrast, the major players in yeast cells against heat and oxidative stress are the heat shock transcription factor 1 (HSF) protein family, the primary modulator of the heat shock response, and Msn2/4 – all stress-responsive transcriptional activators. Besides, mild heat shock can activate the cell wall integrity pathway which can give an advantage for further activation of Hsf1 or Msn2/4 (Levin, 2005; Morano et al., 2012).

Evolutionary engineering, also known as adaptive laboratory evolution (ALE), is an experimental strategy mimicking nature's own engineering principle *via* variation and selection. Evolutionary selection principles have been used for the improvement of biotechnologically important characteristics, including novel catabolic activities, improved enzyme properties, plasmid functions, and stress resistance (Sauer, 2001; Çakar et al., 2005, 2012). *S. cerevisiae* strains that are resistant against diverse stress types have been successfully obtained by evolutionary engineering, including nickel-resistant (Küçükgöze et al., 2013), cobalt-resistant (Çakar et al., 2009; Alkim et al., 2013), iron-resistant (Balaban et al., 2020), coniferyl aldehyde-resistant (Hacısalihoğlu et al., 2019), caffeine-resistant (Surmeli et al., 2019), ethanol-tolerant (Turanlı-Yıldız et al., 2017), chronologically long-lived (Arslan et al., 2018a,b), and silver-resistant (Terzioğlu et al., 2020) *S. cerevisiae*.

The major advantage of evolutionary engineering is that it does not require any detailed prior information about the desired phenotypes. The only requirement is a selection scheme that will favor the desired phenotype (Sauer, 2001). Thus, it is highly advantageous to obtain genetically complex phenotypes, such as oxidative stress-resistant yeasts. Any selective condition that may show an oxidative stress effect such as H_2O_2 can be used as the selective pressure. Another advantage of evolutionary engineering is the ability to analyze evolved strains at genomic and transcriptomic levels, owing to the rapid development in omics technologies. This allows identification of the key changes in the evolved strains that are associated with the desired phenotype (Çakar et al., 2012). Despite the various studies on oxidative stress responses and resistance, the complex molecular mechanisms are unclear. Further, to the best of our knowledge, there are no studies on oxidative stress-resistant *S. cerevisiae* strains obtained by evolutionary engineering and their characterization. Moreover, to our knowledge, there are also no reports comparing the efficiencies of different evolutionary selection strategies in obtaining oxidative stress-resistant *S. cerevisiae* strains, particularly to elucidate the role of heat and oxidative pretreatment.

In this study, we first generated a genetically stable, oxidative stress-resistant *S. cerevisiae* strain using evolutionary engineering strategies. These included gradually increased and continuously applied selective oxidative stress levels over populations of selection, with and without heat and oxidative stress pretreatment. Prior to the evolutionary engineering selection, yeast cells were treated with the chemical mutagen ethyl methane sulfonate (EMS), to increase the genetic diversity of the initial population of selection by random mutagenesis. The phenotypic and physiological characteristics and the transcriptomic profile of the evolved strain showed that the acetate consumption and maltose accumulation increased, with elevated gene expression levels related to stress response; carbohydrate, lipid, and protein metabolic processes including anabolic and catabolic reactions; generation of precursor metabolites and energy; transportation and autophagy. In addition, we found down-regulated genes that were associated with nuclear transport, organelle assembly, tRNA, cell cycle function and mitosis. The genomic profile of the evolved strain showed that mutations mainly accumulated in genes directly associated with the stress response, cell wall organization, and carbohydrate metabolism/transport, which are in accordance with the physiological and transcriptomic results. Overall, our study shows how yeast can evolve by altering its genomic profile to cope with an experimental oxidative stress condition and how these genetic alterations can be beneficial in different stress environments. It also indicates the key molecular factors that are associated with oxidative stress resistance in yeast.

MATERIALS AND METHODS

Strain, Media, and Growth Conditions

The *S. cerevisiae* CEN.PK 113-7D strain (MATa, MAL2-8c, SUC2), kindly provided by Prof. Dr. Jean Marie François and Dr. Laurent Benbadis (University of Toulouse, France), was used as the reference strain (*905*). Unless otherwise stated, yeast cultivations were performed in yeast minimal medium (YMM), containing 0.67% "w/v" yeast nitrogen base without amino acids (Difco, New Jersey, United States) and 2.0% (w/v) glucose (VWR BDH PROLABO, Leicestershire, United Kingdom) as the sole carbon source, under aerobic conditions at 30°C. Cell growth was monitored spectrophotometrically by optical density measurements at 600 nm (OD_{600}).

Ethyl methane sulfonate (Sigma, St. Louis, MO, United States) mutagenesis of the reference strain was carried out as described previously (Lawrence, 1991; Balaban et al., 2020), under conditions that resulted in a 10% survival rate after treatment to obtain a randomly mutated initial *S. cerevisiae* population

(*906*) with increased genetic diversity. That population was used directly as the starting population for all selection experiments.

Selection Strategy for Obtaining Evolutionary Engineered–Continuous Oxidative Stress Resistant Yeast Cells

Three different evolutionary engineering strategies were employed to select for oxidative stress-resistant evolved strains (**Figure 1**).

i Oxidative continuous (OC) stress selection: the EMS-mutagenized *S. cerevisiae* population called *906* was initially cultivated in YMM containing 0.5-mM H_2O_2 and the successive population surviving that oxidative stress was then exposed to increasing H_2O_2 levels, up to 10 mM H_2O_2. Each successive population was named as OC X^{th} Population (O and C stand for Oxidative and Continuous, respectively and X shows the population number).

ii Oxidative pulse (OP) stress pretreatment selection: the EMS-mutagenized *S. cerevisiae 906* population was initially cultivated in YMM containing 0.3-mM H_2O_2 and incubated for 1 h as a pulse oxidative stress. Our initial pulse oxidative stress tests with the *906* culture showed that there was about 30% decrease in survival upon 0.3-mM H_2O_2 stress. Thus, 0.3-mM H_2O_2 was used as a mild, but effective stress level for oxidative stress pre-conditioning. Following pre-conditioning, the culture was subjected to continuous oxidative stress as in (i). Each successive population was named as OP X^{th} Population (O and P stand for Oxidative and Pulse, respectively and X shows the population number). The pre-conditioning step was repeated at each successive population of selection.

iii Heat pulse (HP) stress pretreatment selection: the EMS-mutagenized *S. cerevisiae 906* population was initially incubated in YMM at 37°C for 1 h as a pulse heat stress. It was then subjected to continuous oxidative stress as in (i). Each successive population was named as HP X^{th} Population (H and P stand for Heat and Pulse, respectively and X shows the population number). The pre-conditioning step was repeated at each successive population of selection.

During these selection experiments, for each population a parallel control group was incubated in YMM at 30°C. At the end of each selection experiment, 10 randomly chosen individual strains were picked from solid YMM plates of the final populations and the cultures were stored at –80°C in 30% "v/v" glycerol.

Estimation of Stress Resistance Levels of the Evolved Strains

For the quantitative estimation of stress resistance, viable cell counts were made both by the most probable number (MPN) method and colony counting on YMM agar plates, as described previously (Russek and Colwell, 1983; Çakar et al., 2005). For the MPN method, dilutions were made in the range of 10^{-1} to 10^{-8} for five parallel samples in 96-well plates and the MPN of cells surviving the stress condition was estimated, as described previously (Çakar et al., 2005). In addition, cultures grown in the absence of any stress condition were used as controls. MPN scores were determined after 48 and 72 h of incubation. Each score refers to the "number of organisms per unit volume" of the original sample and was calculated from the tables indicated (Lindquist, 2016). The survival rates of the cultures were determined by calculating the ratio between the number of cells/mL under stress condition and those under control conditions.

To estimate the oxidative stress resistance levels, cells were cultivated until their mid-logarithmic phase (OD_{600} of 1–1.5) and were subjected to either continuous oxidative stress (YMM containing 1-mM and 2-mM H_2O_2, 72 h, 30°C) or pulse oxidative stress (YMM containing 0.1 M and 0.3 M H_2O_2 for 90 min followed by incubation in YMM, 72 h, 30°C). The survival rates were then determined by calculating the ratio between the number of viable cells in stress conditions and that under control conditions.

The cross-resistances to other stress conditions such as $CoCl_2$, salt, ethanol, heat, and freeze-thaw stress were also determined using the same method for the estimation of oxidative stress resistance. Briefly, the following stress conditions were applied during the cross-resistance tests:

- Heat stress by incubating strains in YMM at 60°C for 10 min,
- Freeze-thaw stress by placing strains in liquid nitrogen and at –20°C for 25 min and thawing at room temperature,
- Ethanol stress by incubating strains in YMM containing 5 and 7% "v/v" ethanol,
- Salt stress by incubating strains in YMM containing 5 and 7% "w/v" NaCl,
- Metal stress by incubating strains in YMM containing 1 mM $CoCl_2$.

Additionally, cross-resistances to some other metal and non-metal stress conditions were also determined using the semi-quantitative spot assay by culturing serially diluted samples (up to 10^{-5} dilution) on YMM-agar medium containing a variety of stress factors at a final concentration of $CoCl_2$ (1.5-mM), $NiCl_2{\cdot}6H_2O$ (0.1-mM), $CuSO_4{\cdot}5H_2O$ (0.1-mM), $ZnCl_2{\cdot}6H_2O$ (7.5-mM), NaCl (0.5-M), $(NH_4)2Fe(SO_4)_2{\cdot}6H_2O$ (25-mM), $MnSO_4$ (1-mM), and ethanol (8% "v/v"). Resistance profiles were documented upon 72 h incubation at 30°C.

Physiological Analysis of Evolved Strains Obtained From Different Selection Strategies

Some of the evolved strains that are resistant to continuously applied oxidative stress condition and cross-resistant to other stress conditions were used for further growth physiological analyses, including cell dry weight (CDW) measurements, catalase activity tests, metabolite analysis by high-performance liquid chromatography (HPLC), and trehalose and glycogen analyses.

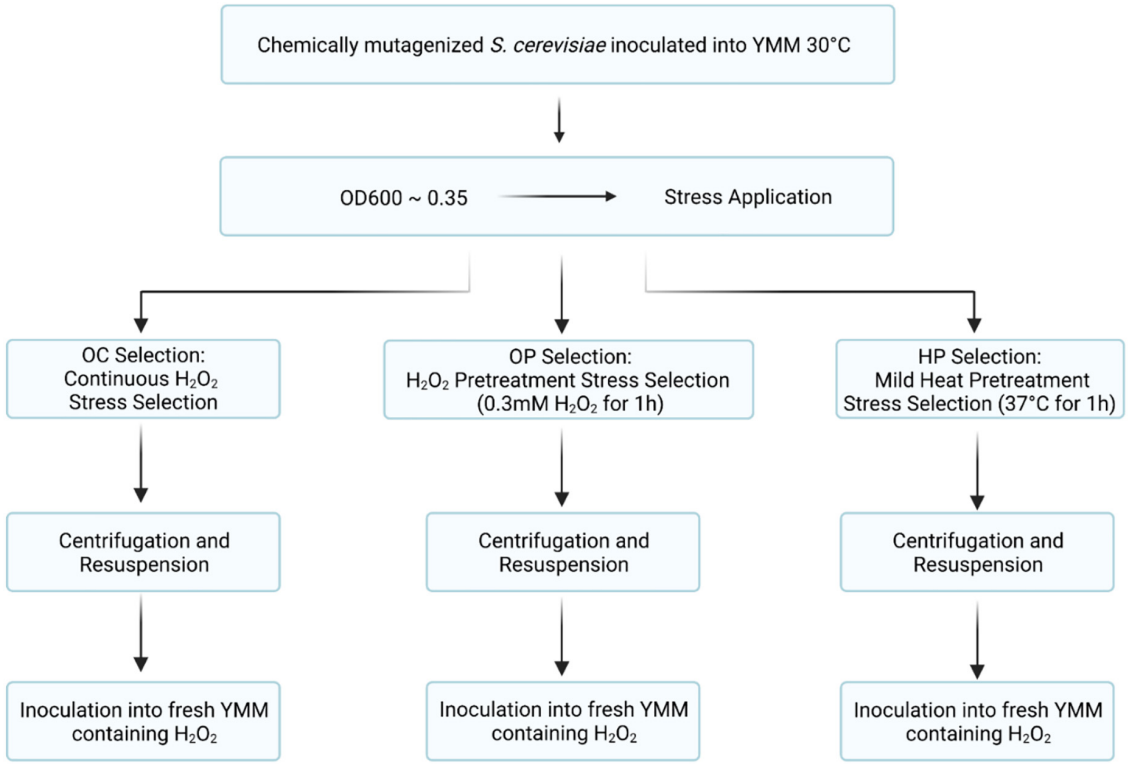

FIGURE 1 | Flow charts of evolutionary selection and preconditioning strategies. Generation and selection of oxidative stress-resistant *S. cerevisiae* populations using different evolutionary engineering strategies are shown (OC, oxidative continuous; OP, oxidative pulse; HP, heat and pulse).

Growth Physiological Experiments and Sample Collection

Overnight cultures of the reference strain and the evolved strain were inoculated in YMM (YMM containing 0-, 0.5-, and 1-mM H_2O_2 in 2-L flasks. They were then incubated at 30°C and 200 rpm for 48 h. Samples were withdrawn every 1.5 h for monitoring growth, CDW and metabolites (residual glucose, ethanol, glycerol, acetate, and maltose) and trehalose/glycogen contents.

Cell Dry Weight Analysis

A 10 ml cultures of the reference strain and the evolved strain harvested after 48 h of growth in YMM containing 0, 0.5, and 1 mM H_2O_2 were used for CDW analysis. After the cell pellets were obtained by centrifugation (5,000 *g*, 5 min), they were dried for 2 h at 90°C, cooled in a desiccator for 30 min and weighed, as described previously (Küçükgöze et al., 2013).

Metabolite Analysis by High-Performance Liquid Chromatography

Residual glucose and extracellular metabolites including ethanol, acetate, glycerol, and maltose were analyzed using HPLC, as described previously (Küçükgöze et al., 2013). Briefly, precultures were grown overnight in 100 mL YMM at 30°C and 150 rpm. Cultivations were performed as one control flask containing YMM and two test flasks with YMM containing 0.5 mM and 1 mM H_2O_2. The cultures were incubated at 30°C and 150 rpm for 48 h. HPLC samples were prepared by centrifugation of 1.5 mL culture samples at 10,000 g for 5 min, and subsequent filtration of supernatants using 0.2 μm filters. The HPLC system consisted of a system controller (SCL-10A, Shimadzu, Kyoto, Japan), liquid chromatography unit (LC-10AD, Shimadzu, Kyoto, Japan), degasser (DGU-14A, Shimadzu, Kyoto, Japan), refractive index detector (RID-10A, Shimadzu, Kyoto, Japan), auto injector (SIL-10AD, Shimadzu, Kyoto, Japan), and column oven (CTO-10AC, Shimadzu, Kyoto, Japan). An Aminex© HPX-87H column was used at 60°C with a flow rate of 0.6 mL min^{-1}, with 20 μL sample injections. 5 mM H_2SO_4 solution was used as the mobile phase/eluent (Küçükgöze et al., 2013).

Trehalose and Glycogen Determination by Enzymatic Reaction

Reserve carbohydrate (trehalose and glycogen) contents were determined as described previously (Parrou and François, 1997). 25 OD_{600} units of cells were collected, treated with 250-μl 0.25-M sodium carbonate, and placed at 95°C for 4 h. Cell suspensions were then adjusted to pH 5.2 with 1 M 150-μl acetic acid and 0.2 M 600-μl sodium acetate buffer (pH 5.2).

A 10-μl trehalase or 20-μL amylo-glycosidase (solubilized in 0.2 M sodium acetate pH 5.2) was added to cell suspensions for trehalose or glycogen determination, respectively. The intracellular glucose release was then quantified upon oxidase/peroxidase reagent treatment of the cells, using

the glucose oxidase/peroxidase method (Cramp, 1967). Absorbance of the samples was measured, as described previously (Küçükgöze et al., 2013).

Catalase Activity Measurement

Catalase activity was assayed as described previously (Ueda et al., 1990). Briefly, 680-μl of 50-mM potassium phosphate buffer (pH 7.2) and 480-μl of 40-mM H_2O_2 were mixed and incubated in a quartz cuvette (2.5 min, 30°C). After incubation, 40-μl cell extract was added into this mixture to initiate the reaction. The decrease in absorbance at 240 nm was recorded and ΔA240/min/mg protein was calculated to determine the specific catalase activity.

Lyticase Sensitivity Assay

Lyticase sensitivity assay was adapted from Kuranda et al. (2006) and performed as described previously (Balaban et al., 2020), using the reference and the evolved strain cultured both under control and 0.5-mM H_2O_2 stress conditions. The cultures were then harvested (10 min; 10,000 g) and resuspended in 10-mL of 10-mM Tris/HCl buffer (pH 7.4), containing 40 mM β-mercaptoethanol (Merck, Hohenbrunn, Germany). Following incubation at 25°C for 30 min, 2 U/mL lyticase (Sigma-Aldrich, St. Louis, MO, United States) was added into each sample and then incubated at 30°C and 150 rpm. The lyticase resistance of the cells was calculated as the ratio of the OD_{600} value upon lyticase treatment to the initial OD_{600} value before lyticase treatment. Experiments were performed as three biological repeats.

Transcriptomic Analysis by Microarray

Overnight cultures of the reference strain and the evolved strain were inoculated into fresh 2% YMM (0 mM and 0.5 mM H_2O_2) in 100 mL flasks to an initial OD_{600} of 0.1 and incubated at 30°C. At mid-exponential phase of growth, 1 OD_{600} unit of cells (2×10^7 cells/mL) were harvested by centrifugation (Arslan et al., 2018a). Total RNA isolation of the harvested cultures was performed using RNeasy Mini Kit (Qiagen, Hilden, Germany), according to the manufacturer's instructions. The experiment was repeated three times.

The RNA concentrations and quality were assessed by a NanoDrop 2000 UV-Vis spectrophotometer (Thermo Fisher Scientific, Waltham, MA, United States) and BioAnalyzer 2100 (Agilent Technologies, Santa Clara, CA, United States).

Agilent yeast microarrays, Yeast (V2) Gene Expression Microarray (Design ID:016322), were used to monitor mRNA transcript of *S. cerevisiae* open reading frames. Hybridization, washing, staining and scanning were performed according to the instructions in the Agilent One Color RNA Spike-in Kit manual. Gene expression profile was visualized, clustered hierarchically and expression fold changes of the evolved strain with respect to the reference strain were calculated using the Agilent GeneSpring GX software supplied by Agilent Technologies, Santa Clara, CA, United States as described previously (Arslan et al., 2018a).

KEGG pathways for stress tolerance were identified using DAVID Bioinformatics Resources (v6.8) (Huang et al., 2009), and the differentially expressed genes ($p \leq 0.05$ and fold change ≥ 2) were determined, as described previously (Hacısalihoğlu et al., 2019). GO analysis ($p \leq 0.05$ and fold change ≥ 2) was performed using Saccharomyces Genome Database SGD Gene Ontology Slim Mapper.[1]

The complete microarray data are available at GEO repository under accession number GSE184952.[2]

Whole Genome Sequencing

Prior to sequencing, the reference strain and the evolved strain were grown and harvested as described before (Surmeli et al., 2019). DNA extraction was carried out using a MasterPure™ DNA Purification Kit (Epicenter, San Diego, United States), following the manufacturer's instructions. Concentration and purity of isolated DNA samples was assessed by NanoDrop 2000 UV-Vis spectrophotometer (Thermo Fisher Scientific, Waltham, MA, United States) and Qubit® Fluorometer 3.0 (Thermo Fisher Scientific).

The Ion Torrent Sequencing Systems were used for the whole genome sequencing of the strains. Library preparation involved four main phases: (i) Digestion and fragmentation of genomic DNA by using Ion Shear™ Plus Reagents Kit (Thermo Scientific, United States), (ii) ligation of adapters *via* use of IonXpress™ Plus Fragment Library Kit (Thermo Scientific, United States) and Ion Xpress™ Barcode Adapters, (iii) size selection with usage of E-Gel System (Thermo Scientific, United States and (iv) amplification and purification by using Ion Xpress™ Plus Fragment Library Kit (Thermo Scientific, United States) and Agencourt AMPure XP (Beckman Coulter, Carlsbad, CA, United States) reagent. All steps were carried out according to the manufacturer's instructions.

Template preparation was carried out by the Ion Chef™ Instrument and high-throughput sequencing was performed by the Ion S5 Sequencing System (Thermo Scientific, United States). Briefly, 20 ng/mL of the prepared library was then loaded into Ion Chef™ (Thermo Fisher Scientific, Waltham, MA, United States). Ion 540™ Chip Kit was used for sample tracking and sequencing, using Ion S5™ Sequencer (Thermo Fisher Scientific, Waltham, MA, United States). Whole genome sequencing data were created and analyzed on Torrent Suite Software by using *S. cerevisiae* CEN.PK113-7D reference genome (GCA_000269885.1; ASM26988v1). The Torrent Suite Software was then used to perform raw data analysis at all stages including quality control, trimming adaptor, removing low-quality sequences, alignment of raw data to reference strain data and variant calling. Data from this work have been deposited in the NCBI Sequence Read Archive (SRA) under BioProject PRJNA768245.

Statistical Analysis

All experiments were performed using at least three biological replicates. The data analyses were performed using the R software "stats" package (R Core Team, 2020). Statistical significance was calculated using a two-tailed, unpaired Student's *t*-test. $p < 0.05$ was considered as statistically significant except for analyses of microarray and whole genome sequencing.

[1] http://www.yeastgenome.org

[2] https://www.ncbi.nlm.nih.gov/geo/query/acc.cgi?acc=GSE184952

RESULTS

Identification of the Evolved Strains With the Highest Oxidative Stress Resistance Within the Final Populations of Diverse Evolutionary Selection Strategies

Evolutionary engineering strategies consisted of successive batch selection in the presence of gradually increasing continuous oxidative stress with and without pre-treatments. The starting oxidative stress level was set as 0.5 mM H_2O_2. As the growth of the 21st–24th populations was as low as 0.1–0.4 OD_{600}, the selection experiments to obtain oxidative stress-resistant evolved strains ended with these final populations.

The oxidative stress resistance levels of individual evolved strains isolated from the final populations of these different evolutionary engineering strategies were then determined. Three evolved strains called C8 (OC strategy), P4 (OP strategy), and H7 (HP strategy) were identified as the highest oxidative stress-resistant strains, upon continuous or pulse oxidative stress tests, using the MPN method. The genetic stability of the evolved strains C8, P4, and H7 was verified by 10 successive batch cultivations in the absence of oxidative stress as the selection pressure (data not shown). The survival rates of the evolved strains H7 and P4 were higher than those of the reference strain and C8, under both continuous and pulse oxidative stress conditions, despite a relatively better survival of C8 under continuous stress condition, compared to the pulse stress condition. Besides, H7 had the highest survival rate under most of the stress conditions tested, except for 1 mM continuous H_2O_2 stress (**Figure 2**).

Cross-Resistance to Other Stress Factors

Cross-resistance of evolved strains C8, P4, and H7 to different stress types including cobalt (1 mM $CoCl_2$), heat (60°C for 10 min), freeze-thaw [−196°C (liquid nitrogen) and −20°C for 25 min], ethanol [5 and 7% (v/v)], and salt [5 and 7% (w/v) NaCl] stress were also tested (**Figure 3**).

The results showed that the evolved strain H7 had the highest cross-resistance to cobalt and heat stress, compared to C8 and P4 (**Figures 3A,B**). H7 was also cross-resistant to freeze-thaw stress (**Figure 3C**), and highly cross-resistant to ethanol stress (5 and 7% "v/v") (**Figure 3D**). Similar results were also observed for salt stress-resistance (5 and 7% "w/v" NaCl) (**Figure 3E**).

Semi-quantitative cross-resistance test results of the evolved strain H7 were also generally in line with the quantitative, MPN-based cross-resistance results. Additionally, H7 was cross-resistant to iron [25 mM $(NH_4)2Fe(SO_4)_2$] as shown by the semi-quantitative cross-resistance test results (**Figure 4**).

Physiological and Metabolic Characterization of the Evolved Strain

Growth physiology of the reference (*905*) and the evolved strain (H7) was analyzed using batch cultures in YMM and YMM containing 0.5-mM and 1-mM H_2O_2 as the oxidative stress factor (**Figure 5**).

The maximum specific growth rates and doubling times of the cultures are indicated in **Table 1**.

It was observed that the oxidative stress levels (up to 1 mM H_2O_2) applied in these experiments had no significant inhibitory effect on the growth of H7. However, the reference strain was significantly inhibited at these oxidative stress levels. At 1 mM H_2O_2 in particular, the reference strain had a considerably longer lag phase and doubling time, as well as a significantly lower maximum specific growth rate (**Figure 5** and **Table 1**).

The metabolite profiles of both strains were generally in line with their growth data (**Figure 6**). The reference strain had a significantly decreased glucose consumption rate at 1 mM H_2O_2, whereas the glucose consumption rate of H7 did not significantly decrease during oxidative stress. Glycerol production (g/L) profiles of the reference strain *905* and H7 cultures varied in line with their growth curves. Interestingly, it was observed that under oxidative stress conditions, the glycerol levels of H7 slightly decreased after the first 24 h of cultivation, during the stationary phase of growth. Acetate was produced by both reference strain and H7, although at significantly lower levels in H7, compared to the reference strain. Additionally, after the exponential phase of growth, acetate levels decreased in H7 cultures, both in the presence and absence of oxidative stress. In the presence of oxidative stress, ethanol production of H7 was higher than that of the reference strain. François and Parrou (2001) reported that, under harsh environmental conditions, glycogen production and degradation occurs in yeast which leads to the liberation and accumulation of maltose. For this reason, maltose levels of H7 and the reference strain were also measured. Interestingly, H7 accumulated maltose, unlike the reference strain. As the H_2O_2 concentration (oxidative stress level) in the culture medium increased, the maltose production levels of H7 also increased (**Figure 6**).

As glycogen and trehalose function both as storage carbohydrates and stress protectants (François and Parrou, 2001), the glycogen and trehalose profiles of the reference strain and the evolved strain H7 were obtained (**Figure 7**). The results revealed that H7 had significantly higher glycogen and trehalose content than the reference strain throughout the cultivation, both in the presence and absence of oxidative stress. Both glycogen and trehalose contents of H7 increased until the end of the exponential phase of growth (approximately at the 18th hour of cultivation), after which it decreased. The maximum glycogen and trehalose contents of H7 at the 18th hour of cultivation were 17-fold and 10-fold higher than those of the reference strain (**Figure 7**).

To test if the oxidative stress-resistant evolved strain also had increased catalase activity, the catalase activity measurements were made for the evolved strain and the reference strain. It was observed that the specific catalase activity of H7 was about fourfold of that of the reference strain, both in the presence and absence of oxidative stress (**Figure 8**), without induction of catalase activity by H_2O_2 in H7.

The lyticase sensitivity assay was also applied to test if there were differences in cell wall integrity between the evolved

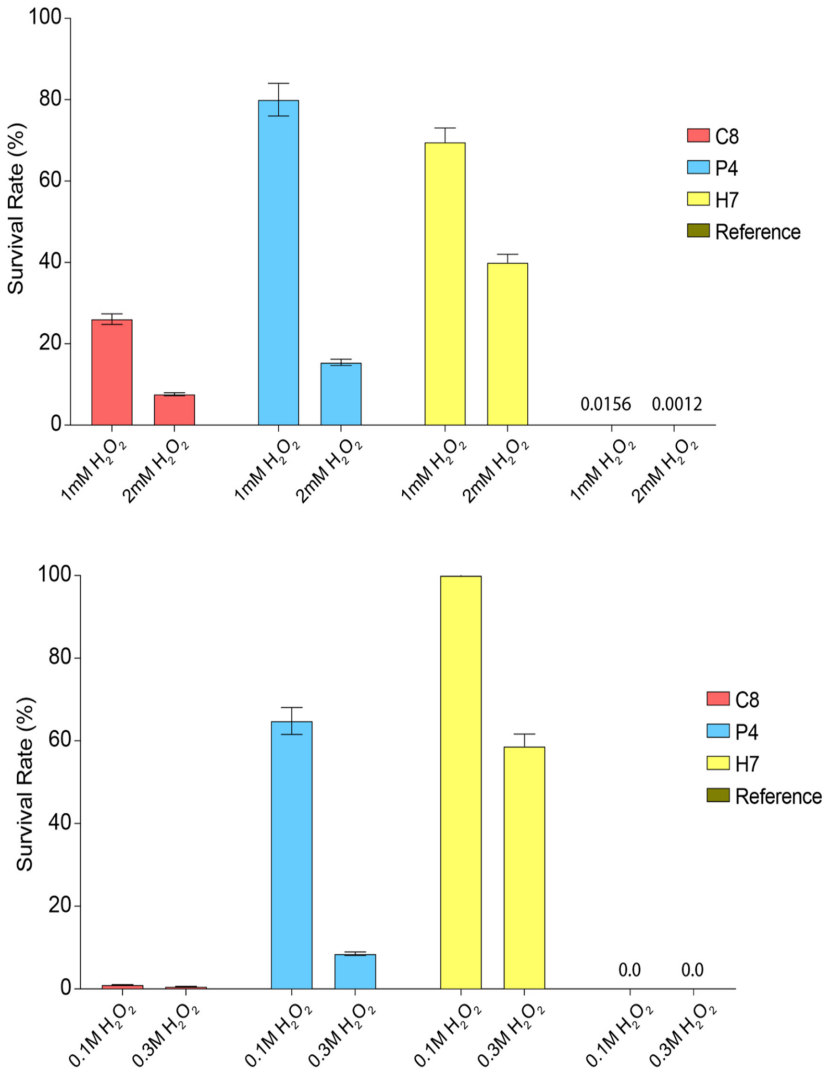

FIGURE 2 | Oxidative stress survival rates of the reference and most resistant strains C8, P4, and H7 obtained from OC, OP, and HP selection approaches, respectively. The cultures were **(top figure)** continuously exposed to 1 or 2 mM H_2O_2 or **(bottom figure)** exposed to 0.1 and 0.3 M H_2O_2 as pulse oxidative stress. The survival rates (%) were determined upon incubation (72 h, 30°C).

strain and the reference strain. The results revealed that H7 had significantly higher lyticase resistance than the reference strain, both in the presence and absence of oxidative stress (**Figure 9**), indicating a significantly higher cell wall integrity or robustness of H7. Interestingly, the lyticase resistance of H7 did not increase in the presence of oxidative stress, although the lyticase resistance of the reference strain slightly increased upon oxidative stress (**Figure 9**).

Comparative Gene Expression Profile of the Oxidative Stress-Resistant Evolved Strain H7

To investigate the molecular basis of oxidative stress resistance, global transcriptomic profiles of H7 and the reference strain were analyzed during mid-exponential growth phase and in the absence of oxidative stress, by using DNA microarray technology. $p < 0.05$ was applied as the cut-off value. 1911 ORFs were differentially expressed by at least two-fold in the evolved strain. Of these, 897 were up-regulated and 1014 were down-regulated. Genes of H7 which were up-regulated by sevenfold or higher and down-regulated by at least fivefold are shown in **Tables 2**, **3** respectively. Gene ontology analysis was carried out by GO Slimmapper of the Saccharomyces Genome Database. Genes that were up- and down-regulated by at least twofold in H7 are listed in **Supplementary Tables 1, 2**, respectively.

Table 2 and **Supplementary Table 3**, show many of the up-regulated genes are associated with the response to stress conditions such as oxidative, heat, chemical, osmotic, and starvation stress. In addition, genes related to metabolite production and modification process such as the carbohydrate metabolic process, generation of precursor metabolites and

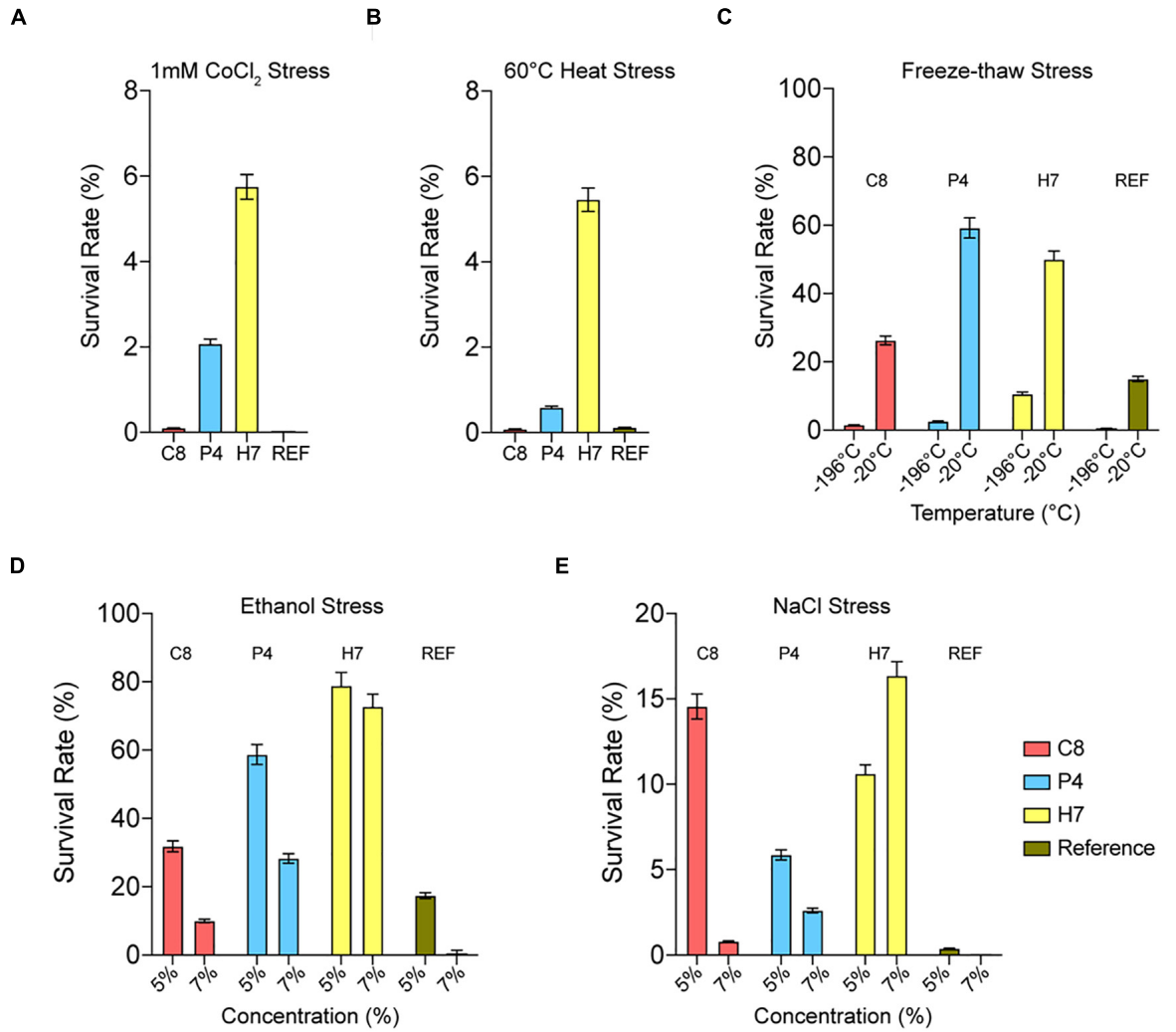

FIGURE 3 | Quantitative cross-resistance analysis (MPN) results of the highest oxidative-stress resistant strains C8, P4, H7 and the reference strain. The cultures were exposed to **(A)** 1 mM $CoCl_2$, **(B)** 60°C for 10 min, **(C)** –196°C (liquid nitrogen) and –20°C for 25 min, **(D)** 5 and 7% (v/v) ethanol and **(E)** 5 and 7% (w/v) NaCl. The survival rates (%) were determined upon incubation (72 h, 30°C). The results were obtained using the MPN analysis under various stress conditions.

energy, the monocarboxylic acid metabolic process, the cofactor metabolic process, the lipid metabolic process, protein phosphorylation, protein complex biogenesis, cell wall organization or biogenesis, oligosaccharide metabolic process, and protein modification by small protein conjugation or removal and protein folding were also up-regulated in H7. Mitochondrion and peroxisome organization-related genes were also up-regulated. Transport-related genes such as ion transport, transmembrane transport, protein targeting, carbohydrate transport, Golgi vesicle transport, membrane invagination, membrane fusion, lipid transport, amino acid transport and organelle fusion were also generally up-regulated, excluding nuclear transportation. Further, genes related to cellular respiration were also up-regulated. Interestingly, the meiotic cell cycle and sporulation-related genes were also overexpressed. **Table 3** and **Supplementary Table 2** indicate that a major group of down-regulated genes in H7 belongs to ribosome biosynthesis. The down-regulated genes also have a role in RNA biosynthesis and modification processing, such as tRNA biosynthesis, snoRNA processing, RNA modification, translation and RNA splicing. A considerable number of genes down-regulated play a role in processes related to nucleotide metabolism such as production, assembly and transport. Genes associated with nuclear transport and transport of nucleobase-containing metabolites were mostly down-regulated in H7. Transcription of genes for organelle and ribosome assembly processes were also down-regulated. Other down-regulated genes in H7 were related to mitosis and cell cycle. Conversely, sporulation and stationary phase-related genes were strongly up-regulated in H7.

As shown in **Supplementary Table 3**, genes related to stress response; metabolic processes of carbohydrates, lipids, and proteins including anabolic and catabolic reactions; generation of precursor metabolites and energy; and transportation of metabolites and ions were up-regulated in H7. However,

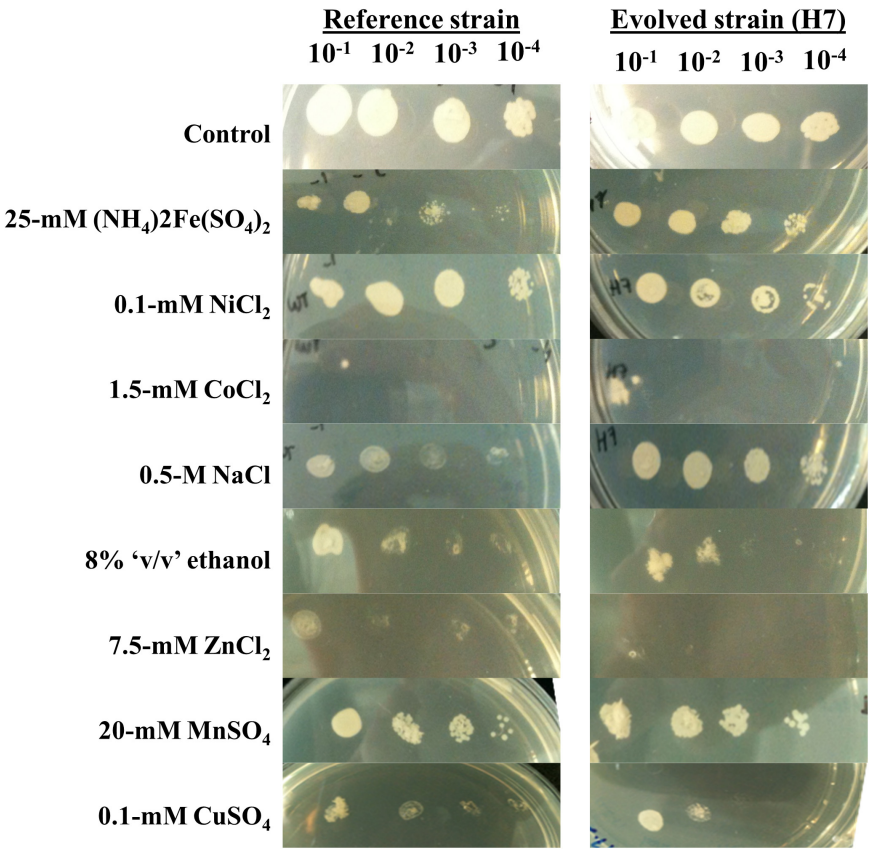

FIGURE 4 | Semi-quantitative cross-resistance analysis (spot assay) results of H7 and the reference strain, upon 72 h of growth. The strains were cultured on YMM plates containing various stress factors, at four serial dilutions (10^{-1} to 10^{-4}). YMM plates without any stress factor were used as the control.

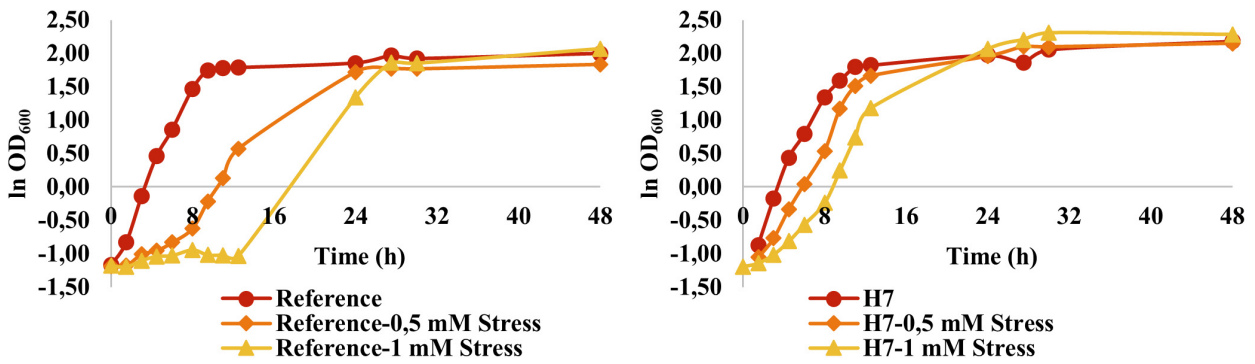

FIGURE 5 | Growth behavior of the reference strain and H7 in the absence and presence of 0.5-mM and 1-mM H_2O_2 as the oxidative stress factor. The cultures were grown in YMM at 30°C and 150 rpm for 48 h.

expression levels of the genes that belong to processes related to ribosome, RNA, nuclear transport, organelle assembly, tRNA, cell cycle, mitosis and transcription from RNA polymerases decreased in H7.

A KEGG pathway mapping analysis was performed for the up- and down-regulated gene sets using DAVID v6.8 Bioinformatics Resources (Huang et al., 2008, 2009) to assess their biological significance. The analysis identified nucleobase metabolism, RNA polymerase and ribosome biogenesis, amino acids biosynthesis and steroid biosynthesis as significantly enriched pathways in the down-regulated gene sets. Moreover, pathway analysis showed that the up-regulated genes in H7 were enriched primarily with those associated with carbon metabolism, oxidative phosphorylation, peroxisome, fatty acid degradation and endocytosis pathways (**Figure 10**).

TABLE 1 | Maximum specific growth rates (μ_{max} "h^{-1}") and doubling times (h) of the reference strain (905) and the evolved strain (H7) in the absence and presence of 0.5-mM and 1-mM H_2O_2 stress.

	μ_{max} (h^{-1})	Doubling time (h)
905	0.35	2.00
905 0.5-mM stress	0.24	2.92
905 1-mM stress	0.15	4.77
H7	0.33	2.12
H7 0.5-mM stress	0.28	2.47
H7 1-mM stress	0.30	2.32

Single Nucleotide Variation Analysis

Variant analysis was carried out for more than 20 million reads for both strains with an average coverage depth of 350. Coverage and quality data are given in **Supplementary Table 4**. We have detected 33 missense, 2 nonsense, and 1 frameshift deletion mutations in the evolved strain H7. Further, 12 silent mutations, 12 intergenic mutations, and 1 nucleotide substitution on Long Terminal Repeat were observed (**Table 4**).

DISCUSSION

In this study, we particularly focused on oxidative stress, one of the most common stress factors in industrial applications using yeast. We investigated the genetic and molecular mechanisms that provide yeast cells an advantage over previous generations to cope with this stress condition (Gasch et al., 2000; Alexandre et al., 2001; Morano et al., 2012). We first constructed oxidative stress-resistant and genetically stable evolved strains, using an evolutionary engineering approach under oxidative stress conditions, with or without heat pretreatment and oxidative stress (hydrogen peroxide) pretreatment. We then performed comparative genomic, transcriptomic, and physiological analyses with the most efficient oxidative stress-resistant evolved strain (H7) and the reference strain, to elucidate the molecular resistance mechanisms to this stress condition.

The results revealed that the evolutionary engineering strategy under oxidative stress conditions and heat pretreatment yielded a genetically stable, evolved strain (H7) with the highest oxidative stress resistance level and with cross-resistance to many other stress types including cobalt, freeze-thaw, heat, ethanol, iron,

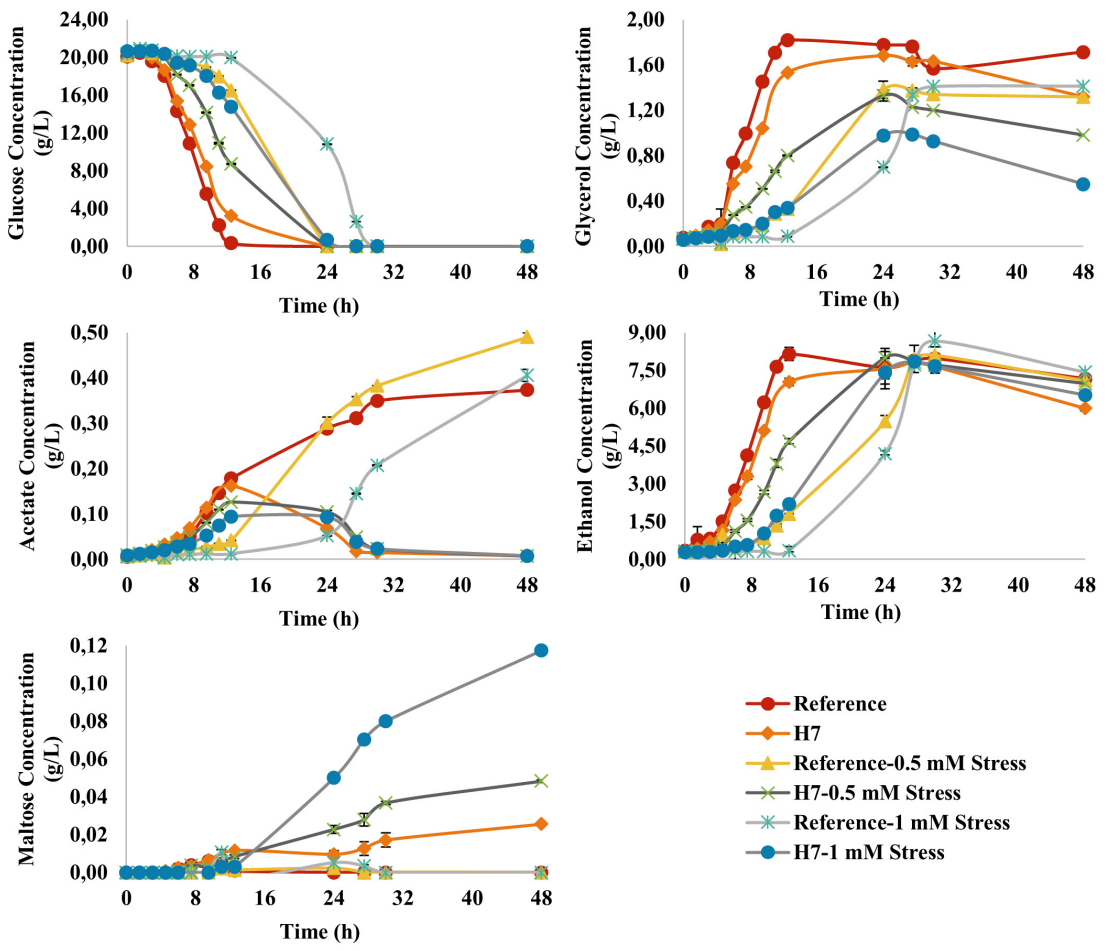

FIGURE 6 | Residual glucose concentration, glycerol, ethanol, acetate and maltose production (g L^{-1}) profiles of the reference strain and H7 in the absence and presence of 0.5-mM and 1-mM H_2O_2 as the oxidative stress factor. The cultures were grown in YMM at 30°C and 150 rpm for 48 h.

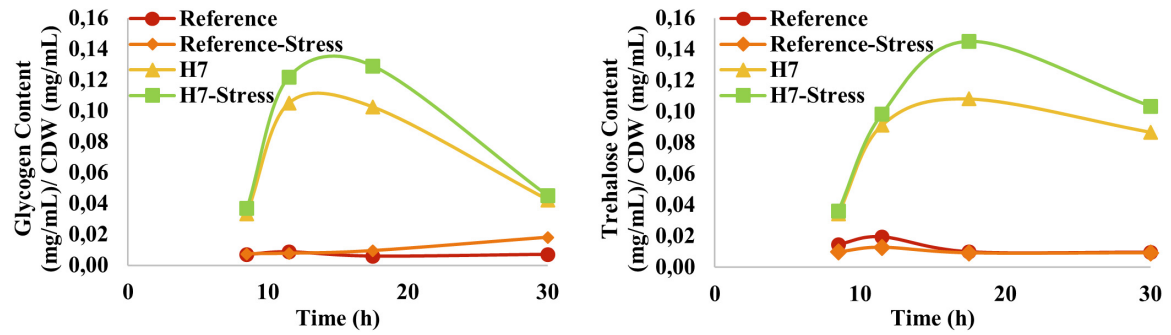

FIGURE 7 | Glycogen and trehalose production (mg mL^{-1}) per CDW (mg mL^{-1}) profiles of the reference strain and H7 in the absence and presence of 0.5-mM H_2O_2 as the oxidative stress factor. The cultures were grown at 30°C and 150 rpm, using YMM. Glycogen and trehalose contents of the samples were determined enzymatically, between the 10th and 30th hour of cultivation.

and salt stress (**Figures 2**, **3**). This evolutionary advantage may be associated with gaining thermotolerance *via* heat shock factors and stress response element pathways that regulate the synthesis of heat shock proteins (Hsps) and with increasing the robustness of the cells to withstand the damaging effects of oxidative stress (Morano et al., 1998; Verghese et al., 2012; Rikhvanov et al., 2014). Indeed, many *HSP* genes were upregulated in our evolved strain H7 (**Supplementary Table 1**) and 11 upregulated genes were found in the "response to heat" category for H7 (**Supplementary Table 3**). Many Hsps can be induced in cells recovering from mild heat shock; they are responsible for the refolding of heat-denatured proteins and survival which can help survive under various stress conditions (Seppä and Makarow, 2005). In line with this notion, an early adaptive response provides almost immediate protection against sublethal stress conditions by activating preexisting defenses; while a late adaptive response provides more efficient protection against a severe stress and also allows cells to return to non-stress conditions, as reported previously (Costa and Moradas-Ferreira, 2001).

The maximum specific growth rate/doubling time of H7 were unaffected by oxidative stress conditions, and the catalase activity of H7 was higher than the reference strain even in the absence of H_2O_2 stress. This strongly suggests the effective resistance of H7 to oxidative stress. Among the many environmental stress response genes that were upregulated in the evolved strain H7, *CTT1* that encodes cytosolic catalase T was up-regulated by 5.37-fold in H7, compared to the reference strain. Cytosolic catalase T is known to have a role in protection from oxidative damage caused by H_2O_2 (Wieser et al., 1991). Another adaptation that is most likely associated with heat pretreatment dependent adaptation was observed in the stress-regulatory transcription factors Msn2 and Msn4. Many genes that are regulated by Msn2 and Msn4 were highly up-regulated in H7 (**Table 2**). These transcription factors, as alternatives to *CTT1*, activate expression of the genes involved in fatty acid oxidation. Even in their absence, *CTT1* can take control over the entire resistance mechanism machinery against oxidative stress (Hasan et al., 2002; Rajvanshi et al., 2017). In addition, physiological analyses showed that, unlike the reference strain, the concentrations of glycerol produced by H7 decreased during the stationary phase of growth, possibly indicating glycerol consumption by

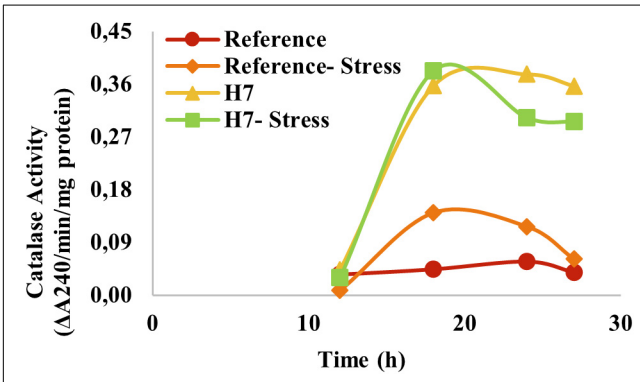

FIGURE 8 | Specific catalase activity (ΔA_{240}/min/mg protein) of the reference strain and H7 in the absence and presence of 2-mM H_2O_2 as the oxidative stress factor. The cultures were grown in YMM at 30°C and 150 rpm.

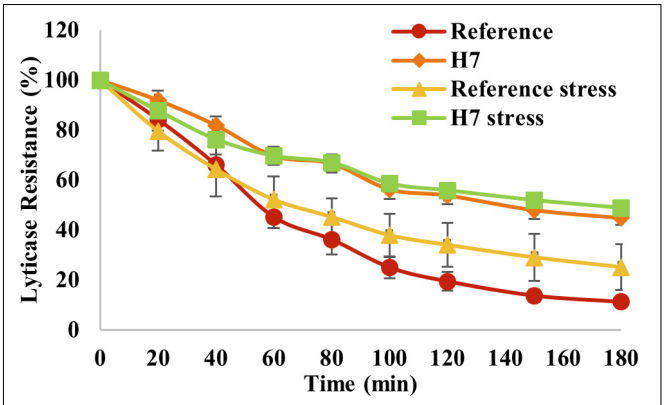

FIGURE 9 | Lyticase sensitivity assay results of the evolved strain H7 and the reference strain under oxidative stress (0.5-mM H_2O_2) and control conditions. Lyticase sensitivity was calculated as the percent decrease in lyticase resistance from 100% as the initial value.

TABLE 2 | Genes which were up-regulated by at least sevenfold in H7.

Systematic gene symbol	Standard gene symbol	Gene name	Fold change	Regulatory genes that are known to regulate the stated gene
YMR107W	*SPG4*	Stationary phase gene	9.52	*CST6, FKH1, GCR1, LEU3, MED2, RAP1, SPT10, SRB5, UME6, YAP5*
YEL039C	*CYC7*	CYtochrome C	9.09	*TUP1, FKH1, FKH2, HAP1, HIR3, MSN2, PHD1, SFP1, SIR2, SIR3, SIR4, SUA7, TFC7*
YMR206W		Putative protein of unknown function	8.44	*GCR2, SFP1, SIR2, SIR3, SIR4, SUA7, UGA3, UME6, XBP1*
YFL014W	*HSP12*	Heat shock protein	8.44	*CLA4, BAS1, CBF1, CSE2, CST6, GCN5, GCR1, HAL9, HCM1, HSF1, IXR1, MED4, MSN2, MSN4, NCB2, RAP1, REB1, RPN4, SFP1, SIR2, SIR3, SIR4, SPT10, SPT3, SRB8, STE20, SUA7, TUP1, UME6, XBP1, YAP5, YAP6, ZAP1*
YNL194C		Integral membrane protein, similar to *SUR7*	8.30	*AFT2, CYC8, MSN2, MSN4, NCB2, RPD3, SPT3, SUA7, UME6, YAP5*
YDL222C	*FMP45*	Found in mitochondrial proteome	7.89	*BUR6, MED4, STE12, SUA7, TEC1, XBP1*
YIL057C	*RGI2*	Respiratory growth induced	7.69	*FKH2, MSN2, MSN4, RAP1, SPT10*
YFR053C	*HXK1*	HeXoKinase	7.63	*BUR6, CYC8, GCN4, GCN5, HSF1, IXR1, MED2, MED4, MSN2, MSN4, RAP1, SFP1, SIN4, SPN1, SPT6, STP1, SUA7, TUP1, YAP1*
YBR072W	*HSP26*	Heat shock protein	7.32	*HCM1, SNF2, BUR6, CIN5, CST6, CYC8, FKH2, GCN5, HSF1, IFH1, MED2, MED4, MET32, MET4, MSN2, MSN4, NCB2, NHP6A, PHO2, RAP1, REB1, SFP1, SPN1, SPT10, SPT20, SPT3, SPT7, SRB5, SUA7, TOA2, TUP1, XBP1, ZAP1*
YNL196C	*SLZ1*	Sporulation-specific protein with a leucine zipper motif	7.27	*SPT10*
YLR327C	*TMA10*	Translation machinery associated	7.23	*BUR6, CAD1, CST6, CUP2, CYC8, FKH1, FKH2, FLO8, GCR1, HSF1, MED2, MED4, MET32, MET4, MSN2, MSN4, NCB2, RAP1, RGM1, RDR1, SFP1, SPT10, SPT3, SPT7, SRB5, SUA7S, WI4, SWI6, TUP1, YAP1*
YAL061W	*BDH2*	Putative medium-chain alcohol dehydrogenase	7.15	*BUR6, CST6, CYC8, MET32, MET4, SOK2, SPT10, SUA7, YAP1*
YBR285W		Putative protein of unknown function	7.13	*FKH1, GCN5, LEU3, RPD3, SFP1, SPT10, SUA7, UME6, ZAP1*
YOL052C-A	*DDR2*	DNA damage responsive	7.00	*CBF1, CST6, GCR1, HSF1, IXR1, LEU3, MET32, MET4, MSN2, MSN4, RAP1, REB1, SIR2, SIR3, SIR4, SPT10, SRB8, SSN2, SUA7*

TABLE 3 | Genes that were down-regulated by at least fivefold in H7.

Systematic gene symbol	Standard gene symbol	Gene name	Fold change	Regulatory genes that are known to regulate the stated gene
YJL167W	*ERG20*	ERGosterol biosynthesis	7.00	*CBF1, INO4, RAP1, REB1, SFP1*
YDR035W	*ARO3*	AROmatic amino acid requiring	6.45	*FKH1, FKH2, GCN4, SPT6, UME6*
Q0110	*BI2*	Cytochrome b mRNA maturase bI2	6.36	
YGR245C	*SDA1*	Severe depolymerization of actin	5.70	*SPF1*
YGL255W	*ZRT1*	Zinc-regulated transporter	5.64	*MOT3, ROX1, ADA2, FKH1, GCN4, GZF3, IXR1, MOT3, RFX1, RIM101, ROX1, SFP1, SIN3, SIR2, SIR3, SIR4, SRB8, SSN2, STP1, SWI4, UME1, XBP1, YAP6, ZAP1*
YGL256W	*ADH4*	Alcohol DeHydrogenase	5.36	*FKH1, FKH2, SFP1, SPT10, TYE7, YAP5, ZAP1*
YNL112W	*DBP2*	Dead box protein	5.24	*CDC73, FKH1, FKH2, RFX1, SFP1, ZAP1*
YAR075W		Non-functional protein with homology IMP dehydrogenase	4.48	*CST6, GCR1, HSF1, RAP1, SFP1, SFP1, SIR2, SIR3, SIR4, SPT10, XBP1, YAP1, YAP6*

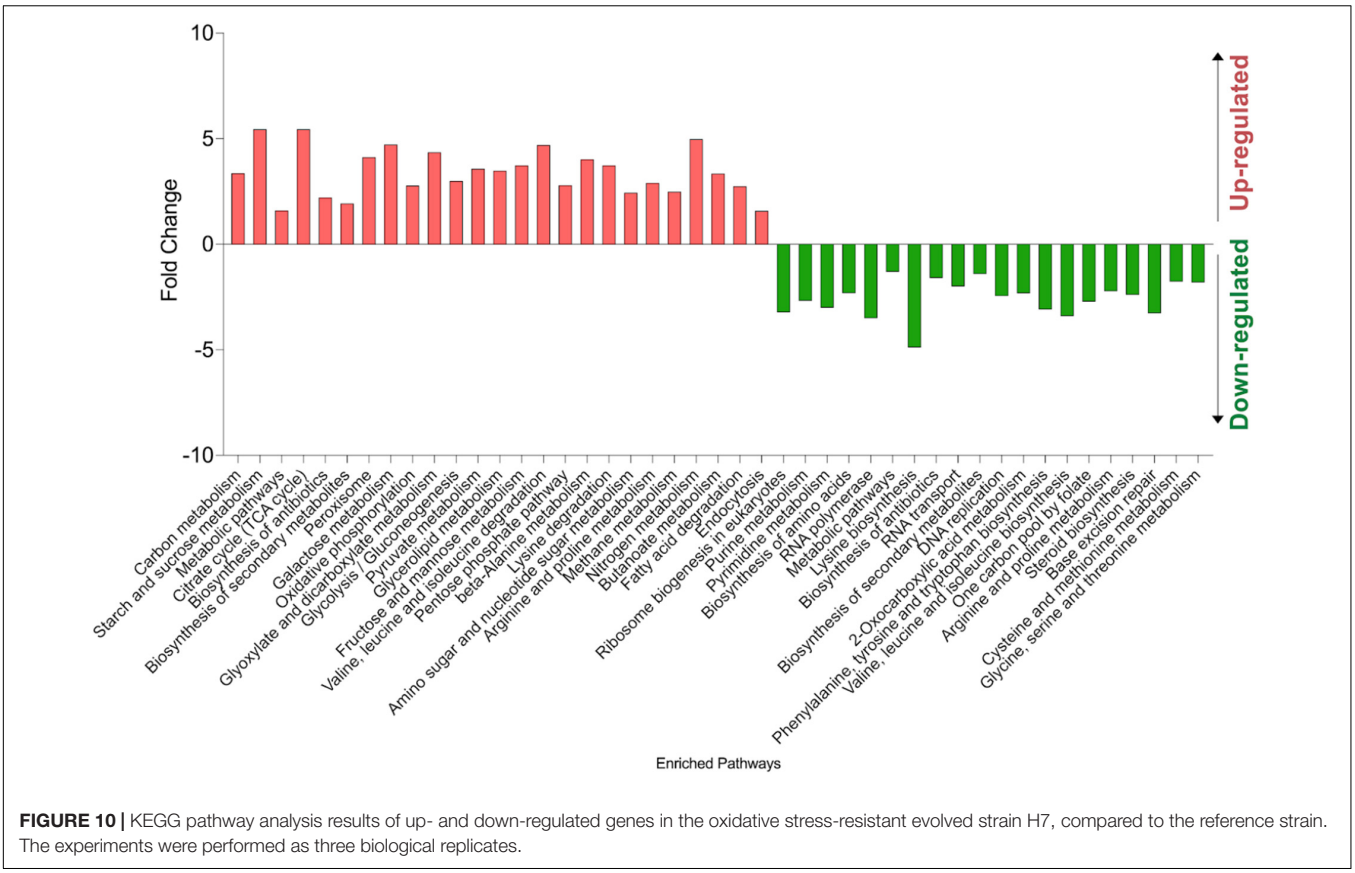

FIGURE 10 | KEGG pathway analysis results of up- and down-regulated genes in the oxidative stress-resistant evolved strain H7, compared to the reference strain. The experiments were performed as three biological replicates.

H7 (**Figure 6**). Transcriptomic data also supports the concept of elevated glycerol utilization in the evolved strain H7 for energy production *via* upregulation of *GUT1* (Glycerol kinase, involved in glycerol utilization) (Pavlik et al., 1993), *GUT2* (responsible for binding to the inner mitochondrial membrane glycerol-3-phosphate dehydrogenase) (Rønnow and Kielland-Brandt, 1993), *GCY1* (glycerol dehydrogenase, plays a role in an alternative pathway for glycerol catabolism under microaerobic conditions) (Jung et al., 2012), and *DAK1* (Dihydroxyacetone kinase, involved in stress adaptation by using dihydroxyacetone as the carbon and energy source) (Molin et al., 2003). Meanwhile, trehalose-associated genes *TPS1, TPS2,* and *TSL1* were up-regulated by 2.4, 3.0, and 5.4-fold in H7, compared to the reference strain, respectively (**Supplementary Table 1**). These findings also support the significantly higher trehalose levels observed in H7 (**Figure 7**). Changes in gene expression profile related to glycerol metabolism and trehalose production could also be associated with protecting yeast against oxidative stress which warrants further investigation. In addition, the potential relationship between oxidative stress resistance and acetate levels is yet to be clarified. Acetate levels of H7 decreased after the exponential phase of growth, both in the presence and absence of oxidative stress, which was not observed in the reference strain (**Figure 6**). It is known that unused acetate is released into the culture medium as acetic acid (Walkey et al., 2012). Up-regulation of *ADY2* (6.2-fold) and *JEN1* (6.1-fold) in H7 support this condition, as *ADY2* encodes an acetate transporter required for sporulation and Jen1p has a role in a lactate–pyruvate–acetate–propionate transport (Paiva et al., 2004). The strong up-regulation of these two genes in H7 may allow for a large amount of acetate uptake into the cell. Further, up-regulation of *ACS1* (1.7-fold) might indicate the utilization of acetate, as Acs1p has a role in acetate utilization and is required for growth on acetate under glucose starvation (Takahashi et al., 2006). The notable upregulation of the acetate transporter genes and the decrease in acetate concentrations may indicate that H7 might accumulate acetate inside the cell. Interestingly, a previous study showed that pre-incubation of yeast cells with low amounts of H_2O_2 caused protection against high acetate levels (Semchyshyn et al., 2011).

The decreased levels of glycerol and acetate during late phases of growth may also suggest that the evolved strain H7 might have adapted itself to grow on non-fermentable carbon sources. Our transcriptomic data also supports this, where *HXK1*, *GLK1,* and *MPC3* genes – that are known to be expressed during growth on non-fermentable carbon sources (Rodríguez et al., 2001; Cherry et al., 2012) – were up-regulated in H7 by 7.6, 3.9, and 6.8-fold, respectively. Another major physiological difference between the evolved strain H7 and the reference strain was the significantly higher maltose levels observed in H7, particularly during the late phases of growth (**Figure 6**). The higher maltose levels in H7 may be associated with the up-regulation of *SGA1* (by 4.8-fold), as *SGA1* encodes a protein involved in glycogen breakdown and the release of maltose (Pugh et al., 1989). It is known that glycogen metabolism is enhanced in response to a wide variety

TABLE 4 | Mutation positions and types in the genome of the oxidative stress-resistant evolved strain H7.

Gene name	Genetic change	Mutation positions	Description (Cherry et al., 2012)
AIM19	c.154G > A	p.P52S	Protein of unknown function; mitochondrial protein that physically interacts with Tim23p
ATG40	c.-602G > A		Autophagy receptor with a role in endoplasmic reticulum degradation
Between RPS14A and snR189	III:177852 G > A		
CDC25	c.1601T > A	p.I534K	Membrane bound guanine nucleotide exchange factor; also known as a GEF or GDP-release factor
CFT2	c.1945G > A	p.G145S	Subunit of the mRNA cleavage and polyadenylation factor (CPF); required for pre-mRNA cleavage,
CIP1	c.1010G > A	p.R337K	Cyclin-dependent kinase inhibitor; activated by environmental stress
DUF1	c.2164G > A	p.Q722*	Ubiquitin-binding protein of unknown function; contains one WD40 repeat in a beta-propeller fold
DYN1	c.10724C > T	p.G3575E	Cytoplasmic heavy chain dynein; involved in spindle assembly, chromosome movement, and spindle orientation during cell division, targeted to microtubule tips by Pac1p
FIS1	c.193G > A	p.L65F	Protein involved in mitochondrial fission and peroxisome abundance; may have a distinct role in tethering protein aggregates to mitochondria in order to retain them in the mother cell
FTH1	c.211delC	p.Q71K#	Putative high affinity iron transporter; involved in transport of intravacuolar stores of iron
GDH2	c.1880C > T	p.G627D	NAD(+)-dependent glutamate dehydrogenase; degrades glutamate to ammonia and alpha-ketoglutarate
HAT2	c.892G > A	p.V298M	Subunit of the Hat1p-Hat2p histone acetyltransferase complex; required for high affinity binding of the complex to free histone H4, thereby enhancing Hat1p activity
HOM3	c.800G > A	p.P267L	Aspartate kinase (L-aspartate 4-P-transferase); cytoplasmic enzyme that catalyzes the first step in the common pathway for methionine and threonine biosynthesis
HPT1	c.179G > A	p.R60K	Dimeric hypoxanthine-guanine phosphoribosyltransferase
IES1	c.307C > T	p.G103R	Subunit of the INO80 chromatin remodeling complex
IKS1	c.554C > T	p.G185D	Protein kinase of unknown cellular role; putative serine/threonine kinase
IRC15	c.217G > A	p.L73F	Microtubule associated protein; regulates microtubule dynamics; required for accurate meiotic chromosome segregation
LYS14	c.2373 + 53 C > T		Transcriptional activator involved in regulating lysine biosynthesis; involved in the regulation of genes of the lysine biosynthesis pathway
MAK10	c.1906G > A	p.R636K	Non-catalytic subunit of the NatC N-terminal acetyltransferase
MCD4	c.2760 + 918C > T		Protein involved in GPI anchor synthesis; multimembrane-spanning protein that localizes to the endoplasmic reticulum;
MEO1	c.11C > T	p.T4I	Putative protein of unknown function;
MSC3	c.2187 + 234C > T		Protein of unknown function
MSH1	c.2880 + 69C > T		DNA-binding protein of the mitochondria; involved in repair of mitochondrial DNA
NFT1	c.2186C > T	p.T729M	Putative transporter of the MRP subfamily
NOP9	c.1939A > C	p.S647A	Essential subunit of U3-containing 90S preribosome; involved in production of 18S rRNA and assembly of small ribosomal subunit
NRG1	c.245C > T	p.W82*	Transcriptional repressor; mediates glucose repression and negatively regulates a variety of processes including filamentous growth and alkaline pH response
PIG1	c.1892G > T	p.S631N	Putative targeting subunit for type-1 protein phosphatase Glc7p
PPX1	c.567C > T	p.M189I	Exopolyphosphatase; hydrolyzes inorganic polyphosphate (poly P) into Pi residues
PRP16	c.251C > T	p.A84V	DEAH-box RNA helicase involved in second catalytic step of splicing and in exon ligation
PRP5	c.2147A > T	p.K716M	RNA helicase in the DEAD-box family; necessary for prespliceosome formation
RER1	c.567 + 47G > A		Protein involved in retention of membrane proteins
RPF2	c.433C > T	p.G145S	Essential protein involved in rRNA maturation and ribosomal assembly; involved in the processing of pre-rRNA and the assembly of the 60S ribosomal subunit
RRP6	c.1720A > G	p.K574E	Nuclear exosome exonuclease component; involved in RNA processing, maturation, surveillance, degradation, tethering, and export; role in sn/snoRNAs precursor degradation
RSC30	c.1402G > A	p. E68K	Component of the RSC chromatin remodeling complex
RTT10	c.2498G > A	p.S833L	WD40 domain-containing protein involved in endosomal recycling
SDC25 (CDC25p)	c.2204G > A	p.G735D	Pseudogene; localized to the membrane; expressed in poor nutrient conditions and on non-fermentable carbon sources
SPC105	c.83G > A	p.S28N	Subunit of a kinetochore-microtubule binding complex
SPP41	c.2769G > A	p.M923I	Protein of unknown function

(Continued)

TABLE 4 | (Continued)

Gene name	Genetic change	Mutation positions[1]	Description (Cherry et al., 2012)
UFD1	c.634G > A	p.A212T	Substrate-recruiting cofactor of the Cdc48p-Npl4p-Ufd1p segregase
UFO1	c.-591G > A		F-box receptor protein; binds to phosphorylated Ho endonuclease, allowing its ubiquitination by SCF and subsequent degradation
VBA1	c.-31G > A		Permease of basic amino acids in the vacuolar membrane
VTC1	c.248G > A	p.R83K	Regulatory subunit of the vacuolar transporter chaperone (VTC) complex; VTC complex is involved in membrane trafficking, vacuolar polyphosphate accumulation, microautophagy and non-autophagic vacuolar fusion
YCR101C	c.250C > T	p.P84S	Putative protein of unknown function
YGL039W	c.-364 G > A		Aldehyde reductase; shown to reduce carbonyl compounds to chiral alcohols
YGL052W	c. 112G > A	p.A38T	Dubious open reading frame
YHRWdelta13	c.211C > T		Ty1 LTR
YJL127C-B	c.159 + 19		Mitochondrial protein of unknown function
YMR321C	c. 318 + 747G > A		Putative protein of unknown function
YPS1	c.838G > A	p.P280S	Aspartic protease; involved with other yapsins in the cell wall integrity response

[#] *Frameshift mutation.*
**Nonsense mutation.*

of environmental stresses, and glycogen degradation can lead to the liberation and accumulation of maltose (François and Parrou, 2001). The oxidative-stress-resistant evolved strain H7 may have such a profile, and it seems to activate stress response genes even in the absence of oxidative stress, retaining an alertness for any potential stress conditions. *HSP12*, *HSP26,* and *DDR2*, other important environmental stress response genes, were also significantly up-regulated in H7 compared to reference strain. In addition, like with glycogen concentrations, H7 trehalose levels were also high, both in the presence and absence of oxidative stress. Similar observations were made in our previous study with a cobalt-resistant *S. cerevisiae* strain, where the expression level of *COT1*, a gene encoding a major vacuolar cobalt-transporter, significantly increased in the cobalt-resistant strain, even in the absence of cobalt stress (Alkim et al., 2013).

We had shown in a previous chronological life span (CLS) study that H7 was a long-lived strain, compared to the reference strain (Arslan et al., 2018b). The link between oxidative stress-resistance, longevity and autophagy has been reported previously (Orozco et al., 2012). Thirty autophagy-related genes were up-regulated by more than twofold for H7. In particular, *ATG39* was increased 5.6-fold in H7. Atg39p is located in perinuclear ER (or the nuclear envelope) and induces autophagic sequestration in part of the nucleus. Atg39-dependent autophagy in the perinuclear ER/nucleus is required for cell survival under nitrogen-deprived conditions. Atg39p has a major role in perinuclear ER-phagy (Mochida et al., 2015). Although there was no change in expression level in the *ATG40* gene, its upstream mutation in H7 may have caused a significant change in autophagy. Besides the *ATG40* gene, *VTC1* gene of H7, which is vacuole-related, also has a missense mutation. *VTC1* encodes the regulatory subunit of the vacuolar transporter chaperone (VTC) complex which is an important constituent of autophagic tubes required for the scission of microautophagic vesicles from these tubes (Uttenweiler et al., 2006). In a previous study, we showed that an iron-stress-resistant evolved *S. cerevisiae* strain had mutations in *VBA2* (encodes a permease) and *VTC4* (encodes a VTC complex regulatory subunit) genes (Balaban et al., 2020). It is important to note that H7 and this iron-resistant evolved strain, which is also resistant to oxidative stress, have mutations on genes related to vacuolar functions. These mutations could be important for oxidative stress. The up-regulation of autophagy-related genes in H7 may enhance its autophagy activity, and mutations in vacuole-related genes may be useful to eliminate the degraded macromolecules *via* vacuoles.

One of the most important mutations in H7 is the nonsense mutation in the *NRG1* gene. Nrg1p is a transcriptional repressor encoded by *NRG1*. The nonsense mutation might lead to the synthesis of a truncated protein with a total or partial loss of its functionality. *NRG1* regulates 2.41% of the genes that were down-regulated by at least twofold, and 8.97% of the genes that were up-regulated by at least twofold in H7 (**Supplementary Table 5**). Nrg1p is a negative regulator of glucose-repressed genes and nrg1Δ mutants could utilize several different carbon sources (Zhou and Winston, 2001). It is important to note that Nrg1p controls the up-regulated genes in H7 that have a role in oxidative stress tolerance or that are induced by glucose limitation. Ten genes have been down-regulated by more than twofold in H7, and 33 genes have been up-regulated by more than twofold (**Supplementary Table 5**). Up-regulated genes regulated by *NRG1* play a role in oxidative stress tolerance or they are induced by a reaction to limited glucose availability – *CCP1* encodes mitochondrial cytochrome-c peroxidase, and it was up-regulated by 2.5-fold in H7 (**Supplementary Tables 5, 6**). Hydrogen peroxide exposure induces activation of the mitochondrial cytochrome-c peroxidase (Charizanis et al., 1999). *GSY1* encodes glycogen synthase (Farkas et al., 1990), and it was also up-regulated in H7 by 4.8-fold. *HXT2* encodes a high affinity, low-capacity glucose transporter and is induced and expressed under low-glucose conditions (Johnston and Kim, 2005). *HXT2* was up-regulated by 4.8-fold in H7. In addition to the genes that have a role in metabolic maintenance, genes encoding transcription factors were also up-regulated in H7, such as *HAP4*, *NRG2,* and *USV1* which are targets of *NRG1*.

A missense mutation was found in H7 on the *RSC30* gene which encodes a regulatory protein according to the YEASTRACT database (Teixeira et al., 2018). In H7, this gene regulates 5.32% of the down-regulated and 8.18% of up-regulated genes with a fold change higher than 2. *RSC30* is required for the proper regulation of cell wall/stress response and ribosomal protein genes (Neely and Workman, 2002). Our lyticase sensitivity assay results revealed that the evolved strain had significantly higher cell wall integrity than the reference strain (**Figure 10**), which may be associated with the missense mutation in *RSC30*.

Thirteen of the 14 genes that were up-regulated in H7 by at least sevenfold were found to be regulated by *SUA7,* with nine of them regulated by *SPT10*. *SUA7* encodes a yeast transcription factor TFIIB homolog and it has a function in transcription start site selection (Pinto et al., 1992). In addition, *SPT10* is known as a global regulator that binds to the histone upstream activating sequence elements (Eriksson et al., 2005).

AIM19, FIS1, IRC15, IKS1, GDH2, YGL052W, VBA1, FYV6, TPS1, VHS3, and *HSP82* are genes which have a missense point mutation, and which are also up-regulated in H7. According to the regulation enrichment analysis results using YEASTRACT database (Teixeira et al., 2018), it was found that the transcription factors Yap1p, Gcn4p, and Met31p have regulatory control on all these genes. Yap1p is a basic leucine zipper transcription factor required for oxidative stress tolerance and is activated by H_2O_2 (Cherry et al., 2012). Gcn4p is a key transcriptional activator of amino acid biosynthesis genes, and it plays a role in longevity and stress response (Mittal et al., 2017). Met31p is a zinc-finger DNA-binding transcription factor involved in the regulation of the methionine biosynthesis genes (Cherry et al., 2012). Among the genes regulated by these transcription factors, *IKS1* encodes a putative serine–threonine kinase and it is an Ira1p kinase suppressor. Deletion of *IKS1* gene causes hypersensitivity to copper sulfate (Dastidar et al., 2012) and a sorbate- resistant phenotype (Rieger et al., 1999). *IKS1* may be involved in the regulation of key pathways in acute stress defense (Ma et al., 2015). In H7, the mutation that occurred in the protein kinase domain of the protein encoded by *IKS1* could be important for oxidative stress resistance. Gdh2p, the NAD^+-dependent GDH (NAD-GDH; Gdh2) encoded by *GDH2*, catalyzes reversible oxidative deamination of glutamate to α-ketoglutarate and ammonia (Miller and Magasanik, 1990). Gdh2-dependent NAD^+ supply stimulates the growth at low temperature (Ballester-Tomás et al., 2015). In H7 genome, the mutation occurred in a region encoding the Leu/Phe/Val dehydrogenases active site of this gene. To our knowledge, there are no previous studies that describe such a mutation which warrants further investigation.

In this study, we successfully generated an oxidative stress-resistant and genetically stable *S. cerevisiae* strain *via* an evolutionary engineering strategy with heat pretreatment. Due to the nature of the stress and pretreatment condition, this strain is resistant to heat, freeze-thaw, ethanol, salt, iron, and cobalt stress conditions. Underlying mechanistic changes providing this adaptive resistance were elucidated with (i) differences in glycogen degradation, maltose, trehalose, glycerol, and acetate production levels; (ii) lyticase sensitivity assay that strongly supports the potential role of the cell wall in oxidative stress resistance of the evolved strain; (iii) comparative transcriptomic analysis showing changes in expression profiles in genes associated with autophagy, carbon metabolism, peroxisome and cell wall organization or biogenesis; (iv) comparative genomic analysis of the evolved strain showing mutations in diverse genes which are under the control of critical transcription factors. Investigation of the individual effects of the identified mutations in H7 genome *via* genome editing and reverse engineering strategies will be key toward a better understanding of the complex molecular mechanisms of oxidative stress resistance and specific genomic player(s). For this purpose, incorporation of the identified mutations in the reference strain as single mutations and/or their combinations, using novel and powerful genome editing strategies such as CRISPR-Cas9 is planned as the reverse engineering approach.

DATA AVAILABILITY STATEMENT

The datasets presented in this study can be found in online repositories. The names of the repository/repositories and accession number(s) can be found in the article/ **Supplementary Material**.

AUTHOR CONTRIBUTIONS

ZÇ: conceptualization, supervision, and funding acquisition. NK-Ö, BY, CA, MA, AT, HK, and EG: methodology. NK-Ö and BY: resources. NK-Ö, BY, and CA: data curation and writing – original draft preparation. NK-Ö, BY, and ZÇ: writing and review and editing and project administration. All authors contributed to the article and approved the submitted version.

FUNDING

This research was funded by the Scientific and Technological Research Council of Turkey, TUBITAK, (project no: 105T314, PI: ZC).

ACKNOWLEDGMENTS

We thank Hasan Tükenmez and Can Holyavkin for technical assistance with evolutionary engineering experiments and the whole-genome re-sequencing data, respectively. We also thank Ian Young (Department for Biomedical Research, University of Bern) for proofreading the manuscript.

SUPPLEMENTARY MATERIAL

The Supplementary Material for this article can be found online at: https://www.frontiersin.org/articles/10.3389/fmicb.2022.822864/full#supplementary-material

REFERENCES

Alexandre, H., Ansanay-Galeote, V., Dequin, S., and Blondin, B. (2001). Global gene expression during short-term ethanol stress in *Saccharomyces cerevisiae*. *FEBS Lett.* 498, 98–103. doi: 10.1016/s0014-5793(01)02503-0

Alkim, C., Benbadis, L., Yilmaz, U., Cakar, Z. P., and François, J. M. (2013). Mechanisms other than activation of the iron regulon account for the hyper-resistance to cobalt of a *Saccharomyces cerevisiae* strain obtained by evolutionary engineering. *Metallomics* 5, 1043–1060. doi: 10.1039/C3MT00107E

Allakhverdiev, S. I., Kreslavski, V. D., Klimov, V. V., Los, D. A., Carpentier, R., and Mohanty, P. (2008). Heat stress: an overview of molecular responses in photosynthesis. *Photosynth. Res.* 98, 541–550.

Arslan, M., Holyavkin, C., Kısakesen, H. İ, Topaloğlu, A., Sürmeli, Y., and Cakar, Z. P. (2018a). Physiological and Transcriptomic Analysis of a Chronologically Long-Lived *Saccharomyces cerevisiae* Strain Obtained by Evolutionary Engineering. *Mole. Biotechnol.* 60, 468–484. doi: 10.1007/s12033-018-0087-2

Arslan, M., Turanli-Yildiz, B., Yilmaz, B., Kocaefe, N., and Cakar, Z. P. (2018b). An improved semi-quantitative spot assay to analyse chronological lifespan in yeast. *Roman. Biotechnol. Lett.* 23:13551.

Balaban, B. G., Yilmaz, U., Alkim, C., Topaloglu, A., Kisakesen, H. I., Holyavkin, C., et al. (2020). Evolutionary Engineering of an Iron-Resistant *Saccharomyces cerevisiae* Mutant and Its Physiological and Molecular Characterization. *Microorgan.* 8:43. doi: 10.3390/microorganisms8010043

Ballester-Tomás, L., Randez-Gil, F., Pérez-Torrado, R., and Prieto, J. A. (2015). Redox engineering by ectopic expression ofglutamate dehydrogenase genes links NADPH availability and NADH oxidation with coldgrowth in *Saccharomyces cerevisiae*. *Microb. Cell Fact.* 14:100. doi: 10.1186/s12934-015-0289-2

Bayliak, M., Burdyliuk, N., and Lushchak, V. (2017). Growth on alpha-ketoglutarate increases oxidative stress resistance in the yeast *Saccharomyces cerevisiae*. *Internat. J. Microbiol.* 2017:5792192. doi: 10.1155/2017/5792192

Byndloss, M. X., Olsan, E. E., Rivera-Chávez, F., Tiffany, C. R., and Cevallos, S. A. (2017). Microbiota-activated PPAR-γ signaling inhibits dysbiotic *Enterobacteriaceae* expansion. *Science* 357, 570–575.

Çakar, Z. P., Alkım, C., Turanlı, B., Tokman, N., Akman, S., Sarıkaya, M., et al. (2009). Isolation of cobalt hyper-resistant mutants of *Saccharomyces cerevisiae* by in vivo evolutionary engineering approach. *J. Biotechnol.* 143, 130–138. doi: 10.1016/j.jbiotec.2009.06.024

Çakar, Z. P., Seker, U. O. S., Tamerler, C., Sonderegger, M., and Sauer, U. (2005). Evolutionary engineering of multiple-stress resistant *Saccharomyces cerevisiae*. *FEMS Yeast Res.* 5, 569–578. doi: 10.1016/j.femsyr.2004.10.010

Çakar, Z. P., Turanlı-Yıldız, B., Alkım, C., and Yılmaz, U. (2012). Evolutionary engineering of *Saccharomyces cerevisiae* for improved industrially important properties. *FEMS Yeast Res.* 12, 171–182. doi: 10.1111/j.1567-1364.2011.00775.x

Candas, D., and Li, J. J. (2014). MnSOD in oxidative stress response-potential regulation via mitochondrial protein influx. *Antioxid. Red. Signal.* 20, 1599–1617.

Charizanis, C., Juhnke, H., Krems, B., and Entian, K. D. (1999). The mitochondrial cytochrome c peroxidase Ccp1 of *Saccharomyces cerevisiae* is involved in conveying an oxidative stress signal to the transcription factor Pos9 (Skn7). *Mole. Gen. Genet. MGG.* 262, 437–447. doi: 10.1007/s004380051103

Cherry, J. M., Hong, E. L., Amundsen, C., Balakrishnan, R., Binkley, G., Chan, E. T., et al. (2012). Saccharomyces Genome Database: the genomics resource of budding yeast. *Nucleic Acids Res.* 40, D700–D705. doi: 10.1093/nar/gkr1029

Costa, V., and Moradas-Ferreira, P. (2001). Oxidative stress and signal transduction in *Saccharomyces cerevisiae*: insights into ageing, apoptosis and diseases. *Molecular Aspects of Medicine* 22, 217–246. doi: 10.1016/S0098-2997(01)00012-7

Cramp, D. G. (1967). New automated method for measuring glucose by glucose oxidase. *J. Clin. Pathol.* 20, 910L–912. doi: 10.1136/jcp.20.6.910

Dastidar, R. G., Hooda, J., Shah, A., Cao, T. M., Henke, R. M., and Zhang, L. (2012). The nuclear localization of SWI/SNF proteins is subjected to oxygen regulation. *Cell Biosci.* 2:30. doi: 10.1186/2045-3701-2-30

Davidson, J. F., Whyte, B., Bissinger, P. H., and Schiestl, R. H. (1996). Oxidative stress is involved in heat-induced cell death in *Saccharomyces cerevisiae*. *Proc. Natl. Acad. Sci.* 93, 5116–5121.

Eriksson, P. R., Mendiratta, G., McLaughlin, N. B., Wolfsberg, T. G., Mariño-Ramírez, L., Pompa, T. A., et al. (2005). Global regulation by the yeast Spt10 protein is mediated through chromatin structure and the histone upstream activating sequence elements. *Mole. Cell. Biol.* 25, 9127–9137. doi: 10.1128/MCB.25.20.9127-9137.2005

Espey, M. G. (2013). Role of oxygen gradients in shaping redox relationships between the human intestine and its microbiota. *Free Rad. Biol. Med.* 55, 130–140.

Faber, F., and Bäumler, A. J. (2014). The impact of intestinal inflammation on the nutritional environment of the gut microbiota. *Immunol. Lett.* 162, 48–53.

Farkas, I., Hardy, T. A., DePaoli-Roach, A. A., and Roach, P. J. (1990). Isolation of the GSY1 gene encoding yeast glycogen synthase and evidence for the existence of a second gene. *J. Biol. Chem.* 265, 20879–20886.

Finkel, T. (2005). Radical medicine: treating ageing to cure disease. *Nat. Rev. Mole. Cell Biol.* 2005:1763. doi: 10.1038/nrm1763

Finkel, T., and Holbrook, N. J. (2000). Oxidants, oxidative stress and the biology of ageing. *Nature* 408:239.

Förstermann, U. (2008). Oxidative stress in vascular disease: Causes, defense mechanisms and potential therapies. *Nat. Clin. Pract. Cardiovasc. Med.* 2008:1211. doi: 10.1038/ncpcardio1211

François, J., and Parrou, J. L. (2001). Reserve carbohydrates metabolism in the yeast *Saccharomyces cerevisiae*. *FEMS Microbiol. Rev.* 25, 125–145. doi: 10.1111/j.1574-6976.2001.tb00574.x

Gasch, A. P., Spellman, P. T., Kao, C. M., Carmel-Harel, O., Eisen, M. B., Storz, G., et al. (2000). Genomic Expression Programs in the Response of Yeast Cells to Environmental Changes. *Mole. Biol. Cell* 11, 4241–4257. doi: 10.1091/mbc.11.12.4241

Görlach, A., Bertram, K., Hudecova, S., and Krizanova, O. (2015). Calcium and ROS: a mutual interplay. *Redox Biol.* 6, 260–271.

Grant, C. M. (2001). Role of the glutathione/glutaredoxin and thioredoxin systems in yeast growth and response to stress conditions. *Mole. Microbiol.* 2001:2283. doi: 10.1046/j.1365-2958.2001.02283.x

Hacısalihoğlu, B., Holyavkin, C., Topaloğlu, A., Kısakesen, H. İ, and Cakar, Z. P. (2019). Genomic and transcriptomic analysis of a coniferyl aldehyde-resistant *Saccharomyces cerevisiae* strain obtained by evolutionary engineering. *FEMS Yeast Res.* 19:21. doi: 10.1093/femsyr/foz021

Hasan, R., Leroy, C., Isnard, A. D., Labarre, J., Boy-Marcotte, E., and Toledano, M. B. (2002). The control of the yeast H_2O_2 response by the Msn2/4 transcription factors. *Mole. Microbiol.* 45, 233–241. doi: 10.1046/j.1365-2958.2002.03011.x

Hong, S. Y., Roze, L. V., and Linz, J. E. (2013). Oxidative stress-related transcription factors in the regulation of secondary metabolism. *Toxins* 5, 683–702.

Huang, D. W., Sherman, B. T., and Lempicki, R. A. (2008). Bioinformatics enrichment tools: paths toward the comprehensive functional analysis of large gene lists. *Nucleic Acids Res.* 37, 1–13. doi: 10.1093/nar/gkn923

Huang, D. W., Sherman, B. T., and Lempicki, R. A. (2009). Systematic and integrative analysis of large gene lists using DAVID bioinformatics resources. *Nat. Prot.* 4, 44–57. doi: 10.1038/nprot.2008.211

Imlay, J. A. (2015). Transcription Factors That Defend Bacteria Against Reactive Oxygen Species. *Annu. Rev. Microb.* 2015:104322. doi: 10.1146/annurev-micro-091014-104322

Izawa, S., Inoue, Y., and Kimura, A. (1995). Oxidative stress response in yeast: effect of glutathione on adaptation to hydrogen peroxide stress in *Saccharomyces cerevisiae*. *FEBS Lett.* 368, 73–76. doi: 10.1016/0014-5793(95)00603-7

Jamieson, D. J. (1992). *Saccharomyces cerevisiae* has distinct adaptive responses to both hydrogen peroxide and menadione. *J. Bacteriol.* 174, 6678L–6681. doi: 10.1128/jb.174.20.6678-6681.1992

Jamieson, D. J. (1998). Oxidative stress responses of the yeast *Saccharomyces cerevisiae*. *Yeast* 14, 1511–1527. doi: 10.1002/(SICI)1097-0061(199812)14:16<1511::AID-YEA356<3.0.CO;2-S

Johnston, M., and Kim, J.-H. (2005). Glucose as a hormone: receptor-mediated glucose sensing in the yeast *Saccharomyces cerevisiae*. *Biochem. Soc. Trans.* 33, 247–252. doi: 10.1042/BST0330247

Jung, J.-Y., Kim, T.-Y., Ng, C.-Y., and Oh, M.-K. (2012). Characterization of GCY1 in *Saccharomyces cerevisiae* by metabolic profiling. *J. Appl. Microb.* 113, 1468–1478. doi: 10.1111/jam.12013

Küçükgöze, G., Alkım, C., Yılmaz, U., Kısakesen, H. I, Gündüz, S., Akman, S., et al. (2013). Evolutionary engineering and transcriptomic analysis of nickel-resistant *Saccharomyces cerevisiae*. *FEMS Yeast Res.* 13, 731–746. doi: 10.1111/1567-1364.12073

Kuranda, K., Leberre, V., Sokol, S., Palamarczyk, G., and François, J. (2006). Investigating the caffeine effects in the yeast *Saccharomyces cerevisiae* brings new insights into the connection between TOR, PKC and Ras/cAMP signalling pathways. *Mole. Microb.* 61, 1147–1166. doi: 10.1111/j.1365-2958.2006.05300.x

Lawrence, C. W. (1991). [18] Classical mutagenesis techniques. *Methods Enzymol.* 194, 273–281. doi: 10.1016/0076-6879(91)94021-4

Levin, D. E. (2005). Cell wall integrity signaling in *Saccharomyces cerevisiae*. *Microbiol. Mole. Biol. Rev.* 69, 262–291.

Li, J., Wuliji, O., Li, W., Jiang, Z. G., and Ghanbari, H. A. (2013). Oxidative stress and neurodegenerative disorders. *Internat. J. Mole. Sci.* 2013:141224438. doi: 10.3390/ijms141224438

Lih-Brody, L., Powell, S. R., Collier, K. P., Reddy, G. M., Cerchia, R., Kahn, E., et al. (1996). Increased oxidative stress and decreased antioxidant defenses in mucosa of inflammatory bowel disease. *Digest. Dis. Sci.* 1996:2093613. doi: 10.1007/BF02093613

Lindquist, J. (2016). *The Most Probable Number Method*. 1–4. Available online at: https://www.jlindquist.com/generalmicro/102dil3a.html (accessed October 12, 2016).

Lushchak, V. I. (2011). Adaptive response to oxidative stress: Bacteria, fungi, plants and animals. *Comparat. Biochem. Physiol. Part C* 153, 175–190.

Ma, C., Wei, X., Sun, C., Zhang, F., Xu, J., Zhao, X., et al. (2015). Improvement of acetic acid tolerance of Saccharomyces cerevisiae using a zinc-finger-based artificial transcription factor and identification of novel genes involved in acetic acid tolerance. *Appl. Microb. Biotechnol.* 99, 2441–2449. doi: 10.1007/s00253-014-6343-x

Miller, S. M., and Magasanik, B. (1990). Role of NAD-linked glutamate dehydrogenase in nitrogen metabolism in *Saccharomyces cerevisiae*. *J. Bacteriol.* 72, 4927L–4935. doi: 10.1128/jb.172.9.4927-4935.1990

Mittal, N., Guimaraes, J. C., Gross, T., Schmidt, A., Vina-Vilaseca, A., Nedialkova, D. D., et al. (2017). The Gcn4 transcription factor reduces protein synthesis capacity and extends yeast lifespan. *Nat. Comm.* 8:457. doi: 10.1038/s41467-017-00539-y

Mochida, K., Oikawa, Y., Kimura, Y., Kirisako, H., Hirano, H., Ohsumi, Y., et al. (2015). Receptor-mediated selective autophagy degrades the endoplasmic reticulum and the nucleus. *Nature* 522, 359–362. doi: 10.1038/nature14506

Molin, M., Norbeck, J., and Blomberg, A. (2003). Dihydroxyacetone kinases in *Saccharomyces cerevisiae* are involved in detoxification of dihydroxyacetone. *J. Biolog. Chem.* 278, 1415–1423. doi: 10.1074/jbc.M203030200

Morano, K. A., Grant, C. M., and Moye-Rowley, W. S. (2012). The response to heat shock and oxidative stress in *Saccharomyces cerevisiae*. *Genetics* 190, 1157–1195. doi: 10.1534/genetics.111.128033

Morano, K. A., Liu, P. C. C., and Thiele, D. J. (1998). Protein chaperones and the heat shock response in *Saccharomyces cerevisiae*. *Curr. Opin. Microb.* 1, 197–203. doi: 10.1016/S1369-5274(98)80011-8

Morimoto, R. I. (1998). Regulation of the heat shock transcriptional response: cross talk between a family of heat shock factors, molecular chaperones, and negative regulators. *Genes Dev.* 12, 3788–3796.

Mujahid, A., Yoshiki, Y., Akiba, Y., and Toyomizu, M. (2005). Superoxide radical production in chicken skeletal muscle induced by acute heat stress. *Poul. Sci.* 84, 307–314.

Neely, K. E., and Workman, J. L. (2002). The complexity of chromatin remodeling and its links to cancer. *Biochim. et. Biophys. Acta* 1603, 19–29. doi: 10.1016/S0304-419X(02)00067-7

Orozco, H., Matallana, E., and Aranda, A. (2012). Oxidative stress tolerance, adenylate cyclase, and autophagy are key players in the chronological life span of *Saccharomyces cerevisiae* during winemaking. *Appl. Env. Microb.* 78, 2748–2757. doi: 10.1128/AEM.07261-11

Paiva, S., Devaux, F., Barbosa, S., Jacq, C., and Casal, M. (2004). Ady2p is essential for the acetate permease activity in the yeast *Saccharomyces cerevisiae*. *Yeast* 21, 201–210. doi: 10.1002/yea.1056

Park, S. G., Cha, M. K., Jeong, W., and Kim, I. H. (2000). Distinct physiological functions of thiol peroxidase isoenzymes in *Saccharomyces cerevisiae*. *J. Biol. Chem.* 2000:5723. doi: 10.1074/jbc.275.8.5723

Parrou, J. L., and François, J. (1997). A Simplified Procedure for a Rapid and Reliable Assay of both Glycogen and Trehalose in Whole Yeast Cells. *Anal. Biochem.* 248, 186–188. doi: 10.1006/ABIO.1997.2138

Pavlik, P., Simon, M., Schuster, T., and Ruis, H. (1993). The glycerol kinase (GUT1) gene of *Saccharomyces cerevisiae*: cloning and characterization. *Curr. Genet.* 24, 21–25. doi: 10.1007/BF00324660

Pinto, I., Ware, D. E., and Hampsey, M. (1992). The yeast SUA7 gene encodes a homolog of human transcription factor TFIIB and is required for normal start site selection in vivo. *Cell* 68, 977–988. doi: 10.1016/0092-8674(92)90040-J

Pugh, T. A., Shah, J. C., Magee, P. T., and Clancy, M. J. (1989). Characterization and localization of the sporulation glucoamylase of *Saccharomyces cerevisiae*. *Biochim. et Biophys. Acta Prot. Struct.* 994, 200–209. doi: 10.1016/0167-4838(89)90294-X

R Core Team (2020). *R: A language and environment for statistical computing*. Vienna: R Foundation for Statistical Computing.

Rajvanshi, P. K., Arya, M., and Rajasekharan, R. (2017). The stress-regulatory transcription factors Msn2 and Msn4 regulate fatty acid oxidation in budding yeast. *J. Biol. Chem.* 292, 18628–18643. doi: 10.1074/jbc.M117.801704

Reuter, S., Gupta, S. C., Chaturvedi, M. M., and Aggarwal, B. B. (2010). Oxidative stress, inflammation, and cancer: How are they linked? *Free Rad. Biol. Med.* 2010:6. doi: 10.1016/j.freeradbiomed.2010.09.006

Rieger, K.-J., El-Alama, M., Stein, G., Bradshaw, C., Slonimski, P. P., and Maundrell, K. (1999). Chemotyping of yeast mutants using robotics. *Yeast* 15, 973–986. doi: 10.1002/(SICI)1097-0061(199907)15:10B<973::AID-YEA402<3.0.CO;2-L

Rikhvanov, E. G., Fedoseeva, I. V., Varakina, N. N., Rusaleva, T. M., sand Fedyaeva, A. V. (2014). Mechanism of *Saccharomyces cerevisiae* yeast cell death induced by heat shock. Effect of cycloheximide on thermotolerance. *Biochemistry* 79, 16–24. doi: 10.1134/S0006297914010039

Rivera-Chávez, F., Lopez, C. A., and Bäumler, A. J. (2017). Oxygen as a driver of gut dysbiosis. *Free Rad. Biol. Med.* 105, 93–101.

Rodríguez, A., De La Cera, T., Herrero, P., and Moreno, F. (2001). The hexokinase 2 protein regulates the expression of the GLK1, HXK1 and HXK2 genes of *Saccharomyces cerevisiae*. *Biochem. J.* 355, 625–631. doi: 10.1042/bj3550625

Rønnow, B., and Kielland-Brandt, M. C. (1993). GUT2, a gene for mitochondrial glycerol 3-phosphate dehydrogenase of *Saccharomyces cerevisiae*. *Yeast* 9, 1121–1130. doi: 10.1002/yea.320091013

Russek, E., and Colwell, R. R. (1983). Computation of most probable numbers. *Appl. Env. Microb.* 45, 1646–1650.

Sauer, U. (2001). Evolutionary Engineering of Industrially Important Microbial Phenotypes BT - Metabolic Engineering. *Adv. Biochem. Eng. Biotechnol.* 73, 129–169. doi: 10.1007/3-540-45300-8_7

Semchyshyn, H. M., Abrat, O. B., Miedzobrodzki, J., Inoue, Y., and Lushchak, V. I. (2011). Acetate but not propionate induces oxidative stress in bakers' yeast *Saccharomyces cerevisiae*. *Redox Rep.* 16, 15–23. doi: 10.1179/174329211X12968219310954

Seppä, L., and Makarow, M. (2005). Regulation and recovery of functions of *Saccharomyces cerevisiae* chaperone BiP/Kar2p after thermal insult. *Eukaryotic Cell* 4, 2008–2016. doi: 10.1128/EC.4.12.2008-2016.2005

Sokol, H., Leducq, V., Aschard, H., Pham, H.-P., Jegou, S., Landman, C., et al. (2017). Fungal microbiota dysbiosis in IBD. *Gut* 66, 1039L–1048. doi: 10.1136/gutjnl-2015-310746

Steels, E. L., Watson, K., and Parsons, P. G. (1992). Relationships between thermotolerance, oxidative stress responses and induction of stress proteins in human tumour cell lines. *Biochem. Pharm.* 44, 2123–2129.

Storz, G., Tartaglia, L. A., Farr, S. B., and Ames, B. N. (1990). Bacterial defenses against oxidative stress. *Trends Genet.* 1990:90278. doi: 10.1016/0168-9525(90)90278-E

Surmeli, Y., Holyavkin, C., Topaloglu, A., Arslan, M., Kisakesen, H. I., and Cakar, Z. P. (2019). Evolutionary engineering and molecular characterization of a caffeine-resistant *Saccharomyces cerevisiae* strain. *World J. Microb. Biotechnol.* 35, 1–16. doi: 10.1007/s11274-019-2762-2

Takahashi, H., McCaffery, J. M., Irizarry, R. A., and Boeke, J. D. (2006). Nucleocytosolic Acetyl-Coenzyme A Synthetase Is Required for Histone

Acetylation and Global Transcription. *Mole. Cell* 23, 207–217. doi: 10.1016/j.molcel.2006.05.040

Teixeira, M. C., Monteiro, P. T., Palma, M., Costa, C., Godinho, C. P., Pais, P., et al. (2018). YEASTRACT: an upgraded database for the analysis of transcription regulatory networks in *Saccharomyces cerevisiae*. *Nucleic Acids Res.* 46, D348–D353. doi: 10.1093/nar/gkx842

Terzioğlu, E., Alkım, C., Arslan, M., Balaban, B. G., Holyavkin, C., Kısakesen, H. İ., et al. (2020). Genomic, transcriptomic and physiological analyses of silver-resistant *Saccharomyces cerevisiae* obtained by evolutionary engineering. *Yeast* 37, 413–426. doi: 10.1002/yea.3514

Turanlı-Yıldız, B., Benbadis, L., Alkım, C., Sezgin, T., Akşit, A., Gökçe, A., et al. (2017). In vivo evolutionary engineering for ethanol-tolerance of *Saccharomyces cerevisiae* haploid cells triggers diploidization. *J. Biosci. Bioeng.* 124, 309–318. doi: 10.1016/j.jbiosc.2017.04.012

Ueda, M., Mozaffar, S., and Tanaka, A. (1990). [72] Catalase from Candida boidinii 2201. *Methods Enzymol.* 188, 463–467. doi: 10.1016/0076-6879(90)88074-K

Uttenweiler, A., Schwarz, H., Neumann, H., and Mayer, A. (2006). The Vacuolar Transporter Chaperone (VTC) Complex Is Required for Microautophagy. *Mole. Biol. Cell* 18, 166–175. doi: 10.1091/mbc.e06-08-0664

Verghese, J., Abrams, J., Wang, Y., and Morano, K. A. (2012). Biology of the heat shock response and protein chaperones: budding yeast (*Saccharomyces cerevisiae*) as a model system. *Microb. Mole. Biol. Rev.* 76, 115–158. doi: 10.1128/MMBR.05018-11

Wahid, A. (2007). Physiological implications of metabolite biosynthesis for net assimilation and heat-stress tolerance of sugarcane (*Saccharum officinarum*) sprouts. *J. Plant Res.* 120, 219–228.

Walkey, C. J., Luo, Z., Madilao, L. L., and van Vuuren, H. J. J. (2012). The fermentation stress response protein Aaf1p/Yml081Wp regulates acetate production in *Saccharomyces cerevisiae*. *PLoS One* 7:e51551–e51551. doi: 10.1371/journal.pone.0051551

Wieser, R., Adam, G., Wagner, A., Schuller, C., Marchler, G., Ruis, H., et al. (1991). Heat shock factor-independent heat control of transcription of the CTT1 gene encoding the cytosolic catalase T of *Saccharomyces cerevisiae*. *J. Biol. Chem.* 266, 12406–12411.

Yang, L., Tan, G. Y., Fu, Y. Q., Feng, J. H., and Zhang, M. H. (2010). Effects of acute heat stress and subsequent stress removal on function of hepatic mitochondrial respiration, ROS production and lipid peroxidation in broiler chickens. *Comparat. Biochem. Physiol. Part C* 151, 204–208.

Zhou, H., and Winston, F. (2001). NRG1 is required for glucose repression of the SUC2 and GAL genes of *Saccharomyces cerevisiae*. *BMC Genet.* 2:5. doi: 10.1186/1471-2156-2-5

Conflict of Interest: The authors declare that the research was conducted in the absence of any commercial or financial relationships that could be construed as a potential conflict of interest.

Publisher's Note: All claims expressed in this article are solely those of the authors and do not necessarily represent those of their affiliated organizations, or those of the publisher, the editors and the reviewers. Any product that may be evaluated in this article, or claim that may be made by its manufacturer, is not guaranteed or endorsed by the publisher.

Citation: Kocaefe-Özşen N, Yilmaz B, Alkım C, Arslan M, Topaloğlu A, Kısakesen Hİ, Gülsev E and Çakar ZP (2022) Physiological and Molecular Characterization of an Oxidative Stress-Resistant Saccharomyces cerevisiae Strain Obtained by Evolutionary Engineering. Front. Microbiol. 13:822864. doi: 10.3389/fmicb.2022.822864

frontiers in Microbiology

ORIGINAL RESEARCH
published: 02 March 2022
doi: 10.3389/fmicb.2022.825121

Identification and Functional Analysis of GTP Cyclohydrolase II in *Candida glabrata* in Response to Nitrosative Stress

*Ryo Nasuno[1], Soma Suzuki[1], Sayoko Oiki[2], Daisuke Hagiwara[2,3] and Hiroshi Takagi[1]**

[1] Division of Biological Science, Graduate School of Science and Technology, Nara Institute of Science and Technology, Ikoma, Japan, [2] Faculty of Life and Environmental Sciences, University of Tsukuba, Tsukuba, Japan, [3] Microbiology Research Center for Sustainability, University of Tsukuba, Tsukuba, Japan

Reactive nitrogen species (RNS) are signal molecules involved in various biological events; however, excess levels of RNS cause nitrosative stress, leading to cell death and/or cellular dysfunction. During the process of infection, pathogens are exposed to nitrosative stress induced by host-derived RNS. Therefore, the nitrosative stress resistance mechanisms of pathogenic microorganisms are important for their infection and pathogenicity, and could be promising targets for antibiotics. Previously, we demonstrated that the *RIB1* gene encoding GTP cyclohydrolase II (GCH2), which catalyzes the first step of the riboflavin biosynthesis pathway, is important for nitrosative stress resistance in the yeast *Saccharomyces cerevisiae*. Here, we identified and characterized the *RIB1* gene in the opportunistic pathogenic yeast *Candida glabrata*. Our genetic and biochemical analyses indicated that the open reading frame of CAGL0F04279g functions as *RIB1* in *C. glabrata* (*CgRIB1*). Subsequently, we analyzed the effect of *CgRIB1* on nitrosative stress resistance by a growth test in the presence of RNS. Overexpression or deletion of *CgRIB1* increased or decreased the nitrosative stress resistance of *C. glabrata*, respectively, indicating that GCH2 confers nitrosative stress resistance on yeast cells. Moreover, we showed that the proliferation of *C. glabrata* in cultures of macrophage-like cells required the GCH2-dependent nitrosative stress detoxifying mechanism. Additionally, an infection assay using silkworms as model host organisms indicated that *CgRIB1* is indispensable for the virulence of *C. glabrata*. Our findings suggest that the GCH2-dependent nitrosative stress detoxifying mechanism is a promising target for the development of novel antibiotics.

Keywords: ***Candida glabrata*, nitric oxide, GTP cyclohydrolase II, riboflavin, macrophage, silkworm**

OPEN ACCESS

Edited by:
Nuno Pereira Mira, University of Lisbon, Portugal

Reviewed by:
Miguel Cacho Teixeira, University of Lisbon, Portugal
Jorge Amich, Laboratorio de Referencia de Micología, Centro Nacional de Microbiologia, Instituto de Salud Carlos III, Spain
Sascha Brunke, Leibniz Institute for Natural Product Research and Infection Biology, Germany

****Correspondence:***
Hiroshi Takagi
hiro@bs.naist.jp

Specialty section:
This article was submitted to Microbial Physiology and Metabolism, a section of the journal Frontiers in Microbiology

Received: *30 November 2021*
Accepted: *14 January 2022*
Published: *02 March 2022*

Citation:
Nasuno R, Suzuki S, Oiki S, Hagiwara D and Takagi H (2022) Identification and Functional Analysis of GTP Cyclohydrolase II in Candida glabrata in Response to Nitrosative Stress. Front. Microbiol. 13:825121. doi: 10.3389/fmicb.2022.825121

INTRODUCTION

Reactive nitrogen species (RNS) including nitric oxide (NO) function as ubiquitous signal molecules in a variety of biological phenomena in many kinds of organisms including mammals, plants, and microorganisms (Pacher et al., 2007; Wink et al., 2011). For example, NO regulates the relaxation of vascular smooth muscle cells and neurotransmission in mammals

(Ferrer-Sueta et al., 2018). We previously reported that NO conferred high-temperature stress resistance on cells of the yeast *Saccharomyces cerevisiae* (Nishimura et al., 2013; Nasuno et al., 2014). NO exerts its functions by the activation of soluble guanylate cyclase (sGC) through its binding to the heme of sGC in mammals (Francis et al., 2010; Hunt and Lehnert, 2015). NO also mediates post-translational modification, such as *S*-nitrosylation and oxidation of cysteine residues on proteins to induces certain biological activities (Bai et al., 2011; Nakato et al., 2015). The NO_2 radical, one of the most unstable RNS derived from NO, induces the nitration of tyrosine residues on proteins, leading to loss, change or even gain of function (Kang et al., 2015; Porter et al., 2020).

In contrast to the physiological roles of RNS as signals described above, excess concentrations of RNS are toxic and cause nitrosative stress, leading to cellular dysfunction and/or cell death (Boscá and Hortelano, 1999; Pacher et al., 2007; Yoshikawa et al., 2016). Animal defense systems use nitrosative stress induced by RNS as a weapon to kill pathogens. Macrophages activated during infection release NO, and then NO and NO-derived RNS like peroxynitrite attack pathogenic microorganisms (von Bargen et al., 2011). Therefore, the nitrosative stress detoxifying mechanisms in pathogens are important for their infectivity and/or pathogenicity. A previous study showed that one of the important NO-degrading enzymes, NO reductase, is involved in the virulence of *Pseudomonas aeruginosa*, by an infection assay using the silkworm *Bombyx mori* as a model host organism (Arai and Iiyama, 2013). Flavohemoglobin (fHb) is another NO detoxification system, which degrades NO oxidatively or reductively under aerobic or anaerobic conditions, respectively (Gardner et al., 1998; Kim et al., 1999). A previous report using the pathogenic fungus *Candida albicans* indicated that the survival of mice infected with a *C. albicans* strain lacking fHb is significantly higher than that infected with the wild-type strain, suggesting that the fHb deficiency reduces the virulence of *C. albicans* (Hromatka et al., 2005).

Recently, we discovered a novel nitrosative stress resistance system dependent on GTP cyclohydrolase II (GCH2) in the yeast *S. cerevisiae* (Anam et al., 2020). GCH2, the first-step and rate-limiting enzyme of the riboflavin (RF) biosynthesis pathway, converts its substrate GTP into 2,5-diamino-6-(5-phospo-d-ribosylamino)-pyrimidin-4(3H)-one (DARP); then DARP scavenges NO, leading to nitrosative stress resistance. The *RIB1* gene encoding GCH2 is conserved among a wide range of microorganisms including bacteria, yeasts, and fungi, but not in mammals. Therefore, GCH2 would be a promising target protein for development of novel antibiotics.

The asexual and haploid yeast *Candida glabrata* is an opportunistic pathogen causing candidiasis especially in patients with immunocompromised state, with diabetes or cancer, treated with antimicrobials, and using the medical devices in surgery like catheters (Malani et al., 2005; Antinori et al., 2016). After *C. albicans*, *C. glabrata* is the second most frequently isolated *Candida* species causing invasive candidiasis (Hassan et al., 2021). Although *C. glabrata* is less virulent than other *Candida* species, such as *C. albicans*, it causes high mortality when the immune systems of patients are suppressed by underlying diseases like acquired immune deficiency syndrome (AIDS), treatment with immunosuppressive drugs, or aging (Hassan et al., 2021). *Candida* species including *C. glabrata* cause catheter-related bloodstream infections, which is a life-threatening complication, in the patients using catheters for parenteral nutrition (Phua et al., 2019). *C. glabrata* has unique characteristics especially during infection. Several cytokines are produced when organisms are infected with pathogenic microorganisms like *C. albicans* or *Mycobacterium tuberculosis*, leading to the activation of macrophages and maturation of phagolysosomes (Lionakis and Netea, 2013). When macrophages come into contact with pathogenic microbes, various saccharides including mannan, glucan, key structural components of fungi and yeasts, and lipopolysaccharide (LPS), a key component of bacterial membranes, bind to the specific receptors on the macrophage, activating it (Lionakis and Netea, 2013). The cytokine production induced by infection with *C. glabrata* is clearly lower than that by *C. albicans* (Seider et al., 2011). Whereas, the infection with *C. glabrata* does not cause NO production from macrophages unlike *C. albicans* (Kaur et al., 2007), even though human osteoblasts infected with *C. glabrata* produce NO (Muñoz-Duarte et al., 2016). Additionally, an *in vitro* infection assay demonstrated that *C. glabrata* was much less toxic to macrophages than *C. albicans*, despite the fact that *C. glabrata* was more effectively phagocytosed by macrophages than *C. albicans* (Dementhon et al., 2012). Further studies indicated that *C. glabrata* could even replicate inside macrophage cells (Seider et al., 2011). Importantly, *C. glabrata* is relatively resistant to azole type antifungals, the most widely used class of antifungal drugs, due to its energy-dependent efflux system (Parkinson et al., 1995). Therefore, it is highly desirable to discover novel antifungals that would be effective against *C. glabrata*, and/or a feasible drug target for that species.

Here, we identified the gene encoding GCH2 and characterized the GCH2-dependent NO resistance system in *C. glabrata*. Furthermore, we demonstrated that the NO detoxifying mechanism mediated by GCH2 was essential for the virulence of *C. glabrata* with infection assays using macrophage cultures and silkworms.

MATERIALS AND METHODS

Strains, Plasmids, and Medium

Candida glabrata KUE100-1 strain with a CBS138 background (Ueno et al., 2007) was used as a wild-type (WT) strain. The strain lacking CAGL0F04279g was constructed as follows. The DNA fragment from 500 bp upstream to 500 bp downstream of CAGL0F04279g was introduced to a plasmid pUC18 by PCR and InFusion reaction (Clontech, Mountain View, CA, United States) using pUC18 and the genomic DNA of WT strain as templates and primers listed in **Supplementary Table 1**. The resultant plasmid pUC18-CAGL0F04279g was linearized to remove the open reading frame (ORF) of CAGL0F04279g by the inverse PCR and then conjugated to a *natNT2* transformation marker

from pFA6a-natNT2, generating the plasmid pUC18-ΔCAGL0F04279g-natNT2. The DNA fragment consisting of 500 bp upstream region of CAGL0F04279g, a natNT2 transformation marker, and 500 bp downstream region of CAGL0F04279g was amplified by PCR using pUC18-ΔCAGL0F04279g-natNT2 as a template and the primers listed in **Supplementary Table 1**, and then introduced to WT cells for homologous recombination. The conventional colony-direct PCR was performed to analyze the transformants. The clones showing the genotype of recombination were identified as the *rib1*Δ strain, as described in detail in the results section. Subsequently, a plasmid pUC18-CAGL0F04279g was linearized to remove the ORF of CAGL0F04279g by the inverse PCR and then conjugated to a *kanMX6* transformation marker from pFA6a-kanMX6, to generate the plasmid pUC18-ΔCAGL0F04279g-kanMX6 harboring the 500 bp upstream region of CAGL0F04279g, a *kanMX6* transformation marker, and 500 bp downstream region of CAGL0F04279g, tandemly. The *rib1*Δ strain was transformed with the DNA fragment consisting of the DNA sequence of 500 bp upstream of CAGL0F04279g, a *kanMX6* transformation marker, and 500 bp downstream of CAGL0F04279g amplified from pUC18-ΔCAGL0F04279g-kanMX6. The resultant transformants were analyzed by the conventional colony-direct PCR analysis. In order to delete *YHB1*, pUC18-YHB1-natNT2 harboring the 500 bp upstream region of *YHB1,* a *natNT2* transformation marker, and 500 bp downstream region of *YHB1*, tandemly, was constructed using the primers listed in **Supplementary Table 1**, pUC18, and pFA6a-natNT2 in the similar way to the construction of pUC18-ΔCAGL0F04279g-natNT2. The DNA fragment consisting of the DNA sequence of 500 bp upstream of *YHB1*, a *natNT2* transformation marker, and 500 bp downstream of *YHB1* amplified from pUC18-YHB1-natNT2 was introduced to WT cells.

A centromere-type plasmid pRS313 (ATCC) was introduced to complement the histidine auxotrophy of *C. glabrata* used in this study. A centromere-type plasmid pCU-PDC1 was used for gene expression in *C glabrata* (Zordan et al., 2013). The coding region including epitope tag in pET53-CAGL0F04279g, which was constructed as described below, was amplified by PCR using the primers listed in **Supplementary Table 1**, and then introduced into pCU-PDC1, generating pCU-PDC1-CAGL0F04279g to express CAGL0F04279g under the control of the *PDC1* promoter. The plasmid pCU-PDC1-CAGL0F04279g was also used to overexpress CAGL0F04279g in the WT strain. In order to express *RIB1* from *S. cerevisiae*, the previously constructed plasmid pET53-RIB1 (Anam et al., 2020) was used as a template, followed by the same manipulation as the case of CAGL0F04279g.

Candida glabrata strains were cultured in a nutrient-rich medium YPD (1% yeast extract, 2% peptone, and 2% glucose) or a synthetic medium SD (2% glucose, 0.5% ammonium sulfate, 0.17% yeast nitrogen base without ammonium sulfate and amino acids) with pH 5.5 at 37°C in the presence of 50 μM RF, 200 μg/mL G418, 200 μg/mL nourseothricin, or 2% agar if necessary.

The primers, yeast strains, and plasmids used in this study were listed in **Supplementary Tables 1–3**, respectively.

Quantitative PCR to Determine the Copy Number of CAGL0F04279g

The ORF of the *ACT1* gene was amplified from the genomic DNA of the WT and then inserted into the plasmid pUC18-CAGL0F04279g by PCR using the primer listed in **Supplementary Table 1** and InFusion reaction, generating the plasmid pUC18-CAGL0F04279g-*ACT1*. The genomic DNA of each strain of *C. glabrata* was extracted using Dr. GenTLE^{TM} (from Yeast) High Recovery (TaKaRa Bio, Shiga, Japan) following the manufacturer's instruction. A quantitative PCR with Real-Time PCR System QuantStudio 3 (Qiagen, Hilden, Germany) and SsoAdvanced Universal SYBR Green Supermix (Bio-Rad, Hercules, CA, United States), using the genomic DNA as a template and primers listed in **Supplementary Table 1**, was performed in order to determine the copy number of CAGL0F04279g in each strain. The copy number of CAGL0F04279g and *ACT1* were calculated from each *Ct* value using the standard curve using the plasmid pUC18-CAGL0F04279g-*ACT1* as a template. The obtained copy number of CAGL0F04279g was normalized by that of *ACT1*.

Phenotypic Analysis of *Candida glabrata* on Solid Medium

Yeast cells were cultured in SD medium containing 50 μM RF until exponential growth phase. The serial dilutions were spotted on to SD solid medium with pH 5.5 and then cultured at 37°C. Fifty μM RF or the indicated concentration of sodium nitrite was added to solid medium to analyze the RF auxotrophy or nitrosative stress resistance, respectively.

Analysis of GTP Cyclohydrolase II Enzymatic Activity

The CAGL0F04279g ORF was cloned into a plasmid pET53 by BP and LR reactions in Gateway technology (Invitrogen, Carlsbad, CA, United States) and PCR with the primers listed in **Supplementary Table 1**. The resultant plasmid pET53-CAGL0F04279g was introduced into *Escherichia coli* BL21 (DE3) strain. The transformant cells were cultured in LB medium with 100 μg/mL ampicillin until 0.8 of OD_{600} and then 0.1 mM isopropyl-β-D-thiogalactopyranoside was added, followed by further incubation at 30°C for 16 h. The harvested cells were washed with and suspended in 20 mM sodium phosphate (pH 7.4), 500 mM NaCl (Buffer A) and then disrupted by sonication. The supernatant after centrifugation was subjected to purification using Ni Sepharose 6 Fast Flow (Cytiva, Tokyo, Japan). Eluate with Buffer A containing 500 mM imidazole was dialyzed against 50 mM Tris–HCl (pH 8.0), 1 mM TCEP, 10% glycerol and then the sample containing the recombinant protein from CAGL0F04279g was used further analyses. The purity was analyzed by SDS-PAGE and CBB staining.

The recombinant enzyme was incubated in the mixture containing 100 mM Tris–HCl (pH 8.8), 5 mM $MgCl_2$, 2.5 mM dithiothreitol, and 1 mM GTP at 37°C for 30 min. Fifty μL of

the stop solution containing 1% diacetyl and 15% trichloroacetic acid was added and then incubated at 37°C for 70 min. The fluorescence intensity of the supernatant after centrifugation was measured using a microplate reader TriStar LB942 (Berthold Technologies, Bad Wildbad, Germany) with an excitation filter F355 and emission filter F460. The standard curve of 6,7-dimethylpterin was drawn to quantify generated DARP. One unit of the specific activity of GTPCH2 was defined as the amount of enzyme to produce 1 μmol of DARP per min, which was calculated using the value at 15 min incubation.

Yeast cells cultured in SD with RF for 24 h were resuspended in 20 mM sodium phosphate buffer (pH 7.4) containing 0.5 M NaCl, followed by cell disruption using Multi-beads shocker (Yasui Kikai, Osaka, Japan) with glass beads. The supernatant after centrifuge was collected and then the GCH2 activity in it was analyzed as described above.

In vitro Nitric Oxide Quenching Assay

The recombinant protein expressed from CAGL0F04279g was incubated for 30 min at 37°C with or without GTP in the same condition as the GCH2 activity assay described above. Subsequently, 7 μM 4-amino-5-methylamino-2′;,7′-difluorofluorescein (DAF-FM) and 400 μM 1-hydroxy-2-oxo-3-(3-aminopropyl)-3-isopropyl-1-triazene (NOC-5) was added and then further incubated at room temperature and the fluorescence intensity was monitored to estimate the remaining NO in solution over time using a microplate reader TriStar LB942 (Berthold Technologies, Bad Wildbad, Germany) with an excitation filter F485 and emission filter F535.

Culture of Macrophage-Like Cells

Dulbecco's modified Eagle medium (DMEM) with 4.5 mg/L glucose, 4 mM L-glutamine, 15 mg/L phenol red, and 25 mM HEPES (FUJIFILM Wako Pure Chemical, Osaka, Japan) supplemented with 1/100 volume of Antibiotic-Antimycotic Mixed Stock Solution (100×) (Stabilized) (Nacalai Tesque, Kyoto, Japan), 1/100 volume of MEM Non-Essential Amino Acids Solution (100×) (Nacalai Tesque), and 1/10 volume of Fetal Bovine Serum, French (FBS, French) (MP Biomedicals, Irvine, CA, United States) was used as DMEM-A in this study. DMEM with 4.5 mg/L glucose, 4 mM L-glutamine, and 25 mM HEPES (FUJIFILM Wako Pure Chemical, Osaka, Japan) supplemented with 1/10 volume of FBS, French was also used as DMEM-B.

Macrophage-like cells RAW264.7 (ATCC) were cultured in DMEM-A at 37°C with 5% CO_2. After 3 passages, cells were resuspended in DMEM-B and then 2.5×10^4 cells adhered to a polystyrene cell culture plate were further cultured for 24 h in the presence of 100 ng/mL LPS, 100 μM NOS inhibitor N^G-nitro-L-arginine methyl ester (NAME), or 100 μg/mL RF if necessary. The supernatant of RAW264.7 cell culture in DMEM-B was reacted with 2.5 μM DAF-FM and then the fluorescence was measured using a microplate reader TriStar LB942 (Berthold Technologies, Bad Wildbad, Germany) with an excitation filter F485 and emission filter F535.

Each strain of *C. glabrata* cultured in SD medium with RF was washed and then 1.2×10^5 cells of yeast were added to 2.5×10^4 cells of RAW264.7, which were cultured in DMEM-A and resuspended in DMEM-B as described above, followed by further culture in DMEM-B for 2 h in the presence of LPS, NAME, and RF if necessary. Subsequently, RAW264.7 cells were washed with 1 mL of PBS twice and cultured in DMEM-B for the indicated time in the presence of LPS, NAME, and RF if necessary. After removal of medium, macrophage-like cells were incubated in 0.1% Triton X-100 for 1 min for cell lysis and the supernatant was spread onto YPD plate. The number of colonies generated after a few days culture at 37°C were counted to estimate the viable cell number of yeast inside macrophage.

Silkworm Infection Assay

Candida glabrata strains were cultured in SC-Ura-His medium containing 50 μM RF (WT, *rib1*ΔΔ, *yhb1*Δ) at 37°C for 2 days. Cells were harvested and resuspended in 0.05% Tween 20/0.6% NaCl at 2×10^8/mL. Red food coloring agent was added to the suspensions.

Four-molt silkworms and SILKMATE 2S were purchased from Ehime Sansyu (Ehime, Japan). Silkworms (the first day of fifth-instar larvae) were fed with SILKMATE 2S at 25°C for 2 days, followed by fasting for a day. The larvae were injected with 50 μL of fungal suspensions into intra-hemolymph using a 29-gage needle. After infection, the larvae were maintained without food at 30°C and survival percent was monitored for 4 days. Twelve silkworms were used for each strain. Statistical analyses of the survival percent were performed using the Kaplan-Meier method (Cochran–Mantel–Haenszel).

RESULTS

Candida glabrata Harbors Two Copies of Putative *RIB1* Gene CAGL0F04279g

A previous study determined the genomic DNA sequence of the *C. glabrata* CBS138 strain, indicating that the ORF of CAGL0F04279g in *C. glabrata* is homologous to the *RIB1* gene in *S. cerevisiae* (Dujon et al., 2004). Our BLAST search using an expected amino acid sequence translated from CAGL0F04279g, whose length is 296 amino acids, indicated that the protein encoded by CAGL0F04279g exhibited 79.6% of identity and 1.0×10^{-177} of *e*-value against GCH2 encoded by *RIB1* gene in *S. cerevisiae*, which consists of 345 amino acids. Therefore, we hypothesized that the ORF of CAGL0F04279g functions as the *RIB1* gene encoding GCH2 in *C. glabrata* and then analyzed a *C. glabrata* strain lacking CAGL0F04279g.

First, we deleted CAGL0F04279g by homologous recombination with a *natNT2* transformation marker using a WT strain as a host. The resultant transformants were analyzed by conventional PCR. Surprisingly, all candidate clones of the CAGL0F04279g disruptants exhibited not only the genotype of recombination with a *natNT2* marker but also the same genotype as the WT strain (**Figure 1A**). These results suggest that *C. glabrata* CBS138 strain possesses two or more copies of CAGL0F04279g, even though the previous genomic analysis suggested that there is only one copy of CAGL0F04279g.

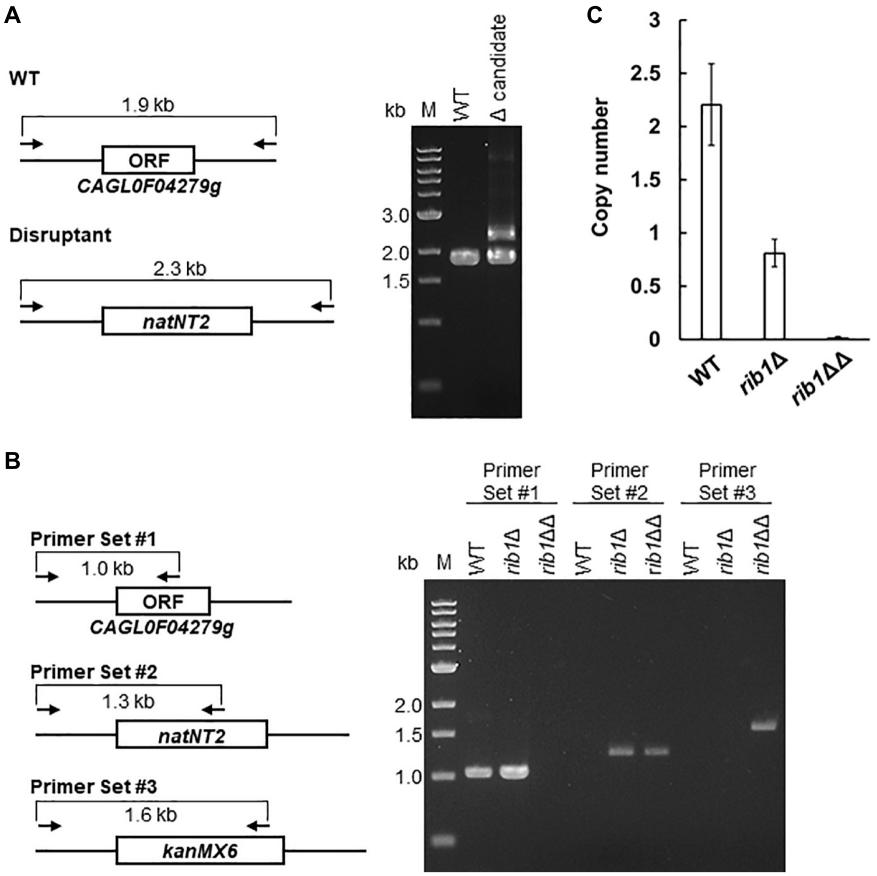

FIGURE 1 | Deletion and copy number determination of CAGL0F04279g. **(A)** The result of PCR analysis of the transformants generated by the homologous recombination with a *natNT2* marker using the WT rain as a host is shown, with the expected genetic structure in the locus of CAGL0F04279g in WT and disruptant strains. Each arrow indicates the primers for PCR analysis. The expected length of amplified DNA fragment is indicated. **(B)** The result of PCR analysis of the candidate clones generated by the additional transformation with a *kanMX6* marker was shown, with the expected genetic structure in the locus of CAGL0F04279g in WT and disruptant. Each arrow indicates the primers for PCR analysis. The expected length of amplified DNA fragment was indicated. **(C)** Quantitative PCR analysis to determine the copy number of CAGL0F04279g. The copy number of CAGL0F04279g calculated using a standard curve was normalized to the copy number of *ACT1*. The values are the means and standard deviations of three independent experiments.

Subsequently, we deleted an additional copy of CAGL0F04279g using the clones showing both WT and disruptant genotypes (*rib1*Δ) as a host strain by a homologous recombination using a *kanMX6* transformation marker. As a result of PCR analysis, the resultant transformants (*rib1*ΔΔ) exhibited both the genotype of recombination with *natNT2* and that with *kanMX6*, indicating that the ORF of CAGL0F04279g no longer existed in the genome of the *rib1*ΔΔ strain (**Figure 1B**). We further measured the copy number of CAGL0F04279g by a quantitative PCR. An absolute quantification of the copy numbers of CAGL0F04279g with a standard curve, which was drawn with the plasmid harboring CAGL0F04279g using *ACT1* as a reference gene, demonstrated that the WT strain possessed two copies of CAGL0F04279g; in contrast, the *rib1*Δ strain possessed only one copy of CAGL0F04279g (**Figure 1C**). Next, we determined whether the DNA sequences of the two copies of CAGL0F04279g were the same or different. A DNA fragment from 509 bp upstream to 504 bp downstream of the ORF of CAGL0F04279g was cloned into plasmid pUC18. The independent clones of resultant plasmids were subjected to DNA sequencing analysis, and 8 independent clones exhibited the exact same DNA sequences. This suggests that the two copies of CAGL0F04279g in *C. glabrata* harbor the same DNA sequence.

The finding that *C. glabrata* harbors two copies of CAGL0F04279g in its genome is inconsistent with a previous report (Dujon et al., 2004). For further analyses in the present study, the *rib1*ΔΔ strain, from which both copies of CAGL0F04279g were deleted, was used as a CAGL0F04279g disruptant. The *rib1*Δ strain, from which one copy of CAGL0F04279g was deleted, was also used as a single-copy disruptant in additional experiments described below.

CAGL0F04279g Functions as the *RIB1* Gene Encoding GTP Cyclohydrolase II in *Candida glabrata*

The RF auxotrophic phenotypes of the WT, *rib1*Δ, and *rib1*ΔΔ strains were analyzed (**Figure 2A**). All strains grew

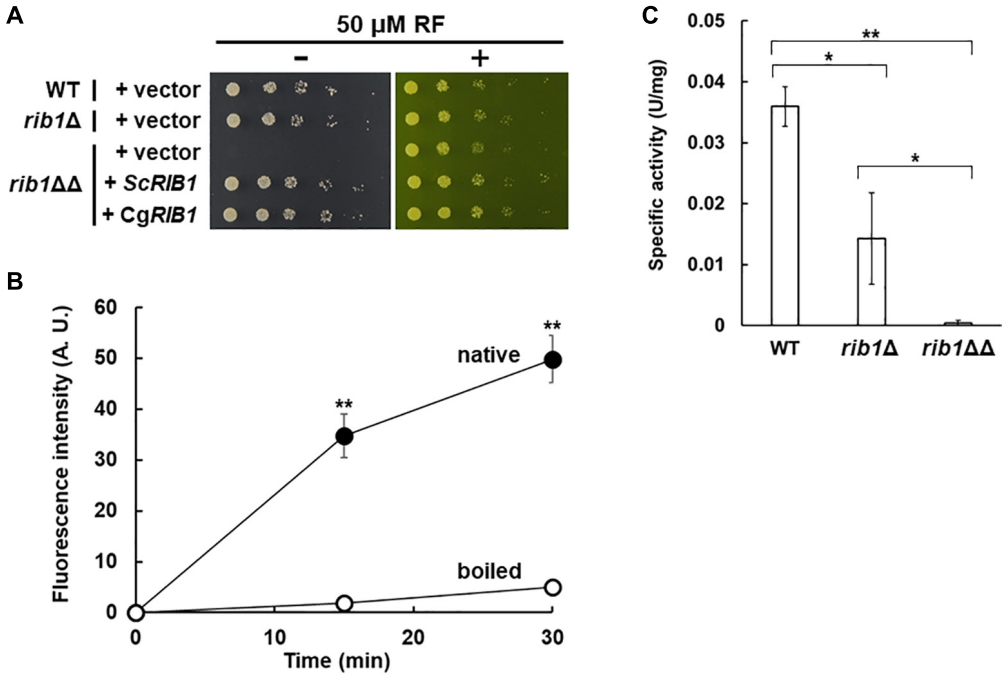

FIGURE 2 | Identification of *CgRIB1* encoding GCH2 in *C. glabrata*. **(A)** Yeast cells were cultured in SD medium until exponential phase. Serial dilutions of each strain were spotted onto SD medium with pH 5.5 in the presence or absence of RF and then further cultured. **(B)** The protein expressed from CAGL0F04279g in *E. coli* was purified. The purified protein was incubated in the reaction mixture over time, with or without pre-boiling. The resultant solution was reacted with diacetyl and then the fluorescence was measured. The fluorescence at time of 0 min was used as a blank in each sample. **(C)** Yeast cell-free extract prepared from cells cultured in SD medium for 24 h was used as a crude enzyme. The values in panels **(B,C)** are the means and standard deviations of three independent experiments. $^{*}p < 0.05$; $^{**}p < 0.001$ by Student's *t*-test.

at almost the same growth rate on a medium containing RF. However, in the absence of RF, the *rib1*ΔΔ strain did not grow while the WT and *rib1*Δ strains grew at the same rate. Importantly, the growth defect of the *rib1*ΔΔ strain was compensated for by the expression of the *RIB1* gene from *S. cerevisiae* (*ScRIB1*) or CAGL0F04279g. Subsequently, the enzymatic activity of the gene product of CAGL0F04279g was analyzed using the recombinant protein purified from *E. coli* cells expressing CAGL0F04279g by monitoring fluorescence derived from its reaction product (**Figure 2B**). When the native recombinant enzyme was included in the reaction mixture, the fluorescence increased in a time-dependent manner. On the other hand, the pre-boiled enzyme did not show increased fluorescence. These findings indicate that the recombinant protein exhibits GCH2 activity, which was calculated as 1.25 U/mg. Therefore, we concluded that CAGL0F04279g functions as *RIB1* encoding GCH2 in *C. glabrata* (*CgRIB1*).

Additionally, the GCH2 activity in yeast cell-free lysate was evaluated (**Figure 2C**). The WT and *rib1*Δ strains showed clear GCH2 activity, but the activity in the *rib1*Δ strain was almost 40% of that of the WT. Interestingly, there was no detectable GCH2 activity in the lysate from the *rib1*ΔΔ strain. These results suggest that the two copies of *CgRIB1* function to fully express active GCH2 almost equally, which is not surprising because the DNA sequences of the two copies of *CgRIB1* were identical as shown above.

RIB1 Is Essential for Nitrosative Stress Resistance in *Candida glabrata*

A previous study reported that the presence of nitrite induced nitrosative stress under acidic conditions (Zhou et al., 2013). Therefore, we evaluated the growth of *C. glabrata* on minimal medium containing sodium nitrite at pH 5.5 (**Figure 3A**). The growth of the WT strain decreased in a nitrite dose-dependent manner while the strain lacking the *YHB1* gene encoding fHb exhibited a more severe growth defect than the WT strain at a high concentration of nitrite. These results indicate that nitrosative stress induced by nitrite is toxic to *C. glabrata* under the conditions tested in this study. The growth of the *rib1*ΔΔ strain on medium containing nitrite was dramatically inhibited, which was compensated for by the plasmid carrying the *CgRIB1* gene. Indeed, overexpression of *CgRIB1* increased the growth of *C. glabrata* cells in the presence of nitrite (**Figure 3B**). These results indicate that *CgRIB1* is critical for nitrosative stress resistance in *C. glabrata*. Furthermore, we measured the NO-quenching activity of the reaction product of GCH2 encoded by *CgRIB1* (CgGCH2) using a fluorescent NO probe DAF-FM and an NO donor NOC-5 (**Figure 3C**). The time-dependent increase in fluorescence by the addition of NOC-5 was clearly

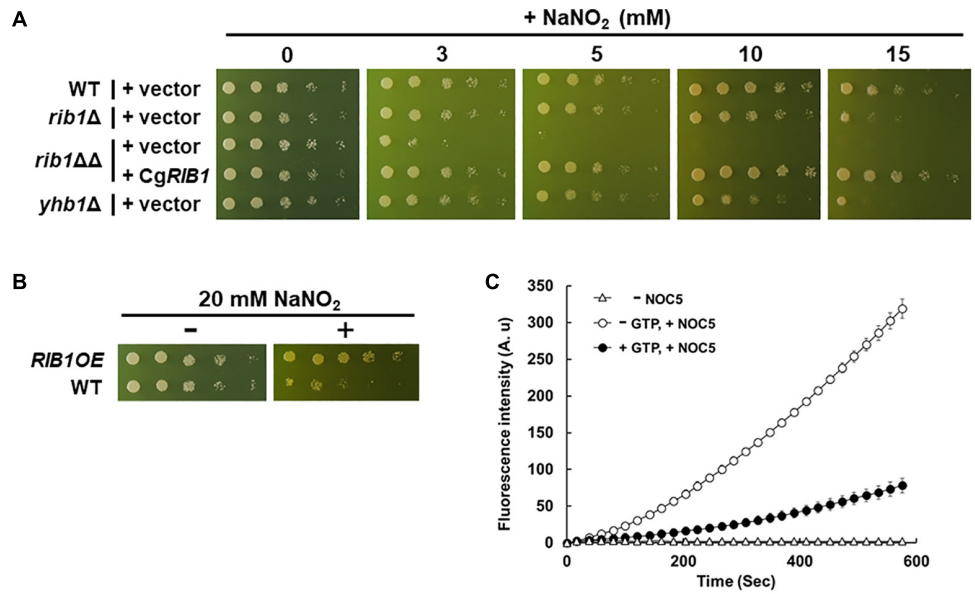

FIGURE 3 | Nitrosative stress resistance mechanism mediated by *CgRIB1* in *C. glabrata*. **(A,B)** Yeast cells cultured in SD medium containing RF until exponential phase were spotted onto the SD medium with pH 5.5 containing RF with or without various concentration of sodium nitrite, followed by further cultivation. **(C)** The enzymatic reaction mixture using the recombinant CgGCH2 protein with or without its substrate GTP was mixed with DAF-FM, followed by the addition of NOC-5. The fluorescence intensity was monitored over time. The fluorescence intensity at the time of 0 min was used as a blank in each sample. The mixture of reaction buffer with DAF-FM lacking NOC-5 was used as a negative control. The values are the means and standard deviations of three independent experiments.

inhibited by the enzymatic reaction mixture of CgGCH2; this effect was canceled out by the omission of GTP from the reaction mixture, suggesting that the product of CgGCH2 enzymatic reaction scavenges NO before it reacts with DAF-FM. These results indicate that *CgRIB1* confers nitrosative stress resistance on *C. glabrata* cells in the same way as in *S. cerevisiae* cells. Interestingly, the growth of the *rib1*Δ strain was also impaired by exposure to nitrite; however, the degree of its growth defect was milder than in the *rib1*ΔΔ strain (**Figure 3A**). This finding indicates that the effect of nitrosative stress depends on the copy number of *CgRIB1*.

RIB1-Dependent Nitrosative Stress Resistance Is Important for Proliferation of *Candida glabrata* in Macrophage-Like Cells

In order to examine the effect of CgGCH2 on the virulence of *C. glabrata*, we evaluated the replication of yeast in a culture of RAW264.7 cells, a model of activated macrophages. At first, NO production was induced from RAW264.7 cells by LPS treatment using DAF-FM (**Figure 4A**). The fluorescence derived from NO was increased when RAW264.7 cells were treated with LPS, which was clearly suppressed by the additional treatment with the NOS inhibitor NAME. These results showed that the LPS treatment and NAME addition performed in this study efficiently induced and inhibited NO production from RAW264.7 cells, respectively. Subsequently, *C. glabrata* cells were incorporated into the culture of LPS-treated RAW264.7 cells, and the viable cell numbers of yeast were analyzed (**Figure 4B**). The viable cell number of the WT strain increased over time. The strain lacking *YHB1* grew in the RAW264.7 cells culture more slowly than the WT strain, probably due to nitrosative stress induced by the treatment with LPS. The cell number of the *rib1*ΔΔ strain increased slightly until 24 h incubation; however, it decreased during the next 24 h. In order to exclude the effect of RF auxotrophy on the phenotype of the *rib1*ΔΔ strain, the macrophage infection assay was performed in the presence of 100 μg/mL RF, which has been reported to increase the RF concentration inside macrophage cells to 100 μM (Dey and Bishayi, 2016; **Figure 4C**). The result showed that for the first 24 h, the *rib1*ΔΔ strain grew better in the presence than in the absence of RF; however, its viable cell number dropped in the following 24-h incubation. When the mammalian NOS inhibitor NAME was added to evaluate the inhibitory effect of NO produced from RAW264.7 cells on the growth of yeast (**Figure 4D**), the growth of *yhb1*Δ cells was recovered to almost the same level as WT cells, suggesting that the growth defect of *yhb1*Δ cells had been due to nitrosative stress. Importantly, the decrease in cell number of the *rib1*ΔΔ strain during the second 24 h incubation was dramatically rescued by treatment with NAME, which indicates that the severe growth defect of the *rib1*ΔΔ strain was also induced by nitrosative stress.

RIB1 Is Important for Virulence of *Candida glabrata* in a Silkworm as a Model Host Organism

The silkworm has a similar innate immune system to that of mammals (Panthee et al., 2017); thus it is often used as a

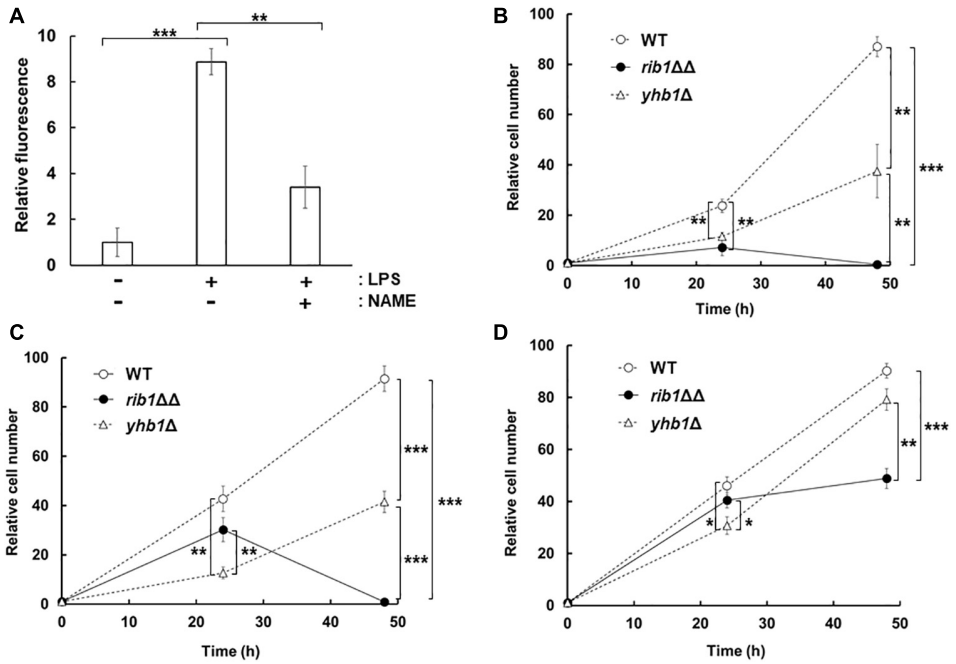

FIGURE 4 | Proliferation of *C. glabrata* in macrophage-like cell. **(A)** NO production from RAW264.7 cells activated by LPS. The supernatant of cells incubated with LPS and/or NAME was reacted with DAF-FM and then the fluorescence intensity was measured. The fluorescence intensity before the incubation was used as a blank. **(B–D)** RAW264.7 cells infected with *C. glabrata* were washed and resuspended in DMEM-B, followed by further incubation for 24 or 48 h. After incubation, macrophage-like cells were lysed and the extracted solution were plated onto YPD with RF solid medium. Colonies formed after further cultivation for a few days at 37°C were counted. Relative cell number using that at 0 h as 1 was shown. The macrophage-like cells were pretreated with LPS **(B)**, LPS and RF **(C)**, or LPS, RF, and NAME **(D)**, respectively, and then further incubated in the presence of these additives. The values are the means and standard deviations of three independent experiments. *$p < 0.05$; **$p < 0.01$; ***$p < 0.001$ by Student's *t*-test.

model organism for infection assays. The effect of *CgRIB1* on the virulence of *C. glabrata* was analyzed with an infection assay using silkworms. All silkworms died within 67 h after infection with the WT strain. On the other hand, silkworms infected with the *rib1*ΔΔ strain died at a significantly slower rate than those infected with the WT strain, indicating that *CgRIB1* is critical for the virulence of *C. glabrata* cells (**Figure 5A**). The survival rate of silkworms was not changed by the presence of the *YHB1* gene in *C. glabrata* (**Figure 5B**). These results suggest that *CgRIB1* is more important than *YHB1* for the virulence of *C. glabrata*.

DISCUSSION

We demonstrated that the CAGL0F04279g ORF functions as the *CgRIB1* gene encoding CgGCH2 and confers nitrosative stress resistance on *C. glabrata* cells. It was also shown that CgGCH2 is important for the proliferation of *C. glabrata* cells in macrophage-like cells *via* nitrosative stress resistance. The effect of NO on the virulence of *C. glabrata* has not been clarified previously, even though the lower NO production from macrophages activated by infection with *C. glabrata* was reported (Kasper et al., 2015). Thus, this is the first report to demonstrate the importance of nitrosative stress on infection by *C. glabrata*. Our findings provide new strategies for anti-bacterial and fungal therapies through the inhibition of CgGCH2 activity. Specific inhibitors of CgGCH2 should be considered as candidates for novel antifungals.

Furthermore, we found that *CgRIB1* is important for the virulence of *C. glabrata* by an infection assay using silkworms. We did not measure the RF content in silkworms; thus, we cannot exclude the possibility that the *rib1*ΔΔ strain had reduced its virulence because of RF auxotrophy inside silkworms. Previous studies have reported the importance of nitrosative stress in killing pathogens and protecting host organisms from pathogens during infection (Hromatka et al., 2005; Arai and Iiyama, 2013). Therefore, the increased survival rate of silkworms infected with the *rib1*ΔΔ strain could be caused by the decrease in nitrosative stress resistance of the *rib1*ΔΔ strain, at least partially.

Our DNA sequencing analysis suggested that the nucleotide sequences of two copies of *RIB1* were identical, from 509 bp upstream to 504 bp downstream of ORF. Although we did not determine the promoter region of each copy of *RIB1*, the GCH2 enzymatic activity in the cell-free extract from the *rib1*Δ strain was almost half of that from WT (**Figure 2C**), suggesting that the expression level of each *RIB1* copy is almost the same.

We showed that the nitrosative stress resistance of *C. glabrata* cells is dependent on the copy number of *CgRIB1* (**Figure 3A**). On the other hand, one copy of *CgRIB1* was enough to synthesize RF required for the growth of yeast cells (**Figure 2A**). These results raise the possibility that the function of CgGCH2

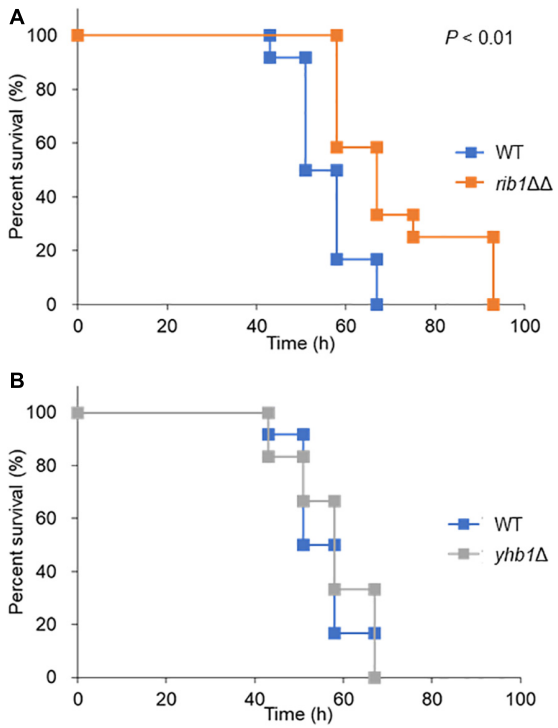

FIGURE 5 | Infection assay using silkworm as a model host organism. **(A)** Survival rate of silkworm infected with *C. glabrata* strains. The *C. glabrata* strains (WT and *rib1*ΔΔ) were cultured in SC-Ura-His containing RF for 2 days. Resuspended yeast cells were injected to fifth-instar larvae using a needle. The larvae (n = 12) were maintained at 30°C, and survival rate was monitored for 4 days. Statistical significance was examined by Log-rank test using a statistical analysis software BellCurve. The P value for comparison between WT and *rib1*ΔΔ was lower than 0.01. **(B)** Survival rate of silkworm infected with *C. glabrata* strains. The *C. glabrata* strains (WT and *yhb1*Δ) were injected to fifth-instar larvae, and the survival rate was monitored for 4 days. There was no statistical significance between WT and *ybh1*Δ.

as an inducer for nitrosative stress resistance, not as an enzyme involved in RF synthesis, would be a selection pressure for evolution, as various situations including infection and symbiosis with other microbes generating NO can easily be imagined, even though the *CgRIB1* gene was unexpectedly duplicated during the construction of KUE100-1 strain from its host strain CBS138. The copy number variation of the *CgRIB1* gene might be a determinant for the virulence and pathogenicity of each strain in the same pathogenic microbe species.

The growth of the *yhb1*Δ strain on medium containing nitrite was better than that of *rib1*ΔΔ strain. This indicates that *CgRIB1* is more critical than *YHB1* for the nitrosative stress resistance of *C. glabrata*, at least under acidified nitrite conditions. The previous studies reported that the NO formation from nitrite under acidic conditions (pH 5.5) is extremely rapid (Opländer et al., 2012; Rayson et al., 2012). Linde et al. (2015) demonstrated that the NO donor *S*-nitrosoglutathione induced *YHB1* but not *CgRIB1* in *C. glabrata*. However, *CgRIB1* would be expressed for RF biosynthesis in the absence of RF without NO stress. Therefore, a constitutively active *CgRIB1*-dependent mechanism could alleviate the rapid and short-term NO stress derived from acidified nitrite more efficiently than *YHB1*, which might take a longer time to fully function. An inducible nitrosative stress-resistance system like *YHB1* is upregulated only after exposure to stress stimuli; it cannot function effectively at the beginning of stress exposure. In contrast, a constitutively active NO detoxifying mechanism such as *CgRIB1* is capable of modulating stress more rapidly. Although the constitutive activations of stress resistance mechanisms generally waste organismal resources, the activation of *CgRIB1* is required for the growth of yeast cells in the absence of RF thus that strategy is not a waste. A constitutive stress resistance mechanism that bifunctionally contributes to both stress response and basal growth, such as *CgRIB1*, would be a more effective and reasonable strategy for cell survival than an inducible strategy, especially under rapid stress conditions.

In contrast to the growth test on the solid medium containing nitrite, our infection assay with macrophages indicated that the *rib1*ΔΔ strain grew better than the *YHB1*-deleted strain at 24 h in the presence of RF (**Figure 4C**). The NO synthesis from the LPS-activated macrophage was much slower than that from acidified nitrite (Amura et al., 1998). The long-term nitrosative stress induced by the activated macrophage could be detoxified by the *YHB*-dependent resistance mechanism which was upregulated during exposure to NO for 24 h. However, the cell number of the *rib1*ΔΔ strain dropped at 48-h incubation, even though the *YHB1*-deficent strain still grew (**Figure 4C**). This implies that *CgRIB1* is more important than *YHB1* for the proliferation inside macrophage at this time point. Although the *CgRIB1*-dependent NO resistance mechanism should be involved in the proliferation in macrophage at 48 h incubation at least partly, the growth of the rib1ΔΔ strain was still worse than WT, thus other unknown mechanisms than NO resistance mediated by *CgRIB1* could contribute additionally. For example, it is possible that the RF concentration in macrophage at 48 h incubation is not enough to culture the RF auxotroph and then inhibits the growth of the *rib1*ΔΔ strain, since we did not determine the intramacrophage RF content. Whereas, *CgRIB1* might be induced more strongly than *YHB1* in macrophage at 48 h incubation, even though no researches to analyze the expression of *CgRIB1* inside macrophages have been reported.

We activated macrophage-like cells by treatment with LPS. Several pathogenic microorganisms, not only yeasts and fungi but also bacteria, co-infect. Polymicrobial infections of *Candida* species and bacteria are getting frequently in recent years (Klotz et al., 2007). Whereas, Coco et al. (2008) reported that the mixed infection of *C. glabrata* and *C. albicans* were important for the severe inflammation in denture wearers. These facts indicate that the coinfection of *C. glabrata* with other pathogenic microbes are not rare and the important situations to be examined. The infection of RAW264.7 cells activated by LPS with *C. glabrata* performed in this study can mimic such coinfection situations, even though the macrophage activation by infection with *C. glabrata* produces only a lower level of NO. Recently,

it was reported that *C. glabrata* induced NO production from human osteoblasts (Muñoz-Duarte et al., 2016). Our infection analysis with the LPS-treated macrophage could also be a model system to examine the interaction with other types of cells.

CONCLUSION

We identified the *RIB1* gene encoding GCH2 in *C. glabrata* (*CgRIB1*) by the RF auxotrophy test and the enzymatic analysis of the *CgRIB1* gene product. The growth test on the acidic medium containing nitrite indicated that *CgRIB1* was involved in nitrosative stress resistance in *C. glabrata*, which was dependent on its copy number. Our infection assay demonstrated that the *CgRIB1*-dependent nitrosative stress resistance is indispensable for the proliferation of yeast cells in macrophage-like cells and that *CgRIB1* plays a role for the virulence of *C. glabrata*. The findings in this study imply that the *CgRIB1*-dependent NO resistance system is a promising target for novel antifungals.

DATA AVAILABILITY STATEMENT

The raw data supporting the conclusions of this article will be made available by the authors, without undue reservation.

AUTHOR CONTRIBUTIONS

RN and HT conceived the study and designed the experiments. SS performed the experiments except for the infection assay with silkworms. SO and DH performed the infection assay with silkworms. RN, SS, DH, and HT analyzed the data. RN, DH, and HT wrote the manuscript. All authors read and approved the final manuscript.

FUNDING

This work was supported by grants for a Grant-in-Aid for Young Scientists (19K16129) from the Japan Society for the Promotion of Science (JSPS) and the Mochida Memorial Foundation for Medical and Pharmaceutical Research to RN, and also by a Grant-in-Aid for Scientific Research (S) (19H05639), from JSPS to HT.

SUPPLEMENTARY MATERIAL

The Supplementary Material for this article can be found online at: https://www.frontiersin.org/articles/10.3389/fmicb.2022.825121/full#supplementary-material

REFERENCES

Amura, C. R., Kamei, T., Ito, N., Soares, M. J., and Morrison, D. C. (1998). Differential regulation of lipopolysaccharide (LPS) activation pathways in mouse macrophages by LPS-binding proteins. *J. Immunol.* 161, 2552–2560.

Anam, K., Nasuno, R., and Takagi, H. (2020). A novel mechanism for nitrosative stress tolerance dependent on GTP cyclohydrolase II activity involved in riboflavin synthesis of yeast. *Sci. Rep.* 10:6015. doi: 10.1038/s41598-020-62890-3

Antinori, S., Milazzo, L., Sollima, S., Galli, M., and Corbellino, M. (2016). Candidemia and invasive candidiasis in adults: a narrative review. *Eur. J. Intern. Med.* 34, 21–28. doi: 10.1016/j.ejim.2016.06.029

Arai, H., and Iiyama, K. (2013). Role of nitric oxide-detoxifying enzymes in the virulence of *Pseudomonas aeruginosa* against the silkworm, Bombyx mori. *Biosci. Biotechnol. Biochem.* 77, 198–200. doi: 10.1271/bbb.120656

Bai, X., Yang, L., Tian, M., Chen, J., Shi, J., Yang, Y., et al. (2011). Nitric oxide enhances desiccation tolerance of recalcitrant *Antiaris toxicaria* seeds via protein *S*-nitrosylation and carbonylation. *PLoS One* 6:e20714. doi: 10.1371/journal.pone.0020714

Boscá, L., and Hortelano, S. (1999). Mechanisms of nitric oxide-dependent apoptosis: involvement of mitochondrial mediators. *Cell. Signal.* 11, 239–244. doi: 10.1016/S0898-6568(98)00064-3

Coco, B. J., Bagg, J., Cross, L. J., Jose, A., Cross, J., and Ramage, G. (2008). Mixed *Candida albicans* and *Candida glabrata* populations associated with the pathogenesis of denture stomatitis. *Oral Microbiol. Immunol.* 23, 377–383. doi: 10.1111/j.1399-302X.2008.00439.x

Dementhon, K., El-Kirat-Chatel, S., and Noël, T. (2012). Development of an in vitro model for the multi-parametric quantification of the cellular interactions between *Candida* yeasts and phagocytes. *PLoS One* 7:e32621. doi: 10.1371/journal.pone.0032621

Dey, S., and Bishayi, B. (2016). Riboflavin along with antibiotics balances reactive oxygen species and inflammatory cytokines and controls *Staphylococcus aureus* infection by boosting murine macrophage function and regulates inflammation. *J. Inflamm. (Lomd)* 13:36. doi: 10.1186/s12950-016-0145-0

Dujon, B., Sherman, D., Fischer, G., Durrens, P., Casaregola, S., Lafontaine, I., et al. (2004). Genome evolution in yeasts. *Nature* 430, 35–44.

Ferrer-Sueta, G., Campolo, N., Trujillo, M., Bartesaghi, S., Carballal, S., Romero, N., et al. (2018). Biochemistry of peroxynitrite and protein tyrosine nitration. *Chem. Rev.* 118, 1338–1408. doi: 10.1021/acs.chemrev.7b00568

Francis, S., Busch, J., Corbin, J., and Sibley, D. (2010). cGMP-dependent protein kinases and cGMP phosphodiesterases in nitric oxide and cGMP action. *Pharmacol. Rev.* 62, 525–563. doi: 10.1124/pr.110.002907.525

Gardner, P. R., Gardner, A. M., Martin, L. A., and Salzman, A. L. (1998). Nitric oxide dioxygenase: an enzymic function for flavohemoglobin. *Proc. Natl. Acad. Sci. U.S.A.* 95, 10378–10383. doi: 10.1073/pnas.95.18.10378

Hassan, Y., Chew, S. Y., and Than, L. T. L. (2021). *Candida glabrata*: pathogenicity and resistance mechanisms for adaptation and survival. *J. Fungi (Basel)* 7:667. doi: 10.3390/jof7080667

Hromatka, B. S., Noble, S. M., and Johnson, A. D. (2005). Transcriptional response of *Candida albicans* to nitric oxide and the role of the *YHB1* gene in nitrosative stress and virulence. *Mol. Biol. Cell* 16, 4814–4826. doi: 10.1091/mbc.E05

Hunt, A. P., and Lehnert, N. (2015). Heme-nitrosyls: electronic structure implications for function in biology. *Acc. Chem. Res.* 48, 2117–2125. doi: 10.1021/acs.accounts.5b00167

Kang, J. W., Lee, N. Y., Cho, K. C., Lee, M. Y., Choi, D. Y., Park, S. H., et al. (2015). Analysis of nitrated proteins in *Saccharomyces cerevisiae* in mating signal transduction. *Proteomics* 15, 580–590. doi: 10.1002/pmic.201400172

Kasper, L., Seider, K., and Hube, B. (2015). Intracellular survival of *Candida glabrata* in macrophages: immune evasion and persistence. *FEMS Yeast Res.* 15:fov042. doi: 10.1093/femsyr/fov042

Kaur, R., Ma, B., and Cormack, B. P. (2007). A family of glycosylphosphatidylinositol-linked aspartyl proteases is required for virulence of *Candida glabrata*. *Proc. Natl. Acad. Sci. U.S.A.* 104, 7628–7633. doi: 10.1073/pnas.0611195104

Kim, S. O., Orii, Y., Lloyd, D., Hughes, M. N., and Poole, R. K. (1999). Anoxic function for the *Escherichia coli* flavohaemoglobin (Hmp): reversible binding of nitric oxide and reduction to nitrous oxide. *FEBS Lett.* 445, 389–394. doi: 10.1016/S0014-5793(99)00157-X

Klotz, S. A., Chasin, B. S., Powell, B., Gaur, N. K., and Lipke, P. N. (2007). Polymicrobial bloodstream infections involving *Candida* species: analysis of patients and review of the literature. *Diagn. Microbiol. Infect. Dis.* 59, 401–406. doi: 10.1016/j.diagmicrobio.2007.07.001

Linde, J., Duggan, S., Weber, M., Horn, F., Sieber, P., Hellwig, D., et al. (2015). Defining the transcriptomic landscape of *Candida glabrata* by RNA-Seq. *Nucleic Acids Res.* 43, 1392–1406. doi: 10.1093/nar/gku1357

Lionakis, M. S., and Netea, M. G. (2013). *Candida* and host determinants of susceptibility to invasive Candidiasis. *PLoS Pathog.* 9:e1003079. doi: 10.1371/journal.ppat.1003079

Malani, A., Hmoud, J., Chiu, L., Carver, P. L., Bielaczyc, A., and Kauffman, C. A. (2005). *Candida glabrata* fungemia: experience in a tertiary care center. *Clin. Infect. Dis.* 41, 975–981. doi: 10.1086/432939

Muñoz-Duarte, A. R., Castrejón-Jiménez, N. S., Baltierra-Uribe, S. L., Pérez-Rangel, S. J., Carapia-Minero, N., Castañeda-Sánchez, J. I., et al. (2016). Candida glabrata survives and replicates in human osteoblasts. *Pathog. Dis.* 74:ftw030. doi: 10.1093/femspd/ftw030

Nakato, R., Ohkubo, Y., Konishi, A., Shibata, M., Kaneko, Y., Iwawaki, T., et al. (2015). Regulation of the unfolded protein response via S-nitrosylation of sensors of endoplasmic reticulum stress. *Sci. Rep.* 5:14812. doi: 10.1038/srep14812

Nasuno, R., Aitoku, M., Manago, Y., Nishimura, A., Sasano, Y., and Takagi, H. (2014). Nitric oxide-mediated antioxidative mechanism in yeast through the activation of the transcription factor Mac1. *PLoS One* 9:e113788. doi: 10.1371/journal.pone.0113788

Nishimura, A., Kawahara, N., and Takagi, H. (2013). The flavoprotein Tah18-dependent NO synthesis confers high-temperature stress tolerance on yeast cells. *Biochem. Biophys. Res. Commun.* 430, 137–143. doi: 10.1016/j.bbrc.2012.11.023

Opländer, C., Volkmar, C. M., Paunel-Görgülü, A., Fritsch, T., Van Faassen, E. E., Mürtz, M., et al. (2012). Dermal application of nitric oxide releasing acidified nitrite-containing liniments significantly reduces blood pressure in humans. *Nitric Oxide* 26, 132–140. doi: 10.1016/j.niox.2012.01.007

Pacher, P., Beckman, J. S., and Liaudet, L. (2007). Nitric oxide and peroxynitrite in health and disease. *Physiol. Rev.* 87, 315–424. doi: 10.1152/physrev.00029.2006

Panthee, S., Paudel, A., Hamamoto, H., and Sekimizu, K. (2017). Advantages of the silkworm as an animal model for developing novel antimicrobial agents. *Front. Microbiol.* 8:373. doi: 10.3389/fmicb.2017.00373

Parkinson, T., Falconer, D. J., and Hitchcock, C. A. (1995). Fluconazole resistance due to energy-dependent drug efflux in *Candida glabrata*. *Antimicrob. Agents Chemother.* 39, 1696–1699. doi: 10.1128/AAC.39.8.1696

Phua, A. I. H., Hon, K. Y., Holt, A., O'Callaghan, M., and Bihari, S. (2019). Candida catheter-related bloodstream infection in patients on home parenteral nutrition - Rates, risk factors, outcomes, and management. *Clin. Nutr. ESPEN* 31, 1–9. doi: 10.1016/j.clnesp.2019.03.007

Porter, J. J., Jang, H. S., Haque, M. M., Stuehr, D. J., and Mehl, R. A. (2020). Tyrosine nitration on calmodulin enhances calcium-dependent association and activation of nitric-oxide synthase. *J. Biol. Chem.* 295, 2203–2211. doi: 10.1074/jbc.RA119.010999

Rayson, M. S., MacKie, J. C., Kennedy, E. M., and Dlugogorski, B. Z. (2012). Accurate rate constants for decomposition of aqueous nitrous acid. *Inorg. Chem.* 51, 2178–2185. doi: 10.1021/ic202081z

Seider, K., Brunke, S., Schild, L., Jablonowski, N., Wilson, D., Majer, O., et al. (2011). The facultative intracellular pathogen *Candida glabrata* subverts macrophage cytokine production and phagolysosome maturation. *J. Immunol.* 187, 3072–3086. doi: 10.4049/jimmunol.1003730

Ueno, K., Uno, J., Nakayama, H., Sasamoto, K., Mikami, Y., and Chibana, H. (2007). Development of a highly efficient gene targeting system induced by transient repression of YKU80 expression in Candida glabrata. *Eukaryot. Cell* 6, 1239–1247. doi: 10.1128/EC.00414-06

von Bargen, K., Wohlmann, J., Taylor, G. A., Utermöhlen, O., and Haas, A. (2011). Nitric oxide-mediated intracellular growth restriction of pathogenic *Rhodococcus equi* can be prevented by iron. *Infect. Immun.* 79, 2098–2111. doi: 10.1128/IAI.00983-10

Wink, D. A., Hines, H. B., Cheng, R. Y. S., Switzer, C. H., Flores-Santana, W., Vitek, M. P., et al. (2011). Nitric oxide and redox mechanisms in the immune response. *J. Leukoc. Biol.* 89, 873–891. doi: 10.1189/jlb.1010550

Yoshikawa, Y., Nasuno, R., Kawahara, N., Nishimura, A., Watanabe, D., and Takagi, H. (2016). Regulatory mechanism of the flavoprotein Tah18-dependent nitric oxide synthesis and cell death in yeast. *Nitric Oxide* 57, 85–91. doi: 10.1016/j.niox.2016.04.003

Zhou, S., Narukami, T., Masuo, S., Shimizu, M., Fujita, T., Doi, Y., et al. (2013). NO-inducible nitrosothionein mediates NO removal in tandem with thioredoxin. *Nat. Chem. Biol.* 9, 657–663. doi: 10.1038/nchembio.1316

Zordan, R. E., Ren, Y., Pan, S. J., Rotondo, G., Iluore, A. D. L. P., and Cormack, B. P. (2013). Expression plasmids for use in *Candida glabrata*. *G3 (Bethesda)* 3, 1675–1686. doi: 10.1534/g3.113.006908

Conflict of Interest: The authors declare that the research was conducted in the absence of any commercial or financial relationships that could be construed as a potential conflict of interest.

Publisher's Note: All claims expressed in this article are solely those of the authors and do not necessarily represent those of their affiliated organizations, or those of the publisher, the editors and the reviewers. Any product that may be evaluated in this article, or claim that may be made by its manufacturer, is not guaranteed or endorsed by the publisher.

frontiers in Microbiology

ORIGINAL RESEARCH
published: 04 March 2022
doi: 10.3389/fmicb.2022.812457

Production of Different Biochemicals by *Paenibacillus polymyxa* DSM 742 From Pretreated Brewers' Spent Grains

Blanka Didak Ljubas, Mario Novak, Antonija Trontel, Ana Rajković, Zora Kelemen, Nenad Marđetko, Marina Grubišić, Mladen Pavlečić, Vlatka Petravić Tominac and Božidar Šantek*

Department of Biochemical Engineering, Faculty of Food Technology and Biotechnology, University of Zagreb, Zagreb, Croatia

Brewers' spent grains (BSG) are a by-product of the brewing industry that is mainly used as feedstock; otherwise, it has to be disposed according to regulations. Due to the high content of glucose and xylose, after pretreatment and hydrolysis, it can be used as a main carbohydrate source for cultivation of microorganisms for production of biofuels or biochemicals like 2,3-butanediol or lactate. 2,3-Butanediol has applications in the pharmaceutical or chemical industry as a precursor for varnishes and paints or in the food industry as an aroma compound. So far, *Klebsiella pneumoniae*, *Serratia marcescens*, *Clostridium sp.*, and *Enterobacter aerogenes* are being used and investigated in different bioprocesses aimed at the production of 2,3-butanediol. The main drawback is bacterial pathogenicity which complicates all production steps in laboratory, pilot, and industrial scales. In our study, a gram-positive GRAS bacterium *Paenibacillus polymyxa* DSM 742 was used for the production of 2,3-butanediol. Since this strain is very poorly described in literature, bacterium cultivation was performed in media with different glucose and/or xylose concentration ranges. The highest 2,3-butanediol concentration of 18.61 g l^{-1} was achieved in medium with 70 g l^{-1} of glucose during 40 h of fermentation. In contrast, during bacterium cultivation in xylose containing medium there was no significant 2,3-butanediol production. In the next stage, BSG hydrolysates were used for bacterial cultivation. *P. polymyxa* DSM 742 cultivated in the liquid phase of pretreated BSG produced very low 2,3-butanediol and ethanol concentrations. Therefore, this BSG hydrolysate has to be detoxified in order to remove bacterial growth inhibitors. After detoxification, bacterium cultivation resulted in 30 g l^{-1} of lactate, while production of 2,3-butanediol was negligible. The solid phase of pretreated BSG was also used for bacterium cultivation after its hydrolysis by commercial enzymes. In these cultivations, *P. polymyxa* DSM 742 produced 9.8 g l^{-1} of 2,3-butanediol and 3.93 g l^{-1} of ethanol. On the basis of the obtained results, it can be concluded that different experimental setups give the possibility of directing the metabolism of *P. polymyxa* DSM 742 toward the production of either 2,3-butanediol and ethanol or lactate.

Keywords: *Paenibacillus polymyxa* DSM 742, biochemicals, 2,3-butanediol, lactate, brewers' spent grains

OPEN ACCESS

Edited by:
Aleksandra P. Djukic-Vukovic, University of Belgrade, Serbia

Reviewed by:
Dragana Mladenović, University of Belgrade, Serbia
Victor Ujor, University of Wisconsin–Madison, United States

***Correspondence:**
Božidar Šantek
bsantek@pbf.hr

Specialty section:
This article was submitted to Microbiotechnology, a section of the journal Frontiers in Microbiology

Received: *10 November 2021*
Accepted: *11 January 2022*
Published: *04 March 2022*

Citation:
Didak Ljubas B, Novak M, Trontel A, Rajković A, Kelemen Z, Marđetko N, Grubišić M, Pavlečić M, Tominac VP and Šantek B (2022) Production of Different Biochemicals by Paenibacillus polymyxa DSM 742 From Pretreated Brewers' Spent Grains. Front. Microbiol. 13:812457. doi: 10.3389/fmicb.2022.812457

INTRODUCTION

A focus of the modern industry is to decrease large amounts of by-products and transform them into more environmentally friendly products (Tang et al., 2009). A good example of such industry is beer production in which by-products are available through the whole year. Two main by-products of beer production are spent yeasts (≈125,000 t/y in Europe) and brewers' spent grains (BSG) (≈38.6 million tons worldwide) that can be used as livestock feed, or in different biotechnological processes (Karlović et al., 2020). After mashing and lautering, BSG is separated from wort, and it accounts for 85% of total waste in the beer industry which makes it a very attractive raw material for the biotechnological industry in the production of active coal and biomethane as well as extraction of high-value products. BSG is a lignocellulosic biomass that contains 40–50% of polysaccharides (starch, glucans, arabinoxylans), 30% proteins, 5% ash, and 15% of lignin. The content depends on the brewing process: sweetening and sanding, as well as cereal used in the process (Tang et al., 2009; Ikram et al., 2017; Jackowski et al., 2020). Pretreatment of BSG releases fermentable sugars which can be used as a substrate for the growth of microorganisms and the production of different biochemicals. Except being a carbon source, it is also a good source of amino acids such as tryptophan, phenylalanine, histidine, methionine, and lysine (Ikram et al., 2017). In addition, phenolic compounds from the BSG show immunomodulatory activity in inflammatory processes (McCarthy et al., 2013).

Paenibacillus polymyxa (formally *Bacillus polymyxa*) is a sporogenic, rod-shaped, gram-positive bacterium (Jeong et al., 2019) which is found in different habitats like soil, rhizosphere, plant tissue, and fermented foods (Meena et al., 2017). This bacterium produces a wide range of secondary metabolites like phytohormones, polysaccharides, and antimicrobial substances which are involved in adaptation and survival in different environmental conditions (Grady et al., 2016). Some of the secondary metabolites are antimicrobial lipopeptides, such as antibiotic polypeptins, polymyxins, and fusaricidins, which inhibit plant pathogens and are therefore useful in agronomy (Li and Chen, 2019). Some of the strains synthetize antibiotic polymyxin E1 which is efficient against Gram-negative bacteria, while other strains produce lantibiotic and paenibacillin, antibiotics useful against Gram-positive bacteria (He et al., 2007; Lal and Tabacchioni, 2009). Apart from the antibiotics, *P. polymyxa* produces different peptides which have strong antifungal activity against fungi such as *Aspergillus niger*, *Aspergillus oryzae*, *Fusarium oxysporum*, and yeasts *Saccharomyces cerevisiae* and *Candida albicans* (Kajimura and Kaneda, 1997). Bacterium *P. polymyxa* also promotes plant growth by atmospheric nitrogen fixation and synthesis of plant hormones (Meena et al., 2017).

Paenibacillus polymyxa has potential for production of biochemicals, polymers, and enzymes such as 2,3-butanediol (2,3-BD), exopolysaccharides, cellulases, glucanases, proteases, and xylanases (Lal and Tabacchioni, 2009). These products play a significant role in the agriculture, food, and biotechnological industries (Daud et al., 2019). The market value of 2,3-BD in 2020 was estimated to be around 76 million USD. It is used as a building block in different industries, such as the chemical industry for production of plastics and anti-freeze, in the cosmetic and food industries. Various bacteria, such as *Enterobacter*, *Klebsiella*, and *Serratia* sp., produce 2,3-BD with a higher yield than bacterium *P. polymyxa*. The downside of these bacteria is their pathogenicity which makes the bioprocess more complex and expensive regarding microbial safety. Additionally, they produce *S,S*-2,3-BD or *meso*-BD which is less suitable for industrial application. *P. polymyxa* is a non-pathogenic bacterium with a GRAS status which produces 98% pure optical active *R,R*-2,3-BD (Moo-Young, 2011). Besides 2,3-BD, *P. polymyxa* produces other biochemicals such as ethanol, acetate, lactate, formate, and succinate which can also be very valuable biotechnological products (Hakizimana et al., 2020).

The aim of this work was to define the potential of *P. polymyxa* DSM 742 for sustainable biochemical production. The BSG was selected as a renewable feedstock, and therefore it was hydrolyzed by using dilute sulfuric acid to obtain fermentable sugars. After hydrolysis, the liquid phase of pretreated BSG was detoxified with activated carbon in order to remove bacterial growth inhibitors. The solid phase of pretreated BSG was hydrolyzed with commercial enzymes to maximize the efficiency of fermentable sugar production from this feedstock. In the first stage, the new strain of *P. polymyxa* DSM 742 was cultivated in media with different carbon sources (glucose, xylose, or their mixture) in order to define its potential for 2,3-BD and ethanol or lactate production. In the second stage, *P. polymyxa* was cultivated in the stirred tank bioreactor on the three types of pretreated BSG to define bacterium capacity to use pretreated BSG as a carbon source for 2,3-BD and ethanol or lactate (**Figure 1**).

MATERIALS AND METHODS

Pretreatment of Brewers' Spent Grains

The raw material used for pretreatment was BSG obtained after beer production in the microbrewery of the Laboratory for Biochemical Engineering, Industrial Microbiology and Malting and Brewing Technology, Faculty of Food Technology and Biotechnology, University of Zagreb (Zagreb, Croatia). The material after brewing was dried at 105°C to constant weight and stored in a cool and dry place until further use. Dry BSG contained the following (in %): glucan 40.50, xylan 6.14, arabinan 6.32, soluble lignin 5.50, insoluble lignin and ash 26.22, acetate 1.66, formate 1.35, and furans 2.07. The BSG composition was determined by the NREL method (Sluiter et al., 2012).

Dry BSG (1 kg of BSG was suspended in 10 l of 0.5% w/w H_2SO_4) was hydrolyzed in the high-pressure reactor (Rosing, Zagreb, Croatia) at 180°C during 10 min, as described in Marđetko et al. (2018). After dilute acid hydrolysis, 6.8 l of the liquid phase and 170 g of the solid phase of pretreated BSG were obtained. The composition of the liquid and solid phases of pretreated BSG was determined as described in Marđetko et al. (2018). The obtained liquid phase of pretreated

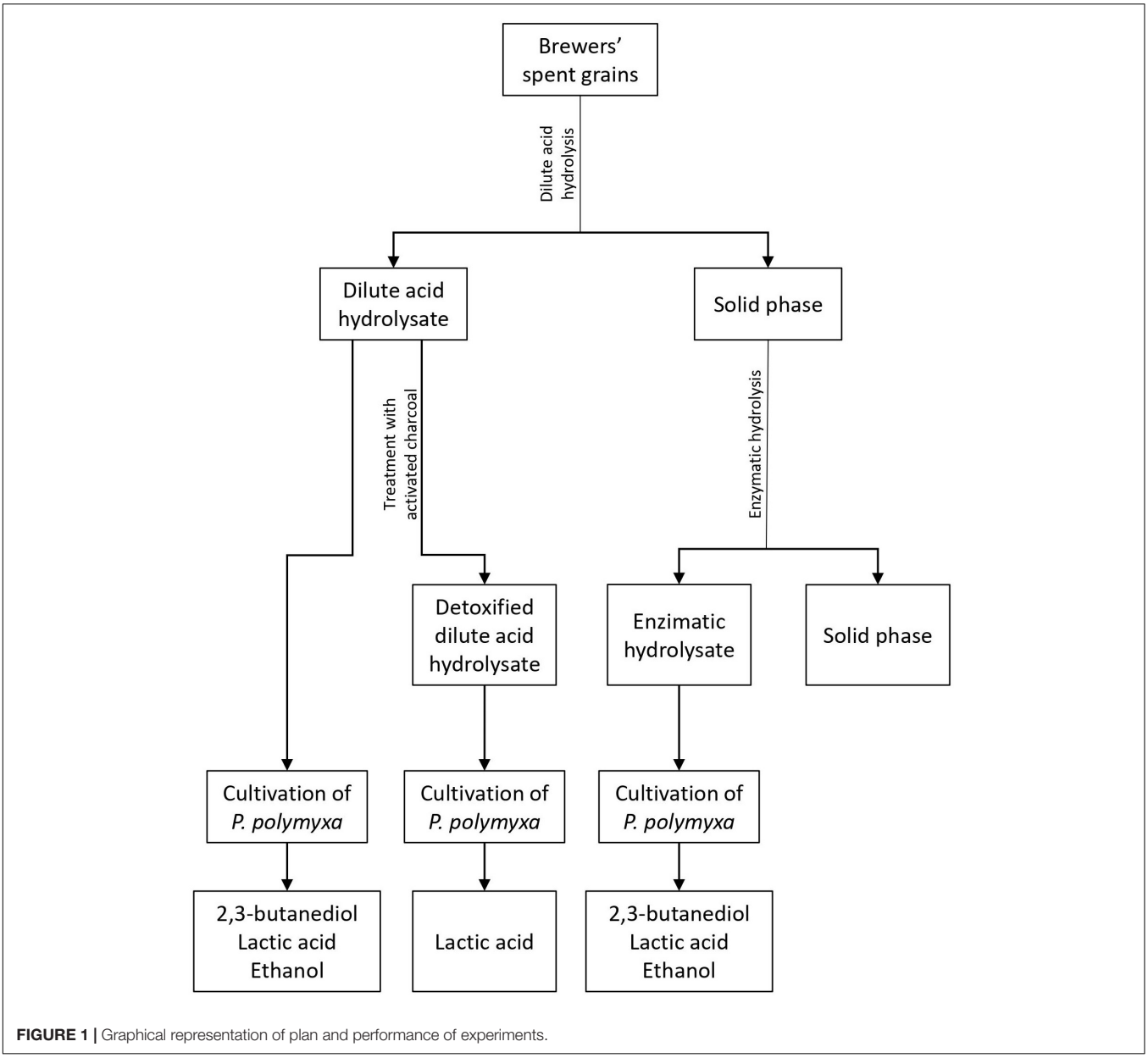

FIGURE 1 | Graphical representation of plan and performance of experiments.

BSG had the following composition (in g l^{-1}): glucose 26.89, xylose 11.57, and acetate 0.77. The liquid phase of pretreated BSG was additionally treated with activated charcoal (Merck KGaA, Darmstadt, Germany) to remove toxic compounds [18 g activated charcoal/1 l of liquid phase at 20°C for 1 h and at a magnetic shaker rotation speed of 250 rpm] (Sampaio et al., 2006; Canilha et al., 2008). Activated charcoal was removed by filtration on a Büchner funnel (filter paper LabExpert, pore size 55 mm, Hilden, Germany). The obtained detoxified liquid phase of pretreated BSG had the same carbohydrate composition as the liquid phase of pretreated BSG prior to detoxification. Both the original liquid phase and detoxified liquid phase of pretreated BSG were used for cultivations of *P. polymyxa* DSM 742.

The composition of the solid phase of pretreated BSG was as follows (in %): glucan 36.69, xylan 2.13, acid insoluble lignin and ash 47.49, and moisture 13.69. The solid phase of pretreated BSG (350 g, obtained from several batches performed in the same pretreatment conditions) was suspended in 5 l of 0.05 mol l^{-1} acetate buffer (pH 5.0), and two commercial enzyme cocktails, Viscozyme L (Novozymes, Bagsvaerd, Denmark) at a concentration of 5% vol vol^{-1} of suspension, and Cellulase SAE0020 (Sigma-Aldrich, St. Louis, MO, United States) at a concentration of 2% vol vol^{-1}, were added. Viscozyme L [≥100 FBG/g of carboxymethyl cellulose] is a blend of β-glucanases, pectinases, hemicellulases, and xylanases, while Cellulase SAE0020 (≥1,000 FPU/g of cellulose) is a blend of celluloses, β-glucosidases, and hemicellulases. Hydrolysis was

performed in a horizontal rotating tubular bioreactor (HRTB; Rosing, Zagreb, Croatia) during 30 h at 40°C and HRTB rotation of 20 rpm. HRTB is made of stainless steel whose interior is characterized by two paddles to homogenize the content of the bioreactor. It is also equipped with temperature and pressure control units, as well as an electric motor and a base unit. The total volume of HRTB is 30 l, and the maximal rotation speed is 60 rpm. After hydrolysis, suspension was filtrated, and 160 g of non-hydrolyzed material and 5 l of hydrolysate were obtained. The obtained hydrolysate of pretreated BSG was used for cultivation of *P. polymyxa* in the stirred tank bioreactor.

Microorganism and Culture Media

Paenibacillus polymyxa DSM 742 was purchased from the German Collection of Microorganisms and Cell Cultures GmbH (Leipzig, Germany). The culture was maintained and propagated regularly in medium with the following composition (in g l^{-1}): peptone 5, meat extract 3, and glucose 1. For the preparation of solid media, agar in a concentration of 15 g l^{-1} was added. Inoculum for cultivations was prepared in the same liquid medium.

Media used for cultivations in Erlenmeyer flasks were reported in Schilling et al. (2020) and were of the following composition (in g l^{-1}): yeast extract 5, tryptone 5, $MgSO_4 \times 7\ H_2O$ 0.2, KH_2PO_4 3.5, K_2PO_4 2.5, NH_4COOH 5, and $(NH_4)_2SO_4$ 4. The solution of trace elements was prepared separately, filtrated through a disposable sterile syringe filter (pore size 0.20 μm, pa 20/25, nylon; CHROMAFIL Xtra, Macherey-Nagel GmbH & Co. KG, Düren, Germany), and added to the media after sterilization. The solution of trace elements contained the following (in g l^{-1}): $FeSO_4 \times 7\ H_2O$ 2.5, $C_4H_4Na_2O_6 \times 2\ H_2O$ 2.1, $Cl_2Mn \times 2\ H_2O$ 1.8, $CoCl_2 \times 6\ H_2O$ 0.075, $CuSO_4 \times 5\ H_2O$ 0.031, boric acid 0.258, $NaMoO_4 \times 2\ H_2O$ 0.023, and $ZnCl_2$ 0.021. Solutions of carbon sources, 500 g l^{-1} glucose and 500 g l^{-1} of xylose, were prepared separately, sterilized, and added to the culture media in different quantities, depending on the experimental setup. The list of media used for cultivations of *P. polymyxa* DSM 742 is shown in **Table 1**. All chemicals used in this work were of p.a. purity and purchased from Sigma-Aldrich (St. Louis, MO, United States) if not stated otherwise.

TABLE 1 | Initial concentration of main carbon sources in media used for cultivations of *P. polymyxa* DSM 742.

Media*	Carbon source concentration (g l^{-1})	
	Glucose	Xylose
glc_{30}	30	–
glc_{50}	50	–
glc_{70}	70	–
xyl_5	–	5
xyl_{10}	–	10
xyl_{20}	–	20
xyl_{30}	–	30
xyl_{50}	–	50
xyl_{70}	–	70
$glc_{10}xyl_{10}$	10	10
$glc_{20}xyl_{20}$	20	20
$glc_{30}xyl_{30}$	30	30
$glc_{27}xyl_{12}$	27	12
$glc_{22}xyl_{10}$	22	10
$glc_{33}xyl_4$	33	4

**All media are supplemented with yeast extract, salts, and trace elements solution as described in section "Microorganism and Culture Media".*

Cultivation of *Paenibacillus polymyxa* DSM 742 in Media With Glucose, Xylose, or a Mixture of Glucose and Xylose in Erlenmeyer Flasks

The bacterium *P. polymyxa* DSM 742 from slant agar was transferred into 20 ml of medium for maintenance. The bacterium was cultivated in a rotary shaker (speed of 130 rpm) overnight at 30°C. 10 ml of culture was transferred into 100 ml of the same media to grow overnight in the same conditions. For the study of biomass growth and kinetics of 2,3-BD production, complex media were prepared with glucose and xylose as carbon source and the mixture of both sugars (**Table 1**) was used. 7.5 ml of previously prepared culture was inoculated in 150 ml of media for Erlenmeyer flask cultivation. Bacterial cultivations were carried out up to 48 h at 30°C with a shaker rotation speed of 130 rpm. 5 ml of the sample was removed each hour. The optical density of biomass was determined on a spectrophotometer (Carry 100, Agilent Technologies, Santa Clara, CA, United States) at 600 nm, while the chemical content of the broth samples was determined by ultra-performance liquid chromatography (UPLC) analysis (Agilent 1290 Infinity II LC System, Santa Clara, CA, United States) after centrifugation (5 min/8,000 rpm). All experiments in Erlenmeyer flasks were done in triplicate, and standard deviations are presented as error bars in figures. The standard deviation of experimental data was calculated by using the standard procedure in the software Statistica 12.0 (StatSoft, Tulsa, OK, United States).

Cultivation of *Paenibacillus polymyxa* on Different Hydrolysates of Pretreated Brewers' Spent Grains in the Stirred Tank Bioreactor

For the cultivation of *P. polymyxa* DSM 742 in the stirred tank bioreactor (Biostat Cplus, Sartorius Stedim Biotech GmbH, Göttingen, Germany), the hydrolysates of pretreated BSG with 5 g l^{-1} of yeast extract were used. The carbohydrate composition of the obtained hydrolysates of pretreated BSG is presented in **Table 2**. The working volume of the bioreactor was 5.5 l, and it was inoculated with 7% (vol/vol) of previously prepared bacterial culture. Cultivations of *P. polymyxa* DSM 742 in the bioreactor were performed at 30°C, pH = 6.5 with pH control (addition of 3 M NaOH or 2 M H_2SO_4), and a stirrer rotation speed of 250 rpm, in microaerobic conditions during 96 h. The culture samples were taken each hour in sterile conditions after which optical density was determined by a spectrophotometer (Carry 100,

TABLE 2 | Carbon source concentrations in different media with pretreated BSG hydrolysates.

Sugar	LP-BSG medium (g l^{-1})	DLP-BSG medium (g l^{-1})	SP-BSG medium (g l^{-1})
Cellobioses	6.97	/	3.69
Glucose	26.89	22.04	33.27
Xylose	11.57	9.67	3.68
Arabinose	5.62	4.73	0.52
Acetate	0.77	0.77	5.65

LP-BSG, liquid phase of pretreated BSG supplemented with 4 g l^{-1} yeast extract; DLP-BSG, detoxified liquid phase of pretreated BSG supplemented with 4 g l^{-1} yeast extract; SP-BSG, enzymatic hydrolysate of solid phase of pretreated BSG supplemented with 4 g l^{-1} yeast extract.

Agilent Technologies, Santa Clara, CA, United States) at 600 nm. The chemical content of the broth sample was determined by UPLC analysis (Agilent 1290 Infinity II LC System, Santa Clara, CA, United States) after centrifugation (5 min/8,000 rpm). All *P. polymyxa* DSM 742 cultivations in the stirred tank bioreactor were repeated, and the average values of all bioprocess parameters are presented in figures.

Analytical Methods

Biomass growth during cultivations was monitored by determination of optical density at 600 nm (Carry 100, Agilent Technologies, Santa Clara, CA, United States; Das et al., 2021). The broth samples were centrifuged (see sections "Cultivation of *Paenibacillus polymyxa* DSM 742 in Media With Glucose, Xylose, or a Mixture of Glucose and Xylose in Erlenmeyer Flasks" and "Cultivation of *Paenibacillus polymyxa* on Different Hydrolysates of Pretreated Brewers' Spent Grains in the Stirred Tank Bioreactor"), and the obtained supernatant was used for UPLC determination of medium compound concentration.

An aliquot of 750 μl of supernatant was mixed with 750 μl of 10% w/w $ZnSO_4$. The obtained mixture was vortexed for 20 s and left standing for 10 min, after which the sample was centrifuged at 13,500 rpm during 5 min (CF-10, witeg Labortechnik GmbH, Offenburg, Germany) to remove proteins. A volume of 1.5 ml of supernatant was filtrated through a 0.20-μm nylon syringe filter (Macherey-Nagel GmbH & Co. KG, Düren, Germany) in a vial.

The concentrations of glucose, xylose, lactate, acetate, ethanol, and 2,3-BD in samples were determined by UPLC using the Agilent Technologies 1290 Infinity II LC system (Santa Clara, CA, United States) with a Carbo-H++ precolumn (4 mm × 3 mm; Phenomenex, Des Plaines, IL, United States), Rezex ROA column (15 cm × 7.8 mm; Phenomenex, Des Plaines, IL, United States), and a refractive index detector. The mobile phase was 0.0025 M H_2SO_4, the volume of the analyzed sample was 10 μl, and the flow rate was 0.6 ml min^{-1}. The temperature of the column was 60°C. The results were analyzed with OpenLab CDS software.

Bioprocess Efficiency Parameters

Bioprocess efficiency parameters were calculated according to the following equations (the average values of the monitored bioprocess parameters were used in these calculations):

$$Y_S = S_0 - S \quad (1)$$

$$Y_P = P - P_0 \quad (2)$$

$$Y_{P/S} = \frac{Y_P}{Y_S} = \frac{P - P_0}{S_0 - S} \quad (3)$$

$$r_S = \frac{dy_P}{dt} \quad (4)$$

$$\mu = \frac{dOD_{600}}{dt} \quad (5)$$

S_0, P_0 – initial concentration of the substrate or product (g l^{-1})

S, P – final concentration of the substrate or product (g l^{-1})

Y_S – total consumption of substrates (glucose and/or xylose) (g l^{-1})

Y_P – total product yield of 2,3-BD, ethanol, or lactate (g l^{-1})

$Y_{P/S}$ – conversion coefficient of substrate in the product (g g^{-1})

r_S – maximal consumption rate of the substrate (h^{-1})

r_P – maximal production rate of 2,3-BD, ethanol, or lactate (h^{-1})

μ – specific growth rate of *P. polymyxa* (h^{-1})

t – time (h).

RESULTS

Growth Kinetics and Biochemicals Production During Cultivation of *Paenibacillus polymyxa* DSM 742 on Media With Glucose, Xylose, or Their Mixture in Erlenmeyer Flasks

Glucose and xylose are the main carbohydrates that can be obtained after pretreatment of residual lignocellulosic raw materials. The choice of the pretreatment method greatly influences the concentration of the aforementioned fermentable sugars (Marđetko et al., 2018, 2021). Bacterium *P. polymyxa* can use glucose and xylose for its metabolic needs (Okonkwo et al., 2021). Therefore, it was of great importance to determine the influence of different carbon sources on the growth *P. polymyxa* DSM 742 and production of 2,3-BD and other metabolic products. For this research, different media were prepared, containing glucose and/or xylose as a carbon source. **Figure 2** shows the results of cultivation with glucose or xylose as a sole carbon source, while **Figures 3**, **4** show the results of cultivation with glucose and xylose as carbon sources in nutrient media. As it is shown in **Figure 2**, the exponential growth phase began after approximately 6 h. The highest rate of glucose consumption was observed between hours 10 and 35 of cultivation with glucose as a sole carbon source (**Figure 2** and **Table 3**). During the cultivation in the media that had an initial glucose concentration of 30 or 50 g l^{-1}, all glucose was consumed after 36 h of the bioprocess. The cultivation had an initial glucose concentration of 70 g l^{-1}; approximately 18% of the carbon source remained (13.2 g l^{-1}) at the end of the cultivation. The biomass concentration

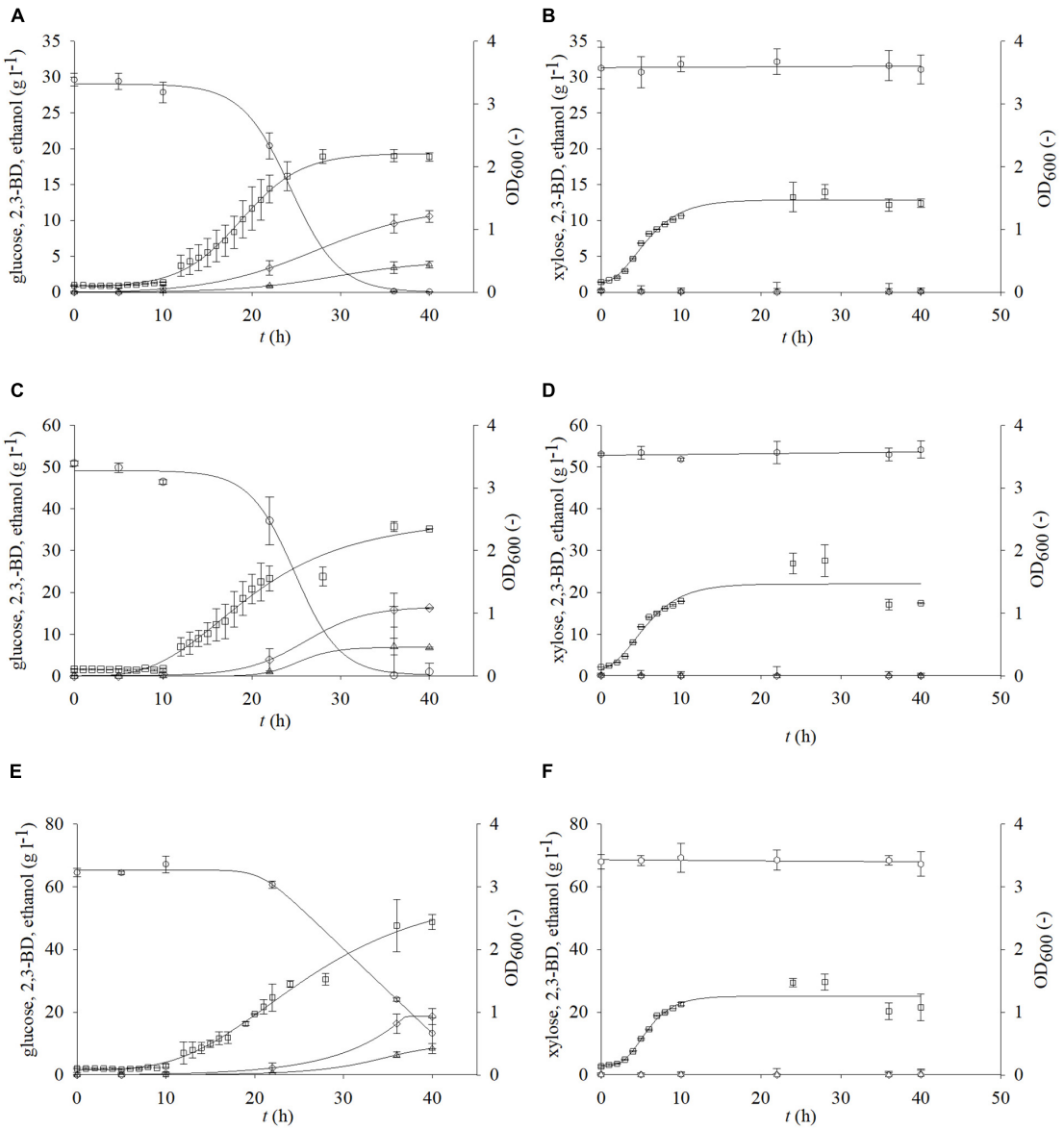

FIGURE 2 | Changes in optical density (OD_{600},□) and concentration of glucose (○) or xylose (●), 2,3-BD (◇), and ethanol (△) during cultivation of bacterium *P. polymyxa* DSM 742 in media with different carbon sources and their concentrations (**A,C,E** – glucose; **B,D,F**—xylose).

was evaluated as optical density determined at 600 nm (OD_{600}) according to Das et al. (2021). Furthermore, optical density was also used for bacterial growth rate determination according to Koller et al. (2019). The maximum values of optical density (OD_{600}) achieved at the end of *P. polymyxa* DSM 742 cultivation were 1.790 for initial glucose concentration of 30 g l^{-1}, 1.589 for 50 g l^{-1}, and 1.663 for 70 g of l^{-1}, respectively. The determined specific growth rates were 0.318 h^{-1} for 30 g l^{-1}, 0.219 h^{-1} for 50 g l^{-1}, and 0.216 h^{-1} for 70 g l^{-1} glucose.

At the initial glucose concentration of 30 g l^{-1}, the maximal 2,3-BD concentration was 10.57 g l^{-1}, while the ethanol concentration was 3.85 g l^{-1}. A 53.8% (16.26 g l^{-1}) of more 2,3-BD was produced in media with an initial glucose concentration of 50 g l^{-1} compared to the media with 30 g l^{-1} and 43% more ethanol than with 30 g l^{-1} (6.75 g l^{-1}). The highest concentration of 2,3-BD (18.61 g l^{-1}) was obtained during cultivation with 70 g l^{-1} of glucose, which is 12.62% more than 50 g l^{-1} and 42.2% more than 30 g l^{-1}. Since xylose is also present in the pretreated BSG, the growth kinetics and synthesis of products on media with xylose were also determined. The highest OD_{600} value (1.781) was observed with an initial xylose concentration of 50 g l^{-1} after 28 h of cultivation (**Figure 2**). With 30 g l^{-1} of xylose, in the same hour of the bioprocess, 13% lower value (1.536) was observed in comparison with 50 g l^{-1} of xylose, while the lowest concentration of biomass was observed with 70 g l^{-1} of the initial xylose concentration (1.416). During *P. polymyxa* cultivation on

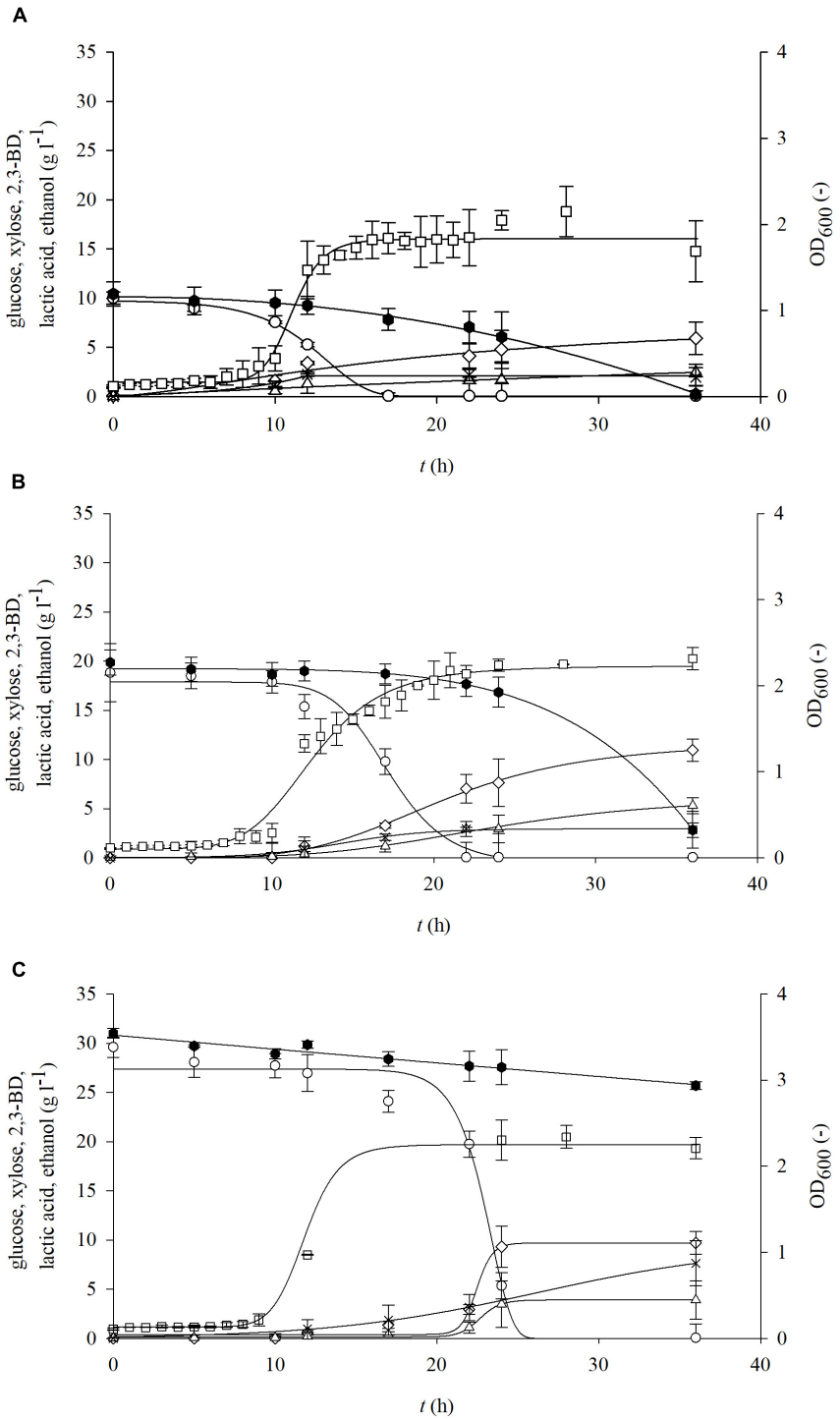

FIGURE 3 | Changes in optical density (OD_{600},□) and concentration of glucose (○), xylose (●), 2,3-BD (◇), lactate (▲), and ethanol (△) during cultivation of bacterium *P. polymyxa* DSM 742 in media with different initial glucose and xylose concentrations [**(A)** 10 g l^{-1} glucose and 10 g l^{-1} xylose; **(B)** 20 g l^{-1} glucose and 20 g l^{-1} xylose; **(C)** 30 g l^{-1} glucose and 30 g l^{-1} xylose].

media with 5, 10, and 20 g l^{-1} of xylose, slightly lower optical densities were observed than in previous experiments (data not shown). In these cases, the following concentrations of 2,3-BD were obtained: 5 g l^{-1} of xylose (1 g l^{-1} 2,3-BD), 10 g l^{-1} (2.92 g l^{-1} 2,3-BD), and 20 g l^{-1} (0.34 g l^{-1} 2,3-BD). At the same time, the ethanol concentrations were 1.16 g l^{-1} for 5 g l^{-1}

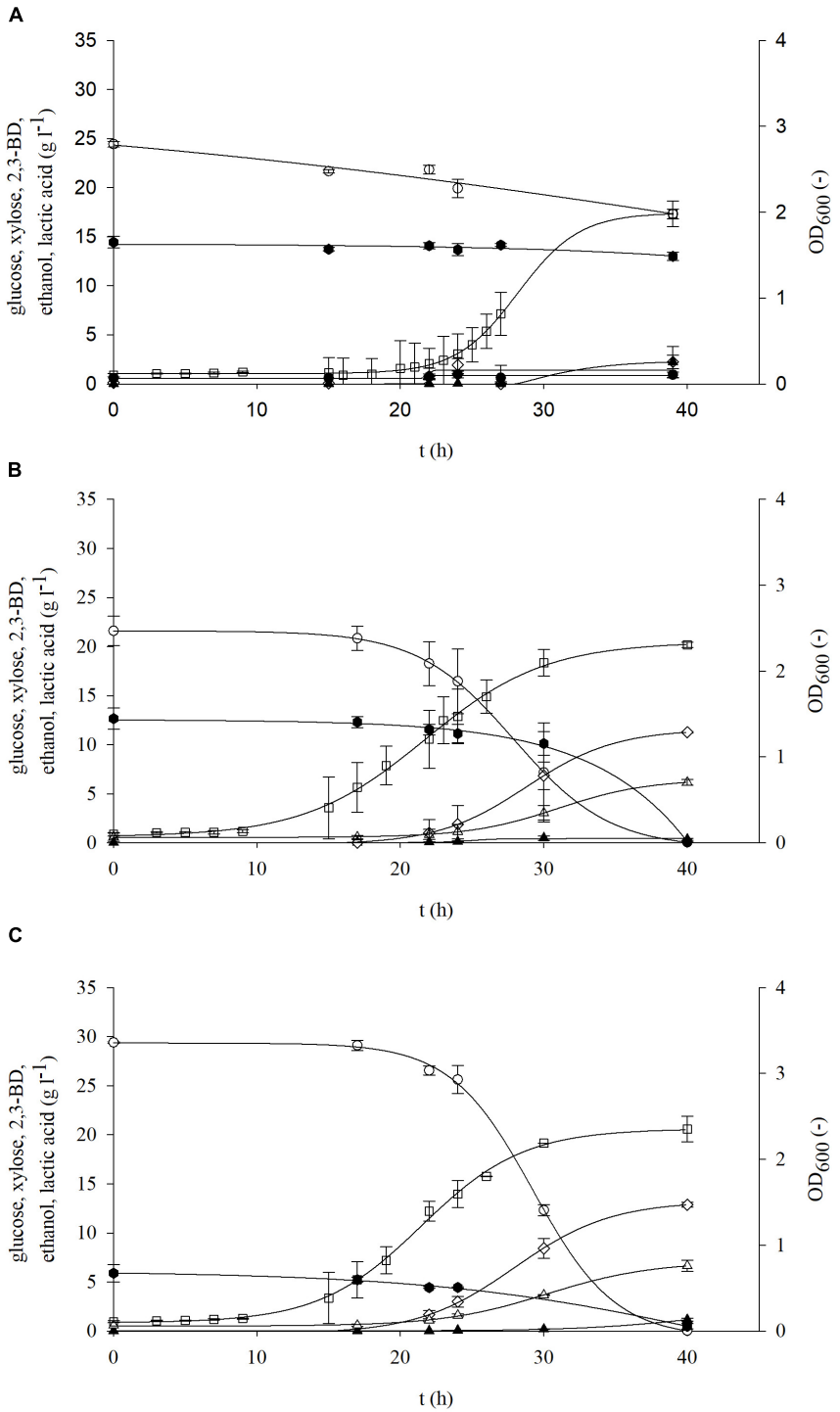

FIGURE 4 | Changes in optical density (OD_{600},□) and concentration of glucose (○), xylose (●), 2,3-BD (◇), lactate (▲), and ethanol (△) during cultivation of bacterium *P. polymyxa* DSM 742 in media with different initial glucose and xylose concentrations [**(A)** 27 g l^{-1} glucose and 12 g l^{-1} xylose; **(B)** 22 g l^{-1} glucose and 10 g l^{-1} xylose; **(C)** 33 g l^{-1} glucose and 4 g l^{-1} xylose].

of xylose, 1.84 g l^{-1} for 10 g l^{-1}, and 0.89 g l^{-1} for 20 g l^{-1}, respectively. The increase in initial xylose concentration (5–70 g l^{-1}) in medium did not show a clear impact on the bioprocess efficiency parameters (**Table 3**), although a slight increase in medium optical density was observed. Furthermore, the xylose consumption during *P. polymyxa* DSM 742 cultivation was also

TABLE 3 | Specific growth rate, consumption of substrate and synthesis of product, and yield of cultivation of *P. polymyxa* DSM 742 on media with different carbon sources.

Type of media	μ [h^{-1}]	$r_{S\ glc}$ [h^{-1}]	$r_{S\ xyl}$ [h^{-1}]	r_{BD} [h^{-1}]	r_{EtOH} [h^{-1}]	$Y_{P/S\ BD}$ [g g^{-1}]	$Y_{P/S\ EtOH}$ [g g^{-1}]
Glucose 30 g l^{-1}	0.318	0.341	/	0.102	0.109	0.012	0.130
Glucose 50 g l^{-1}	0.219	0.384	/	0.120	0.154	0.007	0.135
Glucose 70 g l^{-1}	0.216	0.053	/	0.130	0.162	0.005	0.164
Xylose 5 g l^{-1}	0.136	/	0.036	0.028	0.022	0.189	0.220
Xylose 10 g l^{-1}	0.124	/	0.244	0.088	0.045	0.262	0.166
Xylose 20 g l^{-1}	0.074	/	/	/	/	/	/
Xylose 30 g l^{-1}	0.204	/	/	/	/	/	/
Xylose 50 g l^{-1}	0.213	/	/	/	/	/	/
Xylose 70 g l^{-1}	0.184	/	/	/	/	/	/
Glucose (10 g l^{-1}) + xylose (10 g l^{-1})	0.297	0.778	0.248	0.840	/	0.291	0.122
Glucose (20 g l^{-1}) + xylose (20 g l^{-1})	0.291	1.056	0.137	0.356	/	0.304	0.148
Glucose (30 g l^{-1}) + xylose (30 g l^{-1})	0.220	0.410	/	0.256	/	0.277	0.112
Glucose (27 g l^{-1}) + xylose (12 g l^{-1})	0.241	0.008	/	0.042	0.022	0.041	0.104
Glucose (22 g l^{-1}) + xylose (10 g l^{-1})	0.093	0.083	0.277	0.124	0.107	0.331	0.181
Glucose (33 g l^{-1}) + xylose (4 g l^{-1})	0.154	0.393	0.128	0.108	0.097	0.370	0.191

μ, *specific growth rate;* r_{Sglc}, *glucose consumption rate;* r_{Sxyl}, *xylose consumption rate;* r_{BD}, *production rate for 2,3-BD;* r_{EtOH}, *production rate for ethanol;* $Y_{P/SBD}$, *product yield for 2,3-BD;* $Y_{P/SEtOH}$, *product yield for ethanol.*

at relatively low levels and therefore no significant formation of products (such as 2,3-BD or ethanol) was observed. Application of physiochemical pretreatment methods such as pretreatment of lignocellulosic raw materials in a high-pressure reactor using dilute acid (Marđetko et al., 2018) allows to obtain liquid hydrolysates containing predominantly carbohydrates such as glucose and xylose and some other sugars (e.g., arabinose, galactose or mannose) in significantly smaller (or negligible) concentrations. As hydrolysates of lignocellulosic feedstocks contain multiple carbon sources, it is also necessary to investigate the growth kinetics of *P. polymyxa* in such media. The initial concentrations of both sugars (glucose and xylose) were therefore adjusted so that each medium contains the defined sugar concentration (**Table 1** and **Figures 3**, **4**). The selected sugar concentrations are similar to concentrations in the hydrolysate of lignocellulosic raw materials.

During bacterial cultivation in media with 10 g l^{-1} glucose and 10 g l^{-1} xylose and with 20 g l^{-1} glucose and 20 g l^{-1} xylose, the exponential phase started after 7 h of cultivation, while in media with 30 g l^{-1} glucose and 30 g l^{-1} xylose it started after 9 h (**Figure 3**). After 17 h of cultivation with 10 g l^{-1} glucose and xylose, glucose was completely exhausted, while xylose was depleted after 40 h. In media with 20 g l^{-1} of each sugar, glucose was consumed after 24 h, while 14% (2.82 g l^{-1}) of the initial concentration of xylose remained at the end of cultivation. Glucose was also completely exhausted in the media with an initial concentration of 30 g l^{-1} after 24 h, while at the end of cultivation, 85% of the initial xylose concentration (25.68 g l^{-1}) remained. The rate of glucose uptake (**Table 3**) is 2–3 times higher in media with both carbon sources than in substrates containing only glucose. Also, in contrast to the media which contain only xylose, when both carbon sources are present, xylose is partially exhausted especially at lower initial concentrations (10 and 20 g l^{-1}). During bacterial cultivation on media with non-equal glucose-to-xylose ratios (similar to the BSG hydrolysates), a similar bioprocess behavior (**Figure 4**) was observed as in the previous set of experiments. As it is shown in **Figure 4A**, both sugars were not consumed during bacterial cultivation at 27 g l^{-1} glucose and 12 g l^{-1} of xylose in the period of 40 h probably due to the prolonged bacterial lag phase (cca. 20 h). In other two cases (**Figures 4B,C**), the bacterial lag phase was shorter (cca. 10 h) and consequently both sugars were consumed in the 40-h period. In both sets of the experiment, it was observed that *P. polymyxa* DSM 742 consumed sugars sequentially. The consumption of xylose started when glucose was almost exhausted.

During the cultivation of *P. polymyxa* DSM 742 on media with combination of the two carbon sources, the following products were obtained: 2,3-BD, ethanol, and lactate. As expected, the highest concentrations of products were determined at the end of the bioprocess. Synthesis of products starts at the beginning of the exponential phase and continues during the stationary bacterial growth phase. The highest concentration of 2,3-BD (10.95 g l^{-1}) was achieved in media with an equal glucose-to-xylose ratio at the combination of 20 g l^{-1} of glucose and 20 g l^{-1} xylose (**Figure 3B**). In media with 10 g l^{-1} of the initial concentration, the highest obtained concentration of 2,3-BD was 5.92 g l^{-1}, while 9.70 g l^{-1} of 2,3-BD was produced with 30 g l^{-1}, which is 50 and 22% less compared to the media with 40 g l^{-1} of total sugars, respectively. Compared to cultivations performed on glucose as the only carbon source, the specific production rate of 2,3-BD (**Table 3**) is multiple times higher: 0.840 h^{-1} (10 g l^{-1} glucose and 10 g l^{-1} xylose), 0.356 h^{-1} (20 g l^{-1} glucose and 20 g l^{-1} xylose), and 0.256 h^{-1} (30 g l^{-1} glucose and 30 g l^{-1} xylose). Except 2,3-BD, as a product of cultivation, ethanol was also determined in samples. In cultivation with 10 g l^{-1} glucose and xylose (**Figure 3A**), the ethanol concentration of 2.48 g l^{-1} was achieved, while twice as much (5.32 g l^{-1}) was achieved in media with 20 g l^{-1} sugars. The increased total sugar concentration (30 g l^{-1} glucose + 30 g l^{-1} xylose; **Figure 3C**) yielded 26.6% less ethanol in comparison with the media with

20 g l^{-1} (**Figure 3B**), but 57% more than on the media with 10 g l^{-1} (**Figure 3A**). The highest concentration of lactate (7.63 g l^{-1}) was produced in media with 30 g l^{-1} of glucose and xylose (**Figure 3C**), 62.6% less (2.85 g l^{-1}) lactate was produced with 20 g l^{-1} of glucose and xylose (**Figure 3B**), while 1.94 g l^{-1} (74.6 % less) of lactate was produced in media containing 10 g l^{-1} of glucose and xylose (**Figure 3A**). During the cultivation of *P. polymyxa* DSM 742 in media with a non-equal glucose-to-xylose ratio, the highest 2,3-BD concentration (12.88 g l^{-1}) was observed in medium with 33 g l^{-1} of glucose and 4 g l^{-1} of xylose together with the ethanol concentration of 6.63 g l^{-1} and lactate concentration of 1.16 g l^{-1} (**Figure 4C**). A slightly lower 2,3-BD concentration (11.26 g l^{-1}) was obtained during bacterial cultivation on the medium with 22 g l^{-1} of glucose and 10 g l^{-1} of xylose together with the ethanol concentration of 6.16 g l^{-1} and lactate concentration of 0.36 g l^{-1} (**Figure 4B**). In this set of experiments, the lowest 2,3-BD concentration (2.40 g l^{-1}) was observed during bacterial cultivation in medium with 27 g l^{-1} of glucose and 12 g l^{-1} of xylose together with the ethanol concentration of 0.92 g l^{-1} and lactate concentration of 2.22 g l^{-1} (**Figure 4A**). It is known in literature that bacteria *P. polymyxa* can also produce lactate during cultivation (Dai et al., 2014; Cao et al., 2017; Okonkwo et al., 2020). In our research, lactate was not determined during cultivation with glucose or xylose as a sole carbon source, but when two carbon sources were used, lactate production was observed. Also, it can be observed that the concentration of produced lactate increases with the increase of the total initial sugar concentration by an equal glucose-to-xylose ratio in cultivation media. However, the non-equal ratio of glucose and xylose (2.25:1, 2.2:1, and 8.25:1) in media is related to the considerably lower lactate production during *P. polymyxa* DSM 742 cultivations. Therefore, further research is required to define the optimal glucose-to-xylose ratio for *P. polymyxa* DSM 742 cultivation for 2,3-BD production.

Growth Kinetics and Biochemicals Production During Cultivation of *Paenibacillus polymyxa* DSM 742 on Different Brewers' Spent Grains Hydrolysates in a Stirred Tank Bioreactor

In the first part of this research, the main focus was to determine growth kinetics and biochemical production during cultivation of *P. polymyxa* DSM 742 in media with glucose and/or xylose, that is, carbohydrates that can be obtained after dilute acid pretreatment of BSG. Physiochemical and enzymatic pretreatment methods, as described in "Materials and Methods," yielded three different cultivation media. First, BSG were hydrolyzed with dilute acid (0.5% w/w H_2SO_4) in a high-pressure reactor, using the method by Marđetko et al. (2018), in order to obtain a liquid hydrolysate rich in fermentable sugars and a solid part in which remain non-hydrolyzed complex sugars. The obtained liquid phase of pretreated BSG was detoxified with active coal in order to remove possible inhibitory compounds, and thus second cultivation media were obtained. The solid part of pretreated BSG was hydrolyzed with commercially available lignocellulolytic enzymes to produce third cultivation media. After obtaining the media, batch cultivation of *P. polymyxa* DSM 742 in a stirred tank bioreactor was conducted on non-detoxified and detoxified liquid phases and an enzymatic hydrolyzed solid phase of pretreated BSG. The results are shown on **Figures 5**–**7**.

From the obtained results, it can be observed that the adaptation phase of *P. polymyxa* to non-detoxified, detoxified, and enzymatic hydrolysates of BSG was approximately the same and lasted around 10 h. During the cultivation of *P. polymyxa* DSM 742 on the non-detoxified liquid phase of pretreated BSG (**Figure 5**), it was observed that glucose was completely consumed after 72 h of cultivation and the maximum

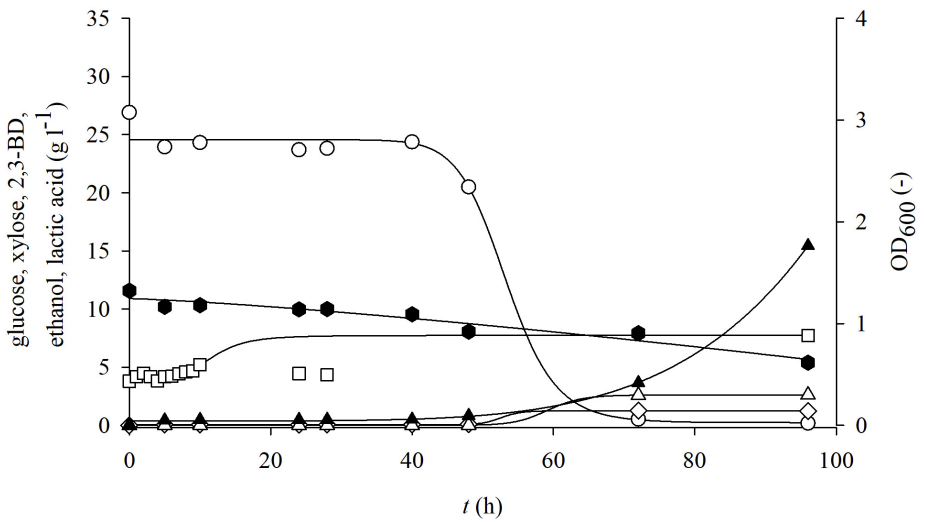

FIGURE 5 | Changes in optical density (OD_{600},□) and concentration of glucose (○), xylose (●), 2,3-BD (◇), ethanol (△), and lactate (▲) during cultivation of bacterium *P. polymyxa* DSM 742 in media with liquid phase of dilute acid BSG hydrolysate in the stirred tank bioreactor.

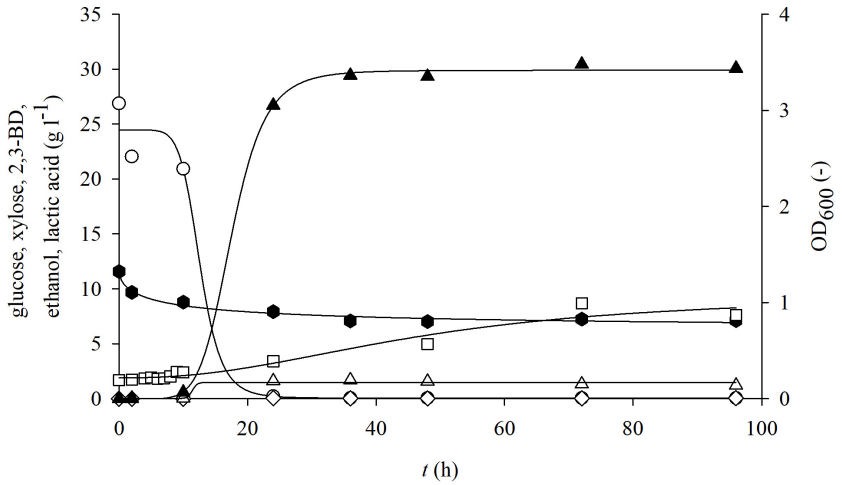

FIGURE 6 | Changes in optical density (OD_{600},□) and concentration of glucose (○), xylose (●), 2,3-BD (◇), ethanol (△), and lactate (▲) during cultivation of bacterium *P. polymyxa* DSM 742 in media with liquid phase of detoxified dilute acid BSG hydrolysate in the stirred tank bioreactor.

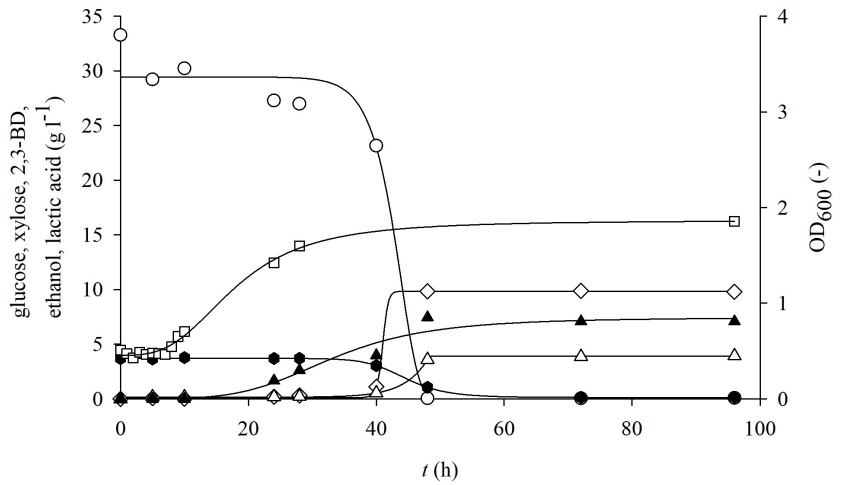

FIGURE 7 | Changes in optical density (OD_{600},□) and concentration of glucose (○), xylose (●), 2,3-BD (◇), ethanol (△), and lactate (▲) during cultivation of bacterium *P. polymyxa* DSM 742 in media with enzymatically hydrolyzed solid phase of dilute acid BSG hydrolysate in the stirred-tank bioreactor.

consumption rate was 0.127 h^{-1}. Xylose was consumed slower than glucose, so a final concentration of xylose was 46.5% of the initial concentration (11.58 to 5.38 g l^{-1}) with a specific consumption rate of 0.0089 h^{-1}. The highest concentration of 2,3-BD was reached after 72 h as well as maximal ethanol concentration. The majority of ethanol was produced during first 48 h, while its concentration was slightly increased with prolonged cultivation. After 72 h of cultivation, 1.26 g l^{-1} of 2,3-BD, 2.5 g l^{-1} of ethanol, and 3.6 g l^{-1} of lactate were produced. At the end of cultivation (96 h), there was a decrease in the concentration of 2,3-BD (1.22 g l^{-1}), while the concentrations of other metabolic products increased (15.43 g l^{-1} of lactate and 2.61 g l^{-1} of ethanol).

The results of cultivation of the bacterium *P. polymyxa* DSM 742 in the liquid detoxified phase of pretreated BSG are shown in **Figure 6**. The initial total phenol concentration in the liquid phase of pretreated BSG was 1.40 g l^{-1}, but after the detoxification process it was only 0.40 g l^{-1}. As it is shown in **Figure 6**, glucose is completely exhausted until the end of the exponential phase, while the concentration of xylose at the end of the bioprocess was 61.5% of the initial concentration (decrease from 11.58 to 7.12 g l^{-1}). After 24 h of cultivation, 26.7 g l^{-1} of lactate was produced, which makes 87.7% of the total synthesis. At the end of the bioprocess, at 96 h, 30.07 g l^{-1} lactate and 3.96 g l^{-1} acetate were synthetized on the detoxified pretreated BSG.

After separation at the end of the physiochemical pretreatment, the solid part of lignocellulosic raw materials is usually discarded as a waste (Macheiner et al., 2003). The solid phase of pretreated BSG, after pretreatment in our research, contains 36.69% w/w of glucans and 2.13% w/w of xylans, meaning that it still has complex sugars that can be used for obtaining fermentable sugars. Therefore, the solid part of

pretreated BSG was enzymatically hydrolyzed in acetic buffer in the HRTB. After enzymatic treatment, 33.27 g l^{-1} of glucose and 3.68 g l^{-1} of xylose were obtained, thus increasing the overall carbohydrate yield from BSG. During cultivation in such media, it was observed that the lag phase was approximately 7 h (**Figure 7**). The maximal specific glucose consumption rate was 0.758 h^{-1} (**Table 4**). After 48 h of cultivation, products that were determined were 9.84 g l^{-1} 2,3-BD, 3.58 g l^{-1} ethanol, and 7.45 g l^{-1} lactate. The specific product concentration did not significantly change with prolongation of cultivation.

DISCUSSION

In beer production, BSG is generated in large quantities during the whole year. Due to its high protein and carbohydrate content, it can be used as a raw material in biotechnology for the production of phenolic acids, lactate, biogas, bioethanol, or xylitol or as a medium for cultivation of various microorganisms, for production of enzymes, or as a carrier for immobilizing yeast during a beer fermentation. It is most often used as livestock feed, as an additive to products intended for human consumption, or as a raw material for production of construction materials, coal, paper, and energy, but also it has the potential to be used as an adsorbent (Mussatto, 2014). The economy of the production of chemicals like 2,3-BD mostly depends on the used renewable raw material which is also a carbon source. The use of cheap residual materials such as BSG can greatly reduce production costs and thus make the production process economically and environmentally sustainable (Amraoui et al., 2021). Due to its high content of polysaccharides, BSG have a great potential for application in the biotechnological industry (Ferraz et al., 2013; Mussatto, 2014; Paz et al., 2019; Jackowski et al., 2020). In addition to the biobased materials, a major role in the production of biochemicals plays selection of an appropriate microorganism as a producer of biochemicals, biofuels, or biomaterials.

Unlike other bacteria that produce 2,3-BD, for example *Klebsiella* sp., *Serratia marcescens*, *Escherichia coli*, and *Enterobacter aerogenes* (Lee et al., 2015; Schilling et al., 2020; Chu et al., 2021), *P. polymyxa* DSM 742 used in this research has a GRAS status and can also produce various other products such as ethanol, lactate, and acetate (Lal and Tabacchioni, 2009; Okonkwo, 2017; Jeong et al., 2019), thus making this selected microorganism ideal for cultivation and setup biorefinery concept to produce various biochemicals from food or agriculture residues, using different pretreatment methods for raw materials and different cultivation techniques to maximize bioprocess yield and efficiency. To this date, there is not enough research data for this strain of *P. polymyxa* DSM 742 that can qualitatively describe growth kinetics and biochemical production during cultivation of selected strain on sugars stemming from pretreated lignocellulosic raw materials as BSG.

Firstly, for characterization of growth kinetics and biochemicals production by strain of *P. polymyxa* DSM 742, we tested different concentrations of two types of carbon source, glucose and xylose, as well as their combination. It is known that glucose and xylose are main sugars obtained after pretreatment of BSG. In this study, different concentrations of single sugars or their mixture in media were tested (**Table 1**). These sugar concentration ranges and ratios are selected due to their frequent appearances in the hydrolysates of lignocellulosic raw materials (Carvalheiro et al., 2004; Marwoto et al., 2004; Chetrariu and Dabija, 2020). Obtained results have shown that there is an increase in 2,3-BD production with increase in initial glucose concentration. However, it appears that a high concentration of substrate slightly inhibits the growth of selected strain *P. polymyxa*. The highest 2,3-BD concentration was achieved during cultivation with 70 g l^{-1} of glucose and was 18.61 g l^{-1}, and 13% less 2,3-BD was produced with 50 g l^{-1} of glucose, while 44% less was produced with the initial concentration of 30 g l^{-1}. Synthesis of ethanol is increased with the increase in concentration of glucose in media as well. The concentration of ethanol during cultivation with 30 g l^{-1} of glucose was 4 g l^{-1}, 45% more was produced during cultivation on 50 g l^{-1} and 53% more with 70 g l^{-1} of glucose compared to the cultivation on 30 g l^{-1} (**Figure 2** and **Table 3**). During cultivation in media containing only xylose, there was no significant synthesis of any metabolic product 2,3-BD, ethanol, or lactate. The reason for this could be the more demanding uptake of xylose in bacterial cells compared to the glucose uptake. This means that xylose as the only carbon source has negligible impact on the kinetics of product formation. These results need further investigation since literature shows production of acetate or 2,3-BD depending on the sugar content in medium (Marwoto et al., 2004; Okonkwo et al., 2021).

After determination of growth kinetics and production of various biochemicals on glucose and xylose as the only medium carbon sources, a research was conducted where *P. polymyxa* DSM 742 was cultivated in media with combined glucose and

TABLE 4 | Bioprocess efficiency parameters during cultivation of bacterium *P. polymyxa* DSM 742 on media with different BSG hydrolysates.

Type of media	μ [h^{-1}]	$r_{S\ glc}$ [h^{-1}]	$r_{S\ xyl}$ [h^{-1}]	r_{BD} [h^{-1}]	r_{EtOH} [h^{-1}]	r_{LA} [h^{-1}]	$Y_{P/S,\ BD}$ [g g^{-1}]	$Y_{P/S,\ EtOH}$ [g g^{-1}]
LP-BSG	0.0063	0.127	0.0067	0.097	0.17	/	0.254	0.102
DLP-BSG	0.0228	0.235	0.0089	/	/	0.273	0.001	0.000
SP-BSG	0.0528	0.758	0.0958	0.160	0.13	/	0.033	0.070

μ, *specific growth rate;* r_{Sglc}, *glucose consumption rate;* r_{Sxyl}, *xylose consumption rate;* r_{BD}, *production rate for 2,3-BD;* r_{EtOH}, *production rate for ethanol;* r_{LA}, *production rate for lactate;* $Y_{P/SBD}$, *product yield for 2,3-BD;* $Y_{P/SEtOH}$, *product yield for ethanol; LP-BSG, liquid phase of pretreated BSG supplemented with 4 g* l^{-1} *yeast extract; DLP-BSG, detoxified liquid phase of pretreated BSG supplemented with 4 g* l^{-1} *yeast extract; SP-BSG, enzymatic hydrolysate of solid phase of pretreated BSG supplemented with 4 g* l^{-1} *yeast extract.*

xylose as carbon sources, in the range of concentrations of 20 to 60 g l^{-1} of total sugars. During 48 h, the glucose consumption rate was 2–3 times higher compared to the glucose consumption rate in media with glucose as a sole carbon source. Xylose was only partially consumed, especially in media with lower sugar concentrations. Comparison between media with only one sugar type (2,3-BD and ethanol were produced) and media with both sugars shows that lactate was additionally produced. The highest concentrations of 2,3-BD and ethanol were obtained with 33 g l^{-1} of glucose and 4 g l^{-1} xylose, respectively (12.88 g l^{-1} 2,3-BD and 6.63 g l^{-1} ethanol). Production of lactate increases with the increase in total sugar content in media with equal glucose to xylose ratio and the highest lactate concentration (7.63 g l^{-1}) was observed during cultivation with 60 g l^{-1} of total sugar concentration. This phenomenon can be explained by the carbon catabolite repression (CCR) or glucose effect where sugars were sequentially used. Xylose consumption begins when glucose was depleted, which leads to the low 2,3-BD yield and productivity (Li et al., 2015). However, the non-equal glucose-to-xylose ratios (2.25:1, 2.2:1, and 8.25:1; **Figure 4**) in cultivation media are related to the considerably lower lactate concentrations during *P. polymyxa* DSM 742 cultivations in combination with relatively high 2,3-BD concentrations. Additionally, cultivation of the *P. polymyxa* ATCC 12321 strain in media containing non-equal glucose-to-xylose ratios (5:1, 2:1, 1:2, 1:5) shows that the increase in xylose content was related to a decrease in lactate concentrations (Ma et al., 2018). The final lactate concentrations were at similar levels (the range of 0.5–2.5 g l^{-1}) during cultivations of both *P. polymyxa* strains in media with non-equal glucose-to-xylose ratios. A comparison between our study and that of Ma et al. (2018) shows that the acetate concentration was enlarged with the increase in xylose concentration in media with non-equal glucose-to-xylose ratios, but in both studies a similar range of acetate concentrations was observed (up to 1.5 g l^{-1}). It is known that acetate kinase activity in xylose-grown cells on xylose medium was higher than that of glucose-grown cells. Furthermore, the activity of phosphoketolase responsible for ethanol synthesis was relatively low (Marwoto et al., 2004). Glucose is metabolized faster than xylose by *P. polymyxa* due to the longer time required for synthesis of enzymes involved in xylose metabolism, and therefore, the lag phase in xylose consumption was observed (Ma et al., 2018). Based on the above discussion, it is obvious that both strains of *P. polymyxa* (ATCC 12321 and DSM 742) show a similar metabolic behavior on the media containing glucose and xylose as carbon sources.

The diversity of *P. polymyxa* DSM 724 metabolism can be explained by the fact that 2,3-BD and its precursor acetoin are produced from pyruvate, obtained from sugars and other carbohydrates metabolized either by the glycolytic pathway (hexoses) or *via* a combination with the pentose-phosphate metabolic pathway (e.g., xylose). Acetoin and 2,3-BD are obtained in mixed-acid fermentation, which also generates other final metabolites such as lactate, acetate, succinate, and formate, ethanol, and glycerol. This phenomenon can be explained by the carbon catabolite repression which is a consequence of sequentially sugar consumption in media (Petrov and Petrova, 2021). Depending on the type of producer and the cultivation conditions, these metabolites are obtained in different proportions or do not accumulate at all. The same bacterial strain can produce predominantly 2,3-BD or acetoin as alternative final metabolites *via* the manipulation of bioprocess parameters (Ji et al., 2011; Schilling et al., 2020; Petrov and Petrova, 2021) where one mole of glucose is converted into pyruvate by the simultaneous generation of two moles of ATP and NADH *via* glycolysis. Consequently, two moles of pyruvate are converted into α-acetolactate, which is further decarboxylated to acetoin and finally dehydrogenated to 2,3-BD, while simultaneously one redox equivalent of NAD^+ is produced. In the absence of alternative electron acceptors during anaerobic and microaerobic conditions, the redox balance is maintained by the formation of additional side products (Schilling et al., 2020) such as lactate and ethanol. Depending on oxygen concentration, lactate dehydrogenase, pyruvate formate lyase, and the pyruvate dehydrogenase complex compete for the intermediate pyruvate. This finally results in the production of lactate, formate, ethanol, or acetate (Alexeeva et al., 2003; Schilling et al., 2020). Pyruvate formate lyase represents a redox valve, which can compensate for the redox imbalance of the 2,3-BD pathway (Adlakha et al., 2015). Due to the redox imbalance of 2,3-BD synthesis, other pathways are required to ensure NAD^+ equilibrium. When the NAD^+/NADH balance cannot be restored otherwise under microaerobic conditions, glucose is converted to redox-neutral end products such as ethanol and lactate. Pyruvate formate lyase enables the conversion of pyruvate to acetyl-CoA without generating any redox equivalents. Subsequently, two moles of NAD^+ are regenerated by the combined action of aldehyde dehydrogenase and alcohol dehydrogenase. This route represents the most efficient pathway for redox regeneration in *P. polymyxa* DSM 742 which allows for the compensation of the redox imbalance of the 2,3-BD biosynthesis (Adlakha et al., 2015; Schilling et al., 2020). From the technological point of view, these results show that it is possible to obtain more than one useful product with multiple carbon sources present in cultivation media as it can be important for a biorefinery approach.

After appropriate pretreatment of BSG, the liquid phase of pretreated BSG containing glucose and xylose can serve as a carbon source for submerged microbial cultivation. Furthermore, the solid phase of pretreated BSG was subsequently hydrolyzed with commercial lignocellulolytic enzymes to maximize the utilization of fermentable sugars from the feedstock. The obtained substrates were used as a carbon source during the cultivation of *P. polymyxa* DSM 742 for the production of various biochemicals such as 2,3-BD, ethanol, and lactate. From the results, it can be seen that glucose was first exhausted while xylose reached 46.5% of the initial concentration at the end of the process. The concentrations of products were lower in comparison with the concentrations reached in media with glucose and/or xylose. Dilute acid-pretreated BSG contain sugars for microbial cultivation but also different chemicals that can inhibit growth of microorganisms and synthesis of products (Bensah and Mensah, 2013; Mardetko et al., 2018). Treatment of the liquid phase of pretreated BSG with active carbon is a cheap and fast way to remove inhibitors. Active carbon can effectively adsorb furfural, hydroxymetilfurfural

(HMF), various aromatic compounds, and organic acids and to a very low extent adsorb acetate (Sjulander and Kikas, 2020). During detoxification of poplar prehydrolysates with active carbon (5% w/v), 77.9% of initial furan derivatives and 98.6% of initial aromatic monomers were removed (Zhang et al., 2018). Removal of inhibitors can affect bacterial growth and yield as well as product synthesis (Mhlongo et al., 2015). Therefore, cultivation of *P. polymyxa* DSM 742 was conducted on the detoxified liquid phase of pretreated BSG. As it was expected, until the end of the bioprocess, glucose was completely exhausted, while only 38.5% of the initial xylose concentration was consumed. During this cultivation, 30.07 g l^{-1} lactate and 3.96 g l^{-1} acetate were produced, but production of 2,3-BD and ethanol was negligible. During cultivation of *P. polymyxa* DSM 742 on the non-detoxified liquid phase of pretreated BSG, approximately a twice lower lactate concentration was observed. This phenomenon can be explained by the fact that the metabolism of *P. polymyxa* can be affected by different factors like temperature, pH, concentrations of dissolved oxygen and fermentation inhibitors, and exopolysaccharide synthesis (Okonkwo et al., 2020). 2,3-BD is the main metabolic product at pH range 5.0–6.5 and lactate at pH 7.1–8.0, respectively. This fact shows that the metabolism of *P. polymyxa* can be altered due to the pH level, and consequently the efficiency of 2,3-BD production can be improved by the maintenance of an appropriate pH range in the broth (Hakizimana et al., 2020). During cultivation of *P. polymyxa* DSM 742 in the bioreactor, pH was maintained at pH = 6.5, and therefore enzymes involved in organic acid synthesis (lactate dehydrogenase and acetate kinase) have higher activities and consequently higher lactate and acetate concentrations were observed especially during cultivation on detoxified pretreated BSG. It is known that the acetate concentration in media up to 12 g l^{-1} shows a positive effect on 2,3-BD production (Nakashimada et al., 2000), and therefore it can partially compensate for the 4-hydroxybenzoic acid inhibition effect (it is observed at the concentration of 0.169 g l^{-1}) on the 2,3-BD synthesis (Jurchescu, 2014). Adsorption of 4-hydroxybenzoic acid on the active carbon is characterized by a weak bounding (Costa et al., 1988), and consequently, it is can be assumed that its concentration in the detoxified liquid phase of pretreated BSG is still in the inhibitory level. Therefore, 2,3-BD synthesis was on a negligible level during *P. polymyxa* DSM 742 cultivation on this BSG medium.

Recently, it was also discovered that *P. polymyxa* DSM 365 possesses the ability to transform HMF to HMF alcohol and eventually to furoic acid in media with HMF as a sole carbon source. In this study, 95% of HMF was transformed into furoic acid which is further used for notable bacterial growth. The growth of *P. polymyxa* in media with furfural as a sole carbon source was severely inhibited although furfural was converted into furfuryl alcohol (16–50% of the initial concentration), but without notable bacterial growth. Cultivation of *P. polymyxa* DSM 365 on the phenolic compounds as a sole carbon source shows that bacterium has the ability to reduce their concentrations as follows: 94% of p-coumaric acid, 59% of vanillic acid, and 68% vanillin. However, in these experiments bacterial growth was not observed (Okonkwo et al., 2021). It is also known that higher oxygen concentrations have a negative impact on the 2,3-BD production, but positive on the bacterial biomass growth. Our cultivations of *P. polymyxa* DSM 742 were performed in microaerobic conditions due to the fact that relatively low final bacterial biomass concentrations were obtained. During 2,3-BD production, *P. polymyxa* synthesizes the exopolysaccharides (cca 50 g l^{-1}) and therefore 2,3-BD production efficiency is reduced. Furthermore, exopolysaccharides can clog bioreactor pipes, increase energy consumption for broth mixing, and considerably complicate the 2,3-BD downstream process (Okonkwo et al., 2020). Based on the previous consideration, it is obvious that different cultivation factors of *P. polymyxa* DSM 742 have to be carefully considered in order to obtain desirable bacterial metabolic products like 2,3-BD, ethanol, or lactate. On the basis of the obtained results, it is clear that different methods of processing the same raw material, BSG, can be used to obtain several different products. This phenomenon is still not well described in literature; therefore, it needs further investigation on metabolic pathways of the *P. polymyxa* DSM 742 strain.

The solid part that remains after dilute acid pretreatment of BSG contains carbohydrates which are not used (for example, glucans are present at 36.69% w/w). Rather than to dispose this as a waste, it can be processed by enzymatic hydrolysis and consequently increase the overall sugar yield of the raw material for different biotechnological processes. This enzymatically obtained nutrient medium contained 23.73% more glucose and 68.2% less xylose than in the liquid phase of pretreated BSG after dilute acid hydrolysis. The glucose consumption rate was the highest from all studied cultivations on obtained pretreated BSG (0.758 h^{-1}), which is 69% higher in comparison with the detoxified liquid phase of pretreated BSG (0.235 h^{-1}) and 83% higher in comparison with the non-detoxified liquid phase of pretreated BSG (0.127 h^{-1}). The maximum concentrations for all products were reached after 48 h of cultivation (2,3-BD 9.84 g l^{-1}, ethanol 3.58 g l^{-1}, and lactate 7.45 g l^{-1}) and did not change significantly until the end of cultivation. The final concentration of lactate (7.08 g l^{-1}) in enzymatic hydrolysate was 50% lower (15.43 g l^{-1}) in comparison with the lactate concentration obtained on the non-detoxified liquid phase of pretreated BSG and 76% lower (30.07 g l^{-1}) than the lactate concentration obtained on the detoxified liquid phase of pretreated BSG. The production rate of 2,3-BD on the enzymatic hydrolysate of the solid phase of pretreated BSG was 1.65 times higher than on the non-detoxified liquid phase of pretreated BSG, but despite that fact, a higher rate of synthesis was achieved on non-detoxified pretreated BSG than on the enzymatic hydrolysate of the solid phase of pretreated BSG for both 2,3-BD (0.254 vs. 0.033 g g^{-1}) and ethanol (0.102 vs. 0.070 g g^{-1}).

Using different pretreatment methods of residual lignocellulosic materials as BSG, it is possible to obtain nutrient media for microbiological cultivations to produce a range of useful biochemicals. In this study, it was shown that *P. polymyxa* DSM 742 can produce 2,3-BD, ethanol, and lactate with different production rates and product yields. On the basis of the obtained results, it is obvious that the highest impact on

the production of different types of biochemicals have working microorganisms, as well as pretreatment (dilute acid hydrolysis or enzymatic hydrolysis) and detoxification methods. The presented concept of biochemical production, using *P. polymyxa* DSM 742, is of great importance for sustainable development of a biochemicals production which could be included in the biorefinery concept. Furthermore, emphasis should be directed toward usage of new and interesting microorganisms that produce various useful biochemicals from different residual food or agricultural residues.

DATA AVAILABILITY STATEMENT

The raw data supporting the conclusions of this article will be made available by the authors, without undue reservation.

AUTHOR CONTRIBUTIONS

All authors listed contributed to the test performance, data analysis, and writing of the manuscript, and they all approved it for the publication.

FUNDING

This work was financed from the Croatian Science Foundation by project Sustainable Production of Biochemicals from Waste Lignocellulose Containing Feedstocks (HRZZ-IP-2018-01-9717), by the project "BioProspecting of the Adriatic Sea" (KK.01.1.1.01.0002), and by COST project "Understanding and exploiting the impacts of low pH on micro-organisms (EuroMicropH)" (CA18113).

REFERENCES

Adlakha, N., Pfau, T., Ebenhöh, O., and Yazdani, S. S. (2015). Insight into metabolic pathways of the potential biofuel producer, *Paenibacillus polymyxa* ICGEB2008. *Biotechnol. Biofuels* 8:159. doi: 10.1186/s13068-015-0338-4

Alexeeva, S., Hellingwerf, K. J., and Teixeira de Mattos, M. J. (2003). Requirement of ArcA for redox regulation in *Escherichia coli* under microaerobic but not anaerobic or aerobic conditions. *J. Bacteriol.* 185, 204–209. doi: 10.1128/JB.185.1.204-209.2003

Amraoui, Y., Prabhu, A., Vivek, N., Coulon, F., Chandel, A. K., Willoughby, N., et al. (2021). Enhanced 2,3-butanediol production by mutant *Enterobacter ludwigii* using brewers' spent grain hydrolysate: process optimization for a pragmatic biorefinery loom. *Chem. Eng. J.* 427:130851. doi: 10.1021/acssuschemeng.1c03951

Bensah, E., and Mensah, M. (2013). Chemical pretreatment methods for the production of cellulosic ethanol: technologies and innovations. *Int. J. Chem. Eng.* 2013:719607. doi: 10.1155/2013/719607

Canilha, L., Carvalho, W., Giulietti, M., Felipe, M. D. G. A., Almeida, E., and Silva, J. B. (2008). Clarification of wheat straw-derivies medium with ion-exchange resins for xylitol crystallization. *J. Chem. Technol. Biotechnol.* 83, 715–721. doi: 10.1002/jctb.1861

Cao, C., Zhang, L., Gao, J., Xu, H., Xue, F., Huang, W., et al. (2017). Research on the solid state fermentation of Jerusalem artichoke pomace for producing R,R-2,3-butanediol by *Paenibacillus polymyxa* ZJ-9. *Appl. Biochem. Biotechnol.* 182, 687–696. doi: 10.1007/s12010-016-2354-7

Carvalheiro, F., Duarte, L. C., Medeiros, R., and Girio, F. G. (2004). Optimization of brewery's spent grain dilute-acid hydrolysis for the production of pentose-rich culture media. *Appl. Biochem. Biotechnol.* 115:1059. doi: 10.1385/abab:115:1-3:1059

Chetrariu, A., and Dabija, A. (2020). Brewer's spent grains: possibilities of valorization. *Appl. Sci.* 10:5619. doi: 10.3390/app10165619

Chu, W., Jiang, K., Lu, P., Xu, Y., Yang, J., Wei, X., et al. (2021). Metabolic regulation and optimization of oxygen supply enhance the 2,3-butanediol yield of the novel *Klebsiella* sp. isolate FSoil 024. *Biotechnol. J.* 14:e2100279. doi: 10.1002/biot.202100279

Costa, E., Calleja, G., and Marijuán, L. (1988). Comparative adsorption of phenol, p-nitrophenol and p-hydroxybenzoic acid on activated carbon. *Ads. Sci. Technol.* 5, 213–228. doi: 10.1177/026361748800500304

Dai, J.-J., Cheng, J.-S., Liang, Y.-Q., Jiang, T., and Yuan, Y.-J. (2014). Regulation of extracellular oxidoreduction potential enhanced (R,R)-2,3-butanediol production by *Paenibacillus polymyxa* CJX518. *Bioresour. Technol.* 167, 433–440. doi: 10.1016/j.biortech.2014.06.044

Das, A., Prakash, G., and Lali, A. M. (2021). 2,3-butanediol production using soy-based nitrogen source and fermentation process evaluation by a novel isolate of *Bacillus licheniformis* BL1. *Prep. Biochem. Biotechnol.* 51, 1046–1055. doi: 10.1080/10826068.2021.1894443

Daud, N. S., Din, A. R. J. M., Rosli, M. A., Azam, Z. M., Othman, N. Z., and Sarmidi, M. R. (2019). *Paenibacillus polymyxa* bioactive compounds for agricultural and biotechnological applications. *Biocatal. Agric. Biotechnol.* 18, 92–101. doi: 10.1016/j.bcab.2019.101092

Ferraz, E., Coroado, J., Gamelas, J., Silva, J., Rocha, F., and Velosa, A. (2013). Spent brewery grains for improvement of thermal insulation of ceramic bricks. *J. Mater. Civil Eng.* 25, 1638–1646. doi: 10.1061/(ASCE)MT.1943-5533.0000729

Grady, E. N., MacDonald, J., Liu, L., Richman, A., and Yuan, Z. C. (2016). Current knowledge and perspectives of *Paenibacillus*: a review. *Microb. Cell Fact.* 1, 203–215. doi: 10.1186/s12934-016-0603-7

Hakizimana, O., Matabaro, E., and Lee, B. (2020). The current strategies and parameters for the enhanced microbial production of 2,3-butanediol. *Biotechnol. Rep.* 25:e00397. doi: 10.1016/j.btre.2019.e00397

He, Z., Kisla, D., Zhang, L., Yuan, C., Green-Church, K. B., and Yousef, A. E. (2007). Isolation and identification of *Paenibacillus polymyxa* strain that coproduces a novel lantibiotic and polymyxin. *Appl. Environ. Microb.* 73, 168–178. doi: 10.1128/AEM.02023-06

Ikram, S., Huang, L., Zhang, H., Wang, J., and Yin, M. (2017). Composition and nutrient value proposition of brewers spent grain. *J. Food Sci.* 82, 2232–2242. doi: 10.1111/1750-3841.13794

Jackowski, M., Niedźwiecki, Ł, Jagiełło, K., Uchańska, O., and Trusek, A. (2020). Brewer's spent grains—valuable beer industry by-product. *Biomolecules* 10:1669. doi: 10.3390/biom10121669

Jeong, H., Choi, S., Ryu, C., and Park, S. (2019). Chronicle of a soil bacterium: *Paenibacillus polymyxa* E681 as a tiny guardian of plant and human health. *Front. Microbiol.* 10:467. doi: 10.3389/fmicb.2019.00467

Ji, X. J., Huang, H., and Ouyang, P. K. (2011). Microbial 2,3-butanediol production: a state-of-the-art review. *Biotechnol. Adv.* 29, 3. doi: 10.1016/j.biotechadv.2011.01.007

Jurchescu, I.-M. (2014). *2,3–Butanediol Production with GRAS Microorganisms – Screening, Cultivation, Optimization and Scale-up*. dissertation. Braunschweig: Fakultät für Lebenswissenschaften der Technischen Universität Carolo-Wilhelmina.

Kajimura, Y., and Kaneda, M. (1997). Fusaricidins B, C and D, new depsipeptide antibiotics produced by *Bacillus polymyxa* KT-8: isolation, structure elucidation and biological activity. *J. Antibiot.* 50, 220–228.

Karlović, A., Jurić, A., Ćorić, N., Habschied, K., Krstanović, V., and Mastanjević, K. (2020). By-products in the malting and brewing industries - re - usage possibilities. *Fermentation* 6:82. doi: 10.3390/fermentation6030082

Koller, M., Hesse, P., and Braunegg, G. (2019). Application of whey retentate as complex nitrogen source for growth of the polyhydroxyalkanoate producer strain DSM1023. *EuroBiotech J.* 3, 78–89. doi: 10.2478/ebtj-2019-0009

Lal, S., and Tabacchioni, S. (2009). Ecology and biotechnological potential of *Paenibacillus polymyxa*: a minireview. *Indian J. Microbiol.* 49, 2–10. doi: 10.1007/s12088-009-0008-y

Lee, S. J., Lee, J. H., Yang, X., Kim, S. B., Lee, J. H., Yoo, H. Y., et al. (2015). Phenolic compounds: strong inhibitors derived from lignocellulosic hydrolysate for 2,3-butanediol production by *Enterobacter aerogenes*. *Biotechnol. J.* 10, 1920–1928. doi: 10.1002/biot.201500090

Li, L., Li, K., Wang, Y., Chen, C., Xu, Y., Zhang, L., et al. (2015). Metabolic engineering of *Enterobacter cloacae* for high-yield production of enantiopure (2R,3R)-2,3-butanediol from lignocellulose-derived sugars. *Metab. Eng.* 28, 19–27. doi: 10.1016/j.ymben.2014.11.010

Li, Y., and Chen, S. (2019). Fusaricidin produced by *Paenibacillus polymyxa* WLY78 induces systemic resistance against *Fusarium* wilt of cucumber. *Int. J. Mol. Sci.* 20:5240. doi: 10.3390/ijms20205240

Ma, K., He, M., You, H., Pan, L., Wang, Z., Wang, Y., et al. (2018). Improvement of (R,R)-2,3-butanediol production from corn stover hydrolysate by cell recycling continuous fermentation. *Chem. Eng. J.* 332, 361–369. doi: 10.1016/j.cej.2017.09.097

Macheiner, D., Adamitsch, B. F., Karner, F., and Hampel, W. A. (2003). Pretreatment and hydrolysis of brewer's spent grains. *Eng. Life Sci.* 3, 401–405. doi: 10.1002/elsc.200301831

Marđetko, N., Novak, M., Trontel, A., Grubišić, M., Galić, M., and Šantek, B. (2018). Bioethanol production from dilute-acid pre-treated wheat straw liquor hydrolysate by genetically engineered *Saccharomyces cerevisiae*. *Chem. Biochem. Eng. Q.* 32, 483–499. doi: 10.15255/CABEQ.2018.1409

Marđetko, N., Trontel, A., Novak, M., Pavlečić, M., Didak Ljubas, B., Grubišić, M., et al. (2021). Screening of lignocellulolytic enzyme activities in fungal species and sequential solid-state and submerged cultivation for the production of enzyme cocktails. *Polymers* 13:3736. doi: 10.3390/polym13213736

Marwoto, B., Nakashimada, Y., Kakizono, T., and Nishio, N. (2004). Metabolic analysis of acetate accumulation during xylose consumption by *Paenibacillus polymyxa*. *Appl. Microbiol. Biotechnol.* 64, 112–119. doi: 10.1007/s00253-003-1435-z

McCarthy, A. L., O'Callaghan, Y. C., Connolly, A., Piggott, C. O., FitzGerald, R. J., and O'Brien, N. M. (2013). *In vitro* antioxidant and anti-inflammatory effects of brewers' spent grain protein rich isolate and its associated hydrolysates. *Food Res. Int.* 50, 205–212. doi: 10.1039/C3FO60191A

Meena, V., Mishra, P., Bisht, J., and Pattanayak, A. (2017). *Agriculturally Important Microbes for Sustainable Agriculture. Volume I: Plant-Soil-Microbe Nexus*. Berlin: Springer. doi: 10.1007/978-981-10-5343-6

Mhlongo, S., den Haan, R., Viljoen-Bloom, M., and van Zyl, W. (2015). Lignocellulosic hydrolysate inhibitors selectively inhibit/deactivate cellulase performance. *Enzyme Microb. Technol.* 81, 16–22. doi: 10.1016/j.enzmictec.2015.07.005

Moo-Young, M. (2011). *Comprehensive Biotechnology*. Amsterdam: Elsevier.

Mussatto, S. I. (2014). Brewer's spent grain: a valuable feedstock for industrial applications. *J. Sci. Food Agric.* 94, 1264–1275. doi: 10.1002/jsfa.6486

Nakashimada, Y., Marwoto, B., Kashiwamura, T., and Kakizono, T. (2000). Enhanced 2,3-butanediol production by addition of acetic acid in *Paenibacillus polymyxa*. *J. Biosci. Bioeng.* 90, 661–664. doi: 10.1016/S1389-1723(00)90013-6

Okonkwo, C. (2017). *Process Development and Metabolic Engineering to Enhance 2,3-Butanediol Production by Paenibacillus polymyxa DSM 365*. dissertation. Columbus, OH: The Ohio State University.

Okonkwo, C. C., Ujor, V., Cornish, K., and Ezeji, T. C. (2020). Inactivation of the levansucrase gene in *Paenibacillus polymyxa* DSM 365 diminishes exopolysaccharide biosynthesis during 2,3- butanediol fermentation. *Appl. Environ. Microbiol.* 86:e00196-20. doi: 10.1128/AEM.00196-20

Okonkwo, C. C., Ujor, V., and Ezeji, T. C. (2021). Production of 2,3-butanediol from non-detoxified wheat straw hydrolysate: impact of microbial inhibitors on *Paenibacillus polymyxa* DSM 365. *Ind. Crops Prod.* 159:113047. doi: 10.1016/j.indcrop.2020.113047

Paz, A., Outeiriño, D., Pérez Guerra, N., and Domínguez, J. M. (2019). Enzymatic hydrolysis of brewer's spent grain to obtain fermentable sugars. *Bioresour. Technol.* 275, 402–409. doi: 10.1016/j.biortech.2018.12.082

Petrov, K., and Petrova, P. (2021). Current advances in microbial production of acetoin and 2,3-butanediol by *Bacillus* spp. *Fermentation* 7:307. doi: 10.3390/fermentation7040307

Sampaio, F. C., Lopes Passos, F. M., Vieira Passos, F. J., De Faveri, D., Perego, P., and Converti, A. (2006). Xylitol crystallization from culture media fermented by yeasts. *Chem. Eng. Proc.* 45, 1041–1046. doi: 10.1016/j.cep.2006.03.012

Schilling, C., Ciccone, R., Sieber, V., and Schmid, J. (2020). Engineering of the 2,3-butanediol pathway of *Paenibacillus polymyxa* DSM 365. *Metab. Eng.* 61, 381–388. doi: 10.1016/j.ymben.2020.07.009

Sjulander, N., and Kikas, T. (2020). Origin, impact and control of lignocellulosic inhibitors in bioethanol production-a review. *Energies* 13:4751. doi: 10.3390/en13184751

Sluiter, A., Hames, B., Ruiz, R., Scarlata, C., Sluiter, J., Templeton, D., et al. (2012). *Determination of Structural Carbohydrates and Lignin in Biomass, Technical Report NREL/TP-510-42618*. Golden, CO: National Renewable Energy Laboratory.

Tang, D., Yin, G., He, Y., Hu, S., Li, B., Li, L., et al. (2009). Recovery of protein from brewer's spent grain by ultrafiltration. *Biochem. Eng. J.* 48, 1–5. doi: 10.1016/j.bej.2009.05.019

Zhang, Y., Xia, C., Lu, M., and Tu, M. (2018). Effect of overliming and activated carbon detoxification on inhibitors removal and butanol fermentation of poplar prehydrolysates. *Biotechnol. Biofuels* 11:178. doi: 10.1186/s13068-018-1182-0

Conflict of Interest: The authors declare that the research was conducted in the absence of any commercial or financial relationships that could be construed as a potential conflict of interest.

Publisher's Note: All claims expressed in this article are solely those of the authors and do not necessarily represent those of their affiliated organizations, or those of the publisher, the editors and the reviewers. Any product that may be evaluated in this article, or claim that may be made by its manufacturer, is not guaranteed or endorsed by the publisher.

frontiers | Frontiers in Microbiology

ORIGINAL RESEARCH
published: 18 April 2022
doi: 10.3389/fmicb.2022.820067

Mild NaCl Stress Influences Staphylococcal Enterotoxin C Transcription in a Time-Dependent Manner and Reduces Protein Expression

*Danai Etter[1,2], Christina Ukowitz[1], Corinne Eicher[1], Taurai Tasara[1] and Sophia Johler[1]**

[1]Institute for Food Safety and Hygiene, Vetsuisse Faculty University of Zurich, Zurich, Switzerland, [2]Laboratory of Food Microbiology, Institute for Food Nutrition and Health, ETH Zurich, Zurich, Switzerland

Enterotoxins (SEs) produced by *Staphylococcus aureus* are the cause of serious food intoxications. Staphylococcal enterotoxin C (SEC) is one of the main contributors, as it is often highly expressed. *S. aureus* possesses a competitive growth advantage over accompanying bacterial flora under stress conditions encountered in foods, such as high NaCl concentrations. However, the influence of NaCl as an external stressor on SEC expression is still unclear. We investigated the influence of 4.5% NaCl on *sec* mRNA and SEC protein levels. A qRT-PCR assay revealed that NaCl stress leads to time-dependently decreased or elevated *sec* mRNA levels for most strains. SEC protein levels were generally decreased under NaCl stress. Our findings suggest that NaCl stress lowers overall SEC concentration and time-dependently affects *sec* mRNA levels.

Keywords: stress response, superantigen, food intoxication, virulence gene regulation, SEC variants

OPEN ACCESS

Edited by:
Daniela De Biase, Sapienza University of Rome, Italy

Reviewed by:
Agnes Weiss, University of Hohenheim, Germany
Zdenkova Kamila, University of Chemistry and Technology in Prague, Czechia

***Correspondence:**
Sophia Johler
sophia.johler@uzh.ch

Specialty section:
This article was submitted to Food Microbiology, a section of the journal Frontiers in Microbiology

Received: *22 November 2021*
Accepted: *29 March 2022*
Published: *18 April 2022*

Citation:
Etter D, Ukowitz C, Eicher C, Tasara T and Johler S (2022) Mild NaCl Stress Influences Staphylococcal Enterotoxin C Transcription in a Time-Dependent Manner and Reduces Protein Expression. Front. Microbiol. 13:820067. doi: 10.3389/fmicb.2022.820067

INTRODUCTION

Staphylococcus aureus is one of the most common causes of foodborne intoxications. In the EU 2454 cases of Staphylococcal Food Poisoning (SFP), outbreaks were reported in 2015 (EFSA, 2016) and 1,400 cases in 2019 (EFSA, 2021). In the USA, the yearly number of cases is estimated at 241′148 (Scallan et al., 2011). Foods commonly implicated in SFP are meat and meat products, as well as dairy products (EFSA, 2017). SFP is caused by staphylococcal enterotoxins (SEs) that are produced by *S. aureus* directly in the food matrix during growth. These exotoxins are of particular interest due to their extreme resistance toward environmental stress conditions, such as heat, acidity, or irradiation. Thus, even heated foods, in which the organism itself has been inactivated, can lead to severe intoxications, as staphylococcal enterotoxins remain emetically and biologically active (Le Loir et al., 2003). To date, a broad range of SEs has been characterized, comprising the classical SEA-SEE and the newly described SEG-SE*l*Z (Fetsch and Johler, 2018). The investigation of staphylococcal enterotoxin C (SEC) is of particular relevance since this toxin can be produced in up to 10 times higher amounts than other SEs (Spaulding et al., 2013).

In addition, SEC exists in different, often host-specific variants (Etter et al., 2020). This adds further complexity to the already highly complex interconnected regulatory system of SEs.

Hurdle technologies represent a combination of preservation methods. It is a highly effective tool in the inhibition of growth and toxin formation of pathogenic microorganisms (Leistner, 2000). This includes the addition of preservatives, changing pH, lowering the a_w value, and heating or cooling (Rahman, 2020). A common preservation method in foods is the addition of salt. Meat products that are commonly associated with SFP usually have NaCl concentrations ranging from 1–2% for ham or sausages, 2–4.5% for dry fermented sausages, and 5–10% for dried and cured meat (Lilic et al., 2015; Kim et al., 2021). Growth of *S. aureus* is usually inhibited by the surrounding microflora in most food matrices. However, in food matrices with such high salt concentrations, *S. aureus* possesses a remarkable growth advantage over competing bacteria. In fact, *S. aureus* was shown to grow at normal levels in media with up to 20% NaCl (Measures, 1975). While high NaCl concentrations do not effectively impede growth of *S. aureus* in foods, they might still act as a hurdle by influencing SE production. Thus, the presence and even growth of *S. aureus* in foods high in NaCl might not be dangerous to the consumer if enterotoxin formation is sufficiently inhibited. Deciphering the role of NaCl in enterotoxin formation is key to understand the risk related to the presence of *S. aureus* in various foods and could contribute to a reduction in food waste. The WHO aim of reducing sodium content in foods is certainly reasonable regarding dietary requirements (WHO, 2011). Diet-related non-communicable diseases are now the leading cause of mortality worldwide, accounting for more deaths than all other, non-diet-related mortality causes combined (Forouzanfar et al., 2016). Salt reduction may however entail food safety concerns if it facilitates pathogen activity, such as SE production (Doyle and Glass, 2010).

Salt stress acts on bacteria *via* two mechanisms: osmotic effects and specific ion effects (Oren, 1999; Chhabra, 2017). Some of the known stress adaptation mechanisms include accumulation of potassium, amino acids, or sugars to prevent sodium influx and reduce osmotic pressure (Doyle and Glass, 2010). How NaCl stress affects SE expression and regulation has not yet been elucidated. Previous experiments demonstrated a reduction in *sec* under 1.2 M NaCl (*ca.* 7% NaCl) in two strains (Regassa and Betley, 1993). In an older study on the effect of NaCl and pH on SEC protein production, it was not possible to detect SEC in broths with 12% NaCl (Genigeorgis et al., 1971). However, SEC expression has not yet been quantified for different toxin variants and strains from different isolation sources in more realistic circumstances with lower salt concentrations, mimicking those encountered during food production and preservation.

We investigated the influence of 4.5% NaCl stress compared to a low-salt containing control medium on *sec* expression in seven strains from different origins and with different SEC variants and *sec* gene promoters (promoter variants are labeled v1–v4). Potential influence of toxin variants or strain background was assessed on mRNA and protein levels. In addition, quantification on both mRNA and protein levels enabled us to determine whether gene regulation as a NaCl stress response is transcriptional or post-transcriptional. We used 4.5% NaCl containing medium to represent concentrations found in fermented meat products. Our findings contribute to a better understanding of matrix–pathogen interaction that is needed to adapt food production parameters and protect consumer health.

MATERIALS AND METHODS

Bacterial Strains, Growth Conditions, and Sample Collection for *sec* mRNA and SEC Protein Quantification

All *S. aureus* strains and their respective SEC variants in this study are listed in **Table 1**. The strains were grown in LB medium (BD, Pont-de-Claix, France) (non-stress control conditions, 1% NaCl) and in LB supplemented with a total of 4.5% (w/v) NaCl (BD) (0.77 M). Mild salt stress conditions encountered in food were mimicked by adjusting to a salt concentration typical for dried fermented meat. All media were autoclaved before adding stress conditions and then sterile filtered (Bottle-top filter 0.2 µm, Fisher Scientific, Reinach, Switzerland) and stored at 4°C.

Bacteria were grown and sampled according to procedures previously described in Etter et al., 2021. Briefly, colonies from 5% sheep blood agar were cultured in LB broth (16 h at 37°C and 125 rpm). After washing the cultures in 0.85% NaCl suspension, 50 ml of medium (LB and LB + NaCl) were inoculated (OD_{600} = 0.05). Cultures were incubated at 37°C at 125 rpm and sampled after 4 h (exponential phase), 10 h (early stationary phase), and 24 h (late stationary phase). Three independent biological replicates were collected. RNAprotect®Tissue Reagent (Qiagen, Hilden, Germany) was used for mRNA sample stabilization. Low protein binding micro-centrifuge tubes (Thermo Scientific, Waltham, MA USA) were used for protein sample collection.

Growth curves were evaluated by plating serial dilutions on plate count agar (Oxoid, Pratteln, Switzerland) as previously described (Etter et al., 2021).

RNA Extraction

RNA extraction was performed with the RNeasy mini Kit Plus (Qiagen) as previously described (Sihto et al., 2014; Etter et al., 2021) and quantified with Quantifluor (Promega, Madison, WI USA). Quality control was performed by the Agilent 2,100 Bioanalyzer (Agilent Technologies, Waldbronn, Germany). Samples were included in the study if they met the inclusion criteria of RNA integrity numbers >6. RNA integrity numbers ranged from 6.3–8.2.

Reverse Transcription and Quantitative Real-Time PCR

All RNA samples were subjected to reverse transcription and qRT-PCR as previously described (Etter et al., 2021). No reverse

TABLE 1 | Overview of *Staphylococcus. aureus* strains used in this study including their SEC variants, origin, and clonal complex.

Strain	Protein variant	*sec* promoter variant	Origin	Clonal complex	References
BW10	SEC[2]	sec_p v1	SFP	CC45	1
NB6	SEC[2]	sec_p v1	SFP	CC45	2
SAI3	SEC[1]	sec_p v3 (H-EMRSA-15)	Human infection	CC8	Wattinger et al., 2012
SAI48	SEC[2]	sec_p v1 (79_S10)	Human infection	CC5	Wattinger et al., 2012
SAR1	SEC_{bovine}	sec_p v2	Bovine mastitis milk	CC151	Johler et al., 2011
SAR38	SEC_{bovine}	sec_p v2	Bovine mastitis milk	CC151	Johler et al., 2011
OV20	SEC_{ovine}	sec_p v4	Ovine	CC133	Guinane et al., 2010

[1]*Medical Department of the German Federal Armed Forces, Germany.*
[2]*Bavarian State Office of Health and Food Safety, Germany.*

transcription controls were included as controls in each qPCR run to ensure absence of DNA. Relative expression of the target gene *sec* was normalized using the housekeeping genes *rho* and *rplD* (Sihto et al., 2014). Ct values were determined using the Lightcycler®Software version 1.1.0.1320 (Roche, Basel, Switzerland). Data were expressed as Δct values. Statistical analysis was performed with RStudio 1.3.1093 and GraphPad Prism 9.2.0. For RNA analysis, a mixed effect linear model was fitted on the fold change, with a full three-way interaction between reference gene, strain, and time effects. Fold change was log_{10}-transformed to ensure normal distribution in statistical analysis. To determine whether individual mRNA levels were increased (indicated by a fold change significantly larger than 1 we used lsmeans to perform a one-sided effect test, with Holm–Bonferroni-corrected *p*-values). Protein data were log-transformed to ensure normal distribution for statistical analysis. A two-way ANOVA and post-hoc Tukey's multiple comparisons were performed. Results were regarded as significant if $p < 0.05$. All relevant information according to MIQE guidelines are provided in **Supplementary Table 2**.

Protein Quantification

An enzyme-linked immunosorbent assay (ELISA) was performed as previously described (Etter et al., 2021). The protocol was based on Poli and colleagues (Poli et al., 2002) with some modifications according to (Wallin-Carlquist et al., 2010). Antibodies and reference toxins were obtained from Toxin Technology Inc., Sarasota, FL, USA. ELISA measurements were performed in duplicates. Statistical analysis was performed with RStudio 1.3.1093 and GraphPad Prism 9.2.0. Results were regarded as significant if $p < 0.05$.

RESULTS AND DISCUSSION

We measured relative *sec* mRNA levels and quantified SEC protein levels of seven *S. aureus* strains BW10, NB6, SAI3, SAI48, SAR1, SAR38, and OV20 at exponential (4 h), early stationary (10 h), and late stationary (24 h) phase during growth in LB under NaCl (4.5%) stress. Strains BW10 and NB6 (both SEC_2, v1) were isolated from food, SAI3 (SEC_1, v3) and SAI48 (SEC_2, v1) from human infection cases, and SAR1 & SAR38 (both SEC_{bovin}e, v2), and OV20 (SEC_{ovine}, v4) were isolated from bovine and ovine mastitis cases, respectively.

sec mRNA Levels Observed Under NaCl Stress Correlates With Toxin Variant in a Time-Dependent Manner

sec mRNA levels were measured in exponential (4 h), early stationary (10 h), and late stationary phase (24 h) across 7 *S. aureus* strains and expressed normalized to strain growth level (**Supplementary Figure 1**). The expression of *sec* mRNA under NaCl stress tended to be lower compared to control conditions in early growth phases but reached or exceeded control levels in late stationary phase (**Figure 1**). Six out of seven strains (BW10, NB6, SAI48, SAR1, SAR38, OV20) exhibited significantly altered expression while in one strain (SAI3) *sec* mRNA level was not significantly affected by NaCl stress. Isolates BW10, NB6, and SAI48 who express toxin variant SEC_2 and promoter variant v1 (**Table 1**) as well as strains SAR38 and OV20 harboring SEC_{bovine} and promoter variant v3 showed decreased levels of *sec* transcripts in exponential or early stationary phase. Strain SAI3 showed comparable *sec* mRNA level patterns to NB6, although differences observed were not statistically significant. In late stationary phase, all strains either reached (BW10, NB6, SAI3, SAI48, OV20) or surpassed (SAR1, SAR38) control levels. Bovine mastitis isolates SAR1 and SAR38 displayed significantly elevated transcription levels under NaCl stress after 24 h. When the results for the different strains were pooled, there was no significant difference in *sec* expression under NaCl stress at 4 h vs. 10 h. However, at 24 h *sec* transcription was significantly elevated under NaCl stress compared to 10 h as well as 4 h (**Supplementary Table 2**).

Previous experiments demonstrated a reduction in *sec* mRNA levels under 1.2 M NaCl stress (*ca.* 10% NaCl) in two strains carrying non-specified SEC variants after 24 h incubation (Regassa and Betley, 1993). In contrast, our study found equal or elevated *sec* mRNA levels under mild NaCl stress after 24 h for all seven investigated strains. The level of NaCl stress seems to play a role in transcriptional regulation in the observed strains with higher NaCl concentration leading to more pronounced downregulation. Here, we could show that even a minor increase

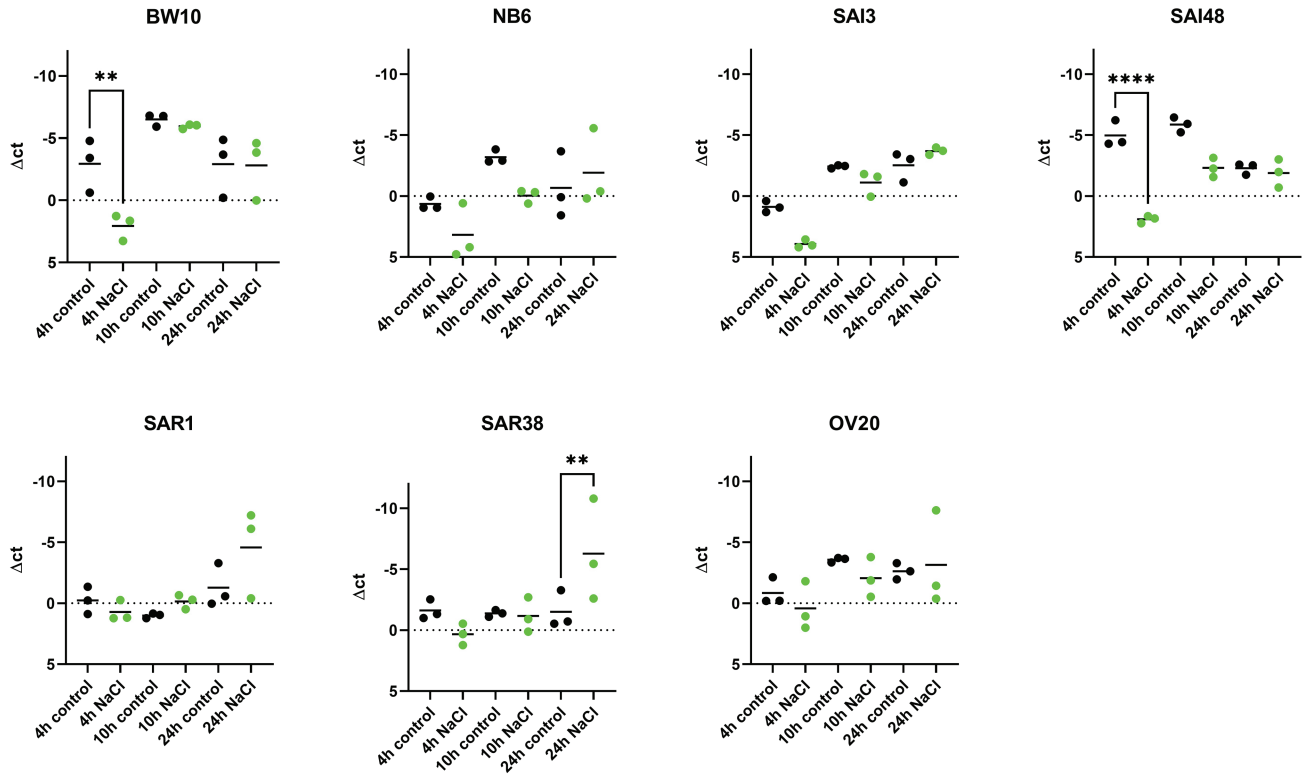

FIGURE 1 | Effect of NaCl stress on *sec* mRNA levels in seven *S. aureus* strains (BW10, NB6, SAI3, SAI48, SAR1, SAR38, OV20) measured by qRT-PCR. qPCR Δct values in exponential (4 h), early stationary (10 h), and late stationary phase (24 h) in LB and LB + 4.5% NaCl for each time point and strain. Control conditions in black and NaCl stress conditions in green. Target mRNA (*sec*) was normalized to two reference genes *rho* and *rplD*. Statistically significant changes in *sec* mRNA levels in LB + 4.5% NaCl compared to LB ($p < 0.05$) are marked by an asterisk.

from 1 to 4.5% NaCl did influence *sec* expression. Therefore, reducing salt in foods could lead to upregulation of *sec* expression and therefore higher SEC concentration in food. The study by Regassa and Betley, 1993, further demonstrated that regulation of SEC occurred at the level of mRNA independently of an intact *agr* allele.

So far, it is not known whether all SEs harbored by a strain react congruently to an external stressor. We included two strains in this study that have previously been tested for transcription of another SE under NaCl stress. Strains BW10 and SAI48 have been investigated in terms of their *sed* transcription under 4.5% NaCl stress. BW10 showed a significant reduction in *sed* mRNA transcription after 24 h, while SAI48 was not affected by NaCl stress (Sihto et al., 2015). In contrast, in the present study *sec* transcription in both strains was significantly reduced in early growth phases but was not affected in late stationary phase. Strains USA300 and HG003 have also been tested for *seb* promoter activity under 4.5% NaCl stress. Promoter activity was significantly downregulated over all time points in both strains (Sihto et al., 2017). In contrast, we observed a downregulation in early growth phases and an upregulation in late stationary phase for *sec*. Comparing the different expression patterns in SEs suggests that each SE can respond differently and that the same stressor can trigger opposing responses in strains that express multiple toxins.

SEC Protein Reduction Is Strain-Dependent Under NaCl Stress

In addition to *sec* mRNA transcript levels, SEC protein concentrations were also measured by ELISA in exponential (4 h), early stationary (10 h), and late stationary phase (24 h). Strains BW10, NB6, SAI48 (all SEC_2, promoter v1), SAR1 (SEC_{bovine}, promoter v2), and OV20 (SEC_{ovine}, promoter v4) produced similar or less SEC under NaCl stress compared to control conditions in some or all growth phases (**Figure 2**). Reductions ranged from 0 to 1.1 log. For low toxin-producing strains, this observation aligns with a study on the effect of NaCl and pH on SEC protein production where it was not possible to detect SEC in broths with 12% NaCl (Genigeorgis et al., 1971). High toxin producers SAI48 and BW10 were affected by NaCl stress in all growth phases, but still expressed the highest amount of SEC (**Table 2**). SAI3 and SAR38 were not affected by salt stress, even though SAR38 had reduced and increased *sec* mRNA levels in early exponential and late stationary phase, respectively, under NaCl stress compared to control conditions. With the exception

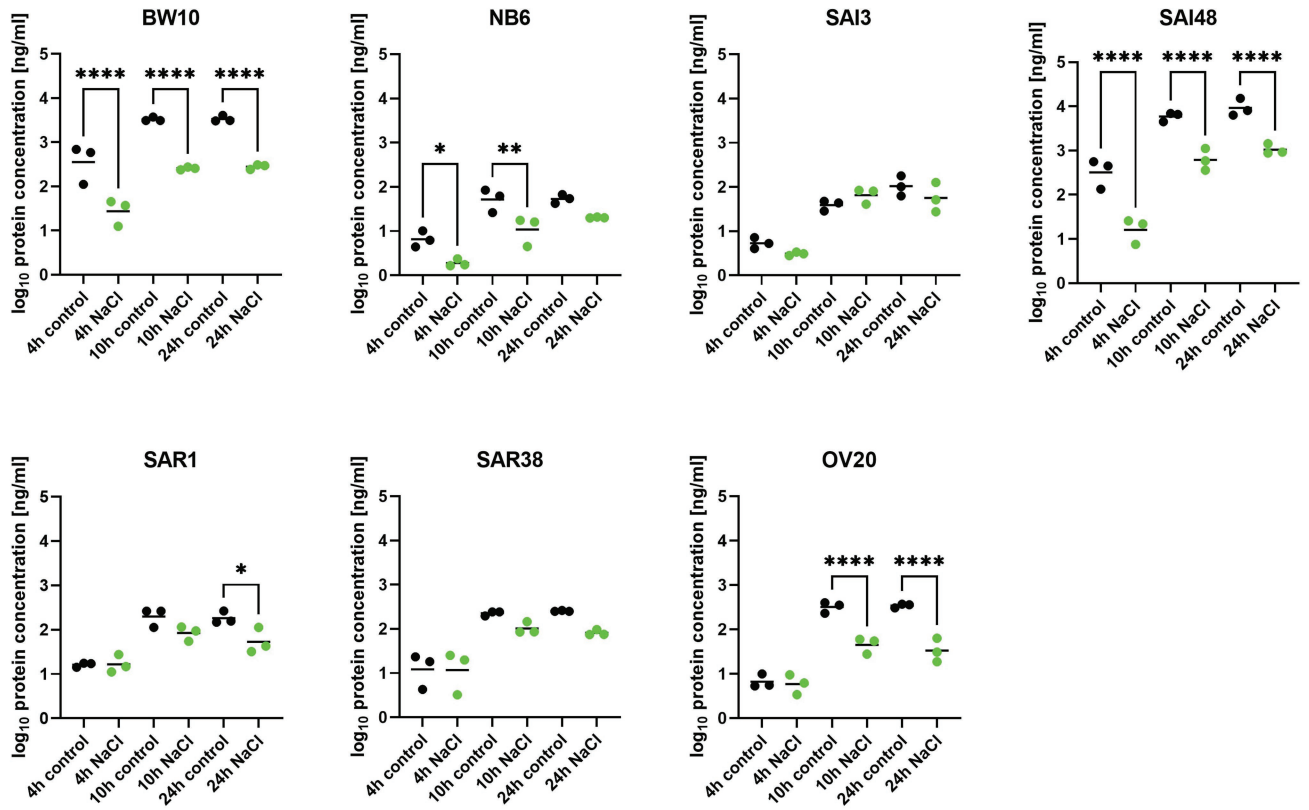

FIGURE 2 | Effect of NaCl stress on SEC protein expression in seven *S. aureus* strains (BW10, NB6, SAI3, SAI48, SAR1, SAR38, OV20) measured by ELISA. Protein concentration is shown in $\log_{10}$ values in exponential (4 h), early stationary (10 h), and late stationary phase (24 h) in LB and LB + 4.5% NaCl for each timepoint and strain. Control conditions in black and NaCl stress conditions in green. Statistically significant changes in SEC concentration in LB + 4.5% NaCl compared to LB ($p < 0.05$) are marked by an asterisk.

of SAR1 and SAR38, all other strains displayed similar patterns in mRNA and protein expression. These two bovine strains showed an increase in *sec* mRNA but not in protein concentration. Presumably, their SE regulation is fine-tuned differently from the other investigated strains. A previous study demonstrated that osmoregulation of SEC under 1.2 M NaCl stress (*ca.* 7% NaCl) occurred at the level of mRNA (Regassa and Betley, 1993). Our data suggest that SEC regulation under NaCl stress takes place at the mRNA level without additional post-transcriptional regulation under the tested conditions. Even though *sec* transcription was overall upregulated in late stationary phase, a downregulation in early growth phases seems sufficient to decrease final toxin concentration in our strains.

A previous study on SEC expression under lactic acid stress showed reductions in SEC protein expressions in a similar range (Etter et al., 2021). Exceptions were observed for strains SAI3 (SEC_1, promoter v3) and SAI48 (SEC_2, promoter v1). SAI3 was only marginally affected by NaCl stress with an overall reduction of −21%, but lactic acid stress had led to a pronounced depletion of −109%. SAI48 on the other hand was significantly affected by NaCl stress with −273% SEC expression reduction, but only showed −29% reduction under lactic acid stress (**Table 2**). Likely, different stress response pathways trigger alternate regulatory elements depending on the genetic background of the strain.

CONCLUSION AND OUTLOOK

Staphylococcus. aureus is commonly present in many foods. Whether presence and growth of this organism is harmful to the consumer heavily depends on its ability to form SEs. It has been shown that food matrix components can influence toxin expression (Alibayov et al., 2015; Sihto et al., 2015; Susilo et al., 2017). We demonstrated here that an increase in NaCl can decrease *sec* transcription mainly at the beginning of growth for many strains. Although, some strains showed elevated transcription levels in late stationary phase. Intriguingly, all strains (BW10, NB6, SAI48) carrying gene variant SEC_2/promoter v1 downregulated *sec* transcription in exponential or early stationary phase. Strains harboring SEC_{bovine}/promoter v2 (SAR1, SAR38) did upregulate *sec* transcription after 24 h. No influence of strain origin or clonal complex was apparent. Due to the limited number of strains used trends related to strain origin or genetic

TABLE 2 | SEC produced under NaCl stress and control conditions. Absolute values in ng/ml including standard deviation. Effect is shown as difference in percent under NaCl stress compared with non-stress control conditions.

Strains	SEC produced under NaCl stress (ng/ml)															Effect of NaCl [%]		
	4 h control			10 h control			24 h control			4 h NaCl			10 h NaCl			24 h NaCl			4 h	10 h	24 h	Sum
BW10	462	±	307	3,325	±	360	3,410	±	562	32	±	17	257	±	19	282	±	35	−93	−92	−92	−277
NB6	7	±	3	58	±	29	54	±	12	2	±	0	13	±	7	20	±	1	−72	−78	−63	−213
SAI3	6	±	2	40	±	10	114	±	59	3	±	0	69	±	24	69	±	52	−44	72	−40	−12
SAI48	380	±	220	5,988	±	1,317	9,868	±	4,688	18	±	10	689	±	391	1,076	±	311	−95	−88	−89	−273
SAR1	16	±	2	213	±	87	189	±	65	18	±	9	88	±	31	62	±	44	10	−59	−67	−116
SAR38	15	±	10	228	±	27	254	±	7	16	±	11	106	±	35	82	±	13	5	−53	−68	−116
OV20	7	±	3	328	±	87	345	±	34	6	±	3	47	±	17	38	±	23	−8	−86	−89	−182

background might not be detectable. SEC protein expression was overall lowered under NaCl stress conditions for all strains. Strains SAI3 and SAI48 showed a different behavior when exposed to NaCl stress than to lactic acid stress. These applied stressors likely trigger different stress response pathways. Different behaviors in *sec* and *sed* expression under NaCl stress might arise from different encoding regions of both SEs. *sec* is encoded on a Staphylococcal pathogenicity island (SaPI), while *sed* is usually encoded on a plasmid. Our results show that findings on transcriptional regulation must not be extrapolated from one SE to another. The different behaviors highlight the importance of investigating a diverse strain set when it comes to virulence factor regulation in *S. aureus*. While transcriptional data does not provide reliable information on the final toxin concentration in foods, it is important to uncover transcriptional regulatory processes. Only by combining transcriptional data and protein expression can a clear picture of stress response and regulatory mechanisms as well as toxic potential be drawn. The investigation of transcriptional and protein expression enabled us to confirm that *sec* regulation under NaCl stress occurs at mRNA level without relevant post-transcriptional modifications in our strain set. Further studies are needed to clarify, which regulatory elements are triggered by the respective stressors. Sequencing of regulatory elements and transcriptomic studies could shed light on the complex interplay of regulators. Our study shows that NaCl could contribute as a hurdle to lower SE concentration in foods containing NaCl. In regard to food, it can be concluded that an increase to 4.5% NaCl leads to lower SEC concentrations for most *S. aureus* strains. Our study highlights the importance of matrix–pathogen interactions in foods and contributes toward a more conscious formulation of food products.

DATA AVAILABILITY STATEMENT

The original contributions presented in the study are included in the article/**Supplementary Material**, further inquiries can be directed to the corresponding author.

AUTHOR CONTRIBUTIONS

SJ, TT, and DE contributed conception and design of the study and wrote sections of the manuscript. DE, CU, and CE analyzed the data and were responsible for data acquisition. DE wrote the first draft of the manuscript. All authors contributed to manuscript revision, read and approved the submitted version.

SUPPLEMENTARY MATERIAL

The Supplementary Material for this article can be found online at: https://www.frontiersin.org/articles/10.3389/fmicb.2022.820067/full#supplementary-material

REFERENCES

Alibayov, B., Karamonova, L., Hollerova, R., Zdenkova, K., and Demnerova, K. (2015). Differences in transcription and expression of staphylococcal enterotoxin C in processed meat products. *LWT – Food Sci. Technol.* 64, 578–585. doi: 10.1016/j.lwt.2015.06.026

Chhabra, R. (2017). *Soil Salinity and Water Quality*. Milton Park: Routledge.

Doyle, M. E., and Glass, K. A. (2010). Sodium reduction and its effect on food safety, food quality, and human health. *Compr. Rev. Food Sci. Food Saf.* 9, 44–56. doi: 10.1111/J.1541-4337.2009.00096.X

EFSA (2016). The European union summary report on trends and sources of zoonoses, zoonotic agents and food-borne outbreaks in 2015. *EFSA J.* 13:4329. doi: 10.2903/j.efsa.2015.4329

EFSA (2017). The European Union summary report on trends and sources of zoonoses, zoonotic agents and food-borne outbreaks in 2016. *EFSA J.* 15:5077. doi: 10.2903/j.efsa.2017.5077

EFSA (2021). The European Union one health 2019 Zoonoses report. *EFSA J.* 19:e06406. doi: 10.2903/j.efsa.2021.6406

Etter, D., Jenni, C., Tasara, T., and Johler, S. (2021). Mild lactic acid stress causes strain-dependent reduction in SEC protein levels. *Microorganisms* 9, 1–10. doi: 10.3390/microorganisms9051014

Etter, D., Schelin, J., Schuppler, M., and Johler, S. (2020). Staphylococcal enterotoxin C—an update on SEC variants, their structure and properties, and their role in foodborne intoxications. *Toxins (Basel)* 12:584. doi: 10.3390/toxins12090584

Fetsch, A., and Johler, S. (2018). Staphylococcus aureus as a foodborne pathogen. *Curr. Clin. Microbiol.* 9, 1–8. doi: 10.1007/s40588-018-0094

Forouzanfar, M. H., Afshin, A., Alexander, L. T., Biryukov, S., Brauer, M., Cercy, K., et al. (2016). Global, regional, and national comparative risk assessment of 79 behavioural, environmental and occupational, and metabolic risks or clusters of risks, 1990–2015: a systematic analysis for the global burden of disease study 2015. *Lancet* 388, 1659–1724. doi: 10.1016/S0140-6736(16)31679-8

Genigeorgis, C., Foda, M. S., Mantis, A., and Sadler, W. W. (1971). Effect of sodium chloride and pH on enterotoxin C production. *Appl. Microbiol.* 21, 862–866. doi: 10.1128/aem.21.5.862-866.1971

Guinane, C. M., Zakour, N. L. B., Tormo-Mas, M. A., Weinert, L. A., Lowder, B. V., Cartwright, R. A., et al. (2010). Evolutionary genomics of *Staphylococcus aureus* reveals insights into the origin and molecular basis of ruminant host adaptation. *Genome Biol. Evol.* 2, 454–466. doi: 10.1093/gbe/evq031

Johler, S., Layer, F., and Stephan, R. (2011). Comparison of virulence and antibiotic resistance genes of food poisoning outbreak isolates of *Staphylococcus aureus* with isolates obtained from bovine mastitis milk and pig carcasses. *J. Food Prot.* 74, 1852–1859. doi: 10.4315/0362-028X.JFP-11-192

Kim, T. K., Yong, H. I., Jung, S., Kim, H. W., and Choi, Y. S. (2021). Technologies for the production of meat products with a low sodium chloride content and improved quality characteristics: a review. *Foods* 10:957. doi: 10.3390/foods10050957

Le Loir, Y., Baron, F., and Gautier, M. (2003). *Staphylococcus aureus* and food poisoning. *Genet. Mol. Res.* 2, 63–76. Available at: http://www.ncbi.nlm.nih.gov/pubmed/12917803

Leistner, L. (2000). Basic aspects of food preservation by hurdle technology. *Int. J. Food Microbiol.* 55, 181–186. doi: 10.1016/S0168-1605(00)00161-6

Lilic, S., Saicic, S., Vranic, D., Trbovic, D., Borovic, B., Velebit, B., et al. (2015). Salt and sodium content in dry fermented sausages and dried meat in Serbia, 8–11.

Measures, J. C. (1975). Role of amino acids in osmoregulation of non-halophilic bacteria. *Nature* 257, 398–400. doi: 10.1038/257398a0

Oren, A. (1999). Bioenergetic aspects of Halophilism. *Microbiol. Mol. Biol. Rev.* 63, 334–348. doi: 10.1128/MMBR.63.2.334-348.1999

Poli, M. A., Rivera, V. R., and Neal, D. (2002). Sensitive and specific colorimetric ELISAs for *Staphylococcus aureus* enterotoxins A and B in urine and buffer. *Toxicon* 40, 1723–1726. doi: 10.1016/S0041-0101(02)00202-7

Rahman, M. S. (2020). *Handbook of Food Preservation, 3rd Edn*. M. S. Rahman Boca Raton: CRC Press.

Regassa, L. B., and Betley, M. J. (1993). High sodium chloride concentrations inhibit staphylococcal enterotoxin C gene (sec) expression at the level of sec mRNA. *Infect. Immun.* 61, 1581–1585. doi: 10.1128/iai.61.4.1581-1585.1993

Scallan, E., Hoekstra, R. M., Angulo, F. J., Tauxe, R. V., Widdowson, M. A., Roy, S. L., et al. (2011). Foodborne illness acquired in the United States-major pathogens. *Emerg. Infect. Dis.* 17, 7–15. doi: 10.3201/eid1701.P11101

Sihto, H.-M., Stephan, R., Engl, C., Chen, J., and Johler, S. (2017). Effect of food-related stress conditions and loss of *agr* and *sigB* on *seb* promoter activity in *S. aureus*. *Food Microbiol.* 65, 205–212. doi: 10.1016/j.fm.2017.03.006

Sihto, H.-M., Tasara, T., Stephan, R., and Johler, S. (2014). Validation of reference genes for normalization of qPCR mRNA expression levels in *Staphylococcus aureus* exposed to osmotic and lactic acid stress conditions encountered during food production and preservation. *FEMS Microbiol. Lett.* 356, 134–140. doi: 10.1111/1574-6968.12491

Sihto, H.-M., Tasara, T., Stephan, R., and Johler, S. (2015). Temporal expression of the staphylococcal enterotoxin D gene under NaCl stress conditions. *FEMS Microbiol. Lett.* 362:24. doi: 10.1093/femsle/fnv024

Spaulding, A. R., Salgado-Pabón, W., Kohler, P. L., Horswill, A. R., Leung, D. Y. M. M., and Schlievert, P. M. (2013). Staphylococcal and streptococcal superantigen exotoxins. *Clin. Microbiol. Rev.* 26, 422–447. doi: 10.1128/CMR.00104-12

Susilo, Y., Sihto, H.-M., Rådström, P., Stephan, R., Johler, S., and Schelin, J. (2017). Reduced enterotoxin D formation on boiled ham in *Staphylococcus aureus* Δagr mutant. *Toxins (Basel).* 9:263. doi: 10.3390/toxins9090263

Wallin-Carlquist, N., Cao, R., Márta, D., Da Silva, A. S., Schelin, J., and Rådström, P. (2010). Acetic acid increases the phage-encoded enterotoxin A expression in *Staphylococcus aureus*. *BMC Microbiol.* 10, 1–10. doi: 10.1186/1471-2180-10-147

Wattinger, L., Stephan, R., Layer, F., and Johler, S. (2012). Comparison of *Staphylococcus aureus* isolates associated with food intoxication with isolates from human nasal carriers and human infections. *Eur. J. Clin. Microbiol. Infect. Dis.* 31, 455–464. doi: 10.1007/s10096-011-1330-y

WHO (2011). The SHAKE technical package for salt reduction. *WHO Doc. Prod. Serv.* 63, 9–31.

Conflict of Interest: The authors declare that the research was conducted in the absence of any commercial or financial relationships that could be construed as a potential conflict of interest.

frontiers | Frontiers in Microbiology

ORIGINAL RESEARCH
published: 12 May 2022
doi: 10.3389/fmicb.2022.802010

Mutations in *degP* and *spoT* Genes Mediate Response to Fermentation Stress in Thermally Adapted Strains of Acetic Acid Bacterium *Komagataeibacter medellinensis* NBRC 3288

*Naoya Kataoka[1,2,3], Minenosuke Matsutani[1,2,4], Nami Matsumoto[1,2], Misuzu Oda[1], Yuki Mizumachi[2], Kohei Ito[1], Shuhei Tanaka[2], Yu Kanesaki[4,5], Toshiharu Yakushi[1,2,3] and Kazunobu Matsushita[1,2,3]**

[1] Department of Biological Chemistry, Faculty of Agriculture, Yamaguchi University, Yamaguchi, Japan, [2] Graduate School of Sciences and Technology for Innovation, Yamaguchi University, Yamaguchi, Japan, [3] Research Center for Thermotolerant Microbial Resources, Yamaguchi University, Yamaguchi, Japan, [4] NODAI Genome Research Center, Tokyo University of Agriculture, Tokyo, Japan, [5] Research Institute of Green Science and Technology, Shizuoka University, Shizuoka, Japan

OPEN ACCESS

Edited by:
Peter Adrian Lund,
University of Birmingham,
United Kingdom

Reviewed by:
Michael Benedik,
Texas A&M University, United States
Maria J. Valera,
Universidad de la República, Uruguay

***Correspondence:**
Kazunobu Matsushita
kazunobu@yamaguchi-u.ac.jp

Specialty section:
This article was submitted to Microbial Physiology and Metabolism, a section of the journal Frontiers in Microbiology

Received: 26 October 2021
Accepted: 13 April 2022
Published: 12 May 2022

Citation:
Kataoka N, Matsutani M, Matsumoto N, Oda M, Mizumachi Y, Ito K, Tanaka S, Kanesaki Y, Yakushi T and Matsushita K (2022) Mutations in degP and spoT Genes Mediate Response to Fermentation Stress in Thermally Adapted Strains of Acetic Acid Bacterium Komagataeibacter medellinensis NBRC 3288. Front. Microbiol. 13:802010. doi: 10.3389/fmicb.2022.802010

An acetic acid bacterium, *Komagataeibacter medellinensis* NBRC 3288, was adapted to higher growth temperatures through an experimental evolution approach in acetic acid fermentation conditions, in which the cells grew under high concentrations of ethanol and acetic acid. The thermally adapted strains were shown to exhibit significantly increased growth and fermentation ability, compared to the wild strain, at higher temperatures. Although the wild cells were largely elongated and exhibited a rough cell surface, the adapted strains repressed the elongation and exhibited a smaller cell size and a smoother cell surface than the wild strain. Among the adapted strains, the ITO-1 strain isolated during the initial rounds of adaptation was shown to have three indel mutations in the genes *gyrB*, *degP*, and *spoT*. Among these, two dispensable genes, *degP* and *spoT*, were further examined in this study. Rough cell surface morphology related to *degP* mutation suggested that membrane vesicle-like structures were increased on the cell surface of the wild-type strain but repressed in the ITO-1 strain under high-temperature acetic acid fermentation conditions. The Δ*degP* strain could not grow at higher temperatures and accumulated a large amount of membrane vesicles in the culture supernatant when grown even at 30°C, suggesting that the *degP* mutation is involved in cell surface stability. As the *spoT* gene of ITO-1 lost a 3′-end of 424 bp, which includes one (Act-4) of the possible two regulatory domains (TGS and Act-4), two *spoT* mutant strains were created: one (ΔTGSAct) with a drug cassette in between the 5′-half catalytic domain and 3′-half regulatory domains of the gene,

and the other (ΔAct-4) in between TGS and Act-4 domains of the regulatory domain. These *spoT* mutants exhibited different growth responses; ΔTGSAct grew better in both the fermentation and non-fermentation conditions, whereas ΔAct-4 did only under fermentation conditions, such as ITO-1 at higher temperatures. We suggest that cell elongation and/or cell size are largely related to these *spoT* mutations, which may be involved in fermentation stress and thermotolerance.

Keywords: DegP, SpoT, acetic acid fermentation, thermotolerance, experimental evolution, cell length, membrane vesicle

INTRODUCTION

Acetic acid bacteria are strictly aerobic Gram-negative bacteria that are known for their ability to oxidize various alcohols, sugars, and sugar alcohols. Vinegar is industrially produced, employing the oxidative fermentation ability of acetic acid bacteria, especially *Acetobacter* and *Komagataeibacter*, and is widely used in many food products. In particular, *Komagataeibacter* sp. has been used to produce high concentrations of acetic acid because of its high acetic acid tolerance. During the fermentation process, acetic acid bacteria are exposed to severe stress by the acetic acid produced and the substrate ethanol. Furthermore, acetic acid fermentation is hindered by fermentation heat, which may worsen the stressor's negative effect, and thus requires strict temperature control. Thus, developing thermotolerant strains of *Komagataeibacter* sp. would be useful to enable efficient high-temperature and high-acidity fermentation.

Experimental evolution is one of the means of obtaining thermotolerant microorganisms. Thermal adaptation has been previously achieved in various microorganisms, including *Escherichia coli* (Rudolph et al., 2010; Rodriguez-Verdugo et al., 2014), *Saccharomyces cerevisiae* (Caspeta et al., 2014), *Acetobacter pasteurianus* (Azuma et al., 2009; Matsutani et al., 2013; Matsumoto et al., 2020), *Komagataeibacter oboediens* (Taweecheep et al., 2019), and *Gluconobacter frateurii* (Hattori et al., 2012; Matsumoto et al., 2018). Furthermore, the mechanism associated with thermotolerance was also analyzed using these strains. However, genomic mutations due to thermal adaptation vary from strain to strain in terms of the mode of gene mutation and the expected functions of the mutated genes. Although highly diverse, the mutated genes have been identified to be related to cell surface functions (peptidoglycan synthesis, outer membrane protein, and lipopolysaccharide synthesis), transporters for ions or amino acids, and two-component signal transduction systems (Matsushita et al., 2016). In addition, the "thermotolerant" genes indispensable for growth at higher temperatures have been examined in the acetic acid bacterium *Acetobacter tropicalis* (Soemphol et al., 2011), *E. coli* (Murata et al., 2011), and *Zymomonas mobilis* (Charoensuk et al., 2017), where, based on gene-disruption-dependent thermosensitive mutant selection, the genes related to membrane stabilization, transport, protein quality control, and cell division have been commonly identified (Charoensuk et al., 2017). In *A. tropicalis* SKU1100, 4 among the 32 transposon-induced thermosensitive mutant strains were identified to be defective in the ATPR_1619 gene encoding serine protease DegP (Soemphol et al., 2011), indicating that DegP is indispensable for growth at temperatures higher than the optimum. This periplasmic protease has been also identified as a "thermotolerant gene" in *E. coli* (Murata et al., 2011) and *Z. mobilis* (Charoensuk et al., 2017), as well as in the plant *Arabidopsis* (Charng et al., 2007), and shown to be related to ethanol tolerance in addition to thermotolerance in *A. tropicalis* (Soemphol et al., 2011) and *Z. mobilis* (Charoensuk et al., 2017).

DegP is known to act as a chaperone at low temperatures but switches to a peptidase (heat shock protein) at higher temperatures (Spiess et al., 1999). Thus, abnormal proteins produced at elevated temperatures can be degraded by DegP, which may recognize improperly folded or denatured proteins that accumulate in the inner membrane and/or periplasmic space (Strauch et al., 1989; Lipinska et al., 1990). Defects in DegP function have been shown to generate a membrane hyper-vesiculation phenotype in several bacteria (McBroom et al., 2006; McBroom and Kuehn, 2007; Schwechheimer et al., 2013).

While the RNA polymerase sigma factor has been listed as a thermotolerant gene in *A. tropicalis* in a previous study (Soemphol et al., 2011), the RNA polymerase RpoH and its-b-subunit (RpoB) were also found to be mutated during thermal adaptation of *K. oboediens* (Taweecheep et al., 2019) and *A. pasteurianus* K-1034 (Matsumoto et al., 2021), respectively. In the latter case, the *spoT* gene, which has been shown to interact with RNA polymerase, was also mutated. The *spoT* mutation was also detected in thermally adapted *E. coli* W3110 (Kosaka et al., 2019), with an associated reduction in the amounts of RNA and DNA. SpoT or RelA (RSH family) catalyzes both the synthesis and degradation of guanosine 3′-diphosphate 5′-diphosphate (ppGpp). Disruption of RelA, an additional ppGpp synthetase to SpoT, in *E. coli* K-12 (Yang and Ishiguro, 2003) has been shown to induce thermosensitivity, which was further stimulated by the additional disruption of SpoT but suppressed by certain mutations of RpoB. Thus, SpoT and RNA polymerase working

Abbreviations: Abbreviations**:** DegP, periplasmic endopeptidase (serine proteinase); SpoT, GTP pyrophosphokinase; ppGpp, guanosine 3′-diphosphate 5′-diphosphate; RSH, RelA/SpoT homology family; CTD, C-terminal regulatory domain of *spoT* gene; TGS, regulatory domain of SpoT suggested to be ligand binding; Act-4, regulatory domain of SpoT suggested to bind to amino acids and regulate associated enzymes; ROS, reactive oxygen species; RpoH, RNA polymerase sigma factor; RpoB, RNA polymerase β-subunit; ΔTGSAct, a mutant strain of NBRC 3288 lacking the whole CTD in *spoT* gene; ΔAct-4, a mutant strain of NBRC 3288 lacking only the Act-4 domain in the *spoT* gene; ΔApAct, a mutant strain of SKU 1108 lacking only the Act-4 domain in the *spoT* gene; YPG, culture medium containing 5-g yeast extract, 5-g polypeptone, and 5-g glycerol per 1 L water; YPGAE, culture medium containing 1% acetic acid and 3% ethanol in the YPG medium.

together are expected to play important roles in developing thermotolerance.

The alarmone (p)ppGpp is a mediator of stringent response that coordinates a variety of cellular activities in response to changes in nutritional conditions or environmental stresses. The alarmone is synthesized and degraded by SpoT or RelA (a long-RSH enzyme), which is composed of an N-terminal catalytic domain and a C-terminal regulatory domain (CTD) thought to be involved in the regulation of the catalytic domain (Irving and Corrigan, 2018). The loss of CTD has been shown to increase ppGpp synthetase activity and decrease hydrolase activity (Mechold et al., 2002), while the overexpression of the CTD reduced the ppGpp levels by disturbing oligomerization (Gropp et al., 2001). Furthermore, a number of studies have shown that ppGpp accumulation is related to cell size reduction (Schreiber et al., 1995; Stott et al., 2015; Vadia et al., 2017).

In this study, to obtain a robust strain able to tolerate several fermentation stresses, such as temperature or acetic acid, *Komagataeibacter medellinensis* NBRC3288 was adapted to higher growth temperatures using an experimental evolution approach in the presence of acetic acid and ethanol (fermentation condition). Three adapted strains, ITO-1, ITO-2, and ITO-3, were obtained from NBRC3288 through continuously repeated cultivations at the early growth phase at 34°C, 34.5°C, and 35°C, respectively. The resultant thermally adapted strains were shown to exhibit considerably increased growth and fermentation ability at higher temperatures, with a trade-off of reduced growth than the wild-type strain under non-fermentation conditions. Furthermore, phenotypic observation indicated that the wild-type strain, but not the adapted strains, was elongated and exhibited an irregular cell surface under stressful high-temperature fermentation conditions. Genome mapping analysis of ITO-3 against the wild-type genome revealed a total of eight mutations in the ITO-3 strain. Among the adapted strains, ITO-1 adapted at the initial stage was the focus of this study because it has three unique indel mutations in the genes of *gyrB* (GLX_00040), *degP* (GLX_19020), and *spoT* (GLX_25720). Among the three mutated genes in ITO-1, *spoT* and *degP* were further examined in this study. The results indicate that the *degP* and *spoT* mutations may be involved in the increased thermotolerance and/or acetic acid fermentation abilities of the ITO-1 strain through their influence on cell surface stability and cell division or cell size regulation, respectively.

MATERIALS AND METHODS

Bacterial Strains and Culture Conditions

Komagataeibacter medellinensis NBRC3288 was used as the parental strain and as a starting strain for thermal adaptation. *Acetobacter pasteurianus* SKU1108 (Chinnawirotpisan et al., 2003) and its thermally adapted strain, TH-3 (Matsutani et al., 2013), were also used for comparison with the strains obtained in this study.

The strains (colonies from potato agar plates) were first inoculated in a 5-ml potato medium (20-g glycerol, 5-g glucose, 10-g yeast extract [Oriental Yeast, Tokyo, Japan], 10-g polypeptone [Nihon Pharmaceuticals Co. Ltd., Osaka, Japan], and 100-ml potato extract [Matsutani et al., 2013] per 1 L water) and cultivated at 30°C and 120 rpm for 24–36 h until the turbidity of the culture reached 150–200 Klett units. Then, 1% (v/v) of the pre-culture was inoculated into a YPG medium (5-g yeast extract, 5-g polypeptone, and 5-g glycerol per 1 L water), or the YPG medium containing 1% acetic acid and 3% ethanol (YPGAE medium). Culturing was done in a 100-ml medium in a 500-ml Erlenmeyer flask or a baffled flask at different temperatures and 200 rpm shaking. Bacterial growth was measured using a Klett-Summerson photoelectric colorimeter. The acidity of the culture medium at different growth phases was measured by alkali-titration of 1-ml culture with.8 N NaOH using 10 μL of 0.025% phenolphthalein (transition pH range: 8.3–10) as a pH indicator. For the cultivation of *A. pasteurianus* strains, the YPGDE medium (the YPG medium containing.5% glucose and 4% ethanol) was used.

Thermal Adaptation of *Komagataeibacter medellinensis* Under Acetic Acid Fermentation Conditions at Higher Temperatures

Thermal adaptation of *K. medellinensis* NBRC 3288 was performed in flask culture (Erlenmeyer flask) under fermentation conditions in which the cells grew in the YPGAE medium. This culture condition was chosen as it facilitated high acetic acid production by this strain. First, repeated cultivation was performed at 34°C, with each inoculation being performed at an early log phase in which the culture acidity was between 1.5 and 2% (w/v) (see **Supplementary Figure 1**). The first cultivation had almost no lag phase, whereas the second and later rounds exhibited long lag phases and low acetic acid production. However, repeated cultivation gradually increased the growth and acidity (**Supplementary Figure 1**). When almost no lag phase for acetic acid production was detected or acidity higher than the first cultivation was observed, repeated cultivation was stopped and the culture medium was spread on potato and YPGAE agar plates. After cultivation at 30°C, two and three colonies were isolated from potato and the YPGAE plates, respectively, and their growth was compared in a 100-ml YPGAE medium. The smallest colony obtained from the YPGAE plate exhibited better growth and acetic acid production than the other strains at 34°C. This strain, named ITO-1, was used in the next step. The next adaptation cycle was performed with ITO-1 at 34.5°C with 15 repeated cultivations. A single colony named ITO-2, which showed better growth and acetic acid production, was isolated by spreading on YPGAE agar and evaluating its growth in the 100-ml YPGAE medium at 34.5°C. Finally, the ITO-2 strain was adapted at 35°C in the YPGAE medium. At 35°C, a longer lag phase appeared during the early repeated cultivation. However, after 20 repetitions, growth and acetic acid production increased, and a single colony (ITO-3) exhibiting better growth and acetic acid production was identified from the YPGAE agar plate. Because the thermal adaptation at 35°C required a considerably

longer time (over 80 days) than the cases of 34°C (23 days) or 34.5°C (35 days), 35°C was judged as the temperature limit for adaptation.

Construction of Plasmids and Recombinant Strains

The bacterial strains and plasmids used in this study are listed in **Supplementary Table 1**, and the primers used for PCR are listed in **Supplementary Table 2**. A putative promoter region of the *adhAB* genes, which encode two subunits of the pyrroloquinoline quinone-dependent alcohol dehydrogenase, was amplified from the genomic DNA of *K. medellinensis* NBRC 3288 with the primers 3288-adhpro-Sac (+) and 3288-adhpro-Xho (−). The *degP* gene (GLX_19020) from NBRC 3288 or ITO-1 strains was amplified from the genomic DNA of *K. medellinensis* NBRC 3288 or ITO-1 with the primers 3288-DegP-PstXho-F and 3288-DegP-HinXba-R. Three fragments, an *adhAB*-gene-promoter construct digested with *Sac*I and *Xho*I, a *degP* gene from NBRC 3288 or ITO-1 digested with *Xho*I and *Xba*I, and the shuttle plasmid pMV24 (Fukaya et al., 1989) digested with *Sac*I and *Xba*I, were ligated to yield p*degP*^{WT} and p*degP*$^{ITO-1}$, respectively.

A recombination plasmid was constructed to generate the Δ*degP* strain of *K. medellinensis* NBRC 3288 by inserting the tetracycline resistance (Tc^R) cassette from pKRP12 (Reece and Phillips, 1995). The *degP* gene was first amplified by PCR from the genomic DNA of *K. medellinensis* NBRC 3288 as described above. The PCR product was digested with *Hin*dIII and cloned into pT7blue cut with *Eco*RV and *Hin*dIII, yielding pT*degP*. Then, a Tc^R fragment prepared from pKRP12 by cutting with *Sal*I was ligated with pT*degP* digested with *Sal*I, yielding pΔ*degP*.

ITO-1 has a deletion in the C-terminal regulatory domain in the SpoT protein, which has two sub-domains, TGS and Act-4 (see **Figure 3A**). In this study, we constructed two mutant strains: one, ΔTGSAct, is a whole regulatory domain deletion mutant, and the other, ΔAct-4, is a mutant missing only the Act-4 domain. The recombination plasmid to generate the ΔTGSAct strain of *K. medellinensis* NBRC 3288 was constructed in the same manner as described above. The *spoT* gene (GLX_25720) was first amplified by PCR from the genomic DNA of *K. medellinensis* NBRC 3288 with the primers 3288-GTPppk-Sal-F and 3288-GTPppk-Xba-R. The PCR product was cloned into a pT7blue cut with *Eco*RV, yielding pT*spoT*. Then, a Tc^R fragment prepared from pKRP12 by cutting with *Sal*I was ligated with pT*spoT* digested with *Xho*I, yielding pΔTGSAct.

For construction of the plasmid to generate the ΔAct-4 strain of *K. medellinensis* NBRC 3288, two fragments (N- and C-terminal sequences of the *spoT* gene) were first amplified by PCR from the genomic DNA of *K. medellinensis* NBRC 3288 with the primers 3288-ITO-spoT-5 (+) and 3288-ITO-spoT-fsn-5 (−), and 3288-ITO-spoT-fsn-5 (+) and 3288-ITO-spoT-3 (−), respectively. Three fragments: N- and C-terminal fragments of the *spoT* gene, and the Tc^R cassette, were combined by overlap extension PCR using the primers 3288-ITO-spoT-5 (+) and 3288-ITO-spoT-3 (−). The resulting PCR product was cloned into pT7Blue cut with *Eco*RV, yielding pΔAct-4. *K. medellinensis* was transformed with these plasmids by electroporation, according to the manufacturer's instructions (Bio-Rad, Hercules, CA, United States).

The markerless deletion system based on pKOS6b was used to generate the ΔApAct strain of *A. pasteurianus* SKU1108 (Kostner et al., 2013). To construct the plasmid, two fragments [N- and C-terminal sequences of the *spoT* gene (APT_00593)] were first amplified by PCR from the genomic DNA of *A. pasteurianus* SKU1108 with the primers, 1108-APT0593RI (+) and 1108-APT0593-TGA-Sac (−), and 1108-APT0593-Xba (−) and 1108-APT0593-Sac (+), respectively. Three fragments: an N-terminal fragment cut with *Eco*RI and *Sac*I, a C-terminal fragment cut with *Xba*I and *Sac*I, and pKOS6b cut with *Eco*RI and *Xba*I, were ligated to yield pΔApAct. *A. pasteurianus* was transformed by triparental conjugation (Figurski and Helinski, 1979). Colonies grown on the YPGD medium containing 50 μg/ml kanamycin were isolated as the first recombinant strains and were confirmed by PCR using primers 1108-APT0593RI (+) and 1108-APT0593-Xba (−) to have a wild-type *spoT* DNA band (2 kbp) or a disrupted *spoT* DNA band (1.6 kbp). Next, the first recombinant strains were spread on a plate of the YPGD medium, containing 60 μg/ml 5-fluorocytosine, which was used as a negative selection marker because pKOS6b contains the *codAB* genes (Kostner et al., 2013). For colony isolation, several colonies grown on this plate were confirmed not to grow on a plate of the YPGD medium containing 50-μg/ml kanamycin. Finally, by confirmation of the disrupted *spoT* DNA band (1.6 kbp), the SKU1108 ΔApAct strain was obtained.

Preparation of Membrane Vesicles

Cells were cultivated in 100 ml of the YPGAE medium in a 500-ml baffled flask at 30°C until the early log phase (Acidity of 1.5∼2%) or the late log to the stationary phase (Acidity of 3.5∼4%). The cell cultures were centrifuged at 10,000 × *g* for 15 min to obtain the supernatants, which were further centrifuged at 133,500 × *g* for 90 min to obtain crude membrane vesicles. The vesicle pellets were resuspended or homogenized with less than 1 ml of a 50-mM potassium phosphate (KPi) buffer (pH 6.5), containing 5-mM $MgSO_4$. The suspensions were centrifuged two times at 6,000 × *g* for 2 min to remove debris. Finally, the supernatants were centrifuged at 221,000 × *g* for 60 min to obtain the vesicle pellets. The pellets were resuspended in a small volume (0.1 to 0.5 ml) of the same buffer and briefly sonicated for use as the membrane vesicles.

Analytical Methods

Dot-Spot Test

The cells were cultivated in a potato medium at 30 or 37°C until the turbidity reached 150–200 Klett units. Then, 1-ml of culture was collected in an Eppendorf tube and centrifuged at 10,000 × *g* for 5 min. The cell pellets from different strains were suspended in 1 ml of 0.85% NaCl solution, and further adjusted by adding NaCl (0.85%) solution to equalize the OD_{600} values. The cell suspensions were then diluted to 10^{-1}, 10^{-2}, 10^{-3}, and 10^{-4} with 0.85% NaCl solution, and 7-μL aliquots were spotted on plates containing three different media, YPG, YPGAE, or YPGDE, and cultured at different temperatures.

Measurement of Cell Size

The cells were cultivated in 100 ml of the YPG, YPGAE, or YPGDE medium in a 500-ml Erlenmeyer flask at different temperatures at 200 rpm. The cells were harvested in the early to mid-log phase (a Klett unit of ∼150 and/or acidity of ∼2.%) by centrifugation at 10,000 × *g* for 5 min, washed with 1 ml of 0.85% NaCl, and resuspended in 0.85% NaCl to an OD_{600} of 1. The cells were placed on a glass slide with a cover slip and observed under a microscope (Eclipse E600, Nikon, Tokyo, Japan) at 400 × magnification, with 3–5 images obtained for each sample. The length of approximately 200 cells was measured using PhotoRuler ver. 1.1.3[1] or ImageJ software (Rasband, W. S., U. S. National Institutes of Health, 1997–2015), and shown as a Box plot, which is composed of a box and a whisker (Dekking et al., 2005). The latter exhibits the upper and lower limits of almost all plots except for some extraordinary plots, which are shown with a circle of each plot, and the box doses the upper and lower limits of averaged plots except for the upper and lower quartile plots (each 25% upper and lower exceptional plots). The median value of the whole plot is depicted as a line inside each box.

Measurement of Intracellular Reactive Oxygen Species Levels

The cells were grown at 30°C or 33 in 100 ml of the YPG or YPDAE medium containing 2-μM H_2DCFDA (dichlorodihydrofluorescein diacetate) as the fluorescence probe in a 500-ml baffled flask. The cells were harvested at the early to mid-log phase by centrifugation at 10,000 × *g* and 4°C for 5 min and washed two times with a 10-mM KPi buffer (pH 7.0). The cells were resuspended in the same buffer at a concentration of 4 ml/g of wet cells and passed two times through a French pressure cell press (American Instrument Co., Silver Spring, MD, United States) at 16,000 psi. After centrifugation at 10,000 × *g* for 10 min to remove intact cells, the supernatant was ultracentrifuged at 100,000 × g for 60 min. The fluorescence intensity of the resulting supernatant was measured at 25°C with excitation at 504 nm and emission at 524 nm. Fluorescence intensity obtained at the same scale or condition was normalized to the protein concentration of the sample used.

Lipid Determination

The lipid content of the membrane vesicles was determined with FM 4-64 (Molecular Probes, Eugene, OR, United States), a lipophilic styryl dye, based on the fact that FM 4-46 fluoresces quickly and in a concentration-dependent manner by binding to liposomes (Wu et al., 2009). The vesicle samples were mixed with 5-mM FM 4-64 in a 50-mM HEPES buffer (pH 7.5), and fluorescence was measured with 630-nm emission and 472-nm excitation in a Hitachi 650 10S fluorescence spectrometer. The vesicle lipid concentration was calculated from a calibration curve prepared with 0–25-mg azolectin. The emission and excitation peaks used were determined to be optimal for both vesicle lipid and azolectin.

[1]http://www.inocybe.info/_userdata/ruler/PhotoRuler.html

ppGpp Measurement

Cell cultures were rapidly filtrated with PVDF membrane, washed, and then extracted by lysis solvent (methanol:acetonitrile:water = 2:2:1), basically according to the published methods (Varik et al., 2017; Ahmad et al., 2019). And then, ppGpp was analyzed by MonoQ HPLC column chromatography as shown in **Supplementary Figure 3**.

Protein Determination

Protein content was determined using a modified Lowry method (Dulley and Grieve, 1975). Bovine serum albumin was used as the standard protein.

Preparation for Scanning Electron Microscopy

The cells were collected from the cultures in YPG and YPGAE media at the early to mid-log phase and washed two times with a 50-mM KPi buffer (pH 6.5). The cell pellets were fixed with 2.5% glutaraldehyde in the same buffer for 2–3 h. After washing two times with the buffer, the pellets were dehydrated in a series of (50–100%) ascending ethanol concentrations and then washed two times with 100% *t*-butyl alcohol by incubating for 1 h each at 35–37°C. Finally, the samples were immersed again in100% t-butyl alcohol, frozen, and then dried under reduced pressure at 5°C in a freeze-drying device (JEOL JFD-300). Then, the samples were coated with gold (thickness: 20 nm) using an ion-sputtering device (JEOL JFC-1500) and observed under a JEOL JSM-6100 scanning electron microscope (JEOL Ltd., Tokyo Japan) operating at 15 kV.

Genome Analysis of Adapted Strains

Genome re-sequencing of the ITO-3 strain was performed using the next-generation sequencing platform Illumina HiSeq 2000 platform at Hokkaido System Science Co., Ltd. (Hokkaido, Japan). Genome mapping was performed to detect mutation points by comparing the draft genome of ITO-3 with the complete genome of the wild-type strain (Ogino et al., 2011).

Transcriptome Analysis

Wild and ITO-1 strains were grown in 100 ml of the following media in a 500-ml Erlenmeyer flask. Cultivation was performed in the YPG medium at 30°C and in the YPGAE medium at 30°C or 34°C at 200 rpm. When the cell growth reached the early to mid-log phase, the cells were collected, and total RNA was extracted using an RNeasy Minikit (Qiagen, Venlo, Netherlands) according to the manufacturer's protocol, and then treated with Ribozero (Qiagen) to remove rRNA from mRNA.

The sequencing cDNA libraries were generated using the TruSeq RNA sample prep Kit v. 3, and sequencing was performed as pair-end reads with 100 base runs using the Illumina HiSeq 2500 platform at NODAI Genome Research Center (NGRC), Tokyo University of Agriculture (Tokyo, Japan). This was kindly performed by Dr. Yu Kanesaki of the NGRC.

The adapter sequence and low-quality terminal regions of row reads were trimmed using Trimmomatic v. 0.35 (Bolger et al., 2014). The resulting paired-end reads generated

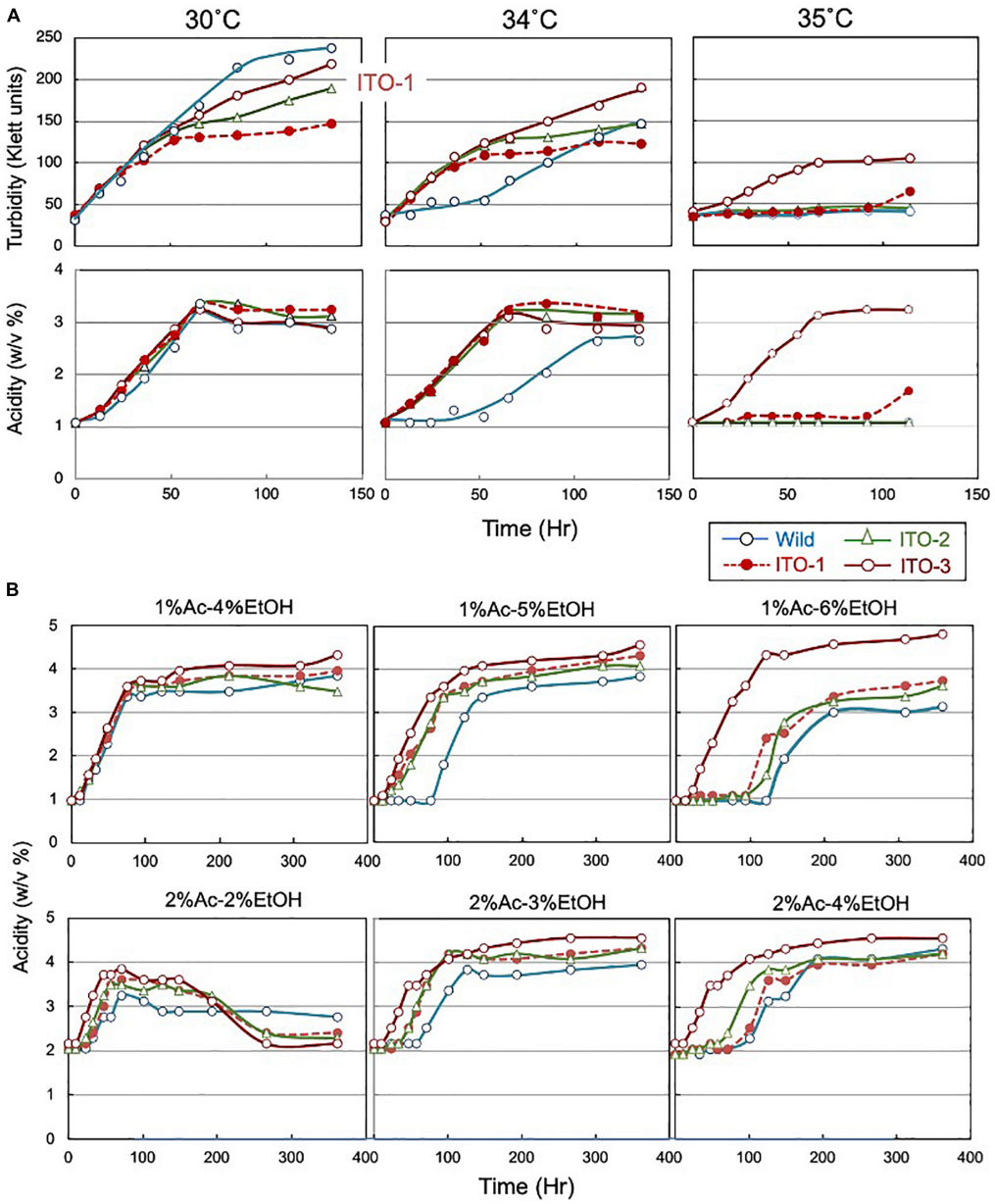

FIGURE 1 | Comparison of growth and acetic acid production of *K. medellinensis* NBRC 3288 and the thermally adapted strains under acetic acid fermentation conditions. **(A)** NBRC 3288 (wild-type strain) and the adapted strains, ITO-1, ITO-2, and ITO-3, were cultivated in the 100-ml of the YPGAE medium in a 500-ml Erlenmeyer flask at 30, 34, and 35°C, with rotary shaking at 200 rpm. Growth (turbidity) and acetic acid concentration (acidity) were measured as described in Materials and methods. This experiment was repeated more than three times, one typical result of which is shown. **(B)** The same strains as **(A)** were cultivated at 30°C in the YPG medium containing different concentrations of acetic acid (Ac) and ethanol (EtOH). In total, 1% Ac-4% EtOH, 1% Ac-5% EtOH, and 1% Ac-6% EtOH show the acetic acid production (acidity) in the YPG medium containing ethanol (4, 5, and 6%, respectively) in the presence of 1% acetic acid, and 2% Ac-2% EtOH, 2% Ac-3% EtOH, and 2% Ac-4% EtOH show the acetic acid production in the YPG medium containing ethanol (2, 3, and 4%, respectively) in the presence of 2% acetic acid.

from the high-throughput sequencing were mapped to the complete genome sequence of *K. medellinensis* NBRC 3288 (GenBank accession: AP012166) as the reference with the program Bowtie2 package using the default setting (Ogino et al., 2011; Langmead and Salzberg, 2012). Read counts were calculated using the htseq-count command included in the HTSeq package based on the gene annotation of the NBRC 3288 genome sequence (Anders et al., 2015). The reads per kilobase million mapped fragments (RPKM) were estimated from read counts per gene using an in-house ruby script. The read counts per gene were used as inputs for the following analysis.

Differentially expressed genes (DEGs) were identified using the edgeR package after normalization using the TCC package (Robinson et al., 2010; Sun et al., 2013). The edgeR package uses a false discovery rate (FDR) to determine DEGs. In this study, genes with FDR < 0.05, and $\log |(\text{fold change})| > 1$ were considered DEGs.

RESULTS

Thermal Adaptation of *Komagataeibacter medellinensis* Under Acetic Acid Fermentation Conditions at Higher Temperatures

The mesophilic acetic acid bacterium, *K. medellinensis* NBRC 3288, produces high quantities of acetic acid at 30°C, but the production diminishes at 34°C, as the growth and fermentation abilities of the NBRC 3288 strain are hindered at higher temperatures. To obtain a strain that can produce acetic acid at higher temperatures, thermal adaptation was performed under fermentation conditions (see **Supplementary Figure 1**), where the culture medium contained acetic acid and ethanol, as described in Materials and methods. Thus, three adapted strains were obtained: one at each adaptation step from 34 to 35°C and named ITO-1 to ITO-3. The growth and acetic acid production abilities of these thermally adapted strains were compared at three different temperatures under fermentation conditions (in the YPGAE medium) (**Figure 1**). As shown, all the adapted strains, but not the wild strain, grew well at 34°C, while only the ITO-3 strain could grow at 35°C. In addition, acetic acid productivity was observed concomitant with their growth behavior. However, turbidity did not always correlate with acetic acid production for reasons described later. In addition, during this thermal adaptation, the tolerance of the adapted strains to ethanol and/or acetic acid, which may be related to the fermentation ability, was also increased (**Figure 1B**). The fermentation rate of the wild-type strain, in the presence of 1% acetic acid, was considerably reduced with 5% ethanol, but not with 4% ethanol, while all the adapted strains fermented well without any lag time with 5% ethanol in the presence of 1% acetic acid. On the other hand, with 6% ethanol in the presence of 1% acetic acid, only ITO-3 could ferment well without any delay. In addition, the presence of 2% acetic acid also reduced the fermentation rate of the wild-type strain, even with only 3% ethanol, whereas the ITO-3 strain could ferment up to 4% ethanol in the presence of 2% acetic acid without any delay. Regardless, even after adaptation, the maximum acetic acid yield from NBRC 3288 did not exceed 5%, even when a much higher substrate concentration was used that theoretically enabled the generation of acetic acid.

Comparison of Cell Size and a Cell Surface Between Wild and the Adapted Strains

As shown in **Figure 1**, cell turbidity and acetic acid productivity were not well correlated; at 30°C, the strains differed in turbidity, despite showing similar acetic acid fermentation ability. In addition, at 35°C, the ITO-3 strain exhibited higher acetic acid productivity, despite exhibiting relatively low turbidity. Therefore, cell sizes were compared between the wild-type and adapted strains (**Figures 2A,B**). Among wild-type, ITO-1, and ITO-3 strains grown on YPGAE (fermentation conditions) at 30°C, the cell sizes of wild-type and ITO-1 cells were almost identical, but ITO-3 cells were a little shorter than the others. In contrast, when grown at 34°C, cell elongation was observed in the wild-type strain but not in ITO-1 and ITO-3. Contrary to their growth on the YPGAE medium, the wild-type strain grew better than ITO-1 on the YPG medium (non-fermentation conditions), especially at higher growth temperatures (**Figure 2C**). Therefore, the cell sizes of wild and ITO-1 strains grown on the YPG medium were also compared (see **Figure 3D**). No cell elongation was observed in either strain at 30°C; in fact, wild-type cells were even shorter than the ITO-1 cells. However, at 34°C, cell elongation was observed to occur in both strains, with ITO-1 cells elongated slightly more than wild-type cells.

We also compared the cell surface morphology of wild-type and ITO-1 strains by Scanning Electron Microscopy (SEM). As shown in **Figure 2D**, a difference in the cell surface was observed between wild and ITO-1 strains grown in the YPGAE medium at 30°C under fermentation conditions; the wild-type strain exhibited a rough surface with some attached vesicles, while ITO-1 exhibited a smooth surface with fewer vesicle-like structures. At 34°C, vesicle-like structures were increased even in the ITO-1 strain, while many debris or vesicle-like structures were seen together with a few intact cells in the wild-type strain. In contrast, under non-fermented conditions (30°C), both strains exhibited smooth cell surfaces and no vesicle-like structures were found. Thus, stress conditions, such as acetic acid production or high growth temperature, appeared to affect the cell surface structure and generate vesicle-like structures on the cell surface.

Thus, *K. medellinensis* thermally adapted under fermentation conditions appears to acquire robustness at higher temperatures in the presence of acetic acid and/or ethanol through genome modification. In the following studies, we focused on the characterization of ITO-1 strain because it had a limited and simple genetic modification as described below.

Stress Response Ability of Wild and ITO-1 Strains Under Fermentation Conditions or High Temperatures

Cells adapted to high temperatures are expected to show a stress-tolerant phenotype, and cells grown under fermentation conditions may also have stress tolerance ability to cope with the substrate ethanol and product acetic acid, both of which are toxic to microbial cells. Such stress tolerance may be related to the generation of reactive oxygen species (ROS). Microbial cells generate a large amount of ROS, especially when grown at growth-limiting high temperatures (Davidson et al., 1996; Matsushita et al., 2016; Chang et al., 2017; Nantapong et al., 2019), and thermally adapted strains have been shown to generate less ROS than the wild-type strain when grown at higher growth temperatures (Matsumoto et al., 2018, 2020).

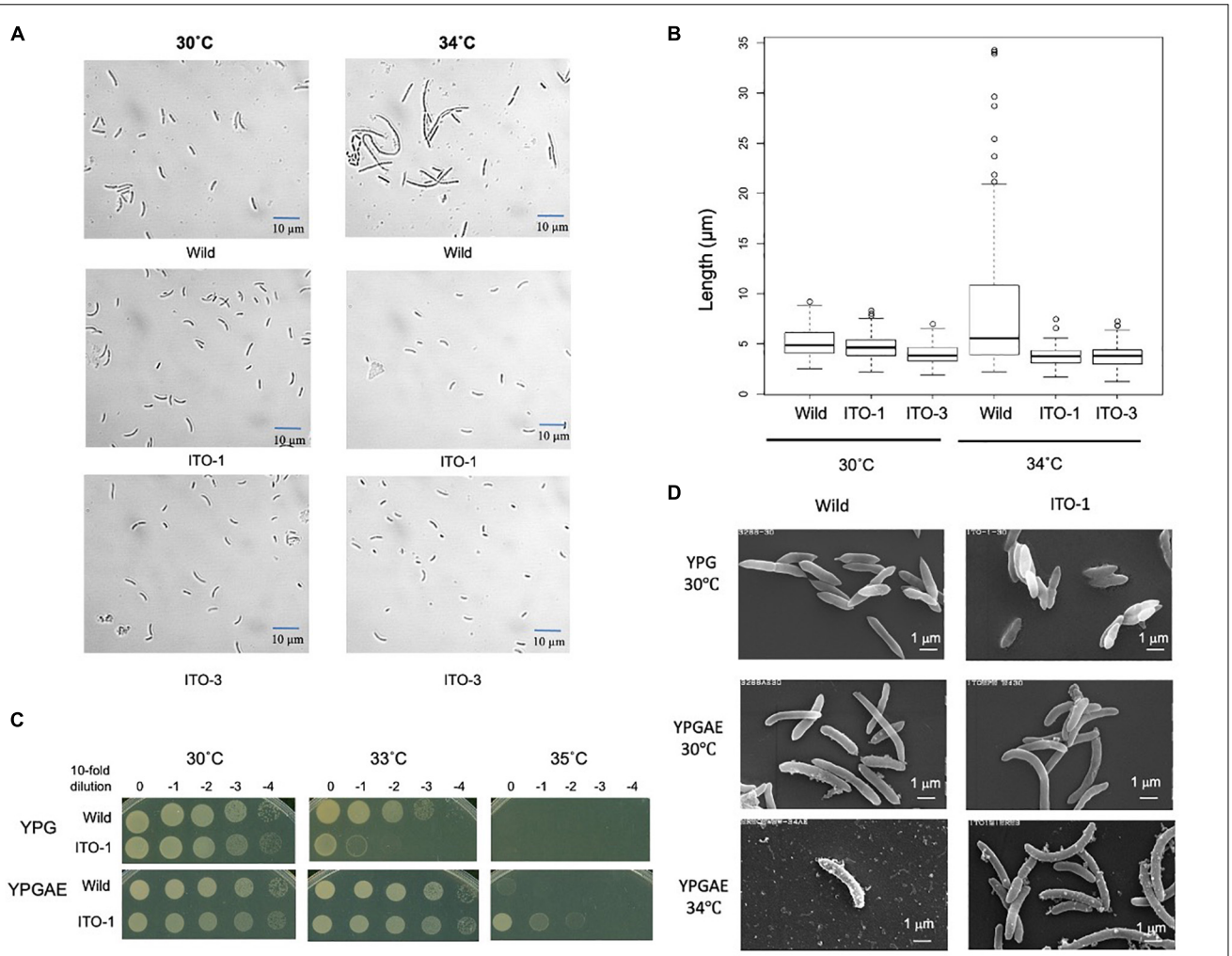

FIGURE 2 | Comparison of cell size and cell surface morphology among NBRC3288, and the adapted strains grown at 30°C and higher temperatures. **(A)** NBRC 3288 (wild-type strain) and the adapted strains, ITO-1 and ITO-3, were cultivated in the 100-ml YPGAE medium in a 500-ml Erlenmeyer flask at 30°C and 34°C with 200-rpm shaking till the early log phase. Cell images were taken under a microscope as described in section "Materials and Methods." **(B)** The box plot shows the cell sizes of wild-type, ITO-1, and ITO-3 strains grown, as in **(A)**, at 30 and 34°C. The box plots were shown by using PhotoRuler, as described in Materials and methods; median values of the cell lengths in the wild-type, ITO-1, and ITO-3 strains were 4.8, 4.6, and 3.8 μm with the cells grown at 30°C, and 5.5, 3.8, and 3.8 μm with those at 34°C, respectively. **(C)** Dot-spot growth comparison was performed, as described in Materials and methods, between wild-type and ITO-1 strains on YPG and YPGAE media at 30, 33, and 35°C. **(D)** Scanning electron microscopic cell surface morphology of NBRC3288 and ITO-1 strains grown on YPG and YPGAE media at 30 and 34°C.

Acetic acid fermentation may similarly generate ROS due to structural damage to the cell membrane caused by acetic acid and/or ethanol. In the present study, the cells grown under fermentation conditions (YPGAE medium) showed extremely higher ROS levels than those grown under non-fermentation conditions (YPG medium) (**Figure 4A**). ROS generation was also increased in the YPGAE medium at higher temperatures in both strains. In addition, ROS generation was repressed in the ITO-1 strain compared to the wild-type strain in the YPGAE medium, but not in the YPG medium at 33°C (**Figure 4A**). Thus, to determine the mechanism behind ROS reduction under fermentation conditions and at higher growth temperatures, transcriptome analysis was performed with the NBRC 3288 strain and the adapted ITO-1 strain. RNA expression levels of both strains were compared during growth on the YPG medium and the YPGAE medium at 30°C, and also of ITO-1 between the cells grown at 30°C and 34°C on the YPGAE medium. Under fermentation conditions, a large number of stress response genes, such as ROS scavenging enzymes, heat shock proteins, chaperonins, and NADPH-generating enzymes, were upregulated in both strains (**Supplementary Table 3**). Typically, several stress response genes upregulated in the fermentation conditions, including peroxidase, Hsp20, DegP, RpoH, G6P dehydrogenase, and aldehyde dehydrogenase, showed a more substantial increase in ITO-1 than in the wild-type strain (**Figure 4B**). On the other hand, when the temperature increased to 34°C, enzymes related to the energy generation system, such as *aptABCDEFGH* (F_1F_0-ATP synthase), *nuoDEFGHIJKLN*

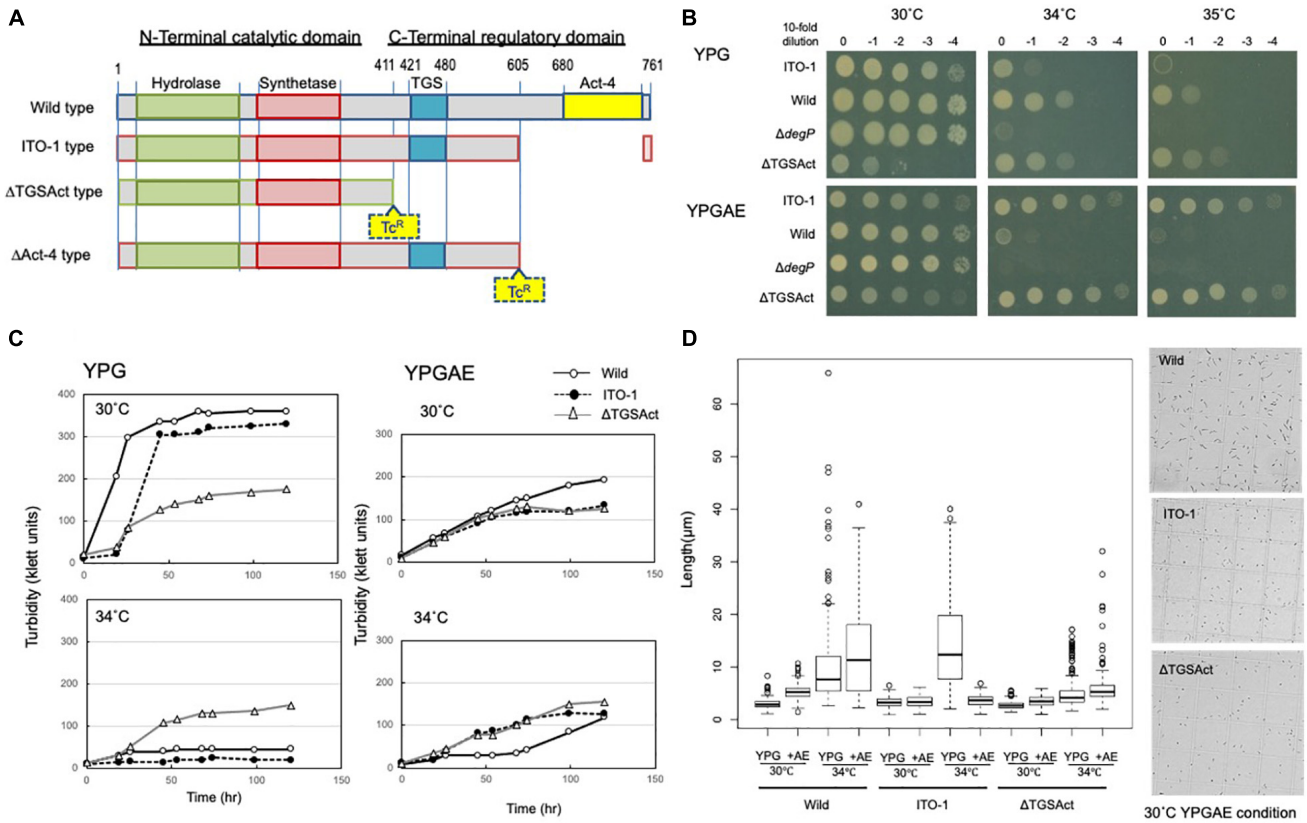

FIGURE 3 | Cell growth and cell length of SpoT mutant strain, ΔTGSAct. **(A)** The *spoT* gene (GLX_25720) domain motif of wild-type and ITO-1 strains, as well as artificial spoT mutant strains, ΔTGSAct, and ΔAct-4. The N-terminal catalytic domain contains metal-dependent hydrolase and synthetase domains, which are thought to constitute a bifunctional enzyme catalyzing (p) ppGpp synthesis, while the C-terminal domain (CTD) is thought to have a TGS domain, which is suggested to be a ligand-binding, regulatory domain, and an Act-4 domain, which may bind to amino acids and regulate associated enzymes. ΔTGSAct and ΔAct-4 were prepared by inserting the Tc^R cassette (Tc), as described in section "Materials and Methods." **(B)** NBRC 3288 (wild-type), ITO-1, Δ*degP*, and ΔTGSAct strains were cultivated in the potato medium containing appropriate antibiotics (25-mg/ml tetracycline for Δ*degP*, and 10-mg/ml ampicillin for ΔTGSAct), and dot-spotted, as described in section "Materials and Methods," on YPG or YPGAE agar plates, and then incubated at 30, 34, and 35°C. **(C)** NBRC 3288 (wild-type), ITO-1, and ΔTGSAct strains were cultivated in 100-ml of the YPG or YPGAE medium in a 500-ml Erlenmeyer flask at 30 and 34°C. Typical results are shown here from at least three independent cultures of each strain. **(D)** Cell length was measured in wild-type, ITO-1, and ΔTGSAct strains grown on YPG or YPGAE (+AE) at 30 and 34°C. Box plots are shown by using PhotoRuler, as described in Materials and methods, and the median values of each cell grown in YPG were 2.8 (30°C) and 7.7 μm (34°C) in wild-type, 3.2 (30°C) and 12.4 μm (34°C) in ITO-1, and 2.6 (30°C) and 4.2 μm (34°C) in ΔTGSAct, and those of each cell grown in YPGAE were 5.3 (30°C) and 11.6 μm (34°C) in wild-type, 3.5 (30°C) and 3.3 μm (34°C) in ITO-1, and 3.6 (30°C) and 5.3 μm (34°C) in ΔTGSAct.

(Type I NADH dehydrogenase), *cyaABCD* (H^+-pumping ubiquinol oxidase), *adhAB* (PQQ-alcohol dehydrogenase), and *aldFGH* (membrane-bound aldehyde dehydrogenase), which were repressed under fermentation conditions, were expressed at higher levels in the ITO-1 strain (**Supplementary Table 3**). Thus, repression of radical generation due to fermentation and energy generation at higher temperatures could be important to survive such stress conditions.

Genome Analysis of Adapted Strains

To determine how thermal adaptation affects the genome, the ITO-3 draft genome was sequenced and compared with the complete genome of the NBRC3288 strain to detect mutations (Ogino et al., 2011). A total of eight mutations, including three deletions, one insertion, and four nucleotide substitutions, were detected in ITO-3 (**Table 1**). Using PCR sequencing, all eight mutations were confirmed in ITO-3, and it was shown that wild, ITO-1 and ITO-2 strains have zero, three, and six mutations of the eight mutations found in ITO-3, respectively. Thus, three mutations occurred in ITO-1, with three and two additional mutations occurring in ITO-2 and ITO-3 strains, respectively (**Table 1**). Some of the mutations seem to confer thermotolerance to the wild strain, while some may have occurred spontaneously by chance. In this study, we focused on mutations in the ITO-1 strain, which has a growth advantage, compared with the wild strain, on the YPGAE medium at 34°C (**Figure 1**), and thus has the ability to produce acetic acid, coping with heat stress as well as ethanol and/or acetic acid stress. ITO-1 had mutations in three genes, with a 12-bp deletion, 12-bp insertion, and a 424-bp deletion in GLX_00040 (*gyrB*), GLX_19020 (*degP*), and GLX_25720 (*spoT*), respectively (**Table 1**). These genes correspond to the enzymes DNA

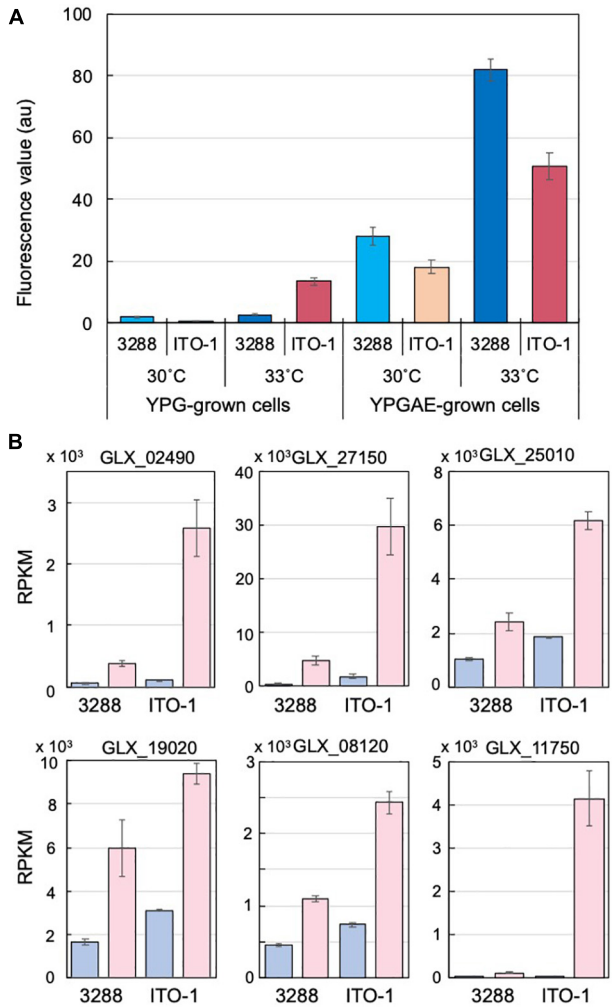

FIGURE 4 | Comparison of stress responses in NBRC3288 and ITO-1 strains grown on YPG and YPGAE media. **(A)** ROS generation was measured, as described in section "Materials and Methods," in NBRC3288 and ITO-1 strains grown on YPG and YPGAE media at 30°C and at 33°C. The fluorescence values obtained are shown by converting the values to one at the same scale or condition. Error bars represent the standard deviation derived from three independent experiments. **(B)** Typical stress response genes were identified from the transcriptome analysis data of NBRC3288 (wild-type strain) and ITO-1 grown on YPG (blue columns) and YPGAE (pink columns) media at 30°C (**Supplementary Table 3**), and their RPKM values are shown. GLX_02490, GLX_27150, GLX_25010, GLX_19020, GLX_08120, and GLX_11750 were annotated as peroxidase, Hsp20, RpoH, DegP, G6P dehydrogenase, and NADPH-dependent aldehyde dehydrogenase, respectively. Error bars represent the standard deviation of RPKM values derived from three different samples.

gyrase, periplasmic endopeptidase, and GTP pyrophosphokinase, respectively (**Table 1**). Among these genes, the *gyrB* mutation was not investigated in this study, because its overexpression had no effect on the growth of the wild and ITO-1 strains (**Supplementary Figure 2**), and disruption of the gene may not be possible due to its indispensability. Thus, in this study, we focused on two genes, *degP* and *spoT*.

Effect of *degP* Mutation on Thermotolerance of *Komagataeibacter medellinensis* NBRC 3288

ITO-1 has a mutation in the *degP* gene, which generates a mutated DegP with additional 4 amino acid residues in the protein sequence. The mutated DegP may play an important role in the cell survival under high temperature or fermentation conditions. As DegP is known to function as a cell surface chaperone or protease (Spiess et al., 1999) and defects in DegP lead to the generation of membrane vesicles (Schwechheimer et al., 2013), the DegP mutation may be involved in modulating the cell surface structure. In fact, such cell surface changes were observed in the wild-type strain but reduced in the ITO-1 strain under stress conditions (**Figure 2D**). This phenomenon could be related to the DegP mutation, which may influence the growth of the ITO-1 strain on the YPGAE medium.

To determine the role of DegP in cell growth under fermentation conditions, its disruptant Δ*degP* was compared with the wild-type and ITO-1 strains in dot-spot analysis (see **Figure 3B**). The Δ*degP* strain grew at 30°C as well as other strains, but not at 34°C on the YPGAE medium. We further studied the effect of *degP* overexpression with a plasmid, p*degP*^{WT} or p*degP*$^{ITO-1}$, containing wild-type or mutated *degP* genes, respectively. p*degP*^{WT}, but not p*degP*$^{ITO-1}$, exhibited a marginal effect on the recovery of the disturbed cell growth of Δ*degP* at 33°C (**Figure 5A**). These plasmids probably produced too much DegP enzymes, especially mutated one, because the cell growth was largely disturbed when expressing them in wild-type and ITO-1 strains (**Supplementary Figure 2**).

When Δ*degP*, wild-type, and ITO-1 strains were grown in Erlenmeyer flasks on the YPGAE medium, there was no clear growth difference at 30°C, whereas at 33°C, only ITO-1 grew well, and the wild and Δ*degP* strains exhibited delayed growth and no growth, respectively (data not shown). The strains were then cultured in baffled flasks, which facilitate high aeration conditions to stimulate cell growth. Here, the Δ*degP* strain exhibited some growth defects at 30°C compared with wild-type and ITO-1 strains, and the Δ*degP* strain harboring p*degP*^{WT}, but not p*degP*$^{ITO-1}$, grew better than Δ*degP* (**Figure 5B**). In contrast, only ITO-1 grew well at 33°C, whereas the wild strain exhibited delayed growth, and both the Δ*degP* strain and the strains harboring p*degP*^{WT} or p*degP*$^{ITO-1}$ did not grow (**Figure 5B**).

DegP may be related to the cell surface structure as shown above and has been shown to be involved in membrane vesicle generation (McBroom et al., 2006; McBroom and Kuehn, 2007). Therefore, to determine the role of DegP in cell growth, all the above strains were grown with high aeration (baffled flask) at 30°C under fermentation conditions, and membrane vesicle generation was compared. Membrane vesicles were isolated from the culture supernatants, as described in section "Materials and Methods," and their lipid and protein contents were examined; they exhibited a fairly high lipid/protein ratio of 1.6∼8.4 compared to the cell membranes (lipid/protein ratio of ∼0.6 to 0.8). As shown in **Figure 5C**, the membrane vesicle content increased from the early log phase (2.1–2.5% acidity)

TABLE 1 | Mutated genes and the mode of mutations in the adapted strains, ITO-1, ITO-2, and ITO-3.

Orf ID	Product	Mutation				ITO-1	ITO-2	ITO-3
		Position	Original sequence	Mutated sequence	Mutational Pattern			
GLX_00040	DNA gyrase subunit B (*gyrB*)	19286	CGCCGCGCGTGAG	C	12 bp deletion	●	●	●
GLX_00820	Hypothetical protein	96323	G	A	D239N			●
GLX_07330	Hypothetical protein	843150	T	TG	1 bp insertion		●	●
GLX_19020	Endopeptidase DegP/Do (*degP*)	2118313	G	GCTTTCCCTTCCC	12 bp insertion	●	●	●
GLX_21880	α, α-trehalose-phosphate synthase	2417396	C	T	A342V		●	●
GLX_25720	GTP pyro-phosphokinase (*spoT*)	2850572–2850989			424 bp deletion	●	●	●
GLX_25830	Outer membrane protein	2862183	C	T	R812C			●
Intergenic	Upstream of GLX_26500	3136818	G	A	SNP		●	●

●, *Mutations occurred in this mutant;* ●, *Mutations retained in these mutants.*

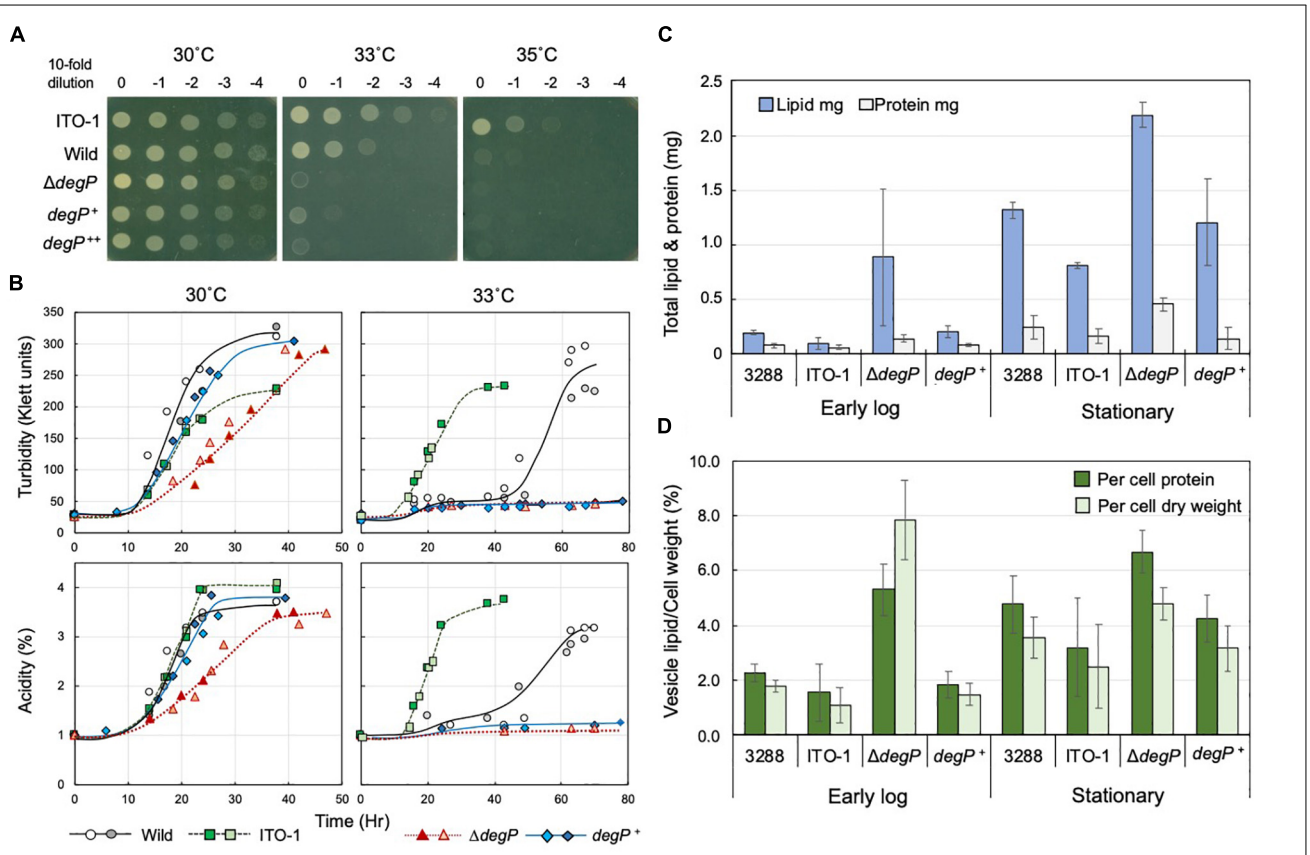

FIGURE 5 | Comparison of cell growth and membrane vesicle generation in NBRC3288, ITO-1, and *degP*-mutated strains grown under fermentation conditions. **(A)** NBRC 3288 (wild-type), ITO-1, and Δ*degP* strains harboring plasmid pMV24, and Δ*degP* strains harboring pP*degP*^{WT} and pP*degP*$^{ITO-1}$ (shown as *degP*$^{+}$ and *degP*$^{++}$, respectively) were cultivated in a potato medium containing 10-mg/ml ampicillin (except for wild and ITO-1 strains) at 30°C. The dot-spot test was then performed, as described in Materials and methods, on YPGAE agar plates at different temperatures. **(B)** NBRC 3288 (wild-type), ITO-1, Δ*degP* strains, and Δ*degP* strains harboring plasmids pMV24, pP*degP*^{WT} (*degP*$^{+}$), or pP*degP*$^{ITO-1}$ were cultivated in 100-ml of the YPGAE medium in a 500-ml-baffled flask at 30 and 33°C. Typical results are shown here from more than three times independent cultures of each strain. As cultures of Δ*degP* (pMV24) and ΔdegP (pP*degP*$^{ITO-1}$) at 30°C grew almost identical to Δ*degP*, *degP*$^{+}$, and also Δ*degP* (pP*degP*$^{ITO-1}$) at 33°C to *degP*$^{+}$ at 33°C, their growth data are not shown here. **(C)** NBRC3288 (wild-type), Δ*degP*, and Δ*degP* harboring pP*degP*^{WT} (*degP*$^{+}$) were cultivated in 100-ml of the YPGAE medium in a baffled flask at 30°C till the early log phase (2.1–2.5% acidity) or till the late log to the stationary phase (3.5–4% acidity). Membrane vesicles were prepared from culture supernatants, as described in section "Materials and Methods." Then, lipids and proteins were determined as described in section "Materials and Methods" and shown as the total content of the whole culture supernatant. Error bars represent the standard deviation derived from three independent experiments. **(D)** Total lipid content is shown as the value (%) per cell protein content or dry cell weight. Lipid content (mg) was the same as shown in **(C)**, and total cell protein (mg) or dry cell weight (mg) was determined from the cell pellets after removal of the culture supernatants, which were used for the preparation of the membrane vesicles. Error bars represent the standard deviation derived from three independent experiments.

to the stationary phase (3.5–4% acidity) in all the strains. In particular, the Δ*degP* strain produced considerably more vesicles than the wild-type strain. When compared with the rate of vesicle generation per biomass (**Figure 5D**), Δ*degP* strain actually produced more, whereas the ITO-1 strain repressed vesicle generation compared to the wild-type strain at all growth phases. Furthermore, the inclusion of p*degP*^{WT} also reduced the vesicle production observed in the Δ*degP* strain. Thus, defects in DegP may induce vesicle generation under stress conditions, such as acetic acid production, and *degP* mutation in ITO-1 may have some gain of function to reduce vesicle generation.

Effect of *spoT* Mutation in the Thermotolerance of ITO-1 Strain

ITO-1 has a mutation in the *spoT* gene, which may generate a C-terminally truncated SpoT protein (**Figure 3A**). Therefore, we first prepared a deletion mutant of the whole SpoTC-terminal regulatory domain (CTD) by inserting the Tc^R cassette between the N-terminal catalytic domain and the CTD (**Figure 3A**). Then, the growth of the resultant disruptant, ΔTGSAct, was compared with that of wild-type and ITO-1 strains on the YPG and YPGAE media at 30, 34, and 35°C by dot spot (**Figure 3B**). Although the growth of the ΔTGSAct strain was slightly worse than that of the other strains at 30°C, it grew well at high temperatures on both media. In contrast, the wild-type strain grew better on the YPG medium and the ITO-1 strain on the YPGAE medium at higher temperatures. Thus, the growth of the ΔTGSAct strain was similar to that of well-growing strains on each medium: wild-type strain on YPG and ITO-1 strain on YPGAE. In terms of cell length, the wild-type strain elongated at a higher growth temperature (34°C) on both media, but cell elongation was observed in the ITO-1 strain only on the YPG medium (**Figure 3D**). Therefore, the growth in flask culture and cell length of the ΔTGSAct strain were compared with those of the wild-type and ITO-1 strains on YPG and YPGAE media (**Figures 3C,D**). On YPG medium, the ΔTGSAct strain exhibited lower turbidity than the other strains at 30°C, but the turbidity was retained at 34°C, unlike the wild-type and ITO-1 strains, both of which displayed reduced growth and elongated cells at 34°C. On the YPGAE medium, the ΔTGSAct strain grew well both at 30 and 34°C, similar to the ITO-1 strain, whereas the wild-type strain showed considerably delayed growth at 34°C. Concomitant with the cell growth behavior, the ΔTGSAct strain maintained a shorter cell length and did not elongate at all, like ITO-1, on YPGAE at 34°C. These results suggest that the truncated SpoT in ΔTGSAct, similar to the mutated SpoT in ITO-1, may repress cell elongation or reduce cell size as observed in both ITO-1 and ΔTGSAct strains. This phenomenon may be mediated by (p) ppGpp accumulation, because it has been shown that the CTD of RelA represses ppGpp synthesis (Gropp et al., 2001; Mechold et al., 2002; Irving and Corrigan, 2018), and that cell size reduction is induced by ppGpp (Schreiber et al., 1995; Stott et al., 2015; Vadia et al., 2017).

Therefore, we examined the ppGpp content of these strains grown on the YPG and YPGAE at 30°C. The nucleotides were extracted directly from the intact cells and analyzed by anion-exchange (Mono-Q column) HPLC, where ppGpp and other nucleotides could be well separated (**Supplementary Figure 3**). However, due to the very low content of ppGpp in the cells compared with other nucleotides, relatively large amounts of culture (80–250 ml) were needed for the extraction before application to HPLC. This is probably due to the difficulty of cell lysis in *K. medellinensis* cells, especially those grown on the YPGAE medium, because *Gluconacetobacter europaeus* (now *Komagataeibacter europaeus*) (Trcek et al., 2007) and *A. pasteurianus* (Kanchanarach et al., 2010) cells grown on high acetic acid concentrations have been shown to be covered with spongy and amorphous materials, respectively, and become tight and hard. Thus, although a quantitative comparison was very difficult among the strains, especially because no data were obtained from the wild cells grown on the YPGAE medium, the ΔTGSAct strain grown on YPG or ITO-1 strain grown on YPGAE exhibited increased levels of ppGpp when compared to other nucleotides like GDP or ATP extracted from the same cells. Thus, it may be said that phenotypic changes, such as cell size reduction observed in the ITO-1 strain and the ΔTGSAct strain, could be induced by increased alarmone production on account of the truncated SpoT protein.

However, there was a difference in growth between ΔTGSAct and ITO-1, especially under non-fermentation conditions (YPG medium) (**Figures 3B,C**). This is probably because only the Act-4 domain in the CTD is deficient in ITO-1, while both TGS and Act-4 domains are deficient in ΔTGSAct (**Figure 3A**). Therefore, we also examined the effect of the Act-4 domain on growth or cell phenotypes.

Deletion of the Act-4 Domain in *Komagataeibacter medellinensis* NBRC 3288

To determine the functional difference between the Act-4 domain and the whole regulatory domain (CTD), the ΔAct-4 mutant was prepared by inserting the Tc^R cassette between the TGS domain and Act-4 domains (**Figure 3A**). Then, the growth of ΔAct-4 strain was compared with that of the ΔTGSAct, wild-type, and ITO-1 strains by dot spot on both non-fermentation (YPG) and fermentation (YPGAE) media at 30, 34, and 35°C (**Figure 6A**). On the YPGAE medium, the ΔAct-4 strain grew better than the wild-type strain at 34 and 35°C but was slightly worse than the ΔTGSAct and ITO-1 strains. In contrast, on the YPG medium, the ΔAct-4 strain grew worse than the ΔTGSAct strain at 34 and 35°C but similar to the wild-type and ITO-1 strains. Thus, the ΔAct-4 strain exhibited thermotolerance under fermentation conditions although slightly weaker than the ITO-1 and ΔTGSAct strains, but not under non-fermentation conditions, like ITO-1 but unlike ΔTGSAct. However, when the cell length was compared, the ΔAct-4 strain displayed a shorter cell length than the wild and ITO-1 strains but almost the same cell length as ΔTGSAct (**Figures 3D**, **6B**) under non-fermentation conditions at 34°C, although thermotolerance was not observed unlike the ΔTGSAct strain.

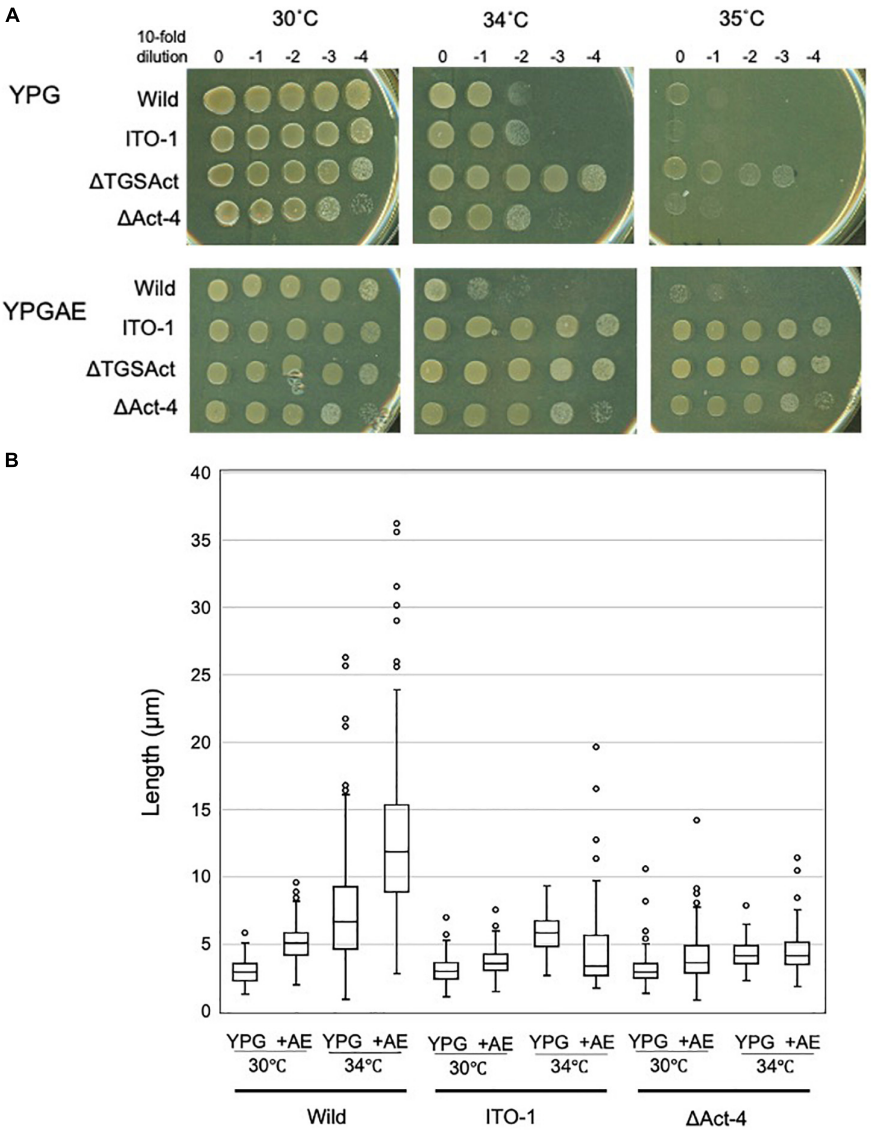

FIGURE 6 | Cell growth and cell length of SpoT mutant strain, ΔAct-4. **(A)** NBRC 3288 (wild-type), ITO-1, ΔTGSAct, and ΔAct-4 strains were cultivated in the potato medium containing appropriate antibiotics (25-mg/ml tetracycline for ΔTGSAct and ΔAct-4 strains), and dot-spotted, as described in Materials and methods, on YPG or YPGAE agar plates, and then incubated at 30, 34, and 35°C. **(B)** Cell length was measured in wild-type, ITO-1, and ΔAct-4 strains grown on YPG or YPGAE (+AE) at 30 and 34°C. Box plots are shown by using the PhotoRuler, as described in Materials and methods, and the median values of each cell grown in YPG were 3 (30°C) and 6.6 μm (34°C) in wild-type, 3.1 (30°C) and 5.9 μm (34°C) in ITO-1, and 3 (30°C) and 4.2 μm (34°C) in ΔAct-4, and those of each cell grown in YPGAE were 5.1 (30°C) and 11.9 μm (34°C) in wild-type, 3.6 (30°C) and 3.5 μm (34°C) in ITO-1, and 3.8 (30°C) and 4.3 μm (34°C) in ΔAct-4.

Effect of Act-4 Domain Deletion in *SpoT* in *Acetobacter pasteurianus* SKU1108

To confirm the role of the Act-4 domain, a similar deletion mutant strain (ΔApAct) was created in another acetic acid bacterium, *A. pasteurianus* SKU1108, *via* a markerless mutation. *A. pasteurianus* SKU1108 is a naturally thermotolerant strain that can perform acetic acid fermentation at 37°C. This strain was further adapted to higher temperatures till 40°C under acetic acid fermentation conditions (the YPGDE medium; the YPGD medium containing 4% ethanol) to generate a thermally adapted strain, TH-3 (Matsutani et al., 2013). As shown in **Figure 7A**, the adapted TH-3 strain showed higher growth and fermentation ability even when grown on the YPGDE medium at 37°C, although a more critical difference was observed at 40°C. The TH-3 strain has 11 mutations, of which the transcriptional regulator MarR, amino acid transporter, C_4-dicarboxylate transporter, and PII uridylyltransferase were shown to be involved in fermentation ability and thermotolerance (Matsutani et al., 2013, unpublished), but it did not have a *spoT* gene mutation. The *spoT* genes of SKU1108 and *K. medellinensis* are homologous to each other, and a sole gene functions as an RSH-enzyme in these a-Proteobacterial

strains (data not shown). Therefore, SpoT in SKU1108 was expected to have a function similar to that in *K. medellinensis*. As shown in **Figures 7A,B**, the ΔApAct strain also showed higher thermotolerance under fermentation conditions. In addition, the ΔApAct strain similar to the TH-3 strain showed a shorter cell length than that of the wild-type SKU1108 strain (**Figure 7C**). Thus, the acetic acid bacterium *A. pasteurianus*, even though from a different genus than *K. medellinensis*, could also acquire thermotolerance *via* the deletion of one of the regulatory domains Act-4 of SpoT protein, which would induce a shorter cell length.

DISCUSSION

In this study, high-temperature-adapted strains, ITO-1, ITO-2, and ITO-3, were obtained sequentially from *K. medellinensis* NBRC3288 by an experimental evolution approach in acetic acid fermentation conditions, where the cells grew at increased temperatures under high concentrations of ethanol and acetic acid. The adapted strain ITO-1 analyzed in this study showed robustness, exhibiting thermotolerance as well as tolerance to resist acetic acid and/or ethanol, while simultaneously exhibiting a trade-off of reduced growth than the wild-type strain under non-fermentation conditions (in the absence of ethanol and/or acetic acid). The adapted ITO-1 strain showed two typical morphological phenotypes related to cell surface structure and cell length. The wild-type NBRC3288 exhibited a rough or irregular cell surface structure and marked cell elongation at higher temperatures, especially under acetic acid fermentation conditions. In contrast, ITO-1 acquired the ability to exhibit a smoother cell surface and smaller cell length than the wild-type strain, even at 30°C. Related to the phenotypic changes, in this study, we focused on the mutations of two genes, *degP* and *spoT*, acquired during the experimental evolution of the ITO-1 strain.

The Role of *degP* Mutation in ITO-1 Strain

Scanning electron microscopy observation indicated that the wild strain grown under fermentation conditions had an irregular cell surface, with attached membrane vesicle-like structures, whereas ITO-1, having a *degP* mutation, exhibited a relatively smooth cell surface where the production of such vesicles may be suppressed. Thus, the membrane vesicle generation was examined under the fermentation conditions employed in this study. The Δ*degP* strain produced a larger number of vesicles than the wild-type strain, whereas the ITO-1 strain repressed vesicle generation throughout its growth. Thus, as expected, a defect in DegP could induce vesicle generation under stressful fermentation conditions, while the mutated DegP in ITO-1 may gain a higher enzyme activity, albeit no direct evidence, to enable the cells to stabilize against such envelope stress by deleting some denatured or abnormal proteins generated on the cell surface. The stable cell surface, including the outer membrane and the periplasm, may confer the cells the ability to tolerate several stresses, especially at higher growth temperatures.

The Role of *spoT* Gene Mutation in ITO-1 Strain

SpoT has four domains: degradation and synthesis domains in the N-terminal half (the catalytic domain) and TGS and Act-4 domains in the C-terminal half (regulatory or the CTD domain) (**Figure 3A**). The ITO-1 strain has a truncated SpoT, which lost a part of the CTD, including the Act-4 domain, and shows thermotolerance under acetic acid fermentation, but not non-fermentation, conditions at 34°C. The ΔTGSAct mutant, with the SpoT lacking the whole CTD, exhibited thermotolerance under both fermentation and non-fermentation conditions, while the other mutant ΔAct-4, lacking only the Act-4 domain in the *spoT* gene, achieved thermotolerance only under fermentation conditions, of which the phenotype is similar to that of the ITO-1 strain. In correlation with the thermotolerance, cell elongation was repressed in these adapted and mutated strains, as opposed to the cell elongation observed in the wild-type strain irrespective of the culture conditions. The ITO-1 strain could repress cell elongation only under fermentation conditions, but both the ΔTGSAct and ΔAct-4 strains repressed cell elongation under both fermentation and non-fermentation conditions. Thus, at least in both ITO-1 and ΔTGSAct strains, it is reasonable to conclude that the thermotolerance phenotype is linked to the ability to repress cell elongation induced by heat stress and partly by fermentation stress. However, there was some uncertainty with the ΔAct-4 strain, as it could not grow well but repressed cell elongation under non-fermentation conditions at 34°C. Thus, to clarify the uncertainty in the function of the Act-4 domain, a similar "Act-4 domain"-deleted mutant (ΔApAct) was created in another acetic acid bacterium, *A. pasteurianus* SKU1108. Results from the ΔApAct strain clearly showed that the mutated SpoT could confer the strain thermotolerance together with the reduced cell size under fermentation conditions (**Figure 7**), thus providing additional supporting information that SpoT missing Act-4 domain functions could reduce the cell size, at least under acetic acid fermentation conditions.

Thus, it is conceivable that the thermotolerance ability is related to cell size regulation, which may be mediated by (p)ppGpp accumulation because the reduction in cell size has been shown to be induced by ppGpp (Schreiber et al., 1995; Stott et al., 2015; Vadia et al., 2017). In this study, our preliminary data suggested that ITO-1 and ΔTGSAct may accumulate ppGpp to a certain level, at least under fermentation conditions (**Supplementary Figure 3**). From the phenotypic differences shown above, it is expected that SpoT of ΔTGSAct, missing the whole CTD, may synthesize ppGpp under both growth conditions, while the variant missing only the Act-4 domain, ITO-1, could accumulate ppGpp by derepressing the catalytic domain only in the presence of acetic acid (or ethanol) (**Figure 8**). Thus, it is conceivable that the ITO-1 strain may acquire the ability to grow better at higher temperatures under fermentation conditions *via* ppGpp-dependent stringent response. This notion is supported by the cell size reduction (**Figures 2B**, **3D**, **6B**)

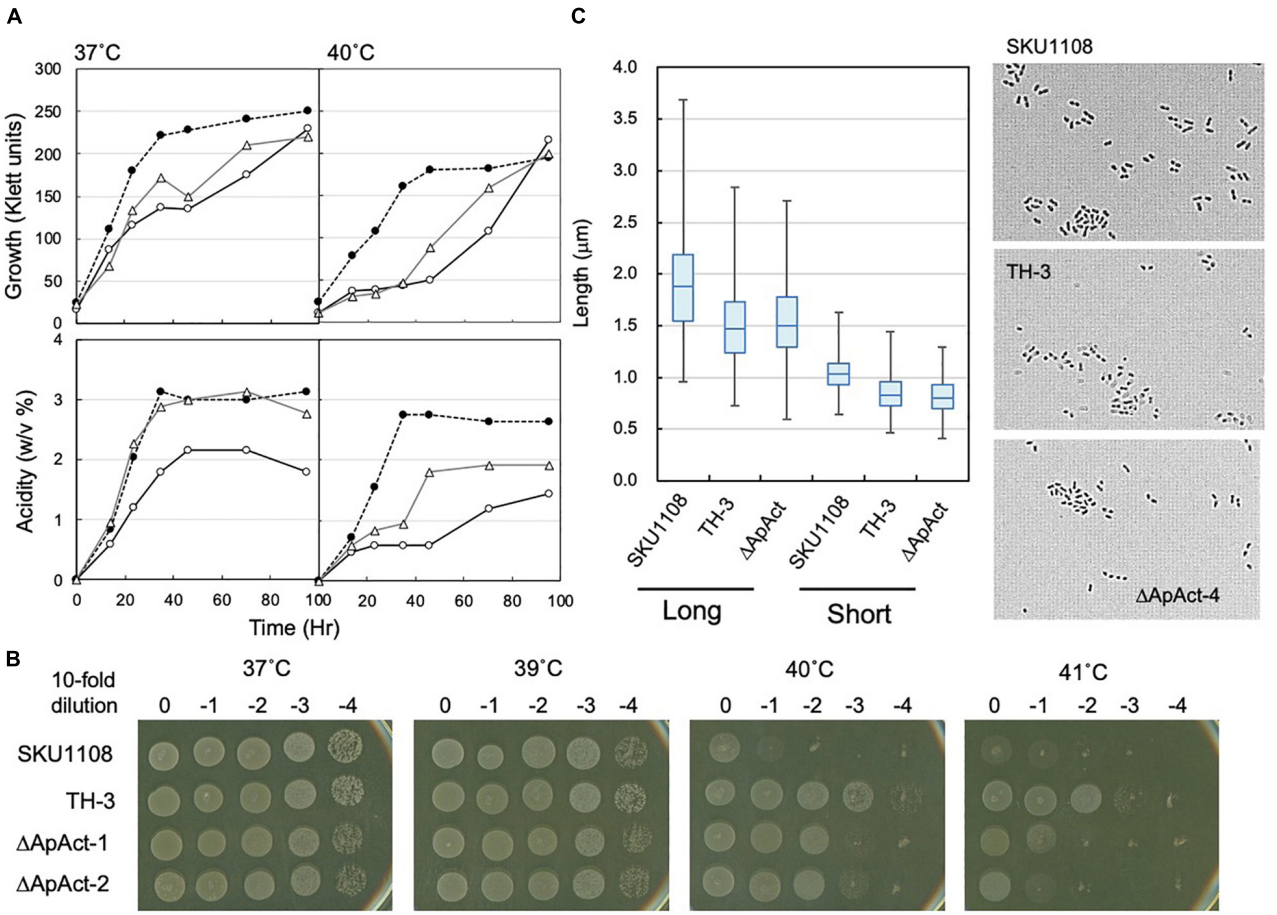

FIGURE 7 | Effect of *spoT* mutation (ΔApAct) on the growth and cell length in *Acetobacter pasteurianus* SKU1108. **(A)** SKU1108 (wild-type), TH-3 (thermally adapted strain), and ΔApAct (Act-4-deleted mutant) were cultivated in 100 ml of the YPGDE medium (containing 4% ethanol) in a 500-ml Erlenmeyer flask at 37 and 40°C. Pre-cultures of these strains were grown in 5 ml of the potato medium at 37°C. Typical results are shown here from three independent cultures of each strain. **(B)** Comparison of dot-spot growth among *A. pasteurianus* SKU1108, TH-3, the same two *spoT* mutant ΔApAct strains, ΔApAct-1 and ΔApAct-2, on the YPGDE agar medium. *A. pasteurianus* strains were cultivated in the 5 ml potato medium at 37°C until 100 Klett units. The strains were diluted with the YPGD medium, spotted on YPGDE (4% ethanol) agar plates, and then incubated for 48 h at 37, 39, 40, and 41°C. **(C)** Cell length was measured in SKU1108, TH-3, and ΔApAct strains grown on the YPGDE medium at 37°C till the mid-log phase (Klett units and acidity of SKU1108, TH-3, and ΔApAct were 135 and 1.2%, 130 and 1.2%, and 100 and 1.2%, respectively). Both the long and short axes of the cells are shown as the box plot by using ImageJ software, as described in section "Materials and Methods." The median values (long axis) of each cell were 1.87, 1.47, and 1.48 μm in SKU1108, TH-3, and ΔApAct, respectively.

and the reduction in expression of translational machinery components, such as ribosomal proteins and t-RNA synthetases under fermentation conditions at 30°C, especially in the ITO-1 strain (**Supplementary Table 3**). The latter phenomenon has already been shown to occur in ppGpp-dependent stringent responses (Paul et al., 2004; Traxier et al., 2008).

Adaptation of ITO-1 Strain via *degP* and *spoT* Mutations

In this study, at least two mutations in the *degP* and *spoT* genes were shown to contribute to stable acetic acid fermentation at higher growth temperatures. The *degP* and *spoT* mutations may contribute to the tolerance ability of the ITO-1 strain *via* cell surface stability and stringent response, respectively, as described above. Since disturbances in the biogenesis of cell surface components, such as outer membrane, lipopolysaccharide, or peptidoglycan, are known to induce stringent response (Roghanian et al., 2019), it is reasonable to assume that the robustness acquired by DegP on account of its mutation could work to repair the cell surface structure in combination with the stringent response induced by *spoT* mutation. In the ITO-1 strain, a large number of stress response genes, such as ROS scavenging enzymes, heat shock proteins, chaperonins, and NADPH-generating enzymes, are upregulated under fermentation conditions, and energy-generating enzymes are upregulated at higher growth temperatures. The former expressional change may also be related to *spoT* mutation in ITO-1 because it has been shown that RpoS-dependent stress response genes could be induced by ppGpp both in *E. coli* (Traxier et al., 2008) and the a-Proteobacterium *Rhizobium etli* (Vercruysse et al., 2011), where heat stress genes

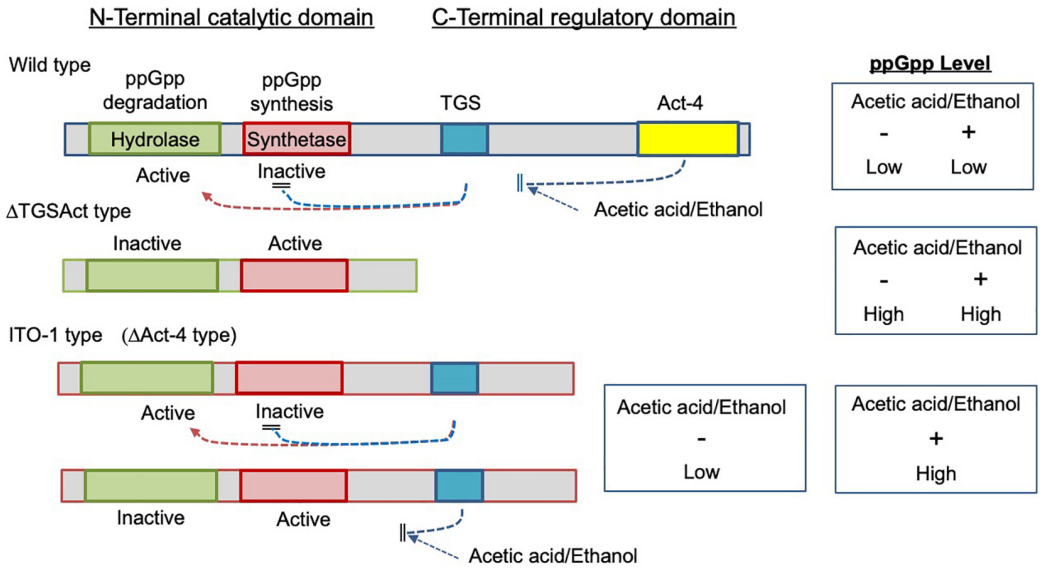

FIGURE 8 | Image for the functional states of the mutated SpoTs from ITO-1 and ΔTGSAct strains. In the wild strain, the hydrolase and synthetase of the catalytic domain (N-terminal) are regulated by the TGS and also by the Act-4 domains (CTD) to be active and inactive, respectively, and thus ppGpp may not be accumulated. In the ΔTGSAct strain, both hydrolase and synthetase of the catalytic domain are derepressed due to the depletion of CTD to be inactive and active, respectively, and thus ppGpp may be accumulated. In the ITO-1 strain, due to the missing of the Act-4 domain, which may control the effect of acetic acid or ethanol, the catalytic domain is regulated solely by the TGS domain, which may be affected by acetic acid or ethanol negatively. Thus, the hydrolase and synthetase of the catalytic domain could be derepressed only in the presence of acetic acid or ethanol.

such as HPS20 and oxidative stress genes are upregulated. These changes may also contribute to stable cell growth or fermentation by reducing ROS generation and increasing energy generation. Thus, the thermally adapted strain, ITO-1, seems to have acquired thermotolerance and acid or alcohol tolerance abilities *via* acquired gene mutations during the experimental evolutionary process.

In conclusion, ITO-1 strain acquired robustness during experimental evolution *via* at least two genes, *degP* and *spoT*, mutations, both of which might be gain-of-function. The former mutation seems to release envelope stress, stabilizing cell surface structure, while the latter seems to induce stringent response, reducing cell size and increasing ROS scavenging ability. The combination of both the phenotypic changes enables ITO-1 to be robust against several fermentation stresses.

DATA AVAILABILITY STATEMENT

The datasets presented in this study can be found in DDBJ Sequence Read Archive repository, accession numbers, DRA012974, for genome resequence and DRA012979 for transcriptome analysis.

AUTHOR CONTRIBUTIONS

KM planned the project. NK, TY, and KM designed the experiments. MO, YM, KI, and NM carried out the experiments with support from NK (genetic work), MM (genome analysis and transcriptome analysis), YK (transcriptome analysis), and ST (microscopy analysis). NK, MM, and NM prepared the manuscript with help from KM and TY. All authors contributed to the scientific discussion throughout the work and have read and approved the manuscript.

FUNDING

This study was funded by the Advanced Low Carbon Technology Research and Development Program (ALCA) of the Japan Science and Technology Agency (JST; JPMJAL1106). This study was also supported by the Cooperative Research Grant of the Genome Research for BioResource, NODAI Genome Research Center, Tokyo University of Agriculture.

ACKNOWLEDGMENTS

We would like to thank Editage (www.editage.com) for English language editing. We also thank Oriental Yeast (Tokyo, Japan) for the kind gift of the yeast extract.

SUPPLEMENTARY MATERIAL

The Supplementary Material for this article can be found online at: https://www.frontiersin.org/articles/10.3389/fmicb.2022.802010/full#supplementary-material

REFERENCES

Ahmad, S., Wang, B., Walker, M. D., Tran, H.-K. R., Stogios, P. J., Savchenko, A., et al. (2019). An interbacterial toxin inhibits target cell growth by synthesizing (p)ppApp. *Nature* 575, 674–678. doi: 10.1038/s41586-019-1735-9

Anders, S., Pyl, P. T., and Huber, W. (2015). HTSeq–a Python framework to work with high-throughput sequencing data. *Bioinformatics* 31, 166–169. doi: 10.1093/bioinformatics/btu638

Azuma, Y., Hosoyama, A., Matsutani, M., Furuya, N., Horikawa, H., Harada, T., et al. (2009). Whole-genome analyses reveal genetic instability of *Acetobacter pasteurianus*. *Nucleic Acids Res.* 37, 5768–5783. doi: 10.1093/nar/gkp612

Bolger, A. M., Lohse, M., and Usadel, B. (2014). Trimmomatic: a flexible trimmer for Illumina sequence data. *Bioinformatics* 30, 2114–2120. doi: 10.1093/bioinformatics/btu170

Caspeta, L., Chen, Y., Ghiaci, P., Feizi, A., Buskov, S., Hallström, B. M., et al. (2014). Biofuels Altered sterol composition renders yeast thermotolerant. *Science* 346, 75–78. doi: 10.1126/science.1258137

Chang, R., Lv, B., and Li, B. (2017). Quantitative proteomics analysis by iTRAQ revealed underlying changes in thermotolerance of *Arthrospira platensis*. *J. Proteomics* 165, 119–131. doi: 10.1016/j.jprot.2017.06.015

Charng, Y., Liu, H., Liu, N., Chi, W., Wang, C., Chang, S., et al. (2007). A heat-inducible transcription factor, HsfA2, is required for extension of acquired thermotolerance in *Arabidopsis*. *Plant Physiol.* 143, 251–262. doi: 10.1104/pp.106.091322

Charoensuk, K., Sakurada, T., Tokiyama, A., Murata, M., Kosaka, T., Thanonkeo, P., et al. (2017). Thermotolerant genes essential for survival at a critical high temperature in thermotolerant ethanologenic *Zymomonasmobilis*TISTR 548. *Biotechnol. Biofuels* 10:204. doi: 10.1186/s13068-017-0891-0

Chinnawirotpisan, P., Theeragool, G., Limtong, S., Toyama, H., Adachi, O., and Matsushita, K. (2003). Quinoprotein alcohol dehydrogenase is involved in catabolic acetate production, while NAD-dependent alcohol dehydrogenase in ethanol assimilation, in *Acetobacter pasteurianus* SKU1108. *J. Biosci. Bioeng.* 96, 564–571. doi: 10.1016/S1389-1723(04)70150-4

Davidson, J. F., Whyte, B., Bissinger, P. H., and Schiestl, R. H. (1996). Oxidative stress is involved in heat-induced cell death in *Saccharomyces cerevisiae*. *Proc. Natl. Acad. Sci. U. S. A.* 93, 5116–5121. doi: 10.1073/pnas.93.10.5116

Dekking, F. M., Kraaikamp, C., Lopuhaä, H. P., and Meester, L. E. (2005). *A Modern Introduction to Probability and Statistics: Springer Texts in Statistics*. London: Springer-Verlag.

Dulley, J. R., and Grieve, P. A. (1975). A simple technique for eliminating interference by detergents in the Lowry method of protein determination. *Anal. Biochem.* 64, 136–141. doi: 10.1016/0003-2697(75)90415-7

Figurski, D. H., and Helinski, D. R. (1979). Replication of an origin-containing derivative of plasmid RK2 dependent on a plasmid function provided in trans. *Proc. Natl. Acad. Sci. U. S. A.* 76, 1648–1652. doi: 10.1073/pnas.76.4.1648

Fukaya, M., Tayama, K., Tamaki, T., Tagami, H., Okumura, H., Kawamura, Y., et al. (1989). Cloning of the membrane-bound aldehyde dehydrogenase gene of *Acetobacter polyoxogenes* and improvement of acetic acid production by use of the cloned gene. *Appl. Environ. Microbiol.* 55, 171–176. doi: 10.1128/aem.55.1.171-176.1989

Gropp, M., Strausz, Y., Gross, M., and Glaser, G. (2001). Regulation of *Escherichia coli* RelA requires oligomerization of the C-terminal domain. *J. Bacteriol.* 183, 570–579. doi: 10.1128/JB.183.2.570-579.2001

Hattori, H., Yakushi, T., Matsutani, M., Moonmangmee, D., Toyama, H., Adachi, O., et al. (2012). High-temperature sorbose fermentation with thermotolerant *Gluconobacterfrateurii* CHM43 and its mutant strain adapted to higher temperature. *Appl. Microbiol. Biotechnol.* 95, 1531–1540. doi: 10.1007/s00253-012-4005-4

Irving, S. E., and Corrigan, R. M. (2018). Triggering the stringent response: signals responsible for activating (p)ppGpp synthesis in bacteria. *Microbiology* 164, 268–276. doi: 10.1099/mic.0.000621

Kanchanarach, W., Theeragool, G., Inoue, T., Yakushi, T., Adachi, O., and Matsushita, K. (2010). Acetic acid fermentation of *Acetobacter pasteurianus*: relationship between acetic acid resistance and pellicle polysaccharide formation. *Biosci. Biotechnol. Biochem.* 74, 1591–1597. doi: 10.1271/bbb.100183

Kosaka, T., Nakajima, Y., Ishii, A., Yamashita, M., Yoshida, S., Murata, M., et al. (2019). Capacity for survival in global warming: adaptation of mesophiles to the temperature upper limit. *PLoS One* 14:e0215614. doi: 10.1371/journal.pone.0215614

Kostner, D., Peters, B., Mientus, M., Liebl, W., and Ehrenreich, A. (2013). Importance of *codB*for new *codA*-based markerless gene deletion in *Gluconobacter*strains. *Appl. Microbiol. Biotechnol.* 97, 8341–8349. doi: 10.1007/s00253-013-5164-7

Langmead, B., and Salzberg, S. L. (2012). Fast gapped-read alignment with Bowtie 2. *Nat. Methods* 9, 357–359. doi: 10.1038/nmeth.1923

Lipinska, B., Zylicz, M., and Georgopoulos, C. (1990). The HtrA (DegP) protein, essential for *Escherichia coli* survival at high temperatures, is an endopeptidase. *J. Bacteriol.* 172, 1791–1797. doi: 10.1128/jb.172.4.1791-1797.1990

Matsumoto, N., Hattori, H., Matsutani, M., Matayoshi, C., Toyama, H., Kataoka, N., et al. (2018). A single-nucleotide insertion in a drug transporter gene induces a thermotolerant phenotype of *Gluconobacterfrateurii* by increasing the NADPH/ $NADP^+$ ratio via metabolic change. *Appl. Environ. Microbiol.* 84:e00354-18. doi: 10.1128/AEM.00354-18

Matsumoto, N., Matsutani, M., Azuma, Y., Kataoka, N., Yakushi, T., and Matsushita, K. (2020). In vitro thermal adaptation of mesophilic *Acetobacter pasteurianus* NBRC 3283 generates thermotolerant strains with evolutionary trade-offs. *Biosci. Biotechnol. Biochem.* 84, 832–841. doi: 10.1080/09168451.2019.1703638

Matsumoto, N., Osumi, N., Matsutani, M., Phathanathavorn, T., Kataoka, N., Theeragool, G., et al. (2021). Thermal adaptation of *acetic acid bacteria* for practical high-temperature vinegar fermentation. *Biosci. Biotechnol. Biochem.* 85, 1243–1251. doi: 10.1093/bbb/zbab009

Matsushita, K., Azuma, Y., Kosaka, T., Yakushi, T., Hoshida, H., Akada, R., et al. (2016). Genomic analyses of thermotolerant microorganisms used for high-temperature fermentations. *Biosci. Biotechnol. Biochem.* 80, 655–668. doi: 10.1080/09168451.2015.1104235

Matsutani, M., Nishikura, M., Saichana, N., Hatano, T., Masud-Tippayasak, U., Theergool, G., et al. (2013). Adaptive mutation of *Acetobacter pasteurianus* SKU1108 enhances acetic acid fermentation ability at high temperature. *J. Biotechnol.* 165, 109–119. doi: 10.1016/j.jbiotec.2013.03.006

McBroom, A. J., Johnson, A. P., Vemulapalli, S., and Kuehn, M. J. (2006). Outer membrane vesicle production by *Escherichia coli* is independent of membrane instability. *J. Bacteriol.* 188, 5385–5392. doi: 10.1128/JB.00498-06

McBroom, A. J., and Kuehn, M. J. (2007). Release of outer membrane vesicles by Gram-negative bacteria is a novel envelope stress response. *Mol. Microbiol.* 63, 545–558. doi: 10.1111/j.1365-2958.2006.05522.x

Mechold, U., Murphy, H., Brown, L., and Cashel, M. (2002). Intramolecular regulation of the opposing (p)ppGpp catalytic activities of Rel(Seq), the Rel/Spo enzyme from *Streptococcus equisimilis*. *J. Bacteriol.* 184, 2878–2888. doi: 10.1128/JB.184.11.2878-2888.2002

Murata, M., Fujimoto, H., Nishimura, K., Charoensuk, K., Nagamitsu, H., Raina, S., et al. (2011). Molecular strategy for survival at a critical high temperature in *Eschierichia coli*. *PLoS One* 6:e20063. doi: 10.1371/journal.pone.0020063

Nantapong, N., Murata, R., Trakulnaleamsai, S., Kataoka, N., Yakushi, T., and Matsushita, K. (2019). The effect of reactive oxygen species (ROS) and ROS-scavenging enzymes, superoxide dismutase and catalase, on the thermotolerant ability of *Corynebacterium glutamicum*. *Appl. Microbiol. Biotechnol.* 103, 5355–5366. doi: 10.1007/s00253-019-09848-2

Ogino, H., Azuma, Y., Hosoyama, A., Nakazawa, H., Matsutani, M., Hasegawa, A., et al. (2011). Complete genome sequence of NBRC 3288, a unique cellulose-nonproducing strain of *Gluconacetobacterxylinus* isolated from vinegar. *J. Bacteriol.* 193, 6997–6998. doi: 10.1128/JB.06158-11

Paul, B. J., Ross, W., Gaal, T., and Gourse, R. L. (2004). rRNA transcription in *Escherichia coli*. *Ann. Rev. Genetics* 38, 749–770. doi: 10.1146/annurev.genet.38.072902.091347

Reece, K. S., and Phillips, G. J. (1995). New plasmids carrying antibiotic-resistance cassettes. *Gene* 165, 141–142. doi: 10.1016/0378-1119(95)00529-f

Robinson, M. D., McCarthy, D. J., and Smyth, G. K. (2010). edgeR: a Bioconductor package for differential expression analysis of digital gene expression data. *Bioinformatics* 26, 139–140. doi: 10.1093/bioinformatics/btp616

Rodriguez-Verdugo, A., Carrillo-Cisneros, D., Gonzalez-Gonzalez, A., Gaut, B. S., and Bennett, A. F. (2014). Different trade-offs result from alternate genetic adaptations to a common environment. *Proc. Nat. Acad. Sci. U. S. A.* 111, 12121–12126. doi: 10.1073/pnas.1406886111

Roghanian, M., Semsey, S., Løbner-olesen, A., and Jalalvand, F. (2019). (p)ppGpp-mediated stress response induced by defects in outer membrane biogenesis and ATP production promotes survival in*Escherichia coli*. *Sci. Rep*. 9:2934. doi: 10.1038/s41598-019-39371-3

Rudolph, B., Gebendorfer, K. M., Buchner, J., and Winter, J. (2010). Evolution of *Escherichia coli* for growth at high temperatures. *J. Biol. Chem.* 285, 19029–19034. doi: 10.1074/jbc.M110.103374

Schreiber, G., Ron, E. Z., and Glaser, G. (1995). ppGpp-mediated regulation of DNA replication and cell division in *Escherichia coli*. *Curr. Microbiol.* 30, 27–32. doi: 10.1007/BF00294520

Schwechheimer, C., Sullivan, C. J., and Kuehn, M. J. (2013). Envelope control of outer membrane vesicle production in Gram-negative bacteria. *Biochemistry* 52, 3031–3040. doi: 10.1021/bi400164t

Soemphol, W., Deeraksa, A., Matsutani, M., Yakushi, T., Toyama, H., Adachi, O., et al. (2011). Global analysis of the genes involved in the thermotolerance mechanism of thermotolerant *Acetobacter tropicalis* SKU1100. *Biosci. Biotechnol. Biochem*. 75, 1921–1928. doi: 10.1271/bbb.110310

Spiess, C., Beil, A., and Ehrmann, M. (1999). A temperature-dependent switch from chaperone to protease in a widely conserved heat shock protein. *Cell* 97, 339–347. doi: 10.1016/S0092-8674(00)80743-6

Stott, K. V., Wood, S. M., Blair, J. A., Nguyen, B. T., Herrera, A., Perez Mora, Y. G., et al. (2015). (p)ppGpp modulates cell size and the initiation of DNA replication in *Caulobacter crescentus* in response to a block in lipid biosynthesis. *Microbiology* 161, 553–564. doi: 10.1099/mic.0.000032

Strauch, K. L., Johnson, K., and Beckwith, J. (1989). Characterization of *degP*, a gene required for proteolysis in the cell envelope and essential for growth of *Escherichia coli* at high temperature. *J. Bacteriol*. 17, 2689–2696. doi: 10.1128/jb.171.5.2689-2696.1989

Sun, J., Nishiyama, T., Shimizu, K., and Kadota, K. (2013). TCC: an R package for comparing tag count data with robust normalization strategies. *BMC Bioinformatics* 14:219. doi: 10.1186/1471-2105-14-219

Taweecheep, P., Naloka, K., Matsutani, M., Yakushi, T., Matsushita, K., and Theeragool, G. (2019). In Vitro thermal and ethanol adaptations to improve vinegar fermentation at high temperature of *Komagataeibacteroboediens* MSKU 3. *Appl. Biochem. Biotechnol*. 189, 144–159. doi: 10.1007/s12010-019-03003-3

Traxier, M. F., Summers, S. M., Nguyen, H.-T., Zacharia, V. M., Hightower, G. A., Smith, J. T., et al. (2008). The global, ppGpp-mediated stringent response to amino acid starvation in *Escherichia coli*. *Mol. Microbiol.* 68, 1128–1148. doi: 10.1111/j.1365-2958.2008.06229.x

Trcek, J., Jernejc, K., and Matsushita, K. (2007). The highly tolerant acetic acid bacterium *Gluconacetobacter europaeus* adapts to the presence of acetic acid by changes in lipid composition, morphological properties and PQQ-dependent ADH expression. *Extremophiles* 11, 627–635. doi: 10.1007/s00792-007-0077-y

Vadia, S., Tse, J. L., Lucena, R., Yang, Z., Kellogg, D. R., Wang, J. D., et al. (2017). Fatty acid availability sets cell envelope capacity and dictates microbial cell size. *Curr. Biol.* 27, 1757–1767.e5. doi: 10.1016/j.cub.2017.05.076

Varik, V., Oliveira, S. R. A., Hauryliuk, V., and Tenson, T. (2017). HPLC-based quantification of bacterial housekeeping nucleotides and alarmone messengers ppGpp and pppGpp. *Sci. Rep*. 7:11022. doi: 10.1038/s41598-017-10988-6

Vercruysse, M., Fauvart, M., Jans, A., Beullens, S., Braeken, K., Cloots, L., et al. (2011). Stress response regulators identified through genome-wide transcriptome analysis of the (p)ppGpp-dependent response in *Rhizobium etli*. *Genome Biol.* 12:R17. doi: 10.1186/gb-2011-12-2-r17

Wu, Y., Yeh, F. L., Mao, F., and Chapman, E. R. (2009). Biophysical characterization of styryl dye-membrane interactions. *Biophys. J.* 97, 101–109. doi: 10.1016/j.bpj.2009.04.028

Yang, X., and Ishiguro, E. E. (2003). Temperature-sensitive growth and decreased thermotolerance associated with *relA* mutations in *Escherichia coli*. *J. Bacteriol.* 185, 5765–5771. doi: 10.1128/JB.185.19.5765-5771.2003

Conflict of Interest: The authors declare that the research was conducted in the absence of any commercial or financial relationships that could be construed as a potential conflict of interest.

Publisher's Note: All claims expressed in this article are solely those of the authors and do not necessarily represent those of their affiliated organizations, or those of the publisher, the editors and the reviewers. Any product that may be evaluated in this article, or claim that may be made by its manufacturer, is not guaranteed or endorsed by the publisher.

Advantages of publishing in Frontiers

OPEN ACCESS
Articles are free to read for greatest visibility and readership

FAST PUBLICATION
Around 90 days from submission to decision

HIGH QUALITY PEER-REVIEW
Rigorous, collaborative, and constructive peer-review

TRANSPARENT PEER-REVIEW
Editors and reviewers acknowledged by name on published articles

Frontiers
Avenue du Tribunal-Fédéral 34
1005 Lausanne | Switzerland

Visit us: www.frontiersin.org
Contact us: frontiersin.org/about/contact

REPRODUCIBILITY OF RESEARCH
Support open data and methods to enhance research reproducibility

DIGITAL PUBLISHING
Articles designed for optimal readership across devices

FOLLOW US
@frontiersin

IMPACT METRICS
Advanced article metrics track visibility across digital media

EXTENSIVE PROMOTION
Marketing and promotion of impactful research

LOOP RESEARCH NETWORK
Our network increases your article's readership